DOE Award Number: DE-FG02-07ER64329

DOE Final Report

Project Title: Aerosol Absorption and Scattering Measurements: Field Measurements and Laboratory Characterizations.

Principal Investigator: Nancy A. Marley
University of Arkansas at Little Rock
Graduate Institute of Technology
501-5698844 email: namarley@ualr.edu

Co-Principal Investigator: Jeffrey S. Gaffney
University of Arkansas at Little Rock
Dept. of Chemistry
501-569-8840 email: jsgaffney@ualr.edu

Project Description and Overview:

Objectives:

Determining the overall impact of atmospheric aerosols on radiative balance requires knowledge of the relative amounts of scattering and absorbing aerosols, their distributions, and their chemical and optical properties. This proposal was a continuation of measurements of aerosol scattering and absorption begun in Mexico City in 2003 in collaboration with MCMA 2003 and continuing in the Atmospheric Science Program field study, Megacity Aerosol Experiment-Mexico City, (MAX-Mex) during March of 2006 aimed at determining the variability of aerosol optical properties.

A suite of instrumentation was deployed in MAX-Mex at site T0, located in the northern part of the Mexico City Metropolitan Area, (MCMA), for the characterization of the aerosol optical properties in the field. Measurements were made of the following aerosol properties: (1) aerosol absorption as a function of wavelength, measured at two minute intervals with a 7-wavelength Aethalometer (2) aerosol scattering as a function of wavelength, measured at one minute intervals with a 3-wavelength nephelometer; 3) aerosol scattering as a function of relative humidity (RH), measured at one minute intervals with 2 single-wavelength nephelometers operated under dry (10% RH) and wet (80% RH) conditions; and 4) collection of size-fractionated aerosol samples on quartz fiber filters at 12 hour intervals (day/night) for further laboratory characterization. Aerosol filter samples were also collected at site T1 (located north of MCMA) for comparison with those collected in the city center. Preliminary results from in situ measurements have indicated an enhanced UV absorption in the afternoon over that expected from black carbon (BC) aerosols alone. These results are directly applicable to both modeling of aerosol radiative forcing and satellite optical depth retrieval algorithms. Both of these applications assume that the aerosol absorption is due only to BC with a wavelength dependence of λ^{-1} whereas results obtained in MAX-Mex show that the aerosol wavelength exponent varies over Mexico City from -0.7 to -1.5.

All of the data collected in the field from the measurement sets 1-3 have been made available to the ASP community via the MILAGRO data site housed at NCAR. The laboratory characterization of aerosol samples collected in the ASP MAX-Mex field study compared results from Mexico City to samples collected at other sites, including Chicago, Little Rock, and Mt. Bachelor, OR. The project focused on obtaining complete spectral characterization of aerosols – especially their absorption characteristics as they relate to basic chemical functional groups. Particular attention was given to organics and from biogenic derived organic compounds. This included determinations of the UV-Visible-NIR characteristics of the aerosol absorption as reported as Angstrom Absorption Exponents. Correlation of these results with IR band observations of carboxylic acid, and carboxylate groups were conducted, along with past correlations with carbon isotopic data that indicated significant enhancements of UV-Visible absorption from biogenic aerosols (both biomass burning and secondary organic aerosols).

Relationships to other ASP Projects

This project collaborated with a number of currently funded ASP projects including research being conducted by Dr. W. Patrick Arnott at the University of Nevada, Reno. Dr. Arnott made use of photoacoustic spectroscopy and light scattering at one or two wavelengths to determine SSA of the aerosol. Comparison of the aethalometer data as well as MAAP instrumentation yielded good to excellent agreement between the instruments and allowed for wider spectral determinations of the carbonaceous aerosol absorptions. A number of collaborative papers have been published with colleagues from Pacific Northwest National Laboratory, the University of Colorado, and Virginia Tech. Collaborations with other MILAGRO participants including Mexican scientists (B. Cardenas and R. Ramos) have also resulted in publications and compared optical aerosol properties at T-0 and T-1 sites with Dr. Telma Castro of UNAM. We are also collaborated with Dr. Emily Fischer who was selected as the Marv Wesely GREF fellow for 2010 in helping to optically and chemically characterize aerosol samples collected at Mt. Bachelor in Oregon, who published the collaborative results as part of her Ph.D. thesis.

Findings

We completed measurements and evaluations of data taken as part of MILAGRO. Data taken at the University of Chicago and that were intercompared with regard to the aerosol absorption with that found here at UALR and in Mexico City found similar results in that where there was indication of biogenic sources of secondary organic aerosols enhanced UV absorption was observed along with infrared spectra that indicated the presence of humic-like substances (HULIS).

In combination with ^{14}C determinations taken in a related project "Natural Radionuclides and Isotopic Signatures for Determining Carbonaceous Aerosol Sources, Aerosol Lifetimes, and Washout Processes", results from this project determined that the source of carbonaceous aerosols in many area studied (Mexico City, Cool, Ca, UALR) had a significant fraction of biogenic carbon in many cases greater than 50% and in the CARES and studies here in the southern U.S. over 75% biogenic origin as determined by the enhanced Angstrom Absorption Extinctions (AAEs) observed were strongly correlated. Data was also obtained for the CARES field study that also clearly show enhanced UV-Vis absorption from carbonaceous aerosols

derived from biogenic sources. Collaborative work with the University of Washington via the Global Change Education Program examining long range transport of aerosols into the U.S. was accomplished examining trace element concentrations determined from PSAP filters, and comparison of AAE's in these samples were also used to "trace" biogenic carbonaceous aerosols from wood smoke events.

Details of the methodologies and results determined were presented at national meetings and papers were published in the peer-reviewed literature. They are listed below:

Data from this project was also used collaboratively by other ASR researchers that produced a number of peer-reviewed papers. These papers included MAX-Mex and CARES efforts that used the data obtained from the project to better interpret aerosol mass spectroscopy, aerosol growth measurements from both field and aircraft studies, as well as modeling efforts. In some of these cases we were asked to assist in the interpretation and were co-authors on the papers. Others the data were used and acknowledged. We have listed collaborative work in the publication list where we were included as co-authors, and have included an invited overview chapter for Atmospheric Environment that the P.I. and Co-P.I. wrote as part of their DOE effort.

This project also helped to train a number of graduate students in the area of climate change science and the students supported are listed below.

Graduate Students supported and trained on this project.
Current:
M. Begum, UALR Applied Science (Chemistry), Ph.D. candidate
A. Sarkar, UALR Applied Science (Chemistry), M.S. candidate, 2013.
A. Marchany-Rivera, UALR Applied Science (Physics) Ph.D. candidate

Graduated Students:
G. Gunawan, Chemistry, M.S. Dec. 2008
A. Mangu, Chemistry, M.S. Dec. 2007;
S. Kilaparty, Chemistry, M.A., May 2009
K.L. Kelly, UALR Chemistry, M.S., Dec. 2010;
G.L. Bridges, Chemistry, M.A., May 2011
E. Alvarez, UALR Applied Science (Physics), M.S. May 2012.

Peer Reviewed Publications (2007-2012):

1. E.J. Dunlea, S.C. Herndon, D. D. Nelson, R.M. Volkamer, F. San Martini, M.S. Zahniser, J.H. Shorter, J.C. Wormhoudt, B.K. Lamb, E.J. Allwine, J.S. Gaffney, N.A. Marley, M. Grutter, C. Marquez, S. Blanco, B. Cardenas, C.R. Ramos Villegas, C.E. Kolb, L.T. Molina and M.J. Molina, "Evaluation of nitrogen dioxide chemiluminescent monitors in a polluted urban environment." Atmos. Chem. Phys. 7, 569-604 (2007).

2. N.A. Marley, J. S. Gaffney, R. Ramos-Villegas and B. Cárdenas González, "Comparison of Measurements of Peroxyacyl Nitrates and Primary Carbonaceous Aerosol Concentrations in Mexico City Determined in 1997 and 2003." Atmos. Chem. Phys., 7, 2277-2285 (2007).

3. D. A. Thornhill, S. C. Herndon, T. B. Onasch, E. C. Wood, M. Zavala, L. T. Molina, J. S. Gaffney, N. A. Marley, and L. C. Marr, "Particulate polycyclic aromatic hydrocarbon spatial variability and aging in Mexico City." Atmos. Chem. Phys. 8, 3093-3105 (2008).

4. N. A. Marley, J. S. Gaffney, T. Castro, A. Salcido, and J. Frederick, "Measurements of Aerosol Absorption and Scattering in Mexico City during the MILAGRO field campaign: A Comparison of Results from the T0 and T1 sites." Atmos. Chem. Phys., 9, 189-206 (2009).

5. Jeffrey S. Gaffney and Nancy A. Marley, "The Impacts of Combustion Emissions on Air Quality and Climate: From Coal to Biofuels and Beyond" Atmos. Env. 43, 23-36 (2009).

6. G. Paredes-Miranda, W. P. Arnott, J. L. Jimenez, A. C. Aiken, J. S. Gaffney, and N. A. Marley, "Primary and secondary contributions to aerosol light scattering and absorption in Mexico City during the MILAGRO 2006 campaign" Atmos. Chem. Phys., 9, 3721-3730 (2009).

7. N. A. Marley, J. S. Gaffney, M. J. Tackett, N. C. Sturchio, L. Heraty, N. Martinez, K. D. Hardy, A. Marchany-Rivera, T. Guilderson, A. MacMillan, and K. Steelman, "The impact of biogenic carbon sources on aerosol absorption in Mexico City" Atmos. Chem. Phy. 9, 1537-1549 (2009).

8. A.C. Aiken, D. Salcedo, M.J. Cubison, J.A. Huffman, P.F. DeCarlo, I.M. Ulbrich, K.S. Docherty, D. Sueper, J.R. Kimmel, D.R. Worsnop, A. Trimborn, M. Northway, E.A. Stone, J.J. Schauer, R. Volkamer, E. Fortner, B. de Foy, J. Wang, A. Laskin, V. Shutthanandan, J. Zheng, R. Zhang, J. Gaffney, N. Marley, G. Paredes-Miranda, W.P. Arnott, L.T. Molina, G. Sosa, and J.L. Jimenez, "Mexico City Aerosol Analysis during MILAGRO using High Resolution Aerosol Mass Spectrometry at the Urban Supersite (T0). Part 1: Fine Particle Composition and Organic Source Apportionment", Atmos. Chem. Phys., 9, 6633-6653 (2009).

9. J. D. Fast, A. C. Aiken, J. Allan, L. Alexander, T. Campos, M. R. Canagaratna, E. Chapman, P. F. DeCarlo, B. de Foy, J. Gaffney, J. de Gouw, J. C. Doran, L. Emmons, A. Hodzic, S. C. Herndon, G. Huey, J. T. Jayne, J. L. Jimenez, L. Kleinman, W. Kuster, N. Marley, L. Russell, C. Ochoa, T. B. Onasch, M. Pekour, C. Song, I. M. Ulbrich, C. Warneke, D. Welsh-Bon, C. Wiedinmyer, D. R. Worsnop, X.-Y. Yu, and R. Zaveri, "Evaluating simulated primary anthropogenic and biomass burning organic aerosols during MILAGRO: implications for assessing treatments of secondary organic aerosols." Atmos. Chem. Phys. 9, 6191-6215 (2009).

10. Fischer, E. V., D. A. Jaffe, N. A. Marley, J. S. Gaffney, and A. Marchany-Rivera (2010), Optical properties of aged Asian aerosols observed over the U.S. Pacific Northwest, J. Geophys. Res., 115, D20209, doi:10.1029/2010JD013943.

11. Molina, L. T. S. Madronich, J. S. Gaffney, E. Apel, B. de Foy, J. Fast, R. Ferrare, S. Herndon, J. L. Jimenez, B. Lamb, A. R. Osornio-Vargas, P. Russell, J. J. Schauer, P. S. Stevens,

R. Volkamer, and M. Zavala. " An overview of the MILAGRO 2006 Campaign: Mexico City emissions and their transport and transformation." Atmos. Chem. Phys., 10, 1–64, 2010.

12. Jeffrey S. Gaffney and Nancy A. Marley, "Climate Impacts from Agricultural Emissions: Greenhouse Species and Aerosols." Chapter 15 in ACS Symposium Volume, "Understanding Greenhouse Gas Emissions from Agricultural Management ." Edited by Lei Guo, Amrith Gunasekara, Laura McConnell, USDA-ARS (2011), pp. 275-295, doi: 10.1021/bk-2011-1072.ch015.

13. R. A. Zaveri, W. J. Shaw, D. J. Cziczo, B. Schmid, R. A. Ferrare, M. L. Alexander, M. Alexandrov5, R. J. Alvarez, W. P. Arnott, D. B. Atkinson, S. Baidar, R. M. Banta, J. C. Barnard, J. Beranek, L. K. Berg, F. Brechtel, W. A. Brewer, J. F. Cahill, B. Cairns, C. D. Cappa, D. Chand, S. China, J. M. Comstock, M. K. Dubey, R. C. Easter, M. H. Erickson, J. D. Fast, C. Floerchinger, B. A. Flowers, E. Fortner, J. S. Gaffney, M. K. Gilles, K. Gorkowski, W. I. Gustafson, M. Gyawali, J. Hair, R. M. Hardesty, J. W. Harworth, S. Herndon, N. Hiranuma, C. Hostetler, J. M. Hubbe, J. T. Jayne, H. Jeong, B. T. Jobson, E. I. Kassianov, L. I. Kleinman, C. Kluzek, B. Knighton, K. R. Kolesar, C. Kuang, A. Kubátová, A. O. Langford, A. Laskin, N. Laulainen, R. D. Marchbanks, C. Mazzoleni, F. Mei, R. C. Moffet, D. Nelson, M. D. Obland, H. Oetjen, T. B. Onasch, I. Ortega, M. Ottaviani, M. Pekour, K. A. Prather, J. G. Radney, R. R. Rogers, S. P. Sandberg, A. Sedlacek, C. J. Senff, G. Senum, A. Setyan, J. E. Shilling, M. Shrivastava, C. Song, S. R. Springston, R. Subramanian, K. Suski, J. Tomlinson, R. Volkamer, H. W. Wallace, J. Wang, A. M. Weickmann, D.R. Worsnop, X.-Y. Yu, A. Zelenyuk, and Q. Zhang. "Overview of the 2010 Carbonaceous Aerosols and Radiative Effects Study (CARES)." Atmos. Chem. Phys., 12, 7647-7687, 2012

Presentations at Scientific Meetings (2007-2012):

1.. Paredes-Miranda, G., Arnott, W. P., Marley, N.A., Gaffney, J. S., "A Tale of two Cities: Photoacoustic and Aethalometer Measurements Comparisons of Light Absorption in Mexico City and Las Vegas, NV, USA" EOS Trans. AGU, 88, (23), Jt. Assem. Suppl. Abstract A41E-08 (2007)

2.. Marley, N.A. and Gaffney, J.S. "The Impact of Rain Events on Aerosol Optical Properties: Mexico City 2003 and 2006" EOS Trans. AGU, 88, (23), Jt. Assem. Suppl. Abstract A41E-03 (2007)

3. Arnott, W. P., Miranda, G. P., Gaffney, J. S., and Marley, N.A. "Aerosol Light Absorption and Scattering at Four Sites in and Near Mexico City: Comparison with Las Vegas, Nevada, USA" EOS Trans. AGU, 88, (23), Jt. Assem. Suppl. Abstract A41E-07 (2007).

4.. Gaffney, J.S., Marley, N.A., Tackett, M.J., Sturchio, N.C., Heraty, L.J., Martinez, N., Hardy, K., Guilderson, T., 2007: Evidence for biomass burning from ^{14}C and $^{13}C/1^{2}C$ Measurements at T0 and T1 during MILAGRO. Eos Trans. AGU, 88(52), Fall Meet. Suppl., Abstract A43C-1420.

5. Marley, N.A., Marchany-Rivera, A., Kelley, K. L., Mangu, A., Gaffney J.S., 2007: Aerosol Angstrom Absorption Coefficient Comparisons during MILAGRO. Eos Trans. AGU, 88(52), Fall Meet. Suppl., Abstract A43C-1421.

6. Mangu, A., Kelley, K.L., Marchany-Rivera, A., Kilaparty, S., Gunawan, G., Gaffney, J.S., and Marley, N.A., 2007. Enhanced UV Absorption in Carbonaceous Aerosols during MILAGRO and Identification of Potential Organic Contributors. Eos Trans. AGU, 88(52), Fall Meet. Suppl., Abstract A43C-1419.

7. Gaffney, J.S., Marley, N.A., Arnott, W.P., Paredes-Miranda, L., Barnard, J.C., Aerosol Absorption Measurements in MILAGRO. 2007. Eos Trans. AGU, 88(52), Fall Meet. Suppl., Abstract A32A-01 Invited.

8. Paredes-Miranda, G., Arnott, W.P., Gaffney, J.S., Marley, N.A., Campbell, D., Fujita, E. Aerosol Light Absorption in Mexico City: Comparison with Las Vegas, NV and Los Angeles, CA. 2007 Eos Trans. AGU, 88(52), Fall Meet. Suppl., Abstract A43C-1422.

9. Aiken, A.C., Salcedo, D., Huffman, J.A., Ulbrich, I., DeCarlo, P.F., Cubison, M., Docherty, K., Sueper, D., Worsnop, D.R., Trimborn, A., Northway, M., Prevot, A., Szidat, S., Wehrli, M.N., Wiedermeyer, C., Wang, J., Zheng, J., Fornter, E., Zhang, R., Gaffney, J.S., Marley, N.A., Sosas Iglesias, G.E., Jimenez, J.L., 2007. Aerosol Analysis with the High Resolution Time-of-Flight Aerosol Mass Spectrometer at the Urban Supersite (T0) in Mexico City during MILAGRO. Eos Trans. AGU, 88(52), Fall Meet. Suppl., Abstract A23C-1467.

10. N. .A. Marley, J.S., Gaffney, T. Castro, and A. Salcido (2008) "A comparison of aerosol optical properties at T1 and T0 during the MILAGRO field study" 88th National Meeting of the American Meteorological Society. Tenth Conference on Atmospheric Chemistry, Conference Proceedings Volume, Paper J1.2, 4 pp.

11. S. P. Kilaparty, K.L. Kelley, A. Mangu, J.S. Gaffney, and N.A. Marley, (2008) "Determination of aerosol absorption constants from MILAGRO and MCMA 2003 field samples by using integrating sphere spectrometry" 88th National Meeting of the American Meteorological Society. Tenth Conference on Atmospheric Chemistry, Conference Proceedings Volume, Paper P1.8, 5 pp.

12. K.L. Kelley, A. Mangu, J.S. Gaffney, and N.A. Marley, (2008) "Infrared spectra of aerosol samples from Mexico City during MILAGRO and MCMA 2003." 88th National Meeting of the American Meteorological Society. Tenth Conference on Atmospheric Chemistry, Conference Proceedings Volume, Paper P1.5, 4 pp.

13. J. S. Gaffney, N.A. Marley, M. Tackett, N.Stuchio, L. Heraty, N. Martinez, K. Hardy, and T. Guilderson, (2008) "Biogenic Carbon Dominance Based on 13C/12C and 14C Measurements of Total Carbon at T-0 and T-1 Sites during MILAGRO." 88th National Meeting of the American Meteorological Society. Tenth Conference on Atmospheric Chemistry, Conference Proceedings Volume, Paper J1.1, 5 pp. http://ams.confex.com/ams/pdfpapers/131852.pdf.

14. Marley, N.A., Kelley, K.L., Kilaparty, P.S., Gaffney, J.S., (2008) "Light Absorbing Aerosols in Mexico City" Eos Trans. AGU, 89(53), Fall Meet. Suppl., Abstract A11E-0185.

15. Gaffney, J.S., Marley, N.A., (2008) "Absorption of Visible and Long-wave Radiation by Primary and Secondary Biogenic Aerosols." Trans. AGU, 89(53), Fall Meet. Suppl., Abstract A11E-0182.

16. Nancy A. Marley and Jeffrey S. Gaffney "Formation and transformation of Humic-Like Substances (HULIS) in atmospheric aerosols: Relation to climate forcing" 89th AMS National Meeting Tenth Conference on Atmospheric Chemistry, Conference Proceedings Volume, Paper J1.2, 3 pp. (2009)

17. Jeffrey S. Gaffney and Nancy A. Marley, "Absorbing Aerosols from Agricultural Burning and Biomass Emissions." 89th National Meeting of the American Meteorological Society. Tenth Conference on Atmospheric Chemistry, Conference Proceedings Volume, Paper J1.1, 4 pp. (2009).

18. N.A. Marley, J. S. Gaffney, V. Rajaram, and E. V. Fischer, "Determining Aerosol Angstrom Absorption Coefficients: Comparison of Full Spectrum Integrating Sphere Reflection Spectroscopy with 3 and 7 Wavelength Filter Absorption Methods" 89th National Meeting of the American Meteorological Society. 12th Symposium on Atmospheric Chemistry, Conference Proceedings Volume, Paper J17.5. (2010).

19. Jeffrey S. Gaffney and N. A. Marley, "Anthropogenic Perturbations of Biogenic Aerosols: Climate Impacts and Feedbacks " 89th National Meeting of the American Meteorological Society. 12th Symposium on Atmospheric Chemistry, Conference Proceedings Volume, Paper J17.2. (2010).

20. Nancy A. Marley, Jeffrey S. Gaffney, and Amrita Sarkar, "Further Determination of Humic Like Substance (HULIS) Content in Absorbing Aerosols by FTIR Spectroscopy: CARES and Other Field Results." EOS Traans. AGU 91, Fall Meet. Suppl. Abstract A21B-0052 (2010).

21. Jeffrey S. Gaffney, Nancy A. Marley, Mahbuba Begum, Neil Sturchio, and Thomas P. Guilderson. "Carbon Isotopic Measurements and Aerosol Optical Determinations during CARES: Indications of the Importance of Background Biogenic Aerosols." EOS Trans. AGU 91, Fall Meet. Suppl. Abstract A13C-0304 (2010).

22. Nancy A. Marley and Jeffrey S. Gaffney, "Spectroscopic Characterization of Fine Mode Atmospheric Aerosols." Oral presentation at the ACS Southwest Regional Meeting, November 9-12, 2011 Austin, TX.

23. Amrita Sarkar, Jeffrey S. Gaffney and Nancy A. Marley, "Spectroscopic Characterization of Water Soluble Organic Compounds Present in Precipitation." Oral presentation at the ACS Southwest Regional Meeting, November 9-12, 2011 Austin, TX.

24. Mahbuba Begum, Jeffrey S. Gaffney and Nancy A. Marley, "Natural Radionuclides as Indicators of Atmospheric Aerosol Lifetimes: Measurements made at the University of Arkansas at Little Rock." Oral presentation at the ACS Southwest Regional Meeting, November 9-12, 2011, Austin, TX.

25. Nancy A. Marley, Jeffrey S. Gaffney, and Amrita Sarkar, "Further Determination of Humic Like Substance (HULIS) Content in Absorbing Aerosols by FTIR Spectroscopy: CARES and Other Field Results." Poster Presentation at the Fall Meeting of the American Geophysical Union, December 5-9, 2011, San Francisco, California, Poster No. A21B-0052.

26. Jeffrey S. Gaffney, Nancy A. Marley, Mahbuba Begum, Niel Sturchio, and Thomas P. Guilderson. "Carbon Isotopic Measurements and Aerosol Optical Determinations during CARES: Indications of the Importance of Background Biogenic Aerosols." Poster Presentation at the Fall Meeting of the American Geophysical Union, December 14-18, 2009, San Francisco, California, Poster No. A13C-0304.

Optical properties of aged Asian aerosols observed over the U.S. Pacific Northwest

E. V. Fischer,[1] D. A. Jaffe,[1,2] N. A. Marley,[3] J. S. Gaffney,[4] and A. Marchany-Rivera[5]

Received 27 January 2010; revised 5 May 2010; accepted 10 June 2010; published 29 October 2010.

[1] A suite of gas-phase and aerosol measurements were made during spring 2008 and spring 2009 at the Mount Bachelor Observatory (2763 masl), located in Oregon. Here we focus on multiwavelength observations of low RH submicron (μm) aerosol scattering (σ_{sp}) and absorption (σ_{ap}), made with an integrating nephelometer and a particle soot absorption photometer. Using a combination of in situ observations, trajectory calculations and satellite observations, we identified seven plumes of Asian origin. These plumes included many of the highest σ_{sp} (34.8 Mm^{-1}) and σ_{ap} (5.7 Mm^{-1}) hourly average values observed at MBO over the 2008 and 2009 campaigns. Of interest in this analysis is (1) whether the intensive optical properties differ between these seven plumes, (2) whether these differences can be linked to differences in composition, and (3) whether the intensive optical properties change during transpacific transport. Results show that the plumes clustered in terms of their optical properties; plumes hypothesized to contain a large fraction of mineral dust were the most distinct. We observed variability between plumes in the scattering Ångström ($Å_s$) exponent. The average submicrometer $Å_s$ for all seven plumes was significantly larger than the same parameter observed closer to Asia. Therefore, we hypothesize that the aerosol size distribution shifts toward smaller particles during transpacific transport. The average submicrometer low-RH aerosol single scatter albedo (ω) observed at MBO (0.88) was slightly larger than previous observations closer to the Asian coast, and the average backscatter fraction (b) was smaller, on the order of 20%.

Citation: Fischer, E. V., D. A. Jaffe, N. A. Marley, J. S. Gaffney, and A. Marchany-Rivera (2010), Optical properties of aged Asian aerosols observed over the U.S. Pacific Northwest, *J. Geophys. Res.*, *115*, D20209, doi:10.1029/2010JD013943.

1. Introduction

[2] Aerosols are an important component of the climate system, and the impact of increased atmospheric aerosol loading due to anthropogenic activities has yet to be fully quantified [*Rockström et al.*, 2009]. Aerosols absorb and scatter solar radiation, and this is known as the aerosol direct effect. The present uncertainty in the global aerosol direct effect is of the same magnitude as the effect itself [*Intergovernmental Panel on Climate Change (IPCC)*, 2007]. Over the past decade, several assessments have highlighted the areas of uncertainties in assessing the global aerosol direct effect. One recurring issue is an incomplete in situ observational record [*Diner et al.*, 2004; *Kaufman et al.*, 2002]. To minimize the uncertainties associated with the anthropogenic aerosol effect on climate we need to (1) relate aerosol optical properties to emissions from specific source regions, (2) separate the natural aerosol from the anthropogenic component, and (3) develop a better understanding of how the optical properties of aerosols change with time and processing [*Kaufman et al.*, 2002].

[3] The scattering and absorption properties of atmospheric aerosols consist of the wavelength-dependent scattering coefficient (σ_{sp}), the wavelength-dependent absorption coefficient (σ_{ap}), and the angular distribution of the scattered light. Both of the coefficients (σ_{sp} and σ_{ap}) can be measured by in situ instruments and have units of inverse length (Mm^{-1}). The σ_{sp} (σ_{ap}) is the product of the aerosol scattering (absorption) cross section and the concentration of scattering (absorbing) particles.

[4] The wavelength dependence of aerosol scattering has historically been parameterized as proportional to $\lambda^{-Å_s}$, where $Å_s$ is the aerosol scattering Ångström exponent [*Ångström*, 1929]. The scattering properties of aerosols are a function of particle size. For large particles, such as sea salt and dust, σ_{sp} changes little with wavelength, so $Å_s$ is small. For small particles, such as those generated by gas-to-particle conversion or directly from combustion, σ_{sp} decreases rapidly with wavelength, so $Å_s$ is larger [*Boren and Huffman*, 1983]. The

[1]Department of Atmospheric Sciences, University of Washington, Seattle, Washington, USA.
[2]Science and Technology Program, University of Washington Bothell, Bothell, Washington, USA.
[3]Graduate Institute of Technology, University of Arkansas at Little Rock, Little Rock, Arkansas, USA.
[4]Department of Chemistry, University of Arkansas at Little Rock, Little Rock, Arkansas, USA.
[5]Department of Applied Science, University of Arkansas at Little Rock, Little Rock, Arkansas, USA.

0148-0227/10/2010JD013943

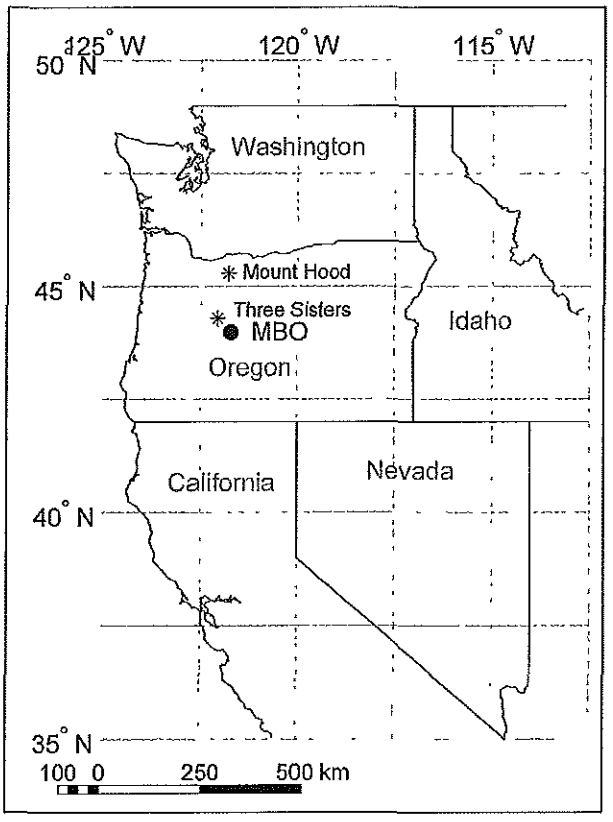

Figure 1. Location of Mount Bachelor and two other relevant IMPROVE monitoring sites: Mount Hood and Three Sisters Wilderness Area.

aerosol absorption coefficient has been parameterized analogously as proportional to $\lambda^{-Å_a}$, where $Å_a$ is the aerosol absorption Ångström exponent. $Å_a$ depends on the size, composition, shape and mixing state of the aerosols [*Bergstrom et al.*, 2007]. Determining the spectral variation of aerosol scattering and absorption is important because it allows measurements of σ_{sp} and σ_{ap} at specific wavelengths to be extrapolated over the solar spectrum. The relationship between $Å_s$ and $Å_a$ varies with aerosol composition, and can be used to stratify in situ data by plume type [*Clarke et al.*, 2007; *Yang et al.*, 2009]. The spectral variation of absorption ($Å_a$) has been used to separate absorption from dust aerosols from combustion-generated carbonaceous aerosols [*Fialho et al.*, 2005].

[5] Two other important intensive properties can be derived from measurements of σ_{ap}, σ_{sp}, and the aerosol backscattering coefficient (σ_{bsp}). The single scatter albedo (ω) is the fraction of total light extinction due to scattering, and the value of ω determines whether an aerosol layer causes net heating or cooling [*Haywood and Shine*, 1995]. The ratio of aerosol scattering directed toward the backward hemisphere to scattering in all directions to is called the backscatter ratio (b). For specific particle types, the angular distribution of scattering can be approximated from b, and thus b can be used to estimate the fraction of incoming solar radiation that aerosols redirect toward space [*Marshall et al.*, 1995].

[6] Atmospheric aerosols in the free troposphere over the west coast of the United States can be broadly classified into three categories by their sources: industrial, dust and biomass burning. Industrial aerosols can have a North American source or they can be advected across the Pacific from Asia [*Anderson et al.*, 1999; *Heald et al.*, 2006; *Jaffe et al.*, 1999]. There is strong evidence that aerosols from East Asia significantly impact air quality and regional climate over North America, especially during spring [*VanCuren*, 2003; *Wuebbles et al.*, 2007; *Yu et al.*, 2008]. The direct emissions of aerosols and their gas-phase precursors will continue to rise in East Asia due to increases in energy consumption and a continued reliance on coal [*Carmichael et al.*, 2009].

[7] The springtime transport of Asian dust across the Pacific has been well documented [*Husar et al.*, 2001; *Jaffe et al.*, 2003a]. Although Asian dust impacts the United States throughout the year [*VanCuren and Cahill*, 2002] spring is the preferred season due to the intense frontal activity that allows for lofting and enhanced outflow from Asia. Dust plumes are generally transported higher than pollution plumes, this combined with a lower wet scavenging efficiency can allow up to ~3 times more fine dust aerosols to reach the United States from Asia than other types of aerosols [*Chin et al.*, 2007]. The impact of dust is not isolated to large plumes. Approximately 50% of the interannual variability in springtime average $PM_{2.5}$ in remote areas of the U.S. Pacific Northwest can be explained by year-to-year changes in Asian dust emissions [*Fischer et al.*, 2009].

[8] Biomass burning is one of the largest global sources of accumulation mode (<1 μm diameter) particles, implying radiative and geochemical impacts [*Reid et al.*, 2004, 2005]. The largest number of fires in the western United States occurs from May to October [*Westerling et al.*, 2003]. However, in the Northern Hemisphere the biomass burning maximum occurs in spring, largely dominated by African and Southeast Asian sources [*Duncan et al.*, 2003]. Siberian biomass burning plumes can travel to western North America and the North American Arctic relatively quickly, on the order of a week, and boreal fires generally take place from May to September [*Duncan et al.*, 2003; *Jaffe et al.*, 2004]. In spring 2008 the Russian boreal forest fire season started unusually early due to low snow amounts (http://rapidfire.sci.gsfc.nasa.gov/firemaps/) [*Warneke et al.*, 2009].

[9] Since its establishment, the Mount Bachelor Observatory (MBO) (2763 m amsl) has proven to be well positioned to observe the transpacific transport of Asian industrial, dust and biomass burning plumes [*Weiss-Penzias et al.*, 2007, 2006]. We report here on springtime observations of submicrometer aerosol optical properties from MBO, located in the lower free troposphere over the Pacific Northwest. These observations are valuable for a number of reasons. The submicrometer aerosol observations at MBO integrate aerosol size, shape, chemistry and mixing state, and therefore apply to the entire fine mode aerosol population. Second, the observations at MBO were made over a relatively long time scale (>1000 h for each spring campaign) and with a high enough time resolution to allow separation of plume conditions from background aerosol. We identify seven well-defined plumes of Asian origin and use a variety of supporting in situ data, satellite observations and model analysis to gain information on plume composition. Owing to the close proximity of anthropogenic, biomass burning and dust aerosol sources,

each plume leaving Asia reflects a different mixture of aerosols. Relationships between the observed optical properties are noted for plumes observed at MBO, and we attempt to identify plumes with a large mineral dust component. Finally, the optical properties for the seven plumes observed at MBO are compared to similar observations closer to the Asian source region.

2. Methods

2.1. Site Description and Sampling Configuration

[10] The observations used in this paper were made in April–May 2008 and April–May 2009 at the Mount Bachelor Observatory (MBO). MBO is located on the summit of a dormant volcano in central Oregon (43.98°N 121.7°W, 2763 m amsl) (Figure 1). Separate aerosol and gas sampling inlets were located 3 m above the roof of the summit lift building, and the instruments were located in a room within the building, situated approximately 15 m below the inlet. The aerosol sample line was situated such that the last 2.5 m were located within the space which was temperature controlled at 20 ± 3°C, typically 10°–20°C warmer than ambient. The aerosol inlet line was constructed of 0.688″ ID conductive tubing. The inlet faced down and there were no sharp bends in the line where aerosols could accumulate. Total flow through the aerosol line was ~35 L min^{-1}. Carbon monoxide (CO), ozone (O_3), NO_x ($NO_x = NO + NO_2$), PAN and total reactive nitrogen (NO_y) were sampled through a 1/4″ internal diameter PFA Teflon line, with a 1 μm Teflon filter located at the inlet. Temperature (T), relative humidity (RH), pressure (P), and wind direction were also measured at the summit. The methods pertaining to the ongoing gas-phase measurements (CO and O_3) have been described previously [*Weiss-Penzias et al.*, 2006]. The methods pertaining to the reactive nitrogen measurements are described separately [*Fischer et al.*, 2010; *Reidmiller et al.*, 2010]. All data are reported in GMT which is 7 h later than local Pacific Daylight Time (GMT = PDT + 7).

2.2. Aerosol Measurements

2.2.1. Overview of Aerosol Measurements

[11] The aerosol stream was split approximately 14 m downstream of the inlet into two air streams (both constructed of 0.688″ ID conductive tubing), from one a Radiance Research (M903) nephelometer measured midvisible (530 nm) submicrometer dry aerosol scattering. The methods pertaining to the single wavelength scattering measurements have been described previously [*Weiss-Penzias et al.*, 2006].

[12] Multiwavelength submicrometer aerosol light scattering and absorption were measured from the second air stream. An integrating nephelometer (Model 3563, TSI Inc., St. Paul, Minnesota) was used to measure submicrometer dry (RH < 30%) light scattering (σ_{sp}) and hemispheric backscattering (σ_{bsp}; i.e., 90°–180° scattering) at three wavelengths (450, 550, and 700 nm) [*Anderson et al.*, 1996; *Heintzenberg and Charlson*, 1996]. Backscattering was measured during spring 2009 but not in spring 2008. Preceding the integrating nephelometer was a Berner impactor [*Berner et al.*, 1979] run at 30 L min^{-1} and employing a greased substrate to prevent particle bounce. This flow rate gives a 50% aerodynamic cutoff diameter of 1 μm. The airstream was not intentionally dried; instead the temperature increase from outdoors into the heated building reduced the RH of the incoming airstream.

[13] Aerosol absorption (σ_{ap}) at three wavelengths was measured with a Particle Soot Absorption Photometer (PSAP) (Radiance Research, Shoreline, Washington). This device responds to differential light transmission through a glass fiber filter (E70–2075W, Pallflex Products Corp., Putnam, Connecticut) as particles are loaded onto the filter. The absorption measurement was made immediately downstream of the nephelometer, ensuring that the scattering and absorption properties were measured on the identical aerosol.

[14] The raw scattering and absorption data were collected as 20 s averages and then reduced to 1 h averages. Periods of likely snowcat contamination, identified by simultaneous drastic spikes in NO and aerosol absorption, were removed from the raw data prior to averaging. All scattering and absorption coefficients are reported at a wavelength of 550 nm, 273.15 K and 1013.25 hPa.

2.2.2. Calibration, Data Reduction, and Uncertainty

[15] The TSI nephelometer calibration protocol differed slightly between spring 2008 and spring 2009. Instrument noise was periodically measured and traced throughout the spring 2008 campaign using an inline HEPA filter. The filter was put in-line for a minimum of 30 min at approximately two week intervals. No trend was noted in the zero data. Multiple calibrations following the manufacturer's protocol were performed, and we used data from these calibrations to estimate the drift uncertainty following equation (8) of *Anderson and Ogren* [1998] with the manufacturer's calibration constants. The measured data were corrected for angular nonidealities, which cause particle scattering in the near forward direction to be underestimated.

[16] The TSI nephelometer was serviced and calibrated by the manufacturer just prior to the spring 2009 campaign. During the spring 2009 campaign the TSI nephelometer was periodically switched to measure both particle free air and CO_2. The measured values were corrected for offset and calibration drift in addition to angular nonidealities [*Anderson and Ogren*, 1998]. The filtered air and CO_2 were measured approximately every two weeks [*Anderson and Ogren*, 1998]. The data reduction and uncertainty analysis that we followed for the scattering data are outlined by *Anderson and Ogren* [1998]. Sources of uncertainties associated with the nephelometer include photon counting noise, zeroing and calibration, and the correction for angular nonidealities. Combined these errors yielded a total uncertainty of ±8% for a scattering coefficient of 30 Mm^{-1}, a 60 min averaging time and a wavelength of 550 nm.

[17] The three-wavelength PSAP is a relatively new instrument, and it is a modified version of the single-wavelength PSAP. The single-wavelength PSAP has been calibrated and intercompared with other filter based aerosol absorption techniques [*Bond et al.*, 1999]. A prototype version of the three-wavelength PSAP was calibrated against two other absorption standards in 2002. The goal was to derive loading correction functions and filter/aerosol scattering correction factors for each of the three wavelengths [*Sheridan et al.*, 2005; *Virkkula et al.*, 2005]. A similar study has not been performed with the commercially available model, but the only difference between the commercially available model and that used by *Virkkula et al.* [2005] is in the light source geometry. The prototype used an elliptical grating to par-

Table 1. Absorption Data Adjustments and Uncertainties[a]

Source	Correction	Uncertainty (Mm^{-1})	Notes
Flow rate	σ_{PSAP}*(F_{PSAP}/F_{meas})	δF_{meas}*σ_{PSAP}	δF_{meas} in this case was 0.01 for a Sensidyne Gilibrator flowmeter
Spot size	User enters the correct spot size for that particular instrument. Instrument calculates correction.	0.08*σ_{PSAP}	4% uncertainty on the measured diameter results in an 8% uncertainty in the spot area, and thus the absorption coefficient [*Virkkula et al.*, 2005].
Noise	–	0.18 $\sqrt{(\tau_o/\tau)}$ Clean Filter 0.3$\sqrt{(\tau_a/\tau)}$ Dirty Filter 0.3*5 $\sqrt{(\tau_a/\tau)}$	PSAP noise does not depend on σ_{ap}. τ_0 is 24 min, τ is 60 min for this study. The first correction factor is the reported noise for the single wavelength PSAP operated at constant altitude [*Anderson et al.*, 1999]. *Anderson et al.* [2003] performed duplicate absorption measurements to examine instrumental noise. Noise is larger when the PSAP is exposed to changing altitudes and changing humidity. Noise also increases with filter loading. They found that noise for a clean filter at a constant pressure is 0.3 for a 30 s time resolution (τ_a = 30 s). Noise for a dirty filter is 5 times higher [*Anderson et al.*, 2003]. Consistent results were found during a comparison of three three-wavelength PSAPs prior to INTEX-B [*McNaughton et al., 2009*].
Drift	–	0.06 σ_{am}	Drift corrections cannot be made because calibrations were not made in the field. This value is based on parallel measurement from 3 single wavelength PSAPs [*Anderson et al.*, 1999]. *Anderson et al.* [2003] report a 5% systematic discrepancy from 2 single wavelength PSAPs operated in parallel. Similar unpublished tests with the three wavelength PSAPs are consistent.
Calibration	–	0.20*σ_{ap}	*Bond et al.* [1999]
Scattering response	$-S_\lambda$*σ_{spm} 467 nm S_λ mean(min, max) = 0.012 (0.009, 0.020) 530 nm S_λ mean(min, max) = 0.016 (0.011, 0.023) 660 nm S_λ mean(min, max) = 0.021 (0.016, 0.029)	0.07*σ_{spm}	The scattering response was determined for a prototype model [*Virkkula et al.*, 2005]. The scattering data are adjusted to PSAP wavelengths. $\sigma_{spmx} = \sigma_{spm1}(\lambda_1/\lambda_x)\alpha^{12}$ $\alpha_{12} = -\log(\sigma_{spm1}/\sigma_{spm2})/\log(\lambda_1/\lambda_2)$

[a]Applies to data collected with a three-wavelength PSAP. The correction to the PSAP data can be summarized as $\sigma_{ap} = \sigma_{PSAP}$*($F_{PSAP}/F_{meas}$) − S_λ*σ_{spm} (equation (1)). Notation: σ_{ap}, absorption photometer measurement after flow rate and scattering corrections; σ_{am}, absorption photometer measurement after flow rate and spot area corrections; σ_{PSAP}, absorption photometer measurement prior to any corrections; σ_{spm}, nephelometer measurement after adjustment for measurements of calibration gases; F_{PSAP}, PSAP flow as reported by PSAP internal flowmeter; F_{meas}, PSAP flow as measured by Sensidyne Gilibrator flowmeter; δF_{meas}, uncertainty in flow rate measured by Sensidyne Gilibrator flowmeter; τ = 60 min averaging time.

tially collimate the light from the LEDs into the light path to the filter. The commercial model uses an integrating hemisphere to produce a uniform high-intensity LED light source. The light source illuminates the cylindrical port and sample flow path to the filter holder. The LED wavelengths are the same. There are no significant differences in the rest of the filter and light path geometry of the two instruments. We do not expect significant performance differences between the prototype three-wavelength PSAP used in the *Virkkula et al.* [2005] study and the instruments used at MBO.

[18] *Bond et al.* [1999] present several important observations of the single-wavelength PSAP, all of which are applicable to the three-wavelength version of the PSAP. (1) The flowmeter in the PSAP can be in error by as much as 20%; therefore it is necessary for the operator to periodically measure and record the flow independently with a high-accuracy flowmeter. (2) There is variation in the sample spot size between instruments. The spot size must be measured on each individual instrument. (3) Aerosol loading onto the *filter can magnify the absorption and create a nonlinear* response in the absorption signal. (4) The PSAP interprets a small amount of aerosol scattering as absorption.

[19] The software in the commercially available three-wavelength PSAP includes a transmission correction function, and this function does an adequate job at low absorption values and at ω values above ~0.80 [*Sheridan et al.*, 2005; *Virkkula et al.*, 2005]. It also allows the user to enter the correct spot size for that particular instrument. Therefore, *many users only need to apply two corrections when pro*cessing the data that is output from the instrument: a flow rate correction and a scattering correction. During the spring 2008 and 2009 campaigns at MBO, the instrument flow was accurately measured on a biweekly basis with a Sensidyne Gilibrator flowmeter (reading accuracy: ±1%), and a correction factor was applied as described by *Bond et al.* [1999]. Then the scattering corrections summarized by *Virkkula et al.* [2005] were applied (1.3%, 1.6%, and 2.1% for 467 nm, 530 nm, and 660 nm, respectively). The scattering data used in the corrections (measured with a TSI nephelometer at 450, 550, and 700 nm) were adjusted to the PSAP measurement wavelengths as described by *Virkkula et al.* [2005].

[20] Finally, we assumed a power law relationship between absorption and wavelength so both the absorption and scattering data could be reported at the same wavelengths. The 467–530 nm pair was used to adjust absorption at 467 nm to 450 nm. The 467–660 nm pair was used to adjust absorption at 530 nm to 550 nm. Finally, the 530–660 nm pair *was used to adjust absorption at 660 nm to 700 nm. Similar* to the single-wavelength PSAP, sources of uncertainty in the three-wavelength PSAP measurement include noise, drift, errors in the loading function, the correction for the scattering artifact, and uncertainty in the flow and spot size corrections [*Anderson et al.*, 2003, 1999; *Bond et al.*, 1999; *Virkkula et al.*, 2005]. Combined these errors yielded a total uncertainty of ~20%. We have summarized the corrections and the main known sources of uncertainty in the PSAP

measurements in Table 1. The correction to the PSAP data can be summarized as

$$\sigma_{ap} = \sigma_{PSAP}{}^{*}(F_{PSAP}/F_{meas}) - S_{\lambda}{}^{*}\sigma_{spm} \quad (1)$$

and all variables are defined in Table 1.

[21] It is important to be aware of the correction scheme that is used to correct the PSAP measurements from various campaigns. A full set of calibration factors for the three-wavelength PSAP is provided by *Virkkula et al.* [2005]. At the low ω and low filter loadings characteristic of MBO, the absorption coefficients would be ~30% lower if the Virkkula scheme was used. This would yield the higher ω values presented in auxiliary material Table S1.[1] The reasons for the discrepancy are not clear and have been noted by other authors [*Sierau et al.*, 2006]. Previous studies have also not used the full *Virkkula et al.* [2005] correction scheme, and have instead relied on the manufacturer's transmission function as was done here. For example, *Sierau et al.* [2006] chose to adapt the findings of *Bond et al.* [1999] to the three-wavelength absorption data. This choice includes an additional 22% correction than applied here. *McNaughton et al.* [2009] used the full *Virkkula et al.* [2005] correction scheme in processing airborne absorption measurements from INTEX-B. We have processed our data in each way (Table 2 and auxiliary material Table S1), and although the magnitude of ω is impacted, the choice of correction scheme does not impact our major findings.

[22] Finally significant consideration should be given to where filter-based absorption measurements are deployed and how they are eventually interpreted. A major drawback to filter based measurements is that the aerosols are deposited onto the filter before the absorption is measured, and this can alter their physical state. This is especially true for liquid-like organic aerosols which can be redistributed around filter fibers, modifying the filter surface and increasing the scattering artifact beyond that accounted for in the *Bond et al.* [1999] and *Virkkula et al.* [2005] corrections [*Subramanian et al.*, 2007]. Liquid-like organic material can also coat any absorbing material already present on the filter and enhance absorption [*Lack et al.*, 2008]. *Lack et al.* [2008] show that the PSAP can overestimate absorption and this bias is dependent on the amount of organic aerosol present. The PSAP has also recently been shown to have a systematic size-dependent bias, and absorption is under reported for the case of coated absorbing spheres [*Lack et al.*, 2009]. Despite these concerns, the PSAP can provide reasonable aerosol absorption measurements in remote regions with relatively low organic mass loadings. MBO fits the requirements of a location where the PSAP provides reasonable measurements.

[23] We present both precision uncertainty and total uncertainty as described by *Anderson et al.* [1999]. Briefly, precision uncertainty includes uncertainty associated with noise and calibration drift. It allows for the comparison of measurements collected using the same instruments and protocols to be statistically compared. This is the appropriate uncertainty to consider when comparing optical properties among the individual Asian aerosol plumes observed at MBO during this study period. It is also appropriate to use this uncertainty to compare measurements made in other locations with similar instruments and protocols. Total uncertainty includes precision uncertainty, the uncertainty associated with the corrections we applied to the data, and the uncertainty associated with the calibration method. This is the appropriate uncertainty to consider when comparing the measurements presented in this study with optical data collected using other measurement methods. We do not include uncertainty for the sampling efficiency in any of the calculations; this includes aerosol loss in the inlet or sampling line which should be insignificant compared to the other uncertainties for the submicrometer aerosol fraction.

2.2.3. Derived Intensive Properties

[24] The scattering and absorption coefficients were converted to the dimensionless intensive optical properties of $\mathring{A}_s$, $\mathring{A}_a$, ω, and b as follows:

$$\mathring{A}_s = -\log\left(\sigma_{sp}^{450}/\sigma_{sp}^{700}\right)/\log(450/700), \quad (2)$$

$$\mathring{A}_a = -\log\left(\sigma_{ap}^{450}/\sigma_{ap}^{700}\right)/\log(450/700), \quad (3)$$

$$\omega = \sigma_{sp}/\left(\sigma_{ap} + \sigma_{sp}\right), \quad (4)$$

$$b = \sigma_{bsp}/\sigma_{sp}, \quad (5)$$

where ω, and b are referenced to 550 nm wavelength and the superscripts in (2) and (3) refer to the other wavelengths measured by the nephelometer. $\mathring{A}_s$ was also calculated using the 550 and 700 nm pair to facilitate comparison with previously published measurements. Uncertainties in the intensive properties are calculated from the uncertainties in the extensive properties. The uncertainty is propagated such that the uncertainty in intensive property X(y, z), δX, is given by

$$\delta X = \left\{[(\delta y)^{*}(\partial X/\partial y)]^2 + [(\delta z)^{*}(\partial X/\partial z)]^2\right\}^{1/2}, \quad (6)$$

where δy and δz are the uncertainties in the extensive properties y and z.

2.3. Compositional Analysis of the PSAP Filters

[25] After the filters were removed from the PSAP, trace element analyses were performed by using reflectance X-ray fluorescence (XRF) spectroscopy (S2 Picofox, Bruker Instruments). This instrument uses a molybdenum X-ray tube with Ni/C multilayer grating to generate a monochromatic X-ray excitation beam that is focused on the sample using very low grazing angle (0.3–0.6 degrees). This allows for total reflection of the beam. The fluorescence spectrum is obtained at a 90 degree angle from the sample using an XFlash detector (Bruker, 10 mm^2 area, FWHM: <160 eV @ Mn Kα line). The use of reflectance XRF minimizes matrix effects in the aerosol samples without extensive sample pretreatment. Elements from sodium to uranium are accessible with this system with the exception of zirconium, niobium, molyb-

[1] Auxiliary materials are available in the HTML. doi:10.1029/2010JD013943.

Table 2. Optical Measurements for Each of the Seven Asian Air Masses Observed at MBO in Spring 2008 and Spring 2009[a]

	σ_{sp} (Mm^{-1})	σ_{ap} (Mm^{-1})	ω	$Å_s$	$Å_a$	b
Plume A: 17 April 2008 1900 GMT to 18 April 2008 1800 GMT[b]						
Peak	33.78	5.67	—	—	—	—
Average	16.11	2.53	0.862	2.33	1.30	—
S.D.	8.29	1.33	0.014	0.15	0.11	—
Prec uncer	0.20	0.06	0.004	0.10	0.08	—
Tot uncer	0.29	0.23	0.006	0.11	0.13	—
Plume B: 25 April 2008 1500 GMT to 28 April 2008 2300 GMT[c]						
Peak	34.76	4.11	—	—	—	—
Average	19.61	2.57	0.889	1.99	1.38	—
S.D.	5.98	0.75	0.019	0.12	0.08	—
Prec uncer	0.13	0.16	0.007	0.04	0.04	—
Tot uncer	0.21	0.17	0.017	0.05	0.09	—
Plume C: 12 May 2008 1000 GMT to 13 May 2008 1200 GMT[d]						
Peak	12.71	1.35	—	—	—	—
Average	9.84	1.17	0.892	2.61	1.41	—
S.D.	1.73	0.14	0.010	0.07	0.08	—
Prec uncer	0.19	0.03	0.013	0.12	0.10	—
Tot uncer	0.24	0.10	0.019	0.14	0.15	—
Plume D: 17 April 2009 0500 to 0800 GMT[e]						
Peak	30.80	4.32	—	—	—	—
Average	24.45	3.43	0.875	1.99	1.18	0.115
S.D.	5.05	0.64	0.023	0.06	0.02	0.001
Prec uncer	0.49	0.14	0.005	0.08	0.13	0.008
Tot uncer	1.00	0.38	0.013	0.14	0.35	0.010
Plume E: 18 April 2009 0200 GMT to 19 April 2009 0500 GMT[f]						
Peak	20.11	2.73	—	—	—	—
Average	10.48	1.57	0.868	2.22	1.27	0.129
S.D.	4.82	0.66	0.011	0.08	0.05	0.007
Prec uncer	0.23	0.05	0.005	0.09	0.11	0.012
Tot uncer	0.34	0.17	0.008	0.13	0.22	0.013
Plume F: 25 April 2009 0200 to 2300 GMT[g]						
Peak	21.33	2.91	—	—	—	—
Average	17.70	2.27	0.886	2.07	1.09	0.117
S.D.	2.28	0.37	0.012	0.04	0.10	0.004
Prec uncer	0.24	0.06	0.003	0.05	0.09	0.006
Tot uncer	0.41	0.24	0.006	0.08	0.19	0.007
Plume G: 15 May 2009 0500 GMT to 16 May 2009 1400 GMT[h]						
Peak	14.02	1.23	—	—	—	—
Average	9.34	0.92	0.909	1.78	1.28	0.114
S.D.	1.60	0.16	0.012	0.39	0.26	0.007
Prec uncer	0.16	0.03	0.003	0.06	0.10	0.008
Tot uncer	0.21	0.10	0.005	0.08	0.17	0.009

[a]Data were corrected for the filter spot size, the flow rate and the scattering response as described in section 2.2.2. The averages are based on hourly data, and the uncertainty pertains to the average. Aerosol scattering (σ_{sp}) and absorption coefficients (σ_{ap}) are at STP and represent submicrometer dry aerosol. The average values exclude data from 1100–1900 Local Time when the local mixed layer may have been influencing MBO. S.D., standard deviation; Prec uncer, precision uncertainty; Tot uncer, total uncertainty.

[b]HYSPLIT trajectories and GEOS—Chem suggest a predominantly biomass burning source near Lake Baikal. Plume traveled over great circle in ~5–6 days.

[c]Satellite images, CALIPSO and IMPROVE data suggest a mixture of dust and smoke, primarily dust. Plume travelled over the great circle in ~7–9 days.

[d]Trajectories passed over NE China and Northern Japan ~7–9 days back from MBO, then over a region of fires near Lake Baikal ~9–10 days back from MBO.

[e]HYSPLIT trajectories pass over Northeastern China and Northern Japan ~7–9 days back from MBO.

[f]HYSPLIT trajectories initialized 19 April 0300–0600 UTC pass through boundary layer in Northeastern China 5 days back from MBO.

denum, and technetium due to their use in the excitation source.

[26] For the XRF analysis, the PSAP filters were fixed to acrylic sampling discs using a thin layer of silicon grease (Dow Corning® 7 Release Compound) and placed into a sample tray. These discs were inserted into the XRF instrument with the sample side facing the X-ray excitation beam. Blank filters were handled and analyzed in the same manner as the samples, and the blank concentration levels were subtracted from the sample concentrations. For this analysis, the elemental concentrations were determined using argon as an internal standard. The quantification was performed automatically by the Picofox Software using the concentration of this internal standard, the net pulse number, and the relative sensitivity of both argon and the element to be analyzed within the measurement spectrum. The detection limits are based on the three-sigma criterion.

[27] The composition information derived from the PSAP filters was only used qualitatively in our analysis to support other sources of information on aerosol composition. Isolating the elemental concentrations for the specific plumes presented here is not possible because the PSAP filters were changed on irregular time intervals. Many filters were collected over several day periods, which often included both plume and nonplume conditions. The elemental information was most useful when filter changes coincided closely with plume boundaries, which occurred once on 17–18 April 2008. Unlike for the absorption measurements, we were not able to correct these filter measurements for snow cat contamination. However, these filters represent the only in situ measurements of aerosol chemical composition, so we have chosen to include them here.

2.4. Description of Backward Trajectories

[28] We calculated two sets of backward trajectories to establish the transport history of the aerosol plumes. The first set included 10 day back trajectories initialized each hour from the summit of MBO using the Hybrid Single-Particle Lagrangian Integrated Trajectory (HYSPLIT-4) model (R. R. Draxler and G. D. Rolph, 2003, http://www.arl.noaa.gov/ready/hysplit4.html). These 10 day trajectories were calculated using global meteorological data from the GDAS (Global Data Assimilation System) archive, which has a time resolution of 3 h, a spatial resolution of 1 degree latitude by 1 degree longitude, and a vertical resolution of 23 pressure surfaces between 1000 and 20 hPa. Trajectories were run at multiple heights surrounding the summit of MBO as in work by *Weiss-Penzias et al.* [2006].

[29] The second set of backward HYSPLIT trajectories were run for 3 days using meteorological data from the EDAS (Eta Data Assimilation System) archive. The EDAS archive grid covers the continental United States after 2004, has a horizontal resolution of 40 km and a vertical resolution of 26 pressure surfaces between 1000 and 50 hPa. These tra-

Notes to Table 2:

[g]HYSPLIT trajectories show air passed through BL in a region of intense agricultural fires in southwest Russia ~8–10 days back from MBO. Plume travelled over the great circle.

[h]NAAPS indicates the presence of dust over the Pacific Northwest. HYSPLIT trajectories show air mass passed through NE China ~10 days prior to reaching MBO.

jectories were initialized from 1200 m above model ground level for each hour of the spring campaign. The trajectories were initialized above the ground since both the GDAS and the EDAS model define the terrain for the grid box containing MBO significantly below the actual altitude of Mount Bachelor. Error in HYSPLIT trajectory calculations normal to the direction of flow are 10–30% of the distance traveled after 24 h [*Draxler and Hess*, 1998].

2.5. Other Supporting Measurement Networks and Platforms

[30] We considered several ground based networks, satellite platforms, and model output as supporting data in our analysis of individual aerosol plumes. Supporting data are described here, and it was only included in our analysis if it coincided with observations at MBO. Thus different data sets were explored for each aerosol plume as needed. We do not attempt a quantitative comparison with the supporting data sets, and they are primarily used as a source of qualitative information on the chemical composition of the aerosols observed at MBO.

[31] IMPROVE monitoring sites are situated in National Parks and Class I Wilderness Areas across the United States (http://vista.cira.colostate.edu/improve/). Speciated fine aerosol (<2.5 μm), $PM_{2.5}$ mass and PM_{10} mass are measured at all IMPROVE sites. Samples are collected every three days [*Malm et al.*, 1994]. We used aerosol chemical speciation data from the two IMPROVE sites located nearest to MBO (Figure 1): Mount Hood (45.288°N, 121.7837°W, 1531m amsl) and Three Sisters Wilderness Area (44.291°N, 122.0434°W, 885 m amsl).

[32] Data from the Cloud-Aerosol Lidar and Infrared Pathfinder Satellite Observation (CALIPSO) [*Liu et al.*, 2009] were used to corroborate plume height and type when an overpass coincided with a period of interest at MBO and an aerosol plume was clearly defined in the CALIPSO data swath. CALIPSO uses the layer integrated attenuated backscatter, the volume depolarization ratio, surface type and elevation to determine aerosol type [*Omar et al.*, 2009]. The six aerosol types (clean continental, clean marine, dust, polluted continental, polluted dust, and smoke) are representative of aerosol mixtures most frequently observed at AERONET sites (AErosol RObotic NETwork, http://aeronet.gsfc.nasa.gov/) [*Omar et al.*, 2005]. CALIPSO orbits in the "A-Train" satellite constellation which includes the Aqua, CloudSat, CALIPSO, PARASOL, and the Aura satellite missions.

[33] The Naval Research Laboratory Aerosol Analysis and Prediction System (NAAPS, http://www.nrlmry.navy.mil/aerosol/) uses real-time satellite observations to forecast the distribution of tropospheric aerosols resulting from biomass burning, dust storms, and anthropogenic SO_2 emissions. These forecasts have been archived since 2000 are readily available on line. The NAAPS simulations are useful because they use operational dynamics, are operated in real time, and provide simulations with global coverage. Keeping in mind the constraints on the input (satellite estimates of smoke and dust), the NAAPS output provides one of the only opportunities to continuously identify periods and geographic regions potentially impacted by pollution, biomass burning smoke or dust plumes. Similar to several previous studies, we used NAAPS forecasts qualitatively to identify regions and time periods potentially impacted by upwind aerosol source regions [*Jaffe et al.*, 2004; *Lapina et al.*, 2006; *Morris et al.*, 2006].

3. Results

3.1. Identification of Asian Pollution Episodes

[34] Presented here is a general overview of the MBO aerosol data, and how the Asian aerosol plumes were identified. Figure 2 presents a time series of hourly averaged 1 μm σ_{sp} and σ_{ap} measured at MBO during spring 2008 and 2009. The seven Asian aerosol plumes are highlighted in Figure 2. We used the HYSPLIT trajectories calculated using the global GDAS meteorological grid to define periods of likely Asian influence. In each case, the air mass impacting MBO descended during the final 24 h of transport to the site as confirmed by the HYSPLIT back trajectories calculated using the 40 km EDAS meteorological grid. Local minimums in water vapor (WV) mixing ratio were also observed at MBO simultaneous with the peaks in aerosol scattering. The air mass may have traveled through the lower troposphere over the Pacific en route to North America, but interaction with the North American boundary layer was unlikely. There were other periods during each measurement campaign where the backward trajectories indicated rapid transport from East Asia. However, because the aerosol and gas-phase (CO, O_3, PAN) observations showed minimal enhancements or there was not an aerosol plume distinguishable from the relatively low background observations, we chose not to focus on these periods. Instead we focused on the seven highlighted plumes because they clearly showed an enhanced aerosol load, and were often also accompanied by enhancements in gas-phase species. Note that the defined plumes include many of the highest peaks in aerosol scattering and absorption observed at MBO.

[35] Table 2 presents the aerosol optical measurements for each of the Asian air masses based on the hourly averaged data. The data in Table 2 exclude data from 1100–1900 Local Time when the afternoon upslope mountain flow may have caused the local mixed layer to reach the summit of Mount Bachelor [*Reidmiller et al.*, 2010; *Weiss-Penzias et al.*, 2006]. This conservative choice reduces the amount of data included in the statistics, but it ensures that we do not include aerosol with a local source in our analysis. This choice does not change the main conclusions of our analysis.

[36] Of interest in this analysis is (1) whether the intensive optical properties differ between these seven Asian plumes, (2) whether these differences can be linked to differences in chemical composition or source region, and (3) whether the intensive optical properties differ from those measured during previous campaigns using similar instruments closer to the Asian source region.

3.2. Plume A: 17–18 April 2008

[37] Elevated σ_{sp}, σ_{ap}, CO, O_3, and PAN mixing ratios were observed from 17 April 1300 GMT to 18 April 1900 GMT (Figure 3a). For example, observed hourly averaged CO at MBO reached 195 ppbv; the monthly mean CO for April 2008 was 138 ppbv. This plume has been described in detail by *Fischer et al.* [2010], and they concluded that it had a Siberian biomass burning source. Figure 3 presents a time series of the measured and calculated aerosol optical properties for this plume and the other plumes discussed

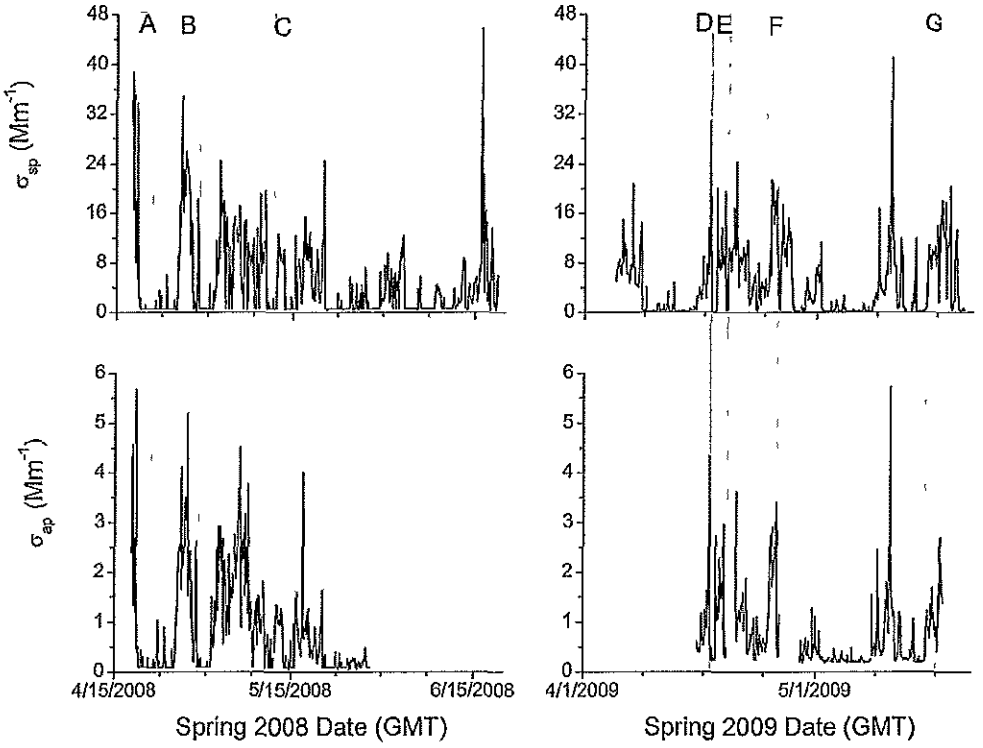

Figure 2. Time series of hourly averaged (top) submicrometer aerosol scattering (σ_{sp}) and (bottom) absorption coefficients (σ_{ap}) at 550 nm measured at Mount Bachelor during (left) spring 2008 and (right) spring 2009. The gray vertical bars show the time boundaries of the 7 Asian aerosol plumes discussed in this paper.

in sections 3.3–3.8. Biomass burning tracers were also enhanced on the PSAP filters during this time (see auxiliary material Figure S1) [*Echalar et al.*, 1995; *Gaudichet et al.*, 1995; *Viana et al.*, 2008].

[38] The 10 day HYSPLIT back trajectories indicate that transpacific transport was relatively efficient; the plume crossed the Pacific Rim in approximately 5 days. Prior to reaching MBO, the trajectories passed through a region of active fires in southeastern Russia near Lake Baikal and the Chinese border. A global chemical transport model (GEOS-Chem) simulated the timing and magnitude of the observed PAN and CO well, and the model supports a Siberian biomass burning source for these aerosols [*Fischer et al.*, 2010]. The air mass containing the aerosol plume arrived at MBO from the northwest under strongly subsiding conditions during a period of cold air advection over the Pacific Northwest.

3.3. Plume B: 25–28 April 2008

[39] Although interpretation of the HYSPLIT back trajectories during this period is not straightforward, there is strong evidence that this aerosol plume was a mix of dust and smoke from Asia. Aerosol scattering and absorption began to rise at MBO late on 25 April 2008 and remained above 15 Mm^{-1} for 48 h (Figure 3b). This was the longest period of elevated σ_{sp} observed at MBO during spring 2008. After a 12 h period where σ_{sp} was below detection limit, MBO intercepted a second plume with similar intensive optical properties for 5 h on 28 April 2008. The peak in σ_{sp} and σ_{ap} was observed at ~0400 GMT on 26 April 2008. This hourly averaged peak was accompanied by 140 ppbv CO; CO reached 171 ppbv later on 26 April. Averaged over the duration of this plume, both CO and O_3 were lower during this plume than they were for either of the other Asian plumes (A and C) we observed during spring 2008, consistent with dust as a main aerosol type [*Price et al.*, 2004]. This plume had a low average $Å_s$, indicating a larger aerosol size distribution within the submicrometer portion of the aerosol (Table 2).

[40] Aerosols were also enhanced at lower elevation surface sites across WA and OR coincident with the elevated σ_{sp} and σ_{ap} at MBO. Figure 4b presents a time series of $PM_{2.5}$ (by nephelometer) observed in Bend, OR (1100 m amsl). The Bend data show pronounced daily afternoon peaks in aerosol concentration, which support entrainment of aerosol into the BL from above. The dashed lines in Figure 4b surround the same time period that is displayed in the MBO time series presented in Figure 4a (and Figure 3b). It is interesting to note the period of elevated $PM_{2.5}$ centered on 18 April coincident with Plume A. Unlike Plume B, during Plume A coincident elevated $PM_{2.5}$ was observed only at some stations in OR and not in WA. The scale of Plume B, observed at widely separated sites, argues against a local aerosol source.

[41] Nearby IMPROVE aerosol data provide evidence supporting a dust and smoke source; however, the samples

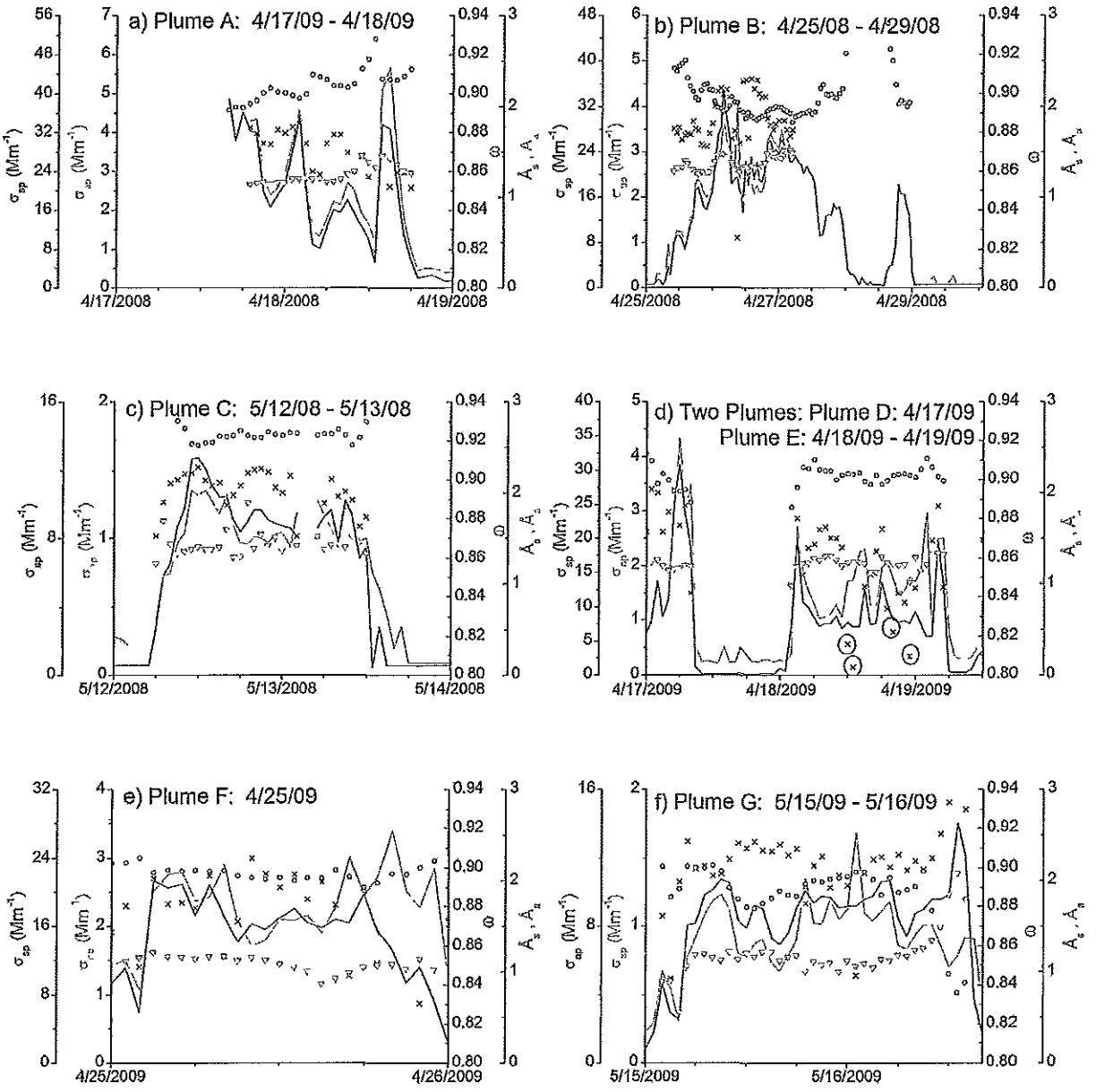

Figure 3. Time series of measured and calculated aerosol optical properties at MBO for the seven plumes highlighted in Figure 2. The black line is σ_{sp} at 550 nm and STP. The gray line is σ_{ap} at 550 nm and STP. Hourly averaged ω at 550 nm, $Å_s$, and $Å_a$ are plotted as blue crosses, red circles, and green triangles, respectively. All time is in GMT. Note that the σ_{sp} and σ_{ap} scales vary but are always set to an 8:1 ratio. Therefore overlaying lines indicate $\omega = 8/9 = 0.89$. Two plumes are presented in Figure 3d, where we have circled the points where there was likely local snowcat contamination. In all subplots, the intensive variables were not calculated when either σ_{sp} or σ_{ap} were below detection limit. The light gray shading indicates local sunset to sunrise.

were collected over a period of 24 h and may contain some aerosol not associated with the Asian plume. Figures 4c and 4d present IMPROVE $PM_{2.5}$ speciation data from the Three Sisters (THIS) monitoring site (see Figure 1 for location). Again, the dashed lines in Figures 4c and 4d surround the same time period that is displayed in the MBO time series presented in Figure 4a. There was one IMPROVE sample on 27 April 2008 that is relevant to this discussion, but we show the period from 15 March to 15 May for context. The THIS sample on 27 April had the highest fine ($PM_{2.5}$) elemental carbon (EC), organic carbon (OC) and potassium (K) for this period. Figure 4d presents IMPROVE fine soil and sulfate; both of these constituents were also elevated on 27 April. A time series for the Mount Hood (MOHO) IMPROVE site revealed similar patterns in these constituents. We calculated the elemental ratios between the

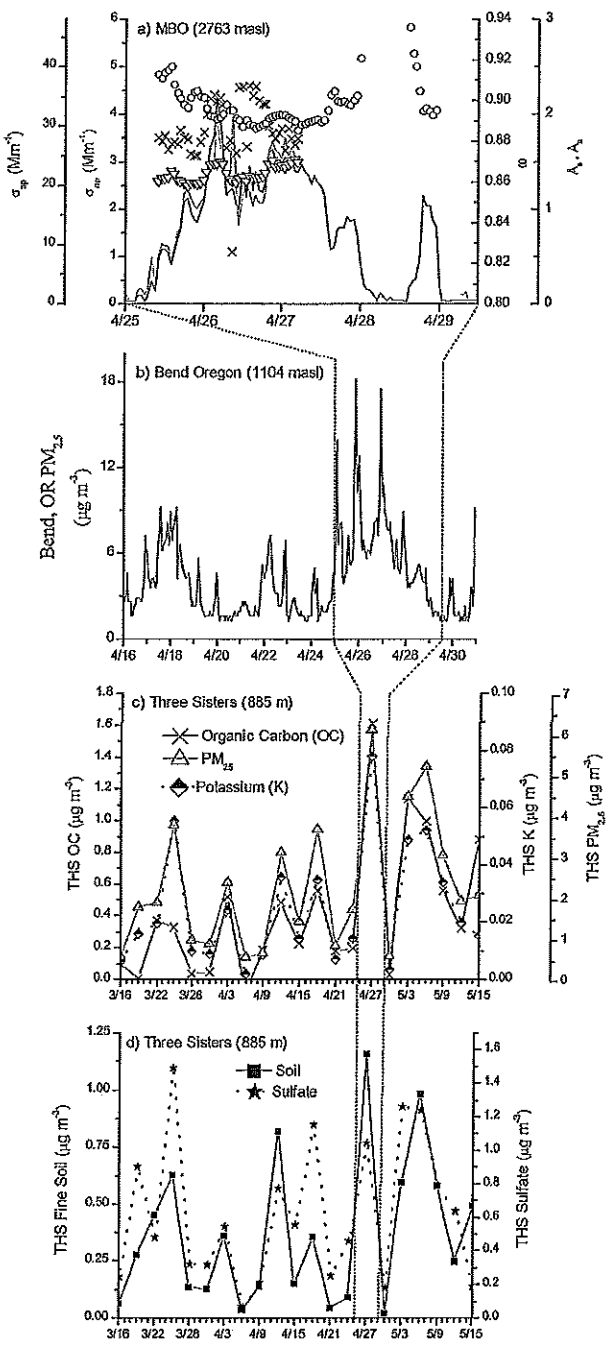

Figure 4. (a) Time series of observed and calculated submicrometer aerosol optical properties at MBO for the period 25 April 2008 0400 GMT to 29 April 2008 0400 GMT (Plume B). As in Figure 3, Hourly averaged ω at 550 nm, $Å_s$, and $Å_a$ are plotted as crosses, circles, and triangles, respectively. (b) Time series of $PM_{2.5}$ observed at Bend, Oregon, for the second half of April 2008. (c) Time series of IMPROVE fine ($PM_{2.5}$) organic carbon (OC), $PM_{2.5}$ mass, and potassium (K) for the Three Sisters monitoring site (44.29°N, 122.043°W, 885 m), and (d) Time series of IMPROVE fine soil and sulfate for the Three Sisters monitoring site. The dashed lines in Figures 4b, 4c, and 4d surround the same time period that is displayed in Figure 4a).

major IMPROVE soil constituents (Fe, Al, Si, Ca, Ti) and K for the 27 April samples at the THIS and MOHO sites. A least squares linear regression between the THIS and MOHO daily elemental ratios yielded a slope of 0.97 and a $R^2 = 0.99$, which indicates a common source [*DeBell et al.*, 2004].

[42] The CALISPO classification for Plume B corroborates the IMPROVE data. There were two relevant CALIPSO overpasses that we considered. The first occurred on 25 April 2008 and identified a dust layer of aerosol off the British Columbia and Washington coast (auxiliary material Figure S2). The second CALIPSO overpass occurred on 27 April and the swath was almost directly over MBO where an aerosol layer near the surface was visible. This layer was classified as a mixture of dust (~37%) and polluted dust (~63%).

[43] The 10 day HYSPLIT backward trajectories associated with this time period were difficult to interpret owing to a strong low-pressure system situated in the Gulf of Alaska. Most of the backward trajectories circled around the Gulf of Alaska, never reaching Asia. The 3-day HYSPLIT backward trajectories calculated using the EDAS grid show rapid descent from the northwest in the 2 days prior to MBO for 26 April. These trajectories show a shift to a southern approach from within the continental boundary layer on April 27, corresponding to the drop in aerosol scattering at MBO. Because the 10 day backward trajectories were unreliable due to the strong cyclone, we used a variety of supporting satellite data and model output to establish the long-range transport history of the air mass impacting MBO.

[44] NAAPS images (not shown) indicate elevated surface concentrations of smoke and dust in the Lake Baikal and Gobi desert regions on 17–18 April. The plume can be seen in visible images over this region at this time, and crossing the Kamchatka Peninsula 2 days later. A period of elevated aerosol load centered on 21 April was observed at the surface in Anchorage, Fairbanks, and Juneau, Alaska. Several CALIPSO swaths identify a deep (~5 km) layer of aerosol over Alaska coincident with these surface measurements. It is unclear whether the majority of the plume traveled south over the Gulf of Alaska or over interior BC. At least a portion of the plume can be seen in MODIS and MISR images approaching the Washington and Oregon coast on 24 and 25 April (auxiliary material Figure S2). On the basis of these various data sources, we hypothesize that the majority of the plume traveled to MBO over the Pacific Rim and not over interior British Columbia.

3.4. Plume C: 12–13 May 2008

[45] Here we focus our attention on the last distinct Asian aerosol plume observed during the spring 2008 campaign. Similar to Plume A, the observed gas-phase species in this plume have been described in detail by *Fischer et al.* [2010] so only a brief summary will be presented here. Carbon monoxide, O_3 and PAN mixing ratios rose throughout 11 May, with a sharp rise in σ_{sp} and σ_{ap} observed on 12 May (Figure 3c). The plume ended abruptly 13 May 1200 GMT. The hourly averaged CO reached 168 ppbv; the average CO mixing ratio observed at MBO during May 2008 was 127 ppbv. The small standard deviations reported in Table 2 and Figures 6, 8, and 9 reflect that the extensive and intensive aerosol optical properties were very consistent

throughout this plume. This plume had the largest average $Å_s$, indicating that this was the smallest size distribution that we observed in the Asian plumes. In contrast to the previous two plumes we have discussed thus far, this plume took a more southerly route straight across the Pacific. Some of the 10 day backward trajectories passed through industrialized regions of East Asia, while many actually passed north of the major industrialized regions of China, and through a region of southeastern Russia and northeastern China impacted by biomass burning. The source of these aerosols was likely a mixture of biomass burning and industrial pollution. The plume descended strongly under high pressure in the 48 h prior to reaching MBO.

3.5. Plume D: 17 April 2009

[46] Plumes D and E were observed very close in time, so they could have the same source. We decided to consider these two plumes separately because the rapid drop in σ_{sp} at ~1000 GMT 17 April was not due to local scavenging. It was accompanied by a simultaneous drop in CO, PAN and O_3 indicating a larger air mass change.

[47] CO, PAN and σ_{sp} were elevated throughout the day on 16 April. A brief simultaneous 3 h peak in these species was observed overnight (auxiliary material Figure S3). Coincident WV mixing ratios at MBO were low (~1.5 g/kg). Three day backward HYSPLIT trajectories initialized from MBO at the time of the maximum σ_{sp} (not shown) show that the air mass descended from the southwest over the previous 24 h. The 10 day backward HYSPLIT trajectories suggest that the air mass crossed the Pacific Ocean in approximately 9 days via the Gulf of Alaska.

3.6. Plume E: 18–19 April 2009

[48] A 22 h period of elevated σ_{sp} and σ_{ap} was observed from 18–19 April at MBO. The plume was bounded by ~20 Mm^{-1} peaks in σ_{sp} (Figure 3d) simultaneous with low WV mixing ratios. The initial spike in σ_{sp} (0300 GMT 18 April) was accompanied by 174 ppbv CO, 70 ppbv O_3 and 534 pptv PAN. The backward trajectories initialized from MBO at the time of the initial σ_{sp} spike (not shown) suggest that the air mass left southeast Russia and northeast China approximately 7 days before arriving at MBO. Some of the trajectories show looping in the Gulf of Alaska. The final spike in σ_{sp} (0400 GMT 19 April 2009) was accompanied by 153 ppbv CO, 70 ppbv O_3 and 465 pptv PAN. The trajectories initialized from MBO at the time of the final σ_{sp} spike (auxiliary material Figure S4) suggest rapid transpacific transport from northeast China approximately 5 days prior.

[49] There is strong evidence that aerosols with a non-Asian source were likely also observed during Plume E. There was an increase in WV and T accompanied by a drop in O_3 during the local afternoon hours of 18 April, possibly indicating the local BL reached the summit. There is a corresponding drop in ω during this time as well. Periods of likely local snow cat contamination were noted in the raw data sporadically during 1200–1300 GMT 18 April, and these points are circled in Figure 3d. We do attempt to remove all data that are impacted by local snow cat emissions, but positively identifying this type of contamination can be difficult. These points are plotted in Figure 3d, but were not included in Table 2 or in the summary Figures 6–9 presented in section 4.

3.7. Plume F: 25 April 2009

[50] The trajectories suggest that the source of these aerosols may have been agricultural fires in western Russia, primarily located south of Moscow (auxiliary material Figure S5). The aerosols were accompanied by elevated PAN and CO, and by very low WV mixing ratios (<1 g/kg). The trajectories suggest that the plume traveled over the great circle to MBO and the transport time from western Russia to MBO was 9–10 days.

3.8. Plume G: 15–16 May 2009

[51] Figure 3f presents a 36 h period of elevated submicrometer aerosols observed at MBO on 15–16 May 2009. There is strong evidence that this aerosol plume had a large dust component. The 10 day backward trajectories (not shown) indicate that the air mass observed during this time traveled across the Pacific via the great circle. The air mass was lofted out of the Asian boundary layer over eastern Mongolia. The travel time from northeastern China to the U.S. Pacific Northwest was 7–9 days. High O_3 (up to 94 ppbv hourly average) was observed during the first several hours of the plume; PAN and CO mixing ratios were also elevated although O_3 was the most extreme. Auxiliary material Figure S6 presents the NAAPS model predicted AOD for the region at 1800 GMT 15 April 2009. A wide band of dust can be seen impacting the Pacific Northwest and continuing further east. CALIPSO passed almost directly over MBO at ~1000 GMT 16 April 2009. A band of aerosol, which CALIPSO classified as dust, can be seen extending from 50°N to 28°S. In the region near MBO, CALIPSO indicates the aerosol layer extended from approximately 1–3.5 km amsl.

4. Optical Properties of Asian Plumes

[52] Scatterplots of the relationship between the intensive aerosol optical properties are presented in Figure 5. The plumes clustered in terms of their scattering and absorption Ångström exponents, indicating a range of sizes and materials present (Figure 5a). Plumes where mineral dust likely made a larger contribution to extinction (Plume B and G) had the lowest $Å_s$, which suggests that the tail of the coarse mode aerosol extends below 1 μm. The MBO $Å_s$ distributions during Plume B and G indicate that dust aerosol has a detectable influence on the observed submicrometer aerosol optical properties. Plume C stands apart from the other plumes, exhibiting the highest $Å_s$; based on backward trajectory calculations, this plume had one of the longest travel times across Pacific. There is also some evidence that portions of this plume descended over the mid-Pacific possibly interacting with the marine boundary layer and precipitation. Both of these factors suggest activation and scavenging of the larger aerosol particles.

[53] Using a plot analogous to Figure 5a, *Clarke et al.* [2007] showed that biomass burning smoke, pollution and dust aerosols observed over North America could be stratified by their combined spectral scattering and absorption properties for the total aerosol sample. The optical measurements presented by *Clarke et al.* [2007] were accompanied by chemical measurements which confirmed the source apportioning. A similar analysis was performed by *Yang et al.* [2009] on aerosol plumes observed in Beijing,

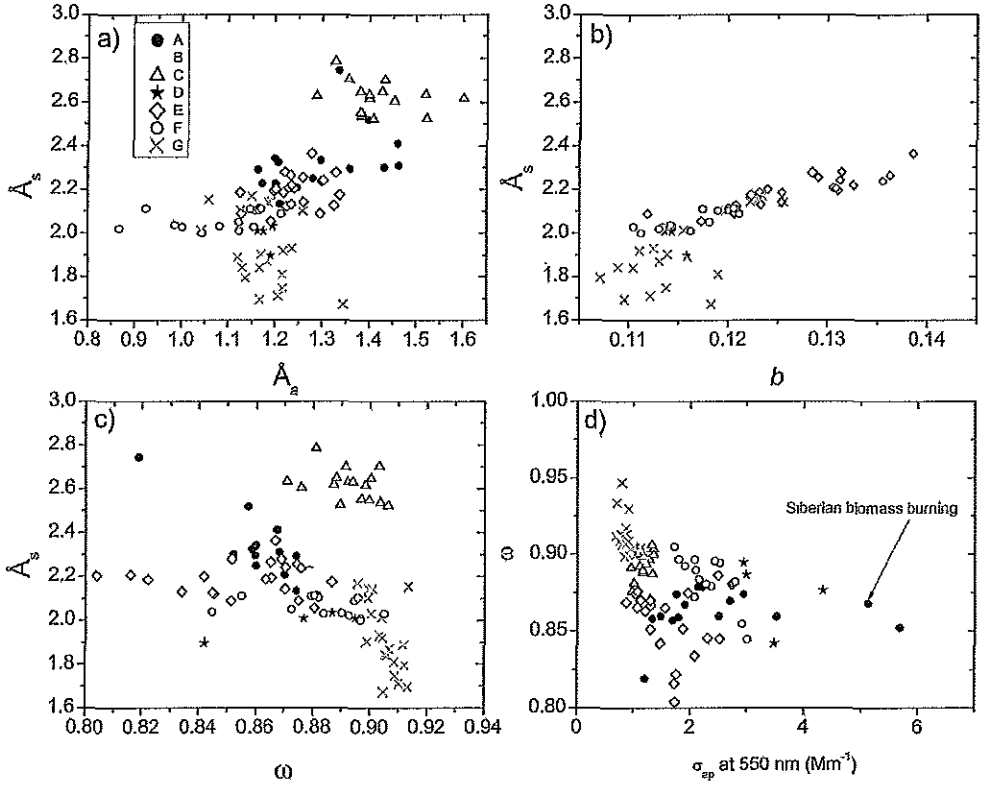

Figure 5. (a–c) Scatterplots of the intensive aerosol optical properties of each Asian air mass. Ångström exponents were calculated using the 450–700 nm pair. Backscatter fraction (b) and single scatter albedo (ω) are at 550 nm. (d) Single scatter albedo versus absorption. None of these plots include data from 1100–1900 Local Time when the local mixed layer may have been influencing MBO. There is strong evidence that dust made a large contribution to the aerosol scattering in plumes B and G, and Siberian biomass burning smoke made a large contribution to plume A.

and again dust plumes were easily identified by lower $Å_s$ distributions (mean $Å_s = 1.72$ for submicrometer aerosols). In addition to size differences, dust aerosols can also have enhanced absorption at short wavelengths [*Patterson*, 1981] and thus plumes containing mineral dust can have a higher total aerosol $Å_a$ than plumes primarily composed of biomass burning smoke or anthropogenic pollution [*Bergstrom et al.*, 2007]. Figure 5a suggests that spectral signatures may offer a way to differentiate aerosol plumes observed at MBO without in situ measurements of chemical composition. We hypothesize that this approach would be more useful if it was extended from the submicrometer to the full aerosol size distribution.

[54] There was a positive relationship between b and $Å_s$; b was larger for smaller particles (Figure 5b). The spring 2009 dust plume (G) had the lowest b. Model calculations suggest that the scattering phase function of sharp and irregularly shaped particles, such as dust, is larger than those of spherical particles at forward scattering angles ($\theta < 10°$) and smaller at backscattering angles ($\theta > 150°$) [*Kalashnikova and Sokolik*, 2002]. The observations of b at MBO are broadly consistent with these modeling results.

[55] Hourly averaged ω ranged from 0.83 to 0.93 within the aged Asian plumes (Figures 5c and 5d). Plume C and the plumes hypothesized to contain large amounts of dust (B and G) had the highest ω values. See auxiliary material Table S1 for MBO ω values calculated with several PSAP correction schemes.

[56] There is a relatively large amount of variability in ω compared to the variability in $Å_s$. There are several points to note when interpreting Figure 5c: (1) The PSAP has more uncertainty than the TSI nephelometer, so we would expect more variability in the intensive properties calculated using the PSAP absorption measurements. (2) The variability in $Å_s$ is somewhat constrained by the imposed 1 μm size cutoff. (3) Plumes can be layered, and contain several types of aerosols with different scattering to absorption ratios. CALIPSO provides strong satellite evidence that plume B contained layers of dust and smoke. *Yang et al.* [2009] observed a similar standard deviation in their ω measurements of polluted submicrometer dust.

[57] Figure 5d is a plot of ω versus absolute absorption at 550 nm. *Clarke et al.* [2007] used a similar plot (Figure 9a) along with measurements of the size distribution to show that they observed a larger absorption to scattering ratio for smaller particles. Although direct measurements of the aerosol size distribution were not made at MBO, the plumes with a larger size distribution based on their $Å_s$ distributions do exhibit a higher range of ω values. This is qualitatively consistent with the *Clarke et al.* [2007] analysis. Following

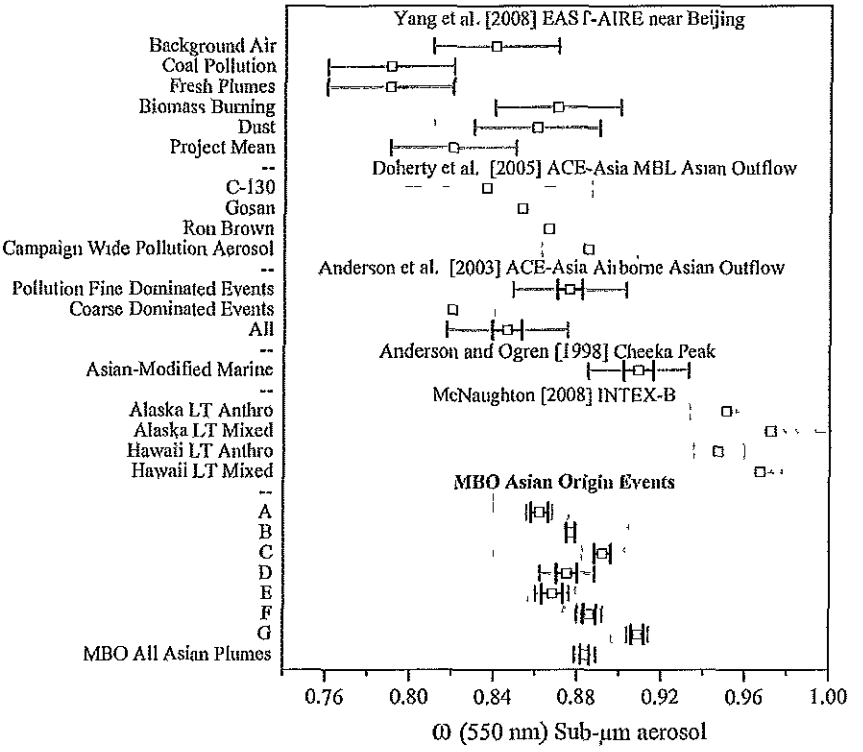

Figure 6. Comparison of single scatter albedo (ω) during Asian Origin aerosol plumes measured at MBO during spring 2008 and spring 2009 with other data sets. All values are reported at 550 nm. Light gray, dark gray, and black bars are 1 standard deviation, the total uncertainty of the average, and the precision uncertainty of the average, respectively. This plot does not include data from 1100–1900 Local Time when the local mixed layer may have been influencing MBO. The classifications for the *McNaughton* [2008] data are presented by *McNaughton et al.* [2009]. Briefly, "LT Mixed" represents a mixture of pollution and dust observed in the lower troposphere, and "LT Anthro" represents fine mode dominated aerosol observed in the lower troposphere. The PSAP data from *McNaughton* [2008] were corrected following the full *Virkkula et al.* [2005] correction scheme. See auxiliary material Table S1 for ω values calculated for MBO using this correction scheme.

from the analysis of *Clarke et al.* [2007] we expect Plume E to have a smaller size distribution compared to the other plumes. Plume C is possibly inconsistent with the *Clarke et al.* [2007] analysis. Plume C, which likely contains the smallest size distribution based on its $Å_s$, also has a relatively high scattering to absorption ratio.

[58] *Clarke et al.* [2007] also observed a horizontal spread in absorption for the biomass burning plume they encountered, and they concluded that σ_{sp} and σ_{ap} scale together in biomass burning plumes. A similar pattern is evident in plume A, which likely has a Siberian biomass burning source. However, we observed a much smaller range of σ_{ap}.

[59] The optical properties presented here were measured on low-RH submicrometer aerosol. Differences in the observed optical properties reflect variations in aerosol composition rather than humidity. To gain information on how the optical properties of Asian aerosols change when they cross the Pacific, we compare observations of the intensive optical properties at MBO with observations closer to the Asian coast. The comparison is with literature observations of intensive aerosol properties which were not made in the same years as the MBO measurements. Interannual variability is a major issue, but our main conclusions appear to be robust across different years of measurements made on either side of the Pacific Ocean.

[60] Figures 6–10 are not intended to be Lagrangian studies of the changing optical properties of aerosols within individual plumes. Scarcity of cloud-free satellite data and the difficulty of tracking individual plumes across the Pacific prevent this type of approach. Rather, our goal is to identify patterns in how aerosol modification during transport changes the average intensive aerosol optical properties. We restrict the comparison to data collected using similar instrument configurations during spring months. This type of comparison is inherently difficult, and this type of analysis would certainly be served by additional data.

[61] *Doherty et al.* [2005] present a comparison of the aerosol optical properties measured from multiple platforms during the spring 2001 ACE-Asia field campaign [*Doherty et al.*, 2005; *Huebert et al.*, 2003]. Scattering and absorption were universally measured with TSI integrating nephelometers and single-wavelength PSAPs, respectively. We compare the observations from MBO with observation of Asian outflow made both in the FT [*Anderson et al.*, 2003]

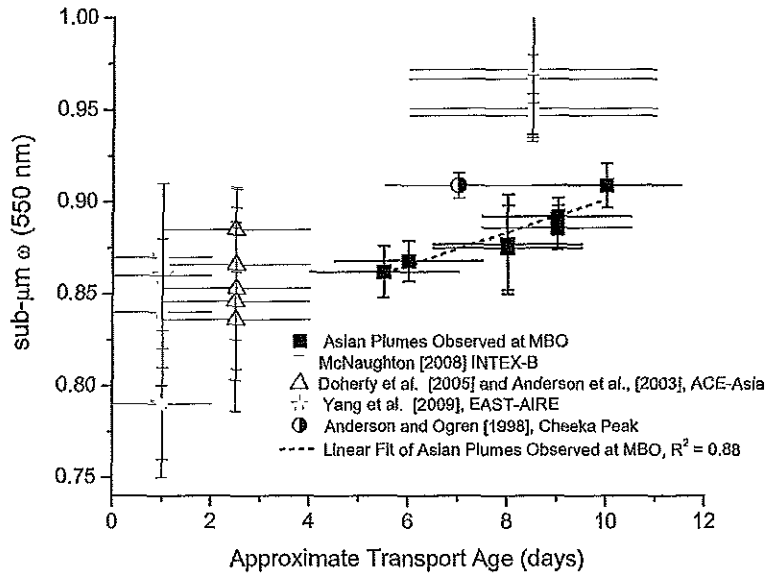

Figure 7. Summary plot for single scatter albedo (ω) during Asian origin aerosol plumes measured at MBO during spring 2008 and spring 2009 with the same data sets presented in Figure 6. Here ω is plotted as a function of processing time or atmospheric transport age. See text in section 4.1 for a detailed description of how transport age was assessed for each data set. Note the positive relationship between transport time and ω. This relationship also holds for plumes observed at MBO, and the linear fit shown here was calculated using only plumes observed at MBO. We remind readers that *McNaughton et al.* [2009] used the full *Virkkula et al.* [2005] correction scheme in processing airborne absorption measurements from INTEX-B. See section 2.2.2 for a discussion of PSAP correction schemes. We have processed our data using several correction schemes (auxiliary material Table S1). When processed using the *Virkkula et al.* [2005] scheme, the resulting ω values are larger, closer to those reported by *McNaughton et al.* [2009].

and within the marine BL [*Carrico et al.*, 2003; *Quinn et al.*, 2004]. The scattering and absorption data collected from the cruise are presented by *Quinn et al.* [2004] and were made at a constant RH (~55%), but the data are presented by *Doherty et al.* [2005] at low RH (~30%). The observations presented by *Doherty et al.* [2005] from the marine BL represent several aerosol classes: pollution, marine, dust and volcanic [*Carrico et al.*, 2003]. The full set of aircraft observations, presented by *Anderson et al.* [2003], were separately classified by their sources and the relative contributions of the fine and coarse modes to aerosol scattering.

[62] Aerosol light scattering and absorption were also measured more recently near Beijing as part of the EAST-AIRE (East Asian Study of Tropospheric Aerosols: an International Regional Experiment) campaign during March 2005 [*Yang et al.*, 2009]. *Yang et al.* [2009] segregated the data into air masses dominated by dust, biomass burning, "fresh chimney plumes," other coal burning pollution, and relatively clean background air for Northern China.

[63] Finally, we also include previous measurements from the eastern Pacific region. The first set of observations of σ_{sp} and σ_{ap} is from Cheeka Peak [*Anderson et al.*, 1999], a coastal low elevation site in northwest Washington that occasionally sees Asian plumes. We have included data from this site during a period impacted by a plume of Asian origin. The second set of observations was from aircraft flights during the Photochemical Ozone Budget of the Eastern North Pacific Atmosphere (PHOBEA) research campaign [*Jaffe et al.*, 2003b]. The most recent aircraft observations were made during spring 2006 as part of Phase B of the Intercontinental Chemical Transport Experiment (INTEX-B) [*McNaughton*, 2008; *McNaughton et al.*, 2009].

[64] Figures 6 through 10 present the intensive aerosol optical properties of Asian plumes observed at MBO in the context of the other relevant data sets discussed above. As in Figure 5, the optical properties presented only represent periods when MBO was free from local BL influence.

[65] On average, the aerosol plumes observed at MBO had a higher submicrometer dry ω than plumes observed closer to the Asian source region (Figure 6). The σ_{sp} measurements by *Anderson et al.* [2003] and *Yang et al.* [2009] were both made with a TSI integrating nephelometer so we can compare these measurements to those at MBO using the precision uncertainty; however, the σ_{ap} measurements were made with a single-wavelength PSAP. The average ω value reported by *Anderson et al.* [2003] and that reported for MBO in Figure 6 are significantly different if the precision uncertainty is considered.

[66] The choice of correction scheme that is applied to the PSAP data will significantly impact the reported ω. See auxiliary material Table S1 and section 2.2.2 for a discussion of the corrections schemes applied across the literature to PSAP data. If the MBO data presented in Figure 6 were corrected following either of the other two correction schemes cited in the literature, the ω values would be larger and would constitute a larger increase compared to

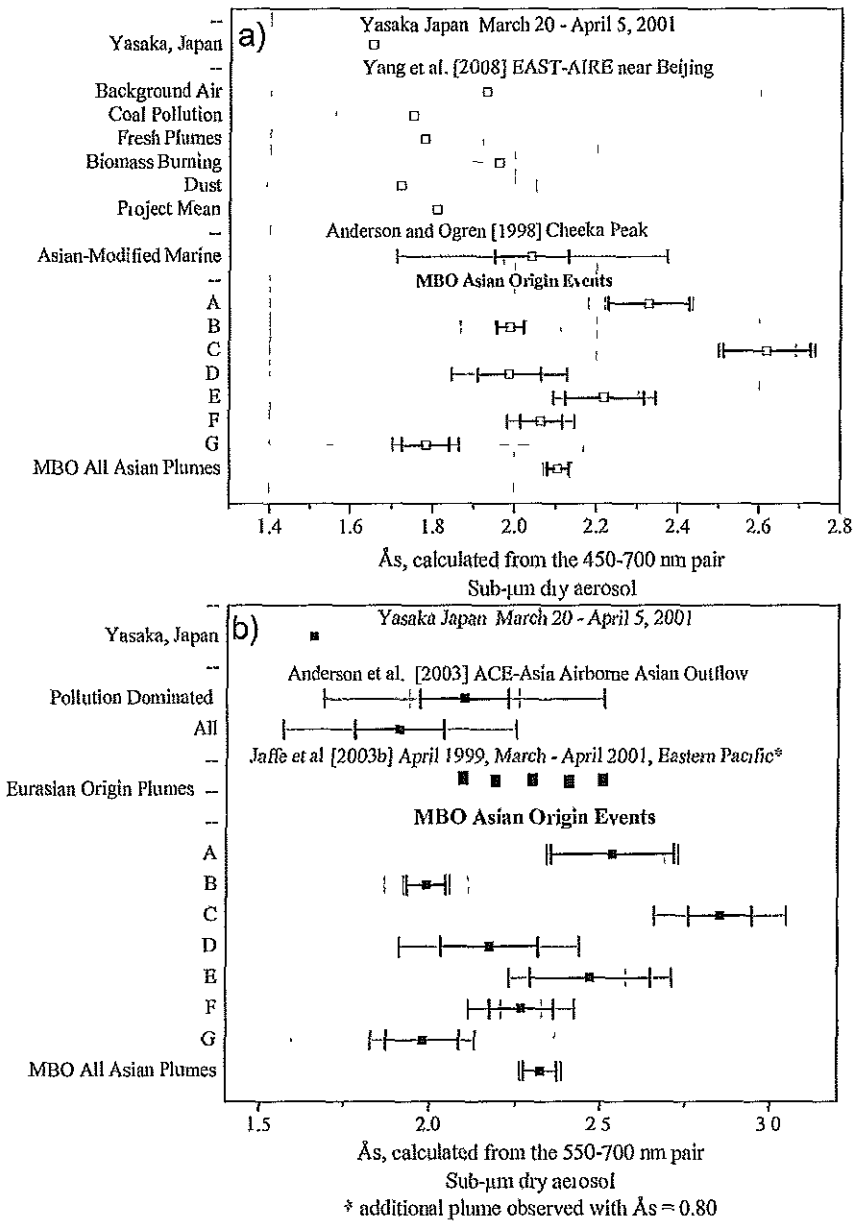

Figure 8. Comparison of the mean scattering Ångström exponent ($Å_s$) during Asian Origin aerosol plumes measured at MBO with other data sets. Light gray, dark gray and black bars are 1 standard deviation, the total uncertainty of the average, and the precision uncertainty of the average respectively. This plot does not include data from 1100–1900 Local Time when the local mixed layer may have been influencing MBO.

observations closer to the Asian source region. In other words, all correction schemes indicate that the submicrometer dry ω values observed at MBO in Asian plumes are larger than those observed closer to the Asian source region, and the difference may be larger than inferred from Figure 6.

[67] Figure 7 presents the same set of data shown in Figure 6 as a function of processing time in the atmosphere. The horizontal axis presents the approximate times downwind from sources as aerosols move from Asia across the Pacific to North America. *Yang et al.* [2009] did not use back trajectories to identify specific emission sources because of the density and proximity of sources. We have assigned a transport age of 0–2 days to this data set. The Asian outflow measurements from the ACE-Asia campaign presented by *Quinn et al.* [2004], *Doherty et al.* [2005], and *Anderson et al.* [2003] were assigned an approximate age of 1 to 4 days based on the discussion and back trajectories presented in these papers. See Figure 1 of *Anderson et al.* [2003] and Figure 1 of *Quinn et al.* [2004]. The *McNaughton* [2008] data were assigned an approximate age of 6–11 days based on the summary plot for the INTEX-B aircraft measurements presented by *Dunlea et al.* [2009]. *Dunlea et al.*

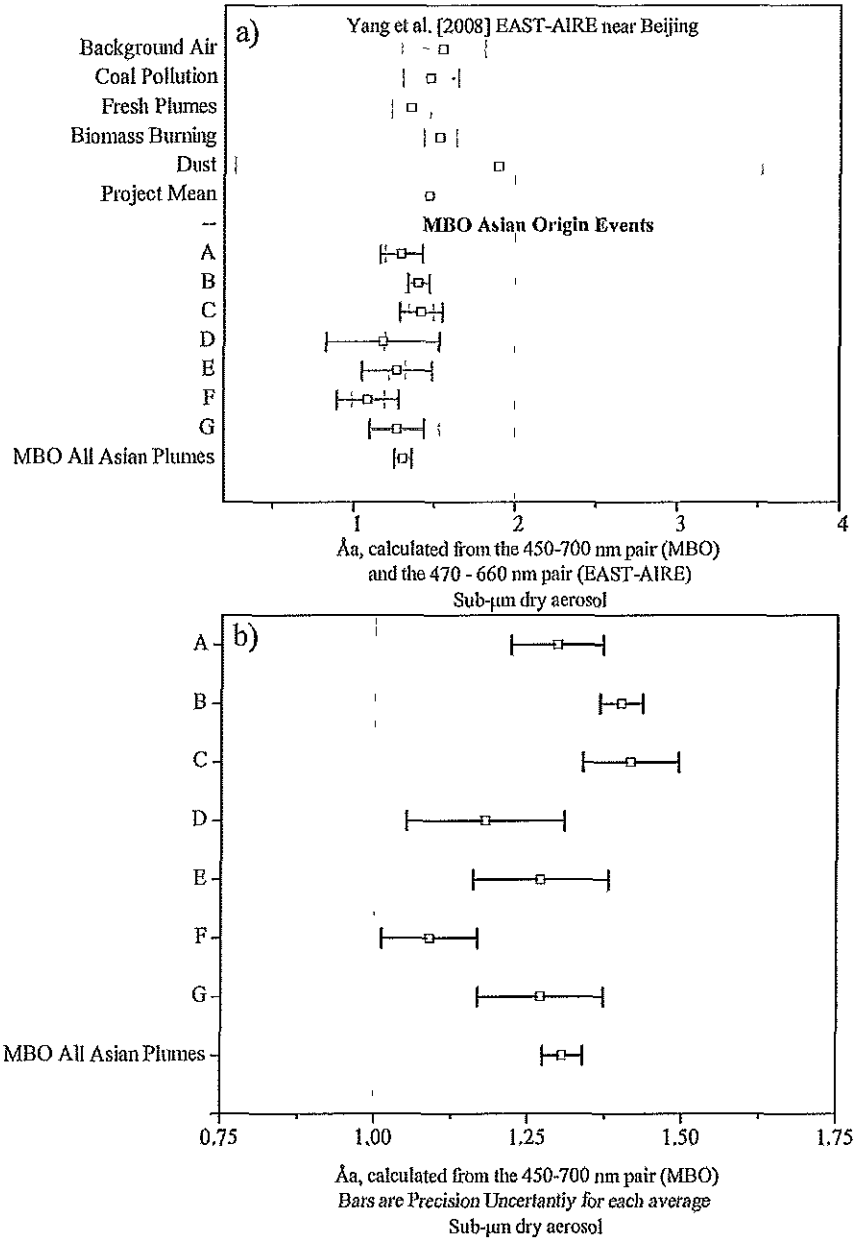

Figure 9. (a) Comparison of the absorption Ångström exponent ($Å_a$) during Asian Origin aerosol plumes measured at MBO during spring 2008 and spring 2009 with data from EAST-AIRE. Light gray and dark gray bars are 1 standard deviation and the total uncertainty of the average, respectively. This plot does not include data from 1100–1900 Local Time when the local mixed layer may have been influencing MBO. This work calculated $Å_a$ from the 450–700 nm pair, and it represents submicrometer aerosol only. *Yang et al.* [2009] calculated $Å_a$ from the 470–660 nm pair, and it represents all aerosol; there was no size cutoff. *Yang et al.* [2009] report the fine absorption fraction at 550 nm for each air mass type. The fine absorption fraction for dust and biomass burning was 0.69 and 0.80 respectively. It was 0.85 for both fresh chimney plumes and coal pollution. The project mean was 0.83. (b) Comparison of ($Å_a$) during Asian Origin aerosol plumes measured at MBO during spring 2008 and spring 2009. Bars are the precision uncertainty of the average for each plume.

[2009] present a summary figure for sulfate and organic aerosol processing as a function of processing time in the atmosphere. Asian plumes observed at MBO were assigned an approximate age based on the back trajectory calculations and supporting satellite images. Figure 7 shows the increase of ω with processing time in the atmosphere. This relationship appears to hold for the individual plumes observed at MBO as well.

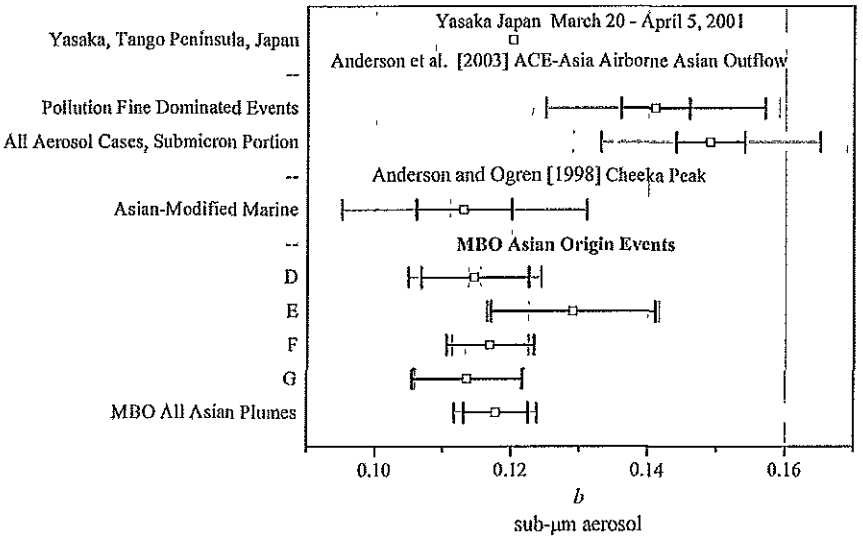

Figure 10. Comparison backscattering ratio (b) during Asian Origin aerosol plumes measured at MBO during spring 2009 with other data sets. All values are reported at 550 nm. Light gray, dark gray, and black bars are 1 standard deviation, the total uncertainty of the average, and the precision uncertainty of the average, respectively. This plot does not include data from 1100–1900 Local Time when the local mixed layer may have been influencing MBO.

[68] The larger average aerosol ω at MBO could be the result of either the addition of a coating of scattering material to the primary aerosols, or the in-transit formation of secondary aerosols. The addition of scattering material to an absorbing core during transpacific transport would increase both scattering and absorption through lensing of incident light [*Bond and Bergstrom*, 2006; *Bond et al.*, 2006; *Fuller et al.*, 1999]. The lensing effect is limited, but the scattering increase is not. The average ω at MBO is larger than that observed in coal pollution and fresh plumes [*Yang et al.*, 2009], but there is a relatively small difference between observations of aged Asian aerosol plumes observed at MBO and observations off the Asian coast [*Anderson et al.*, 2003]. This suggests that the largest changes of ω within aerosol plumes likely occur rapidly, on the time scale of a day.

[69] It should be noted that biomass burning plumes were not specifically identified by *Anderson et al.* [2003] or *Quinn et al.* [2004] in the ACE-Asia aerosol data. MBO plumes A, B and F likely all contain significant amounts of biomass burning smoke. The smoke in plumes A and B likely originated from a similar region (southeastern Russia) and therefore a similar fuel type; this was not the case for plume F which originated further west. The optical properties of aerosols from fires also change with particle size and black carbon content, both of which are dependent on combustion phase [*Reid and Hobbs*, 1998]. Smoke aerosols generally become less absorbing (ω increases) over time as gases and water vapor condense onto the particles [*Haywood et al.*, 2003], but with low-RH sampling at MBO, water is less important.

[70] The MBO $Å_s$ distributions (Figure 8) showed large plume-to-plume variability. From Figure 8 we can infer that there is a shift in the average aerosol size distribution toward maller particles in the submicrometer distribution at MBO compared to the Asian source region. We are referring here to the project means highlighted in yellow in Figure 8. Aside from Plume C, all the Asian plumes observed at MBO had a smaller average $Å_s$ than the North American pollution plume observed by *Anderson et al.* [1999] at Cheeka Peak (not shown in Figure 8).

[71] *Brock et al.* [2004] proposed a conceptual model for transpacific aerosol transport from Asia that could result in dramatic changes to the aerosol size distribution. During the first few days of transport downwind of Asia, gas-phase organic precursors form secondary organic aerosols (SOA) rapidly. This conversion is faster than the SO_2 conversion to sulfate aerosols. Polluted air masses are then lifted out of the boundary layer within warm conveyor belts (WCBs) which are associated with moisture and clouds [*Cooper et al.*, 2004]. The aerosols that have already formed when the air mass is lifted out of the boundary layer are washed out, while less-soluble gas-phase species (e.g., SO_2) are not entirely removed. The remaining gas-phase species are enhanced in SO_2, and sulfate forms in larger concentrations than SOA during transpacific transport [*Brock et al.*, 2004]. This conceptual model is supported by recent observations of sulfate and organic aerosol in aged Asian pollution plumes encountered by the C-130 aircraft during INTEX-B in spring 2006 [*Dunlea et al.*, 2009]. *Dunlea et al.* [2009] provided evidence for a shift in the sulfate size distribution overtime, but did not present the size distribution for the entire aerosol population. Their results showed a decrease in average particle size for a plume recently exported from the BL to the FT, followed by an increase in particle size with processing time during transpacific transport in the FT.

[72] However, there are a number of studies which appear inconsistent with the *Brock et al.* [2004] model. Observations of aerosols in the Northwest Pacific FT in 2001 showed high organic aerosol concentrations [*Heald et al.*, 2005]. Further

downwind, an analysis of surface $PM_{2.5}$ measurements from the U.S. IMPROVE network demonstrated that there is substantial loss and removal of sulfate in Asian plumes during transit across the Pacific [*Jaffe et al.*, 2005]. *Dickerson et al.* [2007] illustrated that dry convection plays an important role in the export of pollutants from the Asian continental BL to the FT. They show that WCBs are more important in cyclonic systems that have moved further east off the coast [*Dickerson et al.*, 2007]. These various BL-FT exchange mechanisms could be one source of the variability in $Å_s$ we observed at MBO.

[73] Figure 9 indicates that the submicrometer aged Asian aerosols observed at MBO showed a strong spectral dependence on absorption, and the plume-to-plume variability was relatively small (refer to Table 2 for values). It should be noted that the $Å_a$ distributions presented for EAST-AIRE in Figure 9a are not directly comparable to those presented for MBO because the EAST-AIRE observations represent all aerosol sizes and the multiwavelength absorption measurements were made with an aethelometer. However, limited relevant measurements of $Å_a$ are available for a direct comparison. See the caption of Figure 9 for details. The range of $Å_a$ values observed at MBO in aged Asian plumes is relatively small compared to reported observations of $Å_a$ closer to sources [*Bergstrom et al.*, 2007; *Yang et al.*, 2009].

[74] Figure 10 indicates that plumes observed at MBO had a lower b than plumes observed closer to the Asian continent. Our data are self consistent, smaller particles are associated with stronger scattering in the backward hemisphere. However, the MBO results are not consistent with data collected closer to Asia. Figure 10 is difficult to interpret because it shows a decrease in the backscattering ratio between plumes observed at MBO and those observed closer to Asia. The results presented in Figure 8, and discussed previously in this section, suggest that on average there is a shift toward a smaller size distribution. Figure 5b confirms the expected inverse relationship between particle size and b. It is possible that the difference in b is driven by a change in the average particle shape more than the average particle size, and b is not a robust indicator of particle size. The mean b for plumes observed at MBO is ~20% lower than that reported by *Anderson et al.* [2003] for Asian outflow intercepted by the C-130 during spring 2001. On the basis of our propagation of uncertainty, these differences are significant. However, *Doherty et al.* [2005] showed that we may not fully understand the precision uncertainty associated with the backscattering measurement in the TSI Model 3563 integrating nephelometer.

[75] We have compared observations of the intensive aerosol optical properties at MBO with those observed closer to the Asian source region in an attempt to better understand how the optical properties change with aerosol age. It should be noted that neither *Anderson et al.* [2003] or *Quinn et al.* [2004] made observations of Siberian biomass burning plumes, and there is strong evidence that such plumes were a major source of aerosols at MBO during spring 2008. Second Asian anthropogenic emissions of aerosols and their gas-phase precursors are dynamic, and the interannual variability is not well quantified. In terms of natural aerosol emissions, specifically dust, we know there can be large interannual variability in the dust source strength and that there is an impact on observed fine particulate concentrations in the western United States [*Fischer et al.*, 2009]. For these reasons, multiple observations in a single plume would certainly be a better way to determine how the average optical properties of Asian aerosols change as they age. However, this type of data is not available at this time.

5. Conclusions and Recommendations for Future Work

[76] We present observations of aerosol optical properties associated with seven well-defined plumes of Asian origin observed at the MBO. When compared to literature observations, these measurements show a significant difference between the optical properties of aerosols over the western versus eastern Pacific. While we understand some aspects of why this is, more data are needed to fully understand this. Key results include the following.

[77] 1. Plumes of Asian origin included many of the highest σ_{sp} (34.8 Mm^{-1} hourly average) and σ_{ap} (5.7 Mm^{-1} hourly average) values observed at MBO over the 2008 and 2009 spring campaigns.

[78] 2. Intensive aerosol properties varied from plume to plume and within some of the plumes. This indicates that even after transpacific transport the aerosols are not necessarily well mixed and the plumes can be layered. It also reinforces the idea that each plume leaving Asia reflects a different mixture of sources.

[79] 3. The plumes clustered in terms of their optical properties. Plumes hypothesized to contain a large fraction of mineral dust were the most distinct, characterized by a relatively higher scattering Ångström ($Å_s$) exponent.

[80] 4. On average the plume mean $Å_s$ at MBO was larger than the project mean $Å_s$ reported for both ACE-Asia aircraft aerosol observations and EAST-AIRE surface observations near Beijing. This suggests a shift toward smaller particles during transpacific transport. The plume-to-plume variability in $Å_s$ could reflect different sources and/or various BL-FT exchange mechanisms.

[81] 5. The average submicrometer dry aerosol ω observed in Asian plumes at MBO (0.88 ± 0.01) was slightly larger than mean observations closer to the Asian coast.

[82] 6. The average submicrometer dry aerosol b observed in Asian plumes at MBO (0.118 ± 0.006) was ~20% smaller than mean observations closer to the Asian coast. This relationship is robust based on our current understanding of measurement uncertainties, but it is not fully understood.

[83] We have presented statistics on aerosol optical properties measured over two spring seasons (April–May) at one location in the lower free troposphere. Addressing the representativeness of observations at MBO would be a productive step toward using these results to address larger research questions such as the regional climate forcing of Asian aerosols. An obvious next step is to systematically connect observations at MBO with concurrent satellite observations to determine plume heights and horizontal extent. However, of the seven plumes presented here, only two (Plumes A and B) were well covered in terms of satellite observations [*Thompson et al.*, 2009] indicating that a longer data set is required for this type of analysis.

[84] Our results suggest a clear path forward for in situ aerosol observations at MBO. In addition to extending the optical measurements to include both the submicrometer

and supermicrometer aerosol fractions, we recommend adding measurements of aerosol chemical composition. Additional measurements of the appropriate chemical tracers could be used to determine if aged Asian smoke, pollution and dust aerosols can be stratified by their combined spectral scattering and absorption properties.

[85] We also need to improve our understanding of the relationship between size and b for nonspherical particles and particles with various mixing states. The interpretation of direct optical measurements of b, like those presented here, will continue to be challenging without a clear understanding of the measurement uncertainty and a better theoretical understanding.

[86] **Acknowledgments.** Emily V. Fischer was supported by a Department of Energy Graduate Research Environmental Fellowship. Support for Mount Bachelor Observatory was provided by the National Science Foundation under grant ATM-0724327. We would like to thank Dave Covert, Patricia Quinn, and Timothy Bates for helpful discussions on the material contained in this manuscript and Nels Laulainen for loaning us a PSAP during spring 2008. We also gratefully acknowledge the support provided by the Mount Bachelor maintenance staff.

References

Anderson, T. L., and J. A. Ogren (1998), Determining aerosol radiative properties using the TSI 3563 Integrating Nephelometer, *Aerosol Sci. Technol., 29*, 57–69, doi:10.1080/02786829808965551.

Anderson, T. L., et al. (1996), Performance characteristics of a high-sensitivity, three-wavelength total scatter/backscatter nephelometer, *J. Atmos. Oceanic Technol., 13*, 967–986, doi:10.1175/1520-0426(1996)013<0967:PCOAHS>2.0.CO;2.

Anderson, T. L., D. Covert, J. D. Wheeler, J. M. Harris, K. D. Perry, B. Trost, D. Jaffe, and J. A. Ogren (1999), Aerosol backscatter fraction and single scattering albedo: Measured values and uncertainties at a coastal station in the Pacific Northwest, *J. Geophys. Res., 104*(D21), 26,793–26,807, doi:10.1029/1999JD900172.

Anderson, T. L., S. J. Masonis, D. Covert, N. C. Ahlquist, S. Howell, A. D. Clarke, and C. McNaughton (2003), Variability of aerosol optical properties derived from in situ aircraft measurements during ACE-Asia, *J. Geophys. Res., 108*(D23), 8647, doi:10.1029/2002JD003247.

Ångström, A. K. (1929), On the atmospheric transmission of Sun radiation and on dust in the air, *Geogr. Ann., 11*, 156–166.

Bergstrom, R. W., P. Pilewskie, P. B. Russell, J. Redemann, T. C. Bond, P. K. Quinn, and B. Sierau (2007), Spectral absorption properties of atmospheric aerosols, *Atmos. Chem. Phys., 7*, 5937–5943, doi:10.5194/acp-7-5937-2007.

Berner, A., C. H. Lurzer, F. Pohl, O. Preining, and P. Wagner (1979), The size distribution of the urban aerosol in Vienna, *Sci. Total Environ., 13*, 245–261, doi:10.1016/0048-9697(79)90105-0.

Bond, T. C., and R. W. Bergstrom (2006), Light absorption by carbonaceous particles: An investigative review, *Aerosol Sci. Technol., 40*, 27–67, doi:10.1080/02786820500421521.

Bond, T. C., T. L. Anderson, and J. R. Campbell (1999), Calibration and intercomparison of filter-based measurements of visible light absorption by particles, *Aerosol Sci. Technol., 30*, 582–600, doi:10.1080/027868299304435.

Bond, T. C., G. Habib, and R. W. Bergstrom (2006), Limitations in the enhancement of visible light absorption due to mixing state, *J. Geophys. Res., 111*, D20211, doi:10.1029/2006JD007315.

Boren, C. F., and D. R. Huffman (1983), *Absorption and Scattering of Light by Small Particles*, John Wiley, Hoboken, N. J.

Brock, C. A., et al. (2004), Particle characteristics following cloud-modified transport from Asia to North America, *J. Geophys. Res., 109*, D23S26, doi:10.1029/2003JD004198.

Carmichael, G. R., et al. (2009), Asian aerosols: Current and year 2030 distributions and implications to human health and regional climate change, *Environ. Sci. Technol., 43*, 5811–5817, doi:10.1021/es8036803.

Carrico, C. M., P. Kus, M. J. Rood, P. K. Quinn, and T. S. Bates (2003), Mixtures of pollution, dust, sea salt, and volcanic aerosol during ACE-Asia: Radiative properties as a function of relative humidity, *J. Geophys. Res., 108*(D23), 8650, doi:10.1029/2003JD003405.

Chin, M., T. Diehl, P. Ginoux, and W. C. Malm (2007), Intercontinental transport of pollution and dust aerosols: Implications for regional air quality, *Atmos. Chem. Phys., 7*, 5501–5517, doi:10.5194/acp-7-5501-2007.

Clarke, A., et al. (2007), Biomass burning and pollution aerosol over North America: Organic components and their influence on spectral optical properties and humidification response, *J. Geophys. Res., 112*, D12S18, doi:10.1029/2006JD007777.

Cooper, O. R., et al. (2004), A case study of transpacific warm conveyor belt transport: Influence of merging airstreams on trace gas import to North America, *J. Geophys. Res., 109*, D23S08, doi:10.1029/2003JD003624.

DeBell, L. J., M. Vozella, R. W. Talbot, and J. E. Dibb (2004), Asian dust storm events of spring 2001 and associated pollutants observed in New England by the Atmospheric Investigation, Regional Modeling, Analysis and Prediction (AIRMAP) monitoring network, *J. Geophys. Res., 109*, D01304, doi:10.1029/2003JD003733.

Dickerson, R. R., et al. (2007), Aircraft observations of dust and pollutants over northeast China: Insight into the meteorological mechanisms of transport, *J. Geophys. Res., 112*, D24S90, doi:10.1029/2007JD008999.

Diner, D. J., et al. (2004), PARAGON: An integrated approach for characterizing aerosol climate impacts and environmental interactions, *Bull. Am. Meteorol. Soc., 85*(10), 1491–1501, doi:10.1175/BAMS-85-10-1491.

Doherty, S., P. K. Quinn, A. Jefferson, C. M. Carrico, T. L. Anderson, and D. A. Hegg (2005), A comparison and summary of aerosol properties as observed in situ from aircraft, ship, and land during ACE-Asia, *J. Geophys. Res., 110*, D04201, doi:10.1029/2004JD004964.

Draxler, R. R., and G. D. Hess (1998), An overview of the HYSPLIT_4 modelling system for trajectories, dispersion, and deposition, *Aust. Meteorol. Mag., 47*, 295–308.

Duncan, B. N., R. V. Martin, A. C. Staudt, R. Yevich, and J. A. Logan (2003), Interannual and seasonal variability of biomass burning emissions constrained by satellite observations, *J. Geophys. Res., 108*(D2), 4100, doi:10.1029/2002JD002378.

Dunlea, E. J., et al. (2009), Evolution of Asian aerosols during transpacific transport in INTEX-B, *Atmos. Chem. Phys., 9*, 7257–7287, doi:10.5194/acp-9-7257-2009.

Echalar, F., A. Caudichet, H. Cachier, and P. Artaxo (1995), Aerosol emissions by tropical forest and savanna biomass burning: Characteristic trace elements and fluxes, *Geophys. Res. Lett., 22*(22), 3039–3042, doi:10.1029/95GL03170.

Fialho, P., A. D. A. Hansen, and R. E. Honrath (2005), Absorption coefficients by aerosols in remote areas: A new approach to decouple dust and black carbon absorption coefficients using seven-wavelength Aethalometer data, *J. Aerosol Sci., 36*(2), 267–282, doi:10.1016/j.jaerosci.2004.09.004.

Fischer, E. V., N. C. Hsu, D. A. Jaffe, M.-J. Jeong, and S. L. Gong (2009), A decade of dust: Asian dust and springtime aerosol load in the U.S. Pacific Northwest, *Geophys. Res. Lett., 36*, L03821, doi:10.1029/2008GL036467.

Fischer, E. V., D. A. Jaffe, D. R. Reidmiller, and L. Jaeglé (2010), Meteorological controls on observed peroxyacetyl nitrate (PAN) at Mount Bachelor during the spring of 2008, *J. Geophys. Res., 115*, D03302, doi:10.1029/2009JD012776.

Fuller, K. A., W. C. Malm, and S. M. Kreidenweis (1999), Effects of mixing on extinction by carbonaceous particles, *J. Geophys. Res., 104*(D13), 15,941–15,954, doi:10.1029/1998JD100069.

Gaudichet, A., F. Echalar, B. Chatenet, J. P. Quisefit, G. Malingre, H. Cachier, P. Baut-Menard, P. Artaxo, and W. Maenhaut (1995), Trace elements in tropical African savanna biomass burning aerosols, *J. Atmos. Chem., 22*, 19–39, doi:10.1007/BF00708179.

Haywood, J. M., and K. P. Shine (1995), The effect of anthropogenic sulfate and soot aerosol on the clear-sky planetary radiation budget, *Geophys. Res. Lett., 22*(5), 22,603–22,606.

Haywood, J. M., S. R. Osborne, P. N. Francis, A. Keil, P. Formenti, M. O. Andreae, and P. H. Kaye (2003), The mean physical and optical properties of regional haze dominated by biomass burning aerosol measured from the C-130 aircraft during SAFARI 2000, *J. Geophys. Res., 108*(D13), 8473, doi:10.1029/2002JD002226.

Heald, C. L., D. J. Jacob, R. J. Park, L. Russell, B. J. Hubert, J. H. Seinfeld, H. Liao, and R. J. Weber (2005), A large organic aerosol source in the free troposphere missing from current models, *Geophys. Res. Lett., 32*, L18809, doi:10.1029/2005GL023831.

Heald, C. L., D. J. Jacob, R. J. Park, B. Alexander, T. D. Fairlie, R. M. Yantosca, and D. A. Chu (2006), Transpacific transport of Asian anthropogenic aerosols and its impact on surface air quality in the United States, *J. Geophys. Res., 111*, D14310, doi:10.1029/2005JD006847.

Heintzenberg, J., and R. J. Charlson (1996), Design and applications of the integrating nephelometer: A review, *J. Atmos. Oceanic Technol., 13*, 987–1000, doi:10.1175/1520-0426(1996)013<0987:DAAOTI>2.0.CO;2.

Huebert, B J, T S Bates, P B Russell, G Shi, Y J Kim, K Kawamura, G R Carmichael, and T Nakajima (2003), An overview of ACE-Asia Strategies for quantifying the relationships between Asian aerosols and their climatic impacts, *J Geophys Res*, *108*(D23), 8633, doi 10 1029/2003JD003550

Husar, R B, et al (2001), Asian dust events of April 1998, *J Geophys Res*, *106*(D16), 18,317–18,330, doi 10 1029/2000JD900788

Intergovernmental Panel on Climate Change (IPCC) (2007), *Climate Change 2007 The Physical Science Basis Working Group I Contribution to the Fourth Assessment*, edited by S Solomon et al, Cambridge Univ Press, Cambridge, U K

Jaffe, D A, et al (1999), Transport of Asian air pollution to North America, *Geophys Res Lett*, *26*(6), 711–714, doi 10 1029/1999GL900100

Jaffe, D A, J A Snow, and O R Cooper (2003a), Asian dust events Transport and impact on surface aerosol concentrations in the United States, *Eos Trans AGU*, *84*(46), 501, doi 10 1029/2003EO460001

Jaffe, D A, I McKendry, T Anderson, and H Price (2003b), Six 'new' episodes of trans-Pacific transport of air pollutants, *Atmos Environ*, *37*, 391–404, doi 10 1016/S1352-2310(02)00862-2

Jaffe, D A, I Bertschi, L Jaegle, P Novelli, J S Reid, H Tanimot, R Vingarzan, and D L Westphal (2004), Long-range transport of Siberian biomass burning emissions and impact on surface ozone in western North America, *Geophys Res Lett*, *31*, L16106, doi 10 1029/2004GL020093

Jaffe, D A, S Tamura, and J Harris (2005), Seasonal cycle and composition of background fine particles along the west coast of the US, *Atmos Environ*, *39*, 297–306, doi 10 1016/j atmosenv 2004 09 016

Kalashnikova, O V, and I N Sokolik (2002), Importance of shapes and composition of wind blown dust particles for remote sensing at solar wavelengths, *Geophys Res Lett*, *29*(10), 1398, doi 10 1029/2002GL014947

Kaufman, Y J, D Tanre, and O Boucher (2002), A satellite view of aerosols in the climate system, *Nature*, *419*, 215–223, doi 10 1038/nature01091

Lack, D A, C D Cappa, D S Covert, T Baynard, P Massoli, B Sierau, T S Bates, P K Quinn, E R Lovejoy, and A R Ravishankara (2008), Bias in filter based aerosol light absorption measurements due to organic aerosol loading Evidence from ambient measurements, *Aerosol Sci Technol*, *42*, 1033–1041, doi 10 1080/02786820802389277

Lack, D A., C D Cappa, E S Cross, P Massoli, A T Ahern, P Davidovits, and T B Onasch (2009), Absorption enhancement of coated absorbing aerosols Validation of the photo acoustic technique for measuring the enhancement, *Aerosol Sci Technol*, *43*, 1006–1012, doi 10 1080/02786820903117932

Lapina, K, R E Honrath, R C Owen, M Val Martin, and G Pfister (2006), Evidence of significant large-scale impacts of boreal fires on ozone levels in the midlatitude Northern Hemisphere free troposphere, *Geophys Res Lett*, *33*, L10815, doi 10 1029/2006GL025878

Liu, Z Y, M Vaughan, D Winker, C Kittaka, B Getzewich, R Kuehn, A Omar, K Powell, C. Trepte, and C Hostetler (2009), The CALIPSO lidar cloud and aerosol discrimination Version 2 algorithm and initial assessment of performance, *J Atmos Oceanic Technol*, *26*, 1198–1213, doi 10 1175/2009JTECHA1229 1

Malm, W C, J F Sisler, D Huffman, R A Eldred, and T A Cahill (1994), Spatial and seasonal trends in particle concentration and optical extinction in the United States, *J Geophys Res*, *99*(D1), 1347–1370

Marshall, S F, D S Covert, and R J Charlson (1995), Relationship between asymmetry parameter and hemispheric backscatter ratio Implications for climate forcing by aerosols, *Appl Opt*, *34*(27), 6306–6311, doi 10 1364/AO 34 006306

McNaughton, C S (2008), Constraining climate model simulations of aerosol size distributions over the North Pacific and North America using in-situ airborne measurements, Ph D thesis, Univ of Hawaii at Manoa, Honolulu

McNaughton, C S, et al (2009), Observations of heterogeneous reactions between Asian pollution and mineral dust over the Eastern North Pacific during INTEX-B, *Atmos Chem Phys*, *9*, 8283–8308, doi 10 5194/acp-9 8283-2009

Morris, G A, et al (2006), Alaskan and Canadian forest fires exacerbate ozone pollution over Houston, Texas, on 19 and 20 July 2004, *J Geophys Res*, *111*, D24S03, doi 10 1029/2006JD007090

Omar, A H, J -G Won, D Winker, S -C Yoon, O Dubovik, and M P McCormick (2005), Development of global aerosol models using cluster analysis of Aerosol Robotic Network (AERONET) measurements, *J Geophys Res*, *110*, D10S14, doi 10 1029/2004JD004874

Omar, A H, et al (2009), The CALIPSO automated aerosol classification and lidar ratio selection algorithm, *J Atmos Oceanic Technol*, *26*, 1994–2014, doi 10 1175/2009JTECHA1231 1

Patterson, E M (1981), Optical properties of crustal aerosol Relation to chemical and physical characteristics, *J Geophys Res*, *86*(C4), 3236–3246, doi 10 1029/JC086iC04p03236

Price, H U, D Jaffe, O R Cooper, and P V Doskey (2004), Photochemistry, ozone production, and dilution during long range transport episodes from Eurasia to the northwest United States, *J Geophys Res*, *109*, D23S13, doi 10 1029/2003JD004400

Quinn, P K, et al (2004), Aerosol optical properties measured on board the Ronald H Brown during ACE-Asia as a function of aerosol chemical composition and source region, *J Geophys Res*, *109*, D19S01, doi 10 1029/2003JD004010

Reid, J S, and P V Hobbs (1998), Physical and optical properties of young smoke from individual biomass fires in Brazil, *J Geophys Res*, *103*(D24), 32,013–32,031, doi 10 1029/98JD00159

Reid, J S, R Koppmann, T F Eck, and D P Eleuterio (2004), A review of biomass burning emissions part II Intensive physical properties of biomass burning particles, *Atmos Chem Phys Discuss*, *4*, 5135–5200, doi 10 5194/acpd 4 5135-2004

Reid, J S, T F Eck, S A Christopher, R Koppmann, O Dubovik, D P Eleuterio, B N Holben, E A Reid, and J Zhang (2005), A review of biomass burning emissions part III Intensive optical properties of biomass burning particles, *Atmos Chem Phys Discuss*, *5*, 827–849

Reidmiller, D R, D A Jaffe, E V Fischer, and B Finley (2010), Nitrogen oxides in the boundary layer and free troposphere at the Mt Bachelor Observatory, *Atmos Chem Phys Discuss*, *10*, 5751–5801, doi 10 5194/acpd-10-5751-2010

Rockstrom, J, et al (2009), A safe operating space for humanity, *Nature*, *461*, 472–475, doi 10 1038/461472a

Sheridan, P J, et al (2005), The Reno Aerosol Optics Study An evaluation of aerosol absorption measurement methods, *Aerosol Sci Technol*, *39*, 1–16, doi 10 1080/027868290901891

Sierau, B, D S Covert, D J Coffman, P K Quinn, and T S Bates (2006), Aerosol optical properties during the 2004 New England Air Quality Study–Intercontinental Transport and Chemical Transformation Gulf of Maine surface measurements—Regional and case studies, *J Geophys Res*, *111*, D23S37, doi 10 1029/2006JD007568

Subramanian, R, C A Roden, P Boparai, and T C Bond (2007), Yellow beads and missing particles Trouble ahead for filter based absorption measurements, *Aerosol Sci Technol*, *41*, 630–637, doi 10 1080/02786820701344589

Thompson, R S, E V Fischer, D A Jaffe, and M Di Perro (2009), Integrating MISR, MODIS, and CALIPSO satellite data with in situ measurements at Mount Bachelor to determine aerosol plume characteristics, *Eos Trans AGU*, *90*(52), Fall Meet Suppl, Abstract A33B 0246

VanCuren, R A (2003), Asian aerosols in North America Extracting the chemical composition and mass concentration of the Asian continental aerosol plume from long term aerosol records in the western United States, *J Geophys Res*, *108*(D20), 4623, doi 10 1029/2003JD003459

VanCuren, R A, and T A Cahill (2002), Asian aerosols in North America Frequency and concentration of fine dust, *J Geophys Res*, *107*(D24), 4804, doi 10 1029/2002JD002204

Viana, M, et al (2008), Tracers and impact of open burning of rice straw residues on PM in eastern Spain, *Atmos Environ*, *42*, 1941–1957, doi 10 1016/j atmosenv 2007 11 012

Virkkula, A., N C Ahlquist, D S Covert, W P Arnott, P J Sheridan, P K Quinn, and D J Coffman (2005), Modification, calibration and filed test of an instrument for measuring light absorption by particles, *Aerosol Sci Technol*, *39*, 68–83, doi 10 1080/027868290901963

Warneke, C, et al (2009), Biomass burning in Siberia and Kazakhstan as an important source for haze over the Alaskan Arctic in April 2008, *Geophys Res Lett*, *36*, L02813, doi 10 1029/2008GL036194

Weiss-Penzias, P, D Jaffe, P Swartzendruber, J B Dennison, D Chand, W Hafner, and E Prestbo (2006), Observations of Asian air pollution in the free troposphere at Mount Bachelor Observatory during spring of 2004, *J Geophys Res*, *111*, D10304, doi 10 1029/2005JD006522

Weiss Penzias, P, D Jaffe, P Swartzendruber, W Hafner, D Chand, and E Prestbo (2007), Quantifying atmospheric mercury emissions from biomass burning and East Asian industrial regions based on ratios with carbon monoxide in pollution plumes at the Mount Bachelor Observatory, *Atmos Environ*, *41*, doi 10 1016/j atmosenv 2007 1001 1058

Westerling, A L, A Gershunov, T J Brown, D R Cayan, and M D Dettinger (2003), Climate and wildfire in the western United States, *Bull Am Meteorol Soc*, *84*(5), 595–604, doi 10 1175/BAMS 84-5-595

Wuebbles, D J, H Lei, and J Lin (2007), Intercontinental transport of aerosols and photochemical oxidants from Asia and its consequences, *Environ Pollut*, *150*, 65–84, doi 10 1016/j envpol 2007 06 066

Yang, M, S G Howell, J Zhuang, and B J Huebert (2009), Attribution of aerosol light absorption to black carbon, brown carbon, and dust in China—Interpretations of atmospheric measurements during EAST-AIRE, *Atmos Chem Phys*, *9*, 2035–2050, doi 10 5194/acp-9-2035-2008

Yu, H., L. A. Remer, M. Chin, H. Bian, R. G. Kleidman, and T. Diehl (2008), A satellite-based assessment of transpacific transport of pollution aerosol, *J. Geophys. Res.*, *113*, D14S12, doi:10.1029/2007JD009349.

E. Fischer and D. A. Jaffe, Department of Atmospheric Sciences, University of Washington, 408 ATG Bldg., Box 351640, Seattle, WA 98195, USA. (efischer@atmos.washington.edu)

J. S. Gaffney, Department of Chemistry, University of Arkansas at Little Rock, Little Rock, AR 72204, USA.

A. Marchany-Rivera, Department of Applied Science, University of Arkansas at Little Rock, Little Rock, AR 72204, USA.

N. A. Marley, Graduate Institute of Technology, University of Arkansas at Little Rock, Little Rock, AR 72204, USA.

Atmos. Chem. Phys., 7, 2277–2285, 2007
www.atmos-chem-phys.net/7/2277/2007/

Atmospheric Chemistry and Physics

Comparison of measurements of peroxyacyl nitrates and primary carbonaceous aerosol concentrations in Mexico City determined in 1997 and 2003

N. A. Marley[1], J. S. Gaffney[1], R. Ramos-Villegas[2], and B. Cárdenas González[3]

[1]Chemistry Department, University of Arkansas at Little Rock, Little Rock, Arkansas, USA
[2]Secretariat of the Environment, Government of the Federal District, Mexico City, D.F., Mexico
[3]El Centro National de Investigation y Capitación Ambiental, Instituto National de Ecologia, Secretaria de Medio Ambiente y Recursos Naturales, Mexico City, D.F., Mexico

Received: 18 December 2006 – Published in Atmos. Chem. Phys. Discuss.: 29 January 2007
Revised: 13 April 2007 – Accepted: 15 April 2007 – Published: 4 May 2007

Abstract. The concentrations of peroxyacetyl nitrate (PAN) in ambient air can be a good indicator of air quality and the effectiveness of control strategies for reducing ozone levels in urban areas. As PAN is formed by the oxidation of reactive hydrocarbons in the presence of nitrogen dioxide (NO_2), it is a direct measure of the peroxyacyl radical levels produced from reactive organic emissions in the urban air shed. Carbon soot, known as black carbon (BC) or elemental carbon (EC), is a primary atmospheric aerosol species and is a good indicator of the levels of combustion emissions, particularly from diesel engines, in major cities. Mexico City is the second largest megacity in the world and has long suffered from poor air quality. Reported here are atmospheric measurements of PAN and BC obtained in Mexico City during the Mexico Megacity 2003 field study. These results are compared with measurements obtained earlier during the *Investigación sobre Materia Particulada y Deterioro Atmosférico – Aerosol and Visibility Research* (IMADA-AVER) campaign in 1997 to obtain an estimate of the changes in emissions in Mexico City and the effectiveness of control strategies adopted during that time. Concentrations of PAN in 1997 reached a maximum of 34 ppb with an average daily maximum of 15 ppb. The PAN levels recorded in 2003 were quite different, with an average daily maximum of 3 ppb. This dramatic reduction in PAN levels observed in 2003 indicate that reactive hydrocarbon emissions have been reduced in the city due to controls on olefins in liquefied petroleum gas (LPG) and also due to the significant number of newer vehicles with catalytic converters that have replaced older higher emission vehicles. In contrast, black/elemental carbon levels were similar in 1997 and 2003 indicating little improvement likely due to the lack of controls on diesel vehicles in the city. Thus, while air quality and ozone production have improved, Mexico City and other megacities continue to be a major source of black carbon aerosols, which can be an important species in determining regional radiative balance and climate.

Correspondence to: J. S. Gaffney
(jsgaffney@ualr.edu)

1 Introduction

Megacities are large urban and suburban complexes whose populations are in the tens of millions of inhabitants (Lynn, 1999). With the rapid growth of the world's population and the continuing industrialization and migration of the populace towards major urban centers, the numbers of these megacities are increasing. Although New York City was the only megacity in the world in 1950, they now number 14 and their distribution is growing most rapidly in the tropical areas of South America and Asia. Today, the largest metropolitan complexes are centered at Tokyo, Japan, and Mexico City, Mexico (Molina and Molina, 2002a). Within the next 10 to 15 years it is predicted that there will be more than 30 megacities worldwide.

Megacities have become important global sources of air pollutants from the associated mobile and stationary sources and the emissions from megacities are leading to regional and global increases in many key trace gases as well as primary and secondary aerosols. The Mexico City metropolitan area (MCMA), which occupies ~1300 km^2 with a population of ~18 M, is one of the largest megacities in the world and is well known for its high levels of air pollution and visibility reduction (Molina and Molina, 2002b). It has been estimated that emissions from the Mexico City basin contribute 15 Mega-tons of fine aerosol ($PM_{2.5}$) per year to the surrounding regions (Gaffney et al., 1999). This fine aerosol is composed of approximately 32% organic carbon, 15% elemental

Published by Copernicus GmbH on behalf of the European Geosciences Union.

carbon, 10% ammonium nitrate and 20% ammonium sulfate (Chow et al., 2002). The emissions of sulfate aerosols alone from the MCMA are estimated to amount to 1% of the total global burden (Barth and Church, 1999). While sulfate is an important light scattering aerosol species, black carbon is an important light absorbing aerosol species. The aerosol emissions from megacities such as Mexico City therefore play potentially important roles in regional radiative balance and climate (Jacobson, 2002; Gaffney and Marley, 2005).

Elevated levels of ozone have been known for some time in Mexico City (Bravo et al., 1989; MARI, 1994; Streit and Guzman, 1996; Fast and Zhong, 1998). Mexico City is located at an altitude of 7200 ft in an air basin surrounded by mountains (Fast and Zhong, 1998; Doran et al., 1998) and at a latitude of 19° of North, which implies high levels of incoming solar radiation all year long. In the past, peak ozone levels exceeding 300 ppb were not uncommon, particularly during the late dry winter months of February and March (The one-hour standard is 0.11 ppm (Molina and Molina, 2002a)). These very high levels of ozone require high levels of reactive hydrocarbons as well as elevated levels of nitrogen oxide (NO) emissions to produce the coupled OH and peroxyradical chemistry that is key to the formation of urban ozone (Finlayson-Pitts and Pitts, 2000). Hydrocarbon measurements taken in Mexico City (Blake and Rowland, 1995) showed that the heavy domestic and commercial use of LPG has led to very high levels of butane and propane in that megacity's air, exceeding parts-per-million (ppm) of carbon in many cases. Indeed, LPG was proposed as an important source of the reactive volatile organic carbon compounds (VOCs) propene and butenes, which could account for an appreciable portion of the observed urban ozone in Mexico City (Blake and Rowland, 1995). Volatile organic carbon samples collected before and during a Mexican national holiday with reduced automobile traffic clearly showed that mobile emissions are equally important as LPG as sources of reactive olefins such as the butenes (Gaffney et al., 1999). In addition, earlier work suggested that mobile sources contribute 75% of the total hydrocarbons to the Mexico City air (Riveros et al., 1998) and that NO_2 was probably the most important contributor to ozone production in Mexico City (Raga et al., 2001a).

Peroxyacyl nitrates (PANs) are important indicator compounds of peroxyradical activity in an urban air shed (Finlayson-Pitts and Pitts, 2000; Gaffney et al., 1989). Formed by the reaction of peroxyacyl radicals with NO_2, they exist in equilibrium with the peroxy radical species according to:

$$RC(=O)-O_2 + NO_2 \rightarrow RC(=O)-O-O-NO_2 \quad (1)$$

where R is typically (in order of importance); CH_3- (peroxyacetyl nitrate, PAN), CH_3CH_2- (peroxypropionyl nitrate, PPN), and $CH_3CH_2CH_2$- (peroxybutryl nitrate, PBN) in an urban environment. The peroxyacyl radicals are formed from the reactive olefins directly or via formation of aldehydes that can react with OH to form the peroxyacyl species. While the PANs are thermally labile, the reverse reaction to reform the PANs is relatively fast leading to no net loss at elevated temperatures in areas of high NO_2 concentrations (Finlayson-Pitts and Pitts, 2000; Gaffney et al., 1989).

Thus, measurements of the temporal variability of the PANs are useful in determining the oxidative reactions involved in the formation of ozone as well as other secondary air pollutants and aerosol species such as nitric acid and ammonium nitrate as they are a direct measure of the peroxyacyl radical formation activity. The PANs therefore serve as a measure of the peroxy radical concentrations in the atmosphere. Since the PANs have low aqueous solubilities, low reactivity with OH, and are slow to photolyze, they can lead to the transport of NO_2 over long distances and can simultaneously act as a reservoir for NO_2 during transport of the urban plume. This can have regional scale impacts on ozone, nitrate aerosols, and other pollutants associated with megacity plumes (Gaffney et al., 1989).

Carbonaceous particulate matter or "soot" particles are produced from the partial combustion of hydrocarbons, particularly from diesel fuels, and are therefore a measure of the combustion emissions in an urban area. Although the elemental composition of these particles is dominated by carbon (>90%), soot particles may be regarded as a complex organic polymer, rather than an amorphous form of elemental carbon (Andreae and Gelencser, 2006). The absolute identification of carbon soot is difficult and the techniques commonly used, such as Raman spectroscopy, electron microscopy, and mass spectrometry are impractical for routine monitoring of this material. Various measurement methods have been developed for the routine quantitation of aerosol soot content that make use of some of its characteristic properties. These methods have created operational definitions such as "black carbon" or "elemental carbon" depending on the key property being measured (Gaffney and Marley, 2006). The term "black carbon" arises from the use of optical attenuation methods and refers to the highly absorbing nature of carbon soot aerosols. In contrast, the term "elemental carbon" is used when thermal combustion methods are employed for detection and refers to the refractory nature of the aerosols at temperatures up to 350–400°C. Comparisons between the optical and thermal combustion methods in different environments have yielded correlation coefficients of 0.99 (Hansen and McMurry, 1990), 0.97 (Allen et al., 1999), and 0.94 (Babich et al., 2000) and the various terms used to identify combustion derived aerosols are commonly used interchangeably.

Although originally identified as a pollutant and a tracer for combustion emissions, carbon soot has more recently gained attention as a major light absorbing species with significant impacts on the radiative balance of the atmosphere (Ramanathan et al., 2005). Some model calculations suggest that the contribution of carbon soot aerosols to global warming may be as much as 0.3–0.4°C, rivaling the contributions from atmospheric methane (Jacobson, 2004; Chung and

Seinfeld, 2005). The ultimate climate effects from carbon aerosols will depend on their physical and chemical properties, as well as their residence times and distributions in the atmosphere (Jacobson, 2001). In order to adequately assess the aerosol impacts on global and regional climate, a better understanding of black carbon aerosol emission rates and atmospheric distributions will be essential.

In an attempt to better understand the Mexico City air chemistry with regard to oxidants and aerosols, a comprehensive collaborative study was carried out during February-March 1997 that included a wide variety of chemistry, aerosol and meteorological measurements (Edgerton et al., 1999; Doran et al., 1998; Fast and Zhong, 1998). This field campaign (IMADA-AVER) was jointly sponsored by the U.S. Department of Energy's Office of Biological and Environmental Research Atmospheric Science Program (DOE/ASP) and *Petrleos Mexicanos* (PEMEX) through the Mexican Petroleum Institute (*Instituto Mexicano de Petroleo*, or IMP).

As part of IMADA-AVER, measurements of near-surface tropospheric PANs were made at the IMP laboratories to determine the concentrations and temporal variability of these species in the megacity (Gaffney et al., 1999). Levels of the PANs were found to approach 40 ppb in the central metropolitan area. Peroxyacetyl nitrate was the major species, although PPN and PBN were also observed in the low ppb ranges. These are the highest values of the PANs seen in any urban area since 50 ppb values were reported for PAN in the late 1970s downwind of Los Angeles in the south coast air basin in southern California (Tuazon et al., 1981). Volatile organic carbon measurements obtained at IMP during the same time indicated that automobiles were responsible for much of the reactive hydrocarbons in the atmosphere (Gaffney et al., 1999). The meteorological measurements demonstrated that the air basin was subject to a strong advection of the boundary layer in the afternoon leading to a clearing out of the pollutants emitted and formed during the day. This regional meteorology leads to very little carryover of the pollutants in Mexico City from day to day and atmospheric chemistry that is dominated by reactions that took place typically over a one day period (Gaffney et al., 1999; Fast and Zhong, 1998; Doran et al., 1998). The application of a simple box model indicated that considerable amounts of air pollutants, both oxidants and aerosols, were being transported out of the Mexico City air basin (Gaffney et al., 1999; Elliott et al., 1997).

In April 2003, the DOE/ASP again conducted a field study in Mexico City (Mexico Megacity 2003) in collaboration with the MCMA 2003 air quality study organized by M. J. Molina and L. T. Molina of the Massachusetts Institute of Technology. Continuous measurements of the PANs and black carbon aerosols were obtained during April 2003 at the National Center for Environmental Research and Training (*Centro Nacional de Investigación y Capacitación Ambiental*, or CENICA), on the Iztapalapa campus of the *Universidad Autónoma Metropolitana* (UAM). Data were collected before and during the Easter holiday to assess changes in PAN and BC loadings as a function of vehicle traffic levels.

Results are presented here for PAN and BC concentrations obtained in Mexico City during the Mexico Megacity 2003 field study. These results are compared with those obtained 6 years earlier during the IMADA-AVER study. Changes in PAN and carbonaceous aerosol levels are presented as an indication of changes in emission levels during that time and the effectiveness of ozone control strategies that have been adopted in Mexico City since 1997. The black carbon aerosol comparisons are of particular importance in the evaluation of the regional impacts of the changing megacity emissions of this key absorbing aerosol species and its importance for regional climate considerations.

2 Experimental methods

Measurements were obtained from February 20 to March 23, 1997 at Building No. 24 (*Refinación y Petroquimica*) of the IMP laboratories (*Eje Central Lazaro Cardenas No. 152, Delegacion Gustavo A. Madero, México, Districto Federale*). This site is located in the north central part of Mexico City (19°29′ 19.392″ N, 99° 08′ 50.258″ W). The PANs were determined using an automated gas chromatograph equipped with an electron capture detection system (GC/ECD). This system has been described in detail elsewhere (Gaffney et al., 1993, 1997, 1998, 1999). A 2-cm^3 sample was injected automatically onto a packed GC carbowax 400 column every 30 min. Data were collected using a recording integrator and processed manually for each of 1380 samples. Calibration of the instrument for the PANs was accomplished by manual injection of standards synthesized by strong acid nitration of the corresponding peracids (Gaffney et al., 1984; Gaffney and Marley, 2005a).

Data for ozone and NO_2 concentrations were obtained from the IMP monitoring station of the Mexico City ambient air monitoring network (*la Red Automática de Monitoreo Atmosférico*, or RAMA), operated at that time by the *Dirección General de Prevencin y Control de la Contaminacin de la Ciudad de México*. Nineteen of the 33 urban RAMA stations measure ozone by UV absorption and nitrogen oxide (NO) and total nitrogen oxides (NO_x) by chemiluminescence among other criteria pollutants, which are reported as hourly averages. As the chemiluminescent nitrogen oxides analyzer in the NO_x mode measures the sum of NO_2, NO and PAN concentrations, the 1997 NO_2 concentrations were estimated by subtraction of the NO and PAN concentrations from NO_x results ($NO_2 \approx NO_x$-NO-PAN).

Measurements of the PANs, NO_2 and fine aerosol black carbon content were obtained from 3 April to 1 May 2003 on the rooftop of the CENICA laboratory building (19° 21′ 44.541″ N, 99° 04′ 16.425″ W) on the UAM Iztapalapa

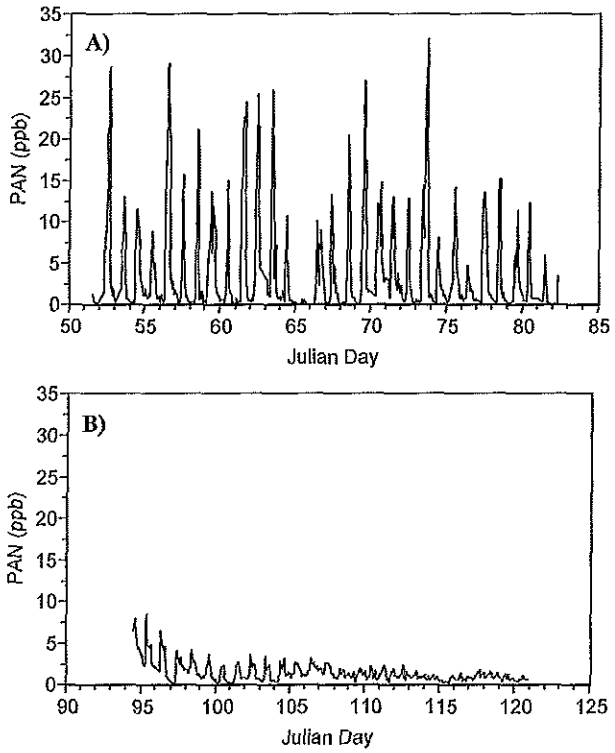

Fig. 1. **(A)** Concentration profiles for peroxyacetyl nitrate (PAN) measured in Mexico City from 20 February to 23 March 1997 and **(B)** from 3 March to 1 April 2003.

campus (*Calle "Sur 10" No. 230, Colonia La Vicentina, Delegación Iztapalapa, México, D.F.*). This site is approximately 16.1 km (10.0 mi) south-southwest of the site at the IMP site that was used in 1997. Measurements of the PANs and NO_2 were obtained by fast gas chromatography with luminol detection. This system has been described in detail elsewhere (Marley, et al., 2004) but will be briefly reviewed here. A 2-cm^3 sample loop was used to automatically inject samples onto a 30-ft. capillary DB-1 column at 1-min intervals. Both NO_2 and PAN were detected by the chemiluminescent reaction with luminol and the intensity of the emission at 425 nm was measured with a photon counting module. The instrument was controlled by a 1.8-GHz Notebook computer with a Windows 2000 operating system and a custom software application programmed in LabVIEW. The instrument was calibrated for NO_2 by dilution of a 2.8-ppm NO_2 tank standard in air with a gas calibrator (Dasibi; Model 1009-CP) and for the PANs with the synthetic standards described above. This instrument has been compared with the GC/ECD method in previous studies and found to give good agreement both in field studies and with synthetic PAN standards (Gaffney et al., 1998, 2005a; Marley et al., 2004).

The black carbon content of fine aerosols was measured by using a seven-channel aethalometer (Andersen) with a sample inlet designed to collect aerosols in the 0.1 to 2 micron size range. The aerosols in the air sample are collected within the instrument by continuous filtration through a paper tape strip. The optical transmission of the deposited aerosol particles is then measured sequentially at seven wavelengths (370, 450, 520, 590, 660, 880, and 950 nm). Since black carbon is a strongly absorbing aerosol species with an absorption coefficient relatively constant over a broad spectral region (Marley et al., 2001) the instrument can automatically calculate the black carbon content from the transmission measurements by assuming black carbon to be the main absorbing aerosol species in the samples with a $1/\lambda$ dependence typical of broadband absorbers and a mass specific absorption coefficient of 16.6 m^2/g at 880 nm (Hansen et al., 1982). The instrument is operated by an embedded computer with a display screen and keypad that controls all instrument functions and automatically records the data to a built-in 3.5″ floppy diskette. Data were recorded for each of the seven channels at a two-minute time resolution. In addition, the analog output of the 520 nm channel was monitored continuously and one minute averages of this channel were recorded separately.

Measurements of total $PM_{2.5}$ mass concentrations were also obtained at the CENICA site by a Tapered Element Oscillating Microbalance (TEOM, Ruppert & Pastashnick) operated at 35°C. This instrument measures the total fine aerosol mass concentration by using a vibrating element whose frequency is dependent on the particle mass collected on a filter located at the end of the element (Hinds, 1999). Hourly averages of ozone for this time period were obtained from the RAMA station at *Cerro de la Estrella* (*Calzada San Lorenzo, Colonia Paraje San Juan, Delegación Iztapalapa, México D.F.*). This site (19° 20′ 09.184″ N, 99° 04′ 28.829″ W) is located 3.0 km (1.8 mi) from the main sampling site at CENICA.

3 Results and discussion

The 30-min concentrations of PAN measured in 1997 are shown in Fig. 1a. The strong diurnal concentration pattern observed is evidence of the regional afternoon clearing of the pollutants from the MCMA basin (see Fig. 3 for expansion of diurnal detail). The PAN concentrations reached a maximum of 34 ppb with an average daily maximum of 15 ppb. The higher PAN analogs were also observed in 1997. Levels of PPN and PBN reached 5 and 1.1 ppb respectively, giving a total maximum concentration for all the PANs of 40 ppb, the highest reported since measurements taken near Los Angeles in the 1970s (Tuazon et al., 1981). Figure 1b shows the time sequence observed for PAN in Mexico City in 2003. The PAN levels recorded in 2003 were quite different, reaching a maximum of only 8 ppb early in the study with an average daily maximum for the time period of 3 ppb. In addition, neither PPN nor PBN were observed above the detection limit

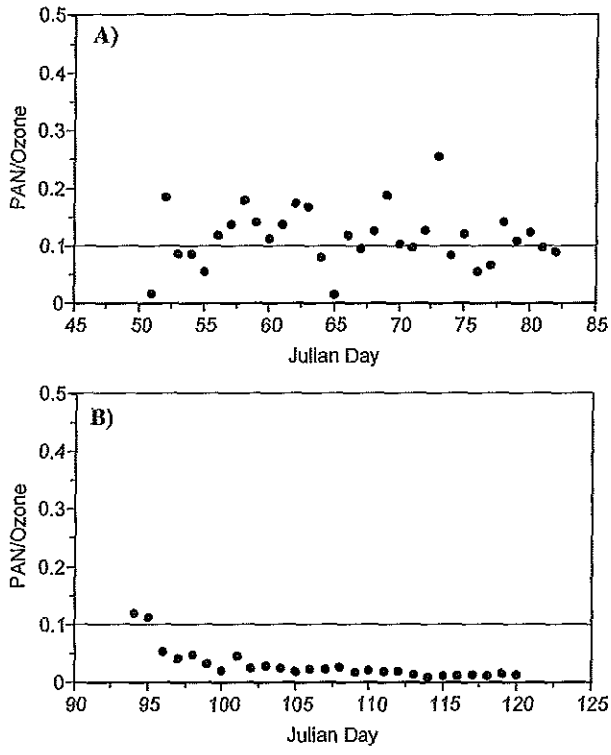

Fig. 2. **(A)** The ratio of PAN to Ozone daily maximum concentrations in Mexico City from 20 February to 23 March 1997 and **(B)** from 3 March to 1 April 2003.

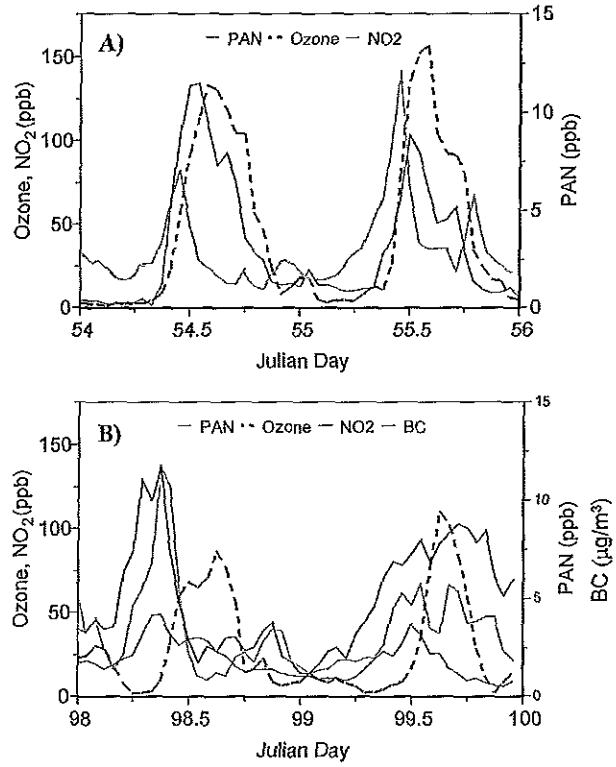

Fig. 3. **(A)** Concentration profiles for ozone, NO_2, and PAN, for Julian Day 55 and 56, 1977 and **(B)** for ozone, NO_2, PAN, and black carbon aerosols for Julian Day 98 and 99, 2003.

of 0.02 ppb at any time during the 2003 study period. The typical diurnal concentration pattern is evident in the first 14 days of the study, indicating the same daily meteorological patterns observed in 1997 leading to a daily clearing of the basin.

18 April 2003 (Julian day 108) was Good Friday marking the beginning of the holiday period accompanied with a decrease in traffic levels and a decrease in mobile and stationary emissions. Average carbon monoxide concentrations dropped by a factor of 2 and peak concentrations dropped by a factor of 4 from the levels reported on the previous Friday. This resulted in even lower PAN levels after that day. The average daily maximum before 18 April was 4 ppb while the average daily maximum afterwards was 1.7 ppb. The IMADA-AVER study in 1997 also incorporated a Mexican national holiday (Benito Juarez's Birthday) on 21 March (Julian Day 80). The maximum PAN concentration observed on that day was 12 ppb.

The hourly average ozone concentrations reached a maximum of 242 ppb during the 1997 study period but only reached 135 ppb in 2003. The ratio of PAN to ozone daily maximum hourly average concentrations is shown in Fig. 2a for 1997 and Fig. 2b for 2003. Past measurements of PAN and ozone concentration in polluted air masses have yielded a ratio of 0.1 (Tuazon et al., 1981; Finlayson-Pitts and Pitts, 2000; Gaffney et al., 1989). The observed ratio of PAN/ozone in 1997 generally agrees with the value of 0.1. However, many days exceeded 0.1 and 6 out of the 32 study days exceeded a ratio of 0.2. This has been attributed to the significant presence of PAN precursors, including higher aldehydes and olefins, in the Mexico City air during that time and also to the fact than the higher PAN levels act to tie up NO_2 thus reducing the ozone production rate and the subsequent atmospheric ozone levels (Gaffney et al, 1999). The PAN/ozone values observed in 2003 only reached the value of 0.1 the first two days of the study. The PAN/ozone ratios after 5 April (Julian Day 95) were significantly below 0.1 with an average daily value of 0.02 for the rest of the study period and an average of 0.03 for the period before the Easter holiday.

As expected, NO_2 levels were also lower in 2003 than in 1997. The maximum NO_2 concentrations reached 205 ppb in 1997 and 137 ppb in 2003. Figure 3a shows the concentration profiles of ozone, NO_2, and PAN for two representative days in 1997. Figure 3b shows similar concentration profiles for 2003. Although the overall concentration levels are lower in 2003 than in 1997, the concentration profiles appear to follow similar patterns. There is a rapid conversion of NO to NO_2 in the Mexico City air in both 1997 and 2003

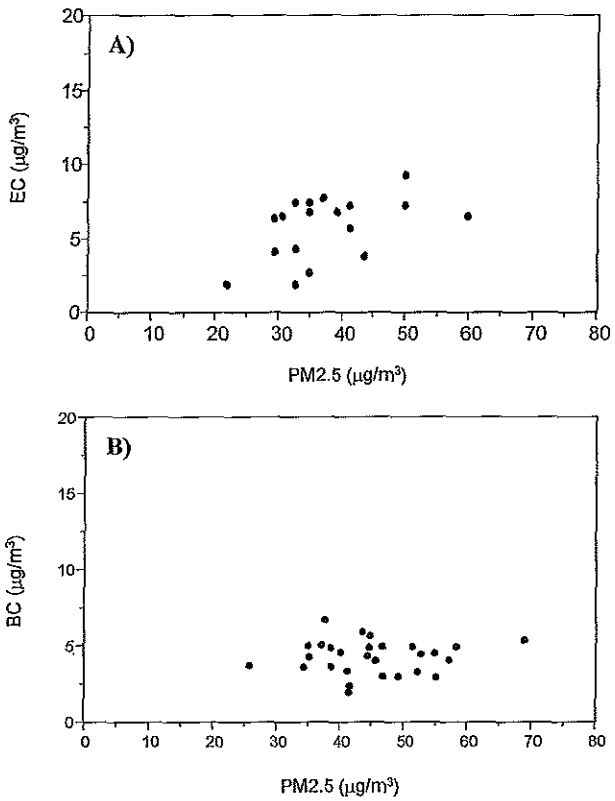

Fig. 4. **(A)** Elemental carbon content of $PM_{2.5}$ particulate samples collected during the IMADA-AVER study, 1997 (Edgerton et al., 1999) and **(B)** black carbon and $PM_{2.5}$ aerosol concentrations measured during the Mexico Megacity 2003 study.

as indicated by the fact that NO_2 reaches a maximum before noon. At this time both ozone and PAN begin to be produced with PAN reaching a maximum earlier than ozone. Shortly after midday the boundary layer height increases leading in a reduction of NO_2 atmospheric concentrations. In late afternoon PAN levels begin to drop faster than ozone. As this rapid decrease in PAN is not likely due to reaction with NO, because this would cause ozone to be lost faster than PAN, it was proposed in 1997 that this behavior might be due to heterogeneous loss of PAN on carbonaceous aerosol surfaces (Gaffney et al., 1999). It has been shown in laboratory studies that PAN can be lost on contact with soot surfaces at low ppb levels during relatively short contact times (Gaffney et al., 1998). Figure 3b also includes the black carbon aerosol profiles obtained in 2003. The NO_2 concentration levels correspond well with the black carbon concentrations as both black carbon and NO, the NO_2 precursor, are produced from combustion. The PAN levels in Fig. 3b begin to drop after the black carbon concentrations reach their maximum supporting the suggestion of heterogeneous PAN loss. This same loss pattern has also been observed in Santiago, Chile where PAN levels have been seen to exceed 20 ppb (Rappengluck et al., 1998, 2000). This city has a large diesel bus fleet and the black carbon levels are likely to be even higher than those observed in Mexico City.

Daily average $PM_{2.5}$ concentrations have been reported elsewhere for *La Merced* site during the AMADA-AVER campaign in 1997 (Edgerton et al., 1999; Chow et al., 2002). These fine aerosol levels ranged from 21–60 $\mu g/m^3$ in 1997 with an average of 36 $\mu g/m^3$. The daily average $PM_{2.5}$ during the 2003 study ranged from 26–69 $\mu g/m^3$ with an average of 45 $\mu g/m^3$. This is not a significant difference in fine atmospheric aerosols from 1997 to 2003. The samples collected in 1997 were also analyzed for elemental carbon content by thermal evolution analysis (Chow et al., 1993, 2001). Figure 4a shows the elemental carbon content of the 1997 $PM_{2.5}$ aerosol fraction as calculated from the previously reported results (Edgerton et al., 1999; Chow et al., 2002). The percent elemental carbon in the fine aerosol samples collected in 1997 varied from 6–23% with an average during the campaign of 15(σ=5)%. Figure 4b shows the daily average black carbon content of fine aerosols as determined from light absorption and TEOM measurements made in 2003 (Salcedo et al., 2006). The daily average percent black carbon in fine aerosols measured in 2003 ranged from 5–18% with an average of 10(σ=3)%. This may represent a slight decrease in black/elemental carbon aerosol content in 2003, especially at higher $PM_{2.5}$ concentrations. However, the thermal evolution method used in 1997 to determine elemental carbon may sometimes result in high values if corrections are not adequately made for charring of the sample during analysis (Chow et al., 2004).

The decreasing trend in PAN levels observed in Mexico City from 1997 to 2003 is similar to that observed in southern California where the maximum PAN concentrations have steadily decreased from 50–70 ppb in the 1960s to 3–10 ppb in the 1990s (Grosjean, 2003). The PPN concentrations in southern California have also decreased from 5–6 ppb in the 1960s to less than 1 ppb in the 1990s. Peak ozone concentrations were about 540 ppb in 1960 and 210 in 1997 (Grosjean, 2003; South Coast Air Quality Management District, 1995; www.aqmd.org). This trend in decreasing atmospheric oxidants reflects the increasingly stringent controls on VOC and NO_x emissions in the state of California. Although the trend for both PAN and ozone in southern California is downward, the ambient levels of PAN have decreased faster than those of ozone yielding a decrease in the PAN/ozone ratio from 0.13 in the 1960s to 0.02 in 1997. Since California's emission controls have focused on reducing the most reactive VOCs thus reducing the overall photochemical reactivity of the emissions (Carter, 1994) it has been suggested that this may have resulted in a larger reduction of the PAN precursors compared to the VOCs that produce ozone but do not produce PAN (Grosjean, 2003).

As the Mexico City and Los Angeles areas have many similarities in their air pollution problems including, a high density of mobile emissions resulting in similar atmospheric

chemistries, the Mexican government utilized a similar approach to improving the air quality in the MCMA as that used by the state of California (Molina and Molina, 2002b). This included the removal of reactive olefins from LPG (Blake and Rowland, 1995; DDF et al., 1996), re-strengthening motor vehicle emission standards with limits on the most reactive VOCs and the introduction of two-way catalytic converters in new vehicles starting with the model year 1991 and three-way catalytic converters stating with 1993 models (Molina and Molina, 2002b). Fuel-based motor vehicle emission inventories for Mexico City have subsequently estimated a decrease in NO_x and hydrocarbon emissions of 26% and 39%, respectively, from 1998 to 2000 (Schifter et al., 2003, 2005). Vehicle remote sensing studies made in 2000 showed that tailpipe hydrocarbon emissions (measured in pounds of HC per pound of fuel) were lowered to one ninth of those emitted by the 1991 fleet (Beaton et al., 1992; CAM/IMP, 2000). Atmospheric measurements have also reported a decrease in ambient hydrocarbon levels from 1992 to 1996 (Arriaga et al., 1997). It is therefore not surprising that results from the recent studies in Mexico City should yield results similar to those observed in the Los Angeles area with respect to atmospheric oxidants, particularly the PANs. However, fine atmospheric aerosols, including black carbon aerosols remain a problem in this megacity. This is primarily due to the lack of controls on diesel particulate emissions.

The presence of the highly absorbing black carbon aerosols in Mexico City leads to a reduction in solar flux of 17.6% locally (Raga et al., 2001b). The mass of these absorbing aerosols exported from this megacity into the surrounding region is estimated to be 6000 metric tons per day or 2 mega-tons per year of black carbon (Gaffney et al., 1999). Since freshly formed black carbon aerosols are hydrophobic, they are expected to be more resistant to washout and have longer lifetimes than more hygroscopic aerosols such as sulfate and nitrate (Gaffney and Marley, 2005b; Dua et al., 1999). In addition, since Mexico City is located at an altitude of 2.2 km above sea level these aerosols are introduced into the atmosphere at altitudes that would be considered to be in the free troposphere 300 km away and are therefore assumed to have longer lifetimes than aerosols released at lower altitudes (Raga et al., 2001b). The Mexico City Metropolitan Area is therefore a major source of black carbon aerosols to the surrounding regions and the release of these highly absorbing aerosols into the surrounding areas will have an impact on the radiative balance and climate on a regional scale.

4 Conclusions and recommendations

A comparison of results for PAN in Mexico City in 2003 with those obtained in 1997 indicate that the overall reactivity of the urban air chemistry has changed consistent with the control strategies that have been put into place in Mexico City, i.e., reduction of olefin content in LPG sources and the replacement of motor vehicles with those that employ the use of catalytic converters to reduce the reactive VOC emissions. Although the levels of PAN are still fairly high for an urban center, PAN and ozone levels are gradually dropping in Mexico City with similar trends to that observed over a number of decades in the Los Angeles air basin (Grosjean, 2003).

The Mexico City urban air is generally transported downwind of the city on a daily basis leading to the strong diurnal cycles observed for PAN at the urban sites. It is apparent that both NO_x and reactive VOC emissions in Mexico City, although still high, are being reduced. Although the reduction of reactive VOCs in the urban emissions leads to the reduction of photochemical oxidants in the MCMA basin, the lower reactivity of the VOCs will certainly lead to the production of PANs downwind of Mexico City as the emissions are transported out of the area. This may lead to regional impacts that were not explored in this study. It is recommended that measurements of PANs in the outflow regions should be undertaken to evaluate the potential impacts of ozone and PAN on ecosystems in the region.

The results for black carbon aerosol content indicate that this pollutant is not being reduced in Mexico City, consistent with no control strategies being put into place. It is clear that this and other megacities continue to be major sources of this key aerosol species on a global scale. As the lifetimes for black carbon aerosols are anticipated to be longer than that for the more hygroscopic aerosol species, the global impact of the emissions from megacities such as Mexico City must continue to be evaluated (Gaffney and Marley, 2005b). Considering the importance of black carbon aerosols in radiative balance, these major sources of absorbing aerosols cannot be ignored if we are to adequately assess their role in climate change.

Acknowledgements. The work at Argonne was supported by the U.S. Department of Energy, Office of Science, Office of Biological and Environmental Research (OBER), Atmospheric Science Program, under contract W-31-109-Eng-38. We wish to thank Mr. Rick Petty of OBER for his continuing encouragement. We also wish to thank the scientists and researchers at CENICA and IMP and the Government of the Federal District, for their hospitality and help with the measurements during the IMADA-AVER and the MCMA-Mexico Megacity 2003 collaborative field studies.

Edited by: L. T. Molina

References

Allen, G. A., Lawrence, J., Koutrakis, P.: Field validation of a semi-continuous method for aerosol black carbon (Aethalometer) and temporal patterns of summertime hourly black carbon measurements in southwestern PA, Atmos. Environ., 33, 817–823, 1999.

Andreae, M. O. and Gelencser, A.: Black carbon or brown carbon? The nature of light-absorbing carbonaceous aerosols, Atmos. Chem. Phys., 6, 3131–3148, 2006, http://www.atmos-chem-phys.net/6/3131/2006/.

Arriaga, J. L., Escalona, S., Cervantes, A. D., Ordúñez, R., and López, T.: Seguimiento de COV en aire urbano de la ZMCM 1992–1996, Contaminación Atmosférica, Vol. 2, edited by: Colin, L. G. and Verela, J. R., Universidad Autonoma Metropolitana-Iztapalapa, 67–98, 1997.

Babich, P., Davey, M., Allen, G., and Koutrakis, P.: Method comparisons for particulate nitrate, elemental carbon, and PM2.5 mass in seven U.S. cities, J. Air Waste Manage. Assoc., 50, 1095–1105, 2000.

Barth, M. C. and Church, A. T.: Regional and global distributions and lifetimes of sulfate aerosols from Mexico City and southeast China, J. Geophys. Res., 104, 30 231–30 239, 1999.

Beaton, S. P., Bishop, G. A., and Stedman, D. H.: Emission Characteristics of Mexico City Vehicles, J. Air Waste Manage. Assoc., 42, 1424–1429, 1992.

Blake, D. R. and Rowland, F. S.: Urban leakage of liquefied petroleum gas and its impact on Mexico City air quality, Science, 269, 953–956, 1995.

Bravo, H. A., Perrin, F. G., Sosa, R. E., and Torres, R. J.: Results of an air pollution strategy (lead reduction in gasoline) on the air quality of Mexico City, in: Proceedings of the 8th Clean Air Congress, Man and his Ecosystem, Elseiver Science Publishers, B.V. The Hague, The Netherlands, pp. 31–37, 1989.

CAM/IMP (Comisión Ambiental Metropolitana/Instituto Mexicano del Petróleo): Auditoría Integral al Programa de Verificación Vehicular, Report published by Comisión Ambiental Metropolitana and Instituto Mexicano del Petróleo, Mexico City, November 2000.

Carter, W. P. L.: Development of ozone reactivity scales for volatile organic compounds, J. Air Waste Manage. Assoc., 44, 881–889, 1994.

Chow, J. C., Watson, J. G., Pritchett, L. C., Pierson, W. R., Frazier, C. A., and Purcell, R. G.: The DRI thermal/optical reflectance carbon analysis system: Description, evaluation and applications in U.S. air quality studies, Atmos. Environ., 27A, 1185–1201, 1993.

Chow, J. C., Watson, J. G., Crow, D., Lowenthal D. H., and Merrifield, T.: Comparison of IMPROVE and NIOSH carbon measurements, Aerosol Sci. Technol., 34, 23–41, 2001.

Chow, J. C., Watson, J. G., Edgerton, S. A., and Vega, E.: Chemical composition of $PM_{2.5}$ and PM_{10} in Mexico City during winter 1997, Sci. Total Environ., 287, 177–201, 2002.

Chow, J. C., Watson, J. G., Chen, L.-W. A., Arnott, W. P., and Moosmüller, H.: Equivalance of elemental carbon by thermal/optical reflectance and transmittance with different temperature protocols, Environ. Sci. Technol., 38, 4414–4422, 2004.

Chung, S. H. and Seinfeld, J. H.: Climate response of direct radiative forcing of anthropogenic black carbon, J. Geophys. Res., 110, D11102, doi:10.1029/2004JD005441, 2005.

DDF (Departamento del Distrito Federal,Gobierno del Estado de México, Secretaría de Medio Ambiente Recursos Naturales y Pesca, and Secretaría de Salud): Programa para mejorar la calidad del aire en el Cvalle de Mèxico, 1995–2000 (PROAIRE), Mexico, 1996.

Doran, J. C., Abbott, S., Archuleta, J., Bian, X., Chow, J., Coulter, R. L., de Wekker, S. F. J., Edgerton, S., Elliott, S., Fernandez, A., Fast, J. D., Hubbe, J. M., King, C., Langley, D., Leach, J., Lee, J. T., Martin, T. J., Martinez, D., Martinez, J. L., Mercado, G., Mora, V., Mulhearn, M., Pena, J. L., Petty, R., Porch, W., Russell, C., Salas, R., Shannon, J. D., Shaw, W. J., Sosa, G., Tellier, L., Templeman, B., Watson, J. G., White, R., Whiteman, C. D., and Wolfe, D.: The IMADA-AVER boundary layer experiment in the Mexico City area, Bull. Amer. Meteorol. Soc., 79, 2497–2508, 1998.

Dua, S. K., Hopke, P. K., and Raunemaa, T.: Hygroscopicity of Diesel Aerosols, Water Air Soil Poll., 112, 247–257, 1999.

Edgerton, S. A., Arriaga, J. L., Archuleta, J., Bian, X., Bossert, J. E., Chow, J. C., Coulter, R. L., Doran, J. C., Doskey, P. V., Elliot, S., Fast, J. D., Gaffney, J. S., Guzman, F., Hubbe, J. M., Lee, J. T., Malone, E. L., Marley, N. A., McNair, L. A., Neff, W., Ortiz, E., Petty, R., Ruiz, M., Shaw, W. J., Sosa, G., Vega, E., Watson, J. G., Whiteman, C. D., and Zhong, S.: Particulate air pollution in Mexico City: A collaborative research project, J. Air Waste Manage. Assoc., 49, 1221–1229, 1999.

Elliott, S., Blake, D. R., Rowland, F. S., Lu, R., Brown, M. J., Williams, M. D., Russell, A. G., Bossert, J. E., Streit, G. E., Santoyo, M. R., Guzman, F., Porch, W. M., McNair, L. A., Keyantash, J., Kao, C-Y. J., Turco, R. P., and Eichinger, W. E.: Ventilation of liquefied petroleum gas components from the valley of Mexico, J. Geophys. Res., 102, 21 197–21 207, 1997.

Fast, J. D. and Zhong, S.: Meteorological factors associated with inhomogeneous ozone concentrations within the Mexico City basin, J. Geophys. Res., 103, 18 927–18 946, 1998.

Finlayson-Pitts, B. J. and Pitts Jr., J. N.: Chemistry of the Upper and LowerAtmospheric, Academic Press, San Diego, California, 2000..

Gaffney, J. S., Fajer, R., and Senum, G. I.: An improved procedure for high purity gaseous peroxyacetyl nitrate production: use of heavy lipid solvents, Atmos. Environ., 18, 215–218, 1984.

Gaffney, J. S., Marley N. A., and Prestbo, E. W.: Peroxyacyl nitrates (PANS): Their physical and chemical properties, in: Handbook of Environmental Chemistry, Volume 4/Part B (Air Pollution), edited by: Hutzinger, O., Springer-Verlag, Berlin, Germany, pp. 1–38, 1989.

Gaffney, J. S., Marley, N. A., and Prestbo, E. W.: Measurements of peroxyacetyl nitrate (PAN) at a remote site in the southwestern United States: Tropospheric implications, Environ. Sci. Technol., 27, 1905–1910, 1993.

Gaffney, J. S., Marley, N. A., Martin, R. S., Dixon, R. W., Reyes, L. G., and Popp, C. J.: Potential air quality effects of using ethanol-gasoline fuel blends: a field study in Albuquerque, New Mexico, Environ. Sci. Technol., 31, 3053–3061, 1997.

Gaffney, J. S., Bornick, R. M., Chen, Y.-H., and Marley, N. A.: Capillary gas chromatographic analysis of nitrogen dioxide and PANs with luminal chemiluminescent detection, Atmos. Environ., 32, 1145–1154, 1998.

Gaffney, J. S., Marley, N. A., Cunningham, M. M., and Doskey, P. V.: Measurements of Peroxyacyl Nitrates (PANs) in Mexico City: Implications for Megacity Air Quality Impacts on Regional Scales, Atmos. Environ., 33, 5003–5012, 1999.

Gaffney, J. S. and Marley, N. A.: Analysis of Peroxyacyl Nitrates (PANs), Organic Nitrates, Peroxides, and Peracids, Chapter 19, in: Chromatographic Analysis of the Environment, 3rd Edition, edited by: Nollett, L., Marcel Dekker/CRC Press, pp. 711–741, 2005a..

Gaffney, J. S. and Marley, N. A.: The Importance of the Chemical and Physical Properties of Aerosols in Determining Their Transport and Residence Times in the Troposphere, Chapter 14, in:

Urban Aerosols and Their Impacts: Lessons Learned from the World Trade Center Tragedy, edited by: Gaffney, J. S. and Marley, N. A., ACS Symposium Book 919, Oxford University Press, pp. 286–300, 2005b.

Gaffney, J. S. and Marley, N. A.: A brief history of aerosol carbon analytical methods. Eighth Conference on Atmospheric Chemistry Symposium: Aerosols – Radiative Impacts and Visibility Reduction, 86th American Meteorological Society National Meeting, Atlanta, GA 2006, Proceedings Volume, Paper 1.5., 2006.

Grosjean, D.: Ambient PAN and PPN in southern California from 1960 to the SCOS97-NARSTO, Atmos. Environ., 37, S221–S238, 2003.

Hansen, A. D. A., Rosen, H., and Novakov, T.: Real-time measurement of the absorption coefficient of aerosol particles, Appl. Opt., 21, 3060–3062, 1982.

Hansen, A. D. A. and McMurry, P. H.: An intercomparison of measurements of aerosol elemental carbon during the 1986 Carbonaceous Species Methods Comparison Study, J. Air Waste Manage. Assoc., 40, 894–895, 1990.

Hinds, W. C.: Aerosol technology: properties, behavior and measurement of airbourne particles, John Wiley and Sons, USA, 1999.

Jacobson, M. Z.: Global direct radiative forcing due to multicomponent anthropogenic and natural aerosols, J. Geophys. Res., 106, 1551–1568, 2001.

Jacobson, M. Z.: Conrol of fossil fuel particulate black carbon and organic matter, possibly the most effective method of slowing global warming, J. Geophys. Res., 107(D19), 4410–4432, doi:10.1029/2001JD001376, 2002.

Jacobson, M. Z.: Climate response of fossil fuel and biofuel soot, accounting for soot's feedback to snow and sea ice albedo and emissivity, J. Geophys. Res.m 109, D21201, doi:10.1029/2004JD004945, 2004.

Lynn, W. R.: Megacities sweet dreams or environmental nightmares, Environ. Sci. Technol., 33, 238A–240A, 1999.

Marley, N. A., Gaffney, J. S., White, R. V., Rodriguez-Cuadra, L., Herndon, S. E., Dunlea, E., Volkamer, R. M., Molina, L. T., and Molina, M. J.: Fast gas chromatography with luminol chemiluminescence detection for the simultaneous determination of nitrogen dioxide and peroxyacetyl nitrate in the atmosphere, Rev. Sci. Instrum., 75, 4595–4605, 2004.

Marley, N. A., Gaffney, J. S., Baird, J. C., Blazer, C. A., Drayton, P. Pj., and Frederick, J. E.: The determination of scattering and absorption coefficients of size-fractionated aerosols for radiative transfer calculations, Aerosol Sci. Technol., 34, 535–549, 2001.

MARI: Mexico City Air Quality Initiative, Los Alamos National Laboratory and the Mexican Petroleum Institute, Los Alamos Report #LA-12699, 1994.

Molina, L. T. and Molina, M. J.: Air quality impacts: Local and global concern, Chapter 1, in: Air quality in the Mexico Megacity, An integrated assessment, edited by: Molina, L. T. and Molina, M. J., Kluwer Academic, Netherlands, 2002a.

Molina, L. T. and Molina, M. J.: Cleaning the air:A comparative study, Chapter 2, in: Air quality in the Mexico Megacity, An integrated assessment, edited by: Molina, L. T. and Molina, M. J., Kluwer Academic, Netherlands, 2002b.

Raga, G. B., Baumgardner, D., Castro, T., Martînez-Arroyo, A., and Navarro-González, R.: Mexico City air quality: a qualitative review of gas and aerosol measurements (1960–2000), Atmos. Environ., 35, 4041–4058, 2001a.

Raga, G. B., Castro, T., and Baumgardner, D.: The impact of megacity pollution on local climate and implications for the regional environment: Mexico City, Atmos. Environ., 35, 1805–1811, 2001b.

Ramanathan, V., Chung, C., Kim, D., Bettge, T., Buja, L., Kiel, J. T., Washington, W. M., Fu, Q., Sikka, D. R., and Wild, M.: Atmospheric brown clouds: Impacts on South Asain climate and hydrological cycle, Proc. Natl. Acad. Sci. USA, 102, 5326–5333, 2005.

Rappengluck, B., Oyola, P., Olaeta, U. I., Schmitt, R., and Fabian, P.: The evolution of photochemical smog in the metropolitan area of Santiago, Chile, Preprint Paper 3.8, 10th Conference on Air Pollution Meteorology, & 8th Annual Meeting of the American Meteorological Society, Phoenix, AZ, pp. 86–90, 1998.

Rappengluck, B., Oyola, P., Olaeta, I., and Fabian, P.: The evolution of photochemical smog in the metropolitan area of Santiago, Chile, J. Appl. Meteorol., 39, 275–290, 2000.

Riveros, H. G., Arriaga, J. L., Tejeda, J., Julián-Sánchez, A., and Riveros-Rosas, H.: Ozone and its precursors in the atmosphere of Mexico City, J. Air Waste Manage. Assoc., 48, 866–871, 1998.

Salcedo, D., Onasch, T. B., Dzepina, K., Canagaratna, M. R., Zhang, J. Q., Huffman, A., DeCarlo, P. F., Jayne, J. T., Mortimer, P., Worsnop, D. R., Kolb, C. E., Johnson, K. S., Zuberi, B., Marr, L. C., Volkamer, R., Molina, L. T., Molina, M. J., Cardenas, B., Bernabé R. M., Márquez, C., Gaffney, J. S., Marley, N. A., Laskin, A., Shutthanandan, V., Xie, Y., Brune, W., Lesher, R., Shirley, T., and Jimenez, J. L.: Characterization of ambient aerosols in Mexico City during the MCMA-2003 campaign with Aerosol Mass Spectrometry: results from the CENICA Supersite, Atmos. Chem. Phys., 6, 925–946, 2006, http://www.atmos-chem-phys.net/6/925/2006/.

Schifter, I., Díaz, L., Múgica, V., and López-Salinas, E.: Fuel-based motor vehicle emission inventory for the metropolitan area of Mexico City, Atmos. Environ., 39, 931–940, 2005.

Schifter, I., Díaz, L., Durán, L., Guzmán, E., Chávez, O., and López-Salinas, E.: Remote sensing study of emissions from motor vehicles in the metropolitan area of Mexico City, Environ. Sci. Technol., 37, 395–401, 2003.

South Coast Air Quality Management District: Air Quality Digest, November, December, 1985.

Streit, G. E. and Guzman, F.: Mexico City air quality: Progress of an international collaborative project to define air quality management options, Atmos. Environ., 30, 723–733, 1996.

Tuazon, E. C., Winer, A. M., Pitts Jr., J. N.: Trace pollutant concentrations in a multiday smog episode in the California south coast air basin by long path length Fourier transform infrared spectroscopy, Environ. Sci. Technol., 15, 1232–1237, 1981.

Atmos. Chem. Phys., 7, 2691–2704, 2007
www.atmos-chem-phys.net/7/2691/2007/

Atmospheric Chemistry and Physics

Evaluation of nitrogen dioxide chemiluminescence monitors in a polluted urban environment

E. J. Dunlea[1,*], S. C. Herndon[2], D. D. Nelson[2], R. M. Volkamer[1,], F. San Martini[1], P. M. Sheehy[1], M. S. Zahniser[2], J. H. Shorter[2], J. C. Wormhoudt[2], B. K. Lamb[3], E. J. Allwine[3], J. S. Gaffney[4], N. A. Marley[4], M. Grutter[5], C. Marquez[6], S. Blanco[6], B. Cardenas[6], A. Retama[7], C. R. Ramos Villegas[7], C. E. Kolb[2], L. T. Molina[1,8], and M. J. Molina[1,**]**

[1]Department of Earth, Atmospheric and Planetary Sciences, Massachusetts Institute of Technology, Bldg. 54, 77 Massachusetts Ave, Cambridge, MA 02139, USA
[2]Aerodyne Research Inc., 45 Manning Road, Billerica, MA 01821-3876, USA
[3]Laboratory for Atmospheric Research, Department of Civil and Environmental Engineering, Washington State University, 101 Sload Hall, Spokane Street, Pullman, WA 99164-2910, USA
[4]University of Arkansas at Little Rock, 2801 South University Avenue, Little Rock, AR 72204-1099, USA
[5]Centro de Ciencias de la Atmysfera, Universidad Nacional Autónoma de México, Mexico, D.F., Mexico
[6]Centro Nacional de Investigacion y Capacitacion Ambiental-INE, Av. Periférico 5000, Col. Insurgentes Cuicuilco, CP 04530, Mexico, D.F., Mexico
[7]Gobierno del Distrito Federal, Agricultura 21, Piso 1, Col. Escandon, Del. M. Hidalgo, CP 11800, Mexico, D. F., Mexico
[8]Molina Center for Energy and the Environment, 3262 Holiday Ct. Suite, 201 La Jolla CA, 92037, USA
[*]now at: University of Colorado at Boulder, Cooperative Institute for Research in Environmental Sciences, UCB 216, Boulder, CO 80309, USA
[**]now at: University of California at San Diego, 9500 Gilman Drive, 0356 La Jolla, CA 92093-0356, USA

Received: 13 December 2006 – Published in Atmos. Chem. Phys. Discuss.: 16 January 2007
Revised: 5 April 2007 – Accepted: 11 May 2007 – Published: 23 May 2007

Abstract. Data from a recent field campaign in Mexico City are used to evaluate the performance of the EPA Federal Reference Method for monitoring the ambient concentrations of NO_2. Measurements of NO_2 from standard chemiluminescence monitors equipped with molybdenum oxide converters are compared with those from Tunable Infrared Laser Differential Absorption Spectroscopy (TILDAS) and Differential Optical Absorption Spectroscopy (DOAS) instruments. A significant interference in the chemiluminescence measurement is shown to account for up to 50% of ambient NO_2 concentration during afternoon hours. As expected, this interference correlates well with non-NO_x reactive nitrogen species (NO_z) as well as with ambient O_3 concentrations, indicating a photochemical source for the interfering species. A combination of ambient gas phase nitric acid and alkyl and multifunctional alkyl nitrates is deduced to be the primary cause of the interference. Observations at four locations at varying proximities to emission sources indicate that the percentage contribution of HNO_3 to the interference decreases with time as the air parcel ages. Alkyl and multifunctional alkyl nitrate concentrations are calculated to reach concentrations as high as several ppb inside the city, on par with the highest values previously observed in other urban locations. Averaged over the MCMA-2003 field campaign, the chemiluminescence monitor interference resulted in an average measured NO_2 concentration up to 22% greater than that from co-located spectroscopic measurements. Thus, this interference has the potential to initiate regulatory action in areas that are close to non-attainment and may mislead atmospheric photochemical models used to assess control strategies for photochemical oxidants.

Correspondence to: E. J. Dunlea
(edward.dunlea@colorado.edu)

1 Introduction

Nitrogen oxides (NO_x = sum of nitrogen oxide (NO) and nitrogen dioxide (NO_2)) are primarily emitted as byproducts of combustion and participate in ozone (O_3) formation and destruction, thus playing a key role in determining the air quality in urban environments (Finlayson-Pitts and Pitts, 2000). NO_2 is designated as one of the United States Environmental Protection Agency's (US EPA) "criteria pollutants", which also include O_3, carbon monoxide (CO), sulfur dioxide (SO_2), airborne lead (Pb) and particulate matter (PM). The US EPA initiates regulatory action if an urban

area has criteria pollutant concentrations that exceed a certain threshold (either one hour averaged daily maxima, eight hour averaged daily maxima or annually averaged concentrations), referred to as being in "non-attainment". While no counties in the US are currently in non-attainment for NO_2, the US EPA has recently announced sweeping new regulations aimed at reducing NO_x levels by 2015 (Environmental Protection Agency, 2005). Therefore, accurately measuring the concentration of NO_2, as mandated under the 1990 Clean Air Act Amendments, Section 182 (c)(1) (Demerjian, 2000), will become increasingly important. Positive interferences in the measurement of NO_2 may lead to the false classification of an urban area as being in non-attainment.

In addition to the regulatory purposes of monitoring, ambient measurements are also used by air quality models (AQM) for characterization and prediction of future high ozone episodes (Demerjian, 2000) and in validations of satellite measurements of NO_2 (Ordóñez et al., 2006; Schaub et al., 2006). Adequate diagnostic testing of AQM's requires uncertainties in NO_2 measurements of less than $\pm 10\%$ Environmental Protection Agency, 2001; McClenny et al., 2002). There has also been considerable attention paid recently to the direct emissions of NO_2 from diesel vehicles (Friedeburg et al., 2005; Jenkin, 2004a; Jimenez et al., 2000; Latham et al., 2001; Pundt et al., 2005) and their resulting health effects (Beauchamp et al., 2004). These and other studies that rely on the data from monitoring networks, such as recent NO_2 source apportionment (Carslaw and Beevers, 2004, 2005) and oxidant partitioning (Jenkin, 2004b) studies, could be significantly affected by interferences in the standard methods for NO_2 measurement. Satellite measurements of NO_2 are often most sensitive to surface NO_2 concentrations; validation of these measurements requires accurate NO_2 surface measurements. In summary, assuring that NO_2 monitors routinely achieve a high level of precision is important for the accurate prediction of air quality and validation of satellite measurements.

Of the various techniques for measuring in situ NO and NO_2 concentrations, the most prevalent, and the Federal Reference Method as designated by the US EPA, is the chemiluminescence instrument (CL NO_x monitors) (Demerjian, 2000). This technique has been described in detail elsewhere (Fontijn et al., 1970; Ridley and Howlett, 1974). Briefly, it is based on the chemiluminescent reaction of NO with O_3 to form electronically excited NO_2, which fluoresces at visible and near infrared wavelengths. The technique is simple and relatively reliable. The detection sensitivity benefits from small background signal levels because no light source is necessary to initiate the fluorescence. Only an O_3-generating lamp and a modestly cooled photomultiplier (typically $\sim -4°C$) are required; thus CL NO_x monitors are relatively inexpensive. Calibration involves the sampling of a known standard to determine the absolute response of the instrument; such standards are readily acquired. CL NO_x monitors typically operate in a mode that alternates between two states: one that measures the concentration of NO by sampling ambient air directly, and one that measures the sum of NO and NO_2 by passing the ambient air stream over a catalyst (usually gold or molybdenum oxide, often heated) to convert NO_2 to NO. The difference of the two values is reported as the NO_2 concentration. Although instruments are available that utilize a flash lamp or laser to convert NO_2 to NO, this study only examines CL NO_x monitors with molybdenum oxide catalysts, which are the most prevalent type (Parrish and Fehsenfeld, 2000).

In addition to the advantages of CL NO_x monitors listed above, however, there are known interferences for this standard technique (see several recent reviews (Cavanagh and Verkouteren, 2001; Demerjian, 2000; Environmental Protection Agency, 1993; McClenny et al., 2002; Parrish and Fehsenfeld, 2000; Sickles, 1992)). The most significant issue with standard CL NO_x monitors is their inability to directly and specifically detect NO_2. It has been well established that other gas phase nitrogen containing compounds are converted by molybdenum oxide catalysts to NO and therefore can be reported as NO_2 by a standard CL NO_x monitor (Winer et al., 1974). As stated by the US EPA, "chemiluminescence $NO/NO_x/NO_2$ analyzers will respond to other nitrogen containing compounds, such as peroxyacetyl nitrate (PAN), which might be reduced to NO in the thermal converter. Atmospheric concentrations of these potential interferences are generally low relative to NO_2 and valid NO_2 measurements may be obtained. In certain geographical areas, where the concentration of these potential interferences is known or suspected to be high relative to NO_2, the use of an equivalent method for the measurement of NO_2 is recommended." (Environmental Protection Agency, 2006) Additionally, manufacturers now use this same technology to make total reactive nitrogen (NO_y) measurements. Molybdenum oxide catalysts are known to efficiently reduce compounds such as NO_2, NO_3, HNO_3, N_2O_5, CH_3ONO_2, $CH_3CH_2ONO_2$, n-$C_3H_7ONO_2$, n-$C_4H_9ONO_2$, and CH_3CHONO and to a lesser extent also reduce HO_2NO_2, HONO, RO_2NO_2, NH_3 and particulate phase nitrate. These catalysts do not efficiently reduce N_2O, HCN, CH_3CN or CH_3NO_2 at typical operating converter temperatures lower than 400°C (Fehsenfeld et al., 1987; Williams et al., 1998). To emphasize this point, consider that the only difference between CL NO_x and NO_y monitors is the position of the catalyst: in a CL NO_y monitor, the catalyst is placed very close to the front of sampling inlet so as to convert all NO_y species, whereas in a CL NO_x monitor, the catalyst is placed after a particulate filter and just before the detection chamber, allowing the conversion and detection as "NO_2" of any gas phase nitrogen containing compounds not removed by passive loss on surfaces upstream of the converter.

Other more specific NO_2 detection techniques have been developed, including a photolysis technique to specifically convert NO_2 to NO that avoids using a metal catalyst while still employing the chemiluminescence reaction (Kley and

McFarland, 1980), an LIF technique (Thornton et al., 2000; Thornton et al., 2003), a fast gas chromatography luminol chemiluminescence detection (Marley et al., 2004), Differential Optical Absorption Spectroscopy (DOAS) (Platt, 1994; Platt and Perner, 1980), cavity ring down (Osthoff et al., 2006) and a Tunable Infrared Laser Differential Absorption Spectroscopy (TILDAS) technique (Li et al., 2004) (also described below). Several recent reviews provide a more complete description of these and other NO_2 measurement techniques (Demerjian, 2000; McClenny et al., 2002; Parrish and Fehsenfeld, 2000). Although several of these instruments have been shown to perform well in intercomparisons (Fehsenfeld et al., 1990; Gregory et al., 1990; Osthoff et al., 2006; Thornton et al., 2003), the majority of these techniques are, at this time, research grade instruments unsuitable for use in routine monitoring. A newer technique, Cavity Attenuated Phase Shift (CAPS) spectroscopy, has shown the potential to provide accurate spectroscopic measurements of NO_2 (0.3 ppb detection limit in <10 s) at a reasonable cost (Kebabian et al., 2005), but it is still in the development phase. Even if these other techniques gain prevalence in the coming years, the current widespread use of CL NO_x monitors makes understanding and quantifying interferences to this technique critical. Recent field studies have begun to quantify the magnitude of interferences to this technique, for example (Li et al., 2004) have shown a consistent positive measurement bias from CL NO_x monitors relative to an absolute TILDAS measurement of NO_2. Additionally, Steinbacher et al. (2007) have shown a persistent bias in CL NO_x monitors with molybdenum oxide converters over a time period of more than 10 years at rural locations in Switzerland. However, our study is one of the first field intercomparisons to directly quantify this interference and characterize the specific compounds responsible for it.

Our study uses data from the recent Mexico City Metropolitan Area (MCMA) field campaign during April of 2003 (MCMA-2003), which featured a comprehensive suite of both gas and particle phase instrumentation from numerous international laboratories, including multiple measurements of NO_2 (Molina et al., 2007). Here, we utilize this unique data set to evaluate the performance of standard CL NO_x monitors in a heavily polluted urban atmosphere, examine possible interferences and make recommendations for monitoring networks in general. Data from an exploratory field mission in the MCMA during February of 2002 are also presented. The meteorology during these campaigns has been discussed in detail elsewhere (de Foy et al., 2005; Molina et al., 2007).

2 Measurements

A major part of the MCMA-2002 and 2003 campaigns was the deployment of the Aerodyne Research, Inc. Mobile Laboratory (ARI Mobile Lab), a van equipped with a comprehensive suite of research grade gas and particle phase instrumentation (Herndon et al., 2005a; Kolb et al., 2004). The ARI Mobile Lab had two modes of operation during the campaigns: mobile and stationary. In mobile mode, the main objectives were either sampling of on-road vehicle exhaust or mapping of emission sources. In stationary mode, the ARI Mobile Lab was parked a chosen site, typically making measurements for several days in a row. Stationary mode data in this study will be presented from four sites from the 2002 and 2003 field campaigns, which are described in detail elsewhere (Dunlea et al., 2006); briefly they are (1) CENICA (Centro Nacional de Investigacion y Capacitacion Ambiental) – the "supersite" for the MCMA-2003 campaign located on a university campus to the south of the city center, which receives a mix of fresh pollution from area traffic corridors and aged pollution from more downtown locations, (2) La Merced – a downtown location near an open market and a large traffic corridor, (3) Pedregal – an affluent residential neighborhood downwind of the city center, and (4) Santa Ana – a boundary site outside of the city, which receives mostly aged urban air during the day and rural air overnight.

The instruments on board the ARI Mobile Lab most relevant to this study were a TILDAS NO_2 instrument and a standard CL NO_x monitor. The TILDAS technique for measuring NO_2 has been described in detail elsewhere (Li et al., 2004) and only a brief description is presented here. TILDAS is a tunable infrared laser differential absorption measurement that employs a low volume, long path length astigmatic Herriott multipass absorption cell (McManus et al., 1995) with liquid nitrogen cooled laser infrared diodes and detectors. The laser line width is small compared to the width of the absorption feature and the laser frequency position is rapidly swept over an entire absorption feature of the molecule to be detected, NO_2 in this case. Accurate line strengths, positions and broadening coefficients are taken from the HITRAN data base (Rothman et al., 2003). Reference cells containing the gas of interest are used to lock the laser frequency position. Of the species in the HITRAN database in the NO_2 ν_2 wavelength region (1600 cm^{-1}), the next strongest absorber (CH_4) has nearby absorption lines which are six orders of magnitude weaker than the NO_2 lines used in these measurements. Additionally, the CH_4 lines are frequency shifted away from the main NO_2 features and this is resolved with the typical linewidth of the lead salt diode lasers used. Therefore, the measurements of NO_2 by tunable diode laser spectroscopy are believed to be interference-free. The mode purity of the diode was verified by measuring 'black' NO_2 lines in a reference cell along another optical path present in the instrument. The absolute accuracy of the concentrations measured by TILDAS is largely determined by how well the line strengths are known. For the absorption lines used in the two instrument channels, measuring NO and NO_2 respectively, the presently accepted band strengths are known to within 6% for NO and 4% for NO_2 (Smith et al., 1985). It is important to note that this

technique is an absolute concentration measurement, which does not require a calibration, and thus served as the benchmark against which to compare other NO_2 measurements. In general, calibrations in the field do greatly improve the confidence in the measurement and assist in evaluating the overall performance of the instrument. Though field calibrations have become routine now, via permeation sources and gas cylinders on the Mobile Lab platform, they were not done during the MCMA-2003 field campaign. On the particular instrument that did go to MCMA-2003, however, the second channel of the instrument was used to measure HCHO (Garcia et al., 2006; Herndon et al., 2005b); calibrations for this species demonstrated the pathlength was correct, and laboratory measurements of the pathlength using a pulsed light source indicate the cell was correctly aligned. Fortunately, for NO_2 measurements, the spectroscopy (and potential other absorbers) near 1600 cm^{-1} is fairly well understood by virtue of being used so commonly.

Standard CL NO_x monitors have been described above and here we briefly describe the calibrations performed during the MCMA-2003 campaign. The standard calibration procedure involves zeroing the monitors while measuring NO_x-free air and then adding several specified amounts of NO to the instrument covering the desired operating range. The CL NO_x monitor on board the ARI Mobile lab was calibrated six times during the campaign, utilizing several different standardized mixtures of NO in nitrogen and NO/CO/SO_2 in nitrogen and resulting in no greater than an 8% deviation. Early in the campaign, technicians from RAMA, Red Automática de Monitoreo Ambiental (RAMA, 2005), calibrated both the CL NO_x monitor on board the Mobile Lab and the one on the CENICA rooftop during the same afternoon for consistency. RAMA operates 32 monitoring sites around the MCMA, many of which are equipped with standard CL NO_x monitors, all of which are calibrated via this same method. The RAMA network has been audited by the US EPA (Environmental Protection Agency, 2003), and was concluded to be "accurate and well-implemented".

For the discussion below, it is important to establish that ambient concentrations of O_3 do not interfere with measured NO_2 concentrations from a CL NO_x monitor. O_3 levels within the detection chamber of these CL NO_x monitors are three orders of magnitude higher than ambient levels (Shivers, personal communication, 2004); thus ambient O_3 levels will not significantly influence the detection of NO in the CL NO_x monitors. The difference in residence time in the sampling lines to the CL NO_x monitor compared to the TILDAS instrument was small enough (<3 s) to preclude the reaction of ambient NO with ambient O_3 from contributing significantly to the measured differences in NO_2 concentrations.

For this study, measurements from the ARI Mobile Lab are used in conjunction with measurements from instruments at the various stationary sites. The instrumentation at the CENICA site included two long-path DOAS (LP-DOAS) instruments (Platt, 1994; Platt and Perner, 1980; Volkamer et al., 1998) which measured NO_2 amongst a suite of other compounds. The detection limits for NO_2 were 0.80 and 0.45 ppb for DOAS-1 and DOAS-2 respectively. The La Merced site also included side-by-side open path Fourier transform infrared (FTIR) and DOAS instruments (Grutter, 2003). Both instruments measured numerous gas-phase compounds, but only data from the FTIR measurement of nitric acid (HNO_3; detection limit of 4 ppb) and from the DOAS measurement of NO_2 (detection limit of 3 ppb) are shown here. See companion paper (Dunlea et al., 2006) for more details on these stationary sites, including information about the inlets used for various measurement locations.

Additional measurements are presented here from Aerodyne Aerosol Mass Spectrometers (AMSs) (Jayne et al., 2000) that were on board the ARI Mobile lab and on the roof of the CENICA building. The AMS measures the size-resolved chemical composition of the non-refractory component of ambient particles smaller than 1.0 μm, including particulate phase nitrate (pNO_3^-).

3 Results and discussions

3.1 Observation of interference

Simultaneous measurements of NO_2 on board the ARI Mobile Lab by the CL NO_x monitor and the TILDAS instrument revealed a recurring discrepancy where the CL NO_x monitor reported a higher NO_2 concentration than the TILDAS instrument. We consider the TILDAS measurement to be an absolute concentration measurement and thus this discrepancy is concluded to be an interference in the CL monitor. We define this "CL NO_x monitor interference" as the CL NO_x monitor NO_2 measurement minus a co-located spectroscopic NO_2 measurement.

$$\text{CL } NO_x \text{ monitor interference} = [NO_2]\,(\text{CLmonitor}) - [NO_2]\,(\text{spectroscopic}) \quad (1)$$

Figure 1 shows the CL NO_x monitor interference as observed during specific periods in both the 2002 and 2003 field campaigns. The periods in Fig. 1 are typical of the observations during both campaigns. The CL NO_x monitor interference was observed to occur daily, peaking in the afternoons during periods when ambient O_3 levels were highest. The CL NO_x monitor interference accounted for as much as 50% of the total NO_2 concentration reported by the CL NO_x monitor (30 ppb out of a reported 60 ppb for the 2002 campaign and 50 ppb out of 100 ppb for the 2003 campaign). The interference was observed at all fixed site locations visited by the ARI Mobile Lab, but was more readily detectable at the urban sites than the Santa Ana boundary site, owing simply to the lower overall NO_2 levels at the boundary site. Additionally, this CL NO_x monitor interference was present when comparing DOAS long path measurements of NO_2 to CL NO_x monitors at both the CENICA and La Merced sites. For

these sites, the CL NO_x monitor interference was more variable in time owing to the loss of spatial coherence when comparing a long path measurement with a point sampling data for a reactive species (for further discussion of open path versus point sampling comparison, see Dunlea et al. (2006) and San Martini et al. (2006a)).

The observation of such large CL NO_x monitor interference levels directly contradicts previous conclusions that this will only be an issue at rural or remote locations (Jenkin, 2004b). In summary, the CL NO_x monitor interference was observed to occur regularly and to roughly correlate with the ambient O_3 concentration; the subsequent section will explore the cause of this interference in more detail.

3.2 Examination of possible sources of interference

Potential sources for the interference in the chemiluminescence NO_2 measurement using the available data from the MCMA 2003 campaign are explored: (1) some portion of the non-NO_x fraction of reactive nitrogen (NO_z) and (2) gas phase olefinic hydrocarbons or gas phase ammonia.

3.2.1 The Non-NO_x Fraction of Reactive Nitrogen (NO_z)

It has been long established that molybdenum converters within standard CL NO_x monitors have a potential interference in the NO_2 measurement due to gas phase reactive nitrogen compounds (Demerjian, 2000; Environmental Protection Agency, 2006; Parrish and Fehsenfeld, 2000). The ARI Mobile Lab as configured for the MCMA-2003 campaign included a total NO_y instrument (TECO 49C), which measures both NO_y and NO using the chemiluminescence technique, but configured differently than a standard CL NO_x monitor so as to purposely exploit the molybdenum converter's ability to detect more gas phase reactive nitrogen species. From the CL NO_y monitor NO_y and NO measurements, along with the TILDAS NO_2 measurement, we calculated the non-NO_x fraction of NO_y, referred to as NO_z. Table 1 lists the results of linear least-squares fits of the correlation plots of the CL NO_x monitor interference versus NO_z at the various locations visited by the ARI Mobile Lab. The CL NO_x monitor interference level varied linearly with the NO_z concentration, and was smaller in magnitude, indicating that some portion of NO_z was responsible for the interference. Fair to good correlation (R^2=0.32–0.79) was observed at all sites visited by the ARI Mobile Lab, with ratios of the CL NO_x monitor interference to NO_z=(0.44–0.66). Thus, the obvious and expected conclusion is that some reactive nitrogen compound or compounds are the cause of the observed CL NO_x monitor interference.

This type of comparison has a number of inherent limitations. Negative values for the CL NO_x monitor interference are often recorded because this calculated value is the subtraction of two measurements. In general, more variance in this subtracted quantity is expected when an open path spec-

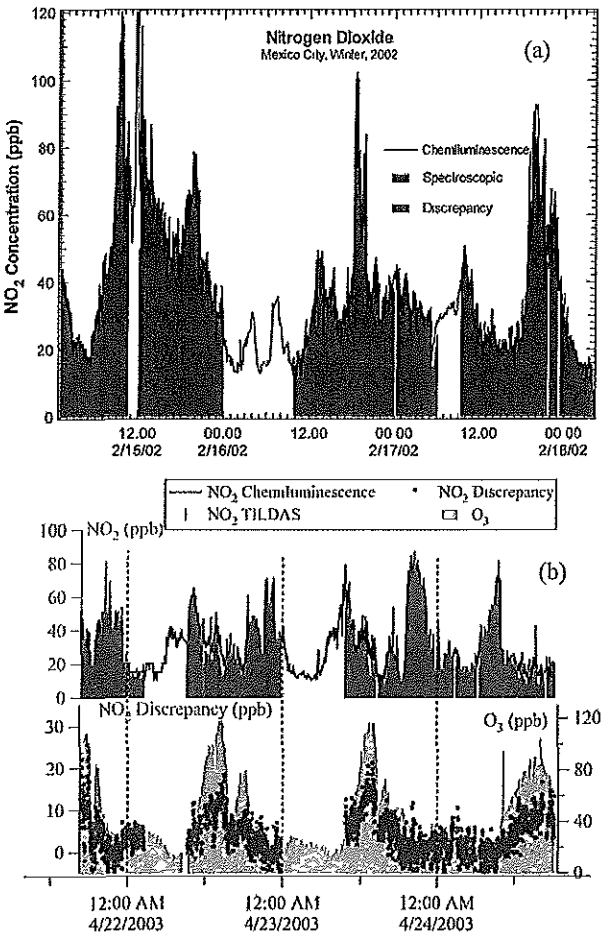

Fig. 1. **(a)** Time series of NO_2 measurements by standard CL NO_x monitor and TILDAS spectroscopic instruments on board ARI Mobile Lab at the Pedregal fixed monitoring site during 2002 campaign for a specific period highlighting when the chemiluminescence instrument showed an interference. **(b)** Time series for one-minute averaged measurements made on board ARI Mobile Lab at the Pedregal fixed monitoring site during MCMA-2003 field campaign for a specific period. The CL NO_x monitor interference is plotted on its own axis in this figure to show the correlation in time with ambient O_3 levels, which indicates a photochemical source of the interfering compound(s).

troscopic measurement is subtracted from a point sampling CL NO_x monitor measurement, limiting the achievable R^2 values for these correlation plots. We also note here that the onset of the daily rise of the CL NO_x monitor at CENICA is delayed relative to the other three sites by ~2 h: from 10 AM onset elsewhere to 12 PM onset at CENICA. CENICA also experiences the highest percentage of negative CL NO_x monitor interference measurements indicating that the open path DOAS light paths may be influenced by NO_x sources, such as roadways underneath the light paths, which do not advect to the CENICA rooftop sampling location. San Martini et

Table 1. Slopes of linear least squares fit of correlation plots of observed CL NO_x monitor interference versus other measured species at series of locations. R^2 values for fits are given in parentheses. All concentrations for correlation plots are 15 min averages and are reported in ppb or equivalent ppb. Maxima, minima, and averages for slopes are listed. Abbreviations: NA = measurement data Not Available at particular location, ID = Insufficient Data available at particular location, ML = data from ARI Mobile Lab in stationary mode, Roof = long path instruments at fixed site locations. Stationary sites are: STA = Santa Ana, PED = Pedregal, MER = La Merced and CEN = CENICA headquarters; see text for description. NO_z, O_3 and HNO_3 are highlighted as showing the best correlations.

Species Correlated with CL NO_x Monitor Interference	ML STA	ML PED	ML MER	ML CEN	Roof CEN	Roof MER	Min	Max	Avg
PTRMS Olefin Proxy m/z 71	1.19 (0.05)	−1.56 (0.03)	−0.86 (0.03)	ID	NA	NA	−1.56	1.19	−0.41
PTRMS Olefin Proxy m/z 43	*0.36 (0.12)*	*−0.2 (0.01)*	*−0.15 (0.06)*	*ID*	*NA*	*NA*	*−0.2*	*0.36*	*0.00*
FIS Monitor Total Olefins	NA	NA	NA	−0.13 (0.04)	−0.15 (0.32)	NA	−0.15	−0.13	−0.14
NH_3	−0.03 (0.03)	0.34 (0.04)	−0.06 (0.17)	0.14	−0.05 (0.01)	0.49 (0.01)	−0.06	0.49	0.14
PAN	NA	NA	NA	ID	4.07 (0.09)	NA			4.07
AMS Particulate Nitrate	2.44 (0.15)	1.74 (0.12)	−0.44 (0.01)	1.68 (0.01)	0.28 (0.01)	NA	−0.44	2.44	1.14
NO_z	**0.54 (0.65)**	**0.66 (0.79)**	**0.44 (0.32)**	**0.49 (0.35)**	**NA**	**NA**	**0.44**	**0.66**	**0.53**
O_3	**0.06 (0.30)**	**0.09 (0.54)**	**0.09 (0.19)**	**ID**	**0.11 (0.21)**	**0.15 (0.21)**	**0.06**	**0.19**	**0.10**
HNO_3	**NA**	**NA**	**NA**	**NA**	**NA**	**1.83 (0.44)**			**1.83**

al. (2006b) have discussed the limitations of this NO_z measurement in more detail.

As shown in Figs. 1 and 3, the CL NO_x monitor interference peaked in magnitude during the afternoons, corresponding to peaks in the ambient O_3 concentration. The CL NO_x monitor interference shows a fair correlation with the co-located measured O_3 concentration at all locations (R^2=0.19–0.54); see Fig. 2 and Table 1. The magnitude of the CL NO_x monitor interference concentration was approximately 10% of the ambient O_3 concentration. We have established above that ambient O_3 does not represent an interference to the NO_2 measurement; this is further corroborated by the poor correlation of the measured CL NO_x monitor interference with the product of ambient concentrations of $[NO]*[O_3]$ (regression R^2=0.03). Thus, we conclude that the CL NO_x monitor interference was primarily due to reactive nitrogen species that are produced photochemically along with O_3.

We now examine the individual species that make up NO_z in order to determine the most likely contributors to the CL NO_x monitor interference. We start by removing from consideration those reactive nitrogen species which are not converted by the molybdenum oxide catalyst, e.g., amines (Winer et al., 1974), or whose concentrations do not peak during the afternoon, specifically nitrous acid (HONO), other organic nitrites, the nitrate radical (NO_3) and N_2O_5. HONO was measured directly by the DOAS instrument at the CENICA supersite and observed to have its highest concentrations during the morning. Other organic nitrites are unlikely to have concentrations that approach ppb levels and will have photolytic loss rates that maximize in the afternoon, making it very unlikely that they could contribute significantly to the observed CL NO_x monitor interferences. Lastly, measured concentrations of NO_3 and N_2O_5 are observed almost exclusively at night, excluding them from possible contribution to the observed daytime interference. Thus, our most likely candidates are (a) particulate nitrate, (b) peroxyacetyl nitrate and other peroxyacyl nitrates, (c) nitric acid (d) alkyl and multifunctional alkyl nitrates and (e) a combination of more than one of these species.

(a) Particulate phase nitrate (pNO_3^-) may be converted by the CL NO_x monitor and reported as NO_2 if sufficiently particles penetrate the particulate filter on the CL NO_x monitor to reach the molybdenum oxide converter. The particulate filter on a CL NO_x monitor typically filters out particles with diameters larger than 200 nm. Measurements from MCMA-2003 with two AMS instruments reveal that only a small fraction of the particle mass was found to be contained in particles with diameters <200 nm (Salcedo et al., 2006). Thus, of the measured levels of submicron pNO_3^-, only a small fraction would be expected to enter a CL NO_x monitor resulting in a potential interference. Additionally, the dissociation of particulate NH_4NO_3 to gas phase HNO_3 from either the filter or surfaces within the instrument and/or sampling line could contribute to this interference. None of the inlets for the NO_2 instruments listed in the experiment section were heated, such that this effect is likely to have been minimal. Thus, we do not expect pNO_3^- do contribute significantly to the CL NO_x monitor interference.

This is confirmed by comparing the diurnal profiles of pNO_3^- and the CL NOx monitor interference (Fig. 3); concentrations of submicron pNO_3^- (as converted to its equivalent gas phase concentration) were significantly smaller than the CL NO_x monitor interference and peaked a few hours before the maximum in the CL NO_x monitor interference. Table 1 reports only a weak correlation (R^2<0.15) of the CL NO_x monitor interference with the measured ambient submicron pNO_3^- levels for all sites. Overall, it is clear that pNO_3^- does not contribute significantly to the observed CL NO_x monitor interference in Mexico City.

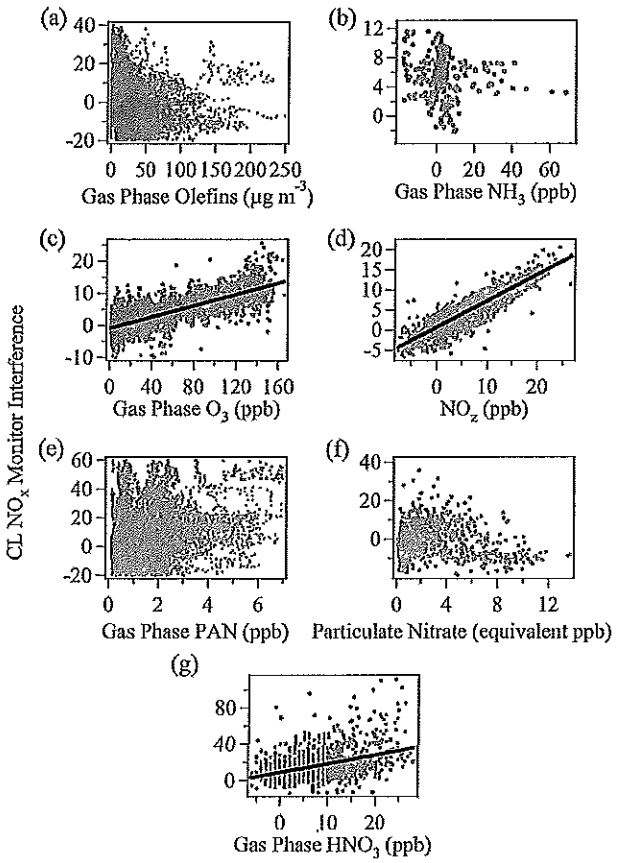

Fig. 2. Linear regression plots for the CL NO_x monitor interference plotted versus **(a)** gas phase olefins (CENICA), **(b)** gas phase NH_3 (Santa Ana), **(c)** gas phase O_3 (Pedregal), **(d)** NO_z (Pedregal), **(e)** gas phase PAN (CENICA), **(f)** particulate nitrate (La Merced), and (g) gas phase HNO_3 (La Merced). See text for description of measurements. Results of the linear regressions are listed in Table 1.

(b) Peroxyacetyl nitrate (PAN) is often found in large quantities in urban atmospheres and concentrations >30 ppb have been observed in the past in Mexico City (Gaffney et al., 1999) The MCMA-2003 field campaign included a PAN measurement at the CENICA supersite (Marley et al., 2007) reveling much lower PAN concentrations (maximum <15 ppb) that peak in mid-morning (Fig. 3b); this does not match the diurnal pattern of the CL NO_x monitor interference. The results of the correlation plots of the CL NO_x monitor interference versus the measured PAN concentrations on the CENICA rooftop show an R^2=0.09. Modeling studies of the outflow of pollution from Mexico City (Madronich, 2006) and more recent measurements downwind of the city (Farmer, D. K., Wooldridge, P. J., and Cohen, R. C., personal communication, 2006) show that peroxyacyl nitrate compounds can account for a significant fraction of the NO_z budget in the outflow from Mexico City. Although PAN is known to be converted to NO_2 on heated surfaces, and as such, PAN may contribute more significantly to this interference in other locations that experience higher PAN concentrations, we conclude that PAN does not contribute significantly to the observed CL NO_x monitor interference in this study because of its low ambient concentrations.

(c) Nitric acid (HNO_3) is photochemically produced within urban atmospheres and has been observed in significant concentrations in Mexico City (Moya et al., 2004). Production of HNO_3 is generally on the same time scale as production of O_3, since both involve the formation of NO_2. O_3 is formed when NO_2 photolyzes via a two step process:

$$NO_2 + h\nu \rightarrow NO + O \quad (2)$$

$$O + O_2 + M \rightarrow O_3 + M \quad (3)$$

(where M represents a third body colliding molecule, presumably N_2 or O_2). HNO_3 is formed from the association reaction of OH with NO_2

$$NO_2 + OH + M \rightarrow HNO_3 + M \quad (4)$$

The measured concentrations of NO_2 and OH during MCMA-2003 (Volkamer et al., 2005) indicate that HNO_3 production rates via reaction (4) are quite large (>15 ppb hr^{-1} at maximum). However, losses for HNO_3 within an urban area are also significant, and the ambient concentration depends on the balance between the production and loss rates. In the presence of NH_3, HNO_3 will readily form particle phase ammonium nitrate (NH_4NO_3). HNO_3 is also readily lost on surfaces by dry deposition (Neuman et al., 1999), but there is a large range of deposition velocities in the literature (4–26 cm s^{-1}) and an exact loss rate is difficult to estimate (Neuman et al., 2004; Wesely and Hicks, 2000). It is thus preferable to rely on measurements of HNO_3 as much as possible. During the MCMA-2003 campaign, the only direct HNO_3 concentration measurements were from the open path FTIR operated by the UNAM group at the La Merced site (Flores et al., 2004; Moya et al., 2004). Although the measured HNO_3 concentrations show reasonably good correlation with the CL NO_x monitor interference concentrations (R^2=0.44), the slope of the correlation plot (1.41) indicates that HNO_3 accounts for ~60% of the CL NO_x monitor interference.

For the locations that did not have a measurement of HNO_3, we use modeled values to estimate the possible contribution of HNO_3 to the CL NO_x monitor. San Martini et al. (2006a, b) have used an ISORROPIA model embedded in a Markov Chain Monte Carlo algorithm to analyze aerosol data and to predict the gas phase HNO_3 concentrations at the locations included in this study. Diurnal profiles of these predicted HNO_3 concentrations are included in Fig. 3. In general, HNO_3 levels are shown to be large enough to account for the measured CL NO_x monitor interference. However, we note that the measured HNO_3 concentrations at La Merced are lower than the predicted levels. We therefore generally

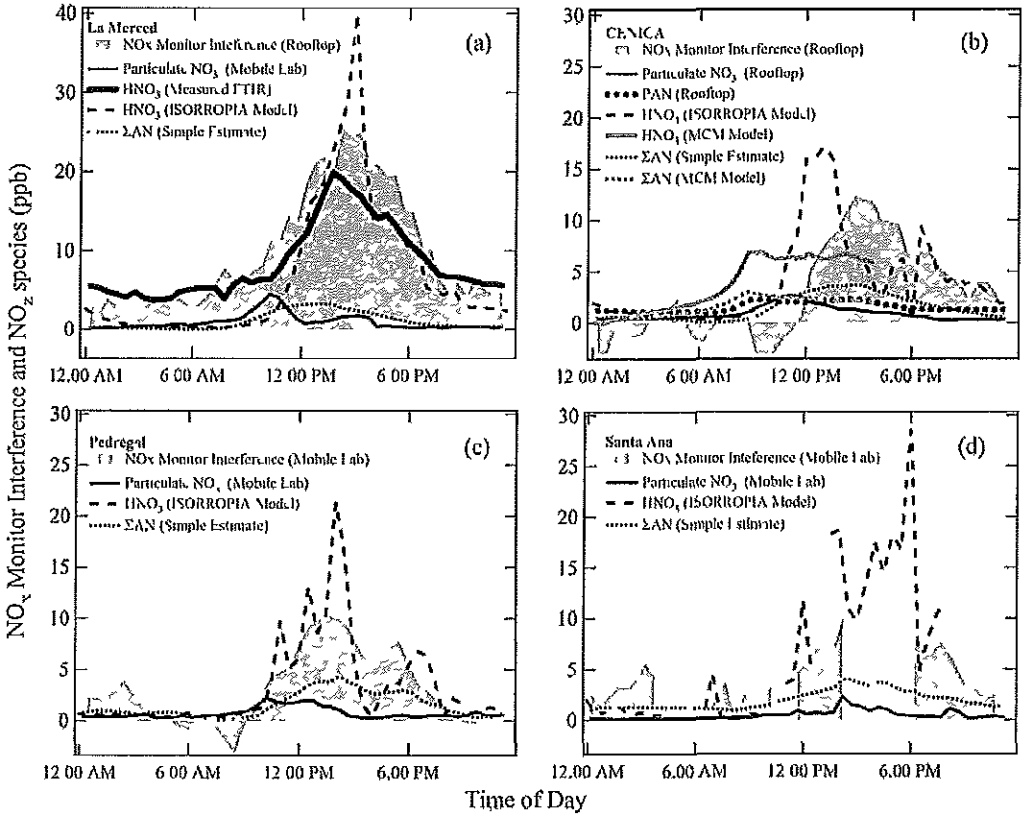

Fig. 3. Diurnally averaged profiles for measured CL NO_X monitor interference, calculated alkyl nitrate concentrations, measured PAN concentrations and measured particulate nitrate in equivalent gas phase concentration as observed at the four fixed sites. Note that only a small fraction of particulate nitrate mass, from particles with diameters <200 nm, could potentially contribute to the NO_X monitor interference. Time of day is for local time. Profiles averaged over the entire MCMA-2003 campaign where possible; exceptions are for Mobile Lab data which were available for several day periods while the Mobile Lab was at particular fixed locations (see text). Gaps in profiles are due to limited data

conclude that HNO_3 accounts for most, but not all, of the observed CL NO_X monitor interference.

As an added complication, HNO_3 is efficiently lost on stainless steel and other surfaces (Neuman et al., 1999). The efficiency with which HNO_3 will reach the molybdenum converter within a particular CL NO_X monitor is then dependent on the amount of stainless steel surface area in the inlet manifold, and thus unique to each monitor. Thus, it is not possible to easily extrapolate this result to all CL NO_X monitors. We generally conclude, however, that HNO_3 accounts for a significant portion of the CL NO_X monitor interference.

(d) Alkyl and multifunctional organic nitrates (from hereon referred to as "alkyl nitrates") are known to be produced simultaneously with O_3 from the minor branch (5b) of the reaction of NO with peroxy radicals (Day et al., 2003; Rosen et al., 2004; Trainer et al., 1991).

$$RO_2 + NO \rightarrow NO_2 + RO \quad (5a)$$

$$RO_2 + NO + M \rightarrow RONO_2 + M \quad (5b)$$

There were no direct measurements of alkyl nitrates as part of the MCMA-2003 campaign of which we are aware. Instead, to study the formation of alkyl nitrates (and HNO_3), we employ a flexible top photochemical box model, which was constrained by measurements conducted at the CENICA supersite for OH sources and sinks from VOC and NO_X. Model simulations were performed with the Master Chemical Mechanism (MCMv3.1) (Jenkin et al., 2003; Saunders et al., 2003) on a 24-h basis constrained with 10-minute averaged measurements of major inorganic species (NO, NO_2, HONO, O_3 and SO_2), CO, 102 volatile organic compounds (VOC), HO_X (=OH+HO_2) measurements, temperature, pressure, water vapor concentration, photolysis frequencies, and dilution. MCMv3.1 is a near-explicit mechanism, i.e. with minimized lumping of VOC reaction pathways, and thus well suited for source-apportionment of organic nitrates and HNO_3 (Sheehy et al., 2007[1]). Figure 3 shows the diurnal

[1]Sheehy, P. M., Volkamer, R. M., Molina, L. T., and Molina, M. J.: Radical Cycling in the Mexico City Metropolitan Area

profile of the modeled concentrations of alkyl nitrates and HNO_3 from the MCM model. Note that the model does not account for horizontal transport and thus modeled concentrations of stable species begin accruing above realistic values after 4 PM local time due to planetary boundary layer dynamics.

Preliminary results from observations from a recent field campaign in 2006 (Farmer, D. K., Wooldridge, P. J., and Cohen, R. C., personal communication, 2006) as well as modeling of the outflow of pollution from Mexico City (Madronich, 2006) show that the sum of all alkyl nitrates, ΣAN, comprises roughly (10–30)% of NO_z in the outflow of Mexico City. Additionally, preliminary results from aircraft measurements of alkyl nitrates made during this same field campaign confirm the presence of alkyl nitrates in the outflow from Mexico City (Blake, D. R. and Atlas, E. L., personal communication, 2006). Alkyl nitrates are thus a non-negligible part of the NO_z budget.

For the locations where measurements of OH and other radicals were not available to constrain the MCM model, we make simple estimates of the alkyl nitrate concentrations based on the measured $[O_3]$. Using the notation of Day et al. (2003), the branching ratio for the formation of an alkyl nitrate in channel (5b) is defined as α. A general correlation of alkyl nitrates with O_3 is expected because both are photochemically generated in the atmosphere. Subsequent reactions of the alkoxy radical (RO_2) in channel (5a) with O_2 lead to the formation of an HO_2 molecule which reacts to form a second NO_2 molecule, which then produces O_3 via reactions (2) and (3) above. Thus, for each reaction of RO_2 with NO in reaction (5), there is either the formation of one alkyl nitrate or two O_3 molecules. As a result, the slope of a plot of ambient $[O_3]$ versus calculated $[\Sigma AN]$ is $2(1-\alpha)/\alpha$. We use this relationship to make a simple estimate of $[\Sigma AN]$ based on the measured $[O_3]$.

We estimate a value for α within Mexico City (α_{MCMA}) based on the measured volatile organic carbon (VOC) speciation. The MCMA-2003 campaign included numerous measurements of the overall VOC loading and speciation thereof (Velasco et al., 2007). Using average speciated VOC concentrations as measured during the campaign and measurements and/or estimates for the branching ratios for channel (5b) of the individual VOC compounds, we calculate α_{MCMA} in a similar manner to the calculations of Rosen et al. (2004) for La Porte, Texas. The ambient VOC mix in Mexico City is heavily dominated by propane (29% by volume) and lighter alkanes ($\leq$C5, 25%), with additional contributions from alkenes (9%), aromatics (8%), heavier alkanes (8%), acetylene (3%) and MTBE (2%), with 15% of the VOC loading left as unidentified. This unidentified portion of the VOC mixture most likely consists of oxygenated VOCs, with branching ratios for reaction (5b) similar to the analogous alkanes and alkenes. We assume a value of α for this unidentified portion of the VOC loading equal to the average of the identified VOCs. We then weight the value of α for each VOC compound by its OH reactivity to determine a best estimate for α_{MCMA}=0.063. Multiplying the measured $[O_3]$ by this α_{MCMA} gives a time series of the estimated total concentration of alkyl nitrates, $[\Sigma AN]$, for the various locations in this study. Diurnal profiles of the estimated $[\Sigma AN]$ are shown in Fig. 3. This simple estimate reveals maxima in $[\Sigma AN]$ of nearly 5 ppb, which are as large as the largest observed $[\Sigma AN]$ in other locations (Rosen et al., 2004). Although ambient VOC concentrations in MCMA are larger than in other urban locations, the MCMA VOC speciation is dominated by light alkanes that do not form alkyl nitrates as readily as longer chain VOCs. For the CENICA supersite, the MCM modeled profile of alkyl nitrates shows a maximum value in the morning, while this simple estimate based on the measured $[O_3]$ shows a peak in afternoon (corresponding to the peak in the O_3 concentration). This is likely due to the suppression of O_3 concentrations at the CENICA site during the morning hours due to nearby NO_x sources mentioned earlier. Overall, the simple estimate provides a rough gauge to the magnitude of $[\Sigma AN]$ expected in a given location.

(e) From the previous sections, we have concluded that HNO_3 and alkyl nitrates contribute to the CL NO_x monitor interference in Mexico City. There is an observable trend in going from "fresh" to "aged" sites, where the contribution of alkyl nitrates relative to the magnitude of the CL NO_x monitor increases moving from the sites in closest proximity to high emissions levels (La Merced and then CENICA) to the sites that are furthest away from large emission sources (Pedregal and then Santa Ana). The estimated $[\Sigma AN]$ is roughly constant at all locations such that the decreasing magnitude of the CL NO_x monitor interference in going from fresh to aged sites is explained by decreasing amounts of HNO_3, i.e., as the air parcel ages, HNO_3 is lost from the gas phase to either particulate nitrate or via dry deposition. If we examine the La Merced (the "freshest" site), the sum of the measured HNO_3 and the estimated ΣAN results in a significantly better agreement of the linear correlation plot (slope=0.97, R^2=0.53). The diurnal profile shown in Fig. 4 closely matches that of the interference. In summary, we conclude that close to the sources of the emissions, the combination of HNO_3 and ΣAN account for the CL NO_x monitor interference, and as the urban air parcel ages, ΣAN comprises a larger percentage of the interference.

3.2.2 Gas phase olefins and ammonia

The chemiluminescent reaction of ambient gas phase olefins with excess O_3 within the CL NO_x monitor reaction chamber, where the resulting fluorescence is recorded as NO_2, is a potential interference to the CL NO_x monitor. However, no correlation of the measured CL NO_x monitor interference was observed with olefin concentrations measured during the

(MCMA): Modeling ROx Using a Detailed Mechanism, to be submitted, 2007.

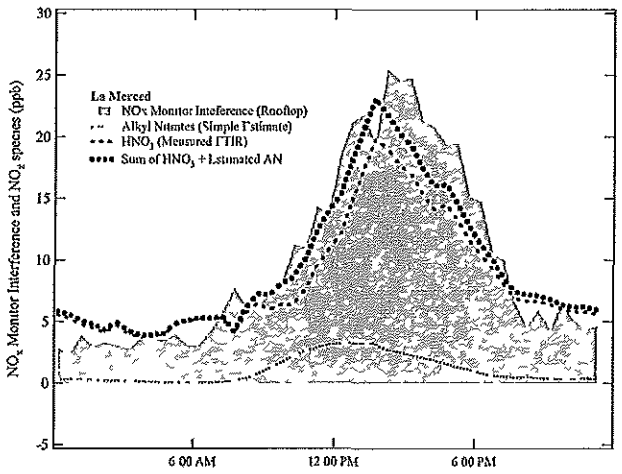

Fig. 4. Diurnally averaged profiles for measured CL NO_X monitor interference, measured HNO_3 concentrations and calculated alkyl nitrate concentrations at La Merced site. Profiles averaged over the entire MCMA-2003 campaign. Also included is a profile of the sum of the measured HNO_3 concentration plus the estimated alkyl nitrate concentration (see text). Time of day is for local time.

MCMA-2003 field campaign from either a Proton Transfer Reaction Mass Spectrometer (PTRMS) on board the ARI Mobile Lab (Rogers et al., 2006) or a Fast Isoprene Sensor (FIS) at the CENICA supersite (Velasco et al., 2007). Results from the linear correlation plots are listed in Table 1. The daily peak in the olefin levels was observed during the morning hours, which does not coincide with the afternoon peak in the CL NO_X monitor interference.

Another possibility for the cause of the CL NO_X monitor interference is gas phase ammonia (NH_3), which has been shown to be converted by molybdenum oxide catalysts with an efficiency somewhere between a few percent (Williams et al., 1998) and 10% (Shivers, personal communication, 2004). A TILDAS system utilizing a Quantum Cascade Laser (QCL) to monitor gaseous ammonia was deployed on board the ARI Mobile Lab for the MCMA-2003 campaign. Measured ambient NH_3 concentrations were not sufficient to account for the observed CL NO_X monitor interferences (typical $[NH_3]<30$ ppb) and NH_3 concentrations peaked during the morning before the break up of the boundary layer (earlier than 11 AM local time), indicating a significant source from automobiles (San Martini et al., 2006a), which does not correspond to the afternoon maxima in the CL NO_X monitor interference. The slopes of correlation plots of the CL NO_X monitor interference versus the measured NH_3 concentrations were less than 0.34 and R^2 values did not exceed 0.17, indicating no significant correlation (see Table 1).

Based on these observations, we conclude that neither gas phase olefins nor ammonia contributed significantly to the observed CL NO_X monitor interference.

3.3 Impact of CL NO_X monitor interference

The CL NO_X monitor interference has been shown to account for up to 50% of the measured NO_2 concentration in Mexico City; interferences of this order could impact the non-attainment status of urban areas. The diurnal profile of the CL NO_X monitor interference peaks in the afternoon when NO_2 concentrations are relatively low, impacting annual standards for NO_2, such as those used by Canada and the United States (Demerjian, 2000), more so than daily 1-h maxima standards. For the MCMA-2003 campaign, the averaged NO_2 concentration (the closest comparison to the annual standard we can do with this data) as measured by CL NO_X monitors was higher than co-located spectroscopic techniques by up to 22% at the four sites in this study (see Table 2). For example, the averaged NO_2 concentration measured at La Merced by the CL NO_X monitor was 49.5 ppb versus 40.6 ppb measured by the co-located DOAS instrument; the former measurement comes much closer to the 53 ppb US EPA annually averaged threshold for non-attainment (Environmental Protection Agency, 1993). (We note that our maximum observed NO_2 concentration in this study for a 1-h averaged of 185 ppb was significantly lower than the Mexican air quality standard of 210 ppb for a 1-h averaged concentration (Finlayson-Pitts and Pitts, 2000).)

Air quality models require uncertainties in NO_2 measurements of roughly $\pm 10\%$. As such, the observed interferences of up to 50% are unacceptable for the proper evaluation of air quality models (McClenny et al., 2002). In the following section we make several recommendations for how to avoid this interference in the future.

4 Conclusions

It has been shown that high levels of ambient reactive nitrogen species can lead to a severe overestimation of ambient NO_2 concentrations by standard chemiluminescence monitors equipped with molybdenum oxide converters. This study is one of the first to quantify this CL NO_X monitor interference and explore its causes in detail. In Mexico City, the observed CL NO_X monitor interference was shown to have no significant contribution from gas phase olefins or ammonia. The good correlation of the CL NO_X monitor interference with ambient O_3 and NO_z concentrations and poor correlation with PAN and particulate nitrate lead to the conclusion that a combination of photochemically produced gas phase nitric acid and alkyl and multifunctional alkyl nitrates is primarily responsible for this interference in this study. It is expected that in other environments with larger ambient PAN concentrations, PAN will contribute to this CL NO_X monitor interference even though it did not in this study. The percentage contribution of HNO_3 to the interference decreases as the air parcel moves away from fresh emission sources. Modeling and calculations reveal that ambient alkyl nitrates

Table 2. Averaged measured NO_2 concentrations for 5 week MCMA-2003 campaign by spectroscopic techniques compared to co-located CL NO_x monitors at 4 locations.

Site	Spectroscopic Instrument	MCMA Campaign Average	CL NO_x Monitor	MCMA Campaign Average	% Difference
La Merced	DOAS-UNAM	40.6	RAMA	49.5	+22%
CENICA	DOAS-1	34.1	CENICA	31.0	−9%[a]
	DOAS-2	28.0			+11%
Pedregal	TILDAS-ML[b]	27.6	ML[b]	29.4	+7%
			RAMA	30.7	+11%
Santa Ana	TILDAS-ML[b]	3.8	ML[b]	9.1	140%

[a] DOAS-1 believed to have larger NO_x concentrations than CENICA rooftop owing to major roadway beneath the light path, see discussion above and (Dunlea et al., 2006).
[b] The ARI Mobile Lab visit each location for only a few days, which may not be a representative sample of the average NO_2 concentration at each location.

concentrations in the MCMA are significant, up to several ppb, which is as high as those observed in other urban locations, and plausible given the high VOC loadings in Mexico City. During the MCMA-2003 field campaign, the CL NO_x monitor interference caused the average measured NO_2 concentration to be larger than co-located spectroscopic measurements by up to 22%. This magnitude of interference is inappropriately large for use in modeling studies and may lead to a non-attainment status for NO_2 to be incorrectly assigned in certain urban areas.

To finish, we make several recommendations: (1) There exists the possibility that currently employed CL NO_x monitors could be retrofitted with photolytic converters to replace molybdenum oxide converters. Such photolytic converters have been shown to perform well in the field (Thornton et al., 2003; Williams et al., 1998). (2) In order to avoid this interference in the long term, instrument manufacturers should pursue low-cost, interference-free techniques for measuring NO_2, which would significantly improve the quality of data from ambient monitoring networks. These include photolytic converters and spectroscopic techniques, including instruments that are already on the market (www.ecophysics.com and www.dropletmeasurement.com). We are not aware, however, of any that have been thoroughly tested in a polluted urban environment. (3) CL NO_x monitors are capable of measuring NO reliably; rather than discard currently in-use CL NO_x monitors, it is possible that those instruments with molybdenum oxide converters could be configured to exploit the ability of the molybdenum oxide converter to reduce reactive nitrogen species to NO, i.e., to measure NO and NO_y. As mentioned above, commercially instruments are currently available that do just this. Monitoring networks could then report NO and NO_y with this instrument instead of NO and NO_2. (4) Post-correction of NO_2 measurements from CL NO_x monitors with molybdenum oxide converters may prove effective in certain circumstances, but must be done carefully, as discussed in Steinbacher et al. (2007).

Acknowledgements. The authors would like to thank M. J. Elrod, K. Dzepina, and J. L. Jimenez for helpful discussions. Financial support from Comision Ambiental Metropolitana (Mexico), the National Science Foundation (ATM-308748, ATM-0528170 and ATM-0528227) and the Department of Energy (DE-FG02-05ER63980 and DE-FG02-05ER63982) is gratefully acknowledged. R. Volkamer is a Dreyfus Postdoctoral Fellow. J. Gaffney and N. Marley acknowledge support of the Department of Energy's Atmospheric Science Program.

Edited by: U. Pöschl

References

Beauchamp, J., Wisthaler, A., Grabmer, W., Neuner, C., Weber, A., and Hansel, A.: Short-term measurements of CO, NO, NO_2, organic compounds and PM_{10} at a motorway location in an Austrian valley, Atmos. Environ., 38, 2511–2522, 2004.

Carslaw, D. C. and Beevers, S. D.: Investigating the potential importance of primary NO_2 emissions in a street canyon, Atmos. Environ., 38, 3585–3594, 2004.

Carslaw, D. C. and Beevers, S. D.: Estimations of road vehicel primary NO2 exhaust emission fractions using monitoring data in London, Atmos. Environ., 39, 167–177, 2005.

Cavanagh, R. R. and Verkouteren, R. M., Improving the Scientific Basis for Informed Decisions on Atmospheric Issues, NIST-NOAA-Industry Workshop on Atmospheric Measures and Standards, National Institute of Standards and Technology, 2001.

Day, D. A., Dillon, M. B., Wooldridge, P. J., Thornton, J. A., Rosen, R. S., Wood, E. C., and Cohen, R. C.: On alkyl nitrates, O_3, and the "missing NO_y", J. Geophys. Res., 108(D16), 4501, doi:10.1029/2003JD003685, 2003.

de Foy, B., Caetano, E., Magaña, V., Zitácuaro, A., Cardenas, B., Retama, A., Ramos, R., Molina, L. T., and Molina, M. J.: Mexico City basin wind circulation during the MCMA-2003 field campaign, Atmos. Chem. Phys., 5, 2267–2288, 2005, http://www.atmos-chem-phys.net/5/2267/2005/.

Demerjian, K. L.: A review of national monitoring networks in North America, Atmos. Environ., 34, 1861–1884, 2000.

Dunlea, E. J., Herndon, S. C., Nelson, D. D., Volkamer, R. M., Lamb, B. K., Allwine, E. J., Grutter, M., Villegas, C. R. R., Mar-

quez, C., Blanco, S., Cardenas, B., Kolb, C. E., Molina, L. T., and Molina, M. J.: Evaluation of Standard Ultraviolet Absorption Ozone Monitors in a Polluted Urban Environment, Atmos. Chem. Phys., 6, 3163–3180, 2006, http://www.atmos-chem-phys.net/6/3163/2006/.

Environmental Protection Agency, U.S.: Air Quality Criteria for Oxides of Nitrogen, Office of Research and Development, http://www.epa.gov/ttn/naaqs/standards/nox/s_nox_index.html, 1993.

Environmental Protection Agency, U.S.: Recommended Methods for Ambient Air Monitoring of NO, NO2, NOy, and Individual NOz Species, National Exposure Research Laboratory, 2001.

Environmental Protection Agency, U.S.: US EPA Audit of RAMA Network, http://www.sma.df.gob.mx/sma/download/archivos/auditoria_epa_ingles.pdf, 2003.

Environmental Protection Agency, U.S.: National Ambient Air Monitoring Strategy, Office of Air Quality Planning and Standards, http://www.epa.gov/ttn/amtic/files/ambient/monitorstrat/naamstrat2005.pdf, 2005.

Environmental Protection Agency, U.S.: Electronic Code of Federal Regulations, ecfr.gpoaccess.gov/, 2006.

Fehsenfeld, F. C., Dickerson, R. R., Hubler, G., Luke, W. T., Nunnermacker, L. J., Williams, E. J., Roberts, J. M., Calvert, J. G., Curran, C. M., Delany, A. C., Eubank, C. S., Fahey, D. W., Fried, A., Gandrud, B. W., Langford, A. O., Murphy, P. C., Norton, R. B., Pickering, K. E., and Ridley, B. A.: A Ground-Based Intercomparison of NO, NO_x, and NO_y Measurement Techniques, J. Geophys. Res., 92(D12), 14 710–14 722, 1987.

Fehsenfeld, F. C., Drummand, J. W., Roychowdhury, U. K., Galvin, P. J. W., E.J., Burh, M. P., Parrish, D. D., Hubler, G., Langford, A. O., Calvert, J. G., Ridley, B. A., Grahek, F., Heikes, B. G., Kok, G. L., Shetter, J. D., Walega, J. G., Elsworth, C. M., Norton, R. B., Fahey, D. W., Murphy, P. C., Hovermale, C., Mohnen, V. A., Demerjian, K. L., Mackay, G. I., and Schiff, H. I.: Intercomparison of NO_2 Measurement Techniques, J. Geophys. Res., 95(D4), 3579–3597, 1990.

Finlayson-Pitts, B. J. and Pitts, J. N.: Chemistry of the Upper and Lower Atmosphere, Academic Press, 2000.

Flores, E., Grutter, M., Galle, B., Mellqvist, J., Samuelsson, J., Knighton, B., Jobson, B. T., Volkamer, R., Molina, L. T., and Molina, M. J., American Geophysical Union Fall Meeting, EOS Trans., 85(47), Abstract A11A-0003, 2004.

Fontjin, A., Sabadell, A. J., and Ronco, R. J.: Homogeneous chemiluminescence measurement of nitric oxide with ozone, Anal. Chem., 42, 575–579, 1970.

Friedeburg, C. v., Pundt, I., Mettendorf, K.-U., Wagner, T., and Platt, U.: Multi-axis-DOAS measurements of NO_2 during the BAB II motorway emission campaign, Atmos. Environ., 39, 977–985, 2005.

Gaffney, J. S., Marley, N. A., Cunningham, M. M., and Doskey, P. V.: Measurements of peroxyacyl nitrates (PANS) in Mexico City: implications for megacity air quality impacts on regional scales, Atmos. Environ., 33, 30, 5003–5012, 1999.

Garcia, A. R., Volkamer, R., Molina, L. T., Molina, M. J., Samuelson, J., Mellqvist, J., Galle, B., Herndon, S. C., and Kolb, C. E.: Separation of emitted and photochemical formaldehyde in Mexico City using a statistical analysis and a new pair of gas-phase tracers, Atmos. Chem. Phys., 6, 4545–4557, 2006, http://www.atmos-chem-phys.net/6/4545/2006/.

Gregory, G. L., Hoell, J. M., Carroll, M. A., Ridley, B. A., Davis, D. D., Bradshaw, J., Rodgers, M. O., Sandholm, S. T., Schiff, H. I., Hastie, D. R., Karecki, D. R., Mackay, G. I., Harris, G. W., Torres, A. L., and Fried, A.: An Intercomparison of Airborne Nitrogen Dioxide Instruments, J. Geophys. Res., 95(D7), 10 103–10 127, 1990.

Grutter, M.: Multi-Gas analysis of ambient air using FTIR spectroscopy over Mexico City, Atmosfera, 16, 1, 1–13, 2003.

Herndon, S. C., Jayne, J. T., Zahniser, M. S., Worsnop, D. R., Knighton, W. B., Alwine, E., Lamb, B., Zavala, M., Nelson, D. D., McManus, B., Shorter, J. H., Canagaratna, M. R., Onasch, T. B., and Kolb, C. E.: Characterization of urban pollutant emission fluxes and ambient concentration distributions using a mobile laboratory with rapid response instrumentation, Faraday Discuss., 130, 327–339, 2005a.

Herndon, S. C., Yongquan, L., Nelson, D. D., and Zahniser, M. S.: Determination of line strengths for selected transitions in the ν_2 band relative to the U_1 and N_2 bands of H_2CO, J. Quant. Spectros. Radiat. Transfer, 90, 207–216, 2005b.

Jayne, J. T., Leard, D. C., Zhang, X., Davidovits, P., Smith, K. A., Kolb, C. E., and Worsnop, D. R.: Development of an Aerosol Mass Spectrometer for Size and Composition Analysis of Submicron Particles, Aerosol Sci. Technol., 33, 1–2, 49–70, 2000.

Jenkin, M. E.: Analysis of sources and partitioning of oxidant in the UK – Part 2: contributions of nitrogen dioxide emissions and background ozone at a kerbside location in London, Atmos. Env., 38, 5131–5138, 2004a.

Jenkin, M. E.: Analysis of sources andpartitioning of oxidant in the UK – Part 1: the NOX-dependence of annual mean concentrations of nitrogen dioxide and ozone, Atmos. Environ., 38, 5117–5129, 2004b.

Jenkin, M. E., Saunders, S. M., Wagner, V., and Pilling, M. J.: Protocol for the development of the Master Chemical Mechanism, MCM v3 (Part B): tropospheric degradation of aromatic volatile organic compounds, Atmos. Chem. Phys., 3, 181–193, 2003, http://www.atmos-chem-phys.net/3/181/2003/.

Jimenez, J. L., McCrae, G. J., Nelson, D. D., Zahniser, M. S., and Kolb, C. E.: Remote Sensing of NO and NO_2 Emissions from Heavy-Duty Diesel Trucks Using Tunable Diode Lasers, Environ. Sci. Technol., 34, 12, 2380–2387, 2000.

Kebabian, P. L., Herndon, S. C., and Freedman, A.: Detection of Nitrogen Dioxide by Cavity Attenuated Phase Shift Spectroscopy, Anal. Chem., 77, 724–728, 2005.

Kley, D. and McFarland, M.: Chemiluminescence detector for NO and NO_2, Atmos. Tech., 12, 63–69, 1980.

Kolb, C. E., Herndon, S. C., Mcmanus, J. B., Shorter, J. H., Zahniser, M. S., Nelson, D. D. J., Jayne, J. T., Canagaratna, M. R., and Worsnop, D. R.: Mobile Laboratory with Rapid Response Instruments for Real-Time Measurements of Urban and Regional Trace Gas and Particulate Distributions and Emission Source Characteristics, Environ. Sci. Technol., 38, 5694–5703, 2004.

Latham, S., Kollamthodi, S., Boulter, P. G., Nelson, P. M., and Hickman, A. J.: Assessment of primary NO_2 emissions, hydrocarbon speciation and particulate sizing on a range of road vehicles, Report PR/SE/353/2001, Transport Research Laboratory (TRL), 2001.

Li, Y. Q., Demerjian, K. L., Zahniser, M. S., Nelson, D. D., McManus, J. B., and Herndon, S. C.: Measurement of formaldehyde, nitrogen dioxide, and sulfur dioxide at Whiteface Moun-

tain using a dual tunable diode laser system, J. Geophys. Res., 109, D16S08, doi:10.1029/2003JD004091, 2004.

Madronich, S.: Chemical evolution of gaseous air pollutants downwind of tropical megacities: Mexico City case study, Atmos. Environ., 40, 6012–6018, 2006.

Marley, N. A., Gaffney, J. S., Ramos-Villegas, R., and Cardenas Gonzalez, B.: Comparison of measurements of peroxyacyl nitrates and primary carbonaceous aerosol concentrations in Mexico City determined in 1997 and 2003, Atmos. Chem. Phys., 7, 2277–2285, 2007, http://www.atmos-chem-phys.net/7/2277/2007/.

Marley, N. A., Gaffney, J. S., White, R. V., Rodriguez-Cuadra, L., Herndon, S. C., Kolb, C. E., Dunlea, E. J., Volkamer, R. M., Molina, L. T., and Molina, M. J.: Fast Gas Chromatography with Luminol Chemiluminescent Detection for the Simultaneous Determination of Nitrogen Dioxide (NO_2) and Peroxyacetyl Nitrate (PAN) in the Atmosphere, Rev. Sci. Inst., 75, 4595–4605, 2004.

McClenny, W. A., Williams, E. J., Cohen, R. C., and Stutz, J.: Preparing to Measure the Effects of the NO_X SIP Call – Methods for Ambient Air Monitoring of NO, NO_2, NO_y, and Individual NO_Z Species, J. Air Waste Manage. Assoc., 52, 542–562, 2002.

McManus, J. B., Kebabian, P. L., and Zahniser, M. S.: Astigmatic mirror multiple pass absorption cells for long pathlength spectroscopy, Appl. Opt., 34, 3336–3348, 1995.

Molina, L. T., Kolb, C. E., De Foy, B., Lamb, B. K., Brune, W. H., Jimenez, J. L., and Molina, M. J.: Air quality in North America's most populous city– overview of MCMA-2003 Campaign, Atmos. Chem. Phys., 7, 2447–2473, 2007, http://www.atmos-chem-phys.net/7/2447/2007/.

Moya, M., Grutter, M., and Baez, A.: Diurnal variability of size-differentiated inorganic aerosols and their gas-phase precursors during January and February of 2003 near downtown Mexico City, Atmos. Environ., 38, 5651–5661, 2004.

Neuman, J. A., Huey, L. G., Ryerson, T. B., and Fahey, D. W.: Study of Inlet Materials for Sampling Atmospheric Nitric Acid, Environ. Sci. Technol., 33, 1133–1136, 1999.

Neuman, J. A., Parrish, D. D., Ryerson, T. B., Brock, C. A., Wiedinmyer, C., Frost, G. J., Holloway, J. S., and Fehsenfeld, F. C.: Nitric acid losss rates measured in power plant plumes, J. Geophys. Res.-Atmos., 109(D23), D23304, doi:10.1029/2004JD005092, 2004.

Ordóñez, C., Richter, A., Steinbacher, M., Zellweger, C., Nüss, H., Burrows, J. P., and Prévôt, A. S. H.: Comparison between 7-years of satellite-borne and ground-based tropospheric NO2 measurements around Milan, Italy, J. Geophys. Res., 111, D05310, doi:05310.01029/02005JD006305, 2006.

Osthoff, H. D., Brown, S. S., Ryerson, T. B., Fortin, T. J., Lerner, B. M., Williams, E. J., Pettersson, A., Baynard, T., Dube, W. P., Ciciora, S. J., and Ravishankara, A. R.: Measurement of atmospheric NO2 by pulsed cavity ring-down spectroscopy, J. Geophys. Res., 111, D12305, doi:12310.11029/12005JD006942, 2006.

Parrish, D. D. and Fehsenfeld, F. C.: Methods for gas-phase measurements of ozone, ozone precursors and aerosol precursors, Atmos. Environ., 34, 1921–1957, 2000.

Platt, U.: Chapter 2, Sigrist, M. W., Monitoring by Spectroscopic Techniques, Wiley & Sons, 1994.

Platt, U. and Perner, D.: Direct Measurements of Atmospheric CH2O, HNO2, O3, NO2 and SO2 by Differential Optical Absorption in the Near UV, J. Geophys. Res., 85, 7453–7458, 1980.

Pundt, I., Mettendorf, K.-U., Laepple, T., Knab, V., Xie, P., Losch, J., Friedeburg, C. v., Platt, U., and Wagner, T.: Measurements of trace gas distributions using Long-path DOAS-Tomography during the motorway campaign BAB II: experimental setup and results for NO_2, Atmos. Environ., 39, 967–975, 2005.

RAMA: Red Automatica de Monitoreo Atmosferico, http://148.243.232.103/imecaweb/base_datos.htm, 2005.

Ridley, B. A. and Howlett, L. C.: An instrument for nitric oxide measurements in the stratosphere, Rev. Sci. Inst., 45, 742–746, 1974.

Rogers, T. M., Grimsrud, E. P., Herndon, S. C., Jayne, J. T., Kolb, C. E., Allwine, E., Westberg, H., Lamb, B. K., Zavala, M., Molina, L. T., Molina, M. J., and Knighton, W. B.: On-road measurement of volatile organic compounds in the Mexico City metropolitan area using proton transfer reaction mass spectrometry, Int. J. Mass Spec., 252, 26–37, 2006.

Rosen, R. S., Wood, E. C., Wooldridge, P. J., Thornton, J. A., Day, D. A., Kuster, W., Williams, E. J., Jobson, B. T., and Cohen, R. C.: Observations of total alkyl nitrates during Texas Air Quality Study 2000: Implications for O_3 and alkyl nitrate photochemistry, J. Geophys. Res., 109, D07303, doi:10.1029/2003JD004227, 2004.

Rothman, L. S., Barbe, A., Benner, D. C., Brown, L. R., Camy-Peyret, C., Carleer, M. R., Chance, K., Clerbaux, C., Dana, V., Devi, V. M., Fayt, A., Flaud, J. M., Gamache, R. R., Goldman, A., Jacquemart, D., Jucks, K. W., Lafferty, W. J., Mandin, J. Y., Massie, S. T., Nemtchinov, V., Newnham, D. A., Perrin, A., Rinsland, C. P., Schroeder, J., Smith, K. M., Smith, M. A. H., Tang, K., Toth, R. A., Vander Auwera, J., Varanasi, P., and Yoshino, K.: The HITRAN molecular spectroscopic database: edition of 2000 including updates through 2001, J. Quant. Spectros. Radiat. Transfer, 82, 5–44, 2003.

Salcedo, D., Onasch, T. B., Dzepina, K., Canagaratna, M. R., Zhang, Q., Huffman, J. A., DeCarlo, P. F., Jayne, J. T., Mortimer, P., Worsnop, D. R., Kolb, C. E., Johnson, K. S., Zuberi, B., Marr, L. C., Volkamer, R., Molina, L. T., Molina, M. J., Cardenas, B., Bernabe, R. M., Marquez, C., Gaffney, J. S., Marley, N. A., Laskin, A., Shutthanandan, V., Xie, Y., Brune, W., Lesher, R., Shirley, T., and Jimenez, J. L.: Characterization of Ambient Aerosols in Mexico City during the MCMA-2003 Campaign with Aerosol Mass Spectrometry: Results at the CENICA Supersite, Atmos. Chem. Phys., 6, 925–946, 2006, http://www.atmos-chem-phys.net/6/925/2006/.

San Martini, F. M., Dunlea, E. J., Grutter, M., Onasch, T. B., Jayne, J. T., Canagaratna, M. R., Worsnop, D. R., Kolb, C. E., Shorter, J. H., Herndon, S. C., Zahniser, M. S., Ortega, J. M., McRae, G. J., Molina, L. T., and Molina, M. J.: Implementation of a Markov Chain Monte Carlo Method to inorganic aerosol modeling of observations from the MCMA-2003 Campaign. Part I: Model description and application to the La Merced Site, Atmos. Chem. Phys., 6, 4867–4888, 2006a.

San Martini, F. M., Dunlea, E. J., Volkamer, R., Onasch, T. B., Jayne, J. T., Canagaratna, M. R., Worsnop, D. R., Kolb, C. E., Shorter, J. H., Herndon, S. C., Zahniser, M. S., Salcedo, D., Dzepina, K., Jimenez, J. L., Ortega, J. M., Johnson, K. S., McRae, G. J., Molina, L. T., and Molina, M. J.: Implementation of a Markov Chain Monte Carlo Method to inorganic aerosol modeling of observations from the MCMA-2003 Campaign. Part

II: Model application to the CENICA, Pedregal and Santa Ana sites, Atmos. Chem. Phys., 6, 4889–4904, 2006b.

Saunders, S. M., Jenkin, M. E., Derwent, R. G., and Pilling, M. J.: Protocol for the development of the Master Chemical Mechanism, MCM v3 (Part A): tropospheric degradation of non-aromatic volatile organic compounds, Atmos. Chem. Phys., 3, 161–180, 2003, http://www.atmos-chem-phys.net/3/161/2003/.

Schaub, D., Boersma, K. F., Kaiser, J. W., Weiss, A. K., Folini, D., Eskes, H. J., and Buchmann, B.: Comparison of GOME tropospheric NO2 columns with NO2 profiles deduced from ground-based in situ measurements, Atmos. Chem. Phys., 6, 3211–3229, 2006, http://www.atmos-chem-phys.net/6/3211/2006/.

Sickles II, J. E. and Nriagu, J. O.: Gaseous Pollutants: Characterization and Cycling, John Wiley & Sons, Inc., 1992.

Smith, M. A. H., Rinsland, C. P., Fridovich, B., and Rao, K. N.: Molecular Spectroscopy: Modern Research, Academic Press, Inc., 1985.

Steinbacher, M., Zellweger, C., Schwarzenbach, B., Bugmann, S., Buchmann, B., Ordóñez, C., Prevot, A. S. H., and Hueglin, C.: Nitrogen Oxides Measurements at Rural Sites in Switzerland: Bias of Conventional Measurement Techniques, J. Geophys. Res., accepted, 2007.

Thornton, J. A., Wooldridge, P. J., and Cohen, R. C.: Atmospheric NO_2: In Situ Laser-Induced Fluorescence Detection at Parts per Trillion Mixing Ratios, Anal. Chem., 72, 528–539, 2000.

Thornton, J. A., Wooldridge, P. J., Cohen, R. C., Williams, E. J., Hereid, D., Fehsenfeld, F. C., Stutz, J., and Alicke, B.: Comparisons of in situ and long path measurements of NO_2 in urban plumes, J. Geophys. Res., 108(D16), 4496, doi:10.1029/2003JD003559, 2003.

Trainer, M., Buhr, M. P., Curran, C. M., Fehsenfeld, F. C., Hsie, E. Y., Liu, S. C., Norton, R. B., Parrish, D. D., Williams, E. J., Gandrud, B. W., Ridley, B. A., Shetter, J. D., Allwine, E. J., and Westberg, H. H.: Observations and modeling of the reactive nitrogen photochemistry at a rural site, J. Geophys. Res., 96(D2), 3045–3063, 1991.

Velasco, E., Lamb, B., Westberg, H., Allwine, E., Sosa, G., Arriaga-Colina, J. L., Jobson, B. T., Alexander, M. L., Prazeller, P., Knighton, W. B., Rogers, T. M., Grutter, M., Herndon, S. C., Kolb, C. E., Zavala, M., Foy, B. d., Volkamer, R., Molina, L. T., and Molina, M. J.: Distribution, magnitudes, reactivities, ratios and diurnal patterns of volatile organic compounds in the Valley of Mexico during the MCMA 2002 & 2003 field campaigns, Atmos. Chem. Phys., 7, 329–353, 2007, http://www.atmos-chem-phys.net/7/329/2007/.

Volkamer, R., Etzkorn, T., Geyer, A., and Platt, U.: Correction of the oxygen interference with UV spectroscopic (DOAS) measurements of monocyclic aromatic hydrocarbons in the atmosphere, Atmos. Environ., 32, 3731–3747, 1998.

Volkamer, R., Molina, L. T., Molina, M. J., Shirley, T., and Brune, B.: DOAS measurement of glyoxal as an indicator for fast VOC chemistry in urban air, Geophys. Res. Lett., 32, L08806, doi:10.1029/2005GL022616, 2005.

Wesely, M. L. and Hicks, B. B.: A review of the current status of knowledge on dry deposition, Atmos. Environ., 34, 2261–2282, 2000.

Williams, E. J., Baumann, K., Roberts, J. M., Bertman, S. B., Norton, R. B., Fehsenfeld, F. C., S.R. Springston, Nunnermacker, L. J., Newman, L., Olszyna, K., Meagher, J., Hartsell, B., Edgerton, E., Pearson, J. R., and Rodgers, M. O.: Intercomparison of ground-based NOy measurement techniques, J. Geophys. Res., 103, 2226–22280, 1998.

Winer, A. M., Peters, J. W., Smith, J. P., and James N. Pitts, J.: Response of Commericial Comiluminescent NO-NO2 Analyzers to Other Nitrogen-Containing Compounds, Environ. Sci. Technol., 8, 13, 1118–1121, 1974.

Atmos. Chem. Phys., 8, 3093–3105, 2008
www.atmos-chem-phys.net/8/3093/2008/

Atmospheric Chemistry and Physics

Spatial and temporal variability of particulate polycyclic aromatic hydrocarbons in Mexico City

D. A. Thornhill[1,4], B. de Foy[2,4], S. C. Herndon[3], T. B. Onasch[3], E. C. Wood[3], M. Zavala[4,5], L. T. Molina[4,5], J. S. Gaffney[6], N. A. Marley[6], and L. C. Marr[1]

[1]Dept. of Civil and Environmental Engineering, Virginia Polytechnic Institute and State University, Blacksburg, VA, USA
[2]Dept. of Earth and Atmospheric Sciences, Saint Louis University, St. Louis, MO, USA
[3]Aerodyne Research Inc., Billerica, MA, USA
[4]Molina Center for Energy and the Environment, La Jolla, CA, USA
[5]Massachusetts Inst. of Technology, Cambridge, MA, USA
[6]Dept. of Chemistry, University of Arkansas, Little Rock, AR, USA

Received: 17 October 2007 – Published in Atmos. Chem. Phys. Discuss.: 9 November 2007
Revised: 19 May 2008 – Accepted: 19 May 2008 – Published: 23 June 2008

Abstract. As part of the Megacities Initiative: Local and Global Research Observations (MILAGRO) study in the Mexico City Metropolitan Area in March 2006, we measured particulate polycyclic aromatic hydrocarbons (PAHs) and other gaseous species and particulate properties, including light absorbing carbon or effective black carbon (BC), at six locations throughout the city. The measurements were intended to support the following objectives: to describe spatial and temporal patterns in PAH concentrations, to gain insight into sources and transformations of PAHs and BC, and to quantify the relationships between PAHs and other pollutants. Total particulate PAHs at the Instituto Mexicano del Petróleo (T0 supersite) located near downtown averaged 50 ng m^{-3}, and aerosol active surface area averaged 80 mm^2 m^{-3}. PAHs were also measured on board the Aerodyne Mobile Laboratory, which visited six sites encompassing a mixture of different land uses and a range of ages of air parcels transported from the city core. A combination of analyses of time series, back trajectories, concentration fields, pollutant ratios, and correlation coefficients supports the concept of T0 as an urban source site, T1 as a receptor site with strong local sources, Pedregal and PEMEX as intermediate sites, Pico Tres Padres as a vertical receptor site, and Santa Ana as a downwind receptor site. Weak intersite correlations suggest that local sources are important and variable and that exposure to PAHs and BC cannot be represented by a single regional-scale value. The relationships between PAHs and other pollutants suggest that a variety of sources and ages of particles are present. Among carbon monoxide, nitrogen oxides (NO_x), and carbon dioxide, particulate PAHs are most strongly correlated with NO_x. Mexico City's PAH/BC mass ratio of 0.01 is similar to that found on a freeway loop in the Los Angeles area and approximately 8–30 times higher than that found in other cities. Evidence also suggests that primary combustion particles are rapidly coated by secondary aerosol in Mexico City. If so, their optical properties may change, and the lifetime of PAHs may be prolonged if the coating protects them against photodegradation or heterogeneous reactions.

1 Introduction

The Mexico City Metropolitan Area (MCMA) is home to some of the highest measured concentrations of particulate polycyclic aromatic hydrocarbons (PAHs) in the world (Marr et al., 2004; Velasco et al., 2004). PAHs are a class of semi-volatile compounds that are formed during combustion. Many are known or suspected carcinogens. In their condensed form, they are associated mainly with fine particles (Eiguren-Fernandez et al., 2004; Miguel et al., 1998). PAH exposure has been associated with low birth weights (Choi et al., 2006; Tang et al., 2006) and respiratory symptoms in infants (Jedrychowski et al., 2005). Thus, the extremely high concentrations of PAHs in Mexico City may pose a serious health hazard and demand more complete information about

Correspondence to: L. C. Marr
(lmarr@vt.edu)

their spatial and temporal patterns, sources, and transformations in the atmosphere.

Like PAHs, light absorbing carbon, also known as black carbon (BC) or elemental carbon depending on the measurement technique, originates from combustion sources (Bond and Bergstrom, 2006). BC is important because of its suspected toxicity, at least in the form of diesel exhaust particulate matter, and its role in radiative forcing. Coating of BC by condensation of non light-absorbing material changes throughout the day in Mexico City and alters the particles' optical properties, typically enhancing absorption (Baumgardner et al., 2007).

Aerosol surface area has also been implicated as an indicator of the health impacts of particulate pollution. Toxicology studies suggest that the dose-response relationship is more closely tied to surface area than to mass, number, or size (Brown et al., 2001; Oberdorster, 2000; Stoeger et al., 2006; Tran et al., 2005). Especially for low-solubility particles, surface area may be a more appropriate measure of exposure (Maynard, 2003). Tandem measurements of both PAHs and surface area in laboratory and field experiments have been shown to discriminate between different types of combustion sources and to indicate the degree of particle aging (Bukowiecki et al., 2002; Burtscher et al., 1993; Marr et al., 2004; Ott and Siegmann, 2006; Siegmann et al., 1999).

In April 2003, a multi-national team of scientists conducted an intensive five-week field campaign in the Mexico City Metropolitan Area (MCMA-2003) to contribute to the understanding of air quality problems in megacities (Molina et al., 2007). Measurements of PAHs by three different techniques suggested that PAH concentrations on the surfaces of particles diminish rapidly during the mid-morning hours due to coating by secondary aerosol in the highly photochemically active environment of Mexico City (Dzepina et al., 2007; Marr et al., 2006). However, detailed PAH measurements in 2003 were limited to a single site, so the spatial and temporal variations in their concentrations, which are important from a standpoint of exposure and control, are not known.

In March 2006, an even larger field campaign in Mexico City took place to study air pollution in megacities not only at the local scale, but also at the regional and global scales. The Megacity Initiative: Local and Global Research Observations (MILAGRO) campaign consisted of four components whose goals ranged from providing the scientific basis for policies that would reduce pollutant levels in Mexico City itself to describing the long-range transport of pollution emitted by a megacity. As part of the MCMA-2006 ground-based component focusing on local impacts, we measured particulate PAHs, aerosol active surface area (AS), and other gaseous, particulate, and meteorological parameters at six locations throughout Mexico City. Measurements were situated at the Instituto Mexicano del Petróleo supersite near the city center and on board the Aerodyne Mobile Laboratory (AML). In addition to visiting the supersite, the AML also traveled to five other suburban, exurban, and rural sites (Fig. 1) that encompassed residential, industrial, commercial, undeveloped, and mixed settings.

The objective of this study is to describe the temporal and spatial variations in PAH, BC, and AS concentrations in Mexico City. Furthermore, we investigate the relationships between ambient PAHs and other pollutants to gain new knowledge about combustion particles' sources and evolution as they are transported throughout the megacity atmosphere. Transformations are important because they could affect the particles' toxicity, optical properties, and long-range transport impacts. We compare and contrast concentrations in fresh, mixed, and aged emissions by considering a busy downtown location, suburban areas, the city outskirts, and a mountaintop location at the edge of the city. The knowledge gained from the study will provide the scientific basis for the development of risk assessments for exposure to these pollutants in Mexico City and the crafting of control strategies to reduce their emissions and health impacts.

2 Experimental

2.1 Particle surface characterization

PAHs were measured using real-time sensors (EcoChem PAS 2000 CE) that photoionize particle-bound PAHs by exposing the aerosol to ultraviolet light at a wavelength of 254 nm, which is specific to condensed-phase PAHs. The current generated by the flow of charged particles is then measured. The analyzer produces a semi-quantitative estimate of total PAHs adsorbed on particles' surfaces at 10-s resolution with a detection limit of $1\,ng\,m^{-3}$. Although the technique does not provide speciation information, its strengths are its sensitivity and high time resolution, both of which are limitations of traditional filter-based methods. Our previous work has shown that the method is sensitive only to PAHs on the surfaces of particles and not those buried under other aerosol components (Marr et al., 2006), so measurements reported by the PAS are henceforth referred to as surface PAHs (SPAHs). In the Results section, we describe an approach for identifying measurements from the PAS that are not confounded by coating of the particles.

Aerosol active surface area, or Fuchs surface, is defined as that which is accessible to a molecule that might diffuse to a particle's surface. It was measured by diffusion charging (EcoChem DC 2000 CE). The DC analyzer generates a corona discharge which produces a cascade of electrons and ions that can attach to particles. As with the photoemission aerosol sensor for PAHs, a sensitive electrometer is then used to measure the current generated by the flow of charged particles. The analyzer reports active surface area of particles smaller than ~100 nm at 10-s resolution with a detection limit of $1\,mm^2\,m^{-3}$. The simultaneous measurement of particle surface properties with the PAS and DC sensors

Table 1. Mobile-laboratory-based SPAH statistics at different sites.

Site (Dates in March)	SPAH (ng m^{-3})	
	Average[a]	Maximum[b]
Pedregal (4th–6th)	7±16	143
Pico Tres Padres (7th–19th)	2±2	18
T1 (19th–22nd)	20±33	229
Santa Ana (22nd–25th)	4±4	29
PEMEX (25th–27th)	13±14	80
T0 (27th–31st)	114±121	604

[a] Mean ± one standard deviation of 1-min concentrations.
[b] Maximum of 1-min concentrations.

has been described as a technique for fingerprinting different types of combustion particles (Bukowiecki et al., 2002).

All the PAH and AS analyzers were factory calibrated three months prior to the field campaign. At the beginning of the field campaign, we co-located and cross-calibrated the instruments against each other while measuring ambient air in Mexico City and then applied the resulting correction factors to all data. To facilitate analysis using diagnostic ratios and multivariate statistics, we averaged all data over a common 2- or 10-min interval. Effective black carbon (BC), operationally defined as the light-absorbing component of particles, was measured at 2-min intervals using an aethalometer (Magee Scientific AE-3) at a wavelength of 880 nm.

2.2 Measurement sites

During the month-long MCMA field campaign in March 2006, we conducted measurements at the Instituto Mexicano del Petróleo (T0 supersite) and on board the Aerodyne Mobile Laboratory (AML), which visited six sites including the T0 supersite (Fig. 1). The supersite is located 10 km north of downtown Mexico City in the midst of a residential, commercial, and services area. It is surrounded by streets that are heavily traveled by light-duty vehicles and modern heavy-duty diesel buses. The PAH and AS analyzers were situated on a building rooftop, approximately 15 m above ground level. The nearest major roads were 40 m away. To fulfill the objective of observing aged plumes, we selected the location and timing of the AML visits (Table 1) on the basis of meteorological analyses that identified sites that were generally downwind of the urban plume on certain days (de Foy et al., 2008).

The AML was designed and built by Aerodyne Research Inc. (Kolb et al., 2004). It was equipped with a comprehensive suite of gas and particle analyzers that measure carbon monoxide (CO), carbon dioxide (CO_2), nitric oxide (NO), nitrogen dioxide (NO_2), total nitrogen oxides (NO_y), speciated volatile organic compounds (VOCs), SPAHs, AS, and BC, among others. The AML's PAH analyzer was identical to that used at T0. BC was measured using a Multi Angle Absorption Photometer (Thermo Electron Model 5012). During the field campaign, the AML drove to six sites and remained parked for 2–12 days at each location (Table 1). These sites encompassed varying environments, including residential, commercial, industrial, undeveloped, and mixed land use areas.

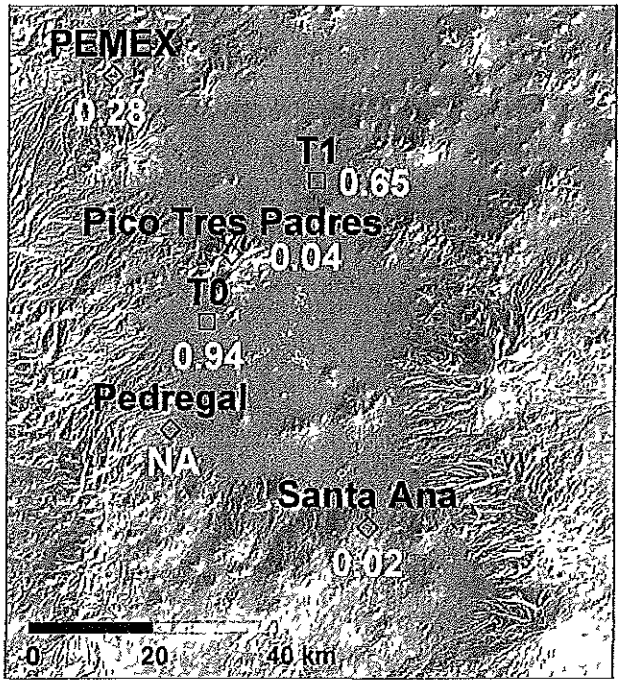

Fig. 1. Supersites (squares) and mobile laboratory measurement sites (diamonds) in the MCMA during the MILAGRO field campaign. The numbers in white are the linear correlation coefficients between SPAH measurements by the mobile laboratory and continuous measurements at T0.

The AML visited the T0 and T1 supersites, Pedregal, Pico Tres Padres, Santa Ana, and PEMEX (Fig. 1). Intended to represent a mixture of fresh emissions and the partially aged Mexico City plume as it drifts downwind under certain meteorological conditions, the T1 supersite is located at the Universidad Technológica de Tecámac ~30 km northeast of T0. Tecámac is a suburb in the State of Mexico and has a mixture of commercial and residential areas. The supersite is within 2 km of the town center, and the nearest road is several hundred meters away. Pedregal is located ~25 km southwest of downtown Mexico City in a suburban residential area whose roads are lightly traveled. The sampling site was the JFK Elementary School, which is also one of the routine air quality monitoring sites for the environmental agency of the Mexico City Federal District Government. Pico Tres Padres, the site of the main television transmitters for the MCMA, is an isolated mountain ~15 km north-northeast of T0 and 3000 m above sea-level, or ~800 m above the valley floor. A single, mostly unused road runs up the mountain, and the

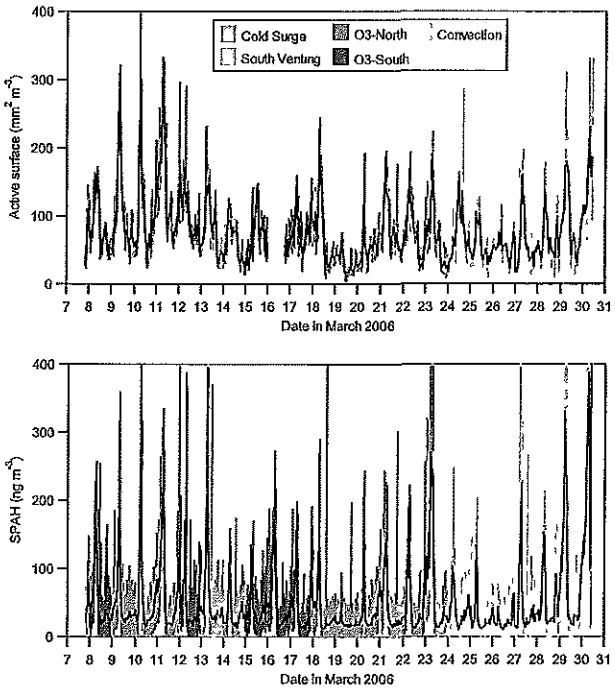

Fig. 2. AS and SPAH concentrations at T0 during the entire field campaign. Raw 1-min measurements are shown by the colored lines, where color indicates the wind transport episode, and 1-h averages are shown in black.

surrounding area is not well traveled. Santa Ana is located in a rural area at the southern tip of the city, ~40 km southeast of T0. Its roads are lightly traveled. Under certain meteorological conditions, Santa Ana represents an outflow receptor for air pollution coming from the city center. Located approximately 40 km north of the city, the PEMEX site is in a highly industrialized area closely situated to a major oil refinery (5 km away), cement plants, chemical factories, agricultural activities, and a power plant.

During the MCMA-2006 field campaign, air flow trajectories within the Mexico City basin and the fate of the urban plume were simulated, and five types of wind circulation patterns were identified (de Foy et al., 2005; de Foy et al., 2008): Cold Surge, South Venting, O_3-North, O_3-South, and Convection (North and South). During the 31 days of the MCMA-2006 field campaign, three were Cold Surge (14, 21, 23 March), eight were South Venting (1–7, 13 March), five were O_3-South (8, 12, 15–17 March), seven were O_3-North (9–11, 18–20, 22 March), and eight were Convection (24–31 March). The prevailing meteorological conditions can strongly influence ambient pollutant concentrations for given emission levels and also determine the regional impacts of the urban plume (de Foy et al., 2006).

To evaluate transport to sites and identify source areas, we carried out residence time analysis and concentration field analysis (Ashbaugh et al., 1985; de Foy et al., 2007; Seibert et al., 1994). Residence time analysis, calculated by summing back trajectories over a grid, produces a time exposure image of the back trajectories for a site, i.e. where the wind was coming from, over multiple hours. Concentration field analysis is the product of residence time analysis and pollutant concentrations at the receptor site each hour. The resulting concentration fields indicate the source areas or transport paths associated with high pollutant levels at a receptor site.

3 Results

Figure 2 displays time series of AS and total particulate SPAH concentrations at the T0 supersite. The raw 1-min measurements are shown by colored lines, whose color indicates the wind transport episode defined for each day. The black lines represent 1-h averages and are intended to highlight diurnal patterns in the measurements. The highest AS concentrations occurred on O_3-North and Convection days, while the highest average SPAH concentrations occurred on Convection days, which are defined by weak winds aloft (de Foy et al., 2008).

Strong diurnal patterns are evident in both AS and SPAHs. AS concentrations at T0 averaged 80 $mm^2\,m^{-3}$ during the campaign, with a maximum 10-s value of 760 $mm^2\,m^{-3}$ on 30 March at 09:58. Typically, concentrations rose above 100 $mm^2\,m^{-3}$ between 06:30–08:30 and then decreased throughout the remainder of the morning and afternoon to ~50 $mm^2\,m^{-3}$. SPAH concentrations averaged 50 $ng\,m^{-3}$ throughout the campaign with a maximum value of 3660 $ng\,m^{-3}$ on 30 March at 10:02, within minutes of the maximum AS observation. During the morning rush hour, SPAH concentrations generally rose to a maximum of ~250 $ng\,m^{-3}$ between 06:30–08:30 and then decreased throughout the remainder of the morning and afternoon to ~20 $ng\,m^{-3}$. The daily minima in AS were more variable than in SPAHs. Overnight concentrations rose as high as 75 $ng\,m^3$. The daily maxima were nearly twice as high as observed at a site 17 km to the southeast in 2003 (Marr et al., 2006) and 1.5 times as high as observed at a site 13 km to the southwest in 2003 and 2005 (Baumgardner et al., 2007). In all three studies, the SPAH concentration measured by aerosol photoionization falls off more rapidly between 08:00–10:00 than do concentrations of other primary pollutants.

Table 1 summarizes SPAH concentrations at each site visited by the AML in chronological order. The highest average SPAH concentration was observed at T0 and the lowest at Pico Tres Padres and Santa Ana, the mountaintop and southern outflow sites, respectively. The maximum SPAH concentration occurred at T0. Figure 3 shows SPAH time series at each site. At Pedregal, SPAH concentrations were highest between 06:00–08:00 on Monday 6 March. They were slightly elevated in the hours before midnight on the evening of Saturday 4 March. These periods probably correspond

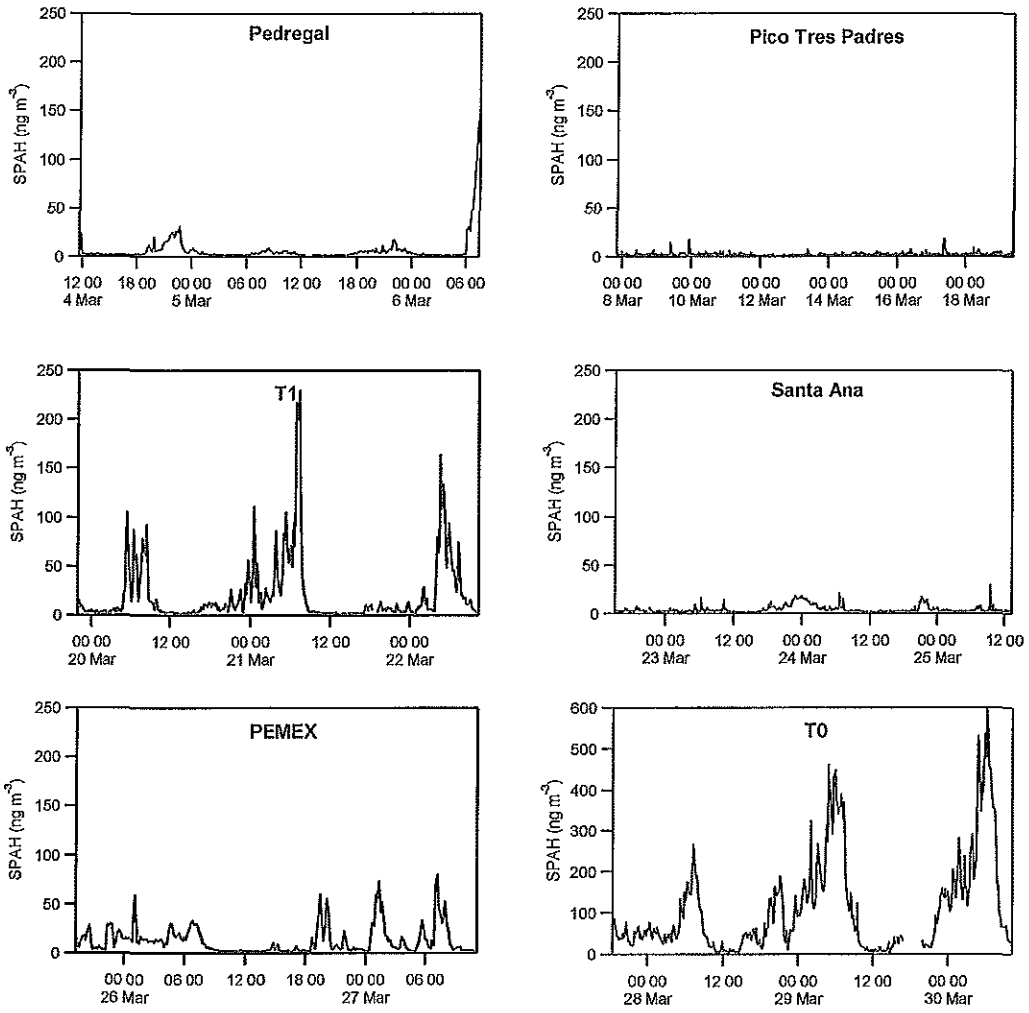

Fig. 3. SPAH concentrations (10-min averages) at sites visited by the AML. The y-axis maximum is larger in the T0 panel.

to the times of heaviest traffic and lowest boundary layer height. At Pico Tres Padres, SPAH concentrations remained below 10 ng m^{-3}, even though fine particulate mass concentrations ($PM_{2.5}$), not shown, routinely rose at approximately 10:00 each day, as the boundary layer lifted up past the site. At T1, SPAH concentrations increased to 100–200 ng m^{-3} in the morning hours, well before 06:00.

Santa Ana lies at the southern edge of the basin, and here SPAH concentrations were always less than 30 ng m^{-3}. Cold Surge conditions, in which the wind flushes from the center of the basin toward the south and past the site late into the evening (de Foy et al., 2008), prevailed on 23 March and may have contributed to the increase in SPAH concentrations centered around midnight of the 24th. At PEMEX, concentrations did not exceed 80 ng m^{-3} and the temporal patterns were irregular. The AML's observation period at T0 coincided with the highest observed concentrations of the field campaign.

The simultaneous measurement of SPAHs at T0 and other sites allows examination of their spatial variability in the MCMA. Figure 1 presents the Pearson correlation coefficients of 10-min SPAH concentrations at various sites visited by the AML against those measured continuously at the T0 supersite during periods of simultaneous measurements. A correlation factor could not be calculated for Pedregal because monitoring at T0 had not yet begun. Of course, the correlation was strongest when the AML was parked at T0. It was moderate at T1 and poor at all other sites. Correlations of BC between T0 and other sites were similar: −0.01 at Pico Tres Padres, 0.70 at T1, −0.06 at Santa Ana, 0.31 at PEMEX, and 0.95 at T0.

Next, we examine transport within the basin. Figure 4 shows the residence time and BC concentration field analyses for T0 during 27–31 March, which were all Convection days, and T1 during 19–22 March, which were O_3-North and Cold Surge days. We chose to use BC as a proxy for PAHs

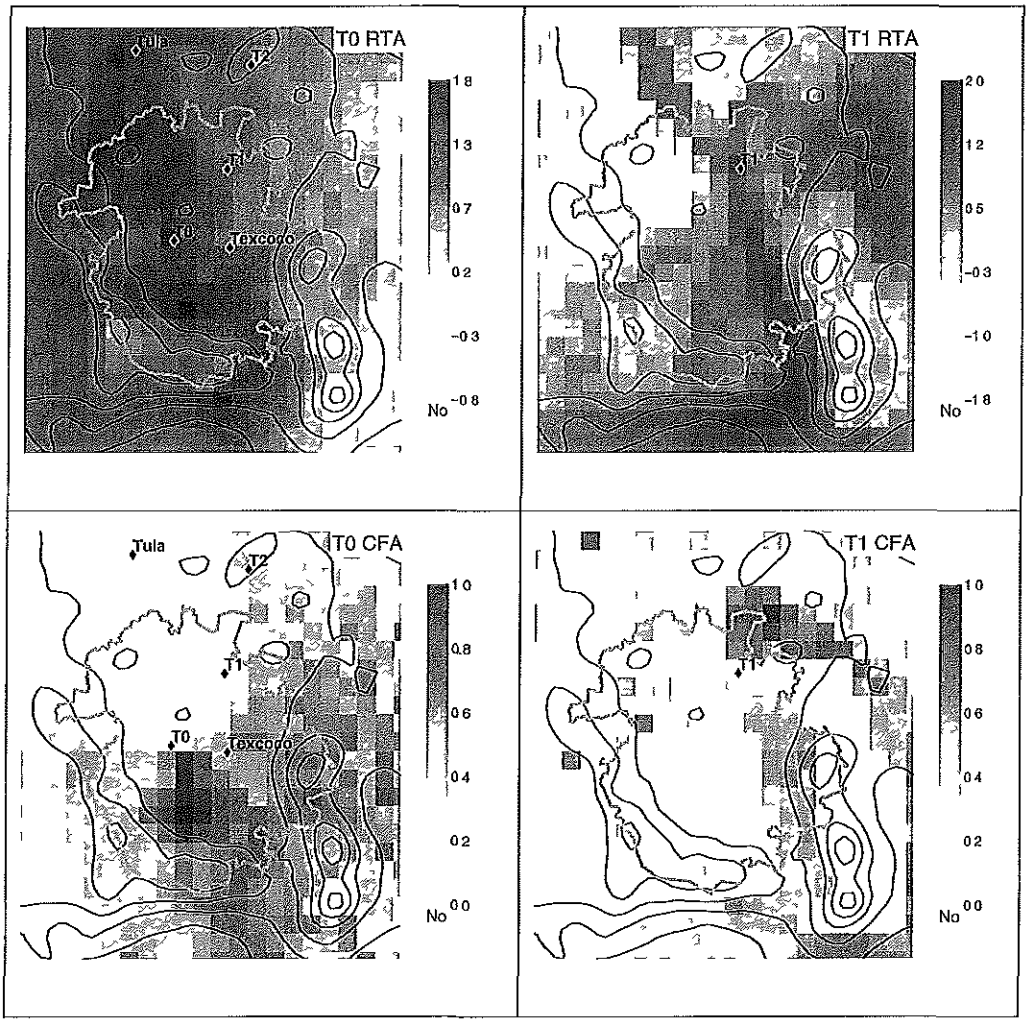

Fig. 4. Residence time (top) and BC concentration field (bottom) analyses at T0 on 27–31 March (left) and T1 on 19–22 March (right) Topography is indicated by black lines and the MCMA border by the pink line.

because SPAHs can be diminished by coating of the aerosol, as described later in the text. In the residence time analysis, the magnitude in each grid cell represents the probability of a back trajectory passing through the cell relative to the total time interval of the trajectory. In the concentration field analysis, areas with high values are the result of back trajectories associated with high concentrations at the receptor site, whereas low values result from back trajectories associated with low concentrations. For both analyses, the values are normalized, with the maximum color value corresponding to the 90th percentile for that grid. The residence time analyses are plotted on a log scale, as they decrease rapidly away from the receptor site; and the concentration field analyses are plotted on a linear scale.

While the residence time analysis shows that air parcels arriving at T0 are coming from all directions but less from the east, the concentration field analysis shows that high BC is associated with transport from the south, the center of the MCMA. For T1, the residence time analysis shows three preferred directions: northwest, east and south (gap flow). However, the concentration field analysis shows that high BC is not associated with transport from the gap flow, but rather with transport from the northeast, where the highway to the MCMA is located. The gap flow is strong and clean. For Pedregal, PEMEX, and Santa Ana, the residence time analyses agree with the wind transport episodes on those days; and the concentration field analyses all show that high BC is associated with transport from the central urban area of the MCMA. The results for Pico Tres Padres–transport from all directions and high BC associated with the urban area–are more uncertain because of the challenges in obtaining accurate trajectories on this hilltop site.

The relationship between SPAHs and AS has been shown to be related to the source type and aging of the particles (Bukowiecki et al., 2002; Marr et al., 2004; Siegmann et al., 1999). Figure 5 illustrates the relationship between SPAH

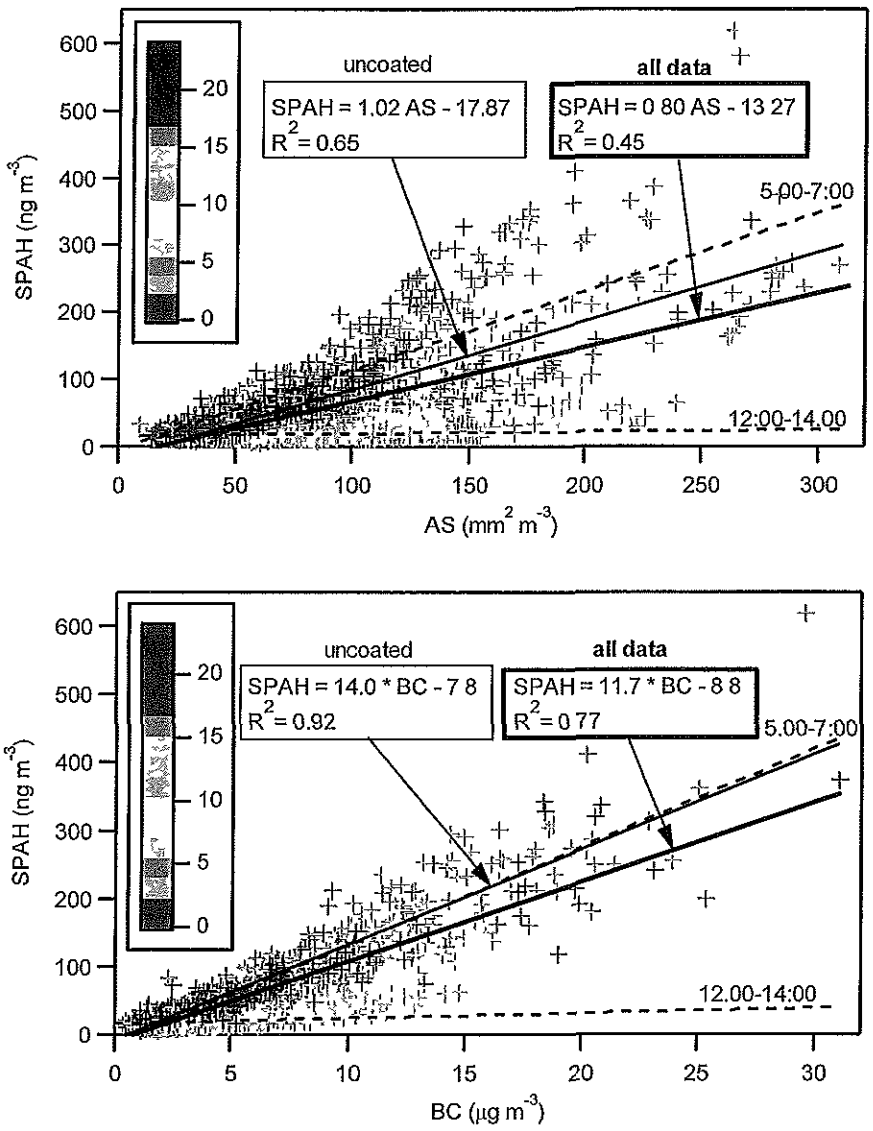

Fig. 5. SPAH v. AS and SPAH v. BC concentrations at T0 colored by hour. The dark solid line is the linear regression for all times, and the lighter solid line is the regression for uncoated particles. The dotted lines labeled 05:00–07:00 and 12:00–14:00 are the regressions for a subset of data specific to these time periods. The equations of these lines are given in the text.

and AS (10-min averages) at T0. The color indicates the time of day of each measurement. There is considerable scatter in the data; the correlation involving all data is fair, with R^2=0.45. For the subset of data between 05:00–07:00, just before sunrise, the equation of the line is SPAH=1.17×AS–3.20 with R^2=0.58. For the subset of data between 12:00–14:00, the equation of the line is SPAH=0.03×AS+16.33 with R^2=0.01. Figure 5 shows that higher SPAH/AS ratios, i.e. those points falling above the regression line, and those with high absolute SPAH and AS values, tend to occur during the early morning hours. The slope of the regression line is 39 times higher in the morning compared to the afternoon. The regression line for the subset of data representing particles that have not been coated by secondary aerosol (described below) falls between the lines for all data and the subset between 05:00–07:00; of the four lines shown, it has the highest R^2. There is no clear relationship between the ratio and wind transport episode.

Figure 5 also shows SPAHs versus BC at T0, classified by time of day. PAHs and BC are expected to be correlated since both originate from combustion sources. For all times, the correlation between SPAHs and BC is stronger (R^2=0.77) than between SPAHs and AS, and the slope of the line, 11.7±0.1 ng μg^{-1}, indicates that SPAHs are 1% of BC by mass. As with SPAH/AS, higher SPAH/BC ratios tend to occur during the morning rush hour period.

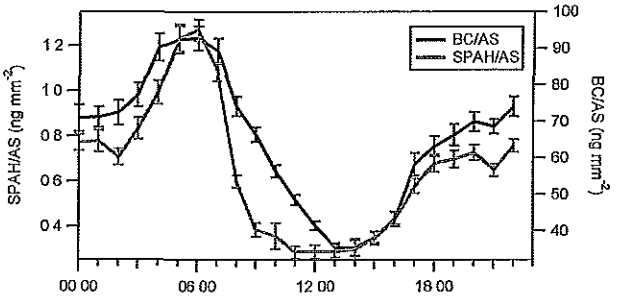

Fig. 6. Weekday average diurnal patterns in SPAH/AS and BC/AS.

As the day progresses, SPAH/BC ratios tend to decrease and are lowest between 12:00–18:00. The equation of the regression line between 05:00–07:00 is SPAH=14.4×BC–13.8 with R^2=0.82, where SPAH is in ng m^{-3} and BC is in μg m^{-3}. Later in the afternoon, between 12:00–14:00, the relationship is SPAH=0.76×BC+16.2 with R^2=0.02. The slope is 19 times higher in the morning. The regression line for the subset of data representing particles that have not been coated by secondary aerosol is similar to that for the hours of 05:00–07:00; of the four lines shown, it has the highest R^2.

Figure 6 shows average weekday diurnal patterns of the ratios SPAH/AS and BC/AS. The latter is an indicator of the fraction of particles that are of combustion origin at any time (Burtscher et al., 1993), as BC is expected to be minimally reactive. The BC/AS ratio peaks around the morning rush hour and then falls off steadily throughout the late morning and early afternoon. During this period, growth of secondary aerosol in Mexico City is considerable (Molina et al., 2007; Salcedo et al., 2006; Volkamer et al., 2006) and contributes to AS but not BC. Even though both PAHs and BC are of combustion origin, their ratios to AS diverge between 07:00–12:00, with SPAH/AS falling off more rapidly than BC/AS. This observation is probably due to physical coating of the particles by secondary aerosol, which shields the PAHs from detection by the photoemission method (Marr et al., 2006).

Pollutant ratios can provide insight into sources of emissions, chemical transformations, and spatial and temporal variability in concentrations. Because of the measurement artifact associated with the photoemission method, i.e. that it does not detect PAHs that are buried under other aerosol components, we must screen out such measurements when calculating ratios. To do so, we assume that the ratio of total PAHs to BC should be approximately constant. Based on the regression results shown in Fig. 5, we examine the time series of (SPAH + 10) / BC, with SPAH in ng m^{-3} and BC in μg m^{-3}. Excluding the period corresponding to the most active photochemistry between 08:00–13:00 when primary combustion particles are most likely to be coated by secondary aerosol, the diurnal average is 13.6±0.6 ng μg^{-1}. The coefficient of variation is only 4.4%. Between 08:00–13:00, the value is significantly lower, ranging from 7.2 to 10.2 ng μg^{-1}. We therefore apply the criterion (SPAH+10) / BC>11 ng μg^{-1} to identify data points representing uncoated particles.

Table 2 shows the slope and standard error of the least-squares linear regression and correlation coefficient (R^2) between SPAHs and carbon monoxide (CO), total nitrogen oxides (NO_y), carbon dioxide (CO_2), and BC measured by the AML. The table presents results calculated using all SPAH data and only uncoated SPAH data, screened using the criterion previously described. In most cases, except for Pico Tres Padres, focusing on fresh SPAH produces higher slopes and stronger correlations. Measurements at Pedregal took place over a weekend, so results from this site may not be representative.

At the remaining sites (T1, Santa Ana, PEMEX, and T0), the strongest correlations and highest slopes tend to be observed at the more urbanized locations, T0 and T1. The different slopes are likely to be indicative of a different mix of sources at each site. Fresh SPAHs are reasonably well correlated with CO, with an R^2 of 0.72 to 0.93. The SPAH/CO slope is similar at T1, PEMEX, and T0 and an order of magnitude lower at Santa Ana. Fresh SPAHs are even more strongly correlated with NO_y; R^2 values range from 0.86 to 0.96 at the last four sites shown in Table 2. The SPAH/NO_y and SPAH/CO_2 slopes are highest at T1 and T0, moderate at PEMEX, and lowest at Santa Ana. The regressions between SPAHs and true NO_x are not significantly different from those with NO_y, so henceforth, we will refer to the relationship as with NO_x. This notation will facilitate comparison with other studies, the majority of which use chemiluminescence and report results as NO_x. When all data are considered, SPAH/BC ratios are highest, approximately 10 ng μg^{-1} at Pedregal, T1, and T0; and the correlations are strongest at these three sites and PEMEX. The correlations improve considerably for uncoated particles.

Table 3 contrasts SPAH/BC ratios at T0 in Mexico City with those measured in three other cities, where the same aerosol photoionization method was used to measure SPAHs. The mass ratio of SPAHs to BC in Mexico City is similar to that measured along a freeway loop in the Los Angeles area and approximately 8–30 times higher than in diluted vehicle exhaust in Ogden, Utah and ambient air in Fresno, California. The correlation factors between SPAHs and BC are similar in all cities. Limiting the analysis to uncoated PAHs in Mexico City does not have a large effect on the ratio.

4 Discussion

4.1 PAH and AS concentrations, sources, and aging

PAH concentrations may vary considerably between cities due to differences in emission sources and meteorological conditions. Mexico City's SPAH concentrations, a lower limit of total particulate PAHs, are substantially higher than those measured in other large cities. Eiguren-Fernandez

Table 2. Least-squares linear regression slope±standard error and R^2 between SPAHs and gaseous pollutants for all SPAH data (top set of numbers) and uncoated particles only (bottom set of numbers).

Site	SPAH/CO slope ($ng\,m^{-3}ppb^{-1}$)	R^2	SPAH/NO_y[a] slope ($ng\,m^{-3}ppb^{-1}$)	R^2	SPAH/CO_2 slope ($ng\,m^{-3}ppm^{-1}$)	R^2	SPAH/BC slope ($ng\,\mu g^{-3}$)	R^2
Pedregal	0.0208±0.0009	0.69	0.12±0.02	0.18	0.61±0.04	0.51	10.4±0.5	0.59
	0.0285±0.0005	0.98	0.2±0.1	0.15	0.94±0.04	0.88	15.7±0.3	0.09
Pico Tres Padres	0.0027±0.0002	0.17	0.060±0.002	0.26	0.121±0.007	0.16	0.077±0.008	0.06
	0.003±0.007	0.04	0.04±0.01	0.03	0.03±0.01	0.02	0.6±0.1	0.04
T1	0.090±0.003	0.77	1.10±0.02	0.87	1.4±0.2	0.38	10.0±0.2	0.88
	0.087±0.005	0.93	1.20±0.04	0.96	4±2	0.72	11.32±0.09	1.00
Santa Ana	0.0122±0.0007	0.44	0.22±0.02	0.34	0.29±0.02	0.33	1.8±0.2	0.17
	0.0171±0.0007	0.80	0.34±0.01	0.86	0.46±0.02	0.68	8.7±0.3	0.87
PEMEX	0.047±0.004	0.34	0.62±0.02	0.86	1.1±0.1	0.37	6.5±0.2	0.77
	0.13±0.01	0.75	0.79±0.02	0.95	3.1±0.2	0.87	11.2±0.3	0.96
T0	0.066±0.004	0.47	1.19±0.03	0.77	3.3±0.1	0.70	10.0±0.2	0.85
	0.096±0.005	0.72	1.45±0.03	0.95	4.3±0.1	0.87	11.5±0.2	0.97

[a] NO_y is total nitrogen oxides measured by chemiluminescence with a molybdenum converter. The ratios are not significantly different when true $NO_x = NO + NO_2$ is used instead.

et al. (2004) measured total particulate PAH concentrations of $0.5\,ng\,m^{-3}$ and $2\,ng\,m^{-3}$ in rural and urban areas of Los Angeles, respectively. In contrast, concentrations in rural and urban areas of Mexico City are nearly 25 times higher. In Hong Kong, particulate PAH concentrations ranged from $0.41\,ng\,m^{-3}$ to $48\,ng\,m^{-3}$ in rural to urban areas (Zheng and Fang, 2000). These values compare more closely with Mexico City; however, PAH concentrations in Mexico City are still higher. PAHs have also been measured in different environments of Greece (Mantis et al., 2005), where total particulate concentrations ranged from $2\,ng\,m^{-3}$ to $52\,ng\,m^{-3}$ in rural to urban areas. Again, these values compare more closely with the results seen in Mexico City, but the values for Mexico City are higher yet.

The database of measurements of ambient AS in other cities is considerably smaller. Mexico City's mean AS concentration of $80\,mm^2\,m^{-3}$ at T0 is comparable to that found in Los Angeles, where mean concentrations of 69 and $53\,mm^2\,m^{-3}$ were recorded at two ambient locations (Ntziachristos et al., 2007). AS in a residential area of Redwood City ranged between 40–300 $mm^2\,m^{-3}$, with the higher concentrations attributed to wood burning and fireplaces in the neighborhood (Ott and Siegmann, 2006). It appears that while particulate PAH loading in Mexico City is higher than in many other cities, its aerosol surface area loading is not comparatively extraordinary.

Vehicular traffic has been recognized as the major contributor to PAH emissions in urban areas (Kittleson et al., 2004; Lee et al., 1995), and therefore it is not surprising that the highest average SPAH and AS concentrations are found at T0, where traffic is heaviest. The timing of SPAH and AS peaks at the more urban locations corresponds to periods of rush hour traffic. Burtscher et al. (1993) also found the highest PAH and AS values in Zurich to occur during rush hour and ascribed them to motor vehicles.

Table 3. Total particulate SPAH/BC mass ratios in Mexico City compared to other locations.

Location	SPAH/BC (mass ratio)	R^2	Reference
Mexico City (T0)			
All data	1.2×10^{-2}	0.77	This study
Uncoated SPAH	1.4×10^{-2}	0.93	This study
Ogden, UT[a]	1.25×10^{-3}	0.75	(Arnott et al., 2005)
Fresno, CA (Winter)	1.2×10^{-3}	0.78	(Arnott et al., 2005)
Fresno, CA (Summer)	3.3×10^{-4}	0.75	(Arnott et al., 2005)
Los Angeles, CA	1×10^{-2}	0.82	(Westerdahl et al., 2005)

[a] Diluted vehicle exhaust, not ambient air.

At some locations, including Pedregal, T1, and PEMEX, increases in SPAH concentrations occur at nighttime between 23:00 and 04:00 (Fig. 3). The increase in SPAHs may be due to transport of particles emitted earlier in the evening during times of high traffic density, or it may indicate the presence of other nighttime sources. Speciation measurements in 2003 suggest that wood and trash burning contribute to PAHs observed at night (Marr et al., 2006). The impact of emissions at nighttime can be magnified because of stable atmospheric conditions. Some industries are thought to switch to using dirtier fuels and processes at night, when enforcement of regulations is less likely. Furthermore, at T1 during the first two weeks of the field campaign, Doran et al. (2007) observed increased organic and elemental carbon during nighttime hours with peak values attained in the morning hours near sunrise.

A similar pattern occurred at T1 on 21 March. The temporal variations imply that at night a buildup of pollution from nearby urban sources is occurring, followed by a subsequent dilution during the next morning as the boundary layer expands.

Spatial and temporal patterns in concentrations indicate not only potential sources of PAHs but also the degree of atmospheric processing the particles undergo. As emissions are transported, they are subject to dilution and other transformations. This behavior is supported by Fig. 3, which shows that in general, higher SPAH concentrations occur at T0 and PEMEX, which are dominated by fresh emissions. Lower concentrations occur at Pico Tres Padres and Santa Ana, which are receptor sites where emissions have undergone dilution and aging by the time they arrive. Intermediate concentrations occur at T1 and Pedregal, which lie between the two extremes.

SPAHs as detected by the surface-specific photoemission method may diminish due to coating by secondary aerosol, and Figs. 4 and 5 support this hypothesis. PAH loss by photodegradation, heterogeneous reactions, or volatilization is less likely because measurements in 2003 showed that even when surface-bound PAHs diminish, PAHs are still detected by aerosol mass spectrometry, a method that is able to detect them anywhere in the particles, not just on the surface (Marr et al., 2006). An increase in secondary aerosol in the mid-morning hours contributes to aerosol surface area and is expected to cause a reduction in both SPAH/AS and BC/AS ratios, but it does not explain the decrease in SPAH/BC ratio (Fig. 5) or the divergence between the two (Fig. 6). Studies using a variety of techniques have shown that primary combustion particles are rapidly coated by secondary aerosol within a few hours in Mexico City (Baumgardner et al., 2007; Dzepina et al., 2007; Johnson et al., 2005; Marr et al., 2006; Salcedo et al., 2006). This finding could explain the temporal patterns observed in SPAH/AS and SPAH/BC ratios because secondary aerosol formation would not increase the total mass of PAHs but could contribute to it being coated. After condensation of secondary aerosol on primary combustion particles, the PAHs on the surfaces of primary particles would no longer be detectable by the photoionization method, but BC would remain detectable by the light absorption method. In contrast, the ratios of SPAH/AS and SPAH/BC were found to be much more constant throughout the day at a port south of Los Angeles (Polidori et al., 2008). The difference may be due to the upwind location of this site, which experiences relatively clean inflow from the Pacific Ocean and thus less secondary aerosol formation.

Pico Tres Padres is of special interest because it sits 800 m above the valley floor, and during the morning hours, it is above the mixing (boundary) layer that contains freshly emitted pollutants. Its diurnal patterns of particulate mass loading differ from those at sites on the valley floor. $PM_{2.5}$ concentrations increase around 10:00 each day, coinciding with the rising of the boundary layer, verified visually, up to the AML's location on the mountain. Particle surface PAH concentrations, however, do not rise concomitantly, further supporting the proposition that initially fresh combustion emissions from the valley below have undergone transformations that inhibit the detection of surface-bound PAHs.

The rapid coating of primary combustion particles in the megacity environment could have important implications for PAH longevity in the atmosphere. Experiments have shown that particulate PAHs can decay in the presence of sunlight (Kamens et al., 1988) and can undergo heterogeneous reactions with the hydroxyl radical, ozone, and NO_x (Esteve et al., 2006; Kwamena et al., 2007; Molina et al., 2004). However, if the PAHs are coated by secondary aerosol, they may be less susceptible to degradation and may persist long enough to be transported to remote areas.

4.2 Intersite correlations of SPAH and BC

Figure 1 shows that SPAH intersite correlation coefficients calculated for other sites versus T0 are quite weak, except for T1. It is possible that the spatial correlations for aged PAHs might be stronger, but the intersite correlations for BC, which serves as a proxy for total particulate PAHs, are similar to those for SPAH. While strong intersite correlations would indicate spatially uniform emission patterns and sources and regional-scale mixing of pollutants, the results for Mexico City suggest that PAHs vary considerably in space. Concentrations at individual sites are largely independent of one another and are instead dominated by local sources, and/or fresh combustion particles have been sufficiently transformed that surface-bound PAHs are no longer present by the time the particles reach other sites. This conclusion is further supported by the lack of a consistent relationship between SPAH and AS concentrations and wind transport episodes (Fig. 2); regional-scale meteorological patterns do not have a strong effect on concentrations.

Mantis et al. (2005) and Siegmann et al. (1999) report generally higher correlation coefficients for their intersite comparisons during studies of PAHs in Greece and Switzerland, respectively. The study in the Greater Athens area of Greece found an intersite correlation of r=0.61 between two urban locations, r=0.76 between an urban location and a background location, and r=0.57 between an urban location and a mixed-urban industrial location. An important implication for risk assessment studies is that a single monitoring site in Mexico City will not adequately represent the population's exposure.

4.3 Correlation of SPAHs with AS, NO_x, CO_2, CO, and BC

The ratio of SPAH to AS concentrations has been described as a fingerprint for different types of combustion particles (Bukowiecki et al., 2002; Matter et al., 1999; Siegmann et al., 1999). The relationship between these parameters provides

a qualitative means of identifying different sources and describing the physical and chemical properties of particles. In contrast to previous studies which have shown tighter relationships between SPAHs and AS for specific sources such as diesel exhaust, roadway vehicle emissions, candles, fires, and cigarettes (Bukowiecki et al., 2002; Marr et al., 2004; Siegmann et al., 1999), the relationship shown in Fig. 5 contains significantly more scatter. For a single source, the relationship between SPAHs and AS is expected to be linear with a characteristic slope. The spread of the data indicates that the aerosol represents a mixture of different sources and particles of different ages. Ambient measurements in complex environments are expected to produce such results.

The stronger correlation of SPAHs with NO_x and BC, versus with CO and CO_2 (Table 2), likely reflects the importance of diesel engines as sources of both PAH and NO_x emissions (Harley et al., 2005; Marr et al., 1999). CO is emitted mainly by gasoline-powered vehicles, which emit far lower particulate PAHs than do diesel engines (Marr et al., 2002). Weak positive correlations between PAHs and NO_x have also been reported in Brisbane, Australia (Muller et al., 1998).

The ratios should be higher and correlations stronger in source areas and receptor sites with a large impact of local sources, and the results shown in Table 2 support this hypothesis. The highest ratios of SPAH to the four other pollutants and strongest correlations occur at T1 and T0. In MILAGRO, T1 is generally considered a receptor site, but concentration field analysis (Fig. 4) shows that it has strong local sources; and T0 is the closest site to the center of the MCMA. Values are intermediate at Pedregal and PEMEX, both of which are located toward the outskirts of the MCMA. Values are lowest at Pico Tres Padres and Santa Ana, the first of which can be thought of as a vertically downwind receptor site and the second of which is an outflow point of the MCMA basin.

Pollutant ratios can be useful for estimating emissions and for describing the evolution of source strengths over decadal time scales (Marr et al., 2002). The mass ratio of particulate SPAH/NO_x measured along roads during the MCMA-2003 field campaign was $4.7\pm5.9\times10^{-4}$ (Jiang et al., 2005). During the MCMA-2006 field campaign, this ratio was $1.09\pm0.05\,ng\,m^{-3}\,ppb^{-1}$, or $7.7\pm0.4\times10^{-4}$ in mass terms, at T0 (and similar at the other urbanized sites T1 and PEMEX). The ratio in 2006 has not changed significantly from that measured in 2003, within the precision of the methods used.

While the mass ratio of SPAH/BC at T0 (Table 3) is similar to that observed along a freeway loop in the Los Angeles area (Westerdahl et al., 2005), lower ratios were found in ambient air in Fresno, California and diluted vehicle exhaust in Ogden, Utah (Arnott et al., 2005). The similarity in SPAH/BC between T0 and the Los Angeles freeway may indicate that vehicular sources are similar in the two locations and dominate measurements at T0 or alternatively, if particles have aged slightly by the time they reach the elevated T0 measurement site, may indicate that the SPAH/BC ratio in fresh emissions in Mexico City is actually higher than in Los Angeles. The ambient ratio in Mexico City is nearly 10 times higher than in Fresno. Direct measurements of exhaust are needed to determine whether particulate emissions from Mexico City's vehicles contain higher amounts of PAHs than in the U.S. If so, PAH emissions could be minimized by reducing the PAH content of fuels (Marr et al., 1999).

5 Conclusions

It is apparent that PAH pollution is a major problem in the more heavily trafficked areas of the MCMA. SPAH concentrations near downtown exhibit a consistent diurnal pattern and routinely exceed $200\,ng\,m^{-3}$ during the morning rush hour. Weak correlations between SPAHs and AS are indicative of the wide variety of sources and ages of particles present in Mexico City. SPAH concentrations are poorly correlated in space, and therefore PAHs should not be treated as a regional-scale pollutant. An important implication of this result is that for risk assessment studies, a single monitoring site will not adequately represent an individual's exposure. The stronger correlation of SPAHs with NO_x, rather than with CO and CO_2, probably reflects the importance of diesel engines as sources of both PAH and NO_x emissions. Mexico City's SPAH/BC ratio is similar to that found along freeways in Los Angeles and 8–30 times higher than that found in two other cities. Aging of primary combustion particles by coating with secondary aerosol appears to result in a decrease in surface SPAH/AS and SPAH/BC ratios over the course of the day and may prolong the lifetime of PAHs in the atmosphere. The photoemission method used in this study to measure PAHs detects only those on particles' surfaces. This specificity can be considered a strength if PAHs' toxicity is mediated via interactions with only the outer surfaces of particles but a weakness if one is attempting to characterize total particulate PAH concentrations. Measurements using other techniques such as aerosol mass spectrometry may be more representative of the total, although photoemission is a more sensitive technique at present.

Acknowledgements. We thank C. Mazzoleni, E. Deustua, X. Yao, M. Cubison, and M. Alexander for their support; the managers of the supersites (T0 and T1) for the use of their facilities; and C. Kolb for the use of the Aerodyne Mobile Laboratory. Financial support was provided by the U.S. National Science Foundation (ATM-0528227) and the U.S. Department of Energy (DE-FG02-05ER63980). This study was also supported by the Molina Center for Strategic Studies in Energy and the Environment. D. Thornhill is supported by a Fulbright Fellowship.

Edited by: S. Madronich

References

Ashbaugh, L. L., Malm, W. C., and Sadeh, W. Z.: A residence time probability analysis of sulfur concentrations at Grand Canyon National Park, Atmos. Environ., 19, 1263–1270, 1985.

Arnott, W. P., Zielinska, B., Rogers, C. F., Sagebiel, J., Park, K. H., Chow, J., Moosmuller, H., Watson, J. G., Kelly, K., Wagner, D., Sarofim, A., Lighty, J., and Palmer, G.: Evaluation of 1047-nm photoacoustic instruments and photoelectric aerosol sensors in source-sampling of black carbon aerosol and particle-bound PAHs from gasoline and diesel powered vehicles, Environ. Sci. Technol., 39, 5398–5406, 2005.

Baumgardner, D., Kok, G. L., and Raga, G. B.: On the diurnal variability of particle properties related to light absorbing carbon in Mexico City, Atmos. Chem. Phys., 7, 2517–2526, 2007, http://www.atmos-chem-phys.net/7/2517/2007/.

Bond, T. C. and Bergstrom, R. W.: Light absorption by carbonaceous particles: an investigative review, Aerosol Sci. Technol., 40, 27–67, 2006

Brown, D. M., Wilson, M. R., MacNee, W., Stone, V., and Donaldson, K.: Size-dependent proinflammatory effects of ultrafine polystyrene particles: a role for surface area and oxidative stress in the enhanced activity of ultrafines, Toxicol. Appl. Pharmacol., 175, 191–199, 2001.

Bukowiecki, N., Kittleson, D. B., Watts, W. F., Burtscher, H., Weingartner, E., and Baltensperger, U.: Real-time characterization of ultrafine and accumulation mode particles in ambient combustion aerosols, J. Aerosol Sci., 33, 1139–1154, 2002.

Burtscher, H., Leonardi, A., Steiner, D., Baltensperger, U., and Weber, A.: Aging of combustion particles in the atmosphere – results from a field study in Zurich, Water Air Soil Poll., 68, 137–147, 1993.

Choi, H., Jedrychowski, W., Spengler, J., Camann, D. E., Whyatt, R. M., Rauh, V., Tsai, W., and Perera, F. P.: International studies of prenatal exposure to polycyclic aromatic hydrocarbons and fetal growth, Environ. Health Perspectives, 114, 1744–1750, 2006.

de Foy, B., Caetano, E., Magaña, V., Zitacuaro, A., Cárdenas, B., Retama, A., Ramos, R., Molina, L. T., and Molina, M. J.: Mexico City basin wind circulation during the MCMA-2003 field campaign, Atmos. Chem. Phys., 5, 2267–2288, 2005, http://www.atmos-chem-phys.net/5/2267/2005/.

de Foy, B., Varela, J. R., Molina, L. T., and Molina, M. J.: Rapid ventilation of the Mexico City basin and regional fate of the urban plume, Atmos. Chem. Phys., 6, 2321–2335, 2006, http://www.atmos-chem-phys.net/6/2321/2006/.

de Foy, B., Lei, W., Zavala, M., Volkamer, R., Samuelsson, J., Mellqvist, J., Galle, B., Martinez, A.-P., Grutter, M., Retama, A., and Molina, L. T.: Modelling constraints on the emission inventory and on vertical dispersion for CO and SO2 in the Mexico City Metropolitan Area using Solar FTIR and zenith sky UV spectroscopy, Atmos. Chem. Phys., 7, 781–801, 2007, http://www.atmos-chem-phys.net/7/781/2007/.

de Foy, B., Fast, J. D., Paech, S. J., Phillips, D., Walters, J. T., Coulter, R. L., Martin, T. J., Pekour, M. S., Shaw, W. J., Kastendeuch, P. P., Marley, N. A., Retama, A., and Molina, L. T.: Basin-scale wind transport during the MILAGRO field campaign and comparison to climatology using cluster analysis, Atmos. Chem. Phys., 8, 1209–1224, 2008, http://www.atmos-chem-phys.net/8/1209/2008/.

Doran, J. C., Barnard, J. C., Arnott, W. P., Cary, R., Coulter, R., Fast, J. D., Kassianov, E. I., Kleinman, L., Laulainen, N. S., Martin, T., Paredes-Miranda, G., Pekour, M. S., Shaw, W. J., Smith, D. F., Springston, S. R., and Yu, X.-Y.: The T1-T2 study: evolution of aerosol properties downwind of Mexico City, Atmos. Chem. Phys., 7, 1585–1598, 2007, http://www.atmos-chem-phys.net/7/1585/2007/.

Dzepina, K., Arey, J., Marr, L. C., Worsnop, D. R., Salcedo, D., Zhang, Q., Onasch, T. B., Molina, L. T., Molina, M. J., and Jimenez, J. L.: Detection of particle-phase polycyclic aromatic hydrocarbons in Mexico City using an aerosol mass spectrometer, Internat. J. Mass Spectrometry, 263, 152–170, 2007.

Eiguren-Fernandez, A., Miguel, A. H., Froines, J. R., Thurairatnam, S., and Avol, E. L.: Seasonal and spatial variation of polycyclic aromatic hydrocarbons in vapor-phase and $PM_{2.5}$ in southern California and rural communities, Aerosol Sci. Technol., 38, 447–455, 2004.

Esteve, W., Budzinski, H., and Villenave, E.: Relative rate constants for the heterogeneous reactions of NO_2 and OH radicals with polycyclic aromatic hydrocarbons adsorbed on carbonaceous particles. Part 2: PAHs adsorbed on diesel particulate exhaust SRM 1650a, Atmos. Environ., 40, 201–211, 2006.

Harley, R. A., Marr, L. C., Lehner, J. K., and Giddings, S. N.: Changes in motor vehicle emissions on diurnal to decadal time scales and effects on atmospheric composition, Environ. Sci. Technol., 39, 5356–5362, 2005.

Jedrychowski, W., Galas, A., Pac, A., Flak, E., Camann, D., Rauh, V., and Perera, F.: Prenatal ambient air exposure to polycyclic aromatic hydrocarbons and the occurrence of respiratory symptoms over the first year of life, European J. Epidemiol., 20, 775–782, 2005.

Jiang, M., Marr, L. C., Dunlea, E. J., Herndon, S. C., Jayne, J. T., Kolb, C. E., Knighton, W. B., Rogers, T. M., Zavala, M., Molina, L. T., and Molina, M. J.: Mobile laboratory measurements of black carbon, polycyclic aromatic hydrocarbons and other vehicle emissions in Mexico City, Atmos. Chem. Phys., 5, 3377–3387, 2005, http://www.atmos-chem-phys.net/5/3377/2005/.

Johnson, K. S., Zuberi, B., Molina, L. T., Molina, M. J., Iedema, M. J., Cowin, J. P., Gaspar, D. J., Wang, C., and Laskin, A.: Processing of soot in an urban environment: case study from the Mexico City Metropolitan Area, Atmos. Chem. Phys., 5, 3033–3043, 2005, http://www.atmos-chem-phys.net/5/3033/2005/.

Kamens, R. M., Guo, Z., Fulcher, J. N., and Bell, D. A.: Influence of humidity, sunlight, and temperature on the daytime decay of polyaromatic hydrocarbons on atmospheric soot particles, Environ. Sci. Technol., 22, 103–108, 1988.

Kittleson, D. B., Watts, W. F., and Johnson, J. P.: Nanoparticle emissions on Minnesota highways, Atmos. Environ., 38, 9–19, 2004.

Kolb, C. E., Herndon, S. C., McManus, J. B., Shorter, J. H., Zahniser, M. S., Nelson, D. D., Jayne, J. T., Carnagaranta, M. R., and Worsnop, D. R.: Mobile laboratory with rapid response instruments for real-time measurements of urban and regional trace gas and particulate distributions and emission source characteristics, Environ. Sci. Technol., 38, 5694–5703, 2004.

Kwamena, N.-O. A., Staikova, M. G., Donaldson, D. J., George, I. J., and Abbatt, J. P. D.: Role of the aerosol substrate in the heterogeneous ozonation reactions of surface-bound PAHs, J. Physical Chem. A, 111, 11 050–11 058, 2007.

Lee, W. J., Wang, Y. F., Lin, T. C., Chen, Y. Y., Lin, W. C., Ku, C. C., and Cheng, J. T.: PAH characteristics in the ambient air of

traffic-source, Sci. Total Environ., 159, 185–200, 1995.

Mantis, J., Chaloulakou, A., and Samara, C.: PM10-bound polycyclic aromatic hydrocarbons (PAHs) in the greater area of Athens, Greece, Chemosphere, 59, 593–604, 2005.

Marr, L. C., Kirchstetter, T. W., Harley, R. A., Miguel, A. H., Hering, S. V., and Hammond, S. K.: Characterization of polycyclic aromatic hydrocarbons in motor vehicle fuels and exhaust emissions, Environ. Sci. Technol., 33, 3091–3099, 1999.

Marr, L. C., Black, D. R., and Harley, R. A.: Formation of photochemical air pollution in central California 1. Development of a revised motor vehicle emission inventory, J. Geophys. Res., 107, 4047, doi:10.1029/2001JD000689, 2002.

Marr, L. C., Grogan, L. A., Wohrnschimmel, H., Molina, L. T., Molina, M. J., Smith, T. J., and Garshick, E.: Vehicle traffic as a source of particulate polycyclic aromatic hydrocarbon exposure in Mexico City, Environ. Sci. Technol., 38, 2584–2592, 2004.

Marr, L. C., Dzepina, K., Jimenez, J. L., Reisen, F., Bethel, H. L., Arey, J., Gaffney, J. S., Marley, N. A., Molina, L. T., and Molina, M. J.: Sources and transformations of particle-bound polycyclic aromatic hydrocarbons in Mexico City, Atmos. Chem. Phys., 6, 1733–1745, 2006, http://www.atmos-chem-phys.net/6/1733/2006/.

Matter, U., Siegmann, H. C., and Burtscher, H.: Dynamic field measurements of submicron particles from diesel engines, Environ. Sci. Technol., 33, 1946–1952, 1999.

Maynard, A. D.: Estimating aerosol surface area from number and mass concentration measurements, Annals of Occupational Hygiene, 47, 123–144, 2003.

Miguel, A. H., Kirchsetter, T. W., Harley, R. A., and Hering, S. V.: On-road emissions of particulate polycyclic aromatic hydrocarbons and black carbon from gasoline and diesel vehicles, Environ. Sci. Technol., 32, 450–455, 1998.

Molina, L. T., Kolb, C. E., de Foy, B., Lamb, B. K., Brune, W. H., Jimenez, J. L., Ramos-Villegas, R., Sarmiento, J., Paramo-Figueroa, V. H., Cardenas, B., Gutierrez-Avedoy, V., and Molina, M. J.: Air quality in North America's most populous city – overview of the MCMA-2003 campaign, Atmos. Chem. Phys., 7, 2447–2473, 2007, http://www.atmos-chem-phys.net/7/2447/2007/.

Molina, M. J., Ivanov, A. V., Trakhtenberg, S., and Molina, L. T.: Atmospheric evolution of organic aerosol, Geophys. Res. Lett., 31, L22104, doi:10.1029/2004GL020910, 2004.

Muller, J. F., Hawker, D. F., and Connel, D. W.: Polycyclic aromatic hydrocarbons in the atmospheric environment of Brisbane, Australia, Chemosphere, 37, 1369–1383, 1998.

Ntziachristos, L., Polidori, A., Phuleria, H., Geller, M. D., and Sioutas, C.: Application of a diffusion charger for the measurement of particle surface concentration in different environments, Aerosol Sci. Technol., 41, 571–580, 2007.

Oberdorster, G.: Toxicology of ultrafine particles: in vivo studies, Phil. Trans. Royal Soc. London Ser. A, 7, 111–124, 2000.

Ott, W. R. and Siegmann, H. C.: Using multiple continuous fine particle monitors to characterize tobacco, incense, candle, cooking, wood burning, and vehicular sources in indoor, outdoor, and in-transit settings, Atmos. Environ., 40, 821–843, 2006.

Polidori, A., Hu, S., Biswas, S., Delfino, R. J., and Sioutas, C.: Real-time characterization of particle-bound polycyclic aromatic hydrocarbons in ambient aerosols and from motor-vehicle exhaust, Atmos. Chem. Phys., 8, 1277–1291, 2008, http://www.atmos-chem-phys.net/8/1277/2008/.

Salcedo, D., Onasch, T. B., Dzepina, K., Canagaratna, M. R., Zhang, Q., Huffman, J. A., DeCarlo, P. F., Jayne, J. T., Mortimer, P., Worsnop, D. R., Kolb, C. E., Zuberi, B., Marr, L. C., Volkamer, R., Molina, L. T., Molina, M. J., Cardenas, B., Bernabé, R. M., Márquez, C., Gaffney, J. S., Marley, N. A., Laskin, A., Shutthanandan, V., Xie, Y., Brune, W., Lesher, R., Shirley, T., and Jimenez, J. L.: Characterization of ambient aerosols in Mexico City during the MCMA-2003 campaign with Aerosol Mass Spectrometry: results from the CENICA Supersite, Atmos. Chem. Phys., 6, 925–946, 2006, http://www.atmos-chem-phys.net/6/925/2006/.

Seibert, P., Kromp-Kolb, H., Baltensperger, U., Jost, D. T., and Schwikowski, M.: Trajectory analysis of high-alpine air pollution data, in: Air Pollution Modeling and its Application X, edited by: Gryning, S.-E. and Millan, M. M., Plenum Press, New York, 1994.

Siegmann, K., Scherrer, L., and Siegmann, H. C.: Physical and chemical properties of airborne nanoscale particles and how to measure the impact on human health, J. Molecular Structure (Theochem), 458, 191–201, 1999.

Stoeger, T., Reinhard, C., Takenaka, S., Schroeppel, A., Karg, E., Ritter, B., Heyder, J., and Schulz, H.: Instillation of six different ultrafine carbon particles indicates a surface area threshold dose for acute lung inflammation in mice, Environ. Health Perspectives, 114, 328–333, 2006.

Tang, D., Li, T.-Y., Liu, J. J., Chen, Y.-H., Qu, L., and Perera, F.: PAH-DNA adducts in cord blood and fetal and child development in a Chinese cohort, Environ. Health Perspectives, 114, 1297–1300, 2006.

Tran, C. L., Buchanan, D., Cullen, R. T., Searl, A., Jones, A. D., and Donaldson, K.: Inhalation of poorly soluble particles. II. Influence of particle surface area on inflammation and clearance, Inhalation Toxicol., 12, 1113–1126, 2005.

Velasco, E., Siegmann, P., and Siegmann, H. C.: Exploratory study of particle-bound polycyclic aromatic hydrocarbons in different environments in Mexico City, Atmos. Environ., 38, 4957–4968, 2004.

Volkamer, R., Jimenez, J. L., San Martini, F., Dzepina, K., Zhang, Q., Salcedo, D., Molina, L. T., Worsnop, D. R., and Molina, M. J.: Secondary organic aerosol formation from anthropogenic air pollution: Rapid and higher than expected, Geophys. Res. Lett., 33, L17811, doi:10.1029/2006GL026899, 2006.

Westerdahl, D., Fruin, S., Sax, T., Fine, P. M., and Sioutas, C.: Mobile platform measurements of ultrafine particles and associated pollutant concentrations on freeways and residential streets in Los Angeles, Atmos. Environ., 39, 3597–3610, 2005.

Zheng, M. and Fang, M.: Particle-associated polycyclic aromatic hydrocarbons in the atmosphere of Hong Kong, Water Air Soil Poll., 117, 175–189, 2000.

Atmos. Chem. Phys., 9, 189–206, 2009
www.atmos-chem-phys.net/9/189/2009/

Atmospheric Chemistry and Physics

Measurements of aerosol absorption and scattering in the Mexico City Metropolitan Area during the MILAGRO field campaign: a comparison of results from the T0 and T1 sites

N. A. Marley[1], J. S. Gaffney[2], T. Castro[3], A. Salcido[4], and J. Frederick[5]

[1]Graduate Institute of Technology, University of Arkansas at Little Rock, Little Rock, AR, USA
[2]Department of Chemistry, University of Arkansas at Little Rock, Little Rock, AR, USA
[3]Centro de Ciencias de la Atmósfera,Universidad Nacional Autónoma de México, México City, México
[4]Instituto de Investigaciones Eléctricas, Gerencia de Sistemas de Calidad Ambiente y Seguridad, Cuernavaca, Morelos, México
[5]Department of Geophysical Sciences, The University of Chicago, Chicago, IL, USA

Received: 29 May 2008 – Published in Atmos. Chem. Phys. Discuss.: 3 July 2008
Revised: 4 December 2008 – Accepted: 4 December 2008 – Published: 13 January 2009

Abstract. In March 2006, a multiagency field campaign was undertaken in Mexico City called the Megacities Initiative: Local and Global Research Observations (MILAGRO). Two of the five field components of the MILAGRO study focused a major part of their efforts on atmospheric particulate emissions from the Mexico City basin and their effects on radiative balance as a function of time, location and processing conditions. As part of these two MILAGRO components, measurements of aerosol optical properties were obtained at a site located in the northern part of Mexico City (T0) and also at a site located 29 km northwest (T1) to estimate the regional effects of aerosol emissions from the basin.

Measurements of aerosol absorption and scattering for fine mode aerosols were obtained at both sites. Aerosol absorption at 550 nm was similar at both sites, ranging from 7–107 Mm^{-1} at T0 and from 3–147 Mm^{-1} at T1. Aerosol scattering measured at 550 nm at T0 ranged from 16–344 Mm^{-1} while the aerosol scattering values at T1 were much lower than at T0 ranging from 2–136 Mm^{-1}. Aerosol single scattering albedos (SSAs) were calculated at 550 nm for the fine mode aerosols at both sites using these data. The SSAs at T0 ranged from 0.47–0.92 while SSAs at T1 ranged from 0.35–0.86. The presence of these highly absorbing fine aerosols in the lower atmosphere of the Mexico City area will result in a positive climate forcing and a local warming of the boundary layer in the region.

Broadband UVB intensity was found to be higher at site T0, with an average of 64 $\mu W/cm^2$ at solar noon, than at site T1, which had an average of 54 $\mu W/cm^2$ at solar noon. Comparisons of clear-sky modeled UVB intensities with the simultaneous UVB measurements obtained at sites T0 and T1 for cloudless days indicate a larger diffuse radiation field at site T0 than at site T1. The determination of aerosol Ångstrom scattering coefficients at T0 suggests that this is due to the predominance of aerosols in the size range of 0.3 micron, which leads to scattering of UVB radiation peaked in the forward direction and to an enhanced UVB radiation observed at ground level. This enhancement of the UVB diffuse radiation field would explain the enhanced photochemistry observed in the Mexico City area despite the reduction in UVB anticipated from light absorbing species.

1 Introduction

Megacities, large urban and suburban centers whose populations exceed ten million inhabitants, are steadily increasing worldwide with the most rapid growth in the tropical

Correspondence to: J. S. Gaffney
(jsgaffney@ualr.edu)

areas of South America and Asia. In 1800 only 3% of the world's population lived in urban areas. This increased to 47% by the end of the 20th century. In 1950 there were 83 cities with populations exceeding one million and New York City was the only megacity (UNEP/WHO, 1992). By 2007 there were 468 urban centers of more than one million and of these 14 are classified as megacities with the largest metropolitan complexes centered at Tokyo, Japan, and Mexico City, Mexico (Molina and Molina, 2002). If this trend continues, the world's urban populations will double every 38 years and within the next 10 to 15 years it is predicted that there will be more than 30 megacities worldwide.

The Mexico City metropolitan area (MCMA) is the largest urban center in North America and the second largest megacity worldwide. It occupies ~3540 km^2 with a population of ~19 million (CAM, 2002). In general, megacities suffer from poor air quality due to the cumulative effects of rapid population growth and industrialization accompanied with increased traffic densities and total energy consumption. However, the topography of the MCMA also acts to exacerbate the poor air quality (Fast et al., 2007; Fast and Zhong, 1998; Doran et al., 1998) as Mexico City is located in a basin on the central Mexican plateau at an altitude of 2240 m and latitude of 19° N. The basin is surrounded on the west, south, and east by mountain ranges that rise up to 1000–3000 m above the basin floor. This topography serves to inhibit dispersion of emissions within the basin during the early morning hours and the high levels of incoming solar radiation at this latitude and elevation promotes atmospheric photochemical reactions that rapidly form secondary pollutants (Whiteman et al., 2000).

Due to the elevation and topography of Mexico City, the height of the boundary layer may reach up to 2–4 km above the surface (Raga et al., 2001a; de Foy et al., 2007). Therefore, pollutants are emitted from the basin at altitudes that are considered to be free troposphere elsewhere and are expected to travel long distances affecting the surrounding regions (Gaffney and Marley, 1998; Williams et al., 2002). Modeling results have indicated that the effects of this exported pollution can impact background levels 300 km or more from the urban area (Barth and Church, 1999; Whiteman et al., 2000). Indeed, past studies have found that the Mexico City air pollutants are typically vented during the late afternoon on a daily basis (Gaffney and Marley, 1998; Whiteman et al., 2000)

Past studies in the Mexico City area have estimated that emissions from the basin contribute 15 megatons of fine aerosol ($PM_{2.5}$) per year to the surrounding regions (Gaffney et al., 1999). This fine aerosol was found to be composed of approximately 32% organic carbon (OC), 15% elemental carbon (EC), 10% ammonium nitrate and 20% ammonium sulfate by elemental and thermal/optical methods (Chow et al., 1993, 2001, 2002; Vega et al., 2004). More recently, in 2003 the composition of fine aerosols was found to be 11% black carbon (BC), 32% OC, 13% ammonium nitrate, and 14% ammonium sulfate by aerosol mass spectrometry and optical attenuation methods (Salcedo et al., 2006; Aiken et al., 2008). This is an indication that although the emissions of reactive hydrocarbon have been reduced in the city due to the significant number of newer vehicles with catalytic converters that have replaced older higher emission vehicles, the aerosol composition has not changed significantly likely due to the lack of controls on diesel vehicles and biomass burning in the region (Marley et al., 2007). Thus, while air quality and ozone production has improved, Mexico City and 25 other megacities continue to be a major source of black carbon aerosols, which can be an important species in determining regional radiative balance and climate.

While sulfate is well known as an important light scattering aerosol species contributing to atmospheric cooling (Charlson et al., 1992), BC and associated OC (including secondary organic aerosol, SOA) have more recently gained attention as major light absorbing aerosol species exerting a positive radiative forcing and reinforcing the atmospheric warming due to increases in the greenhouse gases (Jacobson, 2002; Ramanathan et al., 2005). Some model calculations suggest that the contribution of carbon soot aerosols to global warming may be as much as 0.3–0.4°C, rivaling the contributions from atmospheric methane (Jacobson, 2004; Chung and Seinfeld, 2005). The ultimate climate effects from carbon aerosols will depend on their physical and chemical properties, as well as their residence times and distributions in the atmosphere (Jacobson, 2001).

The presence of the highly absorbing BC aerosols in Mexico City leads to a reduction in overall solar flux of 17.6% locally (Raga et al., 2001b). The mass of these absorbing aerosols exported from this megacity into the surrounding region is estimated to be 6.000 metric tons per day or 2 megatons per year of BC (Gaffney et al., 1999). Since freshly emitted BC aerosols are hydrophobic, they are expected to be more resistant to washout and have longer lifetimes than more hygroscopic aerosols such as sulfate and nitrate (Gaffney and Marley, 2005; Dua et al., 1999). In addition, since the aerosols emitted from the Mexico City basin are introduced into the atmosphere at higher altitudes, they are assumed to have longer lifetimes than similar aerosols released at lower altitudes (Raga et al., 2001b). The MCMA is therefore a major source of BC aerosols to the surrounding regions and the release of these highly absorbing aerosols will have an impact on the radiative balance and climate on a regional scale.

The influences of aerosols on climate are much more complex than those of the greenhouse gasses (Schwartz and Buseck, 2000). Aerosol composition is highly variable, with different species present within the same particle, due to the different sources, production mechanisms and atmospheric transformations (Pósfai et al., 1999). In addition, these different aerosol species can be either internally or externally mixed within the particle yielding different optical and microphysical properties and different radiative effects (Pósfai

et al., 1999; Schnaiter et al., 2005). Aerosol distributions are also variable both spatially and temporally and although aerosol lifetimes are much shorter than those of the greenhouse gases, estimates of their atmospheric residence times range from less than a day to more than a month resulting in transport distances from a few miles to hemispheric scales (Marley et al., 2000; Williams et al., 2002). This variability in composition and distributions makes it difficult to quantify the aerosol impacts on climate and to represent these effects in climate models.

In order to better understand the evolution and transport of pollutant aerosols and gases from emissions in the Mexico City basin and their resulting impacts on regional climate, a multiagency field campaign was undertaken called the Megacities Initiative: Local and Global Research Observations (MILAGRO). The MILAGRO study was composed of five collaborative field experiments. Two of the components of the MILAGRO study focused a major part of their efforts on aerosol emissions. The Megacity Aerosol Experiment, Mexico City 2006 (MAX-Mex) was sponsored by the US Department of Energy (DOE) to investigate the direct radiative effect of aerosols in the Mexico City plume as a function of time, location and processing conditions. The MCMA-2006 study, supported by various Mexican institutions, the US National Science Foundation (NSF) and the DOE, deployed ground based instrumentation to examine fine particles and secondary aerosol precursor gas emissions within the Mexico City Basin. As part of these two MILAGRO components, aerosol scattering and absorption measurements were obtained at a site located at the Instituto Mexicano del Petróleo (IMP- Mexican Petroleum Institute), in the northwestern part of the Mexico City center. This site, known as T0, was chosen to represent the fresh emissions within the MCMA. Measurements were also obtained at the Universidad Tecnológica de Tecamac (Technological University of Tecamac), located approximately 29 km northwest of T0. This site, known as T1, was expected to represent a mixture of both fresh and aged pollutants as they exit the basin.

The evolution of absorbing aerosols downwind of Mexico City has been described previously in a comparison of measurements obtained at site T1 with those obtained at site T2 (Rancho La Bisnaga), located approximately 35 km northnortheast of T1 (Doran et al., 2007, 2008; Doran, 2007). This study focused primarily on the changes in the carbonaceous aerosol composition and the resulting effects on the aerosol mass specific absorption coefficients. It was concluded from this work that emission sources outside the MCMA, including biomass-burning sources, are important contributors to the regional aerosol burden. Other aerosol studies conducted in the Mexico City area have reported similar conclusions (Kleinman et al., 2008; Molina et al., 2007; Stone et al., 2008; Yokelson et al., 2007; DeCarlo et al., 2008; Salcedo et al., 2006).

Presented here is a comparison of measurements of aerosol absorption and aerosol scattering at 550 nm obtained at sites T0 and T1 during the MILAGRO campaign. In addition, the mass specific aerosol absorption coefficients were calculated at 550 nm by using total carbon (TC) measurements taken from high-volume quartz filters. These results are compared with absorption coefficients reported previously by Doran et al. (2007). Also reported here is a comparison of UVB radiation measurements obtained simultaneously at sites T0 and T1, under cloudless conditions, with clear sky modeled UVB values. These data are discussed with regard to the light scattering and absorption measurements obtained at both sites.

2 Experimental methods

2.1 Sample Sites

2.1.1 Site T0

Measurements were obtained from 10 March (day 69) to 29 March (day 88) 2006 at the Instituto Mexicano del Petróleo (IMP) laboratories [Mexico, D. F.]. This site, known as T0, is located in the north central part of Mexico City at latitude 19°29′ N, longitude 99°09′ W, and at an altitude of 2240 m above sea level. The IMP complex is a campus of 33 buildings located in an industrial and commercial area of Mexico City surrounded by streets that are very heavily trafficked by light duty vehicles and diesel buses. The nearest major roads are approximately 300 m away from the measurement site.

Relative humidity and rain intensity at site T0 during the study are shown in Fig. 1 (top). Rain events occurred during the last week of the study period, 23–28 March (days 82–87). Daily maximum relative humidity ranged from a low of 35% during the first week to a high of 89% during the last week of March 2006. Winds ranged from 0.1 to 9 m/s with an average of 2 m/s from the south, southwest.

2.1.2 Site T1

Measurements were also obtained from 1 March (day 60) to 29 March (day 88) 2006 at the Technological University of Tecamac, State of Mexico, 30 km north of Mexico City. This site, known as T1, is at latitude 19°43′ N and longitude 98°58′ W at an altitude of 2340 m a.s.l. Tecamac has a recorded population of 172 410, as of the 2000 census, and is primarily commercial with a total of 3070 small businesses, of which 1923 are food related. The principal mode of transportation in the area consists of light duty vehicles, and small diesel buses. The main transportation route is public road # 85, which runs south to north from Mexico City to Pachuca. The municipality of Pachuca, which is located 94 km northeast of Mexico City and 64 km northeast of Tecamac, is the capital of the state of Hidalgo with a recorded population of 267 751 in 2005.

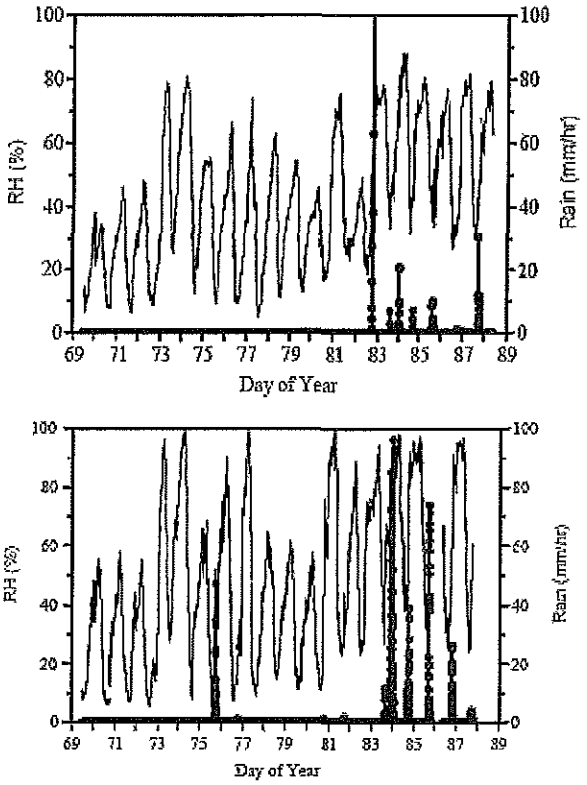

Fig. 1. Relative humidity and rain intensity (blue) measured at sites TO (top) and T1 (bottom) from 10 March (day 69) to 29 March (day 88) 2006 during the MILAGRO field campaign.

Relative humidity and rain intensity at site T0 during the study are shown in Fig. 1 (bottom). Rains events occurred at site T1 on 16, 17, 21, 22, and 24–28 March (days 75, 76, 80, 81, 83–87). Relative humidity ranged from a mid-day low of 40% during the first week to a high of 99% during the last week of March 2006. Winds ranged from 0.1 to 10 m/s with an average of 2 m/s from the south, southwest.

Aerosol Optical Properties

2.1.3 Site T0

The aerosol instrumentation at site T0 was located on the rooftop of Building No. 32 (Héctor Lara Sosa Building, IMP) 15 m above ground level. The sample inlets were designed to collect aerosols in the size range of 0.1 to 2 micron aerodynamic diameter (Hermann et al., 2001). Aerosol scattering was measured with a three wavelength integrating nephelometer (TSI Model 3563) operating at 450, 550, and 700 nm (Anderson and Ogren, 1998). Results obtained at 550 nm are reported here.

The instrument was calibrated by using CO_2 according to the manufacturer's specifications. An internal high efficiency particulate filter (HEPA) is used to provide a clean air measurement periodically for background subtraction. The TSI nephelometer was operated at ambient relative humidity. However, two single wavelength (550 nm) nephelometers (Meteorology Research Incorporated) were operated at low (20%) and high (80%) relative humidity for comparison.

Aerosol absorption was measured with a multi-angle absorption photometer, or MAAP (Thermo Electron Model 5012). The aerosols in the air sample are collected within the instrument by continuous filtration through a glass fiber tape strip and the aerosol absorption is determined by measuring the attenuation of 670 nm light as it passes through the particle laden filter. As the sample is deposited on the filter tape, the light attenuation steadily increases. At high sample loadings the high absorption can cause detection limits to increase. To prevent this, the instrument automatically advances the tape to a new sample spot when light attenuation reaches 25% of its initial value. After the tape advance, a background measurement is taken to correct for variations in filter surfaces and source light intensities.

The use of the filter based aerosol absorption methods have been met with some controversy due to artifacts introduced by depositing the aerosol particles on a filter substrate prior to measurement (Schmid et al., 2005; Arnott et al., 2005). Since these instruments rely on the measurement of light transmitted through a particle laden quartz fiber filter, scattering from the filter surface causes a reduction in light intensity not associated with absorption, which results in a positive error in the attenuation measurement. The MAAP represents a significant improvement over other filter-based methods in that it uses multiple detectors to simultaneously measure the light intensity both transmitted through and scattered from the filter tape. The instrument then uses a two-stream-approximation radiative transfer scheme to determine the aerosol absorption. This explicit treatment of light scattering effects caused by the aerosol and filter matrix in the radiative transfer scheme improves the determination of aerosol absorption considerably over methods that rely on the measurement of transmission alone (Petzold et al., 2005).

The MAAP automatically calculates the BC content in the aerosol samples from the aerosol absorption measurements by assuming BC to be the main absorbing aerosol species in the samples with a mass specific absorption coefficient of 6.6 m^2/g at 670 nm. However, these results are easily reconverted to the initial aerosol absorption measurement using the manufacturer's absorption coefficient.

The aerosol absorption measurements obtained by the MAAP at 670 nm were corrected to 550 nm for direct comparison of the aerosol scattering measurements. The wavelength dependence of the extinction of light by fine aerosol particles (τ) is defined by Ångstrom's turbidity formula as $\tau=\beta\lambda^{-\alpha}$; where β, known as the Ångstrom turbidity coefficient, is the value of τ at a wavelength of 1 μm and α is

the Ångstrom exponent. The total aerosol extinction is the sum of aerosol scattering and absorption as described in the expanded turbidity formula,

$$\tau = \beta_s \lambda^{-\alpha s} + \beta_a \lambda^{-\alpha a} \quad (1)$$

where α_s is the Ångstrom exponent for aerosol scattering, α_a is the Ångstrom exponent for aerosol absorption, and β_s and β_a are the corresponding values of aerosol scattering and absorption at a wavelength of 1 μm. The wavelength dependence of aerosol absorption can be determined independently by

$$A = \beta \lambda^{-\alpha a} \text{ and} \quad (2)$$

$$\ln(A) = -\alpha_a^* \ln(\lambda) \quad (3)$$

Once determined, α_a can then be used to convert absorption measurements made at one wavelength to values at another wavelength.

The aerosol absorption Ångstrom coefficients were calculated from Eq. (2) by using aerosol absorption measurements at 7 wavelengths (370, 450, 520, 590, 660, 880, and 950 nm) made with a 7-channel aethalometer (Hansen et al., 1982). The 7-channel aethalometer is currently the best method available for the determination of α_a in the field. The aethalometer is the only instrument available that allows for the measurement of aerosol absorption at more than 2 wavelengths and includes the UVB spectral range. It is important to include the UV measurement in the determination of α_a since most enhanced absorption occurs in this range (Bergstrom et al., 2002; Kirchstetter et al., 2004; Andreae and Gelencser, 2006; Barnard et al., 2008). Therefore, instruments that use only visible wavelengths to determine α_a will greatly underestimate the wavelength dependence of aerosol absorption.

For small spherical particles with a constant refractive index across the wavelength range of interest, α_a=1 (Bergstrom, 1973). This has been determined to be a good approximation for aerosols composed mostly of BC or for particles containing a significant fraction of OC over a narrow wavelength range <600 nm (Bergstrom et al., 2002; Kirchstetter et al., 2004). However, the aerosol absorption Ångstrom coefficients of mixed carbon aerosols containing BC, secondary OC, and primary OC from biomass burning has been found to be closer to 1.5 (Schmid et al. 2006). In areas impacted heavily by biomass burning, α_a can be closer to 2 to 2.5 (Dubovik et al., 1998; Kirchstetter et al., 2004; Swap et al., 2003). It is therefore important to determine α_a at the same time resolution as the absorption measurements to reduce errors in calculating aerosol absorption at different wavelengths. The aerosol absorption Ångstrom coefficients were calculated simultaneously with the aerosol absorption measurements obtained at 670 nm by the MAAP and these values were used to calculate aerosol absorption at 550 nm. The results obtained for α_a at site T0 varied from 0.54 to 1.52 with an overall average of 0.93 (Marley et al., 2008).

The analog outputs of the MAAP absorption photometer and the nephelometers were monitored continuously and one-minute averages of aerosol absorption and scattering were recorded by a laptop computer operating with LabVIEW software. The data reported here are an hourly running average of the one-minute values for aerosol scattering at 550 nm and aerosol absorption corrected to 550 nm by Eq. (2).

The aerosol scattering measurements made at 550 nm and the aerosol absorption measurements corrected to 550 nm were used to calculate the fine mode aerosol single scattering albedo (SSA). The SSA is defined as the ratio of aerosol scattering to total light extinction (absorption + scattering) as

$$\text{SSA} = \sigma_s/(\sigma_s + \sigma_a) \quad (4)$$

where σ_s is the aerosol scattering coefficient and σ_a is aerosol absorption coefficient. The SSA is therefore the fraction of total light extinction that is due to scattering by aerosols. The results reported here for aerosol SSAs are for the fine mode aerosols only. These are expected to be lower than that for the total aerosol burden due to the fact that the highly absorbing carbonaceous aerosols exist principally in the fine mode. However, the more highly scattering coarse mode aerosols in the size range of 2–10 micron aerodynamic diameter have settling velocities from 60–1000 cm/h and will not be transported as far into the surrounding region unless they are accompanied by high winds and/or are lofted to significant altitude (Finlayson-Pitts and Pitts, 2000).

2.1.4 Site T1

The sample inlet at site T1was located at a height of 10 m above ground level and collected aerosols in the size range of 0.1 to 2 micron aerodynamic diameter at a flow rate of 16.7 l/min at ambient temperature and pressure. Aerosol scattering was measured at site T1 with a portable integrating nephelometer (Radiance Research Model 903) operating at 530 nm, which was calibrated by comparison to a second nephelometer (Radiance Research Model 903) located at the Universidad Nacional Autónoma de México (UNAM). The scattering measurements were recorded by internal data loggers at 1 min intervals. The stored data was retrieved using a personal computer through an RS232 port. These data are reported here as an hourly running average of these one minute values.

Aerosol absorption was obtained by a particle soot absorption photometer, or PSAP (Radiance Research), which is also a filter based measurement technique. The particle laden air stream is first passed through a primary filter and the aerosol absorption is determined by measuring the light attenuation at 550 nm. The clean air stream is then passed through a second filter adjacent to the primary filter, which is used as a reference in order to ensure that the observed change in primary filter transmittance is not due to changes in the intensity of the light source.

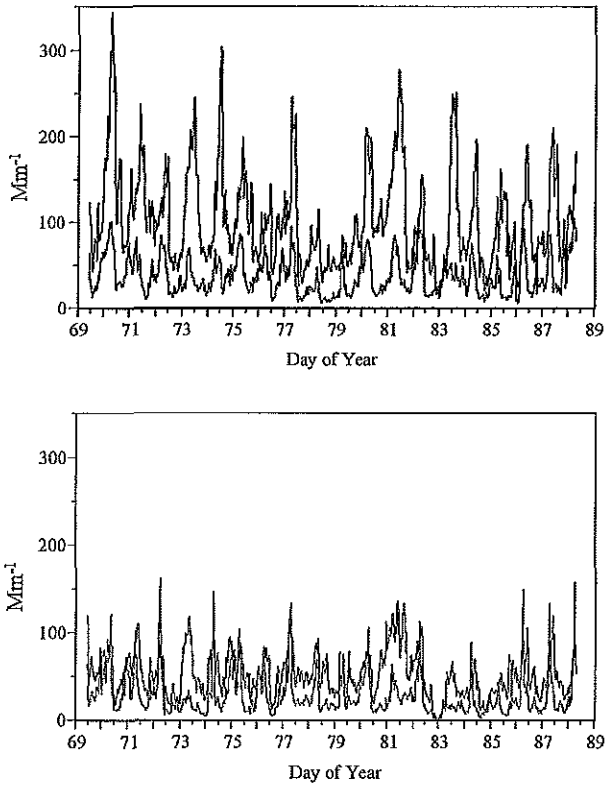

Fig. 2. Measurements of fine (0.1–2 micron) aerosol absorption (red) and scattering (blue) obtained at sites T0 (top) and T1 (bottom) from 10 March (day 69) to 29 March (day 88) 2006 during the MILAGRO field campaign.

The PSAP is also susceptible to errors associated with measuring light transmission through a particle laden filter substrate. Light scattering from the filter surface as well as multiple scattering within the filter medium results in an enhancement of the absorption measurements (Arnott et al., 2005). The instrument manufacturer has empirically determined calibration factors to correct for both the magnification of the absorption by the filter medium as well as for nonlinearities in the instrument response as the filter is loaded with particulates. The aerosol absorbances (σ_a) reported here for 550 nm were calculated from the measured aerosol absorbances (σ_{meas}) by Eq. (5);

$$\sigma_a = (\sigma_{meas} - K_1\sigma_s)/K_2 \quad (5)$$

where σ_s is the measured aerosol scattering, K_1=0.02, and K_2=1.2 (Bond et al., 1999). In addition, transmittance values below 0.5 have been omitted as invalid due to low particle loadings on the filter.

2.2 Meteorology and UV-B measurements

Broadband ultraviolet-B (UV-B) radiation measurements were taken at both site T0 and site T1 with Robertson-Berger (RB) radiometers (Solar Light Co. Model 501). These radiometers record continuous measurement of global (direct + diffuse) broadband ultraviolet radiation from 280–320 nm. Since the output of the detectors vary 1% per degree C, the internal temperatures of the radiometers are maintained at 25±1°C with Peltier elements inside the housings and the internal temperature is monitored to assure stability. Both radiometers were factory calibrated with a 200 W quartz halogen lamp traceable to NIST. After calibration, stability of the detectors has been shown to be excellent over the life of the meter (Deluisi et al., 1992; Weatherhead et al., 1997; Xu and Huang, 2003). The detector has a spectral response that mirrors the erythemal action spectra (McKinlay and Diffy, 1987). They are calibrated in units of minimum erythemal dose per hour (MED/h) where one MED/h is defined as 0.0583 W/m^2. Results reported here have been converted to μW/cm^2.

Measurements of wind speed, wind direction, rain intensity, pressure, temperature, and relative humidity (RH) were obtained at both sites with weather multi-sensor packages (Vaisala, WXT150). Rain intensity measurements reported here were made by the RAINCAP sensor included in the weather package. The sensor detects the impact of individual raindrops by a piezoelectric sensor. The resulting voltage signal is proportional to the volume of the drop and is converted into total accumulated precipitation. All measurements were collected at a five-minute time resolution with a laptop computer operating with LabVIEW software.

2.3 Total Carbon Determinations

Samples of fine (<1.0 micron) aerosols were collected in Mexico City from 1–28 March 2006 (day 60–day 68) at site T0 and site T1. The Aerosol samples were collected on quartz fiber filters by using high volume samplers (Hi-Q Environmental. Products, Model HVP-3800AFC) equipped with cascade impactors (Thermo Anderson). The air samplers were equipped with brushless, three stage centrifugal fan blowers controlled by an electronic mass flow sensor that detects changes in pre-set flow rate caused by changes in temperature, barometric pressure, and pressure drop due to particulate loading on filter media. The high-volume sampler compensates for these changes by adjusting the motor speed to maintain the pre-set flow rate at 1.1 cubic m/min or 40 scfm. Three separate LCD's, display elapsed time, total volume of air sampled, and instantaneous flow rate.

The quartz filter samples were taken at 12-h intervals from 05:30 to 17:30 and from 17:30 to 05:30 local standard time (LST). The volume of air sampled during the 12-h time period averaged 740 m^3. The aerosol samples were analyzed for TC content by thermal combustion. Each sample was

sealed under vacuum in a quartz tube with copper oxide, metallic copper and silver and combusted at 900°C. The CO_2 produced from combustion was cryogenically isolated from other combustion products and its amount measured manometrically (±0.2%).

3 Results and discussion

The results of fine aerosol absorption and scattering at sites T0 and T1 are shown in Fig. 2. Aerosol absorption at site T0 ranged from 7–107 Mm^{-1} with an overall average of 37 Mm^{-1} and followed a diurnal pattern that reached a maximum at around 06:30 (range of 05:00 to 08:00) LST and a minimum at 13:00 (range of 12:00 to 14:00) LST. Previous measurements of aerosol absorption have been reported for the Centro de Ciencias de la Atmósphera inside the campus of UNAM in the southwest quadrant of the Mexico City basin (Baumgardner et al., 2007). Results averaged over 14 days between the years 2003 and 2005 were found to follow a similar diurnal pattern as observed at site T0 but results were much lower than reported here. Aerosol absorption ranged from a low of 7 Mm^{-1} in the early morning (01:00) to a maximum of 33 Mm^{-1} at 06:00 LST. A comparison of the aerosol absorption at T0 showed excellent agreement with data obtained from co-located aethalometer and photoacoustic spectrometer instrumentation (Paredes-Miranda et al., 2008).

The values obtained in this study can also be compared to aerosol absorption measurements reported for Santiago, Chile, which has a similar terrain but a lower altitude. The major sources of absorbing aerosols in both Mexico City and Santiago are motor vehicle traffic, especially diesel buses (Horvath et al., 1997; Molina and Molina, 2002). Aerosol absorption in Santiago was found to reach maximum values of 100–200 Mm^{-1} at around 09:00 LST and correlated with peak traffic hours (Horvath et al., 1997).

Aerosol absorption measurements at site T1 ranged from 3–147 Mm^{-1} with an overall average of 27 Mm^{-1}. The same diurnal pattern observed at T0 was also evident at site T1 (maximum at 06:30 and minimum at 13:00 LST). While the daily maximum absorption values at T1 exceeded those at T0 on 9 of the days studied, these high levels were of much shorter duration, lasting only about 1 to 2 h as compared to 7 to 9 h of peak levels at site T0. In addition, the minimum aerosol absorption observed at site T1 routinely fell below those observed at site T0.

Forty-six minute averages of aerosol absorption obtained from day 74 (15 March) through day 85 (26 March) with a photoacoustic spectrometer operating at 870 nm have been reported previously for site T1 (Doran et al., 2007). A comparison of the daily absorbance maxima reported at 870 nm (Doran et al., 2007) with those recorded by the PSAP at 550 nm, assuming an α_a of 1, yields a difference between the data sets of −0.1 to +83 Mm^{-1} with an average difference of 31 Mm^{-1}. The major source of error in this comparison is probably due to the assumption of α_a=1. During much of the MILAGRO study, site T1 was impacted by local grass fires (Gaffney et al., 2008; Yokelson et al., 2008), which could have contributed significantly to the overall aerosol loadings and to a larger α_a (Kirchstetter et al., 2004). Carbon-14 analysis of 12-h aerosol samples collected at site T1 found that 70% of the carbon in the aerosols was from modern sources (Gaffney et al., 2008), which confirms that much of the carbon aerosol burden in the area arises from biomass derived sources. Determinations of α_a in areas impacted by biomass burning have been shown to be closer to 2 (Dubovik et al., 1998; Kirchstetter et al., 2004; Swap et al., 2003). If α_a=2 is used to convert the values reported at 870 nm to 550 nm, the difference in the two data sets becomes 1 Mm^{-1} ±30 Mm^{-1}. The major source of error in this comparison is most likely due to the differences used in data averaging.

Aerosol scattering measurements obtained at site T0 ranged from 16–344 Mm^{-1} with an overall average of 105 Mm^{-1}. Scattering values generally reached a maximum at 10:30 (range of 07:30 to 13:00) LST. Measurements of aerosol scattering species obtained in Mexico City in April 2003 found that both nitrate and ammonium concentrations showed a sharp diurnal pattern with a maximum of 10–20 $\mu g/m^3$ for nitrate and 4–8 $\mu g/m^3$ for ammonium occurring from 10:00–12:00 LST, while sulfate concentrations did not vary significantly, remaining at round 2–3 $\mu g/m^3$ most of the time (Salcedo et al., 2006). The sharp diurnal pattern of nitrate is due to the photochemical formation of nitric acid from the reaction of NO_2 and OH, and subsequent reaction with ammonia to form the highly scattering aerosol species ammonium nitrate.

Similar rapid photochemical production of secondary organic aerosols (SOA) has also been observed in the Mexico City area (Salcedo et al., 2006; Hennigan et al., 2008; Aiken et al., 2008; Volkamer et al., 2006). The formation of particulate nitrate and SOA were found to be highly correlated suggesting that reaction with OH was also the primary source of the morning rise in SOA (Salcedo et al., 2006; Hennigan et al., 2008). The photochemical SOA formation showed approximately the same enhancement as for ammonium nitrate and occurred between the hours of 08:00–12:45 (Hennigan et al., 2008; Salcedo et al., 2006). This late morning formation of both ammonium nitrate and SOA in Mexico City contributes to the aerosol scattering in the diurnal profile shown in Fig. 2.

Aerosol scattering measured in Denver during the winter reached a maximum of 60–140 Mm^{-1} at approximately 14:00–19:00 LST, 6 h later than observed in Mexico City (Groblicki et al., 1981). The primary aerosol scattering species in Denver is ammonium sulfate formed from the atmospheric oxidation of SO_2, with significant contributions from ammonium nitrate, as well. The photochemical formation of these secondary aerosol species would be expected to be slower in Denver due to the lower actinic flux in the winter

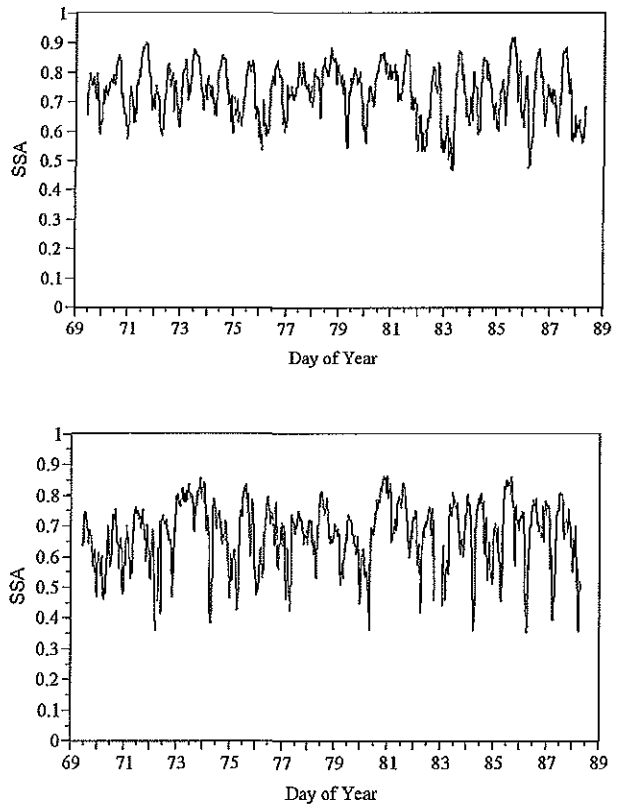

Fig. 3. Aerosol single scattering albedo (SSA) determined at site T0 (top) and T1 (bottom) from 10 March (day 69) to 29 March (day 88) 2006 during the MILAGRO field campaign.

at these higher latitudes, resulting in the later scattering maxima than observed in Mexico City. Aerosol scattering values at T1 were in general much lower than at T0, ranging from 2–136 Mm^{-1} with an overall average of 53 Mm^{-1}, and reached a maximum at 08:30 (range of 06:00 to 13:30) LST. On clear days the boundary layer in Mexico City during March–April grows slowly after sunrise at 06:40 to a height of approximately 1000 m by 11:00 LST (Doran et al., 1998, 2007; de Foy et al., 2008; Fast and Zhong, 1998; Fast et al., 2007). This serves to dilute the pollutants already present in the boundary layer. After 12:00 LST the boundary layer grows rapidly to 3000 m or greater. The maximum scattering values at site T0 occurred 2 h later than the maximum scattering values seen at T1 and 4 h later than the peak aerosol absorption values. This suggests that the high aerosol scattering values measured at T0 were primarily due to rapid SOA formation in the city. Although the overall SOA levels at T1 were found to be similar to those at T0 (Hennigan et al., 2008; Stone et al., 2008), the diurnal pattern of aerosol scattering at site T1 appeared to be controlled primarily by changes in the boundary layer height in the early morning, and by the presence of photochemically aged aerosols in the afternoon (Carabali, 2008; Stone et al., 2008; Aiken, et al., 2008).

The fine mode aerosol SSAs calculated from the ground level absorption and scattering measurements at 550 nm are shown in Fig. 3. The lower aerosol scattering observed at site T1 translates into lower values for fine aerosol SSAs at T1 with a range of 0.35–0.86 and an overall average of 0.68. The very low values for SSAs at site T1 are of very short duration, indicating a local source of absorbing BC aerosol. The fine aerosol SSAs calculated for site T0 ranged from 0.47–0.92 with an overall average of 0.73. While the total aerosol SSAs recorded over most of the Northern Hemisphere are usually about 0.85–0.95 (Jacobson, 2001), values as low as 0.68 have been reported over the southern Atlantic Ocean (Clarke, 1989). The occurrence of lower total aerosol SSAs is an indication of higher levels of more absorbing fine mode aerosols.

The SSA is a function of aerosol chemical composition and morphology. For a completely scattering aerosol, such as sulfate, the SSA~1 and for a highly absorbing aerosol, such as freshly emitted BC, the SSA theoretically would approach zero. The SSA of freshly emitted diesel soot has been reported at 0.2 (Ramanathan et al., 2001; Ban-Weiss et al., 2008). Therefore, aerosols with an SSA>0.95 will have a negative climate forcing and an overall cooling effect on the atmosphere, while an SSA<0.85 will result in a positive climate forcing and an overall warming effect due to the enhanced aerosol absorption (Ramanathan et al., 2001). In addition, the presence of highly absorbing fine mode aerosols in the lower atmosphere will result in heating of the particles and significant local warming of the boundary layer (Hermann and Hanel, 1997; Ramanathan and Carmichael, 2008). This can result in an increase in the convective available potential energy of the boundary layer and a large scale rising motion over time (Chung and Zhang, 2004). This may help to explain the rapid increase in the boundary layer height observed in this area (Shaw et al., 2008; Fast and Zhong, 1998; Whiteman et al., 2000).

Doran et al. (2007) have calculated forward and back trajectories of air masses at 1000 m above ground level (a.g.l.) over site T1 during daylight hours (06:00–18:00 LST) for a 20-day period during the month of March 2006. The most favorable conditions for transport from site T0 to site T1 were seen to occur on days 69, 70, 77, 78, 79, 81, 83, 86 and 87 (10–11, 18–20, 22, 24, 27–28 March). On days 71–76 (12–17 March) and day 82 (23 March) the back trajectories indicate that transport would have likely been from site T1 towards Mexico City and site T0.

The aerosol absorption, scattering, and SSAs obtained at site T0 and T1 have been averaged over the same daylight hours reported by Doran et al. (2007) for direct comparison to their calculated back trajectories. The daily average aerosol absorption at sites T0 and T1 is shown in Fig. 4 along with the measurement ranges observed during each day. The daily average absorption values are similar at both sites ranging from 16–50 Mm^{-1} with an overall average value of 35 Mm^{-1} at T0 and a range of 15–41 Mm^{-1}

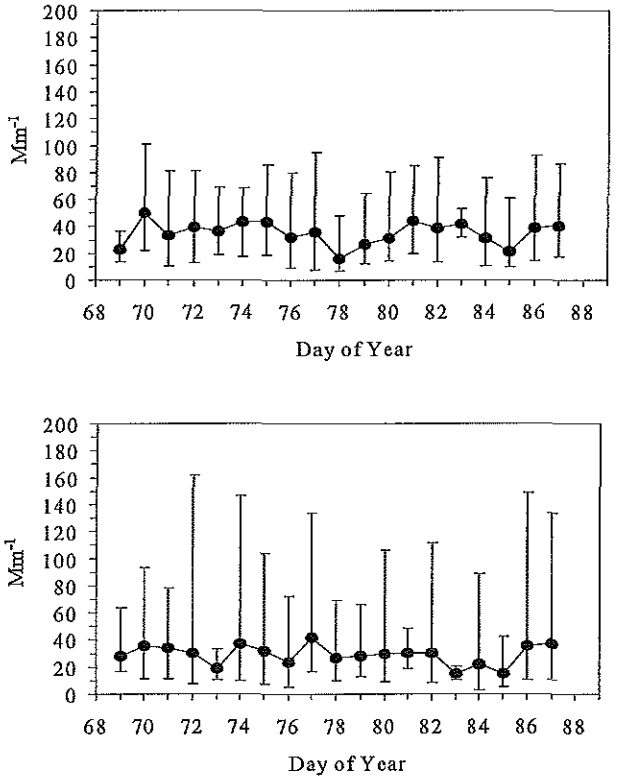

Fig. 4. Daily aerosol absorption averaged from 06:00 18:00 LST and absorption ranges measured at sites T0 (top) and T1 (bottom) from 10 March (day 69) to 29 March (day 88) 2006 during the MILAGRO field campaign.

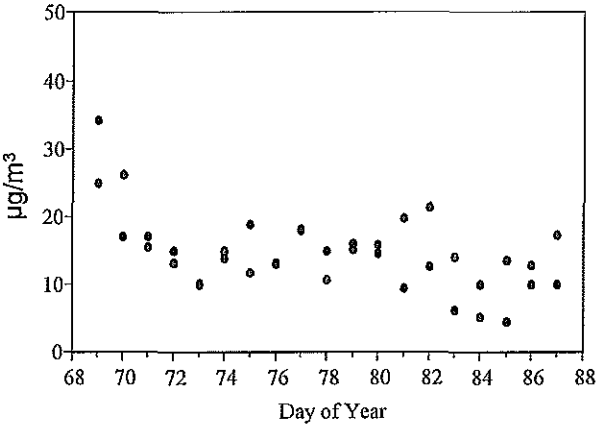

Fig. 5. Total carbon concentrations measured on fine (0.1–1 micron) aerosol samples collected from 05:30–17:30 at site T0 (red) and T1 (blue) from 10 March (day 69) to 29 March (day 88) 2006 during the MILAGRO field campaign.

with an overall average of 29 Mm^{-1} at site T1. The two sites differ primarily in the range of aerosol absorption values observed during the day. While the lower limits on the ranges are similar at both sites, indicating a regional background of around 5 Mm^{-1}, the upper limits of the aerosol absorption measurements are more variable at site T1 with a range of 21–162 Mm^{-1} as compared to site T0 with a range of 36–101 Mm^{-1}. There also appears to be no clear correlation of absorption values with transport from the Mexico City area, again indicating a local source of absorbing aerosols at site T1. Days 77, 86 and 87 (18, 27, 28 March), which were identified as likely transport days from site T0 to site T1, show high maximum aerosol absorbance. However, high maxima were also observed on days 72 and 74 (13 and 14 March) when transport has been identified as from the north. This suggests an impact at site T1 from Pachuca and/or Tizayuca (an important industrial center), which are located 10 and 64 km northeast of T1. Concentrations of TC obtained on fine mode aerosol samples collected over the daylight hours at sites T0 and T1 are shown in Fig. 5. The overall profile of the daily carbon concentrations during the study period is similar at both sites with the highest values (25–35 $\mu g/m^3$) observed on the first two days of the study period and lower values (5–15 $\mu g/m^3$) during the rest of the study. The mass absorption coefficients for BC at 550 nm were estimated assuming that the TC content of the <1 micron aerosols was 30% BC. This is in good agreement with past measurements made in the Mexico City area (Chow et al., 2002; Vega et al., 2004) as well as for measurements made in other urban areas (Tanner et al., 1982; Gaffney et al., 1984). The adjusted values reported for OC/EC ratios measured at site T1 are also in this range (Doran, 2007) as well as estimates made from aerosol mass spectrometry measurements (Aiken et al., 2008; Salcedo et al., 2006). The BC mass absorption coefficients shown in Fig. 6 range from 3.0–12.2 m^2/g with an average of 7.7 m^2/g at T0 and from 2.7–12.3 m^2/g with an average of 7.7 m^2/g at T1.

The mass absorption for EC reported for T1 by continuous OC/EC analysis was 5.6 m^2/g with a range of 1–18 m^2/g at 870 nm and 8.9 m^2/g at 550 nm assuming an α_a of 1 (Doran, 2007). Other reported estimates of BC mass absorption in Mexico City vary from 4.8 m^2/g (Baumgardner et al., 2007) to 9.5 m^2/g (Schuster et al., 2005) at 550 nm. The mass absorption coefficient for BC calculated from a multi-filter rotating shadow-band radiometer (MFRSR) measurements in Mexico City was reported to be 8.2–8.9 m^2/g at 550 nm as (Barnard et al., 2007, 2008). However, these estimations are based on assumptions of BC density, BC refractive index, and aerosol mixing state and may have a "worst case" uncertainty of about 70% (Barnard et al., 2008).

While the mass absorption coefficient of freshly emitted BC aerosols is estimated to be in the range of 6.3–8.7 m^2/g at 550 nm (Bond and Bergstrom, 2006), OC aerosol species such as humic-like substances (HULIS) derived from biomass burning or secondary organic aerosols generated photochemically have mass absorption coefficients <1 m^2/g

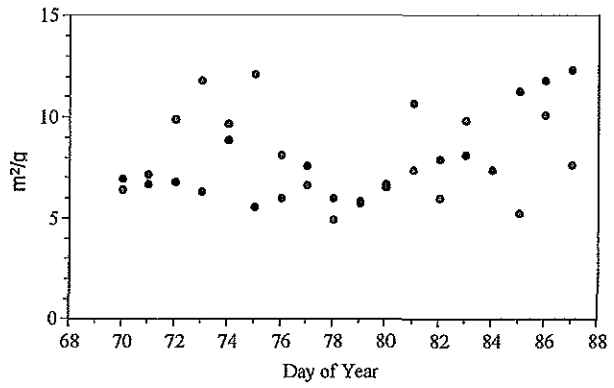

Fig. 6. Daily average mass absorption coefficient calculated for black carbon at site T0 (red) and T1 (blue) from 10 March (day 69) to 29 March (day 88) 2006 during the MILAGRO field campaign.

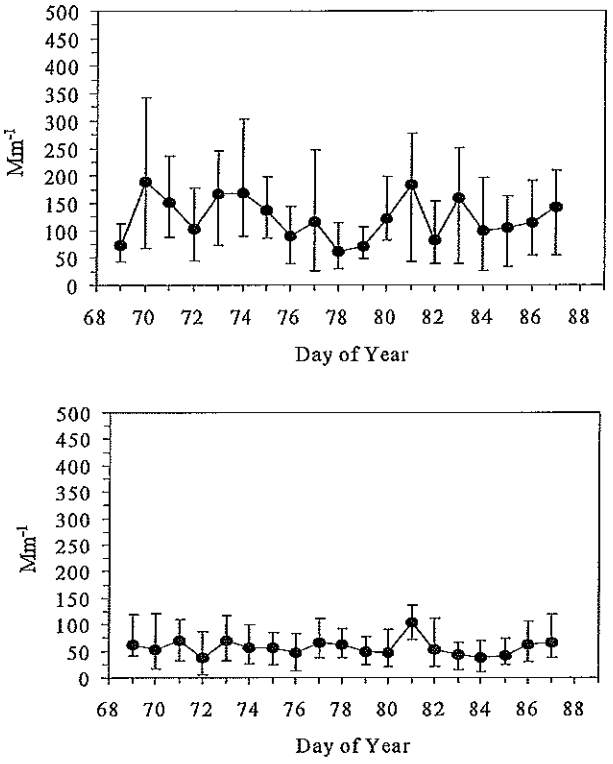

Fig. 7. Daily aerosol scattering averaged from 06:00–18:00 LST and scattering ranges measured at sites T0 (top) and T1 (bottom) from 10 March (day 69) to 29 March (day 88) 2006 during the MILAGRO field campaign.

at 550 nm (Hoffer et al., 2006; Patterson and McMahon, 1984). The overall mass absorption coefficients measured for total carbon (BC+OC) will be dependent on the relative concentrations of BC and OC as well as their mixing state (Hitzenberger and Pauxbaum, 1993; Bond et al., 2006). The similarity of the mass absorption for both sites T0 and T1 suggests that the aerosol carbon composition was similar at both sites. The fine mode aerosol scattering averaged over the daylight hours is shown in Fig. 7 for sites T0 and T1 along with the measurement ranges for each day. The daily averages vary from 60–187 Mm^{-1} with an overall average of 123 Mm^{-1} at T0. The daily average aerosol scattering was lower and more consistent at site T1 with a range of 38–105 Mm^{-1} and an overall average of 57 Mm^{-1}. There also does not seem to be a general trend of major impacts on aerosol scattering at T1 due to transport from Mexico City except for possibly day 81 (22 March). Day 81 was identified as having favorable conditions for transport from site T0 to site T1 (Doran et al., 2007) and that day showed high scattering values for both sites.

The period from day 82 (23 March) to day 87 (24 March) was dominated by heavy regional rains and an overall increase in relative humidity (see Fig. 1). Rain totals before day 82 were 0 mm at site T0 and 6.7 mm at site T1. After day 82 rain totals were 19.2 mm at T0 and 59.5 mm at T1. This was accompanied by an increase in the average daily maximum RH from 59% to 76% at T0 and from 73% to 89% at T1. The increased rains resulted in a decrease in aerosol scattering at both sites by approximately the same amount. The average aerosol scattering at site T0 before the rainy period was 128 Mm^{-1} (range of 62–197 Mm^{-1}) and during the rainy period the aerosol scattering dropped to 118 Mm^{-1} (range of 85–157 Mm^{-1}). The same values for site T1 were 61 Mm^{-1} (range of 39–105 Mm^{-1}) before day 82 and 50 Mm^{-1} (range of 38–66 Mm^{-1}) after day 82. However, the aerosol absorption remained the same at site T0 with a value before day 82 of 35 Mm^{-1} (range of 16–50 Mm^{-1}) and a value of 35 Mm^{-1} (range of 21–42 Mm^{-1}) after day 82. The aerosol absorption at T1 decreased slightly from 30 Mm^{-1} (range of 19–41 Mm^{-1}) before the rainy period to 26 Mm^{-1} (range of 15–37 Mm^{-1}) during the rainy period. Since a significant fraction of highly scattering non-absorbing aerosols are primarily inorganic and hydrophilic, it is expected that they will wash out more readily during rain events than the freshly emitted absorbing BC aerosols that are more hydrophobic in nature (Marley et al., 2000; Gaffney and Marley, 2005; Marley and Gaffney, 2007). However, as the BC aerosols become coated with SOA, they will become more hydrophilic in nature and their washout rates would be expected to increase.

The fine mode aerosol SSAs averaged over the daylight hours at site T0 and T1 are shown in Fig. 8. The average fine aerosol SSA at site T0 ranged from 0.72–0.83 with an overall average of 0.78 while the average fine aerosol SSA at T1 was slightly lower and ranged from 0.63–0.78 with an overall average of 0.70. Doran et al. (2007) reported daily average total column aerosol SSAs at T1 at 500 nm determined by using a MFRSR. These results were reported for days 71, 78 and 86 as 0.84, 0.85 and 0.89 (12, 19, and 27 March) (Doran et

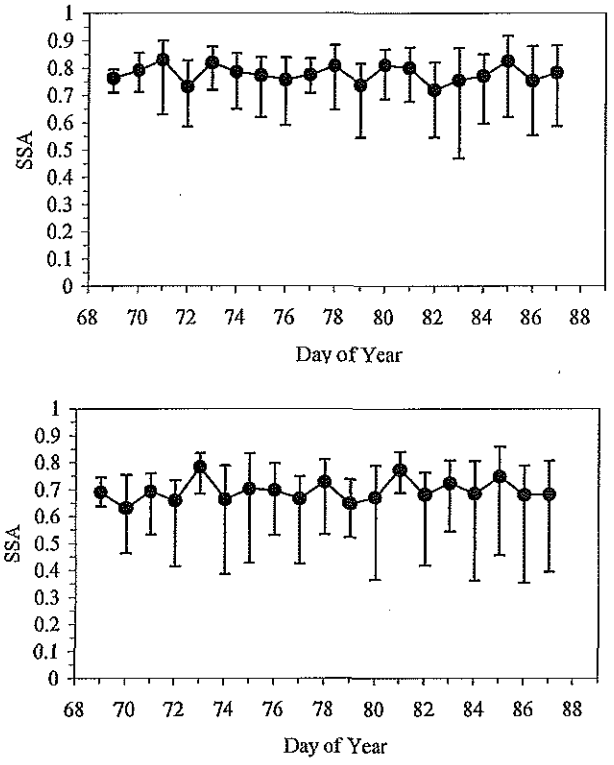

Fig. 8. Daily aerosol single scattering albedo (SSA) averaged from 06:00–18:00 LST and SSA ranges measured at sites T0 (top) and T1 (bottom) from 10 March (day 69) to 29 March (day 88) 2006 during the MILAGRO field campaign.

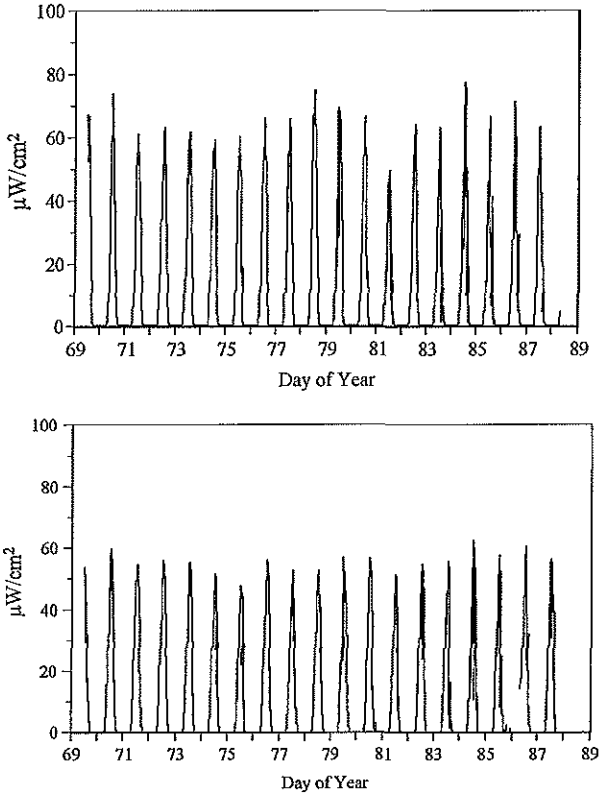

Fig. 9. Broadband UVB measured at sites T0 (top) and T1 (bottom) from 10 March (day 69) to 29 March (day 88) 2006 during the MILAGRO field campaign.

al., 2007). The corresponding average fine aerosol SSAs reported here from ground-based aerosol absorbance and scattering measurements at 550 are 0.69, 0.73, and 0.68. The MFRSR SSA values are for the total aerosol burden while the values calculated in this work represent a surface measurement of fine mode aerosols only. The fine aerosol fraction measured here (0.1 to 2 micron diameter) contains the more highly absorbing carbonaceous aerosols. The much larger mechanically generated coarse mode aerosols (>2 micron), which are included in the MFRSR measurements are very highly scattering species. The total aerosol SSAs are therefore generally expected to be higher than the SSAs measured for the fine aerosol fraction alone.

Daily average fine mode aerosol SSAs have also been reported for La Merced, located in central Mexico City, and Pedregal, a suburban neighborhood in the southwest portion of Mexico City during March of 1997 (Eidels-Dubovoi, 2002). These SSA values were calculated from ground level aerosol absorption measurements obtained with a single channel aethalometer and aerosol scattering measurements obtained by an open air integrating nephelometer at 530 nm. The SSA values reported at La Merced varied from 0.63–0.86 with an average of 0.72 and those reported at Pedregal ranged from 0.60–0.84 with an average of 0.68. These results compare well with the fine mode aerosol SSAs reported here.

Broadband UVB measurements obtained at sites T0 and T1 are shown in Fig. 9. The UVB intensity was higher at site T0, with an average of 64 μW/cm^2 and a range of 50–70 μW/cm^2 at solar noon, than at site T1, which had an average of 54 μW/cm^2 and a range of 48–58 μW/cm^2 at solar noon. In general, UVB reached a maximum at both sites at 12:30 LST. However, the variability of the daily maximum was larger at site T0 (11:30–14:00 LST) than at site T1 (12:00–13:00 LST). A comparison of simultaneous measurements from site T0 and T1 for cloudless days gave a correlation coefficient of 0.931 (slope of 1.18, intercept of 1.01). The measured UVB irradiances have been compared to that expected for clear sky conditions as determined by a radiative transfer model developed at The University of Chicago (Frederick and Lubin, 1988). The input to this model includes column ozone, determined from the Total Ozone Mapping Spectrometer (TOMS) satellite data, atmospheric optical thickness, UVB surface albedo, site location, day of year and time of day. The results of this comparison

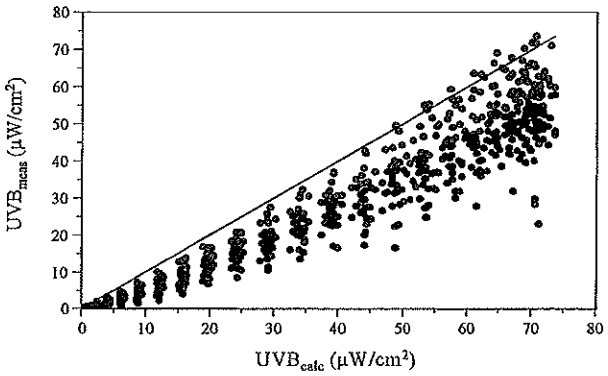

Fig. 10. Broadband UVB measured at sites T0 (red) and T1 (blue) compared to calculated clear sky UVB on days without rain events during the MILAGRO field campaign.

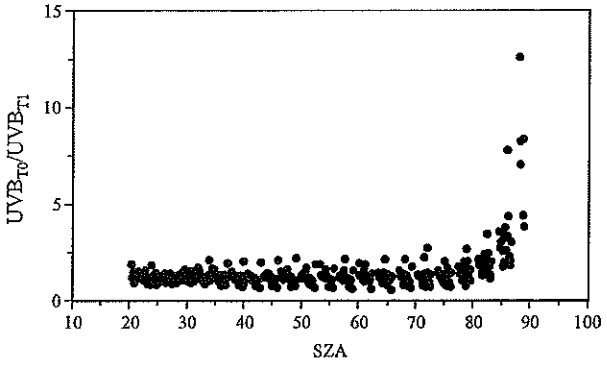

Fig. 11. Ratio of broadband UVB measured at sites T0 and T1 on days without rain events as a function of solar zenith angle (SZA) during the MILAGRO field campaign.

are shown in Fig. 10 for days without rain events. Both sites show reduced UVB radiation when compared to the clear sky modeled values, as expected for sites with significant UVB absorbing gases and aerosols (Castro et al., 2001; Gaffney et al., 2002; Barnard et al., 2008). However, the UVB radiation field observed at site T1 is reduced further than that observed at site T0. The measured UVB at both sites showed good correlation with the modeled UVB values (r^2=0.95, 0.96). However, the slope for site T0 was 0.87 while that for site T1 was 0.72. It should be noted that ozone, an important UVB absorbing gas was at similar or higher levels at T0 than T1, and the difference in observed UVB at the sites was not due to higher ozone at T1 for the clear days examined.

The ratio of UVB measurements obtained simultaneously at site T0 and site T1 for cloudless days are shown in Fig. 11 as a function of solar zenith angle (SZA). This ratio of measured UVB at T0 to UVB at T1 increases dramatically at high SZAs. At high SZAs, when the sun is close to the horizon, the optical path is sufficiently long that the majority of radiation measured by the RB meters is from the diffuse radiation field. The ratio of direct to diffuse insolation measured by the RB meter is 1.3 at a SZA of 20 deg. and reaches 0.1 at an SZA of 70 deg. (Granger et al., 1993). Therefore, since magnitude of the ratio of the UVB radiation at both sites is so strongly tied to the SZA, the data shown in Fig. 11 suggests that the diffuse radiation field at site T0 is much larger than that at site T1.

The aerosol scattering values measured by the three-wavelength nephelometer located at site T0 were used to calculate the average aerosol scattering Ångstrom coefficient (α_s). The Ångstrom coefficient for aerosol scattering is dependent on the particle size distribution with higher values ($\alpha_s > 1$) typically observed for accumulation mode particles (0.1–2 micron diameter) and lower values ($\alpha_s \approx 0$) for coarse mode particles (>2 micron) (Hand et al., 2004). The values calculated for the fine mode particles at site T0 ranged from 0.93 to 1.30 with an average of 1.11 over the entire study period. This corresponds to an average effective particle radius of 0.3 micron. (O'Niell and Royer, 1993; Lenoble and Brogniez, 1985). The direction of light scattered by particles is also dependent on the size of the particle. This is described by the particle scattering asymmetry factor (g). Mie scattering theory predicts that particles that approach the same size as that of the wavelength of the incoming radiation will scatter the radiation most favorably toward the forward direction. The dominant particle size of the fine mode particles at site T0, as determined by the Angstrom coefficient for scattering, is 0.3 micron (300 nm), which is of a similar size as the incoming UVB radiation. Therefore the UVB spectral range will be scattered most efficiently toward this forward direction by these fine mode particles. In addition, the Ångstrom scattering exponent of 1.1 corresponds to a g of 0.7 (Lenoble and Brogniez, 1985), which implies that the aerosol scattering intensity will be peaked 45 deg. toward the forward direction. Therefore, the predominance of highly scattering submicron aerosols at T0 results in a larger amount of diffusely scattered UVB radiation and a higher UVB intensity at ground level than was observed at site T1.

The presence of highly absorbing fine mode aerosols in the Mexico City area, as indicated by the low SSAs, are expected to reduce the UV flux at ground level and therefore to reduce the photochemical production of oxidants such as ozone (Dickerson et al., 1997; Castro et al., 2001). However, as seen in Figs. 10 and 11, the presence of fine mode scattering aerosols in the boundary layer that approach the same size as the wavelength of the incoming UV radiation may also increase the UV flux at ground level due to their ability to strongly scatter light towards the forward direction and this increase in UVB flux also leads to an increase in photochemical oxidant production (Dickerson et al., 1997). Therefore, the larger UVB radiation measured at site T0 than at site T1 helps to explain the high levels of photochemical

activity observed in the Mexico City area during MILAGRO, despite the reduction in UVB anticipated from the presence of light absorbing species (Thompson et al., 2008; Stephens et al., 2008; Shim et al., 2008; Shon et al., 2008; Dusanter et al., 2008; Wood et al., 2008).

4 Conclusions

Measurements of fine mode aerosol absorption and scattering were obtained in Mexico City at site T0 located in the northern part of Mexico City at the IMP (Instituto Mexicano del Petróleo) laboratories and for site T1 located at the Technical University of Tecamac, 29 km northwest of T0. Hourly averages of aerosol absorption at 550 nm was similar at both sites, ranging from 7–107 Mm^{-1} with an average of 37 Mm^{-1} at T0; and from 3–147 Mm^{-1} with an average of 27 Mm^{-1} at T1. Aerosol scattering measured at 550 nm at T0 ranged from 16–344 Mm^{-1} with an average of 105 Mm^{-1}; while the aerosol scattering values at T1 were much lower than at T0 ranging from 2–136 Mm^{-1} with an average of 53 Mm^{-1}. The maximum scattering values at site T0 occurred 2 h later than the maximum scattering values seen at T1 and 4 h later than the peak aerosol absorption values at either site. This suggests that the high aerosol scattering values measured at T0 were primarily due to rapid secondary aerosol formation in the city, while the lower aerosol scattering values at T1 were controlled primarily by changes in the boundary layer height in the early morning.

Fine mode aerosol SSAs were calculated at 550 nm for both sites using these data. The lower aerosol scattering values result in lower values for aerosol SSA at T1. The SSAs at T0 ranged from 0.47–0.92 with an average of 0.73 while SSAs at T1 ranged from 0.35–0.86 with an average 0.68. The low SSA determined for the fine mode aerosols indicate the presence of highly absorbing fine mode aerosols in the lower atmosphere. These fine mode aerosols will have a much slower settling velocity (0.3–60 cm/h) than the more highly scattering coarse mode aerosols (60–1000 cm/h) and will be transported more readily from the Mexico City basin into the surrounding regions (Finlayson-Pitts and Pitts, 2000). The absorption of solar radiation by these highly absorbing fine mode aerosols in the lower atmosphere will result in a heating of the particles and a significant local warming of the boundary layer (Hermann and Hanel, 1997; Ramanathan and Carmichael, 2008). This can result in an increase in the convective available potential energy of the boundary layer and a large scale rising motion over time (Chung and Zhang, 2004) and may help to explain the rapid increase in the boundary layer height observed in past studies in this area (Fast and Zhong, 1998; Whiteman et al., 2000; Shaw et al., 2008). Therefore, studies of boundary layer meteorology processes need to consider absorbing aerosol species when calculating heating rates (Fast and Zhong, 1998; Whiteman et al., 2000).

Comparisons of aerosol absorption averaged over the daylight hours with back trajectories reported by Doran et al. (2007) showed no clear correlation with transport from the Mexico City area, indicating a local source of absorbing aerosols at site T1, as suggested earlier (Doran et al., 2007). Similar comparisons of scattering measurements averaged over the daylight hours also do not seem to show a general trend of major effects on aerosol scattering at T1 due to transport from Mexico City except for possibly day 81 (22 March). Day 81 was identified as having favorable conditions for transport from site T0 to site T1 (Doran et al., 2007) and that day showed high scattering values for both sites.

Broadband UVB intensity was higher at site T0, with an average of 64 $\mu W/cm^2$ and a range of 50–70 $\mu W/cm^2$ at solar noon, than at site T1, which had an average of 54 $\mu W/cm^2$ and a range of 48–58 $\mu W/cm^2$ at solar noon. Comparisons of modeled UVB intensities with the simultaneous UVB measurements obtained at site T0 and at site T1 for cloudless days imply a larger diffuse radiation field at site T0 than at site T1. The determination of aerosol scattering Ångstrom coefficients at T0 suggests the predominance of aerosols at T0 in the size range of 0.3 micron. This results in aerosol scattering peaked 45 deg. toward the forward direction leading to the enhanced diffuse radiation at T0. This enhanced diffuse UVB radiation would help to explain the significant photochemistry observed in the Mexico City area during MILAGRO, despite the reduction in UVB anticipated from the high levels of light absorbing aerosol species (Thompson et al., 2008; Stephens et al., 2008; Shim et al., 2008; Shon et al., 2008; Dusanter et al., 2008; Wood et al., 2008).

The results of this study confirm that the Mexico City megacity environment has significant levels of fine mode absorbing aerosols. The high loadings of BC aerosols from fossil fuel emissions in the urban environment along with biomass burning contributions contribute to significant aerosol absorption, which will lead to local warming in the boundary layer at both the urban and regional sites. The presence of these high concentrations of absorbing aerosols in the urban area will contribute to the urban heat island effects and the transport of these absorbing aerosols into the surrounding areas will result in a positive climate forcing and an overall warming effect in the region.

Acknowledgements. This work was conducted as part of the Department of Energy's Atmospheric Science Program as part of the Megacity Aerosol Experiment – Mexico City, and as part of the MCMA2006 study during MILAGRO. This research was supported by the Office of Science (BER), US Department of Energy Grant No. DE-FG02-07ER64329 and the Mexican Government through SEMARNAT (FOSEMARNAT-2004-01-116) and the Metropolitan Environmental Commission. We wish to thank Mr. Rick Petty and Ashley Willamson of OBER for their continuing encouragement. We also wish to thank Mexican scientists and students from the Instituto Mexicano del Petróleo (IMP) and CENICA, for their assistance, and also to M. I. Saavedra from CCA, UNAM. Thanks also to Neil Sturchio, Ms. Linnea Heraty, and Ms. Nancy Martinez

of the University of Illinois at Chicago for their assistance in obtaining TC measurements reported here, and to Luisa Molina and Sasha Madronich for their organizational assistance with MILAGRO.

Edited by: L. Molina

References

Aiken, A. C., DeCarlo, P. F., Kroll, J. H., Worsnop, D. R., Huffman, J. A., Docherty, K. S., Ulbrich, I. M., Mohr, C. Kimmel, J. R., Sueper, D., Sun, Y., Zhang, Q., Trimborn, A., Northway, M., Zieman, P. J., Canagaratna, M. B., Onash, T. B., Alfarra, M. R., Prevot, A. S. H., Dommen, J., Duplissy, J., Metzger, A., Baltensperger, U., and Jimenz, J. L. O/C and M/OC ratios of primary, secondary, and ambient organic aerosols with high resolution time-of-flight aerosol mass spectrometry, Environ. Sci. Technol., 42, 4478–4485, 2008.

Anderson, T. L. and Ogren, J. A.: Determining aerosol radiative properties using the TSI 3563 integrating nephelometer, Aerosol Sci. Tech., 29, 57–69, 1998.

Andreae, M. O. and Gelencsér, A.: Black carbon or brown carbon? The nature of light-absorbing carbonaceous aerosols, Atmos. Chem. Phys., 6, 3131–3148, 2006, http://www.atmos-chem-phys.net/6/3131/2006/.

Arnott, W. P., Hamasha, K., Moosmuller, H., Sheridan, P. J., and Ogren, J. A.: Towards aerosol light-absorption measurements with a 7-wavelength aethalometer: Evaluation with a photoacoustic instrument and 3-wavelength nephelometer, Aerosol Sci. Tech., 39, 17–29, 2005.

Ban-Weiss, G. A., McLaughlin, J. P., Harley, R. A., Lunden, M. M., Kirchstetter, T. W., Kean, A. J., Strawa, A. W., Stevenson, E. D., and Kendall, G. R.: Long-term changes in emissions of nitrogen oxides and particulate matter from on-road gasoline and diesel vehicles, Atmos. Environ., 42, 220–232, 2008.

Barnard, J. C., Kassianov, E. I., Ackerman, T. P., Johnson, K., Zuberi, B., Molina, L. T., and Molina, M. J.: Estimation of a "radiatively correct" black carbon specific absorption during the Mexico City Metropolitan Area (MCMA) 2003 field campaign, Atmos. Chem. Phys., 7, 1645–1655, 2007, http://www.atmos-chem-phys.net/7/1645/2007/.

Barnard, J. C., Volkamer, R., and Kassianov, E. I.: Estimation of the mass absorption cross section of the organic carbon component of aerosols in the Mexico City Metropolitan Area, Atmos. Chem. Phys., 8, 6665–6679, 2008, http://www.atmos-chem-phys.net/8/6665/2008/.

Barth, M. C. and Church, A. T.Regional and global distributions and lifetimes of sulfate aerosols from Mexico City and southeast China, J. Geophys. Res., 104, 30231–30239, 1999.

Baumgardner, D., Kok, G. L., and Raga, G. B.: On the diurnal variability of particle properties related to light absorbing carbon in Mexico City, Atmos. Chem. Phys., 7, 2517–2526, 2007, http://www.atmos-chem-phys.net/7/2517/2007/.

Bergstrom, R. W.: Extinction and absorption coefficients of the atmospheric aerosol as a function of particle size, Beitraege zur Physik der Atmosphaere, 46, 223–234, 1973.

Bergstrom, R. W., Russell, P. B., and Hignett, P.: Wavelength dependence of the absorption of black carbon particles: Predictions and results from the TARFOX experiment and implications for the aerosol single scattering albedo, J. Atmos. Sci., 59, 567–577, 2002.

Bond, T. C., Anderson, T. L., and Campbell, D.: Calibration and intercomparison of filter-based measurements of visible light absorption by aerosols, Aerosol Sci. Tech., 30, 582–600, 1999.

Bond, T. C. and Bergstrom, R. W.: Light absorption by carbonaceous particles: An investigative review, Aerosol Sci. Tech., 40, 27–67, 2006.

Bond, T. C., Habib, G., and Bergstrom, R. W.: Limitations in the enhancement of visible light absorption due to mixing state, J. Geophys. Res., 111, D20211, doi:10.1029/2006JD007315, 2006.

CAM: Programa para Mejorar la Calidad del aire de la Zona Metropolitana del Valle de Mexico 2002–2010, Capitulo 2, La Zona Metropolitana del Valle de Mexico, 25 pp., online available at: (http://www.paot.org.mx/centro/libros/proaire/cap02.pdf), last access: January 2009, 2002.

Carabalí, G.: Caracterización morfológica, óptica y química de partículas muestreadas en el sitio T1 de la campaña MILAGRO, Tesis de Maestría, Universidad Nacional Autónoma de México, México, 2008..

Castro, T., Madronich, S., Rivale, S., Muhlia, A., and Mar, B.: The influence of aerosols on photochemical smog in Mexico City, Atmos. Environ., 35, 1765–1772, 2001.

Charlson, R. J., Schwartz, S. E., Hales, J. M., Cess, R. D., Coakley Jr., J. A., Hansen, J. E., and Hoffman, D. J.: Climate forcing by anthropogenic aerosols, Science, 255, 423–430, 1992.

Chow, J. C., Watson, J. G., Pritchett, L. C., Pierson, W. R., Frazier, C. A., and Purcell, R. G.: The DRI thermal/optical reflectance carbon analysis system: description, evaluation, and applications in US air quality studies, Atmos. Environ., 27, 1185–1201, 1993.

Chow, J. C., Watson, J. G., Edgerton, S. A., and Vega, E.: Spacial differences in outdoor PM_{10} mass and aerosol composition in Mexico City, J. Air Waste Manage., 52, 423–434, 2001.

Chow, J. C., Watson, J. G., Edgerton, S. A., and Vega, E.: Chemical composition of $PM_{2.5}$ and PM_{10} in Mexico City during winter 1997, Sci. Total Environ., 287, 177–201, 2002.

Chung, C. E. and Zhang, G. J.: Impact of absorbing aerosol on precipitation: Dynamic aspects in association with convective available potential energy and convective parameterization closure and dependence on aerosol heating profile, J. Geophys. Res., 109, D22103, doi:10.1029/2004JD004726, 2004.

Chung, S. H. and Seinfeld, J. H.: Climate response of direct radiative forcing of anthropogenic black carbon, J. Geophys. Res., 110, D11102, doi:10.1029/2004JD005441, 2005.

Clarke, A. D.: Aerosol light absorption by soot in remote environments, Aerosol Sci. Tech., 10, 161–171, 1989.

DeCarlo, P. F., Dunlea, E. J., Kimmel, J. R., Aiken, A. C., Sueper, D., Crounse, J., Wennberg, P. O., Emmons, L., Shinozuka, Y., Clarke, A., Zhou, J., Tomlinson, J., Collins, D. R., Knapp, D., Weinheimer, A. J., Montzka, D. D., Campos, T., and Jimenez, J. L.: Fast airborne aerosol size and chemistry measurements above Mexico City and Central Mexico during the MILAGRO campaign, Atmos. Chem. Phys., 8, 4027–4048, 2008, http://www.atmos-chem-phys.net/8/4027/2008/.

de Foy, B., Varela, J. R., Molina, L. T., and Molina, M. J.: Rapid ventilation of the Mexico City basin and regional fate of the urban plume, Atmos. Chem. Phys., 6, 2321–2335, 2006, http://www.atmos-chem-phys.net/6/2321/2006/.

de Foy, B., Fast, J. D., Paech, S. J., Phillips, D., Walters, J. T., Coulter, R. L., Martin, T. J., Pekour, M. S., Shaw, W. J., Kastendeuch, P. P., Marley, N. A., Retama, A., and Molina, L. T.: Basin-scale wind transport during the MILAGRO field campaign and comparison to climatology using cluster analysis, Atmos. Chem. Phys., 8, 1209–1224, 2008, http://www.atmos-chem-phys.net/8/1209/2008/.

DeLuisi, J., Wendell, J., and Kreiner, F.: An examination of the spectral response characteristics of seven Robertson-Berger meters after long-term field use, Photochem. Photobiol., 56, 115–122, 1992.

Dickerson, R. R., Kondragunta, S., Stenchikov, G., Civerolo, K. L., Doddridge, B. G., and Holben, B. N.: The impact of aerosols on solar ultraviolet radiation and photochemical smog, Science, 31, 827–830, 1997.

Doran, J. C., Abbott, S., Archuleta, J., Bian, X., Chow, J., Coulter, R. L., de Wekker, S. F. J., Edgerton, S., Elliott, S., Fernandez, A., Fast, J. D., Hubbe, J. M., King, C., Langley, D., Leach, J., Lee, J. T., Martin, T. J., Martinez, D., Martinez, J. L., Mercado, G., Mora, V., Mulhearn, M., Pena, J. L., Petty, R., Porch, W., Russell, C., Salas, R., Shannon, J. D., Shaw, W. J., Sosa, G., Tellier, L., Templeman, B., Watson, J. G., White, R., Whiteman, C .D., and Wolfe, D.: The IMADA-AVER boundary layer experiment in the Mexico City area, B. Am. Meteorol. Soc., 79, 2497–2508, 1998.

Doran, J. C., Barnard, J. C., Arnott, W. P., Cary, R., Coulter, R., Fast, J. D., Kassianov, E. I., Kleinman, L., Laulainen, N. S., Martin, T., Paredes-Miranda, G., Pekour, M. S., Shaw, W. J., Smith, D. F., Springston, S. R., and Yu, X.-Y.: The T1-T2 study: evolution of aerosol properties downwind of Mexico City, Atmos. Chem. Phys., 7, 1585–1598, 2007, http://www.atmos-chem-phys.net/7/1585/2007/.

Doran, J. C.: Corrigendum to "The T1-T2 study: evolution of aerosol properties downwind of Mexico City", Atmos. Chem. Phys., 7, 1585-1598, 2007, http://www.atmos-chem-phys.net/7/1585/2007/.

Doran, J. C., Fast, J. D., Barnard, J. C., Laskin, A., Desyaterik, Y., and Gilles, M. K.: Applications of lagrangian dispersion modeling to the analysis of changes in the specific absorption of elemental carbon, Atmos. Chem. Phys., 8, 1377–1389, 2008, http://www.atmos-chem-phys.net/8/1377/2008/.

Dua, S. K., Hopke, P. K., and Raunemaa, T.: Hygroscopicity of diesel aerosols Water Air Soil Poll., 112, 247–257, 1999.

Dubovik, O., Holben, B. N., Kaufman, Y. J., Yamasoe, M., Smirnov, A., Tanre, D., and Slutsker, I.: Single scattering albedo of smoke retrieved from the sky radiance and solar transmittance measured from ground, J. Geophys. Res., 103, 31903–31923, 1998.

Dusanter, S., Vimal, D., Stevens, P. S., Volkamer, R., and Molina, L. T.: Measurements of OH and HO_2 concentrations during the MCMA-2006 field campaign - Part 1: Deployment of the Indiana University laser-induced fluorescence instrument, Atmos. Chem. Phys. Discuss., 8, 13689–13739, 2008, http://www.atmos-chem-phys-discuss.net/8/13689/2008/.

Eidels-Dubovoi, S.: Aerosol impacts on visible light extinction in the atmosphere of Mexico City, Sci. Total Environ., 287, 213–220, 2002.

Fast, J. D. and Zhong, S.: Meteorological factors associated with inhomogeneous ozone concentrations within the Mexico City basin, J. Geophys. Res., 103, 18927–18946, 1998.

Fast, J. D., de Foy, B., Acevedo Rosas, F., Caetano, E., Carmichael, G., Emmons, L., McKenna, D., Mena, M., Skamarock, W., Tie, X., Coulter, R. L., Barnard, J. C., Wiedinmyer, C., and Madronich, S.: A meteorological overview of the MILAGRO field campaigns, Atmos. Chem. Phys., 7, 2233–2257, 2007, http://www.atmos-chem-phys.net/7/2233/2007/.

Finlayson-Pitts, B. J. and Pitts Jr., J. N.: Chemistry of the Upper and Lower Atmosphere, chapter 9, Academic Press, 349–374, 2000.

Frederick, J. E. and Lubin, D.: The budget of biologically active radiation in the earth-atmosphere system, J. Geophys. Res., 93, 3825–3832, 1988.

Gaffney, J. S., Tanner, R. L., and Phillips, M.: Separating carbonaceous aerosol source terms using thermal evolution, carbon isotopic measurements, and C/N/S determinations, Sci. Total Environ., 36, 53–60, 1984.

Gaffney, J. S. and Marley, N. A.: Uncertainties in climate change predictions: Aerosol effects, Atmos. Environ., 32, 2873–2874, 1998.

Gaffney, J. S., Marley, N. A., Cunningham, M. M., and Doskey, P. V.: Measurements of peroxyacyl nitrates (PANs) in Mexico City: Implications for megacity air quality impacts on regional scales, Atmos. Environ., 33, 5003–5012, 1999.

Gaffney, J. S., Marley, N. A., Drayton, P. J., Doskey, P. V., Kotamarthi, V. R., Cunningham, M. M., Baird, J. C. Dintaman, J., and Hart, H. L.: Field observations of regional and urban impacts on NO_2, Ozone, UV-B, and nitrate radical production rates: Nocturnal urban plumes and regional smoke effects, Atmos. Environ., 36, 825–833, 2002.

Gaffney, J. S. and Marley, N. A.: The importance of the chemical and physical properties of aerosols in determining their transport *and residence times in the troposphere, Chapter 14, in: Urban* Aerosols and Their Impacts: Lessons Learned from the World Trade Center Tragedy, edited by: Gaffney, J. S. and N. A., Marley, ACS Symposium Book 919, Oxford University Press, 286–300, 2005.

Gaffney, J. S., Marley, N. A., Tackett, M., Stuchio, N., Heraty, L., Martinez, N. Hardy, K., and Guilderson, T.: Biogenic carbon dominance based on $^{13}C/^{12}C$ and ^{14}C measurements of total carbon at T-0 and T-1 sites during MILAGRO, 88th National Meeting of the American Meteorological Society, Tenth Conference on Atmospheric Chemistry, Conference Proceedings Volume, Paper J1.1, 5 pp., online availabe at: http://ams.confex.com/ams/pdfpapers/131852.pdf, 2008.

Granger, R. G., Basher, R. E., and McKenzie, R. L.: UV-B Robertson-Berger meter characterization and field calibration, Appl. Optics, 32, 343–349, 1993.

Hand, J. L., Kreidenweis, S. M., Slusser, J., and Scott, G.: Comparison of aerosol optical properties derived from Sun photometry to estimates inferred from surface measurements in Big Bend National Park, Texas, Atmos. Environ., 38, 6813–6821, 2004.

Hansen, A. D. A., Rosen, H., and Novakov, T.: Real-time measurement of the absorption coefficient of aerosol particles, Appl. Optics, 21, 3060–3062, 1982.

Hennigan, C. J., Sullivan, A. P., Fountoukis, C. I., Nenes, A., Hecobian, A., Vargas, O., Peltier, R. E., Case Hanks, A. T., Huey, L. G., Lefer, B. L., Russell, A. G., and Weber, R. J.: On the volatility and production mechanisms of newly formed nitrate and water soluble organic aerosol in Mexico City, Atmos. Chem. Phys., 8, 3761–3768, 2008, http://www.atmos-chem-phys.net/8/3761/2008/.

Hermann, P. and Hanel, G.: Wintertime optical properties of atmospheric particles and weather, Atmos. Environ., 24, 4053–4062, 1997.

Hermann, M., Stratmann, M., Wilck, M., and Wiedensohler, A.: Sampling characteristics of an aircraft-borne aerosol inlet system, J. Am. Meterol. Soc., 7–19, 2001.

Hitzenberger, R. and Puxbaum, H.: Comparisons of the measured and calculated specific absorption coefficients for urban aerosol samples in Vienna, Aerosol Sci. Technol., 18, 323–345, 1993.

Hoffer, A., Gelencsér, A., Guyon, P., Kiss, G., Schmid, O., Frank, G. P., Artaxo, P., and Andreae, M. O.: Optical properties of humic-like substances (HULIS) in biomass-burning aerosols, Atmos. Chem. Phys., 6, 3563–3570, 2006, http://www.atmos-chem-phys.net/6/3563/2006/.

Horvath, H., Catalan, L., and Trier, A. A.: study of the aerosol of Santiago De Chile III: Light absorbing measurements, Atmos. Environ., 31, 3737–3744, 1997.

Jacobson, M. Z.: Global direct radiative forcing due to multicomponent anthropogenic and natural aerosols, J. Geophys. Res., 106, 1551–1568, 2001.

Jacobson, M. Z.: Control of fossil fuel particulate black carbon and organic matter, possibly the most effective method of slowing global warming, J. Geophys. Res., 107, ACH 16-1–16-22, doi:10.1029/2001JD001376, 2002.

Jacobson, M. Z.: Climate response of fossil fuel and biofuel soot, accounting for soot's feedback to snow and sea ice albedo and emissivity, J. Geophys. Res., 109, D21201, doi:10.1029/2004JD004945, 2004.

Kirchstetter, T. W., Novakov, T., and Hobbs, P. V.: Evidence that the spectral dependence of light absorption by aerosols is affected by organic carbon, J. Geophys. Res., 109, D21208, doi:10.1029/2004JD004999, 2004.

Kleinman, L. I., Springston, S. R., Daum, P. H., Lee, Y.-N., Nunnermacker, L. J., Senum, G. I., Wang, J., Weinstein-Lloyd, J., Alexander, M. L., Hubbe, J., Ortega, J., Canagaratna, M. R., and Jayne, J.: The time evolution of aerosol composition over the Mexico City plateau, Atmos. Chem. Phys., 8, 1559–1575, 2008, http://www.atmos-chem-phys.net/8/1559/2008/.

Lenoble, J. and Brogniez, C.: Information on stratospheric aerosol characteristics contained in the SAGE satellite multiwavelength extinction measurements, Appl. Optics, 24, 1054–1063, 1985.

Marley, N. A., Gaffney, J. S., Drayton, P. J., Cunningham, M. M., Orlandini, K. A., and Paode, R.: Measurement of ^{210}Pb, ^{210}Po, and ^{210}Bi in size-fractionated atmospheric aerosols: An estimate of fine-aerosol residence times, Aerosol Sci. Tech., 32, 569–583, 2000.

Marley, N. A., Gaffney, J. S., Ramos-Villegas, R., and Cárdenas González, B.: Comparison of measurements of peroxyacyl nitrates and primary carbonaceous aerosol concentrations in Mexico City determined in 1997 and 2003, Atmos. Chem. Phys., 7, 2277–2285, 2007, http://www.atmos-chem-phys.net/7/2277/2007/.

Marley, N. A. and Gaffney, J. S.: The impact of rain events on aerosol optical properties: Mexico City 2003 and 2006, EOS Transactions AGU, 88(23), Joint Assembly Supplement, Abstract A41E-03, 2007.

Marley, N. A., Gaffney, J. S., Tackett, M. J., Sturchio, N. C., Heraty, L., Martinez, N., Hardy, K. D., Machany-Rivera, A., Guilderson, T., MacMillan, A., and Steelman, K.: The impact of biogenic carbon emissions on aerosol absorption in Mexico City, Atmos. Chem. Phys. Discuss., 8, 18499–18530, 2008, http://www.atmos-chem-phys-discuss.net/8/18499/2008/.

McKinlay, A. and Diffy, B. L.: A reference action spectrum for ultraviolet induced erythema in human skin, in: Human exposure to ultraviolet radiation: Risks and regulations, edited by: Passchler, W. R. and Bosnajokovic, B. F. M., Elsevier Science Publishers, Amsterdam, The Netherlands, 83–87, 1987.

Molina, L. T. and Molina, M. J.: Air quality impacts: Local and global concern, Chapter 1, in: Air quality in the Mexico Megacity, An integrated assessment, edited by: Molina, L. T., Molina, M. J., Kluwer Academic, The Netherlands, 2002.

Molina, L. T., Kolb, C. E., de Foy, B., Lamb, B. K., Brune, W. H., Jimenez, J. L., Ramos-Villegas, R., Sarmiento, J., Paramo-Figueroa, V. H., Cardenas, B., Gutierrez-Avedoy, V., and Molina, M. J.: Air quality in North America's most populous city - overview of the MCMA-2003 campaign, Atmos. Chem. Phys., 7, 2447–2473, 2007, http://www.atmos-chem-phys.net/7/2447/2007/.

O'Niell, N. and Royer, A.: Extraction of bimodal aerosol-size distribution radii from spectral and angular slope (Angstrom) coefficients, Appl. Optics, 32, 1642–1645, 1993.

Paredes-Miranda, G., Arnott, W. P., Jimenez, J. L., Aiken, A. C., Gaffney, J. S., and Marley, N. A.: Primary and secondary contributions to aerosol light scattering and absorption in Mexico City during the MILAGRO 2006 campaign, Atmos. Chem. Phys. Discuss., 8, 16951–16979, 2008, http://www.atmos-chem-phys-discuss.net/8/16951/2008/.

Patterson, E. M. and McMahon, C. K.: Absorption characteristics of forest fire particulate matter, Atmos. Environ., 18, 2541–2551, 1984.

Petzold, A., Schloesser, H., Sheridan, P. J., Arnott, W. P., Ogren, J. A., and Virkkula, A.: Evaluation of multiangle absorption photometry for measuring aerosol light absorption, Aerosol Sci. Tech., 39, 40–51, 2005.

Pósfai, M., Anderson, J. R., Buseck, P. R., and Sievering, H.: Soot and sulfate aerosol particles in the remote marine troposphere, J. Geophys. Res., 104, 21685–21683, 1999.

Raga, G. B., Castro, T., and Baumgardner, D.: The impact of megacity pollution on local climate and implications for the regional environment: Mexico City, Atmos. Environ., 35, 1805–1811, 2001a.

Raga, G. B., Baumgardner, D., Castro, T., Martínez-Arroyo, A., and Navarro-González, R.: Mexico City air quality: a qualitative review of gas and aerosol measurements (1960–2000), Atmos. Environ., 35, 4041–4058, 2001b.

Ramanathan, V., Crutzen, P. J., Kiehl, J. T., and Rosenfeld, D.: Aerosols, climate, and the hydrological cycle, Science, 7, 2119–2124, 2001.

Ramanathan, V., Chung, C., Kim, D., Bettge, T., Buja, L., Kiel, J. T., Washington, W. M., Fu, Q., Sikka, D. R., and Wild, M.: Atmospheric brown clouds: Impacts on South Asain climate and hydrological cycle, P. Natl. Acad. Sci. USA, 102, 5326–5333, 2005.

Ramanathan, V. and Carmichael, G.: Global and regional climate changes due to black carbon, Nature Geoscience, 1, 221–227, 2008.

Salcedo, D., Onasch, T. B., Dzepina, K., Canagaratna, M. R., Zhang, Q., Huffman, J. A., DeCarlo, P. F., Jayne, J. T., Mor-

timer, P., Worsnop, D. R., Kolb, C. E., Johnson, K. S., Zuberi, B., Marr, L. C., Volkamer, R., Molina, L. T., Molina, M. J., Cardenas, B., Bernabé, R. M., Márquez, C., Gaffney, J. S., Marley, N. A., Laskin, A., Shutthanandan, V., Xie, Y., Brune, W., Lesher, R., Shirley, T., and Jimenez, J. L.: Characterization of ambient aerosols in Mexico City during the MCMA-2003 campaign with Aerosol Mass Spectrometry: results from the CENICA Supersite, Atmos. Chem. Phys., 6, 925–946, 2006, http://www.atmos-chem-phys.net/6/925/2006/.

Schmid, O., Artaxo, P., Arnott, W. P., Chand, D., Gatti, L. V., Frank, G. P., Hoffer, A., Schnaiter, M., and Andreae, M. O.: Spectral light absorption by ambient aerosols influenced by biomass burning in the Amazon Basin. I: Comparison and field calibration of absorption measurement techniques, Atmos. Chem. Phys., 6, 3443–3462, 2006, http://www.atmos-chem-phys.net/6/3443/2006/.

Schnaiter, M., Linke, C., Möhler, O., Naumann, K.-H., Saathoff, H., Wagner, R., Schurath, U., and Wehner, B.: Absorption amplification of black carbon internally mixed with secondary organic aerosol, J. Geophys. Res., 110, D19204, doi:10.1029/2005JD006046, 2005.

Schuster, G. L., Dubovik, O., Holben, B. N., and Clothiaux, E. E.: Inferring black carbon content and specific absorption from AERONET retrievals, J. Geophys. Res., 101, D10S17, doi:10.1029/2004JD006328, 2005.

Schwartz, S. E. and Buseck, P. R.: Absorbing phenomena, Science, 288, 989–990, 2000.

Shaw, W. J., Pekour, M. S., Coulter, R. L., Martin, T. J., and Walters, J. T.: The daytime mixing layer observed by radiosonde, profiler, and lidar during MILAGRO, Atmos. Chem. Phys. Discuss., 7, 15025–15065, 2007, http://www.atmos-chem-phys-discuss.net/7/15025/2007/.

Shim, C., Li, Q., Luo, M., Kulawik, S., Worden, H., Worden, J., Eldering, A., Diskin, G., Sachse, G., Weinheimer, A., Knapp, D., Montzca, D., and Campos, T.: Characterizing mega-city pollution with TES O_3 and CO measurements, Atmos. Chem. Phys. Discuss., 7, 15189–15212, 2007, http://www.atmos-chem-phys-discuss.net/7/15189/2007/.

Shon, Z.-H., Madronich, S., Song, S.-K., Flocke, F. M., Knapp, D. J., Anderson, R. S., Shetter, R. E., Cantrell, C. A., Hall, S. R., and Tie, X.: Characteristics of the NO-NO_2-O_3 system in different chemical regimes during the MIRAGE-Mex field campaign, Atmos. Chem. Phys., 8, 7153–7164, 2008, http://www.atmos-chem-phys.net/8/7153/2008/.

Stephens, S., Madronich, S., Wu, F., Olson, J. B., Ramos, R., Retama, A., and Muñoz, R.: Weekly patterns of Mxico City's surface concentrations of CO, NO_x, PM_{10} and O_3 during 1986-2007, Atmos. Chem. Phys., 8, 5313–5325, 2008, http://www.atmos-chem-phys.net/8/5313/2008/.

Stone, E. A., Snyder, D. C., Sheesley, R. J., Sullivan, A. P., Weber, R. J., and Schauer, J. J.: Source apportionment of fine organic aerosol in Mexico City during the MILAGRO experiment 2006, Atmos. Chem. Phys., 8, 1249–1259, 2008, http://www.atmos-chem-phys.net/8/1249/2008/.

Swap, R. J., Annegarn, H. J., Suttes, J. T., King, M. D., Platnick, S., Privette, J. L., and Scholes, R. J.: Africa burning: A thematic analysis of the Southern African Regional Science Initiative (SAFARI 2000), J. Geophys. Res./ 108(D13), 8465, doi10.1029/2003JD003747, 2003.

Tanner, R. L., Gaffney, J. S., and Phillips, M. F.: Determination of Organic and Elemental Carbon in Atmospheric Aerosol Samples by Thermal Evolution, Anal. Chem., 54, 1627–1630, 1982.

Thompson, A. M., Yorks, J. E., Miller, S. K., Witte, J. C., Dougherty, K. M., Morris, G. A., Baumgardner, D., Ladino, L., and Rappenglück, B.: Tropospheric ozone sources and wave activity over Mexico City and Houston during MILAGRO/Intercontinental Transport Experiment (INTEX-B) Ozonesonde Network Study, 2006 (IONS-06), Atmos. Chem. Phys., 8, 5113–5125, 2008, http://www.atmos-chem-phys.net/8/5113/2008/.

UNEP/WHO (United Nations Environmental Program/World Health Organization), Urban Air Pollution in Megacities of the World, Blackwell Publisher, Oxford, UK, 1992.

Vega, E., Reyes, E., Ruiz, H., Garcia, J., Sanchez, G., Martinez-Villa, G., Gonzalez, U., Chow, J. C., and Watson, J. G.: Analysis of $PM_{2.5}$ and PM_{10} in the atmosphere of Mexico City during 2000–2002, J. Air Waste Manage., 54, 786–798, 2004.

Volkamer, R., Jimenez, J. L., San Martini, F., Dzpina, F., Zhang, Q., Salcedo, D., Molina, L. T., Worsnop, D. R., and Molina, M. J.: Secondary organic aerosol formation from anthropogenic air pollution: Rapid and higher than expected, Geophys. Res. Lett., 33, L17811, doi:10.1029/2006GL026899, 2006.

Weatherhead, E. C., Tiao, G. C., Reinsel, G. C., Frederick, J. E., DeLuisi, J. J., Choi, D., and Tam, W.: Analysis of long-term behavior of ultraviolet radiation measured by Robertson-Berger meters at 14 sites in the United States, J. Geophys. Res., 102, 8737–8754, 1997.

Whiteman, C. D., Zhong, S., Bian, X., Fast, J. D., and Doran, J. C.: Boundary layer evolution and regional scale diurnal circulations over the Mexican plateau, J. Geophys. Res., 105, 10081–10102, 2000.

Williams, J., de Reus, M., Krejci, R., Fischer, H., and Ström, J.: Application of the variability-size relationship to atmospheric aerosol studies: estimating aerosol lifetimes and ages, Atmos. Chem. Phys., 2, 133–145, 2002, http://www.atmos-chem-phys.net/2/133/2002/.

Wood, E. C., Herndon, S. C., Onasch, T. B., Kroll, J. H., Canagaratna, M. R., Kolb, C. E., Worsnop, D. R., Neuman, J. A., Seila, R., Zavala, M., and Knighton, W. B.: Ozone production, nitrogen oxides, and radical budgets in Mexico City: observations from Pico de Tres Padres, Atmos. Chem. Phys. Discuss., 8, 15739–15789, 2008, http://www.atmos-chem-phys-discuss.net/8/15739/2008/.

Yokelson, R. J., Urbanski, S. P., Atlas, E. L., Toohey, D. W., Alvarado, E. C., Crounse, J. D., Wennberg, P. O., Fisher, M. E., Wold, C. E., Campos, T. L., Adachi, K., Buseck, P. R., and Hao, W. M.: Emissions from forest fires near Mexico City, Atmos. Chem. Phys., 7, 5569–5584, 2007, http://www.atmos-chem-phys.net/7/5569/2007/.

Xu, G. and Huang, X.: Calibration of broadband UV radiometers – methodology and uncertainty evaluation, Metrologia, 40, S21–S24, 2003.

Atmos. Chem. Phys., 9, 3721–3730, 2009
www.atmos-chem-phys.net/9/3721/2009/

Atmospheric Chemistry and Physics

Primary and secondary contributions to aerosol light scattering and absorption in Mexico City during the MILAGRO 2006 campaign

G. Paredes-Miranda[1], W. P. Arnott[1], J. L. Jimenez[2], A. C. Aiken[2], J. S. Gaffney[3], and N. A. Marley[4]

[1]Department of Physics, University of Nevada Reno, and the Desert Research Institute, Reno, NV, USA
[2]Deptartment of Chemistry and Biochemistry and CIRES University of Colorado, Boulder, CO, USA
[3]Department of Chemistry, University of Arkansas, Little Rock, AK, USA
[4]Graduate Institute of Technology, University of Arkansas, Little Rock, AK, USA

Received: 12 August 2008 – Published in Atmos. Chem. Phys. Discuss.: 10 September 2008
Revised: 20 April 2009 – Accepted: 22 April 2009 – Published: 9 June 2009

Abstract. A photoacoustic spectrometer, a nephelometer, an aethalometer, and an aerosol mass spectrometer were used to measure at ground level real-time aerosol light absorption, scattering, and chemistry at an urban site located in North East Mexico City (Instituto Mexicano del Petroleo, Mexican Petroleum Institute, denoted by IMP), as part of the Megacity Impact on Regional and Global Environments field experiment, MILAGRO, in March 2006. Photoacoustic and reciprocal nephelometer measurements at 532 nm accomplished with a single instrument compare favorably with conventional measurements made with an aethalometer and a TSI nephelometer. The diurnally averaged single scattering albedo at 532 nm was found to vary from 0.60 to 0.85 with the peak value at midday and the minimum value at 07:00 a.m. local time, indicating that the Mexico City plume is likely to have a net warming effect on local climate. The peak value is associated with strong photochemical generation of secondary aerosol. It is estimated that the photochemical production of secondary aerosol (inorganic and organic) is approximately 75% of the aerosol mass concentration and light scattering in association with the peak single scattering albedo. A strong correlation of aerosol scattering at 532 nm and total aerosol mass concentration was found, and an average mass scattering efficiency factor of 3.8 m^2/g was determined. Comparisons of photoacoustic and aethalometer light absorption with oxygenated organic aerosol concentration (OOA) indicate a very small systematic bias of the filter based measurement associated with OOA and the peak aerosol single scattering albedo.

Correspondence to: G. Paredes-Miranda
(gparedes@physics.unr.edu)

1 Introduction

About 20% of the Mexican population lives in the Mexico City metropolitan area (MCMA) in a megacity environment with approximately 23 million occupying less than 1% of the Mexican territory according to the 2005 census. Mexico City consists of 125 town councils, and 16 delegations and consists of 23 842 km^2 of territory, although a large part of this area includes mountains and rural zones without urbanization (http://www.inegi.gob.mx). This megacity has developed with a significant dependence on its transportation system. Most of the air pollution in Mexico City comes from the combustion of fossil fuels (gasoline and diesel) in motor vehicles. Approximately 75% of the 4 million tons of pollutants generated yearly in the metropolitan area comes from motor vehicles according to the Mexican emissions inventory (Mar et al., 2001). Biomass burning (BB) can also be a relevant pollution source during the dry season (March–June), especially for particulate matter (PM) (DeCarlo et al., 2008; Molina et al., 2007; Yokelson et al., 2007), although the importance is significantly higher aloft and in the outflow than on the ground inside the city, and BB impacts on the ground were highly variable in time during MILAGRO (Aiken et al., 2009; Stone et al., 2008).

The seasonal variation of the daily maximum vertical component of solar irradiance at the top of the atmosphere above Mexico City varies between 1040 W/m^2 at the winter minimum and 1327 W/m^2 at the summer maximum due to its subtropical location at latitude 19 degrees north. Solar radiation and the relatively high elevation of Mexico City give rise to strong ventilation of the city where residence times for pollutants is on the order of 7 h and the atmospheric boundary layer height can vary from 2 km to 4 km above ground level

(de Foy et al., 2006). Stagnant conditions associated with low wind speeds can produce locally high concentrations of pollutants, depending on the wind direction. The topography surrounding the MCMA basin gives rise to characteristic flow patterns on different days with flow associated with convergence and pollution buildup in the south of MCMA, flow that drains to the northeast, and "cold surges" associated with low atmospheric boundary layer heights where cold air from the north drains through the Chalco passage in the southeast of the MCMA (de Foy et al., 2006). These flow patterns give rise to pollutant concentrations that can vary markedly from day to day; however, it is the purpose of this paper to seek an understanding of the average diurnal behavior of aerosol concentrations and optical properties during the month of March, 2006.

Aerosol light scattering and absorption have considerable radiative impacts that can lead to cooling or heating, respectively. A comparison of the intensity of global radiation in Mexico City with that over a nearby rural area for the same time was performed to estimate attenuation of the solar beam by the smog layer (Jauregui and Luyando, 1999). These authors found that reduction of total solar incoming radiation is on the order of 21–22% on non-cloudy days during both the dry and the rainy seasons. Inorganic and organic aerosols tend to strongly scatter and backscatter visible solar radiation, and are associated with a cooling effect on climate (Charlson et al., 1992; Haywood and Ramaswamy, 1998). Black carbon aerosols strongly absorb radiation from the near infrared through the ultraviolet and tend to have a warming effect on climate (Andreae, 2001; Haywood and Ramaswamy, 1998; Jacobson, 2001). Black carbon has long been associated with "elemental carbon", though other carbonaceous species absorb light as well, particularly at UV wavelengths (Andreae and Gelencsér, 2006; Kirchstetter et al., 2004). A more apt name for aerosol light absorption by organic carbon species is brown carbon because of their selective absorption at shorter wavelengths (Sun et al., 2007).

Filter-based measurement of aerosol light absorption by organic species is complicated because they can exist in the liquid state and wet the filter material (Subramanian et al., 2007). Calibration efforts for the filter-based measurement of aerosol light absorption have only considered aerosol as solids rather than as liquids (Arnott et al., 2005; Bond et al., 1999; Virkkula et al., 2007; Weingartner et al., 2003). A recent review of aerosol light absorption issues is available (Bond and Bergstrom, 2006). Recent measurements in Houston, TX, USA indicate a systematic positive bias of the filter-based instrument, the particle soot absorption photometer in the presence of high secondary organic aerosol concentration (Lack et al., 2008).

Analyses of aerosol measurements during the MCMA-2003 field campaign (Molina et al., 2007; Salcedo et al., 2006; Volkamer et al., 2006, 2007) show that the submicron aerosol mass in Mexico City during the spring is dominated by secondary species (nitrate, sulfate, ammonium, chloride, and secondary organic aerosol or SOA) with the main primary species being primary organic aerosol or POA, black carbon, and crustal material. Salcedo et al. (2006) described the rapid formation of ammonium nitrate in the local Mexico City atmosphere, while ammonium sulfate seemed to be formed more slowly and over larger regional scales. Ammonium chloride was also observed in small concentrations, but its diurnal cycle seemed to reflect primarily its semivolatile character. Volkamer et al. (2006) showed that formation of SOA was rapid and exceeded the predictions of current models by almost an order of magnitude.

This paper reports diurnally averaged aerosol light scattering and absorption measurements made using photoacoustic, nephelometer, and aethalometer instruments during the MILAGRO campaign in March, 2006. Aerosol mass spectrometer measurements of the submicron speciated organics and inorganics were also diurnally averaged. These measurements are combined to show the radiative and chemical impacts of primary and secondary aerosols in the MCMA. The diurnal variation of aerosol chemistry and optics is used to estimate the contributions of secondary aerosol formation to particulate mass and light scattering.

2 Experimental

2.1 Sites

The MILAGRO (Megacity Initiative: Local and Global Research Observations) campaign took place in Mexico City in the MCMA during the month of March 2006 (http://www.eol.ucar.edu/projects/milagro). The campaign was carried out to better understand the local, regional and global impact of pollutants generated in megacities, considering health effects and visibility issues as well as climate impacts. The MILAGRO field experiment involved more than 400 researchers from over 120 institutions in the USA, Mexico, and several other countries. The campaign involved coordinated aircraft and ground-based measurements supported by extensive modeling and satellite observations (de Almeida Castanho et al., 2007). Three main sites were strategically chosen to characterize the transport and transformation of the pollutants carried from the urban area of the city, and to take measurements on the ground; one in the urban area of Mexico City designated T0 located in Northeast Mexico City at the Instituto Mexicano del Petroleo (IMP), and the other two, T1 and T2 were located, respectively at urban and rural locations with approximated 32 km and 63 km north of IMP (Querol et al., 2008).

2.2 Measurement methods

Aerosol light scattering and absorption instruments were calibrated, installed, and operated at the T0 site. Aerosol light absorption was measured by the photoacoustic spectrometer

(PAS) method. The PAS provides a fundamental measurement of aerosol light absorption based on use of a calibrated microphone to measure the sound produced when light absorbing aerosol in the acoustical resonator are heated by laser light absorption and transfer that heat to the surrounding air (Arnott et al., 1999). The PAS instrument accuracy has been evaluated and confirmed using both gaseous light absorption by NO_2 (Arnott et al., 2000) and through the use of the subtraction of aerosol light scattering from aerosol extinction for laboratory generated external mixtures of kerosene soot and ammonium sulfate (Sheridan et al., 2005). The PAS used at IMP was operated at 532 nm, and conveniently allowed for characterization of gaseous (i.e. NO_2) absorption at this wavelength as well when a particle filter was used on the inlet. Simultaneous light scattering measurements are accomplished within the PAS by use of an optical sensor configured to operate as a reciprocal nephelometer (Rahmah et al., 2006). The reciprocal nephelometer measurements of scattering coefficient have a systematic relative uncertainty of 15%, and the photoacoustic absorption coefficient measurements have a 5% relative uncertainty (Lewis et al., 2008) associated with systematic errors noted during repeated calibrations. Independent light scattering measurements were also obtained at the site by using a three-wavelength TSI Model 3550 nephelometer at 450 nm, 550 nm, and 700 nm (Anderson et al. 1996).

Aerosol light absorption data were also obtained with a filter-based method, the 7-wavelength aethalometer (370, 470, 520, 590, 660, 880 and 950 nm). The use of the aethalometer to estimate aerosol light absorption in urban locations has been discussed previously (Arnott et al., 2005). In brief, the aethalometer measurement uses light transmission measurements through an aerosol laden quartz fiber filter. The change of light transmission with time is first used to obtain the aerosol absorption optical depth as affected by multiple scattering enhancements by the fiber media. Then the instrument algorithm computes a black carbon mass concentration (BC) with use of the measured flow rate, sample time, and an assumed filter multiple-scattering-enhanced mass-absorption-efficiency that is about a factor of two larger than would be appropriate for the same particles dispersed in air as an aerosol. The factor of two comes about because it is equally possible for light to be going through the filter in either direction as a consequence of multiple scattering so that for a clean filter, particles deposited on the filter have two chances for absorbing a given photon. Finally, an empirically derived mass absorption efficiency of 8.8 m^2/g was determined, using a PAS and an aethalometer in urban Las Vegas, Nevada, USA, to be relevant for converting the aethalometer BC measurements at 520 nm to aerosol light absorption at 532 nm to correct for the filter enhancement of absorption (Arnott et al., 2005).

Real time chemical characterization of the PM_1 aerosol composition was obtained with a High-Resolution Aerosol Mass Spectrometer (AMS) (Canagaratna et al., 2007; DeCarlo et al., 2006; Jimenez et al., 2003). The AMS provides mass concentration of non-refractory inorganic (nitrate, ammonium, sulfate, and chloride) and organic aerosol (OA). The organic aerosol can be apportioned among different components using factor analysis techniques on the AMS spectra (Zhang et al., 2005, 2007). For this study the Positive Matrix Factorization (PMF) method was applied on the unit-resolution AMS spectra (Paatero and Tapper, 1994; Ulbrich et al., 2008) which allowed the quantification of hydrocarbon-like OA (HOA), oxygenated organic aerosol (OOA) as a surrogate for secondary organic aerosol (SOA), and biomass-burning OA (BBOA). PMF of the high-resolution spectra, which is in progress and will be presented in a future publication, shows similar results with more detail on the apportionment (Aiken et al., 2008; Aiken et al., 2009). The mass concentration measurements obtained with the AMS have an uncertainty of about 20% due to the uncertainty of particle collection efficiency (Huffman et al., 2005; Salcedo et al., 2006).

Aerosol optics measurements were accomplished under dry conditions owing to the generally low relative humidity (below 50%) observed in the instruments. In addition, all measurements are reported at Central Standard Time (CST), the local time in Mexico City. All measurements are reported at ambient pressure and temperature. To convert concentrations to standard temperature and pressure conditions (STP, 1 atm and 273 K) the values reported here should be multiplied by approximately 1.42. It was estimated that the sampling inlets on the instrumentation resulted in an effective size cut of PM_1 (i.e. one micron). The fraction of the $PM_{2.5}$ mass between PM_1 and $PM_{2.5}$ in Mexico City is typically small (Salcedo et al., 2006; Querol et al., 2008), so slight differences in the detailed size cuts of the different instruments should only lead to small differences on the aerosols sampled.

3 Results and discussion

Comparisons of PAS with aethalometer absorption and TSI nephelometer scattering data are presented in Figs. 1 and 2. The data demonstrate good agreement of the PAS measurements for scattering and absorption with these other commonly employed methods. These comparisons are consistent with the accuracy demonstrated in previous comparisons of light absorption and scattering using similar instrumentation (Arnott et al., 2005; Rahmah et al., 2006).

Significant diurnal variations of aerosol light absorption and scattering were observed and are attributed in part due to changes in the meteorology in the Mexico City Basin and the sources of aerosols impacting the IMP site (see Fig. 3). On the diurnal average, the aerosol light absorption and scattering coefficients were found to vary between 20 and 80 Mm^{-1} and between 60 and 170 Mm^{-1}, respectively. Gaseous light absorption at 532 nm, likely associated

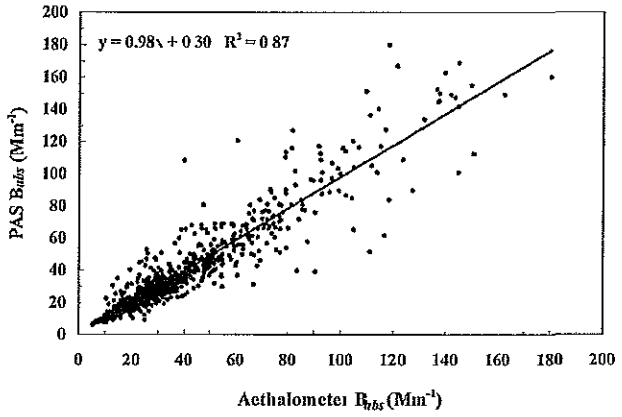

Fig. 1. Light absorption comparison of PAS with Aethalometer at 532 nm and 520 nm at the IMP site. Each point represents a 30 min average.

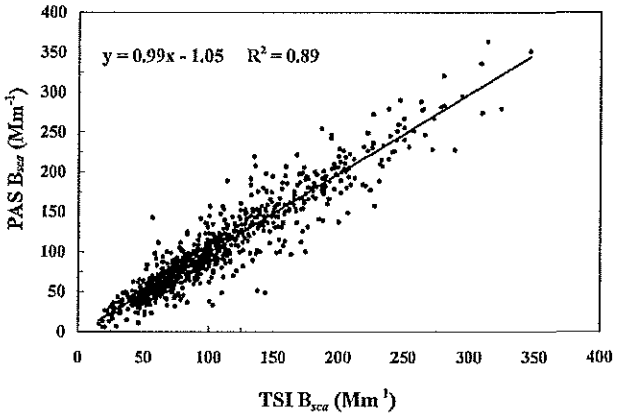

Fig. 2. Light scattering comparison of PAS with TSI at 532 nm and 550 nm at the IMP site. Each point is a 30 min average.

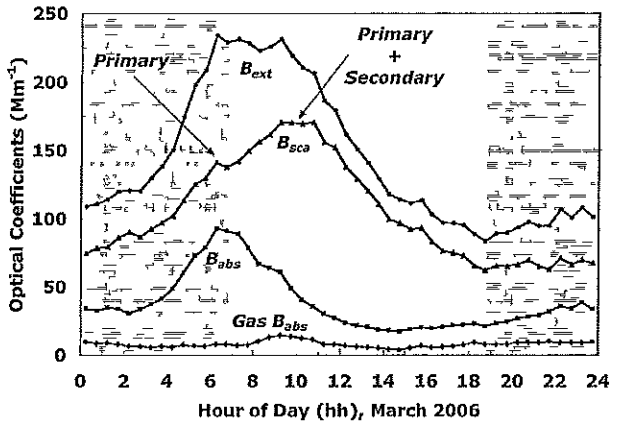

Fig. 3. Diurnal variation of aerosol light absorption, scattering, and extinction at 532 nm.

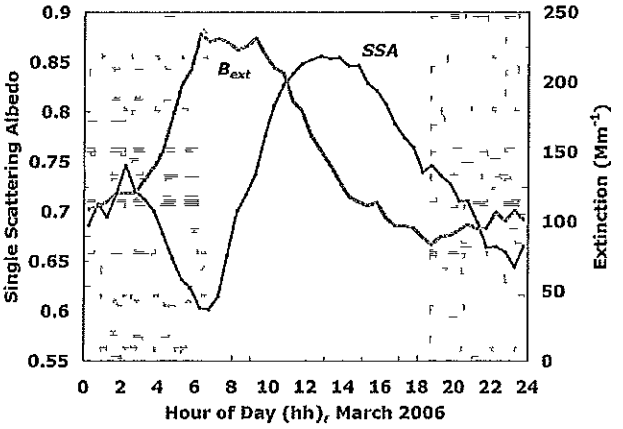

Fig. 4. Diurnal single scattering albedo (dark curve and circles) varies between 0.6 and 0.85 at 532 nm, and begins to flatten out around 10 as extinction (shaded curve and triangles) diminishes. Nighttime is the shaded region.

with NO_2, was less than 20 Mm^{-1} on average. The peak in aerosol light scattering occurs several hours later in the day than the absorption peak because of aerosol light scattering contributions from photochemically-generated secondary aerosol mass and perhaps due to diurnal changes in the primary aerosol sources. Note that the aerosol concentration at night above the boundary layer is typically small (e.g. OOA background levels are $\approx$2–3 μg m^{-3} under ambient conditions (Herndon et al., 2008)) and thus the air which is being mixed down with the urban air during the boundary layer rise in the morning does not greatly perturb the observations presented here. The peak in aerosol light absorption is likely to coincide with the time of early morning traffic rush hour under low atmospheric boundary layer height before sunrise. Previous diurnally averaged aethalometer measurements at the Centro Nacional de Investigación y Capacitación Ambiental (CENICA) supersite located southeast of the T0 site in Mexico City in April 2003 showed an equivalent aerosol light absorption at 532 nm ranging from 22 to 66 Mm^{-1}, with a similar timing of the peak value when the CENICA measurements are converted from Central Daylight Savings Time to Central Standard Time (Salcedo et al., 2006). The 30 min averaged maximum aerosol extinction coefficient on an average day is about 230 Mm^{-1}. It is associated with both primary emissions and secondary formation and extends from around 06:00 a.m. until 10:00 a.m.

The aerosol single scattering albedo (SSA) at 532 nm was calculated from the scattering and extinction measurements shown in Fig. 3. The SSA absolute uncertainty varies somewhat during the day, but it is typically about 0.03, just as in McComiskey et al. (2008). Significant diurnal variation of the aerosol single scattering albedo (SSA) was observed as shown in Fig. 4. Daily averaged minimum SSA values are 0.60 coincident with absorption peaks in the early morning. By noon local time the maximum averaged SSA value

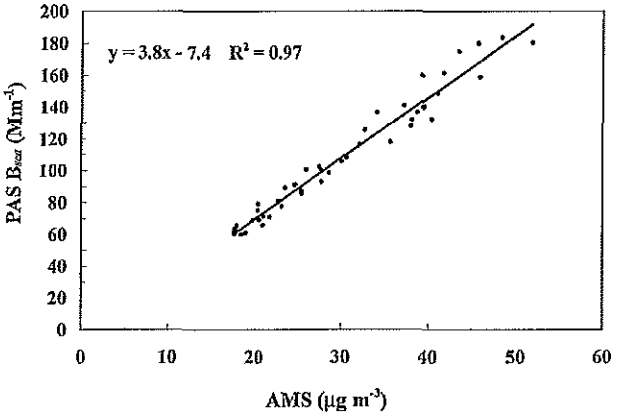

Fig. 5. Correlation of aerosol light scattering at 532 nm with total submicron aerosol mass. The mass scattering efficiency is 3.8 m^2/g. Data are from the diurnal average shown in Fig. 6.

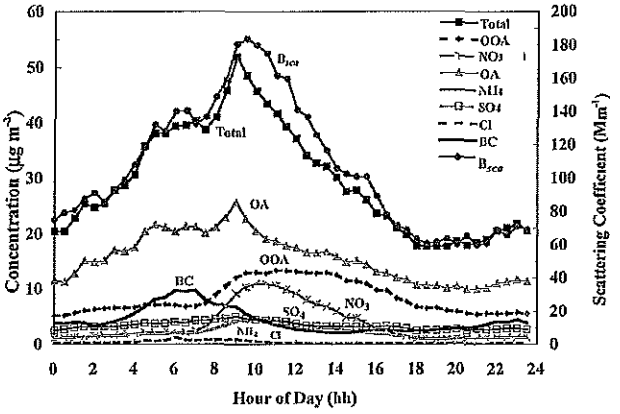

Fig. 6. Diurnal variation of aerosol chemistry and optics.

of 0.85 is observed, coincident with boundary layer height development and ventilation that dilute primary emissions of light absorbing aerosol. Photochemically generated secondary particle mass produces a rapid increase in SSA as soon as the sun rises to a peak around noon. The diurnally averaged single scattering albedo is roughly the same for approximately 3 h centered on local 14:00 as boundary layer dilution is balanced by secondary aerosol formation and continuing primary emissions of scattering and absorbing aerosol. Direct measurements of aerosol single scattering albedo is especially important because of its strong impact on direct aerosol radiative forcing (McComiskey et al., 2008). Aerosol single scattering albedo values are strongly dependent on primary sources and secondary atmospheric chemistry, as well as other parameters such as the combustion intensity and flaming and smoldering fraction of biomass burning events. For example, the flaming stage of bushes such as sage produces smoke with a SSA of around 0.3 at 532 nm (Lewis et al., 2008), very similar to the value found for kerosene and diesel soot (Arnott et al., 2000; Sheridan et al., 2005), while combustion of pines and duffs results in SSAs between 0.9 and 1.0 (Lewis et al., 2008). Aerosol mixing state and chemistry impact optical properties.

Previous measurements of total $PM_{2.5}$ in Mexico City, 2003, have been shown to agree well with the sum of aerosol species from the AMS plus refractory BC and soil (Salcedo et al., 2006), and most of the aerosol mass in MCMA is likely in internally mixed particles by the afternoon (Johnson et al., 2005; Salcedo et al., 2007). In the current study, total aerosol scattering at 532 nm correlates well with total PM_1 aerosol mass as obtained from the AMS plus refractory BC obtained from the photoacoustic measurements of light absorption and use of a mass absorption efficiency factor of 8.8 m^2/gram, as shown in Fig. 5. The mass scattering efficiency of 3.8 m^2/g was determined from the linear regression, which is the same as the value found by DeCarlo et al. (2008) with measurements around the Mexico City region from the NCAR C-130 aircraft. For comparison, other mass scattering efficiency factors at 550 nm found in megacity environments include values of 4.9 m^2/g in India, and 3.4 m^2/g in Beijing (Bergin et al., 2001; Mayol-Bracero et al., 2002). The linear regression shown in Fig. 5 shows a small systematic variation of the aerosol mass scattering efficiency that will be discussed later.

Figure 6 displays the diurnal variation of PM_1 along with its components, and the aerosol scattering coefficient at 532 nm. Figure 6 illustrates the close relationship of PM_1 and aerosol light scattering throughout the average day with a slight tendency of increased aerosol mass scattering efficiency during daylight hours. The PM_1 used here is a sum of BC, the inorganic species, and the total organic aerosol mass (OA). A small negative bias is associated with the omission of crustal material, which however usually only constitutes a few percent of the PM_1 aerosol (Salcedo et al., 2006). BC was estimated by dividing the photoacoustic light absorption measurements at 532 nm by a mass absorption efficiency factor of 8.8 m^2/g. The oxygenated organic aerosol (OOA), NH_4, and NO_3, all have a diurnal trend that is distinctly different from the BC diurnal trend, strongly suggesting that a substantial fraction of the OOA, NH_4, and NO_3 are produced by same-day secondary photochemical processes in addition to a fraction that appears to arise from carryover from the previous day and/or from regional background. It should be noted that the biomass burning organic aerosol (BBOA) and hydrocarbon-like organic aerosol (HOA) (not shown) generally follow a diurnal trend very similar to that of BC (Aiken et al., 2009). In summary, certain species and properties such as BC and aerosol light absorption, HOA, and BBOA tend to follow diurnal emission patterns and atmospheric boundary layer dynamics, while others such as aerosol light scattering, PM_1, OOA, NH_4, and NO_3 have a strong diurnal component. We next develop an estimate of the fraction of aerosol

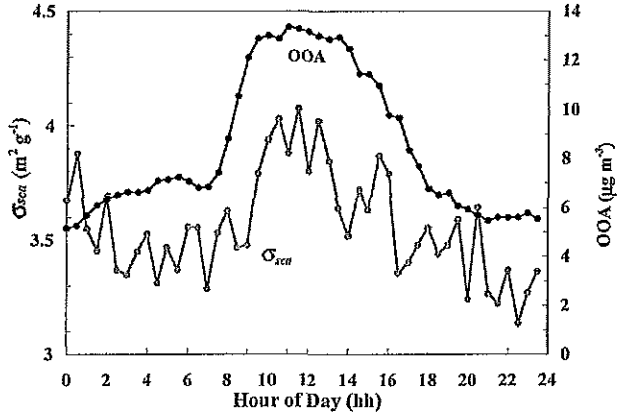

Fig. 7. Mass scattering efficiency as a function of time of day, and the OOA.

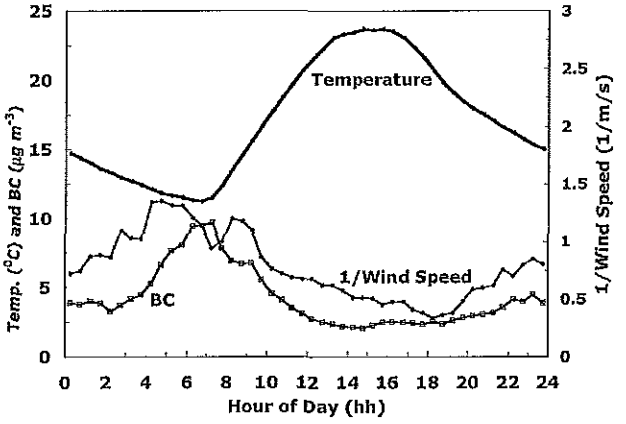

Fig. 8. Average diurnal variation of the air temperature, black carbon mass concentration (BC), and reciprocal wind speed. Reciprocal wind speed is proportional to air parcel residence time in the city and is a measure of stagnation.

light scattering and mass concentration with a diurnal trend suggestive of same-day secondary photochemical processes.

Figure 7 shows the diurnal variation of the mass scattering efficiency and OOA. The peak value of mass scattering efficiency, 4.1 m^2/g, is observed to occur at midday coincident with the peak OOA concentration, while the lowest values ~3.3 m^2/g occur in the late evening and early morning, consistent with the increased fraction of smaller primary particles. Both aerosol size and composition may affect the mass scattering efficiency.

The diurnal variation of some of the planetary boundary layer (PBL) characteristics, and BC are shown in Fig. 8. The reciprocal of wind speed is directly proportional to the residence time of air parcels in the city, and is a measure of stagnation. BC peaks at sunrise when the air temperature is lowest and the air is most stagnant. By 02:00 p.m. the air temperature is maximum, the air is least stagnant, and

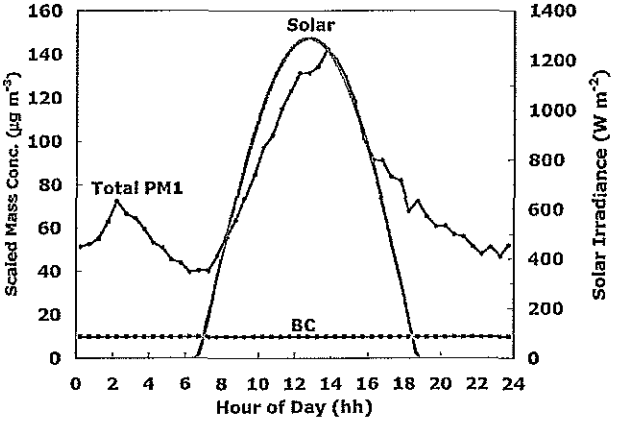

Fig. 9. BC and PM_1 mass concentration scaled to a constant planetary boundary layer. The peak PM_1 lags the peak solar irradiance at the top of the atmosphere by two hours.

black carbon concentration is also lowest. If BC were emitted at a constant rate through out the day, and the deposition rate is constant, then BC would be a measure of the dilution during the day as the PBL develops. Figure 9 shows the PM_1 and BC concentration scaled so that BC is at its peak value all day long. The purpose of this figure is to estimate what the PM_1 concentration would be during the day if only secondary aerosol generation mechanisms were active, but the PBL was otherwise constant at a fixed height. The peak normalized-PM_1 occurs a few hours after the peak solar irradiance during the day due to generation of aerosol of mass by secondary photochemical processes. A second peak occurs in the early morning hours possibly as a consequence of the diminishing air temperature that favors condensation of vapors on existing particles. The effect of biomass burning POA is approximately accounted for by the normalization to BC, since this component has a similar diurnal cycle as BC (Aiken et al., 2009).

In estimating the contributions of aerosol scattering from primary emissions plus carryover from the previous day and same-day secondary mechanisms, we will assume that Mexico City aerosol concentration and optics are due to primary sources that have concentrations determined mostly by diurnal variations in boundary layer dynamics and emission strengths, plus secondary sources that are affected both by boundary layer dynamics and photochemical transformations. Details of the myriad specific emission rates and secondary formation processes and their temporal variations are simplified into these two classes of aerosols. Denote by f_{sca} the fraction of scattering due to secondary as

$$f_{sca} = \frac{B_{sca}^{secondary}}{B_{sca}} = \frac{B_{sca} - \left(\frac{\omega_{prim}}{1-\omega_{prim}}\right) B_{abs}}{B_{sca}}. \quad (1)$$

In Eq. (1), ω_{prim} is the single scattering albedo associated with primary emissions. The numerical value of

$[\omega_{prim}/(1-\omega_{prim})]$=1.16 was determined by best fit of the f_{sca} curve to the f_{mass} curve discussed below. A value of ω_{prim}=0.54 was found, commensurate with 75% of the primary aerosol extinction coming from compression ignition vehicle exhaust having a SSA of 0.4, and 25% of the primary aerosol extinction coming from sources like spark ignition vehicles and biomass combustion having a SSA of 0.95. The value of ω_{prim} is lower than the lowest value of the diurnally averaged SSA in Fig. 4 likely as a result that on the average, some aerosol carryover occurs from day to day. SSA values around ω_{prim} were observed in the morning hours following days with significant wind and rain that cleared out much of the background aerosol. The second term in Eq. (1) is a proxy for the primary emission of light scattering aerosol during all hours of the day. Equation (1) assumes that the sources of primary aerosol emissions that contribute most of the scattering and absorbing aerosols do not dramatically change on average during the course of the day. This assumption is likely to be valid during day light hours associated with the normal business workday since traffic related emissions dominate in Mexico City, and biomass burning impacts appear to have a similar diurnal cycle (Aiken et al., 2009). The quantity f_{sca} is further discussed below after a similar definition of the fraction of aerosol mass concentration due to secondary processes is developed.

The fractional aerosol mass due to photochemical production can also be estimated. Comparisons of the aerosol mass concentration with speciated data given in Fig. 6 are consistent with the secondary aerosol species (NH_4, NO_3, SO_4, and OOA interpreted as a surrogate for SOA) being photochemically produced and are hence correlated to the observed diurnal variations in precursor concentrations and solar radiation, with the exception of sulfate which is produced more regionally as described above. This interpretation is also consistent with previous studies (Salcedo et al., 2006; Volkamer et al., 2007). The total secondary aerosol mass concentration can be obtained from a sum of these species. The ratio, f_{mass}, of the sum of species having sunlight related diurnal variation to the total aerosol mass concentration is given in Eq. 2:

$$f_{mass} = \frac{OOA + NH_4 + NO_3 + SO_4}{OA + BC + IO}, \quad (2)$$

where IO is the sum of all of the inorganic species measured by the AMS as given in Fig. 6. Note that chloride has both primary and secondary sources in Mexico City (Salcedo et al., 2007; DeCarlo et al., 2007) and since its concentration is very small, it is not included in this calculation. This relationship is perhaps specific to Mexico City and may not be applicable to other locations having different geography and aerosol sources, but does give a measure of secondary aerosol production in a tropical megacity. The species in the numerator of Eq. (2) have a carryover from daylight hours and/or a regional background, so that f_{mass} would be non-zero even in nighttime hours.

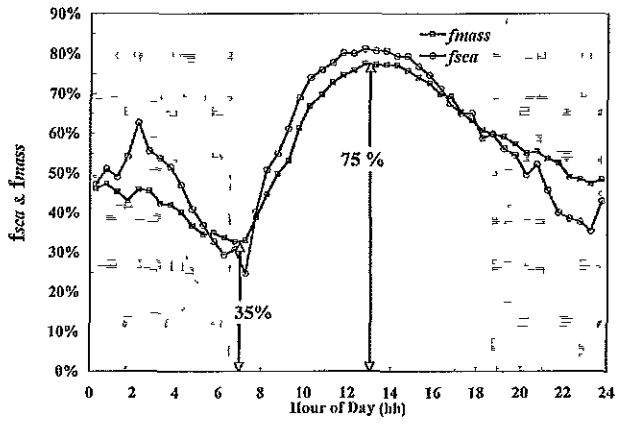

Fig. 10. Diurnal variation of the fraction of aerosol scattering and mass due to secondary photochemically related processes. The minimum occurs at sunrise due to relatively strong aerosol contributions by primary sources compared with carryover of secondary aerosol from the previous day. By noon, about 75% of the aerosol mass and scattering is due to secondary photochemically related production of aerosol.

The diurnal variation of the fraction of aerosol scattering and mass due to secondary photochemically related processes is shown in Fig. 10. The minimum of f_{sca} and f_{mass} is associated with secondary aerosol from regional background or carried over from the previous day. Some of the NH_4 is associated with SO_4 rather than NO_3. The aerosol fraction arising from secondary processes increases abruptly at sunrise, peaks at 11:00 a.m. to 02:00 p.m. and diminishes more gradually into the evening hours. The increase in the secondary contribution during daylight hours is inferred as the part of the curve for f_{mass} in the non-shaded region of Fig. 10. Around 75% of the aerosol scattering and mass is due to same-day secondary aerosol mass. While Fig. 10 is a rough approximation and in particular ignores the impact of crustal species, an estimate of the relative fraction of secondary aerosol impacts is useful to help frame the problem for the modeling community.

Figure 11 shows the diurnal variations of aerosol light absorption measured with the photoacoustic instrument and the aethalometer along with the percentage difference of these values, with the photoacoustic values in the denominator. The aethalometer values are around 15% lower than PAS values from 03:00 a.m. until 06:00 a.m., consistent with a reduction of the multiple scattering enhancement factor of the aethalometer filter media during the time of the lowest SSA (Arnott et al., 2005) . The percentage difference between PAS and aethalometer instruments has a daily variation of about 25% in total (from a maximum of about +15% to a minimum of about −10%). The OOA diurnal variation is also displayed as an indicator of time when secondary organic aerosol concentration is highest. The aethalometer data is about 10% greater than photoacoustic values from 10:00 a.m. to 01:00 p.m. coincident with the peak OOA and

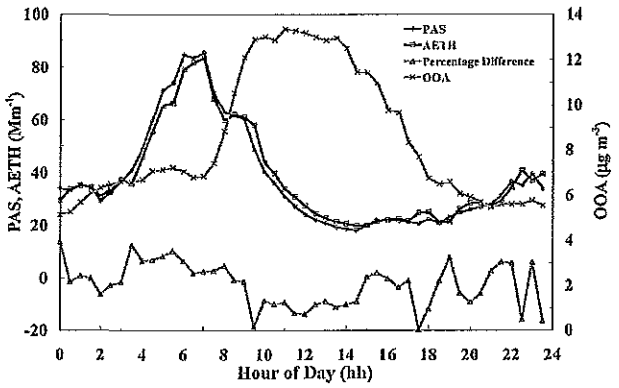

Fig. 11. Percentage difference between PAS and aethalometer instruments as a function of time of day, and the OOA.

SSA. This is in contrast to the report by Lack et al. (2008) of a strong positive bias of greater than 40% for a filter based measurement of aerosol light absorption by the particle soot absorption photometer (PSAP) compared with photoacoustic values when OOA concentration was high in Houston, Texas, USA. The difference in the present work and that reported by Lack may be due to aerosol composition differences and/or PSAP and aethalometer filter media differences (Arnott et al., 2005).

4 Conclusions

Peak absorption in Mexico City occurs early in the morning before boundary layer expansion. Aerosol scattering peaks several hours later than absorption, and photochemically produced aerosol mass is likely the cause of this increase in aerosol light scattering at the Mexico City urban site. Peak scattering occurs as a balance between photochemical production and aerosol dilution as the atmospheric boundary layer extends to larger heights during daylight hours, and average wind speeds increase. Aerosol SSA has a minimum value of 0.60 in the early morning hours as the rush hour traffic is most intense and dilution is limited in a shallow boundary layer. For comparison, the SSA for diesel soot alone would be anticipated to be 0.4 at 532 nm (Sheridan et al., 2005). Values at night are somewhat greater than in the early morning hours, indicating that on average there is some carryover from the previous day to the next. As well, other aerosol sources such as cooking and spark ignition vehicle traffic may contribute to the observed SSA variance. The strong diurnal behavior of the SSA clearly shows that secondary aerosol formation from photochemical processes in Mexico City begins to affect the aerosol radiative forcing values as soon as the sun rises, which is consistent with the strong secondary source observed in previous studies (Salcedo et al., 2006; Volkamer et al., 2006). The SSA values increase at the MCMA site until about 11:00 a.m. when the atmospheric boundary layer height increases and dilutes the accumulated primary and secondary aerosol. At this time, 75% of the scattering and aerosol mass is due to same-day secondary aerosol production during daylight hours. A 10% systematic bias was detected for filter-based measurement of aerosol light absorption in the presence of substantial secondary organic aerosol mass concentration and peak SSA. The average diurnal range of single scattering albedo and secondary aerosol mass and scattering coefficient provide a reasonable estimate of the range of radiative values for aerosols being produced and transported from a tropical megacity. Further work will be needed to make use of this data and other MILAGRO data sets in conjunction with atmospheric models to refine the variability important for assessment of the impact of aerosols on radiative forcing as well as photochemical production of oxidants and secondary aerosols relevant to air quality issues.

Acknowledgements. This work was supported by the Department of Energy Atmospheric Science Program as part of the Megacity Aerosol Experiment- Mexico City (MAX-Mex) and was carried out in collaboration with the MILAGRO project. University of Nevada, Reno (Arnott/Paredes) and University of Arkansas at Little Rock (Gaffney/Marley) field measurements and research efforts were supported by the Office of Science (BER), Department of Energy's Atmospheric Science Program. Arnott/Paredes were also supported in part by the National Science foundation (NSF). The University of Colorado at Boulder (Aiken/Jimenez) effort was supported by NSF, DOE (BER), and a NASA Fellowship to A. Aiken. Arnott/Paredes gratefully acknowledge the assistance of M. Dubey and C. Mazzoleni, during the field campaign. We acknowledge the assistance and encouragement of L. T. Molina. *The authors appreciate the editorial assistance of S. Madronich.*

Edited by: S. Madronich

References

Aiken, A. C., DeCarlo, P. F., Kroll, J. H., Worsnop, D. R., Huffman, J. A., Docherty, K., Ulbrich, I. M., Mohr, C., Kimmel, J. R., Sueper, D., Zhang, Q., Sun, Y., Trimborn, A., Northway, M., Ziemann, P. J., Canagaratna, M. R., Onasch, T. B., Alfarra, R., Prevot, A. S. H., Dommen, J., Duplissy, J., Metzger, A., Baltensperger, U., and Jimenez, J. L.: O/C and OM/OC Ratios of Primary, Secondary, and Ambient Organic Aerosols with High Resolution Time-of-Flight Aerosol Mass Spectrometry, Environ. Sci. Technol., 42, 4478–4485, 2008.

Aiken, A. C., Salcedo, D., Cubison, M. J., de Foy, B., Wiedinmyer, C., Huffman, A., DeCarlo, P. F., Ulbrich, I., Docherty, K., Sueper, D., Kimmel, J. R., Worsnop, D., Trimborn, A., Northway, M., Wehrli, M. N., Szidat, S., Prevot, A. S. H., Baltensperger, U., Noda, J., Wacker, L., Stone, E. A., Schauer, J. J., Volkamer, R., Fortner, E., Knighton, B., Wang, J., Laskin, A., Zheng, J., Zhang, R., Gaffney, J., Marley, N. A., Querol, X., Paredes-Miranda, G., Arnott, W. P., Molina, L. T., Sosa, G., and Jimenez, J. L.: Mexico City Aerosol Analysis during MILAGRO using High Resolution Aerosol Mass Spectrometry at the Urban Supersite (T0). Part 1: Overall Fine Particle Composition and

Organic Source Apportionment., Atmos. Chem. Phys. Discuss., 9, 8377–8427, 2009, http://www.atmos-chem-phys-discuss.net/9/8377/2009/.

Anderson, T. L., Covert, D. S., Marshall, S. F., Laucks, M. L., Charlson, R. J., Waggoner, A. P., Ogren, J. A., Caldow, R., Holm, R. L., Quant, F. R., Sem, G. J., Wiedensohler, A., Ahlquist, N. A., and Bates, T. S.: Performance characteristics of a high sensitivity, three wavelength, total scatter/backscatter nephelometer, Journal of Atmospheric and Oceanic Technology, 13, 967–986, 1996.

Andreae, M. O.: The dark side of aerosols, Nature, 409, 671–672, 2001.

Andreae, M. O. and Gelencsér, A.: Black carbon or brown carbon? The nature of light-absorbing carbonaceous aerosols, Atmos. Chem. Phys., 6, 3131–3148, 2006, *http://www.atmos-chem-phys.net/6/3131/2006/.*

Arnott, W. P., Hamasha, K., Moosmüller, H., Sheridan, P. J., and Ogren, J. A.: Towards aerosol light absorption measurements with a 7-wavelength Aethalometer: Evaluation with a photoacoustic instrument and a 3 wavelength nephelometer, Aerosol Sci. Tech., 39, 17–29, 2005.

Arnott, W. P., Moosmüller, H., Rogers, C. F., Jin, T., and Bruch, R.: Photoacoustic spectrometer for measuring light absorption by aerosols: Instrument description, Atmos. Environ., 33, 2845–2852, 1999.

Arnott, W. P., Moosmüller, H., and Walker, J. W.: Nitrogen dioxide and kerosene-flame soot calibration of photoacoustic instruments for measurement of light absorption by aerosols., Rev. Sci. Inst., 71(7), 4545–4552, 2000.

Bergin, M. H., Cass, G. R., Xu, J., Fang, C., Zeng, L. M., Yu, T., Salmon, L. G., Kiang, C. S., Tang, X. Y., Zhang, Y. H., and Chameides, W. L.: Aerosol radiative, physical, and chemical properties in Beijing during June 1999, J. Geophys. Res., 106(D16), 17969–17980, 2001.

Bond, T. C., Anderson, T. L., and Campbell, D.: Calibration and Intercomparison of Filter-Based Measurements of Visible Light Absorption by Aerosols, Aerosol Sci. Tech., 30(6), 582–600, 1999.

Bond, T. C. and Bergstrom, R. W.: Light absorption by carbonaceous particles: An investigative review., Aerosol Sci. Tech., 40, 27–67, 2006.

Canagaratna, M. R., Jayne, J. T., Jimenez, J. L., Allan, J. D., Alfarra, M. R., Zhang, Q., Onasch, T. B., Drewnick, F., Coe, H., Middlebrook, A., Delia, A., Williams, L. R., Trimborn, A. M., Northway, M. J., DeCarlo, P. F., Kolb, C. E., Davidovits, P., and Worsnop, D. R.: Chemical and Microphysical Characterization of Ambient Aerosols with the Aerodyne Aerosol Mass Spectrometer, Mass Spectrom. Rev., 26, 185–222, 2007.

Charlson, R. J., Schwartz, S. E., Hales, J. M., Cess, R. D., Coakley, J. A., Hansen, J. E., and Hofmann, D. J.: Climate Forcing by Anthropogenic Aerosols, Science, 255, 423–429, 1992.

de Almeida Castanho, A., Prinn, R., Martins, V., Herold, M., Ichoku, C., and Molina, L.: Analysis of Visible/SWIR surface reflectance ratios for aerosol retrievals from satellite in Mexico City urban area., Atmos. Chem. Phys., 7, 5467–5477, 2007, http://www.atmos-chem-phys.net/7/5467/2007/.

de Foy, B., Varela, J. R., Molinta, L. T., and Molina, M. J.: Rapid ventilation of the Mexico City basin and regional fate of the urban plume, Atmos. Chem. Phys., 6, 2321–2335, 2006, http://www.atmos-chem-phys.net/6/2321/2006/.

DeCarlo, P. F., Dunlea, E. J., Kimmel, J. R., Aiken, A. C., Sueper, D., Crounse, J., Wennberg, P. O., Emmons, L., Shinozuka, Y., Clarke, A., Zhou, J., Tomlinson, J., Collins, D. R., Knapp, D., Weinheimer, A. J., Montzka, D. D., Campos, T., and Jimenez, J. L.: Fast Airborne Aerosol Size and Chemistry Measurements with the High Resolution Aerosol Mass Spectrometer during the MILAGRO Campaign, Atmos. Chem. Phys., 8, 4027–4048, 2008, http://www.atmos-chem-phys.net/8/4027/2008/.

DeCarlo, P. F., Kimmel, J. R., Trimborn, A., Northway, M. J., Jayne, J. T., Aiken, A. C., Gonin, M., Fuhrer, K., Horvath, T., Docherty, K., Worsnop, D. R., and Jimenez., J. L.: Field-Deployable, High-Resolution, Time-of-Flight Aerosol Mass Spectrometer, Anal. Chem., 78, 8281–8289, 2006.

Haywood, J. M. and Ramaswamy, V.: Global sensitivity studies of the direct radiative forcing due to anthropogenic sulfate and black carbon aerosols, J. Geophys. Res., 103(D6), 6043–6058, 1998.

Herndon, S. C., Onasch, T. B., Wood, E. C., Kroll, J. H., Canagaratna, M. R., Jayne, J. T., Zavala, M. J. A., Knighton, W. B., Mazzoleni, C., Dubey, M. K., Ulbrich, I. M., Jimenez, J. L., Seila, R., de Gow, J. A., de Foy, B., Fast, J. D., Molina, L. T., Kolb, C. E., and Worsnop, D.: Correlation of secondary organic aerosol with odd oxygen in Mexico City, Geophys. Res. Lett., 35, L15804, doi:10.1029/2008GL034058, 2008.

Huffman, J., Jayne, J., Drewnick, F., Aiken, A., Onasch, T., Worsnop, D., and Jimenez, J.: Design, Modeling, Optimization, and Experimental Tests of a Particle Beam Width Probe for the Aerodyne Aerosol Mass Spectrometer, Aerosol Sci. Tech., 39(12), 21, 2005.

Jacobson, M. Z.: Strong Radiative Heating due to the Mixing State of Black Carbon in Atmospheric Aerosols, Nature, 409, 695–697, 2001.

Jauregui, E. and Luyando, E.: Global radiation attenuation by air pollution and its effects on the thermal climate in Mexico City, Int. J. Climatol., 19(6), 683–694, 1999.

Jimenez, J. L., Bahreini, R., Cocker, D. R., Zhuang, H., Varutbangkul, V., Flagan, R. C., Seinfeld, J. H., O'Dowd, C. and Hoffmann, T.: New Particle Formation from Photooxidation of Diiodomethane (CH2I2), J. Geophys. Res.-Atmos., 108, (D10), 4318, doi:10.1029/2002JD002452, 2003.

Johnson, K. S., Zuberi, B., Molina, L. T., Molina, M. J., Iedema, M. J., Cowin, J. P., Gaspar, D. J., Wang, C., and Laskin, A.: Processing of soot in an urban environment: case study from the Mexico City Metropolitan Area, Atmos. Chem. Phys., 5, 3033–3043, 2005, http://www.atmos-chem-phys.net/5/3033/2005/.

Kirchstetter, T. W., Novakov, T., and Hobbs, P. V.: Evidence that the spectral dependence of light absorption by aerosols is affected by organic carbon, J. Geophys. Res., 109, D21208, doi:10.1029/2004JD00499, 2004.

Lack, D. A., Cappa, C. D., Covert, D. S., Baynard, T., Massoli, P., Sierau, B., Bates, T. S., Quinn, P. K., Lovejoy, E. R., and Ravishankara, A. R.: Bias in Filter Based Aerosol Absorption Measurements Due to Organic Aerosol Loading: Evidence from Ambient Measurements, Aerosol Sci. Tech., 42(12), 1033–1041, 2008.

Lewis, K., Arnott, W. P., Moosmüller, H., and Wold, C. E.: Strong spectral variation of biomass smoke light absorption and single scattering albedo observed with a novel dual wavelength

photoacoustic instrument, J. Geophys. Res., 113, D16203, doi:10.1029/2007JD009699, 2008.

Mar, E., Sheinbaum, N. A., and Luna, N.: Inventario de emisiones y posibles politicas de mitigacion de gases contaminantes provenientes del sector transporte del area metropolitana de la ciudad de Mexico, Preceedings, Contaminacion Atmosferica III, Instituto de Geofisica, UNAM, 313–339, 2001.

Mayol-Bracero, O. L., Gabriel, R., Andreae, M. O., Kirchsteter, T. W., Novakov, T., Ogren, J., Sheridan, P., and Streets, D. G.: Carbonaceous aerosols over the Indian Ocean during the Indian Ocean Experiment (INDOEX): Chemical characterization, optical properties, and probable sources, J. Geophys. Res., 107(D19), 8030, doi:10.1029/2000JD0039, 2002.

McComiskey, A., Schwartz, S. E., Schmid, B., Guan, H., Lewis, E. R., Ricchiazzi, P., and Ogren, J. A.: Direct aerosol forcing: Calculation from observables and sensitivities to inputs, J. Geophys. Res., 113, D09202, doi:10.1029/2007JD009170, 2008.

Molina, L. T., Kolb, C. E., de Foy, B., Lamb, B. K., Brune, W. H., Jimenez, J. L., Ramos- Villegas, R., Sarmiento, J., Paramo-Figueroa, V. H., Cardenas, B., Gutierrez-Avedoy, V., and Molina, M. J.: Air Quality in North America's Most Populous City – Overview of the MCMA-2003 Campaign., Atmos. Chem. Phys., 7, 2447–2473, 2007, http://www.atmos-chem-phys.net/7/2447/2007/.

Paatero, P. and Tapper, U.: Positive matrix factorization: A non-negative factor model with optimal utilization of error estimates of data values, Environmetrics, 5, 111–126, 1994.

Querol, X., Pey, J., Minguillon, M. C., Perez, N., Alastuey, A., Viana, M., Moreno, T., Bernabe, R. M., Blanco, S., Cardenas, B., Vega, E., Sosa, G., Escalona, S., Ruiz, H., and Artinano, B.: PM speciation and sources in Mexico during MILAGRO campaign, Atmos. Chem. Phys., 8, 111–128, 2008, http://www.atmos-chem-phys.net/8/111/2008/.

Rahmah, A. A., Arnott, W. P., and Moosmüller, H.: Integrating nephelometer with a low truncation angle and an extended calibration scheme, Measurement Sci. Technol., 17, 1723–1732, 2006.

Salcedo, D., Onasch, T. B., Canagaratha, M., Dzepina, K., Huffman, J. A., Jayne, J. T., Worsnop, D., Kolb, C., Weimer, S., Drewnick, F., Allan, J., A., D. and Jimenez, J.: Technical Note: Use of a beam width probe in an Aerosol Mass Spectrometer to monitor particle collection efficiency in the field., Atmos. Chem. Phys., 7, 549–556, 2007, http://www.atmos-chem-phys.net/7/549/2007/.

Salcedo, D., Onasch, T. B., Dzepina, K., Canagaratna, M. R., Zhang, Q., Huffman, J. A., DeCarlo, P. F., Jayne, J. T., Mortimer, P., Worsnop, D. R., Kolb, C. E., Johnson, K. S., Zuberi, B., Marr, L. C., Volkamer, R., Molina, L. T., Molina, M. J., Cardenas, B., Bernabe, R. M., Marquez, C., Gaffney, J. S., Marley, N. A., Laskin, A., Shutthanandan, V., Xie, Y., Brune, W., Lesher, R., Shirley, T., and Jimenez, J. L.: Characterization of ambient aerosols in Mexico City during the MCMA-2003 campaign with Aerosol Mass Spectrometry: results from the CENICA Supersite, Atmos. Chem. Phys., 6, 925–946, 2006, http://www.atmos-chem-phys.net/6/925/2006/.

Sheridan, P. J., Arnott, W. P., Ogren, J. A., Anderson, B. E., Atkinson, D. B., Covert, D. S., Moosmuller, H., Petzold, A., Schmid, B., Strawa, A. W., Varma, R., and Virkkula, A.: The Reno aerosol optics study: An Evaluation of Aerosol Absorption Measurement Methods, Aerosol Sci. Tech., 39, 1–16, 2005.

Stone, E. A., Snyder, D. C., Sheesley, R. J., Sullivan, A. P., Weber, R. J., and Schauer, J. J.: Source apportionment of fine organic aerosol in Mexico City during the MILAGRO experiment 2006, Atmos. Chem. Phys., 8, 1249–1259, 2008, http://www.atmos-chem-phys.net/8/1249/2008/.

Subramanian, R., Roden, C. A., Boparai, P., and Bond, T. C.: Yellow beads and missing particles: Trouble ahead for filter-based absorption measurements., Aerosol Sci. Tech., 41, 630–637, 2007.

Sun, H., Biedermann, L., and Bond, T. C.: Color of brown carbon: A model for ultraviolet and visible light absorption by organic carbon aerosol, Geophys. Res. Lett., 34, L17813, doi:10.1029/2007GL029797, 2007.

Ulbrich, I. M., Canagaratna, M. R., Zhang, Q., Worsnop, D. R. and Jimenez, J. L.: Interpretation of Organic Components from Positive Matrix Factorization of Aerosol Mass Spectrometric Data, Atmos. Chem. Phys. Discuss., 8, 6729–6791, 2008, http://www.atmos-chem-phys-discuss.net/8/6729/2008/.

Virkkula, A., Mäkelä, T., Hillamo, R., Yli-Tuomi, T., Hirsikko, A., Hämeri, K., and Koponen, I. K.: A simple procedure for correcting loading effects of aethalometer data, J. Air Waste Manage., 57, 1214–1222, 2007.

Volkamer, R., Jimenez, J. L., Martini, F. S., Dzepina, K., Zhang, Q., Salcedo, D., Molina, L. T., Worsnop, D. R., and Molina, M. J.: Secondary organic aerosol formation from anthropogenic air pollution: Rapid and higher than expected, Geophys. Res. Lett., 33, L178111, doi:10.1029/2006GL026899, 2006.

Volkamer, R., Martini, F. S., Molina, L. T., Salcedo, D., Jimenez, J. L., and Molina, M. J.: A missing sink for gas-phase glyoxal in Mexico City: Formation of secondary organic aerosol, Geophys. Res. Lett., 34, L19807, doi:10.1029/2007GL030752, 2007.

Weingartner, E., Saathoff, H., Schnaiter, M., Streit, N., Bitnar, B., and Baltensperger, U.: Absorption of light by soot particles: determination of the absorption coefficient by means of aethalometers, J. Aerosol Sci., 34, 1445–1463, 2003.

Yokelson, R. J., Urbanski, S. P., Atlas, E. L., Toohey, D. W., Alvarado, E. C., Crounse, J. D., Wennberg, P. O., Fisher, M. E., Wold, C. E., Campos, T. L., Adachi, K., Buseck, P. R., and Hao, W. M.: Emissions from Forest Fires near Mexico City, Atmos. Chem. Phys., 7, 5569–5584, 2007, http://www.atmos-chem-phys.net/7/5569/2007/.

Zhang, Q., Jimenez, J. L., Canagaratna, M. R., Allan, J. D., Coe, H., Ulbrich, I., Alfarra, M. R., Takami, A., Middlebrook, A. M., Sun, Y. L., Dzepina, K., Dunlea, E., Docherty, K., DeCarlo, P. F., Salcedo, D., Onasch, T., Jayne, J. T., Miyoshi, T., Shimono, A., Hatakeyama, S., Takegawa, N., Kondo, Y., Schneider, J., Drewnick, F., Borrmann, S., Weimer, S., Demerjian, K., Williams, P., Bower, K., Bahreini, R., Cottrell, L., Griffin, R. J., Rautiainen, J., Sun, J. Y., Zhang, Y. M., and Worsnop, D. R.: Ubiquity and Dominance of Oxygenated Species in Organic Aerosols in Anthropogenically-Influenced Northern Hemisphere Mid-latitudes, Geophys. Res. Lett., 34, L13801, doi:10.1029/2007GL029979, 2007.

Zhang, Q., Worsnop, D. R., Canagaratna, M. R., and Jimenez, J. L.: Hydrocarbon-like and oxygenated organic aerosols in Pittsburgh: Insights into sources and processes of organic aerosols, Atmos. Chem. Phys., 5, 3289–3311, 2005, http://www.atmos-chem-phys.net/5/3289/2005/.

Atmos. Chem. Phys., 9, 6191–6215, 2009
www.atmos-chem-phys.net/9/6191/2009/

Atmospheric Chemistry and Physics

Evaluating simulated primary anthropogenic and biomass burning organic aerosols during MILAGRO: implications for assessing treatments of secondary organic aerosols

J. Fast[1], A. C. Aiken[2], J. Allan[3], L. Alexander[1], T. Campos[4], M. R. Canagaratna[5], E. Chapman[1], P. F. DeCarlo[6], B. de Foy[7], J. Gaffney[8], J. de Gouw[9], J. C. Doran[1], L. Emmons[4], A. Hodzic[4], S. C. Herndon[5], G. Huey[10], J. T. Jayne[5], J. L. Jimenez[2], L. Kleinman[11], W. Kuster[9], N. Marley[8], L. Russell[12], C. Ochoa[13], T. B. Onasch[5], M. Pekour[1], C. Song[1], I. M. Ulbrich[2], C. Warneke[9], D. Welsh-Bon[9], C. Wiedinmyer[4], D. R. Worsnop[5], X.-Y. Yu[1], and R. Zaveri[1]

[1]Pacific Northwest National Laboratory, Richland, Washington, USA
[2]University of Colorado, Boulder, Colorado, USA
[3]University of Manchester, Manchester, UK
[4]National Center for Atmospheric Research, Boulder, Colorado, USA
[5]Aerodyne Research Inc., Billerica, Massachusetts, USA
[6]Paul Scherrer Institut, Switzerland
[7]Saint Louis University, Saint Louis, Missouri, USA
[8]University of Arkansas – Little Rock, Little Rock, Arkansas, USA
[9]NOAA Earth System Research Laboratory & Cooperative Institute for Research in Environmental Sciences, University of Colorado, Boulder, Colorado, USA
[10]Georgia Institute of Technology, Atlanta, Georgia, USA
[11]Brookhaven National Laboratory, Upton, New York, USA
[12]University of California, San Diego, San Diego, California
[13]Universidad Nacional Autónoma de México, Mexico City, Mexico

Received: 10 January 2009 – Published in Atmos. Chem. Phys. Discuss.: 24 February 2009
Revised: 17 July 2009 – Accepted: 15 August 2009 – Published: 31 August 2009

Abstract. Simulated primary organic aerosols (POA), as well as other particulates and trace gases, in the vicinity of Mexico City are evaluated using measurements collected during the 2006 Megacity Initiative: Local and Global Research Observations (MILAGRO) field campaigns. Since the emission inventories, transport, and turbulent mixing will directly affect predictions of total organic matter and consequently total particulate matter, our objective is to assess the uncertainties in predicted POA before testing and evaluating the performance of secondary organic aerosol (SOA) treatments. Carbon monoxide (CO) is well simulated on most days both over the city and downwind, indicating that transport and mixing processes were usually consistent with the meteorological conditions observed during MILAGRO. Predicted and observed elemental carbon (EC) in the city was similar, but larger errors occurred at remote locations since the overall CO/EC emission ratios in the national emission inventory were lower than in the metropolitan emission inventory. Components of organic aerosols derived from Positive Matrix Factorization of data from several Aerodyne Aerosol Mass Spectrometer instruments deployed both at ground sites and on research aircraft are used to evaluate the model. Modeled POA was consistently lower than the measured organic matter at the ground sites, which is consistent with the expectation that SOA should be a large fraction of the total organic matter mass. A much better agreement was found when modeled POA was compared with the sum of "primary anthropogenic" and "biomass burning" components derived from Positive Matrix Factorization (PMF) on most days, especially at the surface sites, suggesting that the overall magnitude of primary organic particulates released was reasonable. However, simulated POA

Correspondence to: J. D. Fast
(jerome.fast@pnl.gov)

from anthropogenic sources was often lower than "primary anthropogenic" components derived from PMF, consistent with two recent reports that these emissions are underestimated. The modeled POA was greater than the total observed organic matter when the aircraft flew directly downwind of large fires, suggesting that biomass burning emission estimates from some large fires may be too high.

1 Introduction

Most predictions of organic matter made by three-dimensional particulate models are currently significantly too low because the processes contributing to secondary organic aerosol (SOA) formation and transformation are not well understood. One objective of the Megacity Initiative: Local and Global Research Observations (MILAGRO) field campaign (Molina et al., 2008) conducted during March 2006 was to obtain measurements of organic aerosols and precursors of secondary organic aerosols (SOA). Measurements during MILAGRO (e.g. Kleinman et al., 2008; de Gouw et al., 2009) and other field campaigns worldwide (de Gouw et al., 2005; Simpson et al., 2007; Hodzic et al., 2006; Zhang et al., 2007) have indicated that, as a result of secondary organic aerosol (SOA) formation processes, organic aerosol mass is much higher than one would expect from primary emissions and dispersion. However, the understanding of how anthropogenic and biogenic precursors contribute to SOA formation is far from complete. It is therefore not surprising that simulated organic aerosol mass from recent modeling studies have been shown to be a factor of five or more lower than observed (e.g. Volkamer et al., 2006).

Many 3-D chemical transport models employ SOA formulations based on Koo et al. (2003) and Odum et al. (1996). Additional SOA precursors that were previously ignored have been proposed (e.g. Robinson et al., 2007) that can produce significantly more SOA mass (Dzepina et al., 2009) than traditional approaches, but the newer approaches have their own set of assumptions that await additional testing and evaluation. Improving predictions of organic aerosols is important in terms of both air quality and climate applications. For climate applications, the current under-prediction of organic aerosol mass will subsequently affect predictions of direct radiative forcing by affecting scattering and absorption of radiation in the atmosphere. Predictions of indirect radiative forcing will be affected as well because the size distribution and chemical composition will affect aerosol hygroscopic properties, activation of cloud condensation nuclei, ice nuclei, and cloud chemistry.

The goal of this study is to determine whether regional 3-D models operated in a reasonable configuration can adequately predict concentrations of primary organic aerosols (POA). Accurate predictions of POA are needed since it contributes to the total particulate mass and influences the interpretation of total organic matter (OM). Factor analysis methods, such as Positive Matrix Factorization (PMF), combined with mass spectra from the Aerodyne Aerosol Mass Spectrometer (AMS) have recently been applied to derive components of organic aerosols including: hydrocarbon-like organic aerosol (HOA), oxidized organic aerosol (OOA), and biomass burning organic aerosols (BBOA) (e.g. Zhang et al., 2005, 2007; Lanz et al., 2007; Ulbrich et al., 2009). The temporal variation of HOA has been shown to be similar to that of primary emissions of other species in urban areas, whereas OOA is better correlated with species that are formed as a result of photochemical activity (Kondo et al., 2007; Docherty et al., 2008; Herndon et al., 2008). PMF of high-resolution AMS spectra (DeCarlo et al., 2006) results in better separation of the components due to the larger differences in the spectra, especially between HOA and BBOA which have more similar unit-resolution spectra but very different high-resolution spectra (Aiken et al., 2009a; Ulbrich et al., 2009). The BBOA retrieved from PMF is assumed to be composed mainly of primary biomass burning aerosols; the spectra of secondary organic aerosols from biomass burning precursors are more similar to OOA (Grieshop, 2009).

In this study, the WRF-chem model is used with trace gas and particulate release rates derived from gridded versions of the 1999 National Emissions Inventory and the 2002 Mexico City Metropolitan Area (MCMA) as adjusted by Lei et al. (2007) to predict POA and other tracers in the vicinity of Mexico City during the 2006 Megacity Initiative: Local and Global Research Observations (MILAGRO) field campaigns. Uncertainties in both the primary emission estimates and the simulated meteorological processes will affect predictions of total organic matter and consequently total particulate matter; therefore, our objective is to assess the uncertainties in predicted POA before testing and evaluating the performance of SOA treatments. In contrast to many large cities, Mexico City is a challenging location to evaluate particulate models because of the multiple anthropogenic, biomass burning, volcanic, and dust sources of primary particulates and particulate precursors. SOA in the vicinity of Mexico City originating from biogenic precursors are expected to be low in concentration during the dry season, although biogenic SOA formed from emissions on the coastal ranges may make a contribution to background organic aerosols over Central Mexico (Hodzic et al., 2009). A wide range of continuous surface measurements and intermittent aircraft measurements is used to evaluate the model. Organic aerosol predictions are evaluated using data from AMS instruments (e.g. Canagaratna et al., 2007) deployed at four ground sites and onboard two research aircraft. Estimates of POA from PMF analysis are currently available for three of the ground sites and for some aircraft flights.

We first briefly discuss the performance of simulated meteorology and carbon monoxide (CO) to show that transport and mixing is reasonably represented on most days during the simulation period over Mexico and that CO emission

Table 1. Selected WRF-Chem configuration options for this study.

Atmospheric Process	WRF-Chem Option
Advection	Positive Definite
Longwave radiation	RRTM
Shortwave radiation	Goddard
Surface layer	MM5 similarity theory
Land surface	Noah
Boundary layer	YSU
Cumulus clouds	Kain-Fritsch (outer domain only)
Cloud microphysics	Enhanced Purdue Lin
Gas phase chemistry	*CBM-Z*
Aerosol chemistry	MOSAIC
Aqueous chemistry	Fahey and Pandis
Photolysis	Fast-J

estimates are adequate. Then, predictions of black carbon and organic matter are evaluated with the available measurements made during MILAGRO. Modeled POA was consistently lower than the measured organic matter at the ground sites, which is consistent with the expectation that SOA is typically a large fraction of the total organic aerosol mass. A much better agreement was found when modeled POA was compared with the sum of measured HOA and BBOA, suggesting that the emission rates were reasonable overall. A similar conclusion was obtained using the AMS instruments on the aircraft on days with relatively low biomass burning. On days with a significant number of fires, the predicted POA was greater than the total observed organic matter as the aircraft flew directly downwind of the biomass burning sources. One or more factors may contribute to this error including biomass burning emissions that were too high, the validity of assumptions employed to derived biomass burning estimates from satellite remote sensing, and errors in way the model treated plume rise or horizontal mixing of point sources.

2 Model description

Version 3 of the Weather Research and Forecasting (WRF) *community model that simulates trace gases and particulates* simultaneously with meteorological fields (Grell et al., 2005) is used in this study. The chemistry version of WRF, known as WRF-Chem, contains several treatments for photochemistry and aerosols developed by the user community.

Table 1 lists the specific treatments employed for meteorology, trace gas, and particulate processes used in this study that are described elsewhere (Skamarock et al., 2008). Atmospheric chemistry is simulated using the CBM-Z photochemical mechanism (Zaveri and Peters, 1999), the Fast-J photolysis scheme (Wild et al., 2000), and the MOSAIC aerosol model (Zaveri, et al., 2008). MOSAIC employs the sectional approach for the aerosol size distribution in which both mass and number are predicted for each size bin. Eight size bins are used ranging from 0.039 (lower bound) to 10 μm (upper bound). An internal mixture assumption is used so that all particles within a bin have the same chemical composition. There are no separate hydrophilic and hydrophobic species of organic matter and elemental carbon. The hygroscopic properties for all particles within a size bin are computed assuming internal mixing as the volume-weighted bulk hygroscopicity for each chemical composition. MOSAIC includes treatments for nucleation (Wexler et al., 1994), coagulation (Jacobson et al., 1994), and dry deposition (Binkowski and Shankar, 1995). Aerosols influence the scattering and absorption of solar radiation (i.e. the aerosol direct effect) and photolysis rates through the use of extinction, single-scattering albedo, and asymmetry factor parameters. These parameters are computed as a function of wavelength using refractive indices based on predicted particulate mass, composition, and wet radius for each size bin (Fast et al., 2006). Treatments for aqueous chemistry, cloud-aerosol interactions, aerosol indirect effects, and wet deposition (Gustafson et al., 2007; Chapman et al., 2008) are also included; however, these processes were not significant prior to the cold surge on 23 March (Fast et al., 2007) since mostly sunny conditions were observed and simulated over the central Mexican plateau.

It is important to note that MOSAIC does not include a treatment of SOA for version 3 of WRF-Chem and that all organic matter is treated as non-volatile POA. A more recent 0-D version of MOSAIC now incorporates gas-to-particle partitioning processes for SOA similar to the approach used by the MADE/SORGAM aerosol model (Ackermann et al., 1998; Schell et al., 2001); nevertheless, a test simulation using MADE/SORGAM in WRF-Chem produced SOA concentrations less than 1 $\mu g\,m^{-3}$ that were considerably lower than observed SOA during MILAGRO (e.g. Herndon et al., 2008; Kleinman et al., 2008; Aiken et al., 2009). Understanding the specific gas-to-particle partitioning processes responsible for SOA formation and translating those findings into treatments suitable for models is the subject of on-going research.

Therefore, the purpose of this study is to evaluate predictions of POA so that SOA treatments can be evaluated later (*e.g. Hodzic et al., 2009*) *using the current assessment of the* uncertainties in dispersion and the emission inventories. If one assumes POA is non-volatile, then errors in POA predictions will results from uncertainties in the emission inventories, transport and mixing processes, and deposition. Some studies (including those for Mexico City) have recently shown that POA is semi-volatile (Robinson et al., 2007; Huffman et al., 2008, 2009a, b), but this issue and its implementation into models have not been fully resolved. The implications of assuming non-volatile POA are described later.

Table 2. List of MILAGRO instrumentation and measurements employed in this study. All particulate concentrations in this paper are for ambient conditions, rather than at standard temperature and pressure (STP).

Instrument or Platform	Location(s)	Measurements
RAMA air quality monitoring network	Mexico City	winds, CO, $PM_{2.5}$, PM_{10}
Radar wind profiler	T1 and Veracruz	winds. PBL depth
Radiosondes	T1	PBL depth
Micropulse Lidar	T1	PBL depth
Thermo Environmental Systems, Model 48C	T1	CO
Tapered Element Oscillating Microbalance (TEOM)	T1	$PM_{2.5}$ mass
Aethelometer	T0	black carbon
Particle Soot Aerosol Photometer & Photoacoustic Aerosol Spectrometer	Paso de Cortes	black carbon
Sunset Laboratory OC/EC Carbon Aerosol Analyzer	T1, T2	organic and black carbon ($PM_{2.5}$)
Aerodyne Aerosol Mass Spectrometer (AMS)	T0*, T1, Paso de Cortes, Pico Tres Padres	organic matter (PM_1)
Gas chromatograph with flame-ionization (GC-FID)	T1	alkanes, alkenes, acetylene
Proton-transfer Ion Trap Mass Spectrometry (PIT-MS)	T1	aromatics, oxygenated VOCs
G-1 aircraft	variable	winds, CO, organic matter
C-130 aircraft	variable	winds, CO, organic matter
DC-8 aircraft	variable	winds, CO

* AMS instruments deployed at T0 and on the C-130 were high-resolution versions (DeCarlo et al., 2006), while the rest were unit resolution versions (Canagaratna et al., 2007)

3 Experimental method

3.1 MILAGRO measurements

MILAGRO was composed of five collaborative field experiments conducted during March 2006 (Molina et al., 2008). The MCMA-2006 field experiment, supported by various Mexican institutions and the US National Science Foundation (NSF) and Department of Energy (DOE), obtained measurements at several surface sites over the city. Measurements over the city and up to a hundred kilometers downwind of the city were obtained from six research aircraft associated with the Megacities Aerosol Experiment (MAX-Mex) supported by the DOE, the Megacities Impact on Regional and Global Environments – Mexico (MIRAGE-Mex) field experiment, supported by the NSF and Mexican agencies, the Intercontinental Transport Experiment B (INTEX-B), supported by the National Aeronautical and Space Administration (NASA), and a biomass burning effort supported by the USDA Forest Service and the NSF. MILAGRO is the largest of a series of international campaigns in and around Mexico City, which also includes IMADA-AVER in 1997 (Edgerton et al., 1999) and MCMA-2003 (Molina et al., 2007).

One objective of MILAGRO was to collect measurements over a wide range of spatial scales to describe the evolution of the Mexico City pollutant plume from its source and up to several hundred kilometers downwind. The flight paths for three of the research aircraft are shown in Fig. 1a and b. The G-1 aircraft flew primarily over and northeast of the city to obtain information on the local processing of pollutants (Kleinman et al., 2008). Regional-scale measurements over Mexico City, the central Mexican plateau, and the Gulf of Mexico were obtained from the C-130 aircraft (e.g. DeCarlo et al., 2008; Shon et al., 2008). The DC-8 aircraft obtained measurements over the largest spatial scales between Mexico City and Houston (Molina et al., 2008). Extensive surface chemistry and meteorological profiling measurements were made at three "supersites" denoted by T0, T1, and T2 in Fig. 1c (e.g. Doran et al., 2007; Shaw et al., 2007). A more limited set of measurements was obtained at several other sites in the vicinity of Mexico City.

The specific measurements used in this study, listed in Table 2, are discussed later in more detail when compared against model predictions.

3.2 Model configuration

A simulation period between 06:00 UTC (midnight local standard time) 6 March and 06:00 UTC 30 March was chosen that included most of the airborne and surface measurements that were operational during MILAGRO. Two computational domains were employed. The outer domain (Fig. 1a) encompasses Mexico east of Baja California, southern Texas, and a portion of Central America using a 12-km grid spacing. The extent of the inner domain (Fig. 1b), encompassing central Mexico and a large portion of the Gulf of Mexico using a 3-km grid spacing, was chosen to include a large fraction of the aircraft flight paths.

The initial and boundary conditions at 6-h intervals for the meteorological variables were obtained from the National

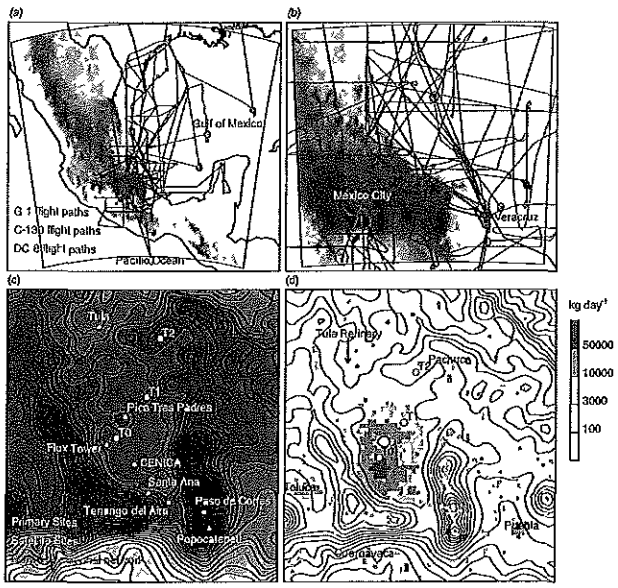

Fig. 1. WRF-chem modeling domains that depict topographic variations over the **(a)** outer domain ($\Delta x = 12$ km) encompassing Mexico and **(b)** inner domain ($\Delta x = 3$ km) encompassing the central Mexican plateau and portions of the Gulf of Mexico. Lines denote local, regional, and synoptic-scale flight paths made by the G-1, C-130 and DC-8 aircraft. The locations of the three supersites, other research sites, and operational monitoring network in the vicinity of Mexico City are shown in **(c)**. Emissions of CO over central Mexico based on the 1999 National Emissions Inventory and the 2002 MCMA emissions inventory is shown in **(d)**, where green dots denote the locations of biomass burning sources during March 2006 obtained from MODIS thermal anomaly satellite data.

Center for Environmental Prediction's Global Forecast System (GFS) model. Initial ocean temperatures, soil temperatures, and soil moisture were also obtained from the GFS model. In addition to constraining the boundary conditions to the large-scale analyzed meteorology, four-dimensional data assimilation was used to nudge (Liu et al., 2006; Doran et al., 2008) the predicted wind, temperature, and specific humidity to the observations obtained from the radar wind profilers and the radiosondes at the T0, T1, T2 sites (Fig. 1c) and the operational radiosondes in Mexico.

The initial and boundary conditions at 6-h intervals for CBM-Z and MOSAIC variables were obtained from 34 trace gases and 12 particulate species produced by the MOZART-4 global chemistry model (Pfister et al., 2008) run with a grid spacing of 2.8×2.8 degrees. Boundary condition values for long-lived species, such as CO and ozone, have an impact on WRF-Chem predictions over central Mexico. The concentrations of most other species are produced primarily by emissions within the modeling domain rather than by long-range transport. For example, ambient background particulate concentrations in the lower to middle troposphere over the Pacific Ocean were typically between 1 and 5 $\mu g\,m^{-3}$. Most of this mass was composed primarily of SO_4, NO_3, NH_4, and dust. Elemental carbon (EC) and organic matter (OM) was usually much less than 0.1 and 0.5 $\mu g\,m^{-3}$, respectively, and consequently contributed little to the overall concentration of carbonaceous particulates over central Mexico.

3.3 Emission inventories

Emissions of trace gases and particulates were obtained from two inventories: the 2002 Mexico City Metropolitan Area (MCMA) inventory as adjusted by Lei et al. (2007) and the 1999 National Emissions Inventory (NEI).

The original 2002 MCMA inventory was developed by the Comisión Ambiental Metropolitana (CAM, 2004). Lei et al. (2007) describe how the annual emissions were mapped into grid cells with a resolution of 2.25 km encompassing the Mexico City Valley. Previous studies have suggested that volatile organic compounds (VOC) emission estimates were too low when compared with measurements made during recent field campaigns (e.g. Molina and Molina, 2002). Consequently, Lei et al. (2007) increased the total mass of VOC released by 65%, although their adjustment factors varied among the specific hydrocarbon species. The resulting Lei et al. (2007) gridded inventory contains diurnally-varying mobile, area, and point source emission rates for 26 trace-gas and 13 particulate species representative of a typical weekday. As in Lei et al. (2007), typical weekday emissions from mobile sources in our investigation were reduced by 10% on Saturdays and 30% on Sundays and holidays to capture weekdays/weekend variations. The $PM_{2.5}$ emissions were composed of four components: primary organic matter, elemental carbon, other inorganic material, and crustal material. The ratio of the mass emitted by each component to the total $PM_{2.5}$ mass varied over the Mexico City basin. Total $PM_{2.5}$ and PM_{10} emissions in this study were not adjusted from the original inventory.

The 1999 NEI inventory was developed by Mexico's Secretariat of the Environment and National Resources, the US Environmental Protection Agency, and several other groups (http://www.epa.gov/ttn/chief/net/mexico.html). Annual emission estimates of CO, NO_x, SO_2, total VOCs, NH_3, $PM_{2.5}$, and PM_{10} were developed for point, area, and mobile sources. This inventory was converted to a ~2.5 km grid that is more useful to modelers by using population and road proxies. Emissions of CO, NO_x, SO_2, VOC, NH_3, $PM_{2.5}$, and PM_{10} are available for point, area, and mobile sources. Due to the absence of speciation recommendations from inventory developers, total VOCs were divided by mass into 13 hydrocarbons using a mean speciation profile derived by averaging over all the grid cells in the Lei et al. (2007) modified 2002 MCMA inventory. Similarly, 1999 NEI inventory estimates of fine and coarse particulate matter was divided into primary organic, black carbon, and inorganic species by computing an average ratio of these species to the total $PM_{2.5}$ emitted over all the grid cells in the 2002 MCMA inventory.

Table 3. *Annual particulate and trace gas emission rates (tons/year) over the MCMA and at the Tula industrial complex, located ~45 km north of the MCMA. Also included are the emission estimates from biomass burning and volcanic sources for March 2006.*

Inventory	PM_{10}	$PM_{2.5}$	SO_2	CO	NO_x	VOC	NH_3
2000 MCMA	10341	6033	10004	2035,425	193451	429755	15446
2002 MCMA[1]	23542	6777	8585	1941593	188262	490100	16933
2004 MCMA	20686	6662	6646	1792,081	179996	532168	17514
2006 MCMA	22951	6089	6913	1990336	191262	576616	19936
1999 NEI[2]	31890	25159	38195	1592665	177599	477137	47651
Tula[3]	17227	12307	382917	5768	203481	2293	–
Biomass[4]	12670	11635	770	86588	6178	5945	890
Volcanic[5]	–	–	52598	–	–	–	–

[1] Estimates from the original MCMA emissions inventory; VOC emissions were increased by 65% in this study as in Lei et al. (2007).
[2] Only for area encompassing the MCMA inventory
[3] Includes multiple stack information
[4] Encompassing the MCMA and surrounding valleys between 100–98° W and 18.5–20.5° N fo March 2006
[5] Only from Popocatepetl, located ~60 km southeast of Mexico City, for March 2006

This ratio is adjusted slightly to include a small amount of SO_4 (2%) and NO_3 (0.2%) emissions based on typical urban emissions in the US While $PM_{2.5}$ emission rates vary over Mexico, the relative amount of organic, black carbon, inorganic, SO_4, and NO_3 is constant. Since the inventory contains annual estimates for each grid cell, we assumed that the hourly and weekend/weekday variations were the same as employed for the 2002 MCMA inventory and Lei et al. (2007).

Gridded versions of the 2006 MCMA inventory were not yet available at the time of this study, but the annual emissions estimates for the 2002 and 2006 inventories were similar as indicated in Table 3. Also listed in Table 3 are values for the subset of the 1999 NEI inventory obtained by summing over the same area covered by the MCMA inventory. The NEI values over Mexico City are all significantly different than those reported by the local inventory for 2000, especially for PM, SO_2 and NH_3. In this study, 2002 MCMA emissions with VOCs adjusted as in Lei et al. (2007) are used in the Mexico Valley and the 1999 NEI emissions are used elsewhere. Figure 1d shows the resulting yearly emission of particulate matter in the vicinity of Mexico City for the 3-km grid in relation to the MILAGRO primary surface sampling sites. T0 is located close to the highest emission rates in the city while T1 is located at the edge of the city. The emission rates in the immediate vicinity of the remote T2 site are low.

In addition to anthropogenic sources within Mexico City, there are also other large emission sources over central Mexico. While most of the point sources within the Mexico City valley are relatively small, the Tula industrial complex located ~45 km north of the MCMA (Fig. 1d) emits large amounts of NO_x, SO_2, and PM, according to the 1999 NEI emission inventory (Table 3). NO_x and PM annual emissions are about the same order of magnitude as in Mexico City, while SO_2 is ~50 times higher than Mexico City. Emissions of CO and VOCs are much lower than Mexico City. When the winds are from the north, emissions from Tula can be transported over Mexico City (e.g. de Foy et al., 2007). When the winds are southerly to southwesterly, it is possible that the Mexico City and Tula pollutant plumes meige as they are transported northeastward.

Biomass burning is also a significant source of trace gas and particulates over Mexico (Yokelson et al., 2007; Molina et al., 2007; DeCarlo et al., 2008; Aiken et al., 2009). Daily estimates of trace gas and particulate emissions from fires were obtained using the MODIS thermal anomalies product on the Terra and Aqua satellites and land cover information as described by Wiedinmyer et al. (2006). A diurnal variation in the emission rates, with a peak value at 20:00 UTC (14:00 LT) and a minimum value at sunrise, was applied to distribute the daily estimates over time. The emissions were distributed uniformly within ~300 m of the ground, because insufficient information was available to perform plume rise calculations. The MODIS thermal anomaly methodology can underestimate the number of fires for two reasons: clouds that obscure fires from the measurements and twice-daily overpass times that do not provide enough temporal information on short-lived fires. For example, many fires sampled by aircraft were small shrub and agricultural clearing fires that were not detected by satellite (Yokelson et al., 2007). The MODIS thermal anomaly methodology may also assume most of a pixel area is burning even when a fire occupies a small portion of the pixel. Flaming versus smoldering combustion that varies during the coarse of a fire is not taken into account as well. While biomass burning estimates derived from MODIS are the most readily available information for models, their uncertainties must be taken into account when assessing smoke plumes predicted by models.

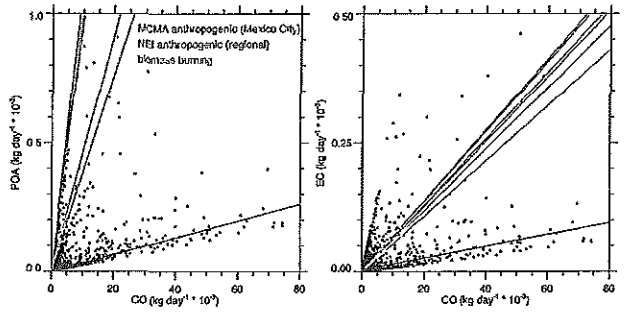

Fig. 2. Scatter plots of POA and EC emissions versus those for CO over the central Mexican plateau where red and blue dots denote grid cells that employ the 2002 MCMA inventory and 1999 National Emissions Inventory, respectively. Green lines denote biomass burning ratios derived from the MODIS "hotspot" inventory during March 2006 and red line denotes best fit of the MCMA grid cells.

The satellite thermal anomaly data indicated many large fires occurred close to Mexico City during March 2006. Most of those fires were located along the mountain ridge just east of Mexico City (Fig. 1d). As indicated by Table 3, PM from biomass burning during this month is estimated to be larger than the annual emissions in Mexico City. This comparison, however, does not account for SOA formation, which is proportionally much larger from the urban emissions (Volkamer et al., 2006; Yokelson et al., 2007) and the possible overestimation of biomass burning emission ratios as discussed later and also by Aiken et al. (2009).

Scatter plots of POA and EC emissions versus those of CO over central Mexico for both anthropogenic and biomass-burning sources are shown in Fig. 2. Over Mexico City, CO emission rates are well correlated with emission rates of POA and EC. The slope of $3.29 * 10^{-3}$ kilogram of urban POA per kilogram of CO from the entire MCMA inventory is similar to values estimated for other urban areas (Zhang et al., 2005; Docherty et al., 2008), but is 30–75% lower than the values of $4.3–5.7 \times 10^{-3}$ observed in ambient air at T0 during 2006 and at CENICA during 2003 (Dzepina et al., 2007; Aiken et al., 2009). Outside of Mexico City, emissions of POA and EC are relatively higher when compared with CO and there is more scatter. The differences between the two inventories are consistent with the total emissions listed in Table 3. The implications of the differences in the emission inventories on CO, EC, and POA predictions will be described later.

Recently Christian et al. (2009) suggested that trash burning at municipal landfills could be responsible for about 29% of the $PM_{2.5}$ present in the urban Mexico City area. However, their estimate has a high uncertainty, since it is based on extrapolating measurements from four short-term trash burning events and the use of antimony (chemical symbol Sb) as a tracer for trash burning. Querol et al. (2008) also attributed their measurements of Sb in Mexico City particulates to a road traffic source, specifically abrasion of motor vehicle brake pads, consistent with a large literature on this source (e.g. Thorpe and Harrison, 2008; Amato et al., 2009). Insufficient activity information (e.g., frequency, duration, location, timing, etc.) is available to modify existing emissions inventories to include trash burning as a potential source of $PM_{2.5}$.

4 Results

Even though a wide range of trace gases and particulates are included in the model, this study focuses on parameters useful to evaluate the simulated transport and mixing of POA over central Mexico. Inorganic particulate matter (i.e. SO_4, NO_3, NH_4, dust) will be described in a subsequent study. The predicted POA will provide information needed to assess the overall magnitude of organic matter emission estimates (the largest component of total particulate matter emissions) from anthropogenic and biomass burning sources.

We first describe the performance of the model in simulating the circulations and boundary layer depth over central Mexico, since transport and mixing processes will directly affect the predicted spatial distribution of particulates. Predictions of CO are then evaluated to further assess simulated transport and mixing. The reactions associated with CO are very slow, thus CO can be treated as a passive scalar for the time scales in this study. Another passive scalar, EC, is evaluated because the sources of EC are similar to those of organic matter. Finally, predictions of primary organic aerosols are evaluated using components of organic matter derived from PMF analysis at the surface and aloft. All particulate concentrations in this paper are for ambient conditions, rather than at standard temperature and pressure (STP).

4.1 Winds and boundary layer depth

The overall meteorological conditions during MILAGRO are described in Fast et al. (2007) and de Foy et al. (2008). Near-surface winds over the central Mexican plateau are influenced by interactions between the heating and cooling associated with terrain variations and the larger-scale synoptic flow. Because Mexico City is located in a basin, the complexity of the local meteorology affects the transport and mixing of trace gases and particulates directly over their emission sources before they are transported downwind.

Several studies have assessed the performance of mesoscale models in simulating near-surface winds and boundary layer structure over Mexico City (e.g. de Foy et al., 2006; Fast and Zhong, 1998; Jazcilevich, et al., 2003). While there are difficulties simulating the details of the near-surface winds at specific locations and times, mesoscale models usually capture the primary thermally-driven circulations and their interactions that are observed, such as diurnally-varying upslope and downslope flows, northerly daytime flow into

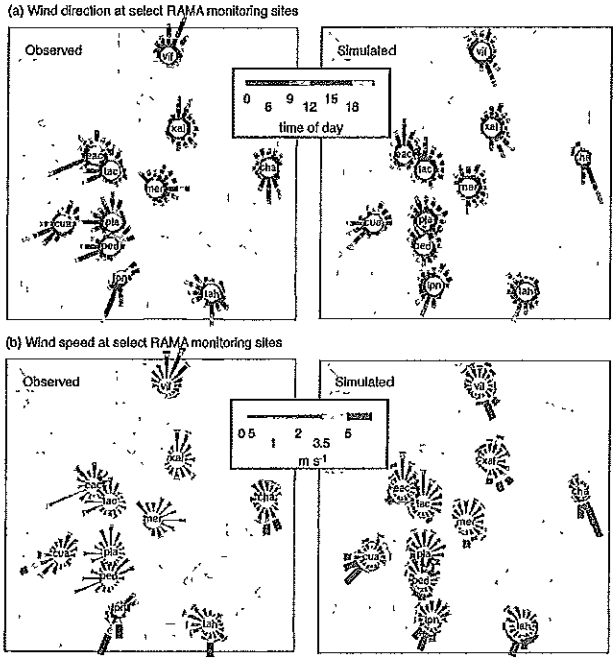

Fig. 3. Observed and predicted wind roses by **(a)** time of day (UTC) and **(b)** wind speed within 22.5 degree wind direction intervals during MILAGRO between 6 and 30 March for selected RAMA stations. Black lines denote terrain contours at 250 m intervals.

the basin, afternoon southerly gap winds through the southeastern end of the basin, and propagating density currents that bring in cool moist air from the coastal plain into the basin late in the afternoon.

Wind roses are employed in Fig. 3 to summarize the observed and predicted winds between 6 and 30 March at select RAMA operational monitoring stations. Inspection of individual time series of wind speed and direction (not shown) indicated that the simulated circulations were often qualitatively consistent with the observations. For example, the simulated north to northeasterly afternoon winds were similar to the observations (Fig. 3a). During the late afternoon, the model tended to over-predict the extent of the gap flow to the XAL and VIF stations as it propagated over the basin. While the winds were predicted reasonably well over the eastern side of the basin at the CHA station, the model propagated this southerly flow over the XLA and VIF stations that usually had northerly winds during the late afternoon. At night, the model produced downslope westerly flows that were observed at CUA; however, the simulated downslope flows did not propagate a few kilometers farther into the basin as observed after midnight at EAC, TAC, PLA, PED, and TPN. The simulated wind speeds were frequently larger than observed over the city center because heat, moisture, and momentum fluxes computed by the surface layer parameterization depend on similarity theory and a single roughness length for urban grid cells. A more complex urban canopy parameterization is required to create additional drag and that would reduce the simulated near-surface wind speeds. WRF does have an urban canopy, but databases that employ Mexico City buildings are still being developed. Surface wind measurements in an urban area are not likely to be representative over a large area, so some caution is needed when comparing observed and simulated quantities at specific locations.

Simulating the details of near-surface winds in areas of complex terrain and urban areas is still challenging for mesoscale models; however, model performance is much better aloft. An example of the simulated winds at the T1 and Veracruz sites compared with radar wind profiler measurements is shown in Fig. 4. Since the model employs the radar wind profiler measurements in the data assimilation scheme, it is not surprising that the simulated multi-day variations in the winds are very similar to the observations. For example, the winds at T1 between 9 and 11 March and 18 and 20 March are associated southwesterly flow ahead of troughs located over western Mexico that are strong enough to suppress local diurnal variability. At Veracruz, the most prominent feature is the passage of cold surges on 14, 22, and 23 March that bring strong northerly flows over the coast of the Gulf of Mexico. These flows occur below the height of the plateau and have a small impact on the winds over central Mexico.

Figure 5 is an example of an independent evaluation of the large-scale wind fields in which the predictions are compared with measurements from three aircraft on March 19 that are not employed by the data assimilation scheme. The aircraft flew at various altitudes: 0–5.5 km MSL for the G-1 and C-130, and 0–11 km MSL for the DC-8. The simulated winds are consistent with the measurements over the largest spatial scales associated with the C-130 and DC-8 aircraft. Somewhat larger differences between the observed and simulated southwesterly winds occurred along the G-1 flight path just downwind of Mexico City. The wind speed correlation coefficients for the G-1, C-130, and DC-8 flights are 0.45, 0.70, and 0.89, respectively. These results suggest that the model captures the overall synoptic scale flows well, but some uncertainties in the simulated local variability of the winds over the central Mexican plateau are associated with the interaction of the synoptic and thermally driven flows.

The continuous measurements of boundary layer (BL) depth at the T0, T1, and T2 sites can be used to assess the simulated depth of vertical mixing that will affect the dispersion of primary trace gas and particulate emissions. An example of the variation in the observed and predicted BL depth at T1 between March 17 and 23 is shown in Fig. 6a. Observed BL depths were obtained from radar wind profiler and lidar measurements as described by Shaw et al. (2007) and there may be uncertainties in the observed BL depth as much as a few hundred meters. The simulated magnitude and multi-day variations in BL depth were similar to the measurements. Observed and simulated BL depths on 17 March

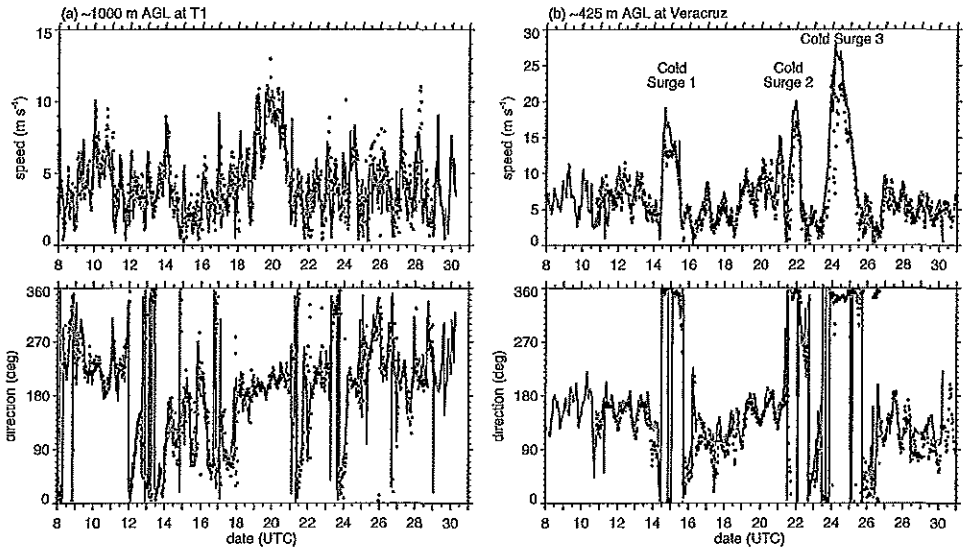

Fig. 4. Observed radar wind profiler wind speed and direction (dots) and predicted wind speed and direction (lines) at (a) T1 and (b) Veracruz, where UTC = local standard time + 6 h.

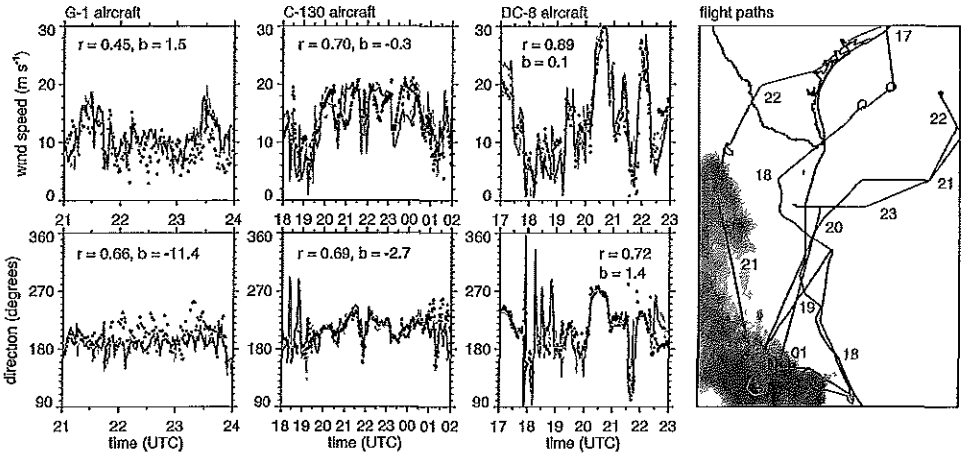

Fig. 5. Observed and predicted wind speed and direction along the G-1, C-130, and DC-8 flight paths on 19 March where gray shading denotes predicted values within one grid cell surrounding the aircraft position. Panel on right depicts the flight paths for each aircraft along positions at select times for the C-130 and DC-8 aircraft.

were as high as 4.3 and 3.8 km AGL, respectively, while observed and simulated BL depths on 19 March were as high as 1.8 and 2.3 km AGL, respectively. There are differences in the rate of BL growth on some days, such as 20 March in which the simulated BL grew too quickly between 16:00 and 20:00 UTC (10:00–14:00 LT). The YSU scheme in version 3 of WRF also had a tendency to collapse the afternoon BL too quickly, such as on 18 March. The typical differences between the observed and simulated BL depth can also be seen by examining the mean and range of BL depths over the entire field campaign at the T0, T1, and T2 sites shown in Figs. 6b, 6c, and 6d, respectively. The simulated BL growth is similar to the observations until about 20:00–21:00 UTC (14:00–16:00 LT), but the tendency to collapse the BL too quickly occurred at all sites. It must be noted that radar wind profilers and lidars have difficulty detecting shallow stable layers that develop around sunset; therefore, the reported BL depths are really the vertical extent of mixing in a decaying residual layer during the transition between day and night.

4.2 Carbon monoxide

We next examine variations in carbon monoxide (CO) to evaluate the impact of simulated winds and BL depth during MILAGRO on the transport and mixing of trace gases in the region.

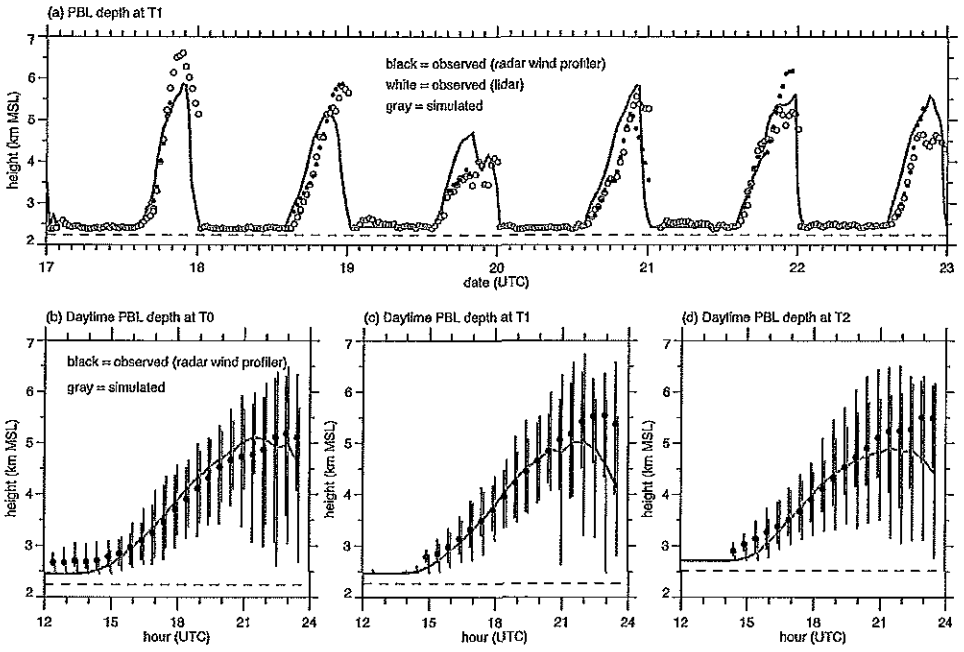

Fig. 6. **(a)** Observed (dots) and simulated (line) boundary layer depth at T1 between 17 and 23 March. Average daytime boundary layer height and range of values during the field campaign at the **(b)** T0, **(c)** T1, and **(d)** T2 sites. Dashed lines denote the elevation of each site.

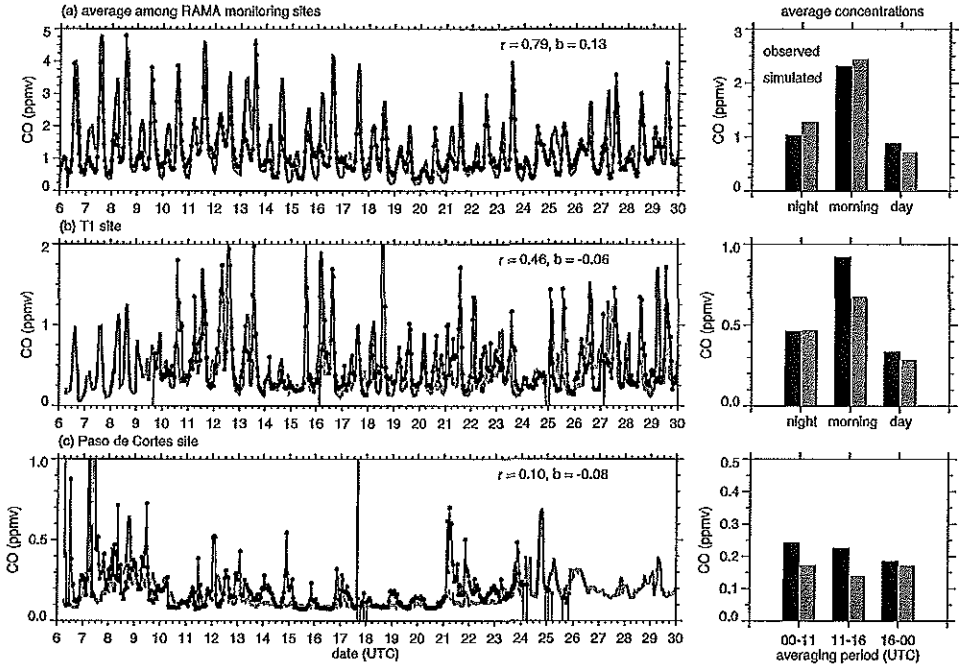

Fig. 7. Observed (dots) and simulated (gray line) **(a)** CO mixing ratio averaged among 25 RAMA operational monitoring stations within the Mexico City basin and CO mixing ratio at the **(b)** T1 site and **(c)** Paso de Cortes site. Correlation coefficient and mean bias denoted by r and b, respectively. The panels on the right are averages the observed (black) and simulated (gray) values during night (18:00–05:00 LST), morning (05:00–10:00 LST), and daytime (10:00–18:00 LST) periods.

The observed and simulated diurnal variation in the average CO computed among the RAMA operational monitors in Mexico City is shown in Fig. 7a. The model reproduced the magnitude and timing of CO reasonably well with a correlation coefficient of 0.79. Observed and simulated peak values occurred just after sunrise and are associated with the morning rush-hour traffic and shallow BL depths. Simulated CO was somewhat too high at night that is likely the result of an underestimation of BL mixing during some nights. While there were no direct continuous measurements of BL depth at night over the city, we suspect that the heating and roughness elements associated with buildings would enhance vertical mixing (e.g. Sarrat et al., 2006) not presently accounted for in the model. Inspection of potential temperature profiles obtained from radiosondes launched several kilometers southwest of T0 at 06 UTC (midnight) indicate that the nocturnal boundary layer could be as high as 500 m AGL on a few nights (not shown); however, a 200 m minimum nocturnal boundary layer depth was employed by the model based on lidar backscatter data at T1 (Fig. 7a). Therefore, the effect of vertical mixing in the city could be about a factor of two too low at times during the night. The CO values are also averaged for nighttime periods between 00:00 and 11:00 UTC (18:00–05:00 LT), morning periods between 11:00 and 16:00 (05:00–10:00 LT) and afternoon periods between 16:00 and 00:00 UTC (10:0–18:00 LT). Simulated CO was ~20% higher that observed when averaged among all the nighttime periods. The simulated errors in CO were less during the day, with morning values being ~7% higher than observed.

The consistency of the monitoring data and simulated CO suggests that the overall emission estimates of CO over the city are reasonable. However, there is evidence to suggest that the diurnally varying emission rates may be off somewhat because CO was somewhat lower than observed during the afternoon. The tendency of the model to collapse the boundary layer 1–2 h before sunset should have produced a positive bias in CO.

The observed and simulated CO just outside of the city at the T1 site is shown in Fig. 7b. While the model qualitatively captured the magnitude and temporal variations in the observed CO, errors in simulated CO are somewhat larger than over the city as indicated by the lower correlation coefficient of 0.46. When the results are averaged over the three time periods, it is evident that most of the errors are associated with the under-predictions during the morning period between 11 and 16 UTC (05:00–10:00 LT). This would suggest that BL depths would be over-predicted, but this is not supported by Fig. 6. We suspect that uncertainties in the emission inventories contribute to uncertainties in predicted CO at this location. Rapid changes in urban growth at the edge of the city and/or traffic along the highway just to the south of T1 during the morning rush hour period may not be represented well.

At the Paso de Cortes site (Baumgarder et al., 2009), located ~1.8 km above the basin, the model captured much of the multi-day variations in CO (Fig. 7c). However, the simulated peak values were too low. Peak CO mixing ratios ranged between 0.4 and 1.0 ppm on twelve days between 6 and 24 March, but simulated CO exceeded 0.4 ppm only on one day. The observed and simulated peaks occurred during both daytime and nighttime periods, but they are not well correlated. The CO averages do not show the same diurnal variations in the city, as expected at this remote site. The lower CO/EC anthropogenic emission ratios outside of Mexico City (Fig. 2) likely contributed to the negative bias in the predicted CO. Additionally, the 3 km horizontal grid spacing may be insufficient to represent local terrain-induced flows along the mountain ridge and subsequently affects the transport and mixing of smoke plumes from nearby fires (Fig. 1d).

Predictions of CO further downwind were also evaluated using data averaged over 10-s intervals from the research aircraft. An example of the spatial and temporal variations on March 19 is shown in Fig. 8, the same time period as the winds shown in Fig. 5. Close to the city, the simulated CO was similar to the measurements along most of the G-1 flight path (Fig. 8a) with a correlation coefficient of 0.63. Simulated CO was higher than observed during four periods in which the aircraft passed over the east side of the Mexico City valley where a large number of fires occurred. Several factors could have contributed to the over-prediction in CO at this location including estimates for biomass burning that were too high, estimates of the peak burning rate that is assumed to occur at 20:00 UTC (14:00 LT) every afternoon, and the simulated vertical mixing that may not loft the CO plume to the correct altitudes. Observed and simulated BL height over the city at the time of the G-1 flight was ~4 km MSL (Fig. 6a) and the aircraft was flying just below this altitude. Measurements of potential temperature also suggest the aircraft was within the BL at this time. While the simulated BL depth is reasonable, the model does not account for enhanced vertical mixing associated with the higher temperatures associated with fires that could account for a portion of the over-prediction in CO close to the location of the fires.

Further downwind along the C-130 flight path (Fig. 8b) the simulated variations in CO between the plateau and the Gulf of Mexico qualitatively similar to the measurements, with a correlation coefficient of 0.58 that was higher than along the G-1 path. The differences are associated primarily with the background mixing ratios and specific biomass burning plumes. The simulated background values of ~80 ppb were about 20 ppb higher than observed, and are likely due to background values obtained from the MOZART model. The peak in simulated CO of ~600 ppb at 01:00 UTC (19:00 LT) was also associated with biomass burning plumes just northeast of Mexico City and was 350 ppb higher than observed. Along the DC-8 flight path (Fig. 8c) the observed and simulated CO increased between 17:00 and 19:00 UTC (11:00 and 13:00 LT) as the aircraft approached Mexico City. Peak values were observed directly over Mexico City, but the simulated values were higher than observed for a short period of

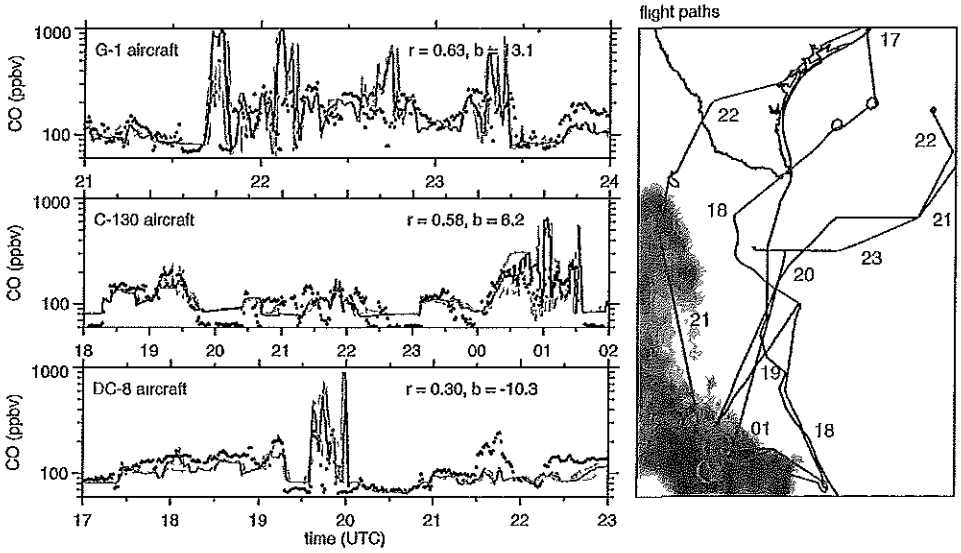

Fig. 8. Observed (dots) and simulated (lines) CO mixing ratio along three aircraft flight paths on 19 March where gray shading denotes predicted values within one grid cell surrounding the aircraft position. Correlation coefficient and mean bias denoted by r and b, respectively. Panel on right depicts the flight paths for each aircraft along positions at select times for the C-130 and DC-8 aircraft.

time. Both the observed and simulated CO was low between 20:00 and 21:00 UTC (14:00–15:00 LT) when the aircraft ascended to high altitudes northwest of Mexico City, but the simulated CO was lower than observed closer to the surface over Texas when the aircraft was flying back to Houston.

A summary of the statistical performance of the simulated CO using percentiles, correlation coefficient (r), and mean bias (b) for all G-1, C-130 and DC-8 flights is shown in Fig. 9. A much larger range for both the observed and simulated percentiles is seen in for G-1 aircraft since it usually flew in the immediate vicinity of the Mexico City and was frequently within the anthropogenic plume. The percentiles show that the model overestimated the measured range of CO on some days and underestimated the range of CO on others. Both the observed and simulated percentiles were lower for the C-130 aircraft since a large fraction of the flight time was spent downwind of Mexico City, and the simulated range of CO was higher and lower than observed depending on the day. In contrast, the simulated range of CO along the DC-8 flight paths was usually less than observed. When averaged among all the aircraft, the percentiles were very similar to the measurements, mean values somewhat lower than observed with a correlation coefficient of 0.61. The correlation coefficients that measure the skill in predicting the magnitude of CO in space and time ranged from 0.30 to 0.89 among the aircraft flights. The results shown in Fig. 9 suggest that the model adequately reproduced the overall transport and mixing of CO downwind of Mexico City, although there were occasional errors in space and time for the exact position of CO plumes and magnitude of smoke plumes.

4.3 Elemental carbon

Observed and predicted concentration of elemental carbon (EC) at the T0, T1, T2, and Paso de Cortes sites is shown in Fig. 10. The model performed the best at T0, the urban site located closest to the highest emission rates. The magnitude and temporal variation of the simulated EC was similar to the measurements with a correlation coefficient of 0.56. The average values during nighttime periods between 00:00 and 11:00 UTC (18:00–05:00 LT) and afternoon periods between 16:00 and 00:00 UTC (10:00–18:00 LT) periods were predicted quite well over the period. However, simulated EC during the morning between 11:00 and 16:00 UTC (05:00–10:00 LT) was significantly underestimated in contrast with CO predictions over the city (Fig. 7a). Since errors in BL depth will affect CO and EC similarly, one must conclude that differences are likely the result of greater uncertainties in EC emissions over the city. One factor could be the relative contribution of diesel vehicles at that time of day in the city, since the CO/EC ratios from the MCMA emission inventory was somewhat higher during the morning rush hours between 12:00 and 15:00 UTC (06:00–09:00 LT) than during the rest of the day.

EC predictions at the T1 site were nearly always lower than observed, although the correlation of 0.45 indicates that the simulated diurnal variation in EC was somewhat similar to the observations. As with CO at this site (Fig. 7b), the largest errors occurred during the morning hours and emission rates of EC may be more problematic at this location than in the city.

Both the observed and simulated EC were usually below 2 $\mu g\,m^{-3}$ further downwind at the remote T2 site. Since the

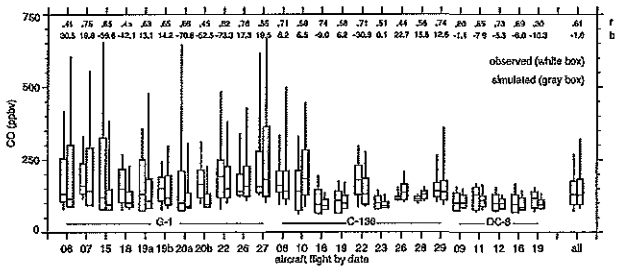

Fig. 9. Comparison of observed and simulated CO along the aircraft flight paths, where horizontal lines denote the median, boxes denote 25th and 75th percentiles, and vertical lines denote 10th and 90th percentiles. Correlation coefficient (r) and mean bias (b) for each flight are included along the top. G-1 and C-130 values were obtained over domain 2 and DC-8 values obtained over domain 1. (a) and (b) denote morning and afternoon flight periods for the G-1 aircraft.

T2 site is remote, the time series of EC indicates multi-day variations and short time scale fluctuations instead of the diurnal variations observed at the T0 and T1 sites. While it is likely that T2 is impacted by Mexico City emissions when the regional winds are southwesterly (e.g. higher EC concentrations between March 18 and 22), transport from Mexico City to T2 does not occur every day (Doran et al., 2008). Instead, EC observed at T2 is from dilute plumes originating from many urban and biomass burning sources. While simulating the exact timing of dilute plumes transported over T2 is challenging, the similarity of the observed and simulated average EC concentrations is nevertheless encouraging.

At the Paso de Cortes remote site, the model reasonably simulated the magnitude and temporal variations in EC prior to 23 March (Fig. 7c). The observed and simulated peaks in EC during the late afternoon on many days (e.g. 16 and 17 March) indicates that some time is required to transport Mexico City EC to this site and that the BL must be sufficiently high since the site located ~1.8 km above the basin floor. After 23 March, the simulated EC is significantly higher than observed. Increased convective activity after the third cold surge on 23 March (Fast et al., 2007) likely led to increased vertical mixing and removal by wet deposition. While the model did produce more cloudiness over the region after 23 March, vertical mixing associated with convection and wet removal were underestimated.

The lower CO/EC anthropogenic emission ratios outside of Mexico City (Fig. 2) likely contributed to the negative bias in the predicted CO at the remote Paso de Cortes site. Both of these sites would be impacted by emissions from cities other than Mexico City during the field campaign, and changing the slope of the regional CO/EC emissions rates to be more like the MCMA inventory (Fig. 2) would improve predictions of both CO and EC at theses locations.

4.4 Organic matter

As described previously, the current version of MOSAIC includes only primary organic aerosols and does not treat SOA. Consequently, predictions of organic matter should be significantly underestimated when compared with the available measurements of total organic matter in the vicinity of Mexico City. If predicted organic matter is higher than observed, then one would conclude that the estimates of primary emissions of organic aerosols are too high because we have shown that transport and mixing is simulated reasonably well during the MILAGRO field campaign period. AMS data in conjunction with PMF analysis also provides a new tool to evaluate POA predicted over both urban and remote locations.

Examples of how PMF analysis can be used to evaluate POA are shown in Fig. 11, in which the time series of observed total organic matter, HOA, HOA+BBOA, and OOA (Aiken et al., 2008, 2009) is compared with predicted POA at the T0 site on 15 and 20 March. Simulated POA is based on the sum of the mass in the first four model size bins (from 0.39 to 0.625 μm), since the number of particles with an estimated volume-equivalent diameter, d_{ve} (DeCarlo et al., 2004), larger than 0.7 μm observed by the AMS instrument was very low. Adding mass from the fifth model size bin (from 0625 to 1.25 μm) did not increase the simulated POA shown in Fig. 11 significantly.

The diurnal variation in HOA on 15 March (Fig. 11a) is similar to primary emissions (e.g. CO) with the highest concentrations shortly after sunrise at the time of peak traffic activity and within a shallow boundary layer. HOA is reduced by vertical mixing as the convective boundary layer grows during the morning after 14:00 UTC (08:00 LT); however, concentrations are quite variable between 14 and 18:00 UTC (08:00–12:00 LT) as a result of light and variable winds that likely transport primary emissions over T0 from different parts of the surrounding urban area. HOA subsequently increases somewhat just before sunset as primary emissions build up within the shallow nocturnal boundary layer. In contrast, OOA increases during the late morning despite increased boundary layer vertical mixing, suggesting that a photochemical secondary process is responsible for the production of OOA. BBOA has the same temporal variation as HOA. There was only one fire reported in the vicinity of Mexico City on this day; therefore, BBOA likely represents dilute smoke from multi-day regional scale transport and many small-scale burning events within the city that cannot be detected by the MODIS hot-spot data.

The diurnal variation of simulated POA on this day was more consistent with HOA, although POA concentrations were higher than HOA concentrations most of the day. Emission rates that were too high, simulated ventilation of the basin that was too weak, and vertical mixing within the nocturnal boundary layer that was too weak could all explain the positive bias in organic aerosols. While the simulated boundary layer depth was similar to estimates from the radar wind

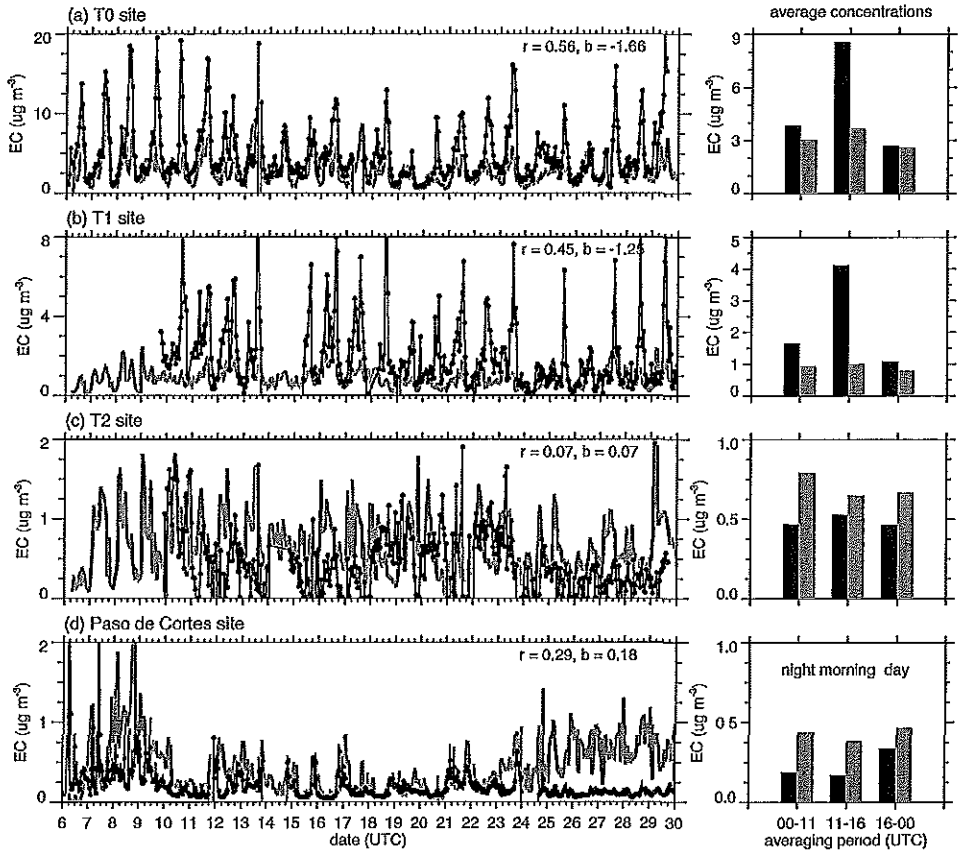

Fig. 10. Time series of observed (black) and modeled (gray) elemental carbon at the **(a)** T0, **(b)** T1, **(c)** T2, and **(d)** Paso de Cortes sites (left) and average concentrations during the night (18:00–05:00 LST), morning (05:00–10:00 LST), and daytime (10:00–18:00 LST) periods (right). Correlation coefficient and mean bias denoted by r and b, respectively.

profiler at T0 during the day, the simulated nocturnal boundary layer depth was 200 m while the sounding launched several kilometers southwest of T0 at 06:00 UTC (midnight) 16 March indicated a neutral layer up to 500 m AGL. Thus, the model likely underestimated the amount of mechanical mixing associated with the urban canopy and/or the basin circulations. This would also explain why simulated CO mixing ratios that were also higher than observed that night (Fig. 7a)

In contrast with 15 March, observed organic aerosol concentrations during the afternoon of 20 March (Fig. 11b) were much lower and the temporal variations of HOA and OOA were not typical of the more frequently observed morning build up of primary emissions followed by increased boundary layer vertical mixing and photochemistry. Instead, relatively strong southwesterly ambient winds ventilated pollutants out of the basin to the north and kept afternoon concentrations relatively low. Observed HOA did have a sharp peak between 12:00 and 14:00 UTC (06:00–08:00 LT) in the morning because observed wind speeds from the radar wind profiler were less than 1 m s^{-1} within the shallow boundary layer (not shown) that likely permitted the build-up of primary emissions, but concentrations dropped rapidly as the boundary layer grew and near-surface winds became coupled with the stronger winds aloft. BBOA increases around sunset as a result of a smoke plume transported from a fire on the mountain ridge south of the city.

Simulated POA was similar to the sum of HOA+BBOA most of the day, except for a brief period shortly after sunrise. While the model captured the increase in organic aerosol associated with a smoke plume late in the day, it failed to capture the peak in anthropogenic organic aerosols between 12:00 and 14:00 UTC (06:00–08:00 LT). At this time near-surface simulated wind speeds were between 2 and 3 m s^{-1} and consequently simulated POA concentrations as high as 9 μg m^{-3} were transported northeast of T0.

Predictions of POA have been compared with organic matter measurements from the available AMS and OC/EC data made at the T0, Pico Tres Padres, T1, T2, and Paso de Cortes sites as shown in Fig 12. Instead of showing the entire time series, mean diurnal variations of organic components are computed for the measurement period at each site. The diurnal variation of organic components over the entire field campaign period at T0 (Fig. 12a) is similar to the 15 March time series shown in Fig. 11a. Predicted POA has a magnitude

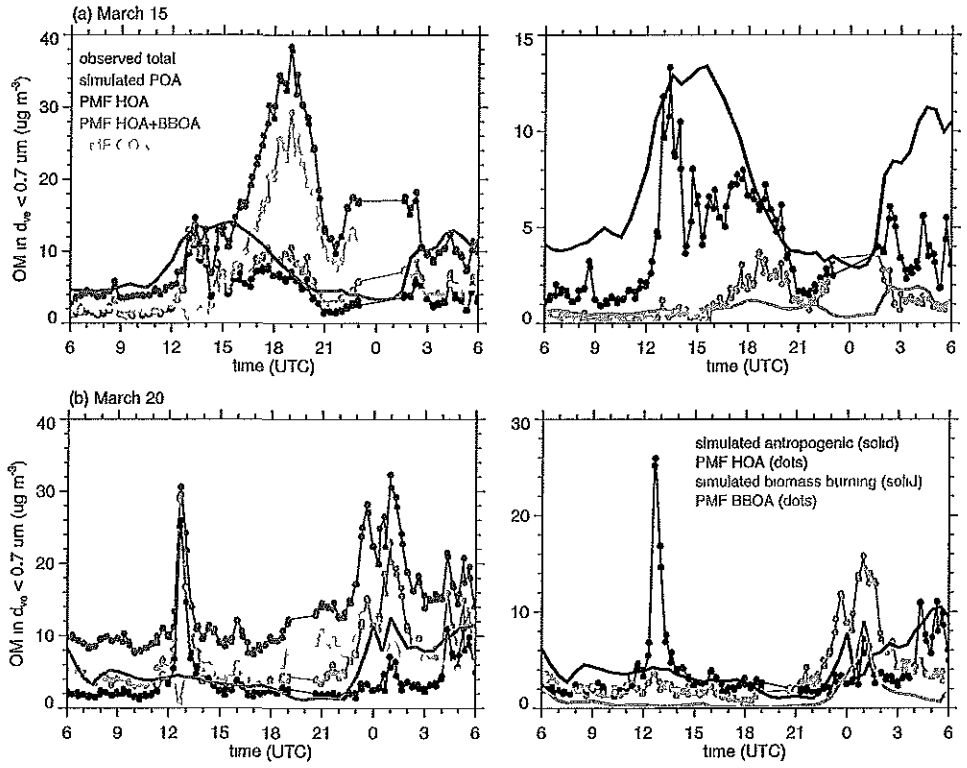

Fig. 11. Time series of observed and modeled average diurnal variations of total organic matter at the T0 site and the components of organic matter derived using the PMF analysis technique on **(a)** 15 March and **(b)** 20 March. Right panels depict simulated POA resulting from anthropogenic and biomass burning sources compared to HOA and BBOA, respectively. Most of the mass from the AMS instrument is assumed to be for particles with diameters less than 0.7 μm.

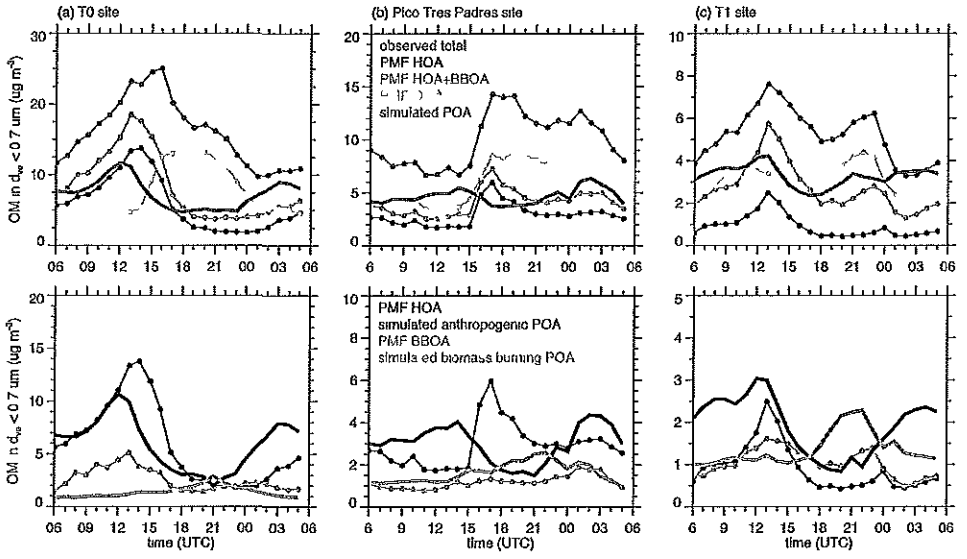

Fig. 12. Time series of observed, PMF components, and modeled average diurnal variations of organic matter at the **(a)** T0, **(b)** Pico Tres Padres, and **(c)** T1 sites. Bottom panels depict simulated anthropogenic and biomass burning POA compared with HOA and BBOA, respectively.

and diurnal variation that is more consistent with HOA or HOA+BBOA, depending on the time of day, than with total organic matter. The simulated peak in POA occurred one or two hours earlier than the peaks in HOA+BBOA and HOA, respectively. The consistent over-prediction of POA at night may be attributed to insufficient vertical mixing within the nocturnal boundary layer in the city.

PMF analysis was also available from the AMS instruments at the Pico Tres Padres (Fig. 12b) and T1 (Fig. 12c) sites. As with T0, the daily averaged predicted POA was between daily averaged HOA and HOA+BBOA concentrations. While the predicted diurnal variations in POA are consistent with variations in HOA at T0, the diurnal variation in predicted POA and measured HOA differ more at Pico Tres Padres and T1. At Pico Tres Padres, the most likely explanation for the discrepancy is that the 3-km grid spacing in the model cannot adequately resolve the local slope flows and boundary layer evolution at the mountain-top sampling site. The observations show a dramatic increase in organics at 15:00 UTC (09:00 LT), which occurs when the convective boundary layer grows above the altitude of the mountain (Herndon et al., 2008). Smoothing of the topography associated with the 3-km grid spacing produced a mountain-top elevation of 2500 m (~400 m lower than the actual elevation); therefore, the simulated atmosphere was not fully decoupled from Mexico City emission sources at night. At the T1 site, the model produced a peak in POA at 13:00 UTC (07:00 LT) similar to the measurements of HOA and HOA+BBOA. But the subsequent decrease in simulated POA reversed at 17:00 UTC (11:00 LT) instead of continuing to decrease for four more hours during the afternoon. As discussed previously with CO and EC, there are likely uncertainties in the local emissions that may contribute to errors on POA at this site, including brick kilns (Christian et al., 2009) and other local sources.

Comparisons of predicted POA and total organic matter from the OC/EC instrument at the T2 site and the AMS instrument at the Paso de Cortes site is shown in Fig. 13a and b, respectively. Predicted POA concentrations were usually less than half the observed total organic matter at both sites. Increases in observed afternoon total organic matter is likely the result of SOA formation as anthropogenic particulates are transported over both of these sites. The increase in observed afternoon total organic matter is more dramatic at Paso de Cortes than at T2 because the Paso de Cortes site is located at a much higher elevation. Measurements at Paso de Cortes during the night are likely to be more representative of the free atmosphere. As the convective boundary layer grows during the morning the site is entrained into the convective boundary layer that contains much higher concentrations of anthropogenic particulates.

The range of total observed organic aerosol, HOA, HOA+BBOA, and predicted POA at the T0, Pico Tres Padres and T1 sites is depicted in terms of percentiles, biases, and correlation coefficients in Fig. 14. The median and range

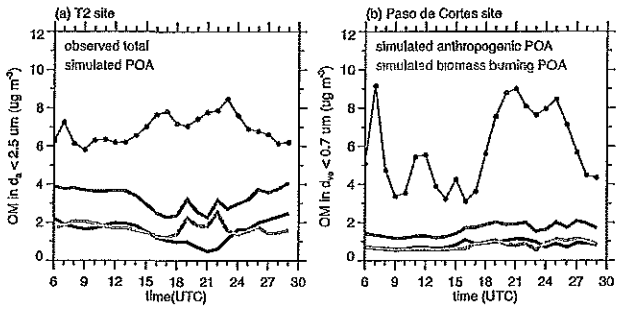

Fig. 13. Time series of observed and modeled average diurnal variations of organic matter at the **(a)** T2 site using Sunset Laboratory EC/OC data and the **(b)** Paso de Cortes site using Aerodyne Aerosol Mass Spectrometer (AMS) data. PMF components not currently available at the Paso de Cortez site.

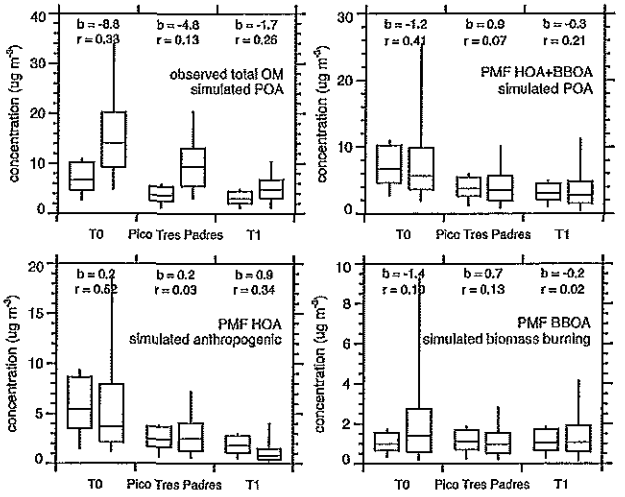

Fig. 14. Box-and-whisker plots of observed organic matter, PMF components, and simulated primary organic matter at the T0, Pico Tres Padres, and T1 sites during the field campaign, where the box denotes the range of the 25th and 75th percentiles, the vertical lines denote the 5th an 95th percentiles, and the horizontal line denotes the median. Mean bias and correlation coefficient for each observed and simulated pair included along the top of each panel.

of predicted POA at each of these sites is more consistent with concentrations of HOA+BBOA. This makes sense because predicted POA contains emissions from both anthropogenic and biomass burning sources. However, the simulated POA temporal variations are not well correlated with HOA+BBOA. A correlation coefficient of 0.41 was obtained in the city at the T0 site, but at the edge of the city the correlation was only 0.21. The correlation of simulated anthropogenic POA and HOA was somewhat higher at both sites. As explained earlier, the poor correlation at the Pico Tres Padres site is likely the result of the 3 km grid spacing poorly representing the small-scale topography. The correlation between simulated biomass burning POA and BBOA was low

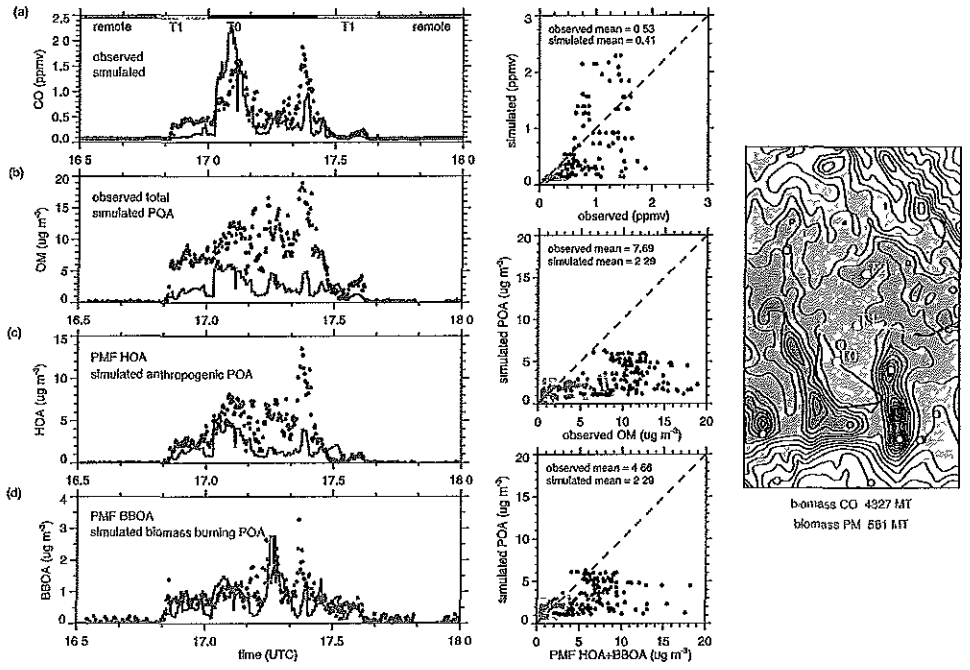

Fig. 15. Observed and simulated **(a)** CO and **(b)** total organic mater, **(c)** anthropogenic organic matter, and **(d)** biomass burning organic matter along the G-1 flight path during the morning of March 15 on a day with relatively low biomass burning over central Mexico. Right panel depicts biomass-burning sources (green dots) and the G-1 flight path divided into transects over the city and T0 (black), north of the city over the T1 site (light blue), and remote regions between Mexico City and Veracruz (purple).

at all sites because the emissions did not include all types of fires and narrow smoke plumes could easily miss the surface sampling sites even with small transport errors. While there are large errors in the timing of predicted POA, the results indicate that the overall simulated POA mass based on the emission inventories from anthropogenic and biomass burning sources is consistent with primary components of observed organic aerosols. Both the simulated biomass burning POA and BBOA are a larger fraction of the total organic matter mass at the edge of the city at T1 than downtown at T0, indicating that biomass burning sources become relatively more important farther away from anthropogenic sources.

AMS instruments were also deployed aboard the G-1 (Kleinman et al., 2008) and C-130 (DeCarlo et al., 2008) aircraft and PMF analysis was performed for a select number of flights. The information on organic components enables predictions of POA to be evaluated further downwind of Mexico City. An example of the observed and predicted CO and organics for the morning flight of the G-1 on 15 March is shown in Fig. 15. Overall, spatial variations of predicted CO were qualitatively similar to the measurements along aircraft flight path (Fig. 15a). The simulated peak of 2.3 ppm just after 17:00 UTC (11:00 LT) was 0.7 ppm higher than observed as the aircraft passed over the T0 site. As the aircraft returned over the city the simulated peak of 1.0 ppm was 0.9 ppm lower than observed. The largest scatter in the observed and simulated CO occurred over the city since timing and location of the simulated plume was not exactly right. As with the analysis of surface organic aerosols, predicted POA was usually less than the concentration of observed total organic aerosols as seen in the time series and scatter plot in Fig. 15. Mean predicted POA was 2.3 $\mu g\,m^{-3}$, while the mean observed total organic matter was 7.7 $\mu g\,m^{-3}$. A somewhat better agreement is reached for the scatter plot of predicted POA with HOA+BBOA (mean value of 4.7 $\mu g\,m^{-3}$), but Fig. 15c and d show that most of the differences result from an underestimation of anthropogenic POA just south and west of the city.

Simulated spatial variations in anthropogenic POA were similar to HOA obtained over the northwestern part of the city as the aircraft passed over T0, although the magnitude of POA was somewhat lower than HOA (Fig. 15c). However, the simulated anthropogenic POA was significantly lower than HOA along the flight legs over the mountains to the south and west of the city. Simulated biomass burning POA and BBOA within the boundary layer along the aircraft flight path over T1 and the city was usually around 1 $\mu g\,m^{-3}$, with no significant peaks to suggest the presence of large fires. Over the city, peak values of biomass burning POA and BBOA were both as high as 2–3 $\mu g\,m^{-3}$. The distribution of predicted biomass burning POA (not shown) suggested that multi-day accumulation of smoke contributed to the boundary layer concentrations, rather than the fires surrounding the city on this day. Note that simulated biomass burning POA

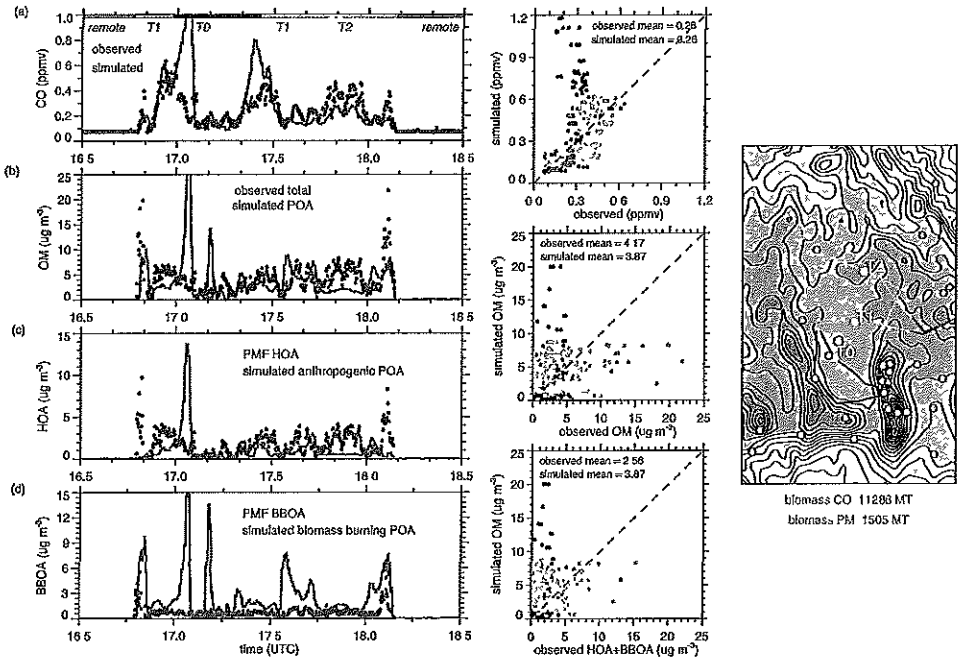

Fig. 16. Same as Fig. 15, except during the morning of 19 March on a day with relatively high biomass burning over central Mexico.

does not include grass fire and other burning sources in the city that may be important.

In contrast to 15 March, 19 March was a day with a many large fires in the vicinity of Mexico City. CO was predicted reasonably well along the G-1 flight path, as shown in Fig. 16a, and CO originating from biomass burning was a significant fraction of the total CO (not shown). Unlike 15 March, predicted POA on this day was equal to or higher than the observed total organic matter over many portions of the flight path (Fig. 16b). The average predicted POA over the central plateau was 3.9 $\mu g\,m^{-3}$, while the observed total organic matter was 4.2 $\mu g\,m^{-3}$ and HOA+BBOA was 2.6 $\mu g\,m^{-3}$. Figure 16c indicates that the simulated anthropogenic POA was much higher than HOA in the vicinity of T0, but was too low in the vicinity of T2 because the simulated wind were too westerly and transport the Mexico City plume just southeast of T2. Simulated biomass burning POA was almost always higher than BBOA (Fig. 16d), except directly north of the mountain ridge east of the city. For example, predicted biomass burning POA over the fire near T0 was 15 $\mu g\,m^{-3}$ even though there was no evidence of smoke from the BBOA time series at that time.

Percentiles are used to summarize the range of observed total organic matter, HOA, HOA+BBOA, and simulated POA along all of the available G-1 and C-130 aircraft flight paths, as shown in Fig. 17. In contrast with the percentiles obtained over many days from the surface sites shown in Fig. 14, the range of simulated POA did not consistently agree better with HOA+BBOA than with observed total organic matter. On some days simulated POA is similar to HOA+BBOA, such as the G-1 flights on March 15. On other days predicted POA was lower than the observed total organic aerosols but still higher than the range of HOA+BBOA (e.g. 29 March C-130 flight). For the G-1 flights on 18 and 20 March, the simulated POA was frequently less than HOA + BBOA. On 18 March, the predicted OM plume was transported several kilometers north of the aircraft flight path. While the location of the observed and predicted OM plume was similar on 20 March, errors in the simulated boundary layer growth near-surface winds may have diluted the Mexico City plume too fast. When all the flights are considered together, the simulated POA was closest to the HOA+BBOA as with the analysis of the surface AMS instrument sites.

Scatter plots that relate primary organic aerosol concentrations and CO mixing ratios for four geographic regions are shown in Fig. 18 including: (a) at the T0 site and G-1 transects over Mexico City, (b) at the Pico Tres Padres site, (c) at the T1 site and G-1 transects in the vicinity of T1, and G-1 transects in the vicinity of T2 and between Mexico City and Veracruz. At the surface, hourly averages are used and the simulated quantities correspond to the measurement period at each site. Scatter plots for the simulated quantities are qualitatively similar to the observations both at the surface and aloft for all four regions, with some exceptions. Modeled POA rarely exceeded 15 $\mu g\,m^{-3}$ in the city (Fig. 18a), although the number of hours observed HOA+BBOA exceeded 15 $\mu g\,m^{-3}$ was a small percentage of the measurement period. Most of the observed peak primary organic aerosols were composed primarily of HOA during the morning, indicating that the modeled POA was too low

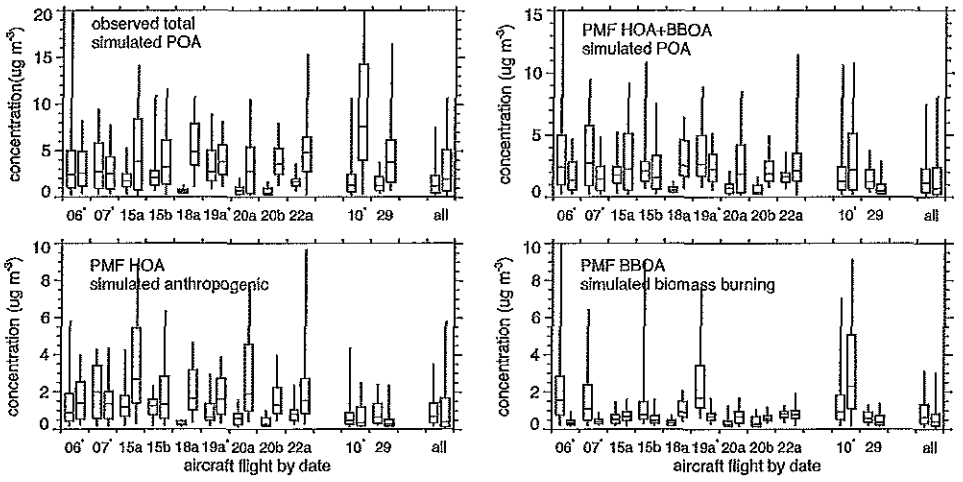

Fig. 17. Comparison of observed organic matter, PMF components, and simulated primary organic matter along the aircraft flight track *where horizontal lines denote the median, boxes denote 25th and 75th percentiles, and vertical lines denote 5th and 95th percentiles. Data at* high altitudes outside of the Mexico City basin have been excluded from the G-1 flight tracks. Asterisk denotes days with five or more large fires within 60 km of Mexico City.

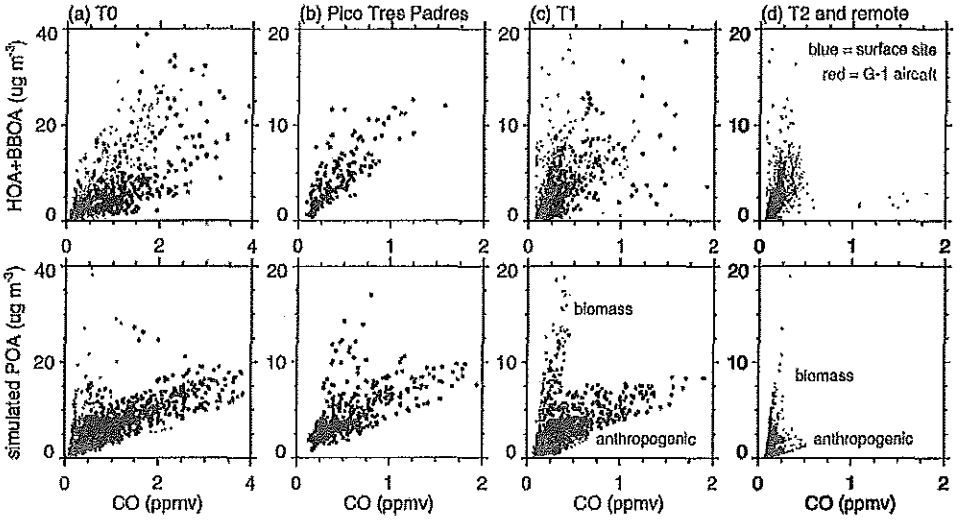

Fig. 18. *Primary organic aerosol concentrations versus CO mixing ratios at surface sampling sites and along G-1 flight paths for four* geographic regions including: (a) at the T0 site and G-1 transects over Mexico City, (b) at the Pico Tres Padres site, (c) at the T1 site and G-1 transects in the vicinity of T1, and G-1 transects in the vicinity of T2 and between Mexico City and Veracruz. Observed and simulated quantities on the top and bottom panels, respectively.

when traffic emissions are the greatest. At Pico Tres Padres (Fig. 18b) and T1 (Fig. 18c), both the observed and simulated scatter plots had points clustered around two slopes. Those with high primary organic aerosol concentrations and low CO mixing ratios originated mostly from biomass burning sources, while those with higher CO mixing ratios originated mostly from anthropogenic sources. The modeled POA/CO for biomass burning exhibited less scatter than the observations, suggesting that there is more variability in the biomass burning POA/CO ratios than indicated in the emission inventory (Fig. 2). Further downwind in the vicinity of the T2 site (Fig. 18d), biomass burning sources contributed a larger fraction of both the observed and simulated total primary organic aerosols. As with Fig. 18c, the modeled POA/CO for biomass burning aerosols exhibited less variability and appeared to represent the upper limit of the observations.

5 Discussion

Predictions of POA depend upon the anthropogenic and biomass burning estimates as well as the representation of transport and mixing that affects downwind dispersion of particulates. While the meteorology was simulated reasonably well overall, errors in the simulated circulations will undoubtedly affect the predicted timing and concentration of trace gas and particulate plumes at times. These errors are usually associated with details of the local circulations, rather than the large-scale synoptic circulations as shown in Fig. 5. But based on the evaluation of predicted scalars using data collected at a number of surface sites and from aircraft over a three-week period, we believe that overall magnitude of POA can be assessed using the present model configuration. For the purposes of evaluating emission inventories, it would have been useful to bring the meteorological quantities into even closer agreement with observations, especially near the surface in the vicinity of Mexico City. Data assimilation cannot solve all these issues, however, even for sophisticated variational techniques (e.g. Bei et al., 2008).

In general, CO was better simulated than EC and POA. All three of these quantities were better simulated in the city at the T0 site than at other locations. This is not surprising since particulate emission estimates are likely to be less understood and more uncertain than emission sources of CO. While the location of T1 at the edge of the city is useful for understanding chemical evolution over a few hours as pollutants are transported out of the city, the spatial and temporal variations of local emissions will affect local-scale variations in predicted trace gases and particulates in the vicinity T1. The diurnal variations in CO and EC was simulated reasonably well at T1, but the EC concentrations were much lower than observed during the morning between 11:00 and 16:00 UTC (05:00–10:00 LT). Although the overall magnitude of modeled POA and the sum of HOA and BBOA at T1 was similar, the simulated temporal variations of these quantities were not correlated as well as modeled and measured CO or EC. Two factors contributing the uncertainties in particulate predictions at T1 could be the characterization of the relative number of gasoline and diesel vehicles along the nearby highway that varies during the day and changes in urban growth at the city edge not accounted for in the emissions inventory.

At remote sites, such as T2 and Paso de Cortes, the simulation results suggest that there would be some improvements in predicted CO and EC if the slope of the regional CO/EC emission rates were closer to those within the metropolitan area. This also implies that the slope of the regional CO/POA emission rates may need to be closer to those within the metropolitan area. This would lead to lowering of simulated POA outside of the city at the remote sampling sites and along the aircraft transects that are not the Mexico City plume.

At remote sites, biomass burning is also expected to contribute a relatively larger fraction of the observed carbonaceous aerosols. However, biomass burning in this study originates only from large fires and it is not currently possible for models to account for numerous smaller fires that occurred in the region (Yokelson et al., 2007). As with the measurements shown in Fig. 14, numerous small burning sources in the city not accounted by metropolitan emission inventory, may also contribute to observed carbonaceous aerosols. For example, grass fires could be important in this region on some days and have significantly lower PM emission factors (e.g. Sinha et al., 2004) even though most of the aircraft measurements focused on pine forest fires (Yokelson et al., 2007).

The horizontal grid spacing employed in this study also affects the conclusions regarding smoke plumes. The grid spacing artificially spreads a smoke plume at the source over a 9 km^2 area; therefore, downwind simulated smoke plumes are likely wider than in reality. While resolution primarily affects the comparisons of model predictions along aircraft flight paths that intersect smoke plumes just downwind of their source (e.g. Fig. 15), uncertainties in the fuel loading for the vegetation types located on the mountains surrounding Mexico City may also contribute to the over-estimations in the emission of particulates for some fires.

Another issue contributing to uncertainties in the POA predictions is volatility. Since emitted organic particulates are semi-volatile (Robinson et al., 2007; Huffman et al., 2008, 2009a, b), then they can evaporate and possibly re-condense further downwind to form SOA. The degree of POA evaporation is unclear. Ambient measurements suggest a volatility somewhat lower than that in the Robinson et al. (2007) model at ambient concentrations (Dzepina et al., 2009), but the volatility under higher concentrations which are most relevant for the evaporation of fresh emissions remains poorly characterized. To the extent that it occurs, evaporation of anthropogenic POA emissions would increase their underestimation, since we assume POA to be non-volatile and predicted POA was similar to HOA + BBOA in the city. On the other hand, the over-prediction of POA downwind of large fires would be improved if a portion of the biomass burning particulates were assumed to be semi-volatile or if lower emission factors were used.

The AMS instrument is now being used widely to obtain information on the composition and size distribution of aerosols (e.g. Zhang et al., 2007). Nevertheless, some caution is warranted when comparing model predictions and AMS measurements. The size cut of the particles that can be measured by the AMS is reported to be 1 μm in vacuum aerodynamic diameter (PM_1 in d_{va}) (e.g. Canagaratna et al., 2007). This size cut corresponds to slightly smaller particles than the 1 μm cut in transition-regime aerodynamic diameter (d_{ta})that is typically used to define PM_1 ambient measurements using cyclone or impactor inlets operated at ambient pressure, with the exact correspondence being dependent on ambient pressure and on particle density and shape and thus

composition (DeCarlo et al., 2004). For example, for the average density of 1.4 g cm^{-3} calculated from the chemical composition measurements at T0 or CENICA (Aiken et al., 2009; Salcedo et al., 2006) and the pressure of Mexico City, a PM_1 cut in d_{va} corresponds to a $PM_{0.9}$ cut in d_{ta}. There can be some variation in individual aerodynamic lenses as well, which in some cases lead to smaller size cuts (Liu et al., 2007). The PM_1 cut in d_{va} corresponds to 0.7 μm physical diameter for spherical particles under the average conditions in Mexico City. Therefore, only predicted organic aerosols from the four size bins below 0.7 μm were to compare with the AMS measurements.

The primary source of uncertainty on the measured AMS mass is the collection efficiency (CE). A CE of 0.5 has been determined from many field inter-comparisons for dry non-highly-acidic particles (e.g. Takegawa et al., 2005; Canagaratna et al., 2007 and references therein) that is expected to apply to the Mexico City conditions, and also with internal AMS light scattering (Cross et al., 2007). This value of CE has been verified with extensive inter-comparisons for Mexico City (Salcedo et al., 2006, 2007; Johnson et al., 2008; DeCarlo et al., 2008; Dunlea et al., 2008; Aiken et al., 2009; Kleinman et al., 2008). However, some uncertainty exists in this value which results in an uncertainty in the measured mass of ~20–25%. Some additional uncertainty on the relative amounts of the PMF components on the order of 5–10% of the total OM arises from the PMF separation (Ulbrich et al., 2009), which is higher for the unit-resolution data (Aiken et al., 2009). Estimates of the temporal variations and relative contribution of primary anthropogenic, primary biomass burning, and secondary organic aerosols seem qualitatively reasonable, but uncertainties in AMS quantification and PMF output need to be reduced for a more precise evaluation of model predictions of organic aerosols.

Finally, comparing modeled POA in the city using data derived from the AMS instrument at the T0 site to draw conclusions regarding whether estimates of organic aerosol emissions are reasonable must be put into perspective. More firm conclusions over the urban area could be drawn once the AMS data from the 'flux tower' site (Fig. 1c) becomes available and another simulation is performed using a much smaller grid spacing to resolve the terrain of Pico Tres Padres and the gradients in emissions around the Pico Tres Padres and T1 sites. In contrast, there are 25 CO monitoring sites located across the metropolitan area. While mesoscale models may not simulate temporal variations in CO at each site perfectly, the spatially averaged observed and simulated values agree reasonably well (Fig. 7) because small errors in transport that move pollutants from one part of the basin to another (Fast and Zhong, 1998) are averaged out.

These issues stress the complexity of modeling organic aerosols and evaluating the predictions of POA using the available measurements. This does not yet consider the additional complexity of understanding SOA processes, such as hydrocarbon precursor photochemistry and gas-to-particle partitioning, and developing schemes that represent those processes in models. Coupling the extensive trace gas hydrocarbon and particulate organic matter measurements to compute the total observed organic carbon (TOOC) in the atmosphere, a concept introduced by Heald et al., (2008), is needed to understand how organic carbon moves between the gas and particle phases. An analysis of TOOC has already been performed using measurements at the T1 site (de Gouw et al., 2009), and comparisons of simulated TOOC with TOOC derived at all the sites that have both hydrocarbon and organic matter data is needed to evaluate treatments of SOA in the future.

6 Summary

This study employs a wide range of measurements made at the surface and aloft to examine the performance of the WRF-Chem chemical transport model in simulating POA in the vicinity of Mexico City during the March 2006 MILAGRO field campaigns. Since the emission inventories and dispersion will affect predictions of total organic matter and consequently total particulate matter, our objective is to assess the uncertainties in predicted POA before testing and evaluating the performance of secondary organic aerosol (SOA) treatments in future studies.

The predicted meteorology was constrained by wind, temperature, and humidity profiles obtained from radar wind profilers and radiosondes by using data assimilation. Independent measurements, such as those from research aircraft, indicate that the model captured the overall local, regional, and synoptic scale circulations. However, errors in the timing and interaction of various thermally driven circulations associated with complex terrain were produced at times near the surface within the Mexico City basin. The growth of the boundary layer depth was predicted reasonably well on most days, except that the afternoon convective boundary layer usually collapsed too quickly around sunset. The model did not include a detailed urban canopy parameterization that would influence local heating and vertical wind shears so that vertical mixing was likely too shallow over the city during some nights.

Before evaluating predicted POA, scalars such as CO and EC were first used to further assess the role of the predicted thermally-driven circulations, boundary-layer mixing, and their interaction with the larger-scale flows on transport and mixing in the region. CO was well simulated on most days both over the city and downwind, indicating that transport and mixing processes were usually consistent with the observed meteorological conditions. Predicted and observed diurnal variations of EC in the city were similar, except that simulated EC concentrations during the morning were half of the observed concentrations. Larger errors in EC occurred at remote locations. If the slope of the CO/EC emission rates in the national emission inventory were changed to be

more consistent with the metropolitan emission inventory, then predictions of both CO and EC would likely improve at remote locations.

In contrast with many previous field campaigns, AMS measurements during MILAGRO were available both at ground sites and on research aircraft so that components of organic aerosols derived from PMF at many locations could be used to evaluate the model. Predicted POA was consistently lower than the measured organic matter at the ground sites, which is consistent with the expectation that SOA should be a large fraction of the total organic matter mass. A much better agreement was found when the overall predicted POA was compared with the sum of "primary anthropogenic" (HOA) and "primary biomass burning" (BBOA), suggesting that the overall magnitude of primary organic particulates released was reasonable. The predicted POA was greater than the total observed organic matter for short periods when the aircraft flew directly downwind of large fires, suggesting that biomass burning emission estimates from some large fires may be too high.

Uncertainties in the predictions of organic aerosols will affect estimates of aerosol direct radiative forcing. Global models with their coarse spatial grid spacing cannot resolve strong gradients in particulates, such as those originating from emissions in the vicinity of megacities, so it is problematic to evaluate global model predictions of organic aerosols using point observations. Regional models, however, should be able to resolve most of the spatially and temporally varying processes responsible for the emission, transport, mixing, and removal of POA in the atmosphere. In this study, the magnitude and diurnal variation of POA was predicted reasonably well in the city, but errors increased downwind of Mexico City. While time-averaged observed and predicted magnitude of POA was similar downwind, errors in the predicted diurnal variability produced differences up to a factor of two. These errors in diurnal variability would likely affect the magnitude of aerosol direct radiative forcing during the day as well as influence the amount secondary species condensing on pre-existing particulates. These issues will be examined in subsequent studies that employ WRF-Chem and new treatments of SOA.

Acknowledgements. We thank Wenfang Lei (Massachusetts Institute of Technology) for providing the 2002 MCMA emissions inventory, Marcelo Mena (Universidad Nacional Andrés Bello) for providing the gridded version of the 1999 NEI, and Darrel Baumgardner (Universidad Nacional Autónoma de México) for providing data from the Paso de Cortes site. This research was supported by the US DOE's Atmospheric Sciences Program of the Office of Biological and Environmental Research (OBER) under Contract DE-AC06-76RLO 1830 at Pacific Northwest National Laboratory (PNNL). Computational resources were provided by EMSL, a national scientific user facility located at PNNL and sponsored by the DOE OBER. PNNL is operated for the US DOE by Battelle Memorial Institute. The National Center for Atmospheric Research is sponsored by the National Science Foundation. Jose Jimenez and his team were supported by DOE ASP (DE-FG02-05ER63981), NSF (ATM-0528634), and EPA STAR (RD-83216101-0).

Edited by: S. Madronich

References

Ackermann, I. J., Hass, H., Memmesheimer, M., Ebel, A., Binkowski, F. S., and Shankar, U.: Modal aerosol dynamics model for Europe: Development and first applications, Atmos. Environ., 32, 2981–2999, 1998.

Aiken, A. C., Salcedo, D., Cubison, M. J., de Foy, B., Wiedinmyer, Huffman, C. J., DeCarlo, P. F., Ulbrich, I. M., Docherty, K. S., Sueper, D., Kimmel, J. R., Worsnop, D. R., Trimborn, A., Northway, M., Wehrli, M. N., Szidat, S., Prevot, A., Baltensperger, U., Noda, J., Wacker, L., Stone, E. A., Schauer, J. J., Volkamer, R., Fortner, E., Knighton, B., Wang, J., Laskin, A., Zheng, J., Zhang, R., Gaffney, J., Marley, N. A., Querol, X., Paredes-Miranda, G., Arnott, W. P., Molina, L. T., Sosa, G., and Jimenez, J. L.: Mexico City aerosol analysis during MILAGRO using high resolution aerosol mass spectrometry at the urban supersite (T0). Part 1: Fine Particle Composition and Organic Source Apportionment, Atmos. Chem. Phys. Discuss., 9, 8377–8427, 2009.

Aiken, A. C., DeCarlo, P. F., Kroll, J. H., Worsnop, D. R., Huffman, J. A., Docherty, K., Ulbrich, I. M., Mohr, C., Kimmel, J. R., Sueper, D., Zhang, Q., Sun, Y., Trimborn, A., Northway, M., Ziemann, P. J., Canagaratna, M. R., Onasch, T. B., Alfarra, R., Prevot, A. S. H. Dommen, J. Duplissy, J., Metzger, A., Baltensperger, U., and Jimenez, J. L.: O/C and OM/OC ratios of primary, secondary, and ambient organic aerosols with high resolution time-of-flight aerosol mass spectrometry, Environ. Sci. Technol., 42, 4478–4485, doi:10.1021/es703009q, 2008.

Amato, F., Pandolfi, M., Viana, M., Querol, X., Alastuey, A., and Moreno, T.: Spatial and chemical patterns of PM10 in road dust deposited in urban environment, Atmos. Environ. 43, 1650–1659, 2009.

Baumgarder, D., Grutter, M., Allan, J., Ochoa, C., Rappenglueck, B., Russell, L. M, and Arnott, P: Evolution of anthropogenic pollution at the top of the regional mixed layer over the central Mexico plateau, Atmos. Chem. Phys., 3265–3306, 2009.

Bei, N., de Foy, B., Lei, W., Zavala, M., and Molina, L. T.: Using 3DVAR data assimilation system to improve ozone simulations in the Mexico City basin, Atmos. Chem. Phys, 8, 7353–7366, 2008.

Binkowski, F. S. and Shankar U.: The Regional Particulate Matter Model, 1, Model description and preliminary results, J. Geophys. Res., 100, 26191–26209, 1995.

CAM (Comisión Ambiental Metropolitana): Inventario de Emisiones 2002 de la Zona Metropolitana del Valle de Mexico, Mexico, 2004.

Canagaratna, M. R., Jayne, J. T., Jimenez, J. L., Allan, J. D., Alfarra, M. R., Zhang, Q., Onasch, T. B., Drewnick, F., Coe, H., Middlebrook, A., Delia, A., Williams, L. R., Trimborn, A. M., Northway, M. J., DeCarlo, P. F., Kolb, C. E., Davidovits, P., and Worsnop, D. R.: Chemical and microphysical characterization of ambient aerosols with the Aerodyne Aerosol Mass Spectrometer, Mass. Spec. Rev., 26, 183–222, 2007.

Christian, T. J., Yokelson, R. J., Cardenas, B., Molina, L. T., Engling, G., and Hsu. S.-C.: Trace gas and particulate emissions from domestic and industrial biofuel use and garbage burning in central Mexico, Atmos. Chem. Phys. Discuss., 9, 10101–10152, 2009.

Chapman, E. G., Gustafson Jr., W. I., Easter, R. C., Barnard, J. C., Ghan, S. J., Pekour, M. S., and Fast, J. D.: Coupling aerosols-cloud-radiative processes in the WRF-chem model: Investigating the radiative impact of large point sources, Atmos. Chem. Phys., 9, 945–964, 2009.

Cross, E. S., Slowik, J. G., Davidovits, P., Allan, J. D., Worsnop, D. R., Jayne, J. T., Lewis, D. K., Canagaratna, M., and Onasch, T. B.: Laboratory and ambient particle density determinations using light scattering in conjunction with aerosol mass spectrometry, Aerosol Sci. Technol., 41, 343–359, doi:10.1080/02786820701199736, 2007.

DeCarlo, P., Slowik, J. G., Worsnop, D. R., Davidovits, P., and Jimenez, J. L.: Particle morphology and density characterization by combined mobility and aerodynamic diameter measurements, Part 1: Theory, Aerosol Sci. Technol., 38, 1185–1205, doi:10.1080/027868290903907, 2004.

DeCarlo, P. F., Kimmel, J. R., Trimborn, A., Northway, M. J., Jayne, J. T., Aiken, A. C., Gonin, M., Fuhrer, K., Horvath, T., Docherty, K., Worsnop, D. R., and Jimenez, J. L.: Field-deployable, high-resolution, time-of-flight aerosol mass spectrometer, Anal. Chem., 78, 8281–8289, 2006.

DeCarlo, P. F., Dunlea, E. J., Kimmel, J. R., Aiken, A. C., Sueper, D., Crounse, J., Wennberg, P. O., Emmons, L., Shinozuka, Y., Clarke, A., Zhou, J., Tomlinson, J., Collins, D. R., Knapp, D., Weinheimer, A. J., Montzka, D. D., Campos, T., and Jimenez, J. L.: Fast airborne aerosol size and chemistry measurements above Mexico City and Central Mexico during the MILAGRO campaign, Atmos. Chem. Phys., 8, 4027–4048, 2008.

de Foy, B., Molina, L. T., and Molina, M. J.: Satellite-derived land surface parameters for mesoscale modeling of the Mexico City basin, Atmos. Chem. Phys., 6, 1315–1330, 2006.

de Foy, B., Lei, W., Zavala, M., Volkamer, R., Samuelsson, J., Mellqvist, J., Galle, B., Martinez, A.-P., Grutter, M., Retama, A., and Molina, L. T.: Modelling constraints on the emission inventory and on vertical dispersion for CO and SO_2 in the Mexico City metropolitan area using solar FTIR and zenith sky UV spectroscopy, Atmos. Chem. Phys., 7, 781–801, 2007.

de Foy, B., Fast, J. D., Paech, S. J., Phillips, D., Walters, J. T., Coulter, R. L., Martin, T. J., Pekour, M. S., Shaw, W. J., Kastendeuch, P. P., Marley, N. A., Retama, A., and Molina, L. T.: Basin-scale wind transport during the MILAGRO field campaign and comparison to climatology using cluster analysis, Atmos. Chem. Phys., 8, 1209–1224, 2008, http://www.atmos-chem-phys.net/8/1209/2008/.

de Gouw, J. A., Middlebrooket, A. M., Warneke, C., al.: Budget of organic carbon in a polluted atmosphere: Results from the New England Air Quality Study in 2002, J. Geophys. Res., 110, D16305, doi:10.1029/2004JD005623, 2005.

de Gouw, J. A., Welsh-Bon, D., Warneke, C., Kuster, W. C., Alexander, A., Baker, A. K., Beyersdorf, A. J., Blake, D. R., Canagaratna, M., Huey, L. G., Onasch, T. B., Schauer, J., Stone, E., Sullivan, A. P., Vargas, O., Weber, R. J., Worsnop, D. R., Xie, Y., and Zaveri, R.: Emission and chemistry of organic carbon in the gas and aerosol phase at a sub-urban site near Mexico City in March 2006 during the MILAGRO study, Atmos. Chem. Phys., 2009.

Doran, J. C., Barnard, J. C., Arnott, W. P., Cary, R., Coulter, R., Fast, J. D., Kassianov, E. I., Kleinman, L., Laulainen, N. S., Martin, T., Paredes-Miranda, G., Pekour, M. S., Shaw, W.J., Springston, and Yu., X.-Y.: The T1-T2 study: Evolution of aerosol properties downwind of Mexico City, Atmos. Chem. Phys., 7, 1585–1598, 2007, http://www.atmos-chem-phys.net/7/1585/2007/.

Doran, J. C., Fast, J. D., Barnard, J. C., Laskin, A., Desyaterik, Y., Gilles, M. K., and Hopkins, R. J.: Applications of Lagrangian dispersion modeling to the analysis of changes in the specific absorption of elemental carbon, Atmos. Chem. Phys., 8, 1377–1389, 2008.

Dzepina, K., Arey, J., Marr, L. C., Worsnop, D. R., Salcedo, D., Zhang, Q., Onasch, T. B., Molina, L. T., Molina, M. J., and Jimenez, J. L.: Detection of Particle-Phase Polycyclic Aromatic hydrocarbons in Mexico City using an aerosol mass spectrometer, Int. J. Mass Spec., 263, 152–170, 2007.

Dzepina, K., Volkamer, R. M., Madronich, S., Tulet, P., Ulbrich, I. M., Zhang, Q., Cappa, C. D., Ziemann, P. J., and Jimenez, J. L.: Evaluation of new secondary organic aerosol models for a case study in Mexico City, Atmos. Chem. Phys., 4417–4488, 2009.

Edgerton, S. A., Bian, X., Doran, J. C., et al.: Particulate air pollution in Mexico City: A collaborative research project, J. Air Waste Manag. Assoc., 49(10), 1221-1229, 1999.

Fast, J. D. and Zhong, S.: Meteorological factors associated with inhomogeneous ozone concentrations within the Mexico City basin, J. Geophys. Res., 103, 18927–18946, 1998.

Fast, J. D, Gustafson Jr., W. I., Easter, R. C., Zaveri, R. A., Barnard, J. C., Chapman, E. G., and. Grell, G. A.: Evolution of ozone, particulates, and aerosol direct forcing in an urban area using a new fully-coupled meteorology, chemistry, and aerosol model, J. Geophys. Res., 111, D21305, doi:10.1029/2005JD006721, 2006.

Fast, J. D., de Foy, B., Acevedo Rosas, F., Caetano, E., Carmichael, G., Emmons, L., McKenna, D., Mena, M., Skamarock, W., Tie, X., Coulter, R. L., Barnard, J. C., Wiedinmyer, C., and Madronich S.: A meteorological overview of the MILAGRO field campaigns, Atmos. Chem. Phys., 7, 2233–2257, 2007.

Grell, G. A., Peckham, S. E., Schmitz, R., and McKeen, S. A., Frost, G., Skamarock, W. C., and Eder, B.: Fully coupled "online" chemistry within the WRF model, Atmos. Environ., 39, 6957–6976, 2005.

Grieshop, A. P., Donahue, N. M., and Robinson, A. L.: Laboratory investigation of photochemical oxidation of organic aerosol from wood fires 2: Analysis of aerosol mass spectrometer data, Atmos. Chem. Phys., 9, 2227–2240, 2009..

Gustafson Jr., W. I., Chapman, E. G., Ghan, S. J., and Fast, J. D.: Impact on modeled cloud characteristics due to simplified treatment of uniform cloud condensation nuclei during NEAQS 2004, Geophys. Res. Lett., 34, L19809, doi:10.1029/2007GL030021, 2007.

Heald, C. L., Goldstein, A. H., Allan, J. D., Aiken, A. C., Apel, E., Atlas, E. L., Baker, A. K., Bates, T. S., Beyersdorf, A. J., Blake, D. R., Campos, T., Coe, H., Crounse, J. D., DeCarlo, P.F., de Gouw, J. A., Dunlea, E. J., Flocke, F. M., Fried, A., Goldan, P., Griffin, R. J., Herndon, S. C., Holloway, J. S., Holzinger, R., Jimenez, J. L., Junkermann, W., Kuster, W. C., Lewis, A. C., Meinardi, S., Millet, D. B., Onasch, T., Polidori, A., Quinn, P. K.,

Riemer, D. D., Roberts, J. M., Salcedo, D., Sive, B., Swanson, A. L., Talbot, R., Warneke, C., Weber, R.J., Weibring, P., Wennberg, P. O., Wittig, A. E., Zhang, R., Zheng, J., and Zheng, W.: Total Observed Organic Carbon (TOOC): A synthesis of North American observations, Atmos. Chem. Phys., 8, 2007–2025, 2008.

Herndon, S. C., Onasch, T. B., Wood, E. C., Kroll, J. H., Canagaratna, M. R., Jayne, J. T., Zavala, M. A., Berk Knighton, W., Mazzoleni, C., Dubey, M. K., Ulbrich, I. M., Jimenez, J. L. Seila, R., de Gouw, J. A., de Foy, B., Fast, J., Molina, L. T., Kolb, C. E., and Worsnop, D. R.: The correlation of secondary organic aerosol with odd oxygen in a megacity outflow, Geophys. Res. Lett., 35, L15804, doi:10.1029/2008GL034058, 2008.

Hodzic, A., Jimenez, J. L., Madronich S., Aiken A. C., Bessagnet, B., Curci, G., Fast, J., Lamarque, J. F., Onasch, T. B., Roux, G., and Ulbrich, I. M., Modeling organic aerosols during MILAGRO: Application of the CHIMERE model and importance of biogenic secondary organic aerosols, Atmos. Chem. Phys. Discuss., 9, 12207–12281, 2009.

Hodzic A., Vautard R., Chazette P., Menut, L., and Bessagnet, B.: Aerosol chemical and optical properties over the Paris area within ESQUIF project, Atmos. Chem. Phys., 6, 3257–3280, 2006.

Huffman, J. A., Ziemann, P. J., Jayne, J. T., Worsnop, D. R., and Jimenez, J. L.: Development and characterization of a fast-stepping/scanning thermodenuder for chemically-resolved aerosol volatility measurements, Aerosol Sci. Technol., 42, 395–407, 2008.

Huffman, J. A., Docherty, K. S., Aiken, A. C., Cubison, M. J., Ulbrich, I. M., DeCarlo, P. F., Sueper, D., Jayne, J. T., Worsnop, D. R., Ziemann, P. J. and Jimenez, J. L.: Chemically-resolved aerosol volatility measurements from two megacity field studies, Atmos. Chem. Phys. Discuss., 9, 2645–2697, 2009a.

Huffman, J. A., Docherty, K. S., Mohr, C., Cubison, M. J., Ulbrich, I. M., Ziemann, P. J., Onasch, T. B., and Jimenez, J. L.: Chemically-resolved volatility measurements of organic aerosol from different sources, Environ. Sci. Technol., 43, 5351–5357, doi:10.1021/es803539d, 2009b.

Jacobson, M. Z.: Modeling coagulation among particles of different composition and size, Atmos. Environ., 28, 1327–1338, 1994.

Jazcilevich, A. D., Garcia, A. R., and Ruiz-Suarez, L. G.: A study of air flow patterns affecting pollutant concentrations in the Central Region of Mexico, Atmos. Environ., 37, 183–193, 2003.

Johnson, K. S., Laskin, A., Jimenez, J. L., Shutthanandan, V., Molina, L. T., Salcedo, D., Dzepina, K., and Molina, M. J.: Comparative analysis of urban atmospheric aerosol by Proton-Induced X-ray Emission (PIXE), Proton Elastic Scattering Analysis (PESA), and Aerosol Mass Spectrometry (AMS), Environ. Sci. Technol., 42, 6619–6624, doi:10.1021/es800393e, 2008.

Kleinman, L. I., Springston, S. R., Daum, P. H., Lee, Y.-N., Nunnermacker, L. J., Senum, G. I., Wang, J., Weinstein-Lloyd, J., Alexander, M. L., Hubbe, J., Ortega, J., Canagaratna, M. R., and Jayne, J.: The time evolution of aerosol composition over the Mexico City plateau, Atmos. Chem. Phys., 8, 1559–1575, 2008.

Kondo, Y., Miyazaki, Y., Takegawa, N., Miyakawa, T., Weber, R. J., Jimenez, J. L., Zhang, Q., and Worsnop, D. R.: Oxygenated and water-soluble organic aerosols in Tokyo, J. Geophys. Res., 112, D01203, doi:10.1029/2006JD007056, 2007.

Koo, B., Ansari, A. S., and Pandis, S. N.: Integrated approaches to modeling the organic and inorganic atmospheric aerosol components, Atmos. Environ., 37, 4757–4768, 2003.

Lanz, V.A., Alfarra, M. R., Baltensperger, U., Buchmann, B., Hüglin, C., and Prévôt, A. S. H.: Source apportionment of submicron organic aerosols at an urban site by factor analytical modelling of aerosol mass spectra, Atmos. Chem. Phys., 7, 1503–1522, 2007.

Lei, W., de Foy, B., Zavala, M., Volkamer, R., and Molina, L. T.: Characterizing ozone production in the Mexico City metropolitan area: A case study using a chemical transport model, Atmos. Chem. Phys., 7, 1347–1366, 2007.

Liu, Y., Bourgeois, A., Warner, T., Swerdlin, S., and Hacker, J.: Implementation of observation-nudging based on FDDA into WRF for supporting AFEC test operations. 6th WRF Conference, NCAR, Boulder, CO, 10.7, 2006.

Liu, P. S. K., Deng, R., Smith, K. A., Williams, L. R., Jayne, J. T., Canagaratna, M. R., Moore, K., Onasch, T. B., Worsnop, D. R., and Deshler, T.: Transmission efficiency of an aerodynamic focusing lens system: Comparison of model calculations and laboratory measurements for the Aerodyne aerosol mass spectrometer, Aerosol Sci. Technol., 41(8), 721–733, 2007.

Molina, L. T., and Molina, M. J. (Eds.): Air Quality in the Mexico Megacity: An integrated assessment, Kluewer Academic Publishers, 2002.

Molina, L. T., Kolb, C. E., de Foy, B., Lamb, B. K., Brune, W. H., Jimenez, J. L., Ramos-Villegas, R., Sarmiento, J., Paramo-Figueroa, V. H., Cardenas, B., Gutierrez-Avedoy, V., and Molina, M. J.: Air Quality in North America's Most Populous City – Overview of MCMA-2003 campaign, Atmos. Chem. Phys., 7, 2447–2473, 2007.

Molina, L. T., Madronich, S., Gaffney, J. S., and Singh, H. B.: Overview of MILAGRO/INTEX-B campaign, IGACtivities Newsletter, Issues 38, 2–15, 2008.

Odum, J. R., Hoffman, T., Bowman, F., Collins, D., Flagan, R. C., and Seinfeld, J. H.: Gas/particle partitioning and secondary organic aerosol yields, Environ. Sci. Technol., 30, 2580–2585, 1996.

Pfister, G. G., Emmons, L. K., Hess, P. G., Lamarque, J.-F., Orlando, J. J., Walters, S., Guenther, A., Palmer, P. I., and Lawrence, P. J.: Contribution of isoprene to chemical budgets: A model tracer study with the NCAR CTM MOZART-4, J. Geophys. Res., 113, D05308, doi:10.1029/2007JD008948, 2008.

Querol, X., Pey, J., Minguillon, M. C., Perez, N., Alastuey, A., Viana, M., Moreno, T., Bernabe, R. M., Blanco, S., Cardenas, B., Vega, E., Sosa, G., Escalona, S., Ruiz, H., and Artinano, B: PM speciation an sources in Mexico during the MILAGRO-2006 Campaign, Atmos. Chem. Phys., 8, 111–128, 2008.

Robinson, A. L., Donahue, N. W., Shrivastava, M. K., Weitkamp, E. A., Sage, A. M., Grieshop, A. P., Lane, T. E., Pierce, J. R., and Pandis, S. N.: Rethinking organic aerosols: Semivolatile emissions and photochemical aging, Science, 315, 1259–1262, 2007.

Salcedo, D., Onasch, T. B., Dzepina, K., Canagaratna, M. R., Zhang, Q., Huffman, J. A., DeCarlo, P. F., Jayne, J.T., Mortimer, P., Worsnop, D. R., Kolb, C. E., Johnson, K. S., Zuberi, B., Marr, L.C., Volkamer, R., Molina, L. T., Molina, M. J., Cardenas, B., Bernabé, R. M., Márquez, C., Gaffney, J. S., Marley, N. A., Laskin, A., Shutthanandan, V., Xie, Y., Brune, W., Lesher, R., Shirley, T., and Jimenez, J. L.: Characterization of ambient aerosols in Mexico City during the MCMA-2003 campaign with Aerosol Mass Spectrometry: results from the CENICA Super-

site, Atmos. Chem. Phys., 6, 925–946, 2006.

Salcedo, D., Onasch, T. B., Canagaratna, M. R., Dzepina, K., Huffman, J. A., Jayne, J. T., Worsnop, D. R., Kolb, C. E., Weimer, S., Drewnick, F., Allan, J. D., Delia, A. E., and Jimenez, J. L.: Technical Note: Use of a beam width probe in an aerosol mass spectrometer to monitor particle collection efficiency in the field, Atmos. Chem. Phys., 7, 549–556, 2007.

Sarrat, C., Lemonsu, A., Masson, V., and Guedalia, D.: Impact of urban heat island on regional atmospheric pollution, Atmos. Environ., 40, 1743–1758, 2006.

Schell, B., Ackermann, I. J., Hass, H., Binkowski, F. S., and Ebel, A.: Modeling the formation of secondary organic aerosol within a comprehensive air quality modeling system, J. Geophys. Res., 106, 28275–28293, 2001.

Shaw, W. J., Pekour, M. S., Coulter, R. L., Martin, T. J., and Walters J. T.: The daytime mixing layer observed by radiosonde, profiler, and lidar during MILAGRO, Atmos. Chem. Phys. Discuss., 7, 15025–15065, 2007.

Shon, Z.-H., Madronich, S., Song, S.-K., Flocke, F. M., Knapp, D. J., Anderson, R. S., Shetter, R. E., Cantrell, C. A., and Hall, S. R.: Characteristics of the NO-NO_2-O_3 system in different chemical regimes during the MIRAGE-Mex field campaign, Atmos. Chem. Phys., 8, 7153–7164, 2008.

Simpson, D., Yttri, K. E., Klimont, Z., Kupiainen, K., Caseiro, A., Gelencsér, A., Pio, C., Puxbaum, H., and Legrand, M.: Modeling carbonaceous aerosol over Europe: Analysis of the CARBOSOL and EMEP EC/OC campaigns, J. Geophys. Res., 112, D23S14, doi:10.1029/2006JD008158, 2007.

Sinha, P., Hobbs, P. V., Yokelson, R. J., et al.: Emissions from miombo woodland and dambo grassland savanna fires, J. Geophys. Res., 109, D11305, doi:10.1029/2004JD004521, 2004.

Skamarock, W. C., Klemp, J. B, Dudhia, J., Gill, D. O., Barker, D. M., Duda, M. G., Huang, X.-Y., Wang, W., and Powers, J. G.: A description of the advanced research WRF version 3, NCAR Technical Note, NCAR/TN-475+STR, 113 pp., 2008.

Takegawa, N., Miyazaki, Y., Kondo, Y., Komazaki, Y., Miyakawa, T., Jimenez, J. L., Jayne, J. T., Worsnop, D. R., Allan, J., and Weber, R. J.: Characterization of an Aerodyne Aerosol Mass Spectrometer (AMS): Intercomparison with other aerosol instruments, Aerosol Sci. Technol., 39, 760–770, 2005.

Thorpe, A. and Harrison, R. M.: Sources and properties of non-exhaust particulate matter from road traffic: A review, Sci. Total Environ., 400, 270–282, 2008

Ulbrich, I. M., Canagaratna, M. R., Zhang, Q., Worsnop, D. R., and Jimenez, J. L.: Interpretation of organic components from positive matrix factorization of aerosol mass spectrometric data, Atmos. Chem. Phys., 9, 2891–2918, 2009.

Volkamer, R., Jimenez, J.L., San Martini, F., Dzepina, K., Zhang, Q., Salcedo, D., Molina, L.T., Worsnop, D., and Molina, M.J.: Secondary organic aerosol formation from anthropogenic air pollution: Rapid and higher than expected, Geophys. Res. Lett., 38, L17811, doi:10.1029/2006GL026899, 2006.

Wexler, A. S., Lurmann, F. W., and Seinfeld, J. H.: Modeling urban and regional aerosols – I. Model development, Atmos. Environ., 28, 531–546, 1994.

Wiedinmyer, C., Quayle, B., Geron, C., Belcoe, A., McKenzie, D., Zhang, X., O'Neill, S., and Klos Wynne, K.: Estimating emissions from fires in North America for air quality modeling, Atmos. Environ., 40, 3419–3432, 2006.

Wild, O., Zhu, X., and Prather, M. J.: Fast-J: Accurate simulation of in- and below cloud photolysis in tropospheric chemical models, J. Atmos. Chem., 37, 245–282, 2000.

Yokelson, R., Urbanski, S., Atlas, E., Toohey, D., Alvarado, E., Crounse, J., Wennberg, P., Fisher, M., Wold, C., Campos, T., Adachi, K., Buseck, P. R., and Hao, W. M.: Emissions from forest fires near Mexico City, Atmos. Chem. Phys., 7, 6687–6718, 2007.

Zaveri, R. A. and Peters, L. K.: A new lumped structure photochemical mechanism for large-scale applications, J. Geophys. Res., 104, 30387–30415, 1999.

Zaveri, R. A., Easter, R. C., Fast, J. D., and Peters, L. K.: Model for simulating aerosol interactions and chemistry (MOSAIC), J. Geophys. Res., D13204, doi:10.1029/2007JD008792, 2008.

Zhang, Q., Worsnop, D. R., Canagaratna, M. R., and Jimenez, J. L.: Hydrocarbon-like and oxygenated organic aerosols in Pittsburgh: Insights into sources and processes of organic aerosols, Atmos. Chem. Phys., 5, 3289–3311, 2005.

Zhang, Q., Jimenez, J. L., Canagaratna, M. R., Allan, J. D., Coe, H., Ulbrich, I., Alfarra, M. R., Takami, A., Middlebrook, A. M., Sun, Y. L., Dzepina, K., Dunlea, E., Docherty, K., DeCarlo, P. F., Salcedo, D., Onasch, T., Jayne, J. T., Miyoshi, T., Shimono, A., Hatakeyama, S., Takegawa, N., Kondo, Y., Schneider, J., Drewnick, F., Borrmann, S., Weimer, S., Demerjian, K., Williams, P., Bower, K., Bahreini, R., Cottrell, L., Griffin, R. J., Rautiainen, J., Sun, J. Y., Zhang, Y. M., and Worsnop, D. R.: Ubiquity and dominance of oxygenated species in organic aerosols in anthropogenically-influenced Northern Hemisphere midlatitudes, Geophys. Res. Lett., 34, L13801, doi:10.1029/2007GL0299792, 2007.

Atmos. Chem. Phys., 9, 6633–6653, 2009
www.atmos-chem-phys.net/9/6633/2009/

Atmospheric Chemistry and Physics

Mexico City aerosol analysis during MILAGRO using high resolution aerosol mass spectrometry at the urban supersite (T0) – Part 1: Fine particle composition and organic source apportionment

A. C. Aiken[1,2,*], D. Salcedo[3], M. J. Cubison[2], J. A. Huffman[1,2], P. F. DeCarlo[2,4,*], I. M. Ulbrich[1,2], K. S. Docherty[2], D. Sueper[2,5], J. R. Kimmel[2], D. R. Worsnop[5], A. Trimborn[5,], M. Northway[5,***], E. A. Stone[6], J. J. Schauer[6], R. M. Volkamer[1,2], E. Fortner[5,7,8], B. de Foy[9], J. Wang[10], A. Laskin[11], V. Shutthanandan[11], J. Zheng[8], R. Zhang[8], J. Gaffney[12], N. A. Marley[12], G. Paredes-Miranda[13], W. P. Arnott[13], L. T. Molina[14], G. Sosa[15], and J. L. Jimenez[1,2]**

[1]Department of Chemistry, University of Colorado at Boulder, 215 UCB, Boulder, CO 80309, USA
[2]Cooperative Institute for Research in the Environmental Sciences (CIRES), University of Colorado at Boulder, 216 UCB, Boulder, CO 80309, USA
[3]Centro de Investigaciones Quimicas, Universidad Autónoma del Estado de Morelos, Cuernavaca Morelos, Mexico
[4]Department of Atmospheric and Oceanic Sciences, University of Colorado at Boulder, UCB 311, Boulder, CO 80309, USA
[5]Aerodyne Research Inc., 45 Manning Rd., Billerica, MA, 01821, USA
[6]Environmental Chemistry and Technology Program, University of Wisconsin-Madison, 660 North Park St., Madison, WI 53706, USA
[7]Montana State University, Bozeman, MT 59717, USA
[8]Texas A&M, 3150 TAMU, College Station, TX 77843, USA
[9]Saint Louis University, St. Louis, MO 63108, USA
[10]Brookhaven National Laboratory, P.O. Box 5000, Upton, NY 11973, USA
[11]Pacific Northwest National Laboratory, Richland, WA, USA
[12]University of Arkansas, 2801 S. University Avenue, Little Rock, AR 72204, USA
[13]University of Nevada Reno and the Desert Research Institute, Reno, NV, USA
[14]Molina Center for Energy and the Environment and Massachusetts Institute of Technology, USA
[15]IMP, Eje Central Norte Lazaro Cardenas 152, Mexico City, DF 07730, Mexico
[*]now at: Institute for Atmospheric and Climate Science, Swiss Federal Institute of Technology Zurich (ETH-Zurich), 8092 Zurich, Switzerland
[**]now at: Paul Scherrer Institut, 5232 Villigen-PSI, Switzerland
[***]now at: Department of Meteorology, University of Reading, Reading, UK

Received: 14 February 2009 – Published in Atmos. Chem. Phys. Discuss.: 30 March 2009
Revised: 7 August 2009 – Accepted: 15 August 2009 – Published: 11 September 2009

Abstract. Submicron aerosol was analyzed during the MILAGRO field campaign in March 2006 at the T0 urban supersite in Mexico City with a High-Resolution Time-of-Flight Aerosol Mass Spectrometer (HR-ToF-AMS) and complementary instrumentation. Mass concentrations, diurnal cycles, and size distributions of inorganic and organic species are similar to results from the CENICA supersite in April 2003 with organic aerosol (OA) comprising about half of the fine PM mass. Positive Matrix Factorization (PMF) analysis of the high resolution OA spectra identified three major components: chemically-reduced urban primary emissions (hydrocarbon-like OA, HOA), oxygenated OA (OOA, mostly secondary OA or SOA), and biomass burning OA (BBOA) that correlates with levoglucosan and acetonitrile. BBOA includes several very large plumes from regional fires and likely also some refuse burning. A fourth OA component is a small local nitrogen-containing reduced OA component (LOA) which accounts for 9% of the OA mass but one third of the organic nitrogen, likely as amines. OOA accounts for almost half of the OA on average, consistent with previous

Correspondence to: J. L. Jimenez
(jose.jimenez@colorado.edu)

observations. OA apportionment results from PMF-AMS are compared to the $PM_{2.5}$ chemical mass balance of organic molecular markers (CMB-OMM, from GC/MS analysis of filters). Results from both methods are overall consistent. Both assign the major components of OA to primary urban, biomass burning/woodsmoke, and secondary sources at similar magnitudes. The 2006 Mexico City emissions inventory underestimates the urban primary $PM_{2.5}$ emissions by a factor of ~4, and it is ~16 times lower than afternoon concentrations when secondary species are included. Additionally, the forest fire contribution is at least an order-of-magnitude larger than in the inventory.

1 Introduction

Ambient aerosols are of interest due to their effects on human health, regional visibility, and climate (Watson, 2002; Pope and Dockery, 2006; IPCC, 2007). As the number and fraction of the global population living in megacities (defined as having >10 million people) are increasing, the effects of megacity aerosols on human health, in addition to downwind chemistry and radiation (Madronich, 2006), are becoming more important. Most megacities are located in the tropics, while most atmospheric chemistry field research has been conducted in the mid-latitudes. The MILAGRO project (Megacity Initiative: Local and Global Research Observations) is the first large-scale field campaign that focuses on a tropical megacity (Molina et al., 2008) and follows smaller campaigns carried out in Mexico City such as IMADA-AVER (Edgerton et al., 1999) and MCMA-2003 (Molina et al., 2007).

The Mexico City Metropolitan Area (MCMA) is the largest megacity in North America and is one of the five largest cities in the world with over 20 million people in ~1500 km^2. The MCMA has a history of severe air quality problems due to a large number of pollution sources with uneven levels of emission control, which can be further exacerbated by the topography and meteorology of the basin (Molina and Molina, 2002). The tropical location (19° N) and high altitude (2240 m above sea level) result in high UV fluxes and intense photochemistry. The basin is surrounded by mountains on three sides, reducing ventilation of pollutants, especially at night and in the early morning. However, the boundary layer grows to several km above ground, where wind speeds tend to be larger, resulting in significant daily ventilation and limited overnight accumulation or pollutant recirculation (Fast and Zhong, 1998; de Foy et al., 2006b, 2009). Basin ventilation patterns are strongly influenced by a gap flow which forms a convergence line over the MCMA (Whiteman et al., 2000; de Foy et al., 2006a). A classification of weather patterns based on the wind shift and convergence line found three characteristic episode types during MCMA-2003 (de Foy et al., 2005), which was expanded to six for MILAGRO (de Foy et al., 2008).

The MCMA-2006 campaign, a component of MILAGRO, focused on measurements within the basin to better quantify emission sources, photochemistry, and air circulation in the basin. Figure S-1 in the Supplemental Information (see http://www.atmos-chem-phys.net/9/6633/2009/acp-9-6633-2009-supplement.pdf) shows the location of the major measurement sites during the campaign. The T0 Supersite was located 9 km NNE of the city center and 16 km NNW of the CENICA (Centro Nacional de Investigación y Capacitación Ambiental) Supersite used during MCMA-2003. Besides providing a local characterization site for urban pollution, T0 was also designed to provide initial conditions for regional evolution studies of the urban plume (e.g. DeCarlo et al., 2008; Kleinman et al., 2008).

Fine particulate matter (PM) is one of the most serious air quality problems in Mexico City (Molina et al., 2007). Previous campaigns have concluded that about half of the fine PM is organic aerosol (OA) (Chow et al., 2002; Salcedo et al., 2006). OA has numerous sources and can be classified as either primary OA (POA), material directly emitted as particles, or secondary OA (SOA), species formed in the atmosphere via chemical reactions (Hallquist et al., 2009). Data from MCMA-2003 indicated the importance of secondary inorganic (i.e. ammonium nitrate) and organic (SOA) production within the city and their resultant large contributions to the fine PM concentrations (Salcedo et al., 2006; Volkamer et al., 2006, 2007; Dzepina et al., 2009). These results are consistent with those from other locations (Zhang et al., 2005c; Lonati et al., 2007; Weber et al., 2007; Zhang et al., 2007a; Docherty et al., 2008; Fine et al., 2008), and the importance of SOA as a fraction of PM is again apparent during MILAGRO (DeCarlo et al., 2008; Herndon et al., 2008; Kleinman et al., 2008; Stone et al., 2008; de Gouw et al., 2009; Paredes-Miranda et al., 2009; Fast et al., 2009; Hodzic et al., 2009). For example, Kleinman et al. (2008) and de Gouw et al. (2009) report a growth in the $OA/\Delta CO(g)$ ratio with photochemical age due to SOA formation that is consistent with previous observations in the US (e.g. de Gouw et al., 2005). Paredes-Miranda et al. (2009) report that on average the secondary species accounts for about 75% of the fine PM mass and light-scattering in the mid-afternoon, while Herndon et al. report a strong correlation between the observed growth of SOA and O_x ($O_3(g)+NO_2(g)$). DeCarlo et al. (2008) report an $OA/\Delta CO$ for urban air that is much greater than that of primary emissions and a rapid increase in the O/C ratio of OA with photochemical age, both indicating strong SOA formation from MCMA emissions. Based on comparisons with water-soluble OC, Stone et al. (2008) attribute the unapportioned OC from CMB-OMM as secondary OC for MCMA, resulting in 39% on average of the OC (and thus a larger fraction of the OA) being secondary at T0. Fast et al. (2009) and Hodzic et al. (2009) report a large underestimation of the measured OA when only POA sources are considered, supporting the importance of SOA.

The MCMA is also impacted by biomass burning (BB) emissions during the dry season (March–June, Bravo et al., 2002; Salcedo et al., 2006; Molina et al., 2007). During the later portion of the MCMA-2003 campaign, an important regional impact from fires in the Yucatan was reported (Salcedo et al., 2006; Molina et al., 2007). During part of MILAGRO, forest fires from pine savannas in the nearby mountains surrounding the city were very intense and resulted in a significant contribution to the outflow of pollutants from the Mexico City region (Yokelson et al., 2007; DeCarlo et al., 2008; Crounse et al., 2009). The relative impact of BB to ground receptor sites in the city appears to have been highly variable and lower than was observed aloft from several afternoon flights (Querol et al., 2008; Stone et al., 2008; de Gouw et al., 2009). The mountain fires tended to start around noon (Yokelson et al., 2007) and were often carried away from the city by the prevailing winds (Yokelson et al., 2007; DeCarlo et al., 2008; Crounse et al., 2009). Stone et al. (2008) report that an average of 12% (range 5–26%) of the organic carbon (OC) in $PM_{2.5}$ at T0 originated from BB sources, and that this impact was highly variable from day to day. Querol et al. (2008) estimate that the BB contribution to total $PM_{2.5}$ at T0 was ~5–15%. Moffet et al. (2008a) report that 40% of the single-particles at the upper end of the accumulation mode showed signatures characteristic of biomass/biofuel burning but do not quantify the fraction of OA due to these particles. Fast et al. (2009) reports a large overestimation of OA downwind of some large wildfires by a model which only includes POA, suggesting that the POA emissions of at least some fires are overestimated. In summary, significant uncertainties still exist in determining the sources and contribution of BB within the MCMA basin.

In this paper, we present results from ground-based measurements inside the MCMA at the T0 Supersite, including: (1) an overview of the species contributing to submicron PM, their diurnal cycles, size distributions, and comparison with MCMA-2003 and IMADA-AVER results; (2) a determination of OA components using Positive Matrix Factorization (PMF) of high-resolution AMS data (PMF-AMS); (3) a comparison of PMF-AMS results with source apportionment results from the chemical mass balance of organic molecular markers (CMB-OMM); and (4) a comparison of our results with the MCMA $PM_{2.5}$ emissions inventory. The impact of biomass burning at T0 is analyzed in detail in the companion paper (Aiken et al., 2009).

2 Methods

2.1 General

Data were collected at the T0 Supersite, located at the Instituto Mexicano del Petroleo (IMP, 19°29′23″ N, 99°08′55″ W, 2240 m altitude, ~780 mbar ambient pressure), 9 km NNE of the city center, near a combination of residential, commercial and light industrial areas. The closest street with significant road traffic was 200 m from the site. Aerosol data were collected from the top of building 32, ~28 m above ground level, from 10 to 31 March 2006, unless otherwise stated. All aerosol data are reported in $\mu g\,m^{-3}$ at local ambient pressure and temperature conditions. To avoid confusion with concentrations reported in other studies that use standard conditions (STP), we use the units symbol of $\mu g\,am^{-3}$ to make it clear that the measurements are reported under ambient conditions. To convert to STP (1 atm, 273 K, $\mu g\,sm^{-3}$), the particle concentrations reported here need to be multiplied by ~1.42. Note that some studies use different standard conditions from those mentioned above, e.g. Kleinman et al. (2008) reported concentrations under 1 atm and 293 K and that volume mixing ratios (ppbv, pptv, etc.) are invariant and do not depend on the pressure or temperature. All measurements are reported in local standard time (LST, equivalent to US CST and UTC minus 6 h, and the same as local time during the campaign). All regression lines are fit by orthogonal distance regression.

2.2 AMS sampling and analysis

A High Resolution Time-of-Flight Aerosol Mass Spectrometer (HR-ToF-AMS, Aerodyne Research Inc., Billerica, MA) sampled from a common inlet using a $PM_{2.5}$ cyclone (URG-2000-30EN, URG, Chapel Hill, NC) at a flowrate of ~10 lpm through a ~3 m insulated copper inlet line (1/2 inch o.d.) located ~5 m above the roof and ~2 m above the roof structure where the instruments where housed. The total inlet residence time was 16s under laminar flow. A nafion drier (Perma-Pure, Toms River, NJ) was used to dry the air prior to sampling with the AMS. The HR-ToF-AMS (abbreviated as AMS hereafter) has been described in detail previously (DeCarlo et al., 2006; Canagaratna et al., 2007). AMS data were saved every 2.5 min, combining total non-refractory (NR) PM_1 concentrations from the mass spectrum (MS) mode and size distributions from the particle time-of-flight (PToF) mode (Jimenez et al., 2003). The main advantage of the HR-ToF-AMS over previous AMS versions (Jayne et al., 2000; Drewnick et al., 2005) is the ability to resolve the elemental composition of most mass fragments, especially for the low m/z (<100) ions. The increased chemical information enables more direct chemical characterization of organic and inorganic species in addition to improved differentiation of organic components with tracer ions and factor analysis. The "V" and "W" ion paths of the AMS (DeCarlo et al., 2006) were alternated every 5 minutes, and this was the first campaign in which such alternation was performed automatically due to the newly developed ability to remotely control the TOF mass spectrometer power supply (TPS). Size distributions were acquired only in V-mode as their signal-to-noise in W-mode is limited. During different periods of the campaign, the AMS also intermittently sampled through a thermal denuder (Huffman et al., 2008,

2009a, b), aerosol concentrator (Khlystov et al., 2005) or CCN selector (Osborn et al., 2008). The analysis here only includes the ambient data as the more specialized alternating data will be presented elsewhere. All data were analyzed using standard AMS data analysis software (SQUIRREL v1.43 and PIKA v.1.03E, Sueper, 2008) within Igor Pro 6 (Wavemetrics, Lake Oswego, OR). A collection efficiency (CE) of 0.5 was used for all data based on the observed composition and the composition-CE relationships observed in previous campaigns (Canagaratna et al., 2007), consistent with other recent studies in Mexico City and during MILAGRO (Salcedo et al., 2006, 2007; DeCarlo et al., 2008; Kleinman et al., 2008), and also consistent with the intercomparisons presented below. Elemental analysis of the OA was carried out with the methods described previously (Aiken et al., 2007, 2008). Positive matrix factorization (PMF, Paatero and Tapper, 1994; Lanz et al., 2007; Ulbrich et al., 2009) was conducted on unit mass-resolution (UMR) spectra and on the combined high mass resolution (HR, for $m/z \leq 100$) and UMR ($m/z > 100$) OA spectra as has been done previously (Docherty et al., 2008). Results from both analyses were similar, but the HR data showed improved separation, as expected given the increased differentiation of HR spectra for the different sources (Ulbrich et al., 2009). Therefore, only results of the PMF analysis including HR data are presented here. The identification of OA components from the AMS data provides high time resolution data and diurnal cycles not possible with source apportionment methods that require off-line analysis of filters.

2.3 Co-located measurements used in this study

Additional measurements were collected at T0 and are used in this analysis. A Scanning Mobility Particle Sizer (SMPS, Wang and Flagan, 1989) measured number distributions between 15 and 436 nm in diameter. Apparent volume distributions were calculated while assuming sphericity, which could lead to an overestimation of the actual volume in the presence of fractal particles from combustion processes (DeCarlo et al., 2004). Black carbon (BC) absorption measurements were made with an aethalometer (Marley et al., 2009). Hourly PM_1, $PM_{2.5}$ and PM_{10} mass concentrations were acquired with an optical particle counter (OPC)/laser spectrometer (Grimm) corrected by gravimetric measurements (Querol et al., 2008). Additional optical measurements, including light scattering and absorption, were made with a nephelometer (Marley et al., 2009) at 530 nm (scattering at 450 nm, 550 nm, 700 nm and absorption at 670 nm shown in Supp. Info.: http://www.atmos-chem-phys.net/9/6633/2009/acp-9-6633-2009-supplement.pdf) and a photoacoustic spectrometer (PAS) for light absorption and reciprocal nephelometer light scattering measurements at 532 nm (Paredes-Miranda et al., 2009). Two sets of filters and impactor samples were collected and analyzed: (1) elemental concentrations with 6-h time resolution using proton-induced X-ray emission (PIXE; (Johnson et al., 2006, 2008); (2) organic molecular markers using gas-chromatography mass-spectrometry (GC-MS) from $PM_{2.5}$ filter samples at 24-h resolution (Stone et al., 2008). The chemical mass balance of organic molecular markers (CMB-OMM) identified and quantified by GC-MS was applied to determine the contributions of various sources to OC (Stone et al., 2008). For comparison with the PMF-AMS results, OC was converted to OM using previously published OM/OC values for the different sources (Turpin and Lim, 2001; Aiken et al., 2008).

Gas-phase measurements include NO_2, O_3, and aromatics by Differential Optical Absorption Spectroscopy (DOAS, Volkamer et al., 1998, 2005), and acetonitrile from two proton-transfer reaction mass spectrometers (PTR-MS, Zhao and Zhang, 2004; Knighton et al., 2007; Fortner et al., 2009). CO was obtained from the Mexico City ambient air monitoring network (RAMA, Red Automatica de Monitoreo Atmosferico, http://www.sma.df.gob.mx/simat/home_base.php) station at IMP at one minute time resolution and compared well with intermittent data acquired by two other groups, D. Blake (UC-Irvine, personal communication, 2008) and M. Dubey (LANL; personal communication, 2008). Meteorological data, including temperature, relative humidity, precipitation, wind speed and direction, pressure, and precipitation were collected by Marley et al. (2009).

3 Results

3.1 Total submicron aerosol – mass concentrations, time series, and size distributions

First, we compare the sum of the chemically-speciated mass concentrations with co-located total fine PM instrumentation to establish the consistency of the different measurements at T0. The non-refractory (NR) species measured by the AMS are summed with soil and metals from PIXE, and BC from the aethalometer to include the refractory species not measured by the AMS ("AMS+Refractory") due to their negligible vapor pressure at 600°C (Canagaratna et al., 2007). Soil mass is estimated from the PIXE measurements by the method of Malm et al. (Malm et al., 1994; Salcedo et al., 2006). Metal concentrations in fine PM are estimated using averaged chemical compositions reported by Moffet et al. (2008b) for those with high concentrations (from highest to lowest cation concentration: Zn: $ZnCl_2$, $Zn(NO_3)_2$ and ZnO; Pb: $PbCl_2$ and $Pb(NO_3)_2$; Na: NaCl and $NaNO_3$; PO_4) and the average soil factor for the metals with very small concentrations (Cu, Cr, Hg, Mg, Mn, Ni, Sn, V, and W). PIXE data are summed for stages B and C (0.07–1.15 μm) of the DRUM impactor used to collect these samples, including some particles beyond the PM_1 cut. Similarly, the BC concentrations are approximately $PM_{2.0}$ (Marley et al., 2009), resulting in an upper limit for their mass contribution as all other measurements are ~PM_1. The total fine PM measurements used for comparison include the Grimm

OPC PM_1, the mass estimated from the SMPS data, and the light scattering at 532 nm from the PAS and 530 nm from the nephelometer. Note that none of these measurements is a true PM_1 mass measurement. The Grimm instrument is based on an optical particle counter, which does not detect particles below ~300 nm in diameter nor use an aerodynamic size cut curve. It attempts to account for these effects by using corrections from gravimetric measurements. The apparent volume calculated from the SMPS number distributions is converted to mass (assuming sphericity) with a composition-dependent density estimated from the AMS+refractory measurements (Fig. S-2: http://www.atmos-chem-phys.net/9/6633/2009/acp-9-6633-2009-supplement.pdf) and only includes particles from 15–436 nm d_m (mobility diameter). Figure S-3 shows the time series, diurnal cycles, and scatter plots of the different measurements. The different measurements are highly correlated and have similar diurnal cycles. The SMPS peaks a few hours earlier in the day, possibly due to an overestimation of the volume from fractal soot particles in the rush hour and to particle growth in the afternoon increasing the fraction of the mass beyond its size range. The OPC PM_1 data have a slightly later peak than the other measurements, likely due to a similar effect of particle growth increasing the fraction of particles above its minimum size range. In Fig. S-3, we show that the AMS CE of 0.5 estimated from the measured composition results in consistent comparisons with all other ~PM_1 measurements. The largest discrepancy is with the SMPS and is most likely due to the lower size cut of that instrument, as is mentioned above. Figure S-4 shows the comparison of the measured size distributions from the AMS and SMPS. To explore the possible causes of the observed differences, different CEs were applied sequentially for each organic PMF-AMS component and also the inorganic components. There was not a clear improvement in the comparison with the other co-located ~PM_1 measurements for the various perturbations of CE. The sum of speciated (AMS+Refractory) fine PM is similar to the OPC PM_1 estimate and higher than the SMPS estimates. The difference between both PM_1 datasets and the SMPS is likely due to the differences in the size cuts. Some of the scatter may also be due to the use of 6-h averages for the dust (a.k.a. soil) and metal concentrations for the speciated fine PM. Overall, this level of agreement is typical for previous studies (Takegawa et al., 2005; Zhang et al., 2005b; DeCarlo et al., 2008; Dunlea et al., 2008), and we conclude that the AMS and the other instruments discussed performed well during MILAGRO. Table S-1 and Fig. S-3(h) show the R^2 values between all the mentioned total fine PM measurements, indicating that the agreement between all instruments, not just the AMS, have similar levels of scatter, with slightly less when comparing two optical measurements, as would be expected. This comparison indicates that the limitations in accuracy and precision evidenced by these comparisons are distributed among the different instruments and not dominated by the AMS.

Figure 1 shows the time series of the different species, while Fig. 2 includes the average mass fractions, size distributions, and diurnal cycles of the different species. On average, the non-refractory species quantified with the AMS account for 80% of the fine PM mass, while the refractory species account for 20%. Figure 1a and f shows the dominance of OA during the majority of the campaign, consistent with previous studies (Chow et al., 2002; Salcedo et al., 2006; DeCarlo et al., 2008). Most species have a clear diurnal cycle (Fig. 2d), with the exception of soil and a weak cycle for sulfate. The diurnal cycle of submicron nitrate is controlled by HNO_3 production from $OH+NO_2$, gas-to-particle partitioning to form ammonium nitrate with abundant gas-phase NH_3, reaction of HNO_3 with dust, and HNO_3 dry deposition, which have been discussed in detail before for Mexico City (Salcedo et al., 2006; DeCarlo et al., 2008; Hennigan et al., 2008; Querol et al., 2008; Zheng et al., 2008; Fountoukis et al., 2009). The submicron nitrate increases during the latter part of the campaign, consistent with the decreased concentration of supermicron dust (Querol et al., 2008) due to precipitation during this period (Fast et al., 2007), resulting in reduced irreversible reactions of HNO_3 with dust to form supermicron nitrates (Querol et al., 2008; Zheng et al., 2008; Fountoukis et al., 2009). Figure S-5 shows the increased precipitation and decreased coarse PM during this latter period that coincides with increased nitrate. Additionally, the slightly lower temperature and increased RH during this period may also favor the partitioning of HNO_3 to fine aerosols, but are insufficient to explain the observed change.

Sulfate is present in a similar fraction to nitrate, yet with a much weaker diurnal cycle and a larger background, consistent with the non-volatile character of sulfate and the more regional character of this species in Mexico City and the Central Mexican Plateau (Salcedo et al., 2006; DeCarlo et al., 2008; Huffman et al., 2009a). The ammonium concentration follows those of nitrate and sulfate, as expected for nearly fully neutralized acids as described in previous studies (Salcedo et al., 2006; DeCarlo et al., 2008). Note that the pH of these aerosols when they are liquid will still be well below 7 (San Martini et al., 2006; Zhang et al., 2007b). The ammonium balance (Fig. S-6) determined from the high resolution ions is consistent with neutralized aerosols within the accuracy of this determination. It also shows a clear reduction in the scatter due to the reduction in NH_4^+ measurement noise, mainly due to the use of a ToF-AMS, compared to Fig. 10 of Salcedo et al. (2006) which used the interference-subtracted UMR ions from a quadrupole-AMS. The reduction in noise due to the use of the directly-measured HR NH_x^+ ions instead of the estimation of the same ions with the fragmentation table (Allan et al., 2004) is minor in this case, although it may be more important at lower NH_4^+ concentrations. In terms of the organic nitrates (ONs), at present we are only able to state that their contribution to total nitrate and total OA is minor based on the ammonium balance. If the AMS nitrate signal was dominated by ONs there would be a large "ammonium

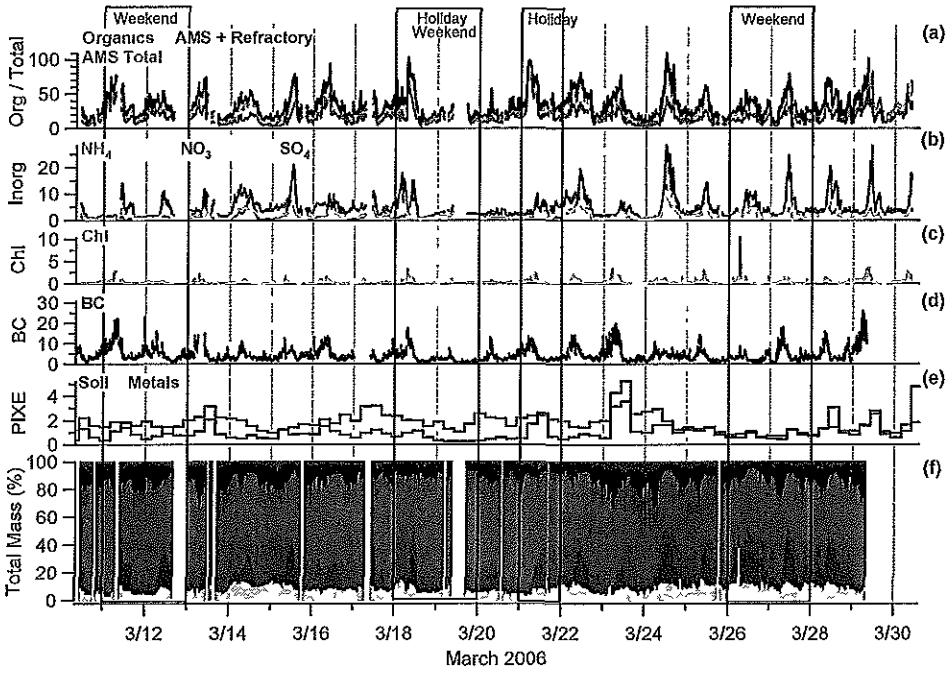

Fig. 1. Time series of mass concentrations as sampled by the AMS in $\mu g\,am^{-3}$: **(a)** OA, AMS total, and AMS+refractory; **(b)** ammonium, nitrate, and sulfate; **(c)** chloride; **(d)** BC; **(e)** metals and soil. Panel **(f)** shows all species in the same colors the same as panels (a–e) as a percentage of the total mass (AMS+BC+metals+soil). Holidays and weekends are indicated with boxes.

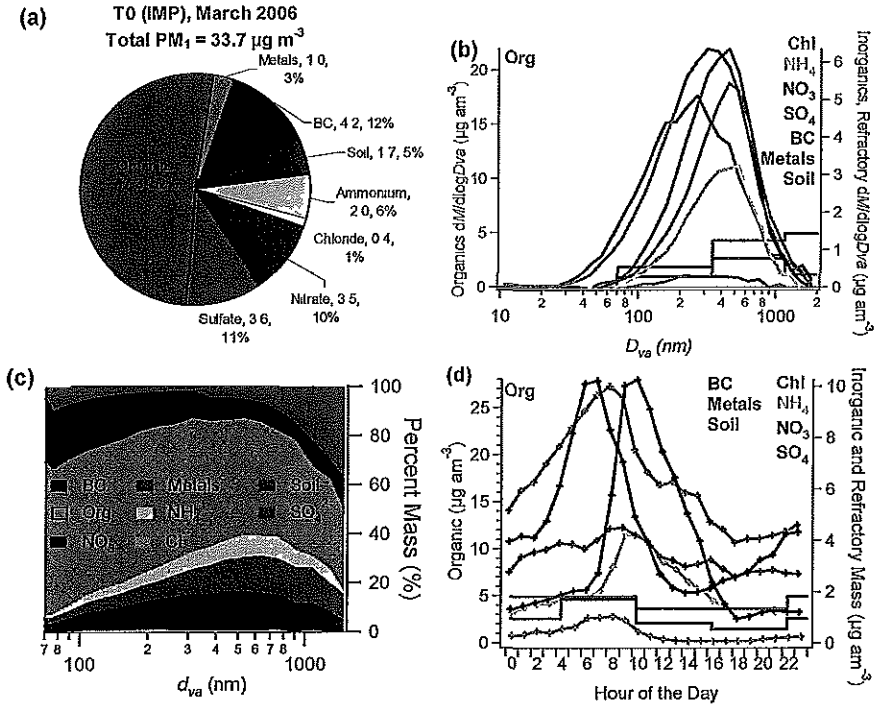

Fig. 2. PM_1 aerosol mass concentrations, size distributions, and diurnal profiles. AMS species plus refractory species **(a)** average mass concentrations, **(b)** size distributions, **(c)** NR-PM_1 size distributions by percent mass, and **(d)** diurnal profiles.

deficit" and large scatter when the ammonium balance analysis is performed assuming that all of the AMS nitrate signal is ammonium nitrate. Neither effect is observed in Fig. S-5, which indicates that ammonium nitrate is the dominant form of nitrate in Mexico City, consistent with the aircraft measurements (DeCarlo et al., 2008), PILS measurements at T1 (Hennigan et al., 2008), and previous studies (Salcedo et al., 2006). This is also consistent with Gilardoni et al. (2009), who report the contribution of ONs and organosulfates to be small based on FTIR measurements on MILAGRO samples at several sites. In Mexico City ONs should make a similar fractional contribution to submicron OA (when the mass of all OA molecules that have a nitrate group is summed) than to submicron nitrate. For example, if 5% of the nitrate signal was due to ONs and we assume a MW of 250 amu for these species, the contribution of ONs to OA mass would be 4%. Additional laboratory calibrations in the HR-ToF-AMS with organonitrate standards are needed before a detailed assessment of their contribution to ambient OA can be performed. Our group and several other groups in the AMS community are active in that area (Farmer et al., 2008).

Chloride is a very small (~1%) fraction of the fine PM observed at T0, as it was during MCMA-2003, but does not show the very numerous and large (up to 40 $\mu g\,am^{-3}$) late night/early morning spikes of NH_4Cl observed during that campaign (Salcedo et al., 2006). Thermal denuder analysis (Huffman et al., 2009a) suggests that approximately two-thirds of the AMS chloride is due to NH_4Cl or species of similarly high volatility, while the rest may be due to more refractory species such as $PbCl_2$, which were identified with the ATOFMS (Moffet et al., 2008b). BC represents a significant fraction, 12% on average, of the aerosol and has a time series indicative of the interaction between primary emissions that peak during the morning traffic hours (~06:00–08:00 a.m. LST) and the boundary layer dilution peaking in the afternoon, as has been reported previously for the area (Salcedo et al., 2006; Marley et al., 2009). The soil fraction, 5%, is similar to that determined during MCMA-2003 and may be due to both urban sources, e.g. dust re-suspension by vehicles, and non-urban sources. The metal concentration represents a small fraction of the fine PM mass with an average of 3%. The range in species fractional composition of the fine PM does not show major deviations from the average composition shown in Fig. 2a. (Fig. S-7 shows histograms of the mass concentrations and the percent of the PM_1 mass contributions for all species mentioned from the sampling period.) OA ranges from 20–80% of the fine PM mass with the NR inorganic species comprising 5–50% of the PM mass and BC rarely exceeding 30% of the fine PM.

The campaign-average mass concentrations and fractional composition are compared with those from two previous campaigns (Chow et al., 2002; Salcedo et al., 2006) and aircraft data aloft over Mexico City during several afternoons during MILAGRO (DeCarlo et al., 2008) in Fig. S-8. (The locations of the three ground sites within the basin can be seen in Fig. S-1). All ground campaigns have similar fine PM mass concentrations and species fractions across the timeframe of the campaigns, 1997–2006. The data from 1997 have ~15% more mass than the later studies, a larger refractory fraction, and a slightly lower OA fraction. The MCMA-2003 data have both the largest OA mass concentration and fraction, likely due to the large impact of BB emissions from the Yucatan during the latter part of that campaign (Salcedo et al., 2006; Molina et al., 2007). However, it is not clear that any interannual trends can be derived from these comparisons due to the different locations and times of the measurements in addition to the short duration of all the campaigns. The aircraft data have less non-refractory mass (19 vs. 25 $\mu g\,am^{-3}$ under T0 conditions) than measurements on the ground. The organic concentration measured by the aircraft in the afternoons is only 2/3 of that observed on the ground as a 24-h average. The nitrate fraction is larger in the aircraft than at T0, likely because the flights were in the afternoon when nitrate is also higher at the ground compared to the 24-h average (Fig. 2) and also likely due to increased partitioning due to the lower temperatures and higher humidities aloft (Neuman et al., 2003; Morino et al., 2006). Species diurnal cycles from MILAGRO are compared with those from MCMA-2003 in Fig. S-9 and are overall similar. Average AMS mass spectra from the entire MCMA-2003 and 2006 campaigns (Fig. S-9) are also similar.

Species size distributions are shown in Fig. 2b. The BC size distribution was estimated from the signal at $m/z57$ (corrected for the OOA signal fraction) and then normalized to the BC mass (Zhang et al., 2005c; Cubison et al., 2008a). The distributions peak at 300–400 nm (d_{va}), and below 100 nm they are overwhelmingly dominated by OA and BC, presumably due to combustion emissions (Slowik et al., 2004). These distributions and mass fractions are very similar to the MCMA-2003 results (Salcedo et al., 2006) (Fig. S-11). Figure S-4 shows a comparison of the size distribution from the speciated measurements with that from the SMPS. The increased mass detected by the AMS under 200 nm d_{va} is likely due to different sizing of fractal particles between the two instruments (DeCarlo et al., 2004; Slowik et al., 2004).

3.2 Investigating OA components/sources with Positive Matrix Factorization (PMF)

Four OA components were identified from AMS spectra using PMF: chemically-reduced urban primary emissions (hydrocarbon-like OA, HOA), oxygenated OA (OOA, mostly a surrogate for secondary OA or SOA), biomass burning OA (BBOA), and a local primary nitrogen-containing source (local OA or LOA) with a hydrocarbon-like backbone and an atomic nitrogen-to-carbon ratio four times higher than for the other factors (N/C~0.06). Figure S-12 includes PMF diagnostic plots (Ulbrich et al., 2009). In this section we describe each component, identify tracer ions, and compare

the component mass spectra (MS) and ambient ratios with components from previous campaigns and the component time series with tracer species from co-located measurements.

3.2.1 Identification of PMF components using MS profiles and comparison with tracer time series

PMF components are identified by their MS signatures and the correlation of their time series with tracers, and then confirmed with additional information such as diurnal cycles and ratios to tracers (Zhang et al., 2005c; Ulbrich et al., 2009). Figure 3 shows the mass spectral (MS) profiles of the four components identified by PMF for the entire campaign, which are similar to those reported in several previous studies (e.g. Zhang et al., 2005c; Lanz et al., 2007; Nemitz et al., 2008; Ulbrich et al., 2009). Figures 4 and 5 compare the time series of the mass concentrations of the four OA components with co-located measurements, while the time series and fractional mass composition of the four PMF factors are shown in Fig. S-13. The elemental compositions of these components are similar to those reported previously (Aiken et al., 2008). The average contribution of each PMF-AMS component to the mass from each element in the OA (C,H,O,N) is shown in Fig. 6. On average, 61% of the OA mass is from carbon, 29% from oxygen, 9% from hydrogen, and 1% from nitrogen. Of the organic oxygen, 2/3 of it is found within the OOA component, while 1/3 of the organic nitrogen is within the LOA component. Compared with a PMF solution using only the UMR spectra, the increased information from the HR ions allows for a more direct separation of the components, especially of HOA and BBOA, as BBOA has some hydrocarbon-like structure in its UMR MS profile. The differences in the mass spectral signatures of HOA and BBOA are enhanced in high-resolution in comparison to unit mass resolution since BBOA has an increased oxygen-content (Aiken et al., 2008), as shown in Fig. 3 and with a scatter plot of the MS profiles in Fig. S-14, (R^2=0.88 in UMR; 0.64 in HR).

The HOA mass spectrum is similar to that determined in Pittsburgh (Zhang et al., 2005a, c), as compared in Fig. S-15. Its O/C is 0.16±0.05, which is higher than the values of 0.03–0.04 determined for motor vehicle exhaust and more similar to the 0.11–0.14 determined for meat cooking aerosols and 0.08 for plastic burning, all of which have hydrocarbon-like mass spectra in UMR (Mohr et al., 2009). This may indicate that the HOA identified here contains some mass from other combustion-related urban sources such as food cooking and trash burning, and possibly also some lightly oxidized SOA formed from e.g. large alkanes (Kroll et al., 2007). Also, it is possible that the HOA still contains some residual BBOA that is not completely separated even in the HR analysis. An upper limit for this effect is that up to 15% of the HOA during the high fire periods may arise from BB sources (Aiken et al., 2009), with this interference being negligible during the low fire periods as is discussed in more detail in the companion paper. The HOA mass concentration shows a high correlation in time with BC (R^2=0.65) and CO(g) (R^2=0.57), which is consistent with the identification of HOA as being dominated by primary combustion sources and consistent with analyses from previous campaigns (e.g. Zhang et al., 2005c; Volkamer et al., 2006). Lastly, the average ratio of HOA/BC is similar to previous US campaigns, while the ratio of HOA/CO(g) is somewhat higher.

The OOA mass spectrum is also similar to what was found in Pittsburgh (Zhang et al., 2005a, c), compared in Fig. S-16. A recent study showed that the AMS mass spectra of several primary sources (meat-cooking, trash-burning, and vehicle emissions; Mohr et al., 2009) were very different from that of OOA and more similar to HOA (and to BBOA in the case of paper burning). OOA has been associated with SOA in multiple previous studies (Zhang et al., 2005a, c; Takegawa et al., 2006; Volkamer et al., 2006; Kondo et al., 2007; Herndon et al., 2008) and SOA is formed very efficiently from urban emissions in Mexico City (Volkamer et al., 2006; Kleinman et al., 2008; de Gouw et al., 2009). Therefore, the time series of OOA is compared with those of two secondary tracers, submicron particulate nitrate and O_x (NO_2(g)+O_3(g)). O_3 has been shown to correlate with SOA production in Mexico City (Volkamer et al., 2006) and elsewhere (Zhang et al., 2005c), but O_x is a better tracer of photochemical oxidant production because it eliminates the effect of the titration of O_3 by fresh NO(g) emissions (Herndon et al., 2008). Particulate nitrate is formed due to photochemistry starting at sunrise and partially evaporates in the afternoons (Salcedo et al., 2006; Hennigan et al., 2008; Zheng et al., 2008). The correlation of OOA with particulate nitrate (R^2=0.71, Fig. 5c) is slightly better than with O_x (R^2=0.55, Fig. 5d), yet both show very similar temporal changes with OOA in the time series comparison (Fig. 4b). This correlation is especially clear during periods with low background concentrations, such as 24 March which follows a cold surge event that brought clean air to the Mexico City area, similar to a case study from MCMA-2003 which has been studied in some detail (Volkamer et al., 2006, 2007; Dzepina et al., 2009). The observed ratio of OOA/O_x is similar to that determined by Herndon et al. (2008) at the Pico Tres Padres site above Mexico City for periods dominated by SOA production for less-aged airmasses, consistent with the relative locations of the two sites (Fig. 5d). All of these pieces of evidence strongly suggest that OOA is dominated by SOA. A fraction of the background OOA, of the order of 1–15 μg am^{-3} is due to regional biogenic SOA formed over the coastal ranges and advected over the Central Mexican Plateau, according to both 3-D modeling and tracer-derived estimates (Hodzic et al., 2009). Some of the SOA may be formed from BB emissions (Grieshop et al., 2009), although field studies report a wide variation of the relative importance of net BB SOA formation from negligible to comparable to the BB POA (Capes et al., 2008; Cubison et al., 2008b; Yokelson et al., 2009). For this

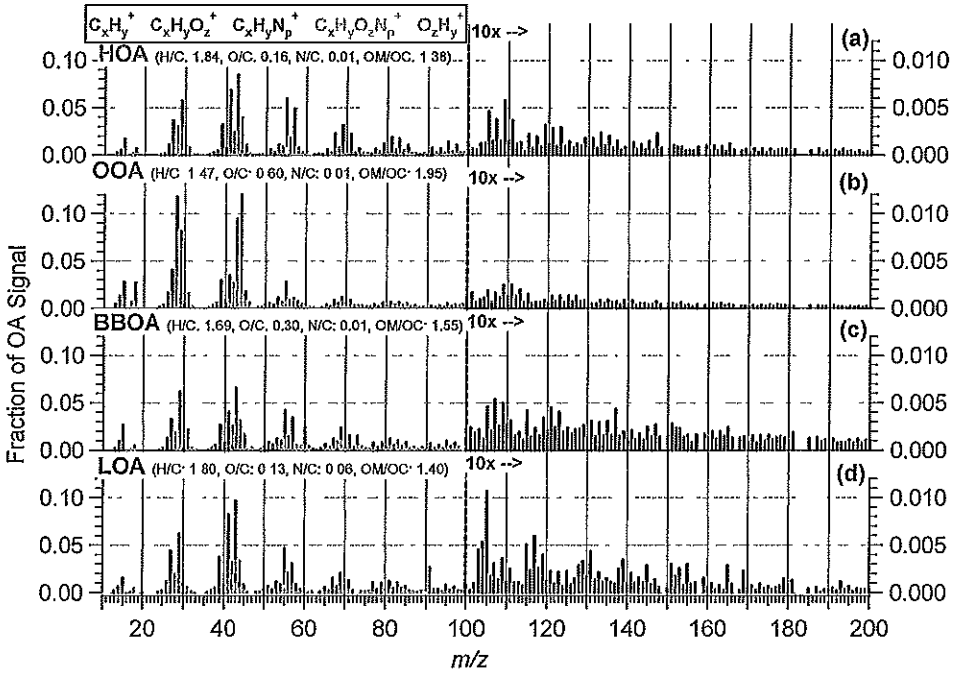

Fig. 3. Mass spectra of four PMF-AMS components with calculated atomic ratios. HR mass spectra under *m/z* 100 and UMR signals above *m/z* 100. HR signals are colored by ion type.

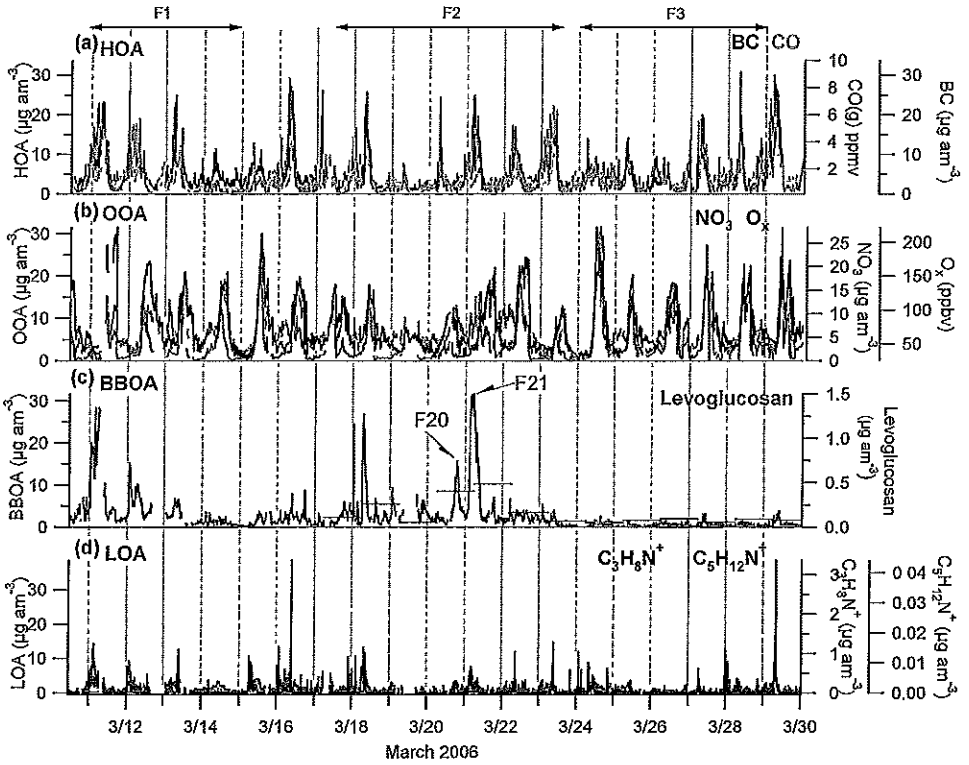

Fig. 4. Time series of PMF-AMS sources and corresponding tracers. Time series of **(a)** HOA, BC, and CO, **(b)** OOA, NO_3, and O_X, **(c)** BBOA, levoglucosan, and **(d)** LOA, $C_3H_8N^+$, $C_5H_{12}N^+$. Periods (F1, F2, F3) are indicated for reference to the fire impact period analysis in Part 2 (Aiken et al., 2009).

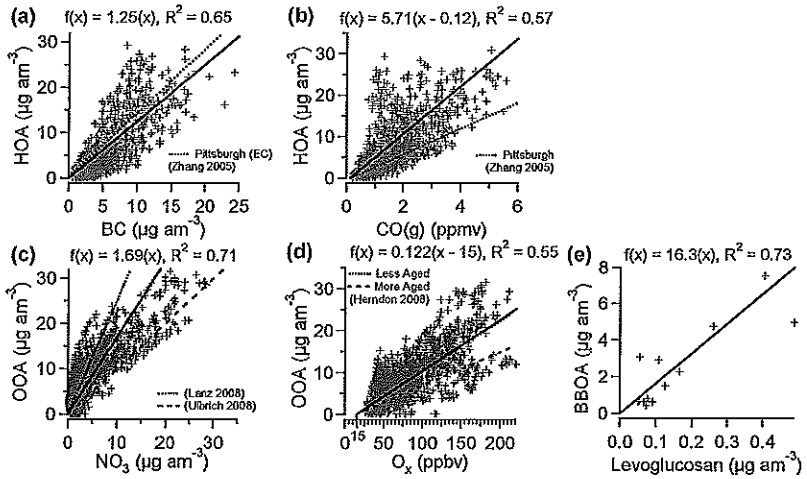

Fig. 5. Scatter plots with linear regressions and R^2 values for **(a)** HOA vs. BC, **(b)** HOA and CO(g), **(c)** OOA and NO_3, **(d)** OOA vs. O_x, and **(e)** BBOA vs. Levoglucosan. Scatter plots include linear regressions determined at other locations in (a, b, d) for comparison. The OOA vs. O_x scatter plot is fitted with an intercept of 15 ppb O_x for OOA=0, consistent with the results of Herndon et al. (2008).

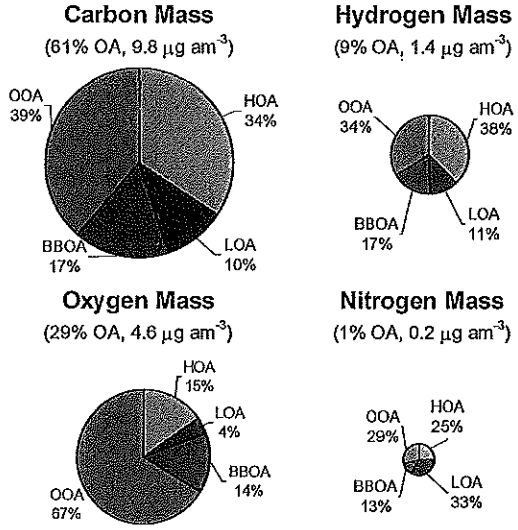

Fig. 6. Average elemental mass of carbon, hydrogen, oxygen, and nitrogen from the whole campaign. Each elemental signal is divided into the percent contribution from the four PMF-AMS components. The relative size of the circles is proportional to the mass concentration of each element.

dataset, several pieces of evidence such as the low levels of the BB tracer acetonitrile during the afternoons when OOA is highest (Fig. 10), and a lack of change of OOA levels between high and low fire periods (Aiken et al., 2009) suggests that the contribution of SOA arising from BB emissions to total OOA at T0 is not major, with the exception of one period described below. This may be due to the fact that the higher BBOA impacts are observed in the early morning (see below), often from plumes emitted from fires burning during the evening and night, and for which photochemistry has not yet acted on the emissions (Aiken et al., 2009).

The background level of OOA at night averages 4.6 $\mu g\,am^{-3}$ during the campaign (defined as the average from 08:00 p.m.–04:00 a.m.), part of which is likely due to some carryover from the previous day, which would be expected to be higher for OOA than particulate nitrate due to the much lower volatility of OOA, resulting in less evaporation (Huffman et al., 2009a). Some of the background OOA is also likely due to regional more aged aerosol from pollution, biomass burning, and biogenic SOA sources. This OOA background does not show major variation across periods of higher and lower BBOA impact (Aiken et al., 2009). One exception occurs during the nights of 20 and 21 March, which follows a period of intense fire impact and has a higher OOA concentration, probably due to SOA formed from BB emissions. Further evidence of this SOA is described in the paper by Stone et al. (2008) where elevated pinonic acid and maximum OC fractions from SOA sources were found in the samples collected during the night of 21 March and the following day. Pinonic acid has been identified in the SOA produced from the photochemical oxidation of α-pinene in chamber studies (Yu et al., 1999). α-pinene is emitted during pine burning (Grieshop et al., 2009), and the correlations in Stone et al. (2008) support the hypothesis that the increased OOA during this period is due to SOA formed from biomass burning emissions.

The BBOA mass spectrum, which is well constrained due to periods of large BB impact at T0, is similar to a source spectrum from a combination of smoldering and flaming pine burning OA (Aiken et al., 2008) as shown in Fig. 7. It is also very similar to the spectrum of paper burning (Mohr et al., 2009) and to spectra from refuse burning sampled at a rural site near Mexico City during MCMA-2003 (not shown; T. Onasch, personal communication, 2009). The BBOA time series is compared with levoglucosan measurements from

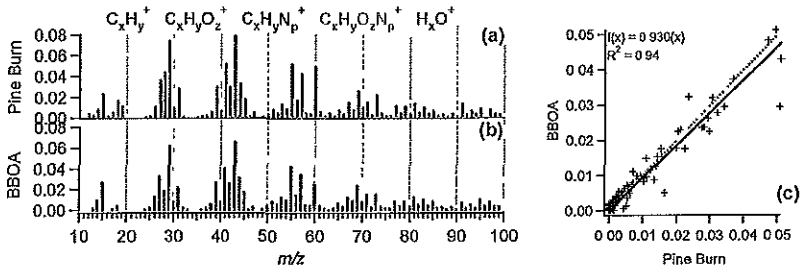

Fig. 7. High resolution mass spectra from (a) primary pine burning emissions and (b) Mexico City BBOA with a (c) scatter plot and linear regression of the high resolution mass spectra. Mass spectral signals are colored by ion type.

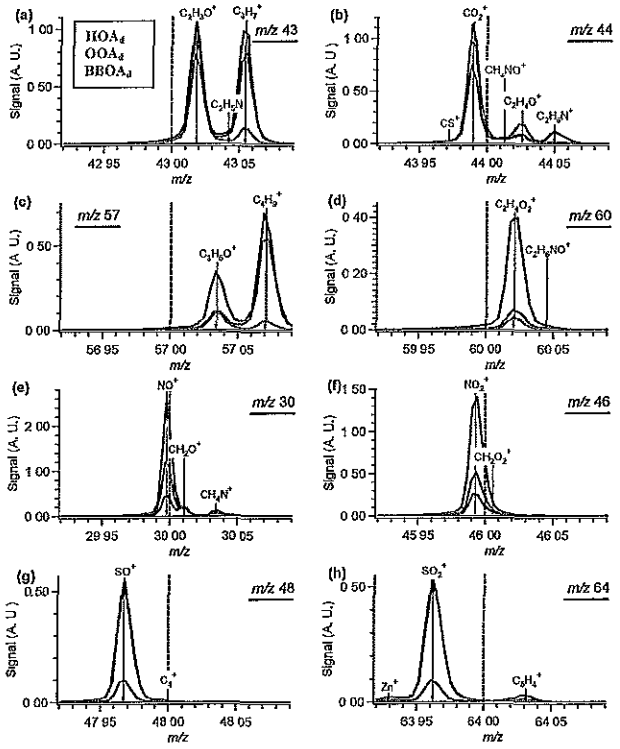

Fig. 8. High resolution ion signals for important (a–d) Organic and (e–h) Inorganic fragment ions. Signals are averaged over ~5 h periods when one PMF factor dominates total OA (e.g. HOA_d=HOA-dominated). (Grey ions are included for reference, but not likely large contributions to the signals.)

GC-MS analysis (Figs. 4c and 5e, Stone et al., 2008). BBOA was averaged onto the filter timescales resulting in an R^2 of 0.73. The slope of the regression indicates that levoglucosan is present at 6.1% of the BBOA mass detected by the PMF-AMS, which falls within the range of previous studies. Sullivan et al. (2008) reports an average mass percentage of 7.0(±3.8)% for levoglucosan/OC from different biomasses, equivalent to ~4.4(±2.4)% of the OM, using a conversion value of 1.6 OM/OC, which encompasses the value determined here.

Additionally, the AMS signal at UMR *m/z*60 has been used previously as a tracer for BBOA (e.g. Alfarra et al., 2007) and can be used to derive a levoglucosan-equivalent concentration from AMS measurements. First, *m/z*60 is almost completely $C_2H_4O_2^+$, as shown in Fig. 8d, consistent with a recent AMS analysis of multiple POA sources (Mohr et al., 2009), and is formed at ~13% of the total signal for levoglucosan standards in the AMS (Aiken et al., 2007). It has been shown to be a clear marker ion for BBOA that is elevated during periods of high smoke impact (Alfarra et al., 2007) and persists despite some reduction with aging in BB plumes measured thousands of km away from the fire locations (Cubison et al., 2008b). This ion is also produced in smaller amounts from some other sources (such as carboxylic acids from SOA formation and also meat cooking; Mohr et al., 2009), and urban areas typically have a level of *m/z*60/OA of ~0.3% in the absence of biomass burning impacts (DeCarlo et al., 2008; Docherty et al., 2008; Ulbrich et al., 2009). We refer to the signal at *m/z*60 after subtraction of 0.3% of the OA as "excess *m/z*60", and define the "levoglucosan-equivalent" ("levog.-eq.") concentration as the concentration of levoglucosan that would be needed to produce the observed level of excess *m/z*60. Figure 9 shows the comparison of levoglucosan from filter-GC/MS measurements (Stone et al., 2008) with the AMS levog.-eq. mass concentrations. The two quantities have an R^2 correlation of 0.79, with the levog.-eq. mass being ~3.2 times that of levoglucosan. Sullivan et al. (2008) identified other carbohydrate anhydrides similar to levoglucosan such as mannosan and galactosan in woodsmoke WSOC for multiple fuel types. Although AMS mass spectra of these species are not available to our knowledge, it is expected that such species also produce *m/z*60 in the AMS as they do in other electron ionization instruments, resulting in an "excess *m/z*60" signal. Therefore, "excess *m/z*60" in the AMS is still a good primary BBOA tracer, but represents a mass that exceeds that of levoglucosan alone. The regression between the AMS levog.-eq. mass and BBOA has a R^2 of 0.93 with a ratio of 0.24 for levog.-eq. mass/BBOA mass, which could potentially be used to approximate BBOA in the absence of PMF-AMS.

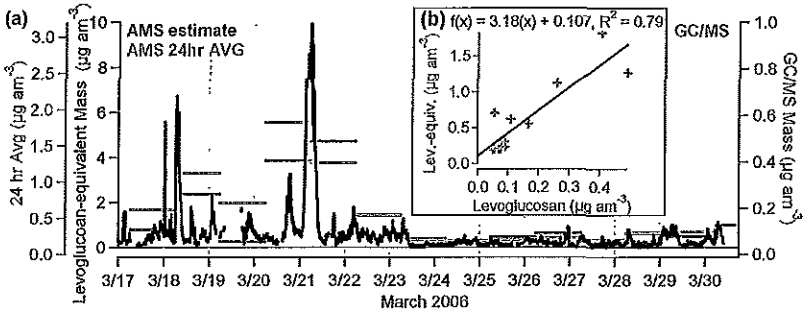

Fig. 9. Mass concentration of levoglucosan-equivalent compounds **(a)** as sampled with the AMS, including averages onto the same time scale as the levoglucosan measured by GC/MS (Stone et al., 2008), and **(b)** a scatter plot with linear regression of the comparison.

Figure 4d shows the time series of the LOA mass concentration along with two nitrogen-containing ions ($C_3H_8N^+$ at *m/z*58 and $C_5H_{12}N^+$ at *m/z*86), which are often large peaks in aliphatic amine spectra (McLafferty and Turecek, 1993), showing that their spiky signals are correlated in time. The highly variable time series (Fig. 4d) and a diurnal cycle enhanced in the morning (Fig. 10b) strongly suggest a primary origin for this source. Further support is provided by the lower autocorrelation values for LOA (compared to other components: PMF-AMS factors, AMS inorganics, gas-phase species) shown in Fig. S-17, which indicates a smaller spatial/temporal extent for this aerosol. Additionally, the LOA time series correlates with the co-located ATOFMS nitrogen-containing organic carbon (NOC) particle type that was "hypothesized to be amines from local industrial emissions based on the time series profile and back trajectory analysis" (Moffet et al., 2008a). Beyond the unusually high nitrogen fraction for the LOA component, of note are the high signals at *m/z*'s 91 ($C_7H_7^+$) and 105 that distinguish its mass spectral profile from the more common primary component, HOA. The LOA component also comprises a high fraction of the OA (~20%) on the night of 23 March and the early morning of 24 March (Fig. S-13e) when the ATOFMS PbZn number count is high and is low during the weekend period of 26 March, where the ATOFMS also reports low concentration of these industrial particles. The source of LOA may or may not be the same as the PbZn source identified by the ATOFMS, and their correlation may reflect instead industrial emissions from the same localized area. Note that the LOA time series does not correlate with AMS NR chloride (R^2=0.09).

The average mass fraction of the PMF OA components is shown in Fig. 10a, which is almost half (46%) OOA and a third (29%) HOA. The diurnal profiles in Fig. 10b point to the formation of OOA/SOA due to photochemistry beginning as early as 07:00–08:00 a.m. and peaking from 09:00 a.m.–03:00 p.m. at ~12.7 $\mu g\,am^{-3}$. HOA shows a peak in the morning consistent with the rush hour and the effects of the low boundary layer height in the morning. BBOA and acetonitrile have similar diurnal profiles (Fig. 10c) which are

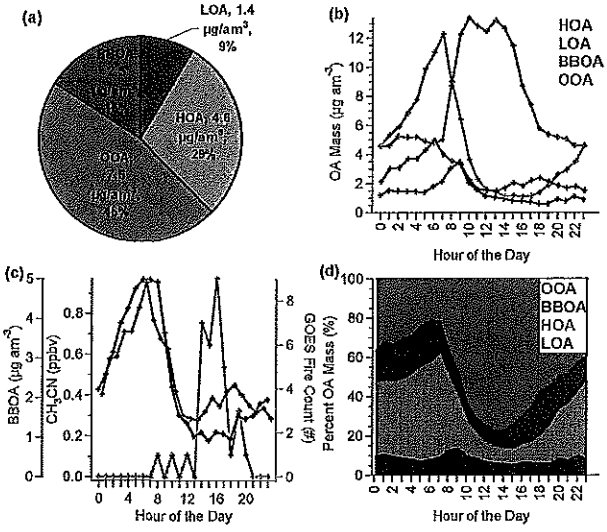

Fig. 10. PMF source **(a)** mass contributions to ~PM_1 OA, **(b)** diurnal profiles, **(c)** BBOA diurnal profile compared with that of acetonitrile and GOES fire counts, and **(d)** diurnal profiles by percent mass.

similar to the rush hour profile but with an earlier start, as was also observed at the T1 site for CH_3CN (de Gouw et al., 2009). There is a second weaker peak in the BBOA diurnal cycle (reaching 2.3 $\mu g\,am^{-3}$ at 06:00 p.m.) in the afternoon to early evening that follows the afternoon peak in fire counts from 02:00–09:00 p.m. as detected by the GOES satellite (http://www.goes.noaa.gov/) using FLAMBE (http://www.nrlmry.navy.mil/flambe/index.html), also shown in Fig. 10c. Figure 10d shows the diurnal cycle for the four components as a fraction of the total OA, indicating that the HOA mass is ~35% during the night and begins to rise at 4 a.m. until 08:00 a.m., when it reaches its fractional peak at 52% of the OA. The OOA mass is ≥70% of the OA from 11:00 a.m. to 05:00 p.m., when SOA production would be expected to peak and when acetonitrile is lowest. BBOA comprises 16% of OA (diurnal range: 8%–23%) on average.

3.2.2 High resolution ion signals – organic and inorganic

The increased mass spectral information content obtained with the HR-ToF-AMS allows for improved separation of OA factors with PMF and increased chemical information of the total and factor OA, e.g. atomic ratios (Aiken et al., 2007, 2008) and ion families (Fig. 3), due to the increased mass resolving power (DeCarlo et al., 2006). Since this is one of the first reports of urban aerosol analysis using the HR-ToF-AMS, the contributions of different ions to some key *m/z*'s of the AMS (which are often used as tracers in AMS studies) are shown in Fig. 8 for periods during the campaign when the OA was dominated by one of the three main PMF sources: HOA (which was 62% of the OA during the selected high-HOA period), OOA (87% during the high-OOA period), BBOA (52% during the high-BBOA period). Signals are in arbitrary units, but all have been scaled to the same air signal at *m/z*28 (N_2^+=100, height). Similar data has been presented previously for aircraft measurements and source profiles (Dunlea et al., 2008; Mohr et al., 2009) and further information on characteristic ions and their contributions to different OA types is discussed by Mohr et al. (2009) and Huffman et al. (2009a) (Fig. S-18 includes all *m/z*'s from 10–100 during the same periods as a reference for this and future studies). As expected, reduced ions such as $C_3H_7^+$ (*m/z* 43) and $C_4H_9^+$ (*m/z*57) are higher during periods dominated by HOA while $C_2H_3O^+$ (*m/z*43) and CO_2^+ (*m/z*44) are higher during OOA-dominated periods. Both types of ions, and also especially $C_2H_4O_2^+$ (*m/z*60), are high during BBOA-dominated periods. The BBOA marker ion at *m/z*60 is an unusual case in which the UMR signal is dominated by a single HR ion, which would allow the correlations discussed above (based on *m/z*60) to be conducted for UMR data without adding increased uncertainty. CO_2^+ dominates the signal within *m/z*44, most markedly during high OOA periods, with the largest fraction of non-CO_2^+ signal occurring during high BBOA periods, consistent with source observations (Mohr et al., 2009). When comparing the main organic ions from the factor-dominated periods (Fig. 8) to the factor mass spectra (Fig. 3) some differences are apparent, such as the high-HOA period has an enhanced fraction of $C_2H_3O^+$ (*m/z*43) due to the presence of 25% OOA during that period. The main inorganic fragment ions from nitrate and sulfate dominate the UMR signal at their respective *m/z*'s almost completely when they are present (Fig. 8e–h and Fig. S-18). The main exceptions are the organic ions at *m/z*30 (CH_2O^+ and CH_4N^+) that occur in both the HOA and BBOA-dominated periods, and $C_5H_4^+$ at *m/z*64 during the BBOA-dominated periods. Additionally, the chloride ions at *m/z*35 and 36 dominate their respective UMR signals, while they do not at *m/z*37 and 38, consistent with the assumptions in the AMS UMR fragmentation table (Allan et al., 2004).

3.2.3 Observed ratio of OA to excess gas-phase carbon monoxide

The total OA/ΔCO, where ΔCO is the gas-phase CO measurement minus a regional boundary layer background of ~120 ppb (Herndon et al., 2008), has been reported during multiple campaigns, e.g. (de Gouw et al., 2005, 2009; Kleinman et al., 2008; de Gouw and Jimenez, 2009). The ratio can yield information about the sources and secondary formation of OA in urban airmasses since POA/ΔCO is low for urban emissions (~5 $\mu g\,sm^{-3}$ ppb-1, Zhang et al., 2005c) and the ratio increases greatly with SOA formation, e.g. de Gouw et al. (2009). Biomass burning can often have high POA/ΔCO ratios, reaching 200 $\mu g\,sm^{-3}\,ppb^{-1}$ (Knighton et al., 2007; DeCarlo et al., 2008; Yokelson et al., 2009), although mid and low ratios have also been reported for some biomasses (Sinha et al., 2004; Knighton et al., 2007). Thus, when urban and biomass emissions mix, the interpretation of OA/ΔCO data is very complex. To document the variation observed here and to allow comparison with other sites and studies, Fig. 11 shows OA/ΔCO observed at T0 along with ratios from previous studies. The T0 data are bounded at the lower end by the low primary emissions ratio for urban HOA (Zhang et al., 2005c; Docherty et al., 2008; this study). The points near the HOA/ΔCO lines are thus likely dominated by urban POA emissions. At the upper end the T0 data are bounded by values observed in both aged urban airmasses dominated by SOA (Volkamer et al., 2006; de Gouw et al., 2009; Kleinman et al., 2008; Dzepina et al., 2009) and forest fire emissions near Mexico City (Yokelson et al., 2007; DeCarlo et al., 2008). T0 is an urban setting and is heavily impacted by HOA emissions, but the dominant presence of higher OA/ΔCO ratios indicates important impacts from SOA formation and/or biomass burning sources. However, since both SOA formation and forest fire emissions can produce the higher OA/ΔCO ratios, their relative contributions cannot be separated with the OA/ΔCO analysis alone. This contrasts with the use of the OA/ΔCO technique in areas where only POA and SOA from urban pollution are thought to be making a major contribution, as under those circumstances the SOA contribution can be estimated with the "CO-tracer method" alone, which estimates POA as the measured ΔCO multiplied by the primary POA/ΔCO ratio, and assigns the rest of the measured OA to SOA (Takegawa et al., 2006; Docherty et al., 2008). Similarly, the contribution of forest fires cannot be reliably estimated in our case with a similar method, since the urban OA/ΔCO is not well-characterized and varies with photochemical age due to SOA formation.

3.3 Comparison of OA apportionment from PMF-AMS and CMB-OMM

PMF-AMS and CMB-OMM results have been compared once previously, and they produced similar results for the fraction of SOA/OA during the summer in Riverside, CA,

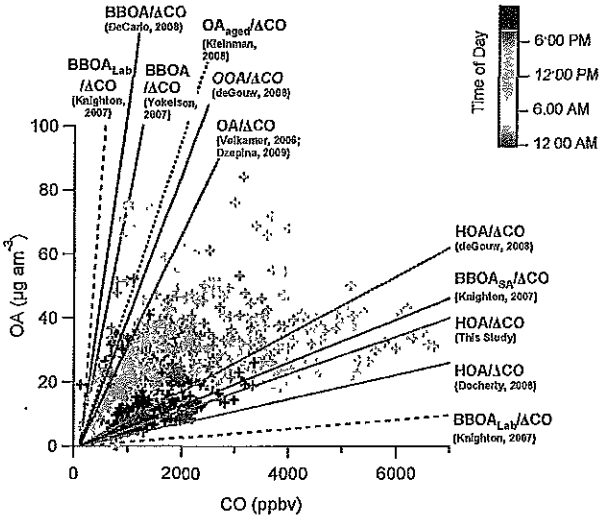

Fig. 11. Scatter plot of AMS Organic Mass (OA) vs. CO(g) for the entire campaign at T0, showing the wide variation in this ratio. Slopes derived from the literature and from this study are also shown (see text). The highest and lowest slopes in the literature are from the study of Knighton et al. (2007) who sampled laboratory BBOA from many different biomasses, the slopes shown are the extremes of their dataset. The $BBOA_{SA}/\Delta CO$ ratio is that sampled by Knighton et al. (2007) for a fire detected at the Santa Ana peripheral site during MILAGRO.

although, with a less pronounced diurnal cycle in CMB-OMM than PMF-AMS (Docherty et al., 2008). CMB-OMM sources are derived as organic carbon mass (OC), which does not include other elements in the organic species such as O, H, N, while PMF-AMS results do include those elements in their OA mass. For comparison, CMB-OMM sources were converted from OC to OA using OM/OC values based on Aiken et al. (2008) (Vegetative Detritus and Woodsmoke, 1.60; Vehicle, 1.20), which are consistent with other methods and the PMF sources found here. The "Other" category of CMB-OMM is calculated here as the difference between the AMS OA measurement and the OA apportioned to primary sources with CMB-OMM to minimize noise in the comparison. The primary CMB-OMM sources were apportioned from $PM_{2.5}$ filters, which could produce a small positive bias in these sources and a negative one in the secondary sources in comparison to the PMF-AMS components. However, the mass concentration between PM_1 and $PM_{2.5}$ is small (Fig. S-5d) and has an increased fraction of dust and a reduced fraction of OA (Fig. 2c) so this bias is expected to be small.

A comparison of the daily average OA apportionment of the two methods and the average composition from the period with overlapping measurements is shown in Fig. 12a–b. Figure 12c–d compares the relative mass fractions for the overlapping sampling period. Most of the components found by both methods are similar and have similar magnitudes: HOA/Vehicle, BBOA/Woodsmoke, and OOA/Other. As discussed above, the PMF-AMS OOA is thought to be dominated by SOA, while Stone et al. (2008) associates the "Other" CMB-OMM component with SOA based on its correlation with WSOC at the near-urban site during MILAGRO (T1, Fig. S-1). The component mass fractions from both methods show similar patterns, e.g. with high BBOA/Woodsmoke on 18, 20, 21 and 22 March and low BBOA/Woodsmoke on most other days during the overlapping period. One difference is that CMB-OMM resolves a small vegetative detritus source (~2%) while PMF-AMS resolves a LOA component (9%) which appears to be more tied to industrial emissions as discussed earlier. It is not surprising that PMF-AMS cannot resolve a source which accounts for only 2% of the mass based on previous method characterization (Ulbrich et al., 2009) and which, since it is likely formed by mechanical processes, may be present mostly in the $PM_{2.5}$-PM_1 size range that the AMS does not sample. Similarly, CMB-OMM cannot retrieve the local LOA primary source since a source profile for it was not available. LOA will likely be lumped as "Other" in CMB. If the average LOA fraction (9%) is subtracted from the "Other" CMB-OMM fraction (58%), we obtain a better estimate of SOA fraction from CMB-OMM (49%) which improves the comparison with the PMF-AMS OOA (46%).

Figure 13 shows scatter plots between the three main components from each method, as well as a hybrid plot showing CMB-OMM Other minus PMF-AMS LOA vs. PMF-AMS OOA to account for the likely attribution of LOA as "Other" in CMB-OMM. These comparisons show reasonable consistency although with significant scatter on a day-to-day basis. The slopes are close to one in most cases, with Woodsmoke/BBOA showing a lower slope (with PMF-AMS>CMB-OMM as indicated by the regression line), yet having the highest level of correlation, likely due to the relatively large dynamic range. The lower estimate of Woodsmoke OA from CMB-OOM may be due to the use of levoglucosan as a tracer based on source measurements, since some degradation of this tracer is observed in ambient studies (Cubison et al., 2008b). The PMF-AMS method conceptually determines the levoglucosan level in BBOA from the ambient measurements and thus is less prone to such underestimation. The lowest R^2 is found for the HOA/Vehicle POA comparison, which may be due to the lower dynamic range of this source which is always present in the urban area and perhaps to the influence of non-vehicle sources of HOA. Additional possible reasons for differences for the daily source contributions include variations in the OM/OC ratios vs. the constant values assumed here for the conversion of CMB sources to OA, uncertainties and noise in both the tracer measurements and AMS spectra, and imperfections in the CMB-OMM and PMF-AMS source attribution algorithms and their application to real data (e.g. Ulbrich et al., 2009). Finally, it is possible that the different PMF-AMS OA components could have slightly different relative ionization efficiencies (RIEs), and/or bounce-related

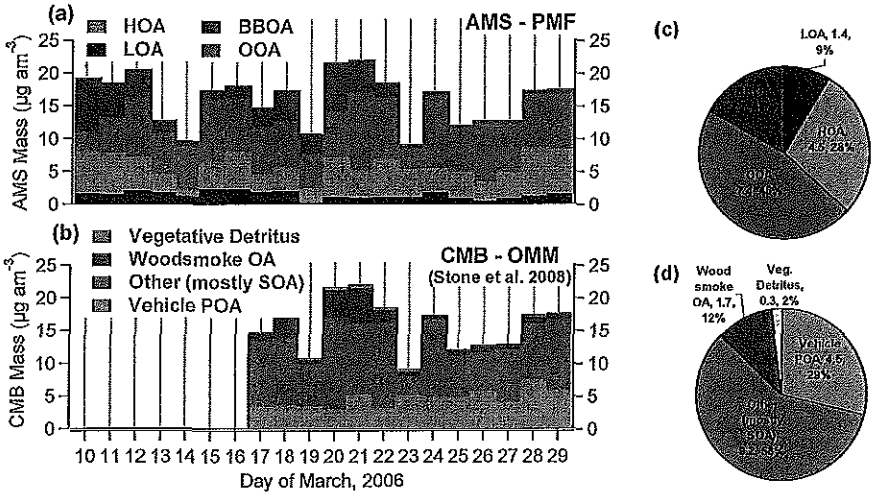

Fig. 12. Daily source apportionment of OA from **(a)** PMF-AMS and **(b)** CMB-OMM with **(c, d)** the average composition of each, respectively, for the overlapping sampling period from 17–30 March. Note: CMB-OMM OC results converted to OM (Aiken et al., 2008).

collection efficiencies (E_b) to the extent that they are present in externally mixed particles. Both of these effects would lead to a positive bias of the chemically-reduced and more volatile components (HOA, BBOA, LOA) and a negative bias against OOA (Jimenez et al., 2003; Huffman et al., 2005, 2009a; Zhang et al., 2005b). We experimented with different E_b*RIE for the different OA components retrieved by PMF, but the comparisons with other measurements (Table S-1 and Figs. S-2, S-3, and S-4) were not significantly improved. Thus, any variations in the product E_b*RIE for the different organic species are estimated to be small and not the main reason for the differences observed in some of the intercomparisons. This is consistent with the analysis by Docherty et al. (2009) for an AMS dataset in Riverside, CA, who estimate that the biases in OA component quantification due to the differences in E_b*RIE between different PMF-AMS OA components are less than 15%. Overall the agreement between both techniques for such a complex urban area given all the remaining uncertainties is very encouraging.

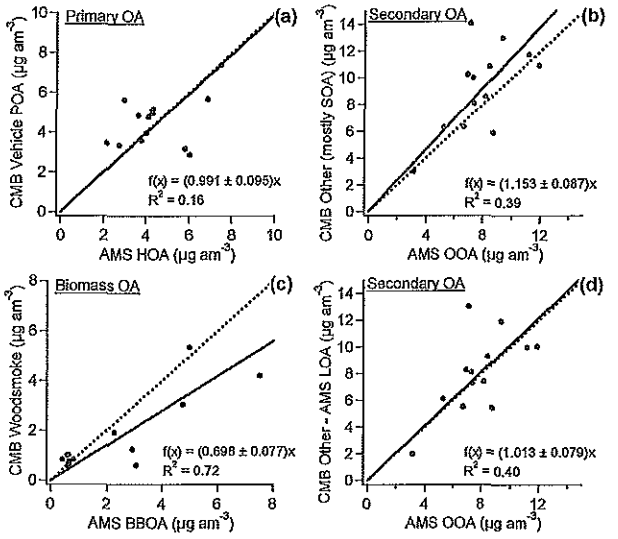

Fig. 13. Scatter plots and linear orthogonal distance regressions of source apportionment factors from CMB-OMM versus the corresponding PMF-AMS source: **(a)** Vehicle POA and HOA, **(b)** Other (mostly SOA) and OOA, **(c)** Woodsmoke and BBOA, **(d)** CMB-Other minus AMS-LOA vs. AMS-OOA. (Dashed lines are 1:1 lines.)

3.4 Comparisons with Mexico City emissions inventory

We can use the PMF-AMS OA results to evaluate the 2006 Mexico City emissions inventory (SMA 2006). Since most of the PM species and components vary slowly in time (Fig. 1), are observed at consistent ratios at different times during the campaign, and show similar fractions and ratios to the data from MCMA-2003 from a different location in the city, we conclude that our observations at T0 are generally representative for Mexico City. The 2006 MCMA emissions inventory attributes 62% of the $PM_{2.5}$ emissions to motor vehicles and most of the rest to a variety of area and point sources, whose activity is not expected to be strongly dependent on the time of the year. When HOA, LOA, submicron soil, metals, and BC mass concentrations are summed during the morning rush hour period (06:00–08:00 a.m.), which is most strongly influenced by direct emissions, we obtain a PM/ΔCO ratio of 11.5 μg am^{-3} ppm^{-1} (13 g/kg). The 2006 emissions inventory has a primary $PM_{2.5}$/ΔCO emission ratio of 3.1 g/kg (equivalent to 2.7 μg am^{-3} ppm^{-1}). Since the CO emissions inventory is thought to be accurate (de Foy et al., 2007), this implies that the primary PM is underestimated by about a factor of four in the 2006 emissions inventory. Since several of the species included in this sum are submicron or (such as BC) do not extend to 2.5 μm, the calculated underestimation of the emission inventory is a lower limit,

as additional small amounts of those species in the PM_1 to $PM_{2.5}$ range would increase the measured-to-inventory ratio. This underestimate is consistent with the results of Zavala et al. (2009) for the mobile source emission inventory. If we add in the secondary aerosol production as determined from the peak in the afternoon by summing the additional OOA, ammonium nitrate and ammonium chloride concentrations (PM/ΔCO ratio of 44 $\mu g\,am^{-3}$ ppm^{-1} for those species), the MCMA PM in the afternoon exceeds the amount that would be predicted with the 2006 emissions inventory by a factor of ~16. Additionally, the forest fire source in the 2006 MCMA emissions inventory is small (2% of the primary $PM_{2.5}$) and is much smaller (by at least an order-of-magnitude) than our observations, which is quantified further in the companion paper (Aiken et al., 2009).

3.5 Rapid estimation of PMF-AMS components from UMR tracer *m/z*

Zhang et al. (2005a) provided a simple approximation to estimate the HOA and OOA concentrations based on the time series of UMR *m/z*44 and 57 (OOA=7.6×*m/z*44 and HOA=12.2×*m/z*57, when *m/z*44 and 57 are in units of org.-eq. $\mu g\,m^{-3}$, Zhang et al., 2005a). Since this is the first study in which PMF has been applied to high-resolution data and also one of the firsts in which BBOA has been explicitly identified in urban air, it is of interest to update the estimation procedure using the results of this study. Figure 14a–d show scatter plots used to derive relationships to estimate OOA, BBOA, and HOA based on linear combinations of *m/z*44, 57, and 60, which are qualitatively consistent with the results of Zhang et al. (2005a, b) although the coefficients are different in this case. OOA is estimated as proportional to UMR *m/z*44, with an offset likely due to ions other than CO_2^+ at this *m/z* (Fig. 14a). BBOA is estimated as proportional to *m/z*60, after subtracting a background of 0.3% of the OA for this ion, mainly due to SOA (Docherty et al., 2008) (Fig. 14b). HOA is estimated as proportional to the $C_4H_9^+$ ion at *m/z*57 (Fig. 14d), which is estimated as the total UMR signal at *m/z*57 minus 10% of UMR *m/z*44 (as an estimate of the $C_3H_5O^+$ ion at *m/z*57, Fig. 14c).

Figure 14e compares the time series of OOA, BBOA, and HOA estimated in this way to those derived with the full PMF analysis of the HR data. It is clear that the tracer-based method with the coefficients determined here is capable of providing a good first-order estimate of the OA components based on the UMR data which can be very useful during field studies and early analyses before the full (and very time-consuming) HR and PMF analyses have been performed. However, the coefficients are not known a priori. Due to the difference in the actual coefficients determined here vs. those determined by Zhang et al. (2005a) for Pittsburgh, it is of great interest to report the results of this analysis for other locations in order to establish the range of variation of the coefficients, as well as dependences on photochemical age, type of POA and BBOA sources, etc.

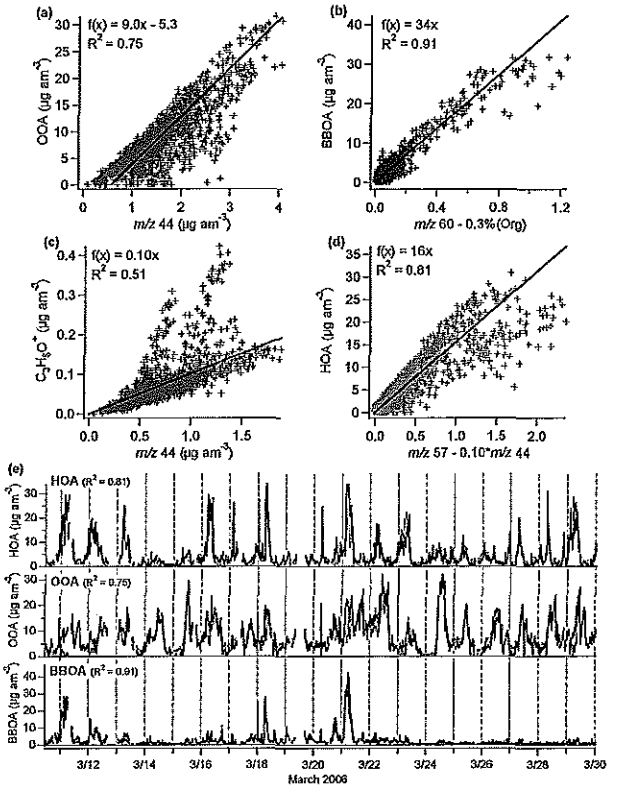

Fig. 14. Relationships between PMF-AMS components and tracer *m/z* from UMR spectra: **(a)** OOA vs. UMR *m/z*44; **(b)** BBOA vs. UMR *m/z*60 minus 0.3%*Org; **(c)** relationship between the $C_3H_5O^+$ ion at *m/z*57 and UMR *m/z*44, which is used to correct for the influence of OOA in UMR *m/z*57; **(d)** HOA vs. OOA-corrected UMR *m/z*57; **(e)** comparison of the time series of the HR PMF-AMS factors (presented in this paper) versus the factors predicted from the UMR tracer *m/z*'s with the relationships derived here.

4 Conclusions

Continuous ambient aerosol measurements were made during MILAGRO at the T0 supersite within Mexico City during March 2006. Intercomparisons confirm that the AMS performed well at T0, and that the scatter of the AMS versus other measurements is similar to that amongst the other measurements. Refractory species account for 20% of the average 33.7 $\mu g\,am^{-3}$ PM_1 (BC: 12%, metals: 3%, soil: 5%). The species mass concentrations, size distributions, and diurnal profiles were similar to those measured during MCMA-2003 at CENICA, with OA accounting for about half of the submicron mass (Salcedo et al., 2006). PMF-AMS analysis of the high-resolution mass spectra was used to separate four organic components, which are consistent with previous studies in Mexico City and elsewhere. The assignments of the four components are supported by their mass spectra,

time series correlations with tracers, and other evidence such as tracer ratios. HOA (primary hydrocarbon-like), OOA (oxygenated, mostly secondary), BBOA (biomass burning, which likely includes both forest fires and some refuse burning), and a small local nitrogen-containing OA (LOA) primary source were identified. LOA likely contains amines and accounts for 1/3 of the detected nitrogen in the OA. Primary emissions and secondary OA formation are both important for this dataset. The impact of biomass burning is significant for OA and is highly variable in time, consistent with other ground-based observations during MILAGRO (Stone et al., 2008; de Gouw et al., 2009). The AMS averages and trends compare well to those from CMB of organic molecular markers, although with significant scatter in the daily comparisons. The 2006 MCMA emissions inventory is underestimated by a factor of ~4 for primary fine PM and lower than the afternoon concentrations by ~16 when secondary species are included. Additional secondary species formation over longer time scales (e.g. Dzepina et al., 2009) will likely increase this ratio. The forest fire PM from the MCMA inventory is at least an order-of-magnitude lower than that estimated from our observations. A simple estimation method based on UMR tracer *m/z*'s can provide a first-order approximation of the PMF components and should be explored for other locations.

Acknowledgements. This study was supported by the following funding, NASA: fellowship NNG04GR06H (ACA), NGT5-30516 (JAH), NNG05GQ50H (IMU); NSF: grants ATM-0528634, ATM-0449815 (CAREER), ATM-0511769 (WPA and GPM), ATM-0528227 (LTM) and ATM-0511803 (LTM); DOE: grants DE-FG02-05ER63981 and DE-FG02-05ER64008 (WPA and GPM); NOAA: grant NA08OAR4310565; and EPA STAR fellowship RD-83216101-0 (PFD). PIXE analysis was performed in the Environmental Molecular Sciences Laboratory, a national scientific user facility sponsored by OBER/DOE and located at Pacific Northwest National Laboratory. Although this research has been partially funded by EPA and NSF, it has not been subject to Agency Review and thus no official endorsement should be inferred. We are grateful to X. Querol for the OPC data. The authors would also like to thank support from and useful discussions with Aerodyne, Tofwerk, J. de Gouw, and the remainder of the Jimenez Group. Finally, we would like to acknowledge IMP for hosting the T0 Supersite and the logistical support from many Mexican government agencies and institutions which made it possible to carry out the MCMA-2006/MILAGRO Campaign.

Edited by: S. Madronich

References

Aiken, A. C., de Foy, B., Wiedinmyer, C., et al.: Mexico City aerosol analysis during MILAGRO using high resolution aerosol mass spectrometry at the urban supersite (T0) – Part 2: Analysis of the biomass burning contribution and the modern carbon fraction, Atmos. Chem. Phys., in preparation, 2009.

Aiken, A. C., DeCarlo, P. F. and Jimenez, J. L.: Elemental Analysis of Organic Species with Electron Ionization High-Resolution, Mass Spectrometry, Anal. Chem., 79(21), 8350–8358, 2007.

Aiken, A. C., DeCarlo, P. F., Kroll, J. H., et al.: O/C and OM/OC Ratios of Primary, Secondary, and Ambient Organic Aerosols with High-Resolution Time-of-Flight Aerosol Mass Spectrometry, Environ. Sci. Technol., 42(12), 4478–4485, doi:10.1021/es703009q, 2008.

Alfarra, M. R., Prevot, A. S. H., Szidat, S., Sandradewi, J., Weimer, S., Lanz, V. A., Schreiber, D., Mohr, M., and Baltensperger, U.: Identification of the mass spectral signature of organic aerosols from wood burning emissions, Environ. Sci. Technol., 41(16), 5770–5777, 2007.

Allan, J. D., Delia, A. E., Coe, H., et al.: Technical note: A generalised method for the extraction of chemically resolved mass spectra from aerodyne aerosol mass spectrometer data, J. Aerosol Sci., 35(7), 909–922, 2004.

Bravo, A. H., Sosa, E. R., Sanchez, A. P., Jaimes, P. M., and Saavedra, R. M. I.: Impact of wildfires on the air quality of Mexico City, 1992–1999, Environ. Pollut., 117(2), 243–253, 2002.

Canagaratna, M. R., Jayne, J. T., Jimenez, J. L., et al.: Chemical and microphysical characterization of ambient aerosols with the aerodyne aerosol mass spectrometer, Mass Spectrom. Rev., 26(2), 185–222, 2007.

Capes, G., Johnson, B., McFiggans, G., Williams, P. I., Haywood, J., and Coe, H.: Aging of biomass burning aerosols over West Africa: Aircraft measurements of chemical composition, microphysical properties, and emission ratios, J. Geophys. Res.-Atmos., 113, D00C15, doi:10.1029/2008JD009845, 2008.

Chow, J. C., Watson, J. G., Edgerton, S. A., and Vega, E.: Chemical composition of PM2.5 and PM10 in Mexico City during winter 1997, Sci. Total Environ., 287(3), 177–201, 2002.

Crounse, J. D., DeCarlo, P. F., Blake, D. R., Emmons, L. K., Campos, T. L., Apel, E. C., Clarke, A. D., Weinheimer, A. J., McCabe, D. C., Yokelson, R. J., Jimenez, J. L., and Wennberg, P. O.: Biomass burning and urban air pollution over the Central Mexican Plateau, Atmos. Chem. Phys., 9, 4929–4944, 2009, http://www.atmos-chem-phys.net/9/4929/2009/.

Cubison, M. J., Ervens, B., Feingold, G., Docherty, K. S., Ulbrich, I. M., Shields, L., Prather, K., Hering, S., and Jimenez, J. L.: The influence of chemical composition and mixing state of Los Angeles urban aerosol on CCN number and cloud properties, Atmos. Chem. Phys., 8, 5649-5667, 2008a, http://www.atmos-chem-phys.net/8/5649/2008/.

Cubison, M. J., Sueper, D., Dunlea, E. J., et al.: Submicron aerosol composition during the ARCTAS campaign: Arctic Haze, Biomass Burning, and California Pollution, Eos Trans. AGU, 89, 53, Fall Meet. Suppl., Abstract A11A-0081, 2008b.

de Foy, B., Caetano, E., Magaña, V., Zitácuaro, A., Cárdenas, B., Retama, A., Ramos, R., Molina, L. T., and Molina, M. J.: Mexico City basin wind circulation during the MCMA-2003 field campaign, Atmos. Chem. Phys., 5, 2267–2288, 2005, http://www.atmos-chem-phys.net/5/2267/2005/.

de Foy, B., Clappier, A., Molina, L. T., and Molina, M. J.: Distinct wind convergence patterns in the Mexico City basin due to the interaction of the gap winds with the synoptic flow, Atmos. Chem. Phys., 6, 1249–1265, 2006a, http://www.atmos-chem-phys.net/6/1249/2006/.

de Foy, B., Fast, J. D., Paech, S. J., Phillips, D., Walters, J. T., Coulter, R. L., Martin, T. J., Pekour, M. S., Shaw, W. J., Kastendeuch, P. P., Marley, N. A., Retama, A., and Molina, L. T.: Basin-

scale wind transport during the MILAGRO field campaign and comparison to climatology using cluster analysis, Atmos. Chem. Phys., 8, 1209–1224, 2008, http://www.atmos-chem-phys.net/8/1209/2008/.

de Foy, B., Lei, W., Zavala, M., Volkamer, R., Samuelsson, J., Mellqvist, J., Galle, B., Martínez, A.-P., Grutter, M., Retama, A., and Molina, L. T.: Modelling constraints on the emission inventory and on vertical dispersion for CO and SO^2 in the Mexico City Metropolitan Area using Solar FTIR and zenith sky UV spectroscopy, Atmos. Chem. Phys., 7, 781–801, 2007, http://www.atmos-chem-phys.net/7/781/2007/.

de Foy, B., Varela, J. R., Molina, L. T., and Molina, M. J.: Rapid ventilation of the Mexico City basin and regional fate of the urban plume, Atmos. Chem. Phys., 6, 2321–2335, 2006b, http://www.atmos-chem-phys.net/6/2321/2006/.

de Foy, B., Zavala, M., Bei, N., and Molina, L. T.: Evaluation of WRF mesoscale simulations and particle trajectory analysis for the MILAGRO field campaign, Atmos. Chem. Phys., 9, 4419–4438, 2009, http://www.atmos-chem-phys.net/9/4419/2009/.

de Gouw, J. and Jimenez, J. L.: Organic Aerosols in the Earth's Atmosphere, Environ. Sci. Technol., in press, 2009.

de Gouw, J. A., Middlebrook, A. M., Warneke, C., et al.: Budget of organic carbon in a polluted atmosphere: Results from the New England Air Quality Study in 2002, J. Geophys. Res.-Atmos., 110, D16305, doi:10.1029/2004JD005623 2005.

de Gouw, J. A., Welsh-Bon, D., Warneke, C., Kuster, W. C., Alexander, L., Baker, A. K., Beyersdorf, A. J., Blake, D. R., Canagaratna, M., Celada, A. T., Huey, L. G., Junkermann, W., Onasch, T. B., Salcido, A., Sjostedt, S. J., Sullivan, A. P., Tanner, D. J., Vargas, O., Weber, R. J., Worsnop, D. R., Yu, X. Y., and Zaveri, R.: Emission and chemistry of organic carbon in the gas and aerosol phase at a sub-urban site near Mexico City in March 2006 during the MILAGRO study, Atmos. Chem. Phys., 9, 3425–3442, 2009, http://www.atmos-chem-phys.net/9/3425/2009/.

de Foy, B., Caetano, E., Magaña, V., Zitácuaro, A., Cárdenas, B., Retama, A., Ramos, R., Molina, L. T., and Molina, M. J.: Mexico City basin wind circulation during the MCMA-2003 field campaign, Atmos. Chem. Phys., 5, 2267–2288, 2005, http://www.atmos-chem-phys.net/5/2267/2005/.

DeCarlo, P. F., Dunlea, E. J., Kimmel, J. R., Aiken, A. C., Sueper, D., Crounse, J., Wennberg, P. O., Emmons, L., Shinozuka, Y., Clarke, A., Zhou, J., Tomlinson, J., Collins, D. R., Knapp, D., Weinheimer, A. J., Montzka, D. D., Campos, T., and Jimenez, J. L.: Fast airborne aerosol size and chemistry measurements above Mexico City and Central Mexico during the MILAGRO campaign, Atmos. Chem. Phys., 8, 4027–4048, 2008, http://www.atmos-chem-phys.net/8/4027/2008/.

DeCarlo, P. F., Kimmel, J. R., Trimborn, A., et al.: Field-deployable, high-resolution, time-of-flight aerosol mass spectrometer, Anal. Chem., 78(24), 8281–8289, 2006.

DeCarlo, P. F., Slowik, J. G., Worsnop, D. R., Davidovits, P., and Jimenez, J. L.: Particle morphology and density characterization by combined mobility and aerodynamic diameter measurements. Part 1: theory, Aerosol Sci. Tech., 38, 1185–1205, 2004.

Docherty, K. S., Stone, E. A., Ulbrich, I. M., et al.: Apportionment of primary and secondary organic aerosols in southern California during the 2005 study of organic aerosols in Riverside (SOAR), Environ. Sci. Technol., 42, 7655–7662, 2008.

Drewnick, F., Hings, S. S., DeCarlo, P., et al.: A new time-of-flight aerosol mass spectrometer (TOF-AMS) – Instrument description and first field deployment, Aerosol Sci. Tech., 39(7), 637–658, 2005.

Dunlea, E. J., DeCarlo, P. F., Aiken, A. C., Kimmel, J. R., Peltier, R. E., Weber, R. J., Tomlison, J., Collins, D. R., Shinozuka, Y., McNaughton, C. S., Howell, S. G., Clarke, A. D., Emmons, L. K., Apel, E. C., Pfister, G. G., van Donkelaar, A., Martin, R. V., Millet, D. B., Heald, C. L., and Jimenez, J. L.: Evolution of Asian aerosols during transpacific transport in INTEX-B, Atmos. Chem. Phys. Discuss., 8, 15375–15461, 2008, http://www.atmos-chem-phys-discuss.net/8/15375/2008/.

Dzepina, K., Volkamer, R. M., Madronich, S., Tulet, P., Ulbrich, I. M., Zhang, Q., Cappa, C. D., Ziemann, P. J., and Jimenez, J. L.: Evaluation of recently-proposed secondary organic aerosol models for a case study in Mexico City, Atmos. Chem. Phys., 9, 5681–5709, 2009, http://www.atmos-chem-phys.net/9/5681/2009/.

Edgerton, S. A., Bian, X., Doran, J. C., et al.: Particulate air pollution in Mexico City: A collaborative research project, J. Air Waste Manage., 49(10), 1221–1229, 1999.

Farmer, D. K., Docherty, K. S., Cubison, M. J., Ziemann, P. J., Matsunaga, A., and Jimenez, J. L.: Aerosol organic nitrate characterization and quantification with the High Resolution-Time of Flight-Aerosol Mass Spectrometer, Fall Meeting Suppl. Abstract A31B-0092, EOS T. Am. Geophys. Un., 2008.

Fast, J. D., de Foy, B., Acevedo Rosas, F., Caetano, E., Carmichael, G., Emmons, L., McKenna, D., Mena, M., Skamarock, W., Tie, X., Coulter, R. L., Barnard, J. C., Wiedinmyer, C., and Madronich, S.: A meteorological overview of the MILAGRO field campaigns, Atmos. Chem. Phys., 7, 2233–2257, 2007, http://www.atmos-chem-phys.net/7/2233/2007/.

Fast, J. D. and Zhong, S. Y.: Meteorological factors associated with inhomogeneous ozone concentrations within the Mexico City basin, J. Geophys. Res.-Atmos., 103(D15), 18927–18946, 1998.

Fast, J., Aiken, A. C., Allan, J., Alexander, L., Campos, T., Canagaratna, M. R., Chapman, E., DeCarlo, P. F., de Foy, B., Gaffney, J., de Gouw, J., Doran, J. C., Emmons, L., Hodzic, A., Herndon, S. C., Huey, G., Jayne, J. T., Jimenez, J. L., Kleinman, L., Kuster, W., Marley, N., Russell, L., Ochoa, C., Onasch, T. B., Pekour, M., Song, C., Ulbrich, I. M., Warneke, C., Welsh-Bon, D., Wiedinmyer, C., Worsnop, D. R., Yu, X.-Y., and Zaveri, R.: Evaluating simulated primary anthropogenic and biomass burning organic aerosols during MILAGRO: implications for assessing treatments of secondary organic aerosols, Atmos. Chem. Phys., 9, 6191–6215, 2009, http://www.atmos-chem-phys.net/9/6191/2009/.

Fine, P. M., Sioutas, C., and Solomon, P. A.: Secondary particulate matter in the United States: Insights from the particulate matter supersites program and related studies, J. Air Waste Manage., 58(2), 234–253, 2008.

Fortner, E. C., Zheng, J., Zhang, R., Berk Knighton, W., Volkamer, R. M., Sheehy, P., Molina, L., and André, M.: Measurements of Volatile Organic Compounds Using Proton Transfer Reaction – Mass Spectrometry during the MILAGRO 2006 Campaign, Atmos. Chem. Phys., 9, 467–481, 2009, http://www.atmos-chem-phys.net/9/467/2009/.

Fountoukis, C., Nenes, A., Sullivan, A., Weber, R., Van Reken, T., Fischer, M., Matas, E., Moya, M., Farmer, D., and Cohen, R. C.:

Thermodynamic characterization of Mexico City aerosol during MILAGRO 2006, Atmos. Chem. Phys., 9, 2141–2156, 2009, http://www.atmos-chem-phys.net/9/2141/2009/.

Gilardoni, S., Liu, S., Takahama, S., Russell, L. M., Allan, J. D., Steinbrecher, R., Jimenez, J. L., De Carlo, P. F., Dunlea, E. J., and Baumgardner, D.: Characterization of organic ambient aerosol during MIRAGE 2006 on three platforms, Atmos. Chem. Phys., 9, 5417–5432, 2009, http://www.atmos-chem-phys.net/9/5417/2009/.

Grieshop, A. P., Donahue, N. M., and Robinson, A. L.: Laboratory investigation of photochemical oxidation of organic aerosol from wood fires 2: analysis of aerosol mass spectrometer data, Atmos. Chem. Phys., 9, 2227–2240, 2009, http://www.atmos-chem-phys.net/9/2227/2009/.

Hallquist, M., Wenger, J. C., Baltensperger, U., Rudich, Y., Simpson, D., Claeys, M., Dommen, J., Donahue, N. M., George, C., Goldstein, A. H., Hamilton, J. F., Herrmann, H., Hoffmann, T., Iinuma, Y., Jang, M., Jenkin, M. E., Jimenez, J. L., Kiendler-Scharr, A., Maenhaut, W., McFiggans, G., Mentel, Th. F., Monod, A., Prévôt, A. S. H., Seinfeld, J. H., Surratt, J. D., Szmigielski, R., and Wildt, J.: The formation, properties and impact of secondary organic aerosol: current and emerging issues, Atmos. Chem. Phys., 9, 5155–5235, 2009, http://www.atmos-chem-phys.net/9/5155/2009/.

Hennigan, C. J., Sullivan, A. P., Fountoukis, C. I., Nenes, A., Hecobian, A., Vargas, O., Peltier, R. E., Case Hanks, A. T., Huey, L. G., Lefer, B. L., Russell, A. G., and Weber, R. J.: On the volatility and production mechanisms of newly formed nitrate and water soluble organic aerosol in Mexico City, Atmos. Chem. Phys., 8, 3761–3768, 2008, http://www.atmos-chem-phys.net/8/3761/2008/.

Herndon, S. C., Onasch, T. B., Wood, E. C., et al.: The Correlation of Secondary Organic Aerosol with Odd Oxygen in a Megacity Outflow, Geophys Res. Lett., 35, L15804, doi:10.1029/2008GL034058, 2008.

Hodzic, A., Jimenez, J. L., Madronich, S., Aiken, A. C., Bessagnet, B., Curci, G., Fast, J., Lamarque, J. F., Onasch, T. B., Roux, G., and Ulbrich, I. M.: Modeling organic aerosols during MILAGRO: application of the CHIMERE model and importance of biogenic secondary organic aerosols, Atmos. Chem. Phys. Discuss., 9, 12207–12281, 2009, http://www.atmos-chem-phys-discuss.net/9/12207/2009/.

Huffman, J. A., Docherty, K. S., Aiken, A. C., Cubison, M. J., Ulbrich, I. M., DeCarlo, P. F., Sueper, D., Jayne, J. T., Worsnop, D. R., Ziemann, P. J., and Jimenez, J. L.: Chemically-resolved aerosol volatility measurements from two megacity field studies, Atmos. Chem. Phys. Discuss., 9, 2645–2697, 2009a, http://www.atmos-chem-phys-discuss.net/9/2645/2009/.

Huffman, J. A., Docherty, K. S., Mohr, C., Cubison, M. J., Ulbrich, I. M., Ziemann, P. J., Onasch, T. B., and Jimenez, J. L.: Chemically-Resolved Volatility Measurements of Organic Aerosol from Different Sources, Environ. Sci. Technol., 43, 5351–5357, doi:10.1021/es803539d, 2009b.

Huffman, J. A., Jayne, J. T., Drewnick, F., Aiken, A. C., Onasch, T., Worsnop, D. R., and Jimenez, J. L.: Design, modeling, optimization, and experimental tests of a particle beam width probe for the aerodyne aerosol mass spectrometer, Aerosol Sci. Tech., 39(12), 1143–1163, 2005.

Huffman, J. A., Ziemann, P. J., Jayne, J. T., Worsnop, D. R., and Jimenez, J. L.: Development and characterization of a fast-stepping/scanning thermodenuder for chemically-resolved aerosol volatility measurements, Aerosol Sci. Tech., 42, 395–407, 2008.

IPCC: Climate Change 2007 – The Physical Science Basis. Working Group I Contribution to the Fourth Assessment Report of the IPCC, Cambridge University Press, Cambridge, UK, 2007.

Jayne, J. T., Leard, D. C., Zhang, X. F., Davidovits, P., Smith, K. A., Kolb, C. E., and Worsnop, D. R.: Development of an aerosol mass spectrometer for size and composition analysis of submicron particles, Aerosol Sci. Tech., 33(1–2), 49–70, 2000.

Jimenez, J. L., Jayne, J. T., Shi, Q., et al.: Ambient aerosol sampling using the Aerodyne Aerosol Mass Spectrometer, J. Geophys. Res.-Atmos., 108(D7), 8425, doi:8410.1029/2001JD001213, 2003.

Johnson, K. S., de Foy, B., Zuberi, B., Molina, L. T., Molina, M. J., Xie, Y., Laskin, A., and Shutthanandan, V.: Aerosol composition and source apportionment in the Mexico City Metropolitan Area with PIXE/PESA/STIM and multivariate analysis, Atmos. Chem. Phys., 6, 4591–4600, 2006, http://www.atmos-chem-phys.net/6/4591/2006/.

Johnson, K. S., Laskin, A., Jimenez, J. L., Shutthanandan, V., Molina, L. T., Salcedo, D., Dzepina, K., and Molina, M. J.: Comparative analysis of urban atmospheric aerosol by Proton-Induced X-ray Emission (PIXE), Proton Elastic Scattering Analysis (PESA), and Aerosol Mass Spectrometry (AMS), Environ. Sci. Technol., 42, 6619–6624, doi:10.1021/es800393e, 2008.

Khlystov, A., Zhang, Q., Jimenez, J. L., Stanier, C., Pandis, S. N., Canagaratna, M. R., Fine, P., Misra, C., and Sioutas, C.: In situ concentration of semi-volatile aerosol using water-condensation technology, J. Aerosol Sci., 36(7), 866–880, 2005.

Kleinman, L. I., Springston, S. R., Daum, P. H., Lee, Y.-N., Nunnermacker, L. J., Senum, G. I., Wang, J., Weinstein-Lloyd, J., Alexander, M. L., Hubbe, J., Ortega, J., Canagaratna, M. R., and Jayne, J.: The time evolution of aerosol composition over the Mexico City plateau, Atmos. Chem. Phys., 8, 1559–1575, 2008, http://www.atmos-chem-phys.net/8/1559/2008/.

Knighton, W. B., Fortner, E. C., Herndon, S. C., et al.: Examination of biomass burning tracer signatures in urban environments, EOS Trans. AGU. Abstract A33D-1569, Fall Meet. Suppl., 88(52), 2007.

Kondo, Y., Miyazaki, Y., Takegawa, N., Miyakawa, T., Weber, R. J., Jimenez, J. L., Zhang, Q., and Worsnop, D. R.: Oxygenated and water-soluble organic aerosols in Tokyo, J. Geophys. Res.-Atmos., 112, D01203, doi:10.1029/2006JD007056, 2007.

Kroll, J. H., Smith, J. D., Wilson, K. R., et al.: Evolution of Diesel Exhaust Aerosol in an Urban Environment, EOS T. Am. Geophys. Un., Abstract A31E-02, Fall Meet. Suppl., 2007.

Lanz, V. A., Alfarra, M. R., Baltensperger, U., Buchmann, B., Hueglin, C., and Prévôt, A. S. H.: Source apportionment of submicron organic aerosols at an urban site by factor analytical modelling of aerosol mass spectra, Atmos. Chem. Phys., 7, 1503–1522, 2007, http://www.atmos-chem-phys.net/7/1503/2007/.

Lonati, G., Ozgen, S., and Giugliano, M.: Primary and secondary carbonaceous species in PM2.5 samples in Milan (Italy), Atmos. Environ., 41(22), 4599–4610, 2007.

Madronich, S.: Chemical evolution of gaseous air pollutants downwind of tropical megacities: Mexico City case study, Atmos. Environ., 40(31), 6012–6018, 2006.

Malm, W. C., Sisler, J. F., Huffman, D., Eldred, R. A., and Cahill, T. A.: Spatial and Seasonal Trends in Particle Concentration and Optical Extinction in the United-States, J. Geophys. Res.-Atmos., 99(D1), 1347–1370, 1994.

Marley, N. A., Gaffney, J. S., Castro, T., Salcido, A., and Frederick, J.: Measurements of aerosol absorption and scattering in the Mexico City Metropolitan Area during the MILAGRO field campaign: a comparison of results from the T0 and T1 sites, Atmos. Chem. Phys., 9, 189–206, 2009, http://www.atmos-chem-phys.net/9/189/2009/.

McLafferty, F. W. and Turecek, F.: Interpretation of mass spectra, *University Science Books, Mill Valley, CA, 1993.*

Moffet, R. C., de Foy, B., Molina, L. T., Molina, M. J., and Prather, K. A.: Measurement of ambient aerosols in northern Mexico City by single particle mass spectrometry, Atmos. Chem. Phys., 8, 4499–4516, 2008a, http://www.atmos-chem-phys.net/8/4499/2008/.

Moffet, R. C., Desyaterik, Y., Hopkins, R. J., et al. Characterization of Aerosols Containing Zn, Pb, and Cl from an Industrial Region of Mexico City, Environ. Sci. Technol., 42(19), 7091–7097, 2008b.

Mohr, C., Huffman, J. A., Cubison, M. J., Aiken, A. C., Docherty, K. S., Kimmel, J. R., Ulbrich, I. M., Hannigan, M., and Jimenez, J. L.: Characterization of primary organic aerosol emissions from meat cooking, trash burning, and motor vehicles with high-resolution aersol mass spectrometry and comparison with ambient and chamber observations, Environ. Sci. Technol., 43, 2443–2449, doi:10.1021/es8011518, 2009.

Molina, L. T., Kolb, C. E., de Foy, B., Lamb, B. K., Brune, W. H., Jimenez, J. L., Ramos-Villegas, R., Sarmiento, J., Paramo-Figueroa, V. H., Cardenas, B., Gutierrez-Avedoy, V., and Molina, M. J.: Air quality in North America's most populous city – overview of the MCMA-2003 campaign, Atmos. Chem. Phys., 7, 2447–2473, 2007, http://www.atmos-chem-phys.net/7/2447/2007/.

Molina, L. T., Madronich, S., Gaffney, J. S., and Singh, H. B.: Overview of MILAGRO/INTEX-B Campaign, IGACtivities Newsletter, 38, 2–15, 2008.

Molina, L. T. and Molina, M. J.: Air quality impacts: Local and global concern, in Mexico megacity: an integrated assessment, Kluwer Academic Press, The Netherlands, 2002.

Morino, Y., Kondo, Y., Takegawa, N., et al.: Partitioning of HNO_3 and particulate nitrate over Tokyo: Effect of vertical mixing, J. Geophys. Res.-Atmos., 111, D15215, doi:10.1029/2005JD006887, 2006.

Nemitz, E., Jimenez, J. L., Huffman, J. A., Ulbrich, I. M., Canagaratna, M. R., Worsnop, D. R., and Guenther, A. B.: An eddy-covariance system for the measurement of surface/atmosphere exchange fluxes of submicron aerosol chemical species – First application above an urban area, Aerosol Sci. Tech., 42(8), 636–657, 2008.

Neuman, J. A., Nowak, J. B., Brock, C. A., et al.: Variability in ammonium nitrate formation and nitric acid depletion with altitude and location over California, J. Geophys. Res.-Atmos., 108(D17), 4557, doi:10.1029/2003JD003616, 2003.

Osborn, R. J., Taylor, N. F., Spencer, C. W., and Collins, D. R.: Isolation of ambient particles of known critical supersaturation: the differential activation separator (DAS), Aerosol Sci. Tech., 42(9), 759–772, 2008.

Paatero, P. and Tapper, U.: Positive Matrix Factorization – a Nonnegative Factor Model with Optimal Utilization of Error-Estimates of Data Values, Environmetrics, 5(2), 111–126, 1994.

Paredes-Miranda, G., Arnott, W. P., Jimenez, J. L., Aiken, A. C., Gaffney, J. S., and Marley, N. A.: Primary and secondary contributions to aerosol light scattering and absorption in Mexico City during the MILAGRO 2006 campaign, Atmos. Chem. Phys., 9, 3721–3730, 2009, http://www.atmos-chem-phys.net/9/3721/2009/.

Pope, C. A. and Dockery, D. W.: Health effects of fine particulate air pollution: Lines that connect, J. Air Waste Manage., 56(6), 709–742, 2006.

Querol, X., Pey, J., Minguillón, M. C., Pérez, N., Alastuey, A., Viana, M., Moreno, T., Bernabé, R. M., Blanco, S., Cárdenas, B., Vega, E., Sosa, G., Escalona, S., Ruiz, H., and Artíiano, B.: PM speciation and sources in Mexico during the MILAGRO-2006 Campaign, Atmos. Chem. Phys., 8, 111–128, 2008, http://www.atmos-chem-phys.net/8/111/2008/.

Salcedo, D., Onasch, T. B., Canagaratna, M. R., Dzepina, K., Huffman, J. A., Jayne, J. T., Worsnop, D. R., Kolb, C. E., Weimer, S., Drewnick, F., Allan, J. D., Delia, A. E., and Jimenez, J. L.: Technical Note: Use of a beam width probe in an Aerosol Mass Spectrometer to monitor particle collection efficiency in the field, Atmos. Chem. Phys., 7, 549–556, 2007, http://www.atmos-chem-phys.net/7/549/2007/.

Salcedo, D., Onasch, T. B., Dzepina, K., Canagaratna, M. R., Zhang, Q., Huffman, J. A., DeCarlo, P. F., Jayne, J. T., Mortimer, P., Worsnop, D. R., Kolb, C. E., Johnson, K. S., Zuberi, B., Marr, L. C., Volkamer, R., Molina, L. T., Molina, M. J., Cardenas, B., Bernabé, R. M., Márquez, C., Gaffney, J. S., Marley, N. A., Laskin, A., Shutthanandan, V., Xie, Y., Brune, W., Lesher, R., Shirley, T., and Jimenez, J. L.: Characterization of ambient aerosols in Mexico City during the MCMA-2003 campaign with Aerosol Mass Spectrometry: results from the CENICA Supersite, Atmos. Chem. Phys., 6, 925–946, 2006, http://www.atmos-chem-phys.net/6/925/2006/.

San Martini, F. M., Dunlea, E. J., Volkamer, R., Onasch, T. B., Jayne, J. T., Canagaratna, M. R., Worsnop, D. R., Kolb, C. E., Shorter, J. H., Herndon, S. C., Zahniser, M. S., Salcedo, D., Dzepina, K., Jimenez, J. L., Ortega, J. M., Johnson, K. S., McRae, G. J., Molina, L. T., and Molina, M. J.: Implementation of a Markov Chain Monte Carlo method to inorganic aerosol modeling of observations from the MCMA-2003 campaign – Part II: Model application to the CENICA, Pedregal and Santa Ana sites, Atmos. Chem. Phys., 6, 4889–4904, 2006, http://www.atmos-chem-phys.net/6/4889/2006/.

Secretaria del Medio Ambiente, G.d.D.F.: Inventario de Emisiones, http://www.sma.df.gob.mx/inventario_emisiones/, 2006.

Sinha, P., Hobbs, P. V., Yokelson, R. J., Blake, D. R., Gao, S., and Kirchstetter, T. W.: Emissions from miombo woodland and dambo grassland savanna fires, J. Geophys. Res.-Atmos., 109, D11305, doi:10.1029/2004JD004521, 2004.

Slowik, J. G., Stainken, K., Davidovits, P., et al.: Particle morphology and density characterization by combined mobility and aerodynamic diameter measurements. Part 2: Application to combustion-generated soot aerosols as a function of fuel equivalence ratio, Aerosol Sci. Tech., 38(12), 1206–1222, 2004.

Stone, E. A., Snyder, D. C., Sheesley, R. J., Sullivan, A. P., Weber, R. J., and Schauer, J. J.: Source apportionment of fine organic

aerosol in Mexico City during the MILAGRO experiment 2006, Atmos. Chem. Phys., 8, 1249–1259, 2008, http://www.atmos-chem-phys.net/8/1249/2008/.

Sueper, D.: ToF-AMS High Resolution Analysis Software – Pika, online available at: http://cires.colorado.edu/jimenez-group/ToFAMSResources/ToFSoftware/PikaInfo/, 2008.

Sullivan, A. P., Holden, A. S., Patterson, L. A., McMeeking, G. R., Kreidenweis, S. M., Malm, W. C., Hao, W. M., Wold, C. E., and Collett, J. L.: A method for smoke marker measurements and its potential application for determining the contribution of biomass burning from wildfires and prescribed fires to ambient $PM_{2.5}$ organic carbon, J. Geophys. Res.-Atmos., 113, D22302, doi:10.1029/2008JD010216, 2008.

Takegawa, N., Miyakawa, T., Kondo, Y., Jimenez, J. L., Zhang, Q., Worsnop, D. R., and Fukuda, M.: Seasonal and diurnal variations of submicron organic aerosol in Tokyo observed using the Aerodyne aerosol mass spectrometer, J. Geophys. Res.-Atmos., 111, D11206, doi:10.1029/2005JD006515, 2006.

Takegawa, N., Miyazaki, Y., Kondo, Y., et al. Characterization of an Aerodyne Aerosol Mass Spectrometer (AMS): Intercomparison with other aerosol instruments, Aerosol Sci Tech., 39(8), 760–770, 2005.

Turpin, B. J. and Lim, H. J.: Species contributions to PM2.5 mass concentrations: Revisiting common assumptions for estimating organic mass, Aerosol Sci. Tech., 35(1), 602–610, 2001.

Ulbrich, I. M., Canagaratna, M. R., Zhang, Q., Worsnop, D. R., and Jimenez, J. L.: Interpretation of organic components from Positive Matrix Factorization of aerosol mass spectrometric data, Atmos. Chem. Phys., 9, 2891–2918, 2009, http://www.atmos-chem-phys.net/9/2891/2009/.

Volkamer, R., Etzkorn, T., Geyer, A., and Platt, U.: Correction of the oxygen interference with UV spectroscopic (DOAS) measurements of monocyclic aromatic hydrocarbons in the atmosphere, Atmos. Environ., 32(21), 3731–3747, 1998.

Volkamer, R., Jimenez, J. L., San Martini, F., Dzepina, K., Zhang, Q., Salcedo, D., Molina, L. T., Worsnop, D. R., and Molina, M. J.: Secondary organic aerosol formation from anthropogenic air pollution: Rapid and higher than expected, Geophys Res. Lett., 33(17), L17811, doi:10.1029/2006GL026899, 2006.

Volkamer, R., Martini, F. S., Molina, L. T., Salcedo, D., Jimenez, J. L., and Molina, M. J.: A missing sink for gas-phase glyoxal in Mexico City: Formation of secondary organic aerosol, Geophys Res. Lett., 34, L19807, doi:10.1029/2007GL030752, 2007.

Volkamer, R., Molina, L. T., Molina, M. J., Shirley, T., and Brune, W. H.: DOAS measurement of glyoxal as an indicator for fast VOC chemistry in urban air, Geophys Res. Lett., 32(8), L08806, doi:10.1029/2005GL022616, 2005.

Wang, S. C. and Flagan, R. C.: Scanning Electrical Mobility Spectrometer, J. Aerosol Sci., 20(8), 1485–1488, 1989.

Watson, J. G.: Visibility: Science and regulation, J. Air Waste Manage., 52(6), 628–713, 2002.

Weber, R. J., Sullivan, A. P., Peltier, R. E., et al.: A study of secondary organic aerosol formation in the anthropogenic-influenced southeastern United States, J. Geophys. Res.-Atmos., 112, D13302, doi:10.1029/2007JD008408, 2007.

Whiteman, C. D., Zhong, S., Bian, X., Fast, J. D., and Doran, J. C.: Boundary layer evolution and regional-scale diurnal circulations over the Mexico Basin and Mexican plateau, J. Geophys. Res.-Atmos., 105(D8), 10081–10102, 2000.

Yokelson, R. J., Crounse, J. D., DeCarlo, P. F., Karl, T., Urbanski, S., Atlas, E., Campos, T., Shinozuka, Y., Kapustin, V., Clarke, A. D., Weinheimer, A., Knapp, D. J., Montzka, D. D., Holloway, J., Weibring, P., Flocke, F., Zheng, W., Toohey, D., Wennberg, P. O., Wiedinmyer, C., Mauldin, L., Fried, A., Richter, D., Walega, J., Jimenez, J. L., Adachi, K., Buseck, P. R., Hall, S. R., and Shetter, R.: Emissions from biomass burning in the Yucatan, Atmos. Chem. Phys., 9, 5785–5812, 2009, http://www.atmos-chem-phys.net/9/5785/2009/.

Yokelson, R. J., Urbanski, S. P., Atlas, E. L., Toohey, D. W., Alvarado, E. C., Crounse, J. D., Wennberg, P. O., Fisher, M. E., Wold, C. E., Campos, T. L., Adachi, K., Buseck, P. R., and Hao, W. M.: Emissions from forest fires near Mexico City, Atmos. Chem. Phys., 7, 5569–5584, 2007, http://www.atmos-chem-phys.net/7/5569/2007/.

Yu, J. Z., Cocker, D. R., Griffin, R. J., Flagan, R. C., and Seinfeld, J. H.: Gas-phase ozone oxidation of monoterpenes: Gaseous and particulate products, J. Atmos. Chem., 34(2), 207–258, 1999.

Zavala, M., Herndon, S. C., Wood, E. C., Onasch, T. B., Knighton, W. B., Marr, L. C., Kolb, C. E., and Molina, L. T.: Evaluation of mobile emissions contributions to Mexico City's emissions inventory using on-road and cross-road emission measurements and ambient data, Atmos. Chem. Phys., 9, 6305–6317, 2009, http://www.atmos-chem-phys.net/9/6305/2009/.

Zhang, Q., Alfarra, M. R., Worsnop, D. R., Allan, J. D., Coe, H., Canagaratna, M. R., and Jimenez, J. L.: Deconvolution and quantification of hydrocarbon-like and oxygenated organic aerosols based on aerosol mass spectrometry, Environ. Sci. Technol., 39(13), 4938–4952, 2005a.

Zhang, Q., Canagaratna, M. R., Jayne, J. T., Worsnop, D. R., and Jimenez, J. L.: Time- and size-resolved chemical composition of submicron particles in Pittsburgh: Implications for aerosol sources and processes, J. Geophys. Res.-Atmos., 110, D07S09, doi:10.1029/2004JD004649, 2005b.

Zhang, Q., Jimenez, J. L., Canagaratna, M. R., et al.: Ubiquity and Dominance of Oxygenated Species in Organic Aerosols in Anthropogenically – Influenced Northern Hemisphere Mid-latitudes, Geophys. Res. Lett., 34(13), L13801, doi:10.1029/2007GL029979, 2007a.

Zhang, Q., Jimenez, J. L., Worsnop, D. R., and Canagaratna, M.: A case study of urban particle acidity and its influence on secondary organic aerosol, Environ. Sci. Technol., 41(9), 3213–3219, 2007b.

Zhang, Q., Worsnop, D. R., Canagaratna, M. R., and Jimenez, J. L.: Hydrocarbon-like and oxygenated organic aerosols in Pittsburgh: insights into sources and processes of organic aerosols, Atmos. Chem. Phys., 5, 3289–3311, 2005c, http://www.atmos-chem-phys.net/5/3289/2005/.

Zhao, J. and Zhang, R. Y.: Proton transfer reaction rate constants between hydronium ion ($H_3O(+)$) and volatile organic compounds, Atmos. Environ., 38, 2177–2185, doi:10.1016/j.atmosenv.2004.01.019, 2004.

Zheng, J., Zhang, R., Fortner, E. C., Volkamer, R. M., Molina, L., Aiken, A. C., Jimenez, J. L., Gaeggeler, K., Dommen, J., Dusanter, S., Stevens, P. S., and Tie, X.: Measurements of HNO_3 and N_2O_5 using ion drift-chemical ionization mass spectrometry during the MILAGRO/MCMA-2006 campaign, Atmos. Chem. Phys., 8, 6823–6838, 2008, http://www.atmos-chem-phys.net/8/6823/2008/.

Atmos. Chem. Phys., 10, 8697–8760, 2010
www.atmos-chem-phys.net/10/8697/2010/
doi:10.5194/acp-10-8697-2010

Atmospheric Chemistry and Physics

An overview of the MILAGRO 2006 Campaign: Mexico City emissions and their transport and transformation

L. T. Molina[1], S. Madronich[2], J. S. Gaffney[3], E. Apel[2], B. de Foy[4], J. Fast[5], R. Ferrare[6], S. Herndon[7], J. L. Jimenez[8], B. Lamb[9], A. R. Osornio-Vargas[10], P. Russell[11], J. J. Schauer[12], P. S. Stevens[13], R. Volkamer[8], and M. Zavala[1]

[1]Molina Center for Energy and the Environment, California, and Massachusetts Institute of Technology, Cambridge, Massachusetts, USA
[2]National Center for Atmospheric Research, Boulder, Colorado, USA
[3]University of Arkansas at Little Rock, Little Rock, Arkansas, USA
[4]Saint Louis University, St. Louis, Missouri, USA
[5]Pacific Northwest National Laboratory, Richland, Washington, USA
[6]National Aeronautics and Space Administration, Langley Research Center, Hampton, VA, USA
[7]Aerodyne Research Inc., Billerica, Massachusetts, USA
[8]Cooperative Institute for Research in the Environmental Sciences (CIRES) and University of Colorado at Boulder, Boulder, Colorado, USA
[9]Washington State University, Pullman, Washington, USA
[10]Instituto Nacional de Cancerología and Universidad Nacional Autónoma de México, México
[11]NASA Ames Research Center, Moffett Field, California, USA
[12]University of Wisconsin-Madison, Madison, Wisconsin, USA
[13]Indiana University, Bloomington, Indiana, USA

Received: 10 March 2010 – Published in Atmos. Chem. Phys. Discuss.: 25 March 2010
Revised: 30 July 2010 – Accepted: 11 August 2010 – Published: 16 September 2010

Abstract. MILAGRO (Megacity Initiative: Local And Global Research Observations) is an international collaborative project to examine the behavior and the export of atmospheric emissions from a megacity. The Mexico City Metropolitan Area (MCMA) – one of the world's largest megacities and North America's most populous city – was selected as the case study to characterize the sources, concentrations, transport, and transformation processes of the gases and fine particles emitted to the MCMA atmosphere and to evaluate the regional and global impacts of these emissions. The findings of this study are relevant to the evolution and impacts of pollution from many other megacities.

The measurement phase consisted of a month-long series of carefully coordinated observations of the chemistry and physics of the atmosphere in and near Mexico City during March 2006, using a wide range of instruments at ground sites, on aircraft and satellites, and enlisting over 450 scientists from 150 institutions in 30 countries. Three ground supersites were set up to examine the evolution of the primary emitted gases and fine particles. Additional platforms in or near Mexico City included mobile vans containing scientific laboratories and mobile and stationary upward-looking lidars. Seven instrumented research aircraft provided information about the atmosphere over a large region and at various altitudes. Satellite-based instruments peered down into the atmosphere, providing even larger geographical coverage. The overall campaign was complemented by meteorological forecasting and numerical simulations, satellite observations and surface networks. Together, these research observations have provided the most comprehensive characterization of the MCMA's urban and regional atmospheric composition and chemistry that will take years to analyze and evaluate fully.

Correspondence to: L. T. Molina
(ltmolina@mit.edu)

Published by Copernicus Publications on behalf of the European Geosciences Union.

In this paper we review over 120 papers resulting from the MILAGRO/INTEX-B Campaign that have been published or submitted, as well as relevant papers from the earlier MCMA-2003 Campaign, with the aim of providing a road map for the scientific community interested in understanding the emissions from a megacity such as the MCMA and their impacts on air quality and climate.

This paper describes the measurements performed during MILAGRO and the results obtained on MCMA's atmospheric meteorology and dynamics, emissions of gases and fine particles, sources and concentrations of volatile organic compounds, urban and regional photochemistry, ambient particulate matter, aerosol radiative properties, urban plume characterization, and health studies. A summary of key findings from the field study is presented.

1 Introduction

The world's population is projected to increase 33% during the next three decades to 8.1 billion. Nearly all of the projected growth is expected to be concentrated in urban centers. Rapidly expanding urban areas and their surrounding suburbs are feeding to the phenomenon of megacities (metropolitan areas with populations exceeding 10 million inhabitants). Well planned and governed, densely populated settlements can reduce the need for land conversion and provide proximity to infrastructure and services. However, many urban areas experience uncontrolled growth leading to urban sprawl, a leading cause of environmental problems. These mega-centers of human population lead to increasing demands for energy, and industrial activity and transportation, all of which result in enhanced, concentrated atmospheric emissions of gases and particulate matter (PM) that impact air quality and climate. Air pollution and climate change are among the most important environmental challenges of this century. This challenge is particularly acute in the developing world where the rapid growth of megacities is producing atmospheric emissions of unprecedented severity and extent (Molina and Molina, 2004; Molina et al., 2004; Lawrence et al., 2007; Gurjar et al., 2008).

There is growing recognition that airborne emissions from major urban and industrial areas influence both air quality and climate on scales ranging from regional to continental and global (Molina and Molina, 2002; Molina et al., 2004; Lawrence et al., 2007; Parrish et al., 2009a). Urban/industrial emissions from the developed world, and increasingly from the megacities of the developing world, change the chemical content of the downwind troposphere in a number of fundamental ways. Emissions of nitrogen oxides (NO_x), carbon monoxide (CO) and volatile organic compounds (VOCs) drive the formation of photochemical smog and its associated oxidants, degrading air quality and threatening both human and ecosystem health and agricultural productivity. On a larger scale, these same emissions drive the production of ozone (a powerful greenhouse gas) in the free troposphere, contributing substantially to global warming. Urban and industrial areas are also major sources of the important directly forcing greenhouse gases, including carbon dioxide (CO_2), methane (CH_4), nitrous oxide (N_2O) and halocarbons, as well as other radiatively important species that contribute to climate change. Nitrogen oxide and sulfur dioxide emissions are also processed to strong acids by atmospheric photochemistry on regional to continental scales, driving acid deposition to sensitive ecosystems. Direct urban/industrial emissions of carbonaceous aerosol particles are compounded by the emission of high levels of secondary aerosol precursors, including: NO_x, VOCs, SO_2, and NH_3, resulting in the production of copious amounts of fine aerosol, affecting the urban source areas and air quality, atmospheric radiation, cloud microphysical properties, and precipitation hundreds to thousands of kilometers downwind.

The geographic redistribution of urban emissions, the evolution of their chemical, physical, and optical properties, the interaction with clouds, and the mechanisms for their eventual removal from the atmosphere are very complex and obviously important, yet only partly understood at the present time.

MILAGRO (Megacity Initiative: Local And Global Research Observations) is an international collaborative project to examine the properties, evolution, and export of atmospheric emissions generated in a megacity. The Mexico City Metropolitan Area (MCMA) – one of the world's largest megacities and North America's most populous city – was selected as the case study to characterize the sources and processes of emissions from the urban center and to evaluate the regional and global impacts of the Mexico City emissions.

MILAGRO is organized under four coordinated components (MCMA-2006, MAX-Mex, MIRAGE-Mex and INTEX-B) that took place simultaneously during March 2006 and involved the participation of more than 150 institutions from Mexico, the United States and Europe and over 450 investigators and technicians representing 30 different nationalities. The measurement campaign was sponsored by the US National Science Foundation (NSF), Department of Energy (DOE), and National Aeronautic and Space Administration (NASA), and by many Mexican agencies, including the Mexican Ministry of the Environment (SEMARNAT), the Metropolitan Environmental Commission of the Valley of Mexico (CAM), *Consejo Nacional de Ciencia y Technología* (CONACyT) and *Petróleos Mexicanos* (PEMEX).

This paper provides an overview of the MILAGRO Campaign in Mexico City and is divided into 9 sections covering the following topics: scope of the MILAGRO Campaign (Sect. 3); meteorology and dynamics (Sect. 4), MCMA emissions of gases and fine particulate matter (Sect. 5); volatile organic compound sources and concentrations (Sect. 6); urban and regional photochemistry (Sect. 7); ambient particulate matter (Sect. 8); aerosol optical properties and radiative

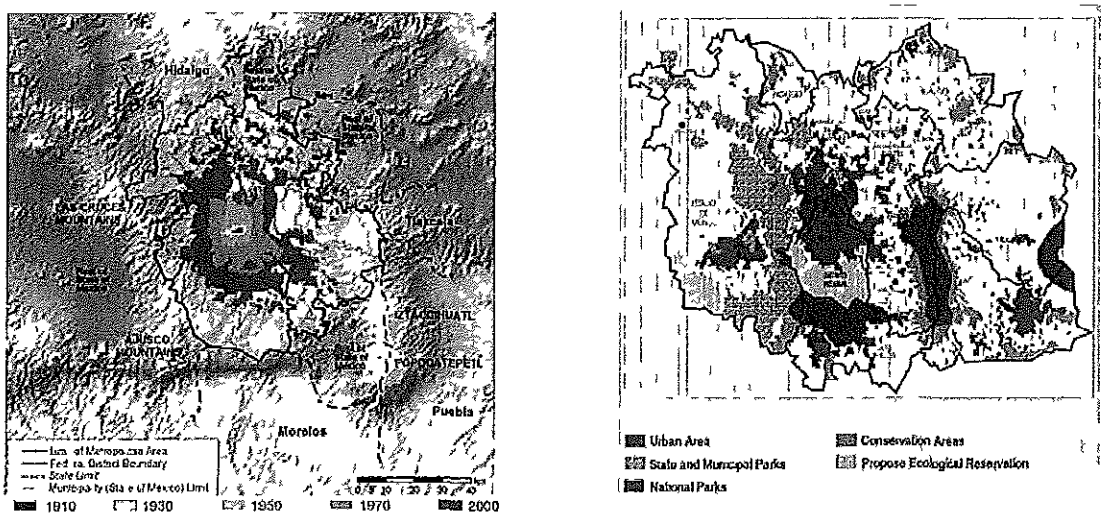

Fig. 1. Left Panel: topographical map of the MCMA; Right Panel Megalopolis in the year 2000 (from Molina and Molina, 2002)

influences (Sect. 9); regional plume from INTEX-B flights over Mexico City and the Gulf (Sect. 10); and health studies (Sect. 11). A summary of key findings is presented in Sect. 12; while some directions for future research are presented in Sect. 13. A list of acronyms is provided in Appendix A.

2 Air quality in the Mexico Megacity

The MCMA lies in an elevated basin 2240 m above sea level. The basin is surrounded on three sides by mountain ridges, but with a broad opening to the north and a narrower gap to the south-southwest. Figure 1a shows the topographical map of the MCMA. During the twentieth century the MCMA experienced huge increases in population and urbanized area as it attracted migrants from other parts of the country and industrialization stimulated economic growth. The population grew from fewer than 3 million in 1950 to over 18 million in 2000; the urbanized area now covers about 1500 km^2 – about 10 times as much land as it occupied just 50 years ago. The expansion of the MCMA is not unique in the region; the neighboring metropolitan areas (Puebla, Tlaxcala, Cuernavaca, Pachuca, and Toluca) are also extending their territories. This multiple expansion has produced a contiguous urban complex known as the Mexico "Megalopolis," which extends beyond the MCMA to include the surrounding "corona" or "crown" of cities including Puebla, Tlaxcala, Cuernavaca, Cuautla, Pachuca, and Toluca, extending 75–150 km from the city center with an estimated population of about 30 million (see Fig. 1b) The growth of the Megalopolis will clearly have important consequences for energy use and the regional ecology and environment (Lezama et al., 2002).

The MCMA's nearly 20 million inhabitants, over 40 000 industries and 4 million vehicles consume more than 40 million liters of petroleum fuels per day and produce thousands of tons of pollutants. The high altitude and tropical insolation facilitate ozone production all year and contribute to the formation of secondary particulate matter. Air quality is generally worse in the winter, when rain is less common and thermal inversions are more frequent (Molina and Molina, 2002, 2004).

During the past decade, the Mexican government has made significant progress in improving air quality. Figure 2 shows the air quality trends of the MCMA; plots show the annual average concentrations for the criteria pollutants (O_3, NO_2, CO, SO_2, Pb, TSP, PM_{10} and $PM_{2.5}$) Substantial reductions in the concentrations of some criteria pollutants (such as lead, CO and SO_2) were achieved by developing and implementing comprehensive air quality management programs and improving air quality monitoring and evaluation programs (Molina et al., 2002). Despite these important gains, MCMA residents remain exposed to concentrations of airborne pollutants exceeding ambient air quality standards, especially PM and ozone, the two most important pollutants from the standpoint of public health (Evans et al., 2002).

2.1 Intensive field studies

As North America's most populated megacity, with a unique combination of meteorology, topography, population and multi-pollutant emission density, the MCMA has attracted a number of air quality field studies. The Mexico City Air Quality Research Initiative (MARI) project gathered surface and vertical profile observations of meteorology and pollutants during 1990–1994 (LANL and IMP, 1994; Streit and Guzman, 1996). The IMADA-AVER (*Investigación*

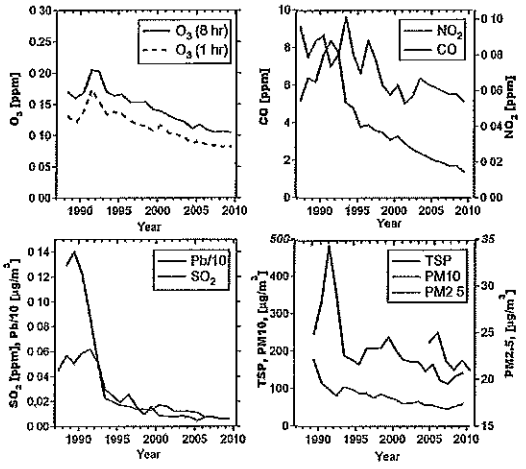

Fig. 2. Air quality trends of the MCMA. Plots show the concentrations estimated as the average of the 5th annual maximum from all stations with valid data for a given year for the following criteria pollutants: O_3, NO_2, CO, SO_2, Pb (divided by 10), TSP (Total Suspended Particles), PM_{10} and $PM_{2.5}$. (Data provided by SMA-GDF, 2009).

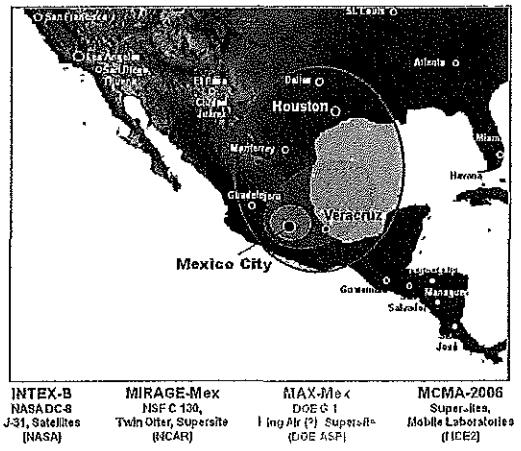

Fig. 3. MILAGRO Campaign: Geographic Coverage. Measurements were performed in the MCMA (see Fig. 4). The size of the circle (MAX-Mex, MIRAGE-Mex and INTEX-B) indicates the geographic coverage of the aircraft deployed.

sobre Materia Particulada y Deterioro Atmosférico, Aerosol and Visibility Evaluation Research) campaign in February–March 1997 yielded comprehensive meteorological measurements in the basin, and provided insights into particulate composition (IMP, 1998; Doran et al., 1998; Edgerton et al., 1999; Molina and Molina, 2002).

The MCMA-2003 measurement campaign was carried out during April 2003 to cover the height of the annual photochemical season just prior to the onset of the rainy season. It involved a highly-instrumented supersite located at the National Center for Environmental Research and Training (*Centro Nacional de Investigatión y Capcitación Ambiental*, CENICA), a component of the National Institute of Ecology (INE) of the Ministry of the Environment (SEMARNAT), with state-of-the-art instrumentation contributed by many US and European teams. A mobile laboratory from Acrodyne Research Inc. was deployed for vehicle-chase sampling measurements, as well as for fixed multi-day measurements at various locations in the MCMA. Many high time resolution instruments were deployed to the MCMA for the first time during this campaign. MCMA-2003 and an exploratory mission in February 2002 generated extensive measurements of many oxidant precursors and photochemical products and intermediates including radicals, speciated VOCs and PM, as well as meteorology and emissions. An overview of MCMA-2003 measurements has been published by Molina et al. (2007).

Observations and modeling studies from MCMA-2003 show that under most conditions, pollutant export from the basin is relatively rapid and that pollutant carryover from day to day is not a major factor in the valley's photochemistry. Emissions studies confirmed that motor vehicles play a major role in supplying the NO_x and VOC precursors that fuel MCMA's extremely active photochemistry. Key results documented in Molina et al. (2007) included a vastly improved speciated emissions inventory from on-road vehicles, showing that the MCMA motor vehicles produce abundant amounts of primary PM, elemental carbon, particle-bound polycyclic aromatic hydrocarbons, carbon monoxide and a wide range of air toxics, including formaldehyde, acetaldehyde, benzene, toluene, and xylenes. The feasibility of using eddy covariance techniques to measure fluxes of volatile organic compounds in an urban core was demonstrated, proving a valuable tool for validating the local emissions inventory. A much better understanding of the sources and atmospheric loadings of VOCs was obtained, including the first spectroscopic detection of glyoxal in the atmosphere and a unique analysis of the high fraction of ambient formaldehyde from primary emission sources. A more comprehensive characterization of ozone formation and its sensitivity to VOCs and NO_x and a much more extensive knowledge of the composition, size distribution and atmospheric mass loadings of both primary and secondary fine PM, including the fact that the rate of MCMA SOA production greatly exceeded that predicted by current atmospheric models were obtained. Intercomparisons between research grade and monitoring instruments demonstrate that significant errors can arise from standard air quality monitors for ozone and nitrogen dioxide. Comparison of aromatic hydrocarbon measurements using three different techniques highlights a potential problem in defining a VOC sampling strategy in urban environment that is meaningful for the comparison with photochemical transport models. Also, the implementation of an innovative Markov Chain Monte Carlo method for inorganic aerosol modeling provided a powerful tool to analyze aerosol data

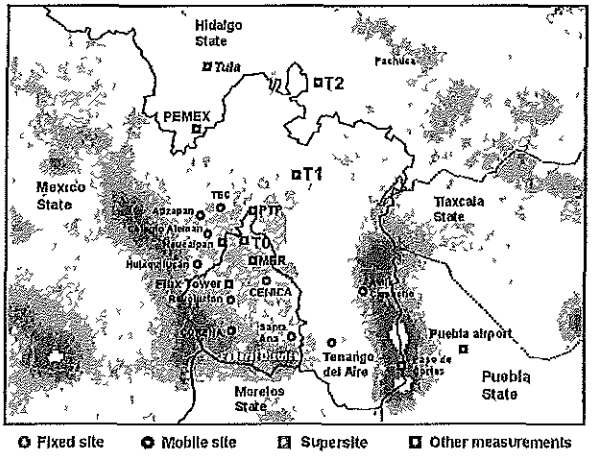

Fig. 4. MCMA-2006: Ground-Based Measurement Sites.

and predict precursor gas phase concentrations where these are unavailable. MCMA-2003 scientific findings were fundamental for the planning of the MILAGRO Campaign, the *largest MCMA-focused field study to date.*

MILAGRO's measurement phase consisted of a month-long series of carefully coordinated observations of the chemistry and physics of the atmosphere in and near Mexico City during March 2006, using a wide range of instruments at ground sites and on aircraft. MILAGRO's measurements were complemented by meteorological forecasting and numerical simulations and data from satellite observations and surface monitoring networks. Together, these research observations have provided a wealth of information on MCMA pollutant emissions and ambient concentrations, their dispersion and transformation processes, and their urban, regional and hemispheric impacts.

Results from MCMA-2003 and from MILAGRO-2006 were presented at special sessions on air quality and climate impacts of megacities at the meetings of the American Geophysical Union in 2004 and 2007 and the European Geosciences Union in 2007–2010. Major findings from the MCMA-2003 and MILAGRO-2006 have been published in two special issues of Atmospheric Chemistry and Physics (ACP) as well as in other peer-reviewed journals. A complete list of publications is available at http://mce2.org/publications.html.

3 Scope of the MILAGRO campaign

The MILAGRO Campaign is a large, international, multi-agency, collaborative project to evaluate the regional impacts of the Mexico City air pollution plume as a means of understanding urban impacts on the regional and global air quality and climate. Specific goals of the campaign included: (i) quantifying the spatial and temporal extent of the urban plume; (ii) analyzing pollutant chemical and physical transformation in the plume; (iii) quantifying the regional impacts of the plume; and (iv) examining the interaction of the urban plume with surrounding sources.

After an initial planning phase which included model simulations of possible dispersion scenarios to guide site selection, the data-collection phase of MILAGRO took place during March 2006. The measurements included a wide range of instruments at ground sites, on aircraft, and satellites. Three supersites, spaced about 30 km apart to examine the pollutant plume evolution, were set up at the Instituto Mexicano del Petróleo (IMP, "T0"), Universidad Tecnológica de Tecámac in the State of Mexico ("T1") and Rancho La Bisnaga in the State of Hidalgo ("T2"). The designations "T0" (initial time), "T1" (first time step), and "T2" (second time step) refer to the timing of transport of the urban plume to different points in space and time. Additional platforms in or near Mexico City included mobile vans containing scientific laboratories and mobile and stationary upward-looking lidars, and fixed mobile units provided by Mexican institutions located at the boundary sites to measure criteria pollutants and meteorological parameters. Tables 1–4 list the key participating institutions and instrumentation deployed at the various surface sites.

Seven instrumented research aircraft participated in MILAGRO: five were based in Veracruz, Mexico, one in Puebla, Mexico and one in Houston, Texas. The five aircraft based in Veracruz were the NCAR/NSF C-130, the DOE Gulfstream-1 (G-1), the US Forest Service Twin Otter, and the NASA J-31 and King Air, while the NASA DC-8 was based in Houston, Texas. The FZK-ENDURO Ultra-light aircraft was stationed at Hermanos Serdán Airport near Huejotzingo, Puebla (Grutter et al., 2008). The scientific payloads of the three larger aircraft are summarized in Table 5 for the C-130, Table 6 for the G-1, and Table 2a of Singh et al. (2009) for the DC-8. The J-31 carried mostly radiometric instruments used to measure aerosols, water vapor, clouds, Earth surface properties, and radiation fields (see Sect. 10 and Table 7), while the King Air carried the high spectral resolution lidar described by Rogers et al. (2009) (see Sect. 9). The Twin Otter focused its sampling on the outflow from biomass burning, with a payload that was described by Yokelson et al. (2007) and included an FTIR instrument, whole air sampling, a nephelometer, and particle sampling for subsequent analysis.

These airborne measurements provided information about the atmosphere over a large region, and at various altitudes. Satellite-based instruments peered down into the atmosphere, providing even larger geographical coverage. Figure 3 shows the geographic coverage and Fig. 4 shows the ground-based measurement sites. The overall campaign was supported by forecasts from meteorological and chemical models, satellite observations, the ambient air quality monitoring network operated by the Atmospheric Monitoring System of the Federal District (*Sistema de Monitoreo Atmosférico,* SIMAT) and meteorological measurements

Table 1. List of participating institutions and instruments deployed at the urban sites.

Institutions	Principal Investigators	Methods	Parameters	References*
T0 (IMP)				
CENICA	B. Cardenas	tethered balloon, ozonesondes, metsondes; pilot balloons with theodolites	O_3 and met parameters up to 1000 m, VOCs up to 200 m; wind speed and wind direction vertical profile	Velasco et al., 2008
CENICA; CSIC (Spain)	B. Cardenas, X. Querol	(5) mini-vol samplers; (2) HiVol, 1 RAAS and 4 mini-vol manual samplers for $PM_{2.5}$, TSP and PM_{10}; Laser spectrometer	OC, EC, thermal optical reflectance and ions in $PM_{2.5}$; metals, morphology by SEM; real time measurement of PM_{10}, $PM_{2.5}$, PM_1	Querol et al., 2008
MIT/MCE2/ UCSD/Heidelberg	L. T. Molina, R. Volkamer, U. Platt	(2) LP-DOAS; Spectroradiometer	NO_2, HONO, VOCs, glyoxal, aromatic VOCs, SO_2; UV actinic fluxes	Volkamer et al., 2007; Dusanter et al., 2009b
Texas A&M	R. Zhang	PTR-MS; CIMS;	VOCs; HNO_3;	Fortner et al., 2009; Zheng et al., 2008
Texas A&M	D. Collins	TDMA; APS; CCN separator	Hygroscopicity; aerosol supermicron size distribution; CCN properties	Wang et al., 2010
MIT/Goteborg U.	J. Pettersson, J. Noda	SPMS; AMS; Aerosol Spectrometer (portable); $PM_{2.5}$ samplers	Aerosol number, size distribution; Na, K, Rb, Cs in PM; 15 size channel count and mass distribution in 0.13–20μm range; $PM_{2.5}$	Aiken et al., 2010
ANL, UALR	J. Gaffney, N. Marley	Aethalometer (7 channel); Multi-angle Absorption Photometer; nephelometer (3 and 1 wavelengths); filter sampler	Aerosol absorption (BC); dry and wet particle scattering; OC/EC, Humic-like substances, ^{14}C, ^{40}K, ^{210}Pb, ^{7}Be, ^{210}Po, ^{210}Bi	Marley et al., 2009a, b
ANL, UALR	J. Gaffney, N. Marley	Vaisala Weather Station, radiometer	Wind speed/direction, rain, T, P, RH; broadband UV radiation	Marley et al., 2009a, b
BNL	J. Wang	CCN Counter; SMPS	CCN; aerosol size distributions	Aiken et al., 2009; Ervens et al., 2010; Wang et al., 2010
MIT/VT	L. T. Molina, L. Marr	EcoChem PAS 2000 CE; DC 2000 CE monitors	PAHs, active surface	Thornhill et al., 2008
U. Colorado	J.L. Jimenez	HR-ToF-AMS; thermal denuder; aerosol concentrator; optical particle counter; SMPS; DustTrak	Aerosol size, composition, number; nanoparticle size distribution; aerosol concentration	Aiken et al., 2008, 2009, 2010; Huffman et al., 2009; Salcedo et al., 2010; Paredes-Miranda et al., 2009;
ARI	D. Worsnop	HR-ToOF-AMS with soft ionization	fine PM organic composition	
DRI, U Nevada	P. Arnott	Photoacoustic spectrometer	Aerosol absorption	Paredes-Miranda et al., 2009
PNNL/EMSL	A. Laskin	DRUM aerosol sampler; TRAC aerosol sampler; Cascade impactor	Sampling for PIXE/PESA/STEM; TEM, SEM/EDX analysis	Johnson et al., 2005; Aiken et al., 2010

Table 1. Continued.

Institutions	Principal Investigators	Methods	Parameters	References*
PNNL	C. Doran, W. Shaw	MFRSR; Eppley B&W radiometer	radiation, aerosol optical depth	Doran et al., 2007
Colorado State U.	J. Slusser	MFRSR	UV filter irradiances (diffuse and total)	Doran et al., 2007
LANL	M. Dubey	H_2/CO/C_2H_4 Monitor	H_2, CO, C_2H_4	
Chalmers	B. Galle	3 MAX-DOAS;	Vertical and horizontal mapping of NO_2	Johansson et al., 2009
U. Alabama at Huntsville (UAH)	J. Walters	wind profiler; ceilometer; 12-channel passive microwave radiometer	Wind speed/direction versus height	Shaw et al., 2007; de Foy et al., 2009
IFU	W. Junkermann	HCHO instrument	HCHO	Dusanter et al., 2009b
UCSD	K. Prather	ATOF-MS	Single particle sice and composition	Moffet et al., 2008a
UW-Madison	J. Schauer	Filter Sampler; Semi-continuous EC/OC	Organic speciation; realtime EC/OC	Stone et al., 2008, 2010a; Aiken et al., 2009, 2010
UW-Madison	J. Schauer	Tekran Ambient Mercury Analyzer	Hg in gas and particulate phase	Rutter et al., 2009
UAM-Azcapotzalco	V. Mugica	High Vol Samplers	PM_{10}, $PM_{2.5}$	Mugica et al., 2009
U-Iowa	C. Stainier	dry-ambient aerosol size spectrometer; SMPS	aerosol water content using RH-controlled SMPS & APS	
U. Iowa	W. Eichinger	Vertically pointing lidar; H_2O/CO_2 sensor; CO monitor; T, P and humidity probes; up and down-welling long & short wave radiation; sonic anemometers	aerosol vertical profile; H_2O, CO_2, CO, T, P, RH, WS, WD, radiation	Lewandowski et al., 2010
Indiana U.	P. Stevens	Laser and supporting equipment for HO_x measurements	HO_x concentrations	Dusanter et al., 2009a
Paul Scherrer Institute	U. Baltensperger	IC-MS	Organic acids (gas & aerosol)	Zheng et al., 2008
SMA-GDF	A. Retama	commercial automatic monitors	NO_x, CO, O_3, SO_2, and PM_{10}	Molina et al., 2007
SIMAT Site				
WSU/MCE2	B. Lamb, T. Jobson L. T. Molina	Flux tower; Fast Olefin Sensor, PTR-MS, CO_2/ H_2O IRGA, met station, GC-FID for VOC flux samples	fluxes of VOCs, CO_2, H_2O,O_3, PAH; sensible and latent heat, radiation; met data: T, RH, P, WS, WD	Velasco et al., 2009, 2010
PNNL/WSU/CEH/U. Colorado	M. Alexander	Quadrupole AMS	Size-resolved composition and fluxes of speciated non-refractory PM_1 aerosols	Yu et al., 2009
UCSD/SIO	L. Russell	Submicron aerosol samples (FTIR and XRF analysis)	Organic functional groups	Gilardoni et al., 2009
UCLA	J. Stutz	LP-DOAS	O_3, NO_2, HCHO, NO_3, HONO, and SO_2	

Table 1. Continued.

Institutions	Principal Investigators	Methods	Parameters	References*
CENICA Site				
CENICA	B. Cardenas	GC-FID	55 speciated hydrocarbons	Wöhrnschimmel et al., 2010
CENICA	B. Cardenas	Commercial automatic monitors at CENICA Monitoring station for criteria pollutants and meteorological parameters	PM_{10}, $PM_{2.5}$, NOx, CO, SO_2, O_3, Total hydrocarbons, carbon in particles; UVA and UVB, WS, WD, RH, *T*	Querol et al., 2008
CENICA, CSIC (Spain)	*B. Cardenas,* X. Querol	*2 Hi-Vol for* PM_{10}	*chemical characterization* of: ions, metals, OC, EC, TC, morphology by SEM	*Querol et al., 2008;* Moreno et al., 2008b
Naucalpan Industrial Sites				
ITESM	G. Mejia	Automatic continuous measurement of particles Thermo DATA RAM, CLIMET, PARTISOL	$PM_{2.5}$, PM_{10}	
ITESM	*D. Tejeda*	*Electron microscope;* Isokinetics	*particle size and shape;* concentration of various combustion gases in stacks	
MAX-DOAS Network				
MIT/MCE2, UCSD, Heidelberg	L. T. Molina, R. Volkamer, U. Platt	5 passive multiple axis DOAS (MAX-DOAS) (at T0, T1, T2, Pico de Tres Padres, Tenango del Aire, Cerro Chiquevite)	Vertical profiles of NO_2, SO_2, HCHO, CHOCHO, O_3, HONO	
Sun Photometer Network				
MCE2/MIT, NASA Goddard	L. T. Molina, V. Martins	5 Microtops II sun photometers and 3 CIMEL AERONET (at Hidalgo, UNAM, Corena, TEC, UAM-I, T0, T1, T2)	Aerosol optical thickness, retrievals of aerosol optical parameters	Castanho et al., 2007

* The related publications where the instruments or methods have been described or mentioned.

provided by the Mexican National Weather Service (*Servicio Meteorológico Nacional,* SMN).

The MILAGRO campaign was organized under the following four coordinated components that took place simultaneously during March 2006:

3.1 The MCMA-2006 (Mexico City Metropolitan Area – 2006 Experiment)

The MCMA-2006 examined emissions and surface concentrations within the Mexico City Basin, their transport and transformation in the atmosphere, and the effects on human health. MCMA-2006 was led by the Molina Center for Energy and the Environment (MCE2) with projects sponsored by NSF, DOE, and several Mexican research agencies, including CAM, INE/SEMARNAT, CONACyT and PEMEX, as well as European agencies. The overall purpose of MCMA-2006 was to strengthen the scientific base for the design and evaluation of policies to improve the air quality in the MCMA by gathering scientific information that helps to better understand the generation and processing of pollutants in the MCMA, their dispersal, transport and transformation in the atmosphere, the exposure patterns of the population to these pollutants and the effects on human health. MCMA-2006 also provided many of the urban measurements needed for understanding the larger scale pollutant evolution which was the focus of its sister campaigns. The required data on particles, VOCs and other gases, meteorology, and solar radiation was gathered at the T0 supersite, a flux tower located at the SIMAT headquarters in the city center (referred to as "SIMAT" site thereafter), measurements at the Tula refinery site and industrial zone in Naucalpan, in combination with a

Table 2. *List of participating institutions and instruments deployed at the T1 site.*

Institutions	Principal Investigators	Methods	Parameters	References*
ANL, UALR	J. Gaffney, N. Marley	Filter Sampler; Filter Samplers for wet aerosols; Precipitation Sampler;	^{14}C, ^{40}K, ^{210}Pb, ^{7}Be, ^{210}Po, ^{210}Bi; OC/EC, Humic Like Substances; C-14, Radionuclides.	Marley et al., 2009a, b
ANL, UALR	J. Gaffney, N. Marley	Vaisala weather station; RB radiometer;	WS, WD, T, RH, precipitation rate; broadband UV radiation	Marley et al., 2009a,b
ANL, U. Alabama at Huntsville	R. Coulter, J. Walters	Radar wind profiler; radiosondes; Sodar; Micropulse lidar	Wind speed, direction vs. height; RH, T vs. height; Lower wind fields; aerosol concentration vs. height;	Doran et al., 2007, 2008; Shaw et al., 2007
CENICA, CSIC (Spain)	B. Cardenas, X. Querol	(5) minivol samplers; (2) HiVol, 1 RAAS and 4 mini-vol manual samplers for $PM_{2.5}$, TSP and PM_10	OC, EC, thermal optical reflectance and ions in $PM_{2.5}$; metals, morphology by SEM	Querol et al., 2008; Moreno et al., 2008b
CENICA	B. Cardenas, G. Solórzano	Tekran 2537[a]	Hg in gas phase	Rutter et al., 2009
DRI–Reno	P. Arnott	photoacoustic spectrometer	aerosol absorption	Doran et al., 2007
Georgia Inst. Tech.	A. Nenes, J. Smith	HTDMA,CCN counter; KSV tensiometer	hygroscopicity size resolved in 10–150 nm range; CCN concentration surface tension	Padró et al., 2010
Georgia Inst. Tech.	G. Huey	CIMS; CLD	OH, HO_2+RO_2, H_2SO_4; NO, SO_2, CO and O_3	Nunnermacker et al., 2008; Smith et al., 2008
Georgia Inst. Tech.	R. Weber	TEOM; Hi Vol	$PM_{2.5}$ mass; filter sampling	Stone et al., 2008; Padró et al., 2010
Georgia Inst. Tech.	R. Weber	PILS and inorganics	Bulk soluble organics Hennigan et al., 2008	Fountoukis et al., 2009;
IFU	W. Junkermann	HCHO instrument (Hantzsch)	HCHO	de Gouw et al., 2009
IIE, Morelos	A. Salcido, A. T. Celada	3-D sonic anemometers	WD, WS, T, RH, fluxes	de Gouw et al., 2009; Moreno et al., 2008b
LBNL (LDRD)	M. Fischer	NIR-TDLAS	NH_3	Fountoukis et al., 2009
NCAR	A. Guenther, J. Greenberg, A. Turnipseed	Continuous profiling tethered balloon system; radiometers	O_3, particles, T, WS, WD, RH, direct diffuse PAR	Greenberg et al., 2009
NCAR	Mike Coffey	mobile Fourier Transform Spectrometer	Column: H_2O, CO_2, CF_2Cl_2, HCN, N_2O, HCL, HDO, CO, $CFCl_3$, OCS, NO, HF, O3, CH4, SO_2, NO_2, C_2H_6, HNO_3, PAN, C_2H_2, CH_2O, CHF_2Cl	
NOAA, Univ Colorado	J. de Gouw. C. Warneke,	GC-FID; PIT-MS	Alkanes, alkenes; VOCs (aromatics, oxygenates, isoprene, monoterpenes, acetonitrile	de Gouw et al., 2009
Penn State	A. Thompson	Ozonesonde ground station	O_3 profile	Thompson et al., 2008

highly capable mobile laboratory, a microlight research aircraft and several fixed mobile units deployed throughout the MCMA at representative urban and boundary sites. In addition, two health studies were carried out during the campaign.

In order to contribute to the education and training of young investigators and to raise public awareness toward atmospheric pollution problems, the Molina Center, in collaboration with the Mexican National Institute of Ecology and other local institutions, set up a series of education and outreach activities, including public lectures, workshops, guided

Table 2. Continued.

Institutions	Principal Investigators	Methods	Parameters	References*
PNNL	C. Doran, W. Shaw, J. Barnard	Eppley B&W radiometers; Nephelometer; PSAP; OCEC analyzer; CPC MFRSR, pyrheliometer, solar tracker	solar radiation; aerosol size and numbers; n light scattering ; Black Carbon (aerosol absorption); OC/EC; aerosol optical depth, solar radiatio	Doran et al., 2007, 2008; Yu et al., 2009
PNNL/EMSL	A. Laskin, M. Alexander	DRUM Aerosol Sampler; TRAC Aerosol Sampler; SMPS; CCN counter	sampling for PIXE/PESA/STEM; sampling for TEM, SEM/EDX analysis; Aerosol size; CCN counter	Moffet et al., 2010
PNNL	M. Alexander	TOF-AMS	aerosol concentration and size distribution	de Gouw et al., 2009; Yu et al., 2009
RAMA	A. Retama	Mobile unit	CO, NO_x, SO_2, O_3, PM_{10}, WD, WS, T, HR	Molina et al., 2007
Texas A&M U.	Don Collins	DMA, H,V-TDMA	aerosol 0.01-1 micron size, size resolved hygroscopicity, volatility, mixing state	Wang et al., 2010
U. C. Berkeley	R. Cohen	TD-LIF	NO_2, NO_3, N_2O_5, HNO_3	Fountoukis et al., 2009
U. Houston, Colorado State U.	B. Lefer, J. Slusser	SAFS, MFRSR, UV-mfr, coud camera, Cimel	Spectral actinic flux, UV irradiances (diffuse and total)	Hennigan et al., 2008; Corr et al., 2009
U. Miami, U. C. Irvine	E. Atlas, D. Blake	VOC Canister sampling; adsorbent and filter samples	anthropogenic and biogenic HCs, $RONO_2$, MTBE, DMS, OCS, halogenated organics; nitrates	de Gouw et al., 2009
U. Minnesota/ NCAR	P. McMurray, J. Smith	TDCIMS; NTDMA; IGMA; High-vol sampler	ultrafine aerosol composition; nanoparticle size distribution, hygroscopicity and volatility; ambient ions and ion clusters; aerosol surface tension	Smith et al., 2008; Iida et al., 2008
U. Wisconsin at Madison	J Schauer	Filter samples with GC-MS and various LC, GCMS	speciated organic content	Stone et al., 2009
U. Wisconsin	J. Schauer	Tekran ambient Hg analyzer	Hg in gas and particulate phase	Rutter et al., 2009
UNAM	A. Muhlia	Pyranometer, AERONET;	spectral irradiance , aerosol optical depth,	Castanho et al., 2007
UNAM	J. Miranda	3 MiniVol	PM_{10}, $PM_{2.5}$	
UNAM	T. Castro	Moudi, nephelometer, particle soot absorption photometer, particle counters, PAH monitor, CO_2 monitor	particles (number, size, chemical composition, optical properties), PAH, CO_2	Marley et al., 2009b
UNAM	M. Moya	Filter samples	PM_1, $PM_{2.5}$	
UNAM, Euphore	G. Ruiz	HONO Long path Absorption Photometer	HONO	

*The related publications where the instruments or methods have been described or mentioned.

tours, essay and poster contests, which were carried out in parallel to the scientific activities by Mexican and international researchers working at the different measurement sites (http://mce2.org/education/milagro.html).

3.2 MAX-Mex (Megacity Aerosol Experiment: Mexico City)

Max-Mex focused on examining how the Mexico megacity aerosol evolves during transport, and how the chemical and physical nature of the aerosol affected scattering and

Table 3. List of participating institutions and instruments deployed at T2 and other sites

Institutions	Principal Investigators	Methods	Parameters	References*
T2 (Rancho La Bisnaga, Hidalgo)				
DRI, U of Nevada-Reno	P. Arnott	Photoacoustic Absorption Spectrometer	Aerosol absorption; light scattering	Paredes-Miranda et al., 2009
PNNL	C. Doran W. Shaw	PSAP, Aethalometer; Nephelometer; PSAP; OCEC analyzer; CPC	Aaerosol size and numbers; light scattering ; Black Carbon (aerosol absorption); OC/EC	Doran et al., 2007;
PNNL	C. Doran, W. Shaw, R. Coulter	Radar wind profiler; radiosondes, Sodar; weather station; radiometer, MFRSR	WS and WD vs. height; RH, T vs. height; Lower Wind fields; solar radiation; aerosol optical depth	Doran et al., 2007; Shaw et al., 2007
ANL	J. Gaffney	Aerosol sampler	Radionuclides	Marley et al., 2009a
PNNL/EMSL	A. Laskin	Time-Resolved Aerosol Collector (TRAC)	XRF, Microscopy at EMSL	Johnson et al., 2006
UNAM	A. Muhlia	Pyranometer	Solar irradiance	
CENICA, CSIC (Spain)	B. Cardenas, X. Querol	Hi-Vol, 1 RAAS and 4 mini-vol manual samplers for $PM_{2.5}$, TSP and PM_{10}	OC, EC, thermal optical reflectance and ions in $PM_{2.5}$; metals, morphology by SEM	Querol et al., 2008 Moreno et al., 2008
Popocatepetl Site				
Chalmers	B. Galle	Scanning Mini-DOAS	SO_2 Emissions from Popocatepetl	Grutter et al., 2008
UNAM	M. Grutter	Scanning imaging infrared spectrometer	Visualizing SO_2 plume from Volcano	Grutter et al., 2008
Altzomoni Site				
UNAM	D. Baumgardner, M. Grutter	FTIR; Dual-column GC; TSI scanning mobility particle sizer (SMPS); LasAir particle size; Nephlometer (1 wavelength)	CO, O_3, SO_2 PANs; condensation nuclei conc.; particle, particle scattering	Baumgardner et al., 2009
UCSD/SIO	L. Russell	Quadrupole AMS Sub-micron filter samples (off line FTIR analysis)	aerosol mass concentration; organic functional group	Gilardoni et al., 2009
Tula Industrial Complex				
IMP	A. Zambrano	Biomonitoring	PAH and metals (Cd, Cr, Cu, Hg, Ni, Pb, V, Zn)	Zambrano García et al., 2009
IMP	E. Gonzales	Moudi, Nephelometer, SMPS, Aethelometer, solar photometer	size distributions, optical properties, carbon concentration, optical depth	
IMP	E. Vega	MOUDI + Mini-vol	$PM_{2.5}$	
IMP	J. L. Arriaga	Canisters and cartridges	VOC/SVOC/Carbonyls	
IMP, Chalmers	G. Sosa, B. Galle	Mobile mini-DOAS	SO_2, NO_2 emissions	Rivera et al., 2009
IMP, CENICA	G. Sosa, H. Wöhrnschimmel	Radiosondes; pilot balloons	WD, WS, T, P, RH,	Wöhrnschimmel et al., 2010

*The related publications where the instruments or methods have been described or mentioned.

Table 4. List of participating institutions and instruments deployed in the mobile labs and mobile units.

Institutions	Principal Investigators	Methods	Parameters	References*
ARI Mobile Laboratory				
ARI	C. Kolb	ToF – AMS; SMPS; Optical Particle Counter; Condensation Particle Counter	PM Size & Composition; PM size distribution; Fine PM mass and number Density	Herndon et al., 2008; Zavala et al., 2009; Wood et al., 2009, 2010
ARI	C. Kolb	Multi-Angle Absorption Photometer (MAAP)	Fine PM BC	See above
ARI	C. Kolb	4 Quantum Cascade Tunable IR Lasers, (QC-TILDAS)	CO, NO_2, NH_3, HNO_3, HCHO	See above
ARI	C. Kolb	UV Absorption Photometer; Chemiluminescent detector; Licor non-dispersive IR	O_3 NO CO_2	See above
ARI	C. Kolb	Anemometer, RH sensor, Pres gauge, thermocouple	Wind Velocity, RH, T, P	See above
MCE2	L. T. Molina	Chemiluminescent Detector	NO_y	See above
Montana State U.	B. Knighton	PTR-MS	VOCs, selected aromatics, oxygenates, olefins, etc.	See above
EPA	R. Seila	VOC canister sampler	VOCs	See above
MCE2, VT	L. T. Molina, L. Marr	Photo-ionization aerosol counter; Diffusion Charger	PAHs; Fine PM surface area	Thornhill et al., 2009
LANL	M. Dubey	Photo-acoustic Instrument; PM filter samples	aerosol absorption & scattering; SEM images	
WSU	B. Lamb	SO_2 fluorescence	SO_2	de Foy et al., 2009b
Chalmers Mobile mini-DOAS				
Chalmers	B. Galle	Mobile Mini-DOAS instruments	SO_2, NO_2, HCHO	Johansson et al., 2009
Iowa Mobile Vertical Lidar System				
University of Iowa	W. Eichinger	mobile upward-looking lidar; Sun photometer	aerosol vertical profile; direct and indirect radiation	Lewandowski et al., 2010
Controlled Meteorological (CMET) Balloons				
Smith College, PNNL	P. Voss, R. Zaveri	Free-floating altitude-controlled balloons with T and humidity sensor	T, P, horizontal winds, relative humidity	Voss et al., 2010

absorption of atmospheric radiation. MAX-Mex was conducted by the Atmospheric Science Program of the DOE Climate Change Research Division in collaboration with scientists supported by NSF, NASA, and Mexican agencies. Measurements were conducted using an airborne lidar operated by NASA scientists with support from DOE, the DOE G-1 airborne platform that obtained gas and aerosol measurements, and also at the three supersites to examine the aerosol plume evolution. The T0 and T1 sites were heavily instrumented in order to characterize atmospheric chemical and physical properties including the scattering and absorption of radiation by particles, particularly in the sub-micrometer fractions that are anticipated to have the longest lifetimes and have the greatest impact on regional and potentially global climate forcing. Although there were fewer instruments at the T2 site, they provided information on aging of pollutant plumes further downwind.

Table 4. Continued.

Fixed Mobile Units				
Institution(s)	Location	Method	Parameters	References
INE – CENICA	Huixquilucan	Mobile unit for criteria pollutants and met. parameters	CO, NO_x, SO_2, O_3, PM_{10}, WD, WS, *T*, RH, *P*, solar radiation	Note: data from the mobile units have been used in various publications
ZMVM	T1	Mobile unit for criteria pollutants and met. parameters	CO, NO_x, SO_2, O_3, PM_{10}, WD, WS, *T*, RH, *P*	See above
Guanajuato	CORENA	Mobile unit for criteria pollutants and met. parameters	NO_x, SO_2, O_3, PM_{10}, WD, WS, *T*, RH, *P*, CH_4, NMHC, THC	See above
Hidalgo	T2	Mobile unit for criteria pollutants and met. parameters	CO, NO_x, SO_2, O_3, PM_{10}, WD, WS, *T*, RH, precipitation	See above
Estado de Mexico	Avila Camacho	Mobile unit for criteria pollutants and met. parameters	CO, NO_x, SO_2, O_3, PM_{10}, WD, WS, *T*, RH, precipitation, P, solar radiation	See above
Nuevo Leon	Santa Ana	Mobile unit for criteria pollutants and met. parameters	CO, NO_x, SO_2, O_3, PM_{10}, $PM_{2.5}$, WD, WS, *T*, RH, precipitation, *P*, solar radiation	See above
Queretaro	Atizapan	Mobile unit for criteria pollutants	CO, NO_x, SO_2, O_3, PM_{10}	See above
UNAM-CCA-FQA, INE, IMK-IFU, MCE2	Tenango del aire	Standard AQ monitors; Surface met parameters; Hantzsch (HCHO), DOAS (NO2), Ceilometer, Pilot balloons Ultra-light plane (flew around the two volcanoes)	CO, NO_x, NO_y, SO_2, O_3, WS, *T*, RH; WD HCHO; NO_2 (Column); PM_{10}, CN, dew point monitors	Melamed et al., 2009

* The related publications where the instruments or methods have been described or mentioned.

3.3 MIRAGE-Mex (Megacity Impacts on Regional and Global Environments – Mexico)

MIRAGE-Mex examined the chemical/physical transformations of gaseous and particulate pollutants exported from Mexico City, providing a case study of the effects of a megacity on regional and global atmospheric composition and climate. MIRAGE-Mex was led by the National Center for Atmospheric Research (NCAR) in collaboration with academic researchers under NSF sponsorship. Specific objectives were to: (i) quantify the spatial extent and temporal persistence of the polluted outflow plume; (ii) identify and quantify the chemical and physical transformations of the gases and aerosols in the plume, especially the processes that lead to the removal of these pollutants from the atmosphere; (iii) quantify the effects of the plume on regional oxidants and radiation budgets, and ultimately on regional climate; and (iv) examine the interactions of the urban plume with background air, as well as pollutants from other sources including regional anthropogenic pollutants, emissions from biomass fires, and biogenic emissions from vegetation. The NCAR/NSF C-130 aircraft carried a payload of state-of-the-art scientific instruments and sampled air above and at different distances from Mexico City to measure how gases and particles age during transport, specifically tracking those chemical, physical, and optical properties that have the potential to affect air quality, weather, and climate on large geographic scales. An additional aircraft (Twin Otter) conducted studies of fire emissions and their effect on the local and regional composition of the atmosphere. Other MIRAGE-Mex researchers were located at the T1 supersite, to examine the chemistry and physics of surface air as it first exits Mexico City.

Table 5. C-130 scientific payload

Parameters	Method	Principal Investigator	Detection Limit/ Response Time
Spectral Actinic flux	*SAFS*	*R. Shetter (NCAR)*	*N/A ; 1 s*
CO	VUV fluorescence	T. Campos (NCAR)	2 ppbv / 2 s
H_2O CO_2		T. Campos (NCAR)	10 ppmv, 1 s 1 ppmv, 1 s
NO NO_2 NO_y O_3	Chemiluminescence	Weinheimer (NCAR)	5 pptv, 3 s 20 pptv, 3 s 50 pptv, 1 s 200 pptv, 1 s
HO_2, $HO_2 + RO_2$	CIMS	C. Cantrell (NCAR)	variable*, 20 s
OH	CIMS	Mauldin, Eisele (NCAR)	$\sim 10^5$ cm^{-3}, 30 s
CH_2O	DFG-TDL	A. Fried (NCAR)	$\sim$ 100 pptv*, 10 s
SO_2	*Modified TECO*	*J. Holloway (NOAA)*	*500 pptv, 1 s*
VOCs, OVOCs	Fast GC-MS (TOGA)	E. Apel (NCAR)	varies by compound*, 2 min
VOCs, OVOCs	PTR-MS	T. Karl (NCAR)	var. by compd.*, 35 s
Organic trace gases	Whole Air Sampling	E. Atlas (U. Miami), D. Blake (U. California/Irvine)	var. by compd.*, variable*
PANs	CIMS	F. Flocke (NCAR)	2 pptv, 2 s
Organic acids (formic, acetic, peracetic, propanoic) H_2O_2 HCN HNO_3 $CH_3(OOH)$ SO_2 CH_3CN HO_2NO_2	CIMS	P. Wennberg (Cal. Tech.)	150 pptv, 15 s *50 pptv, 15 s* 100 pptv, 15 s 50 pptv, 15 s 50 pptv, 15 s 250 pptv, 15 s 200 pptv, 15 s 50 pptv, 15 s
Size-resolved composition of non-refractory submicron aerosols	AMS	J. Jimenez (U. Colorado)	0.05–0.35 ug/m^3, 10–30 s*
Aerosol physio-chemistry and optical properties	Tandem volatility DMA, FMPS, OPCs, nephelometer, PSAP	A. Clarke (U. Hawaii)	Variable by species*, Variable by measurement*
Aerosol physio-chemistry	DMA, Tandem DMA, HTDMA	D. Collins (Texas A&M U.)	var. by spec.*, variable by meas.*
Aerosol composition and optics	CCN, SP2, PASS, filters	L. Russell and G. Roberts (UCSD/SIO); G. Kok (DMT)	var. by spec.*, variable by meas.*
Fine particle composition	PILS	R. Weber (Georgia Tech)	var. by spec.*, variable by meas.*
Soot aerosol	transmission electron microscopy (TEM), tomography	P. Buseck (Arizona State U.)	N/A, N/A*
Aerosol lidar	SABL	Morley (NCAR)	N/A, variable*

* see archived data files for details

3.4 INTEX-B (Intercontinental Chemical Transport Experiment-B)

INTEX-B was an integrated field campaign designed to understand the transport and transformation of gases and aerosols on transcontinental/intercontinental scales and to assess their impact on air quality and climate. Central to achieving this goal was the need to relate space-based observations with those from airborne and surface platforms. Specific INTEX-B/MILAGRO objectives were to: (1) investigate the extent and persistence of the outflow of pollution from Mexico; (2) understand transport and evolution of

Table 6. Scientific payload of the G-1 aircraft.

Parameters	Method	Principal Investigator	Detection Limit/ Response Time
O_3	UV Photometry	S. R. Springston, BNL	2 ppbv/4 s,(+/−5%)
CO	VUV Fluorescence	S. R. Springston, BNL	5 ppbv/1 s (+/−5%)
SO_2	Pulsed Fluorescence	S. R. Springston, BNL	0.2 ppbv/10 s (+/−5%)
NO	O_3 Chemiluminescence	S. R. Springston, BNL	10 pptv/10 s (+/−5%)
NO_2	NO_2 Photolysis/O_3 Chemiluminescence	S. R. Springston, BNL	40 pptv/10 s (+/−5%)
NO_y	Mo Catalyst/O_3 Chemiluminescence	S. R. Springston, BNL	100 pptv/10 s (+/−5%)
H_2O_2, *HMHP*	Scrubber/Derivatization/Fluorescence	J. Weinstein-Lloyd, SUNY Old Westbury	300 pptv/1 min (+/−10%)
K^+,Mg^{++},Na^+,NH_4^+,Cl^-, NO_3^-,SO_4^{--}	PILS	Y.-N. Lee, BNL	$\sim$0.3 ug m^{-3}/3 min (+/−15%)
Particle Incandescence	Single Particle Soot Photometry	G. Senum, BNL	0.2 fg $particle^{-1}$/1 s
Aerosol Size/Composition	Aerosol Mass Spectrometry (CTOF)	E. Alexander, PNNL	TBD/15 s
VOCs	Whole Air Samples/GC-FID	J. Rudolf, York University	Varies/30 s (+/−15%)
VOCs	Proton Transfer MS	E. Alexander, PNNL	Varies/20 s (+/−35%)
Aerosol Count D_P >10 nm	CPC	J.M. Hubbe, PNNL	50% @ 10 nm/1 s
Aerosol Count D_P >3 nm	CPC	J. M. Hubbe, PNNL	50% @ 3 nm/1 s
Aerosol Count (21 bins, 16–444 nm)	Differential Mobility Analyzer	J. Wang, BNL	single particle/$\sim$60 s
N (30 bins, 0.1–3 um)	Optical Probe (PCASP X100)	G. Senum, BNL	single particle/1 s
N (20 bins, 0.6–60 um)	Optical Probe (CAPS probe, CAS)	G. Senum, BNL	single particle/1 s
N (60 bins, 25–1550 um)	Optical Probe (CAPS probe, CIP)	G. Senum, BNL	single droplet/1 s
Liquid Water Content	Hot Wire	G. Senum, BNL	0.01 g m^{-3}/1 s
Total/Back Scatter (3 wavelengths)	Nephelometry	G. Senum, BNL	2 Mm^{-1}/5 s
Aerosol Absorbance (3 wavelengths)	Filter Absorption Spectrometry	S. R. Springston, BNL	2 Mm^{-1}/8 s
Vertical Wind Velocities	200-Hz Gust Probe	G. Senum, BNL	10 cm s^{-1}/0.1 s
Turbulence	200-Hz Gust Probe	G. Senum, BNL	10^{-7} cm^2 s^{-3}/0.1 s

Complete data set, useage guidelines and meta data is available by anonymous ftp at: ftp://ftp.asd.bnl.gov/pub/ASP%20Field%20Programs/2006MAXMex/
Notes:
a) Instruments on board the G-1 also measured zenith and nadir irradiance (UV and spectrally resolved Vis/IR), winds aloft, turbulence, pressure, temperature, dew point, aircraft position and orientation.
b) These are nominal values. Detailed measurement specifications are provided in the headers along with data.

Asian pollution and implications for air quality and climate; (3) map anthropogenic and biogenic emissions and relate atmospheric composition to sources and sinks; (4) characterize effects of aerosols on solar radiation; and (5) validate spaceborne observations of tropospheric composition. INTEX-B/MILAGRO campaign was performed in two parts in the spring of 2006. In the first part, the DC-8 operated from Houston, TX with research flights over Mexico and the Gulf of Mexico (1–21 March) while the J-31 and NSF/NCAR C-130 operated from Veracruz, Mexico. In the second part, the DC-8 was based in Honolulu, HI (17–30 April) and Anchorage, AK (1–15 May) with the NSF/NCAR C-130 operating from Seattle, WA (17 April–15 May) in a coordinated fashion. An overview describing the INTEX-B DC-8 studies over

Table 7. J31 aircraft instrumentation for INTEX-B/MILAGRO.

Instrument Name	Data Products	Technique	Principal Investigator	Detection limit (Nominal accuracy)
Ames Airborne Tracking Sunphotometer (AATS)	Aerosol optical depth and extinction, water vapor column and profile	Tracking Sun photometer, 354–2138 nm	J. Redemann, BAERI/NASA ARC	Slant OD ~0.002 (±0.01) Slant WV ~0.0005 to 0.006 g cm^{-2} (±8%)
Solar Spectral Flux Radiometer (SSFR)	Solar spectral flux	Spectrometer (380–1700 nm) with nadir and zenith hemispheric collectors	P. Pilewskie, U. Colorado	Absolute accuracy 3–5%. Precision 1%
Research Scanning Polarimeter (RSP)	Polarized radiance, , aerosol cloud & Earth surface properties	Angular (along-track downward) scanning polarimeter, 412–2250 nm	B. Cairns, Columbia U.	
Cloud Absorption Radiometer (CAR)	Radiance, aerosol, cloud & Earth surface properties	Angular (cross-track zenith to nadir) scanning , radiometer 340-2301 nm	C. Gatebe, UMBC/NASA GSFC M. King*, NASA GSFC	Radiance absolute accuracy <5%.
Navigation,Meteorology, and Data Acquisition System (NavMet)	Pressure, temperature, humidity	Setra model 470 Vaisala model HMP243	W. Gore, NASA ARC	Uncertainty Pressure: ~0.2 hPa Temperature: 0.1 C RH: 0.5% +2.5%*RH(0 to 1)
Position and Orientation System (POS)	Aircraft position and orientation	Applanix model POS-AV 310	R. Dominguez, UC Santa Cruz/ NASA ARC	Precision lat/lon: 0.000001° pitch/roll/heading: 0.0001° Altitude: 1.0 m DGPS Accuracy Position: 0.5–2.0 m Pitch/roll: 0.030° Heading: 0.080° Altitude: 0.75–3.0 m

* Current affiliation U. Colorado

the Pacific and Gulf of Mexico has been published (Singh et al., 2009). Key results from the INTEX-B flights over Mexico City, as well as J-31 and C-130 flights over the Gulf of Mexico and the Mexico City area, are included in this overview article.

The MILAGRO Campaign has generated very comprehensive data and many interesting results have emerged over the past several years. The observations from MCMA-2003 Campaign were mostly confirmed during MILAGRO; additionally MILAGRO provided more detailed gas and aerosol chemistry, aerosol particle microphysics and optics, and radiation data, as well as vertical and wider regional-scale coverage. In the following sections, we present some key results and a more detailed description of the instrumentation deployed during the campaign. Data sets are available to the entire atmospheric community for further modeling and evaluation:

- MILAGRO Campaign data sets and data sharing policy are available at: http://www.data.eol.ucar.edu/master_list/?project=MILAGRO.
- High spectral resolution lidar (HSRL) data from MILAGRO are shown at: http://science.larc.nasa.gov/hsrl/milagro2.html.
- INTEX-B/MILAGRO data from the DC-8, C-130, King Air, and J-31 are archived at: http://www-air.larc.nasa.gov/cgi-bin/arcstat-b.

4 Meteorology and dynamics

4.1 Observational resources

A wide range of meteorological instrumentation was deployed at T0, T1, and T2 to measure the evolution of wind fields and boundary layer properties that affect the vertical mixing, transport, and transformation of pollutants (see Tables 1–4). As described by Doran et al. (2007), radar wind profilers at each site obtained wind speed and direction profiles up to 4 km above ground level (a.g.l.). A radar wind profiler was also deployed at Veracruz, located on the Gulf of Mexico east of Mexico City to obtain wind information aloft farther downwind of Mexico City. Several radiosondes were launched from T1 and T2 on selected aircraft sampling

days and once per day on other days to obtain temperature and humidity profiles that characterize boundary layer growth (Shaw et al., 2007). Some of these radiosondes also obtained wind profiles that extended above the height of the radar wind profilers measurements. Other radiosondes were released at T1 that obtained profiles of ozone (Thompson et al., 2008) in addition to standard meteorological parameters. Temperature and humidity profiles at T0 were obtained at 1-minute intervals up to 10 km a.g.l. from a microwave radiometer. A micro-pulse lidar and tethersondes were deployed at both T0 and T1 to obtain additional information on boundary layer properties. Semi-Lagrangian measurements of temperature, pressure, and humidity downwind of Mexico City were obtained on several days by Controlled Meteorological (CMET) balloons, also known as tetroons, launched in the vicinity of T1 (Voss et al., 2010). Pilot balloons were released four times a day from a site in the south of the city and one in the mountain gap to the south-east of the MCMA. Further releases took place at the end of the campaign to the north of the basin in conjunction with radiosonde launches (Rivera et al., 2009).

Measurements of the spatially varying wind speed, wind direction, temperature, pressure, and humidity over central Mexico were collected by the G-1 (Kleinman et al., 2008), C-130 (de Carlo et al., 2008), DC-8 (Singh et al., 2009), Twin Otter (Yokelson et al., 2007), and the FZK-ENDURO ultralight aircraft (Grutter et al., 2008). The J-31 (Livingston, et al., 2009) measured temperature, pressure, and humidity. Meteorological stations were deployed at several sites in the vicinity of Mexico City in addition to T0, T1, and T2, including CENICA and Paso de Cortes (Altzomoni) (Baumgardner et al., 2009), Tenango del Aire, Santa Ana, Pico de Tres Padres (Herndon et al., 2008), which measured near-surface wind speed, wind direction, temperature, pressure, humidity, and precipitation. Radiation and cloudiness was measured at T1 and T2 by multi-band rotating shadowband radiometers (MFRSR) and Eppley broadband radiometers (Doran et al., 2007; Fast et al., 2007). Broadband radiometers were also deployed at Paso de Cortes. At T1, all sky photos were acquired between 9 March and 1 April 2006 using a Total Sky Imager (Model #440A Yankee Environmental Systems, Inc.) with 1 min time resolution between 10:15–23:10 UT (Corr et al., 2009). Turbulence parameters were measured using sonic anemometers at T0 and at the SIMAT headquarters (Velasco et al., 2009).

Operational meteorological measurements were collected by the Mexican National Weather Service (SMN) (http://smn.cna.gob.mx/), the Ambient Air Quality Monitoring Network (*Red Automatica de Monitoreo Atmosferico*, RAMA) (http://www.sma.df.gob.mx/simat2) and the *Programa de Estaciones Meteorológicas del Bachillerato Universitario* (PEMBU) http://pembu.atmosfcu.unam.mx/. SMN collected data for the entire country with five stations in the MCMA, while RAMA had fourteen stations in the MCMA. Radiosondes with GPS were launched four times a day at 00:00, 06:00, 12:00 and 18:00 UTC at Mexico City, Veracruz and Acapulco for the duration of the field campaign. Other sites in Mexico continued with the regular, dry-season schedule of one sounding per day at 00:00 UTC.

Semi-Lagrangian measurements of temperature, pressure, and humidity downwind of Mexico City were obtained on several days by CMET balloons launched in the vicinity of T1. These balloons also tracked the long-range transport of pollutants downwind of Mexico City. During the 18–19 March outflow event, a pair of CMET balloons was launched from the north end of the MCMA basin immediately after the DOE G-1 aircraft had sampled the area. The balloons performed repeated soundings as they drifted with the outflow and helped guide the NCAR C-130 aircraft to the outflow 24 h later. The quasi-Lagrangian balloon profile data provided water vapor, potential temperature, and winds (Voss et al., 2010) and in combination with G-1 and C-130 aircraft measurements provided insight into the evolution of trace gases and aerosols over a period of 24 h (Zaveri et al., 2007).

4.2 Meteorological overview

4.2.1 Synoptic conditions

The month of March was selected for the field campaign period because of the dry, mostly sunny conditions observed over central Mexico at this time of the year (Jáuregui, 2000). Clouds and precipitation that usually increase during April would complicate aircraft sampling and scavenge a portion of the pollutants. Cluster analysis of ten years of radiosonde profiles found that synoptic conditions during March 2006 were representative of the warm dry season (de Foy et al., 2008), albeit with an under-representation of clean days and fewer wet or humid days.

As described in Fast et al. (2007), high pressure in the mid to lower troposphere slowly moved from northwestern Mexico towards the east between 1 and 8 March so that the winds over Mexico City were from the north and east. An upper-level trough propagating through the south-central US on 9 March produced westerly winds over Mexico. The winds became southwesterly between 10 and 12 March as a trough developed over the western US. After this trough moved over the north-central US on 13 March, the winds over central Mexico became light and variable. Between 14 and 18 March a series of troughs and ridges propagated from west to east across the US that affected the position of the high pressure system over the Gulf of Mexico and led to variable wind directions over central Mexico. A stronger trough propagated into the south-central US, producing stronger southwesterly winds between 19 and 20 March. After 21 March, high pressure gradually developed over southern Mexico that produced westerly winds at this level over central Mexico for the rest of the month.

Strong northerly near-surface flows associated with the passage of cold fronts over the Gulf of Mexico, known as Cold Surge or El Norte events, occurred on 14, 21, and 23 March. Although cold fronts gradually dissipate as they propagate into the subtropics, the interaction of the southward moving high-pressure systems with the terrain of the Sierra Madre Oriental often accelerates the northerly flow along the coast. While northerly winds occurred briefly over Mexico City after the passage of the fronts, the wind speeds were much lower than those observed along the coast at lower elevations.

In addition to affecting the local transport of pollutants over central Mexico, the cold fronts led to increased humidity, cloudiness, and precipitation. Enhanced mixing and removal processes likely contributed to the observed decrease in background concentrations of organic carbon at T1 (Doran et al., 2007) after the strongest cold front passed over the region on 23 March. Marley et al. (2009a) found that aerosol scattering decreased when rain was observed between 23 and 27 March since scattering aerosols are partially inorganic and hydrophilic and expected to be scavenged more readily. The increases in humidity and the morning clear-sky insolation over the plateau after 14 March were favorable for thermally-driven slope flows so that shallow and deep convective clouds developed preferentially over the highest terrain during the afternoon.

4.2.2 Local circulations

Winds measured by the operational surface monitoring network, radiosondes, and radar wind profilers were analyzed by de Foy et al. (2008) to identify dominant wind patterns in the vicinity of Mexico City. Six types of days were identified according to basin-scale circulations, providing a way for attributing meteorological effects on observed changes in trace gases and particulate matter during the field campaign, in contrast to three episode types for MCMA-2003 (de Foy et al., 2005). Well-defined drainage flows into the basin were observed every morning. Coupling with the evolving synoptic flows aloft led to near-surface convergence zones with high pollutant loadings. Days with the poorest air quality were often associated with the strongest vertical wind direction shear. In contrast, persistent southerly winds at all altitudes (e.g., 18 and 20 March) likely contributed to low pollutant concentrations in the basin. Surface wind clusters were obtained for 10 years of RAMA data, further showing that March 2006 was representative of the warm season, and enabling a comparison of transport events with specific days during MCMA-2003 and 1997 IMADA-AVER field campaigns.

4.2.3 Boundary layer characteristics

Shaw et al. (2007) describe how the radiosondes, radar wind profilers, sodars, and a micropulse lidar were used to estimate boundary layer depths, a key factor affecting near-surface concentrations and chemical transformation of trace gases and aerosols. They showed how various measurement techniques could lead to differences in the estimates of boundary layer depth. An example of convective boundary layer depth estimates during the day derived from lidar and radar wind profiler measurements is shown in Fig. 5. The onset of convection was found to start between 45 and 90 min after sunrise. Although growth of the convective boundary layer was similar among the three sites, the mixing layer was often slightly deeper over Mexico City during the afternoon. Topography variations in the vicinity of T2 did not significantly affect convective boundary layer growth. Maximum daily mixing layer depths were always at least 2 km deep, and frequently extended to 4 km a.g.l., indicating that trace gases and aerosols within the boundary layer are injected directly into the mid-troposphere in contrast to most other urban areas, since the elevation of Mexico City is ~2.2 km. The convective boundary layer growth rate and depth were found to be similar to those observed during the IMADA-AVER campaign (Doran et al., 1998) in the same season during 1997, except that the depths were somewhat higher during MILAGRO after 20:00 UTC.

Herndon et al. (2008) described the effects of convective boundary layer growth on trace gas and aerosol concentrations observed at Pico de Tres Padres. Since this measurement site was ~0.7 km above Mexico City, it sampled air within the residual layer at night that was decoupled from the shallow boundary layer over Mexico City. But concentrations of trace gases and aerosols increased considerably during the late morning as the convective boundary layer grew and enveloped the mountain, consistent with the boundary layer growth observed nearby at T0 and T1. Similarly, Baumgardner et al. (2009) report that diurnal variations in trace gases and particulate matter measured at the Paso de Cortes site were consistent with the convective boundary layer growing above the height of the site (~1.8 km above Mexico City). Boundary layer growth and transport through the mountain pass southeast of Tenango del Aire was measured using a mobile lidar, showing a shallow early morning layer with pollution accumulation, and a residual layer aloft mixing down to the surface as the flow exits the basin (Lewandowski et al., 2010).

Despite the dry conditions usually at the surface over central Mexico, radiosonde profiles showed relative humidity often exceeded 50% in the early morning in the upper boundary layer on many days. The higher relative humidity may result in hygroscopic growth in aerosols and consequently contribute to chemical transformation of aerosols and affect local radiative forcing. Fast et al. (2007) showed that boundary layer over the central plateau was substantially cooler and moister after the second cold front passage on 21 March for the rest of the field campaign, but the peak boundary layer depth did not change significantly.

4.3 Meteorological modeling studies

de Foy et al. (2009a) found that Weather Research Forecasting (WRF) mesoscale model simulations of the basin flows during MILAGRO were an improvement over MM5 simulations and showed that the simulated wind transport was representative of the basin dynamics. Nevertheless, WRF drainage flows within the basin were too weak and the predicted vertical wind shear was too strong. Particle model simulations coupled with WRF showed rapid venting of the basin atmosphere with little recirculation of the urban plume during MILAGRO, similar to previous findings from the IMADA-AVER campaign (Fast and Zhong, 1998) and MCMA-2003 (de Foy et al., 2006a, b). Doran et al. (2008) quantified the transport periods between Mexico City, T1, and T2 using assimilation of radar wind profiler measurements into WRF and a particle dispersion model to simulate transport and mixing of urban and biomass burning sources of elemental carbon. They found that specific absorption did increase as aerosols were transported between T1 and T2. The statistical significance of the result was limited by the number of transport episodes available that did not have significant open biomass burning influence.

The surface meteorological network, boundary layer measurements, and radar wind profiler measurements have also been used to examine the performance of meteorological predictions made by coupled meteorological-chemistry-particulate models, such as WRF-Chem (Fast et al., 2009; Tie et al., 2009; Zhang et al., 2009a; Hodzic et al., 2009), to understand how forecast errors in meteorology affect predictions of trace gases and particulate matter. In general, the synoptic-scale circulations are simulated reasonably well by mesoscale models, although the details (i.e., timing and strength) of local and regional winds affected by terrain variations around Mexico City are more difficult to reproduce by models. Mesoscale modeling studies (e.g., Fast et al., 2009; Hodzic et al., 2009) show that the overall diurnal variation in the simulated boundary layer depth was similar to observation; however, boundary layer parameterizations frequently produced relatively large errors during the afternoon and at night. These errors will affect predicted dilution of trace gases and aerosols. These meteorological observations have also been incorporated into meteorological modeling through data assimilation technique such as Four-Dimensional Data Assimilation (FDDA) and 3-D variational data assimilation (3D VAR) to reduce forecast errors and improve air quality prediction (Bei et al., 2010).

4.4 Meteorological transport studies

Meteorological data are being used to infer transport, mixing, and chemical transformation of pollutants. For example, Doran et al. (2007) employed trajectories based on radar wind profiler measurements to infer periods of transport between Mexico City, T1, and T2. Nocturnal and early morning buildup from local sources was inferred from organic carbon (OC) and elemental carbon (EC) at T1, while transport from the MCMA was seen at T2. Specific absorption during transport periods was lower than during other times, consistent with the likelihood of fresh emissions being found when the winds blew from Mexico City over T1 and T2. Back trajectories were employed by Moffet et al. (2009) to show that organic mass per particle increased and the fraction of carbon-carbon bonds decreased as the Mexico City plume was transported north over the T1 and T2 sites. FLEXPART Lagrangian dispersion modeling was used by several studies to investigate dispersion of SO_2, NO_2, and biomass burning aerosols, with good overall quality in the predictions (Rivera et al., 2009; Aiken et al., 2010; DeCarlo et al., 2010). Yu et al. (2009) also utilized transport categories to explain variations in OC and EC observed at T1 and T2. Melamed et al. (2009) studied the transport of the urban plume in the mountain gap southeast of the Chalco Valley using DOAS columns and surface measurements of NO_2 combined with ceilometer measurements at Tenango del Aire. In addition to the urban plume, NO_2 aloft was detected, possibly due to other factors such as biomass burning, volcanic sources or lightning NO_x. Stremme et al. (2009) measured columns of CO using solar and lunar FTIR and deduced mixing layer heights in the MCMA during both day and night. de Foy et al. (2009b) used SO_2 transport detected by surface networks and OMI satellite retrievals to identify double impacts in the MCMA from stable shallow flow from the north transporting an industrial plume and from southerly winds aloft transporting a volcanic plume.

Concentration Field Analysis (CFA) combines simulated back trajectories with measurement time series to identify potential source regions. This type of analysis was carried out to determine source-receptor relationships of various trace gases and aerosols measured at select sites. Moffet et al. (2008a) used CFA to identify possible urban, point source,

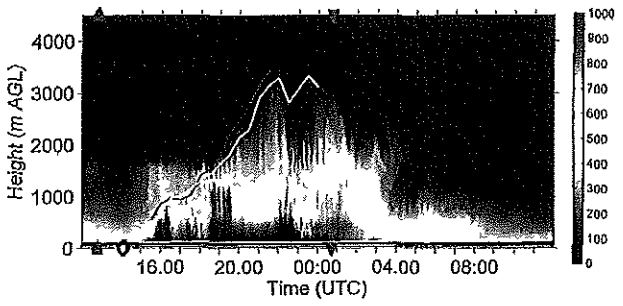

Fig. 5. Backscatter signal strength as a function height on 9 March 2006 for the lidar deployed at the T1 site. The white line denotes the subjectively determined estimate of mixed layer depth from the lidar, while the red line is the same quantity derived from the radar wind profiler. Red triangles denote sunrise and sunset (Source: Shaw et al., 2007).

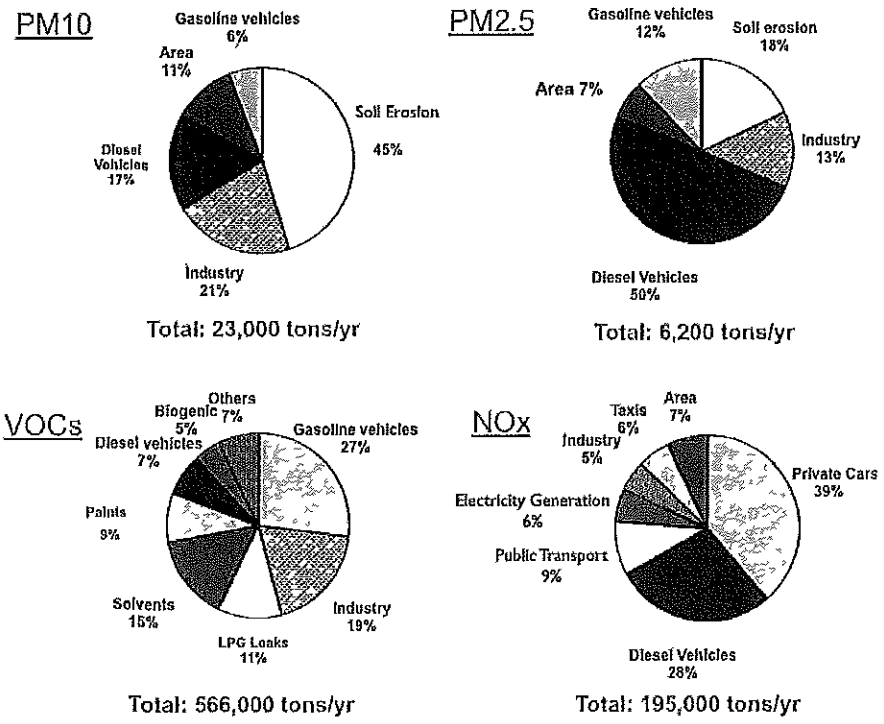

Fig. 6. Emissions Inventory of the MCMA for the year 2006 (Source. www.sma.df.gob.mx/simat).

and biomass burning sources of particulate matter measured by an aerosol time-of-flight mass spectrometry at T0. Rutter et al. (2009) identified possible source regions of gaseous and particulate mercury associated with measurements at T0 and T1. Salcedo et al. (2010) used CFA to identify sources of particulate lead at T0, and found that different chemical forms of lead had very different source footprints.

4.5 Key meteorological results and analyses

The overall synoptic and boundary layer circulations observed during MILAGRO over Mexico City were similar to those reported by previous studies. In contrast to previous field campaigns, the instrumentation at T1 and T2 and onboard the various aircraft during MILAGRO provided a means of quantifying flows over the central plateau. For example, horizontal wind shear was quantified between T0 and T1 that indicated channeling around the Sierra de Guadalupe mountains (de Foy et al., 2008), the timing of propagating density current that transports moist marine air over the central plateau into Mexico was quantified by the measurement network (Fast et al., 2007), and variations in PBL depth over the central plateau were examined (Shaw et al., 2007). The similarity of the boundary layer growth from day to day for both 1997 and 2006 suggests that the boundary layer growth over the central Mexican plateau falls within predictable bounds during the spring dry season.

Surface and airborne lidars, as well as airborne meteorological measurements have shown multiple layers of particulate matter and complex mixing processes (Rogers et al., 2009). These data have yet to be used to evaluate numerical model representations of these layering processes and determine the meteorological factors involved. Improved meteorological understanding and transport simulations are being used to analyze a large range of different measurements from MILAGRO. For example, radar wind profiler data are an invaluable supplement to surface measurements and to model results when determining transport events at the super sites. Furthermore, transport times and impact indexes are being used to relate point measurements to emission inventories and to chemical transformation processes.

5 MCMA emissions of gases and fine PM

Knowledge of gaseous and PM emissions is an important part of an informed air quality control policy. In a megacity, varying economic and social conditions make the characterization of accurate emissions inventories a difficult task; it presents a particularly daunting task in a rapidly developing megacity like the MCMA. The evaluation of bottom-up emissions inventories using dedicated field experiments represents a unique opportunity for reducing the associated uncertainties in the emissions estimates. Figure 6 shows the 2006 MCMA emissions inventory for PM_{10}, $PM_{2.5}$, VOC

and NO_x. Mobile emission sources represent a substantial fraction of the total anthropogenic emissions burden. Observations from MCMA-2003 showed that MCMA motor vehicles produce abundant amounts of primary PM, elemental carbon, particle bound polycyclic aromatic hydrocarbons, CO and a wide range of air toxics, including formaldehyde, acetaldehyde, benzene, toluene, and xylenes (Molina et al., 2007). The MILAGRO campaign has shown the synergy of using multiple measuring platforms, instrumentation, and data analysis techniques for obtaining an improved understanding of the physical and chemical characteristics of emissions in a megacity.

5.1 MCMA emissions inventories

The first emissions inventory for criteria pollutants in the MCMA was completed in 1994. The use of homogenous methodologies was introduced in the 1998 inventory and since then it has been updated every two years. The 2006 inventory (Fig. 6) includes substantial improvements in the description of spatial and temporal emission patterns of the criteria pollutants (SMA-GDF, 2008a). This emissions inventory was created using bottom-up methods and emission factors which were either measured locally or taken from the literature. For example, for mobile sources the MOBILE5 emissions model was adapted to account for local vehicle characteristics, and their emissions were distributed spatially and temporally on the basis of traffic count data for primary and secondary roadways. Emissions from area sources were estimated using geographical statistics, including population density, land use and economic level of each of the districts within the metropolitan area. Emissions from industries, workshops, and commerce and service establishments were obtained from operational permits containing information about their activities, such as processes, working hours, and location. The study region of the inventory (16 delegations in the Federal District and 59 – out of 125 – municipalities of the State of Mexico) covers a total area of about 7700 km^2 or about 0.25% of the Mexican territory. The study region was chosen to include the areas with the highest population densities in the MCMA. However, soil erosion, biomass burning and biogenic emissions are not limited to the city boundaries and their relative contributions depend on the chosen inventory area.

In addition, a 2006-base inventory of toxic pollutants for Mexico City has been produced containing emissions estimates for 109 species (mostly VOCs and metals) from various emission sources (SMA-GDF, 2008b). A greenhouse gas inventory for the emissions of CO_2, CH_4, and N_2O has also been produced for the year 2006 (SMA-GDF, 2008c). At the national level, the first comprehensive national criteria pollutant emissions inventory for the year 1999 was released in 2006 (SEMARNAT, 2006). This inventory suggests that some of the municipalities with largest emissions in the country are located within the MCMA. A new version of the national inventory with base 2005 will be released in 2010 (CEC, 2009).

All these inventories use traditional bottom-up techniques that combine activity data and emission factors for individual sources. Although locally-measured emission factors are used whenever possible, a large fraction of the inventories in Mexico are based on emissions factors compiled and emissions models constructed in the US that are adapted for local conditions (CEC, 2009). This is an important potential source of bias that campaigns such as the MILAGRO/MCMA-2006 study are poised to address.

Anthropogenic emissions dominate the total burden of pollutants in the MCMA emissions inventories for criteria and toxic compounds. As shown in Fig. 6, mobile emissions are a large fraction of the total anthropogenic emissions. In the MCMA criteria pollutant emission inventory, it is estimated that emissions from gasoline and diesel powered vehicles each contribute substantially to the total mass emissions burden for CO (83% and 16%), VOCs (27% and 7%), NO_x (54% and 28%), PM_{10}(6% and 17%), and $PM_{2.5}$(12% and 50%, respectively) (SMA-GDF, 2008a). Other important sources of VOCs are solvents and painting activities (24%), industries (19%), and LPG leaks (11%); whereas for NO_x, industries and other area sources contribute with 11% and 7%, respectively. The estimated emissions of re-suspended particles from paved and unpaved roads suggests that these sources are also important contributors for PM_{10} (51%) and $PM_{2.5}$ (16%).

Several sources of uncertainty are unavoidably present when using bottom-up techniques for the development of emissions inventories, and the MCMA inventories estimates do not escape this issue. These include the uncertainties associated with the representativeness, precision (random error), accuracy (systematic error), variability, and completeness of the databases used for estimating the activity and emissions factors (NARSTO, 2005). In addition, the combination of local conditions of meteorology, topography, altitude, unique source characteristics (e.g., fleet composition, informal commerce activities, etc.), and social practices in Mexico City may introduce further uncertainties when emission factors are obtained by using emission models that were developed and validated elsewhere. It is, therefore, very important to use independent measurement-based ("top-down") evaluations of the local emissions inventories estimates as much as possible. By implementing top-down approaches for the evaluation of emissions, it is possible to identify problems and set priorities for inventory improvements.

In the following sections we summarize the results from the application of top-down techniques in the MCMA with the analysis of data obtained during MILAGRO. Additional emissions measurements are described under Sect. 6 (VOCs) and Sect. 8 (PM).

5.2 Mobile emissions measurements

The vehicle fleet in the MCMA is diverse in both composition and age, and has recently shown a notable increase in its turnover rate. The MCMA experienced a large increase in motor vehicle use between 1996 and 2006. During this interval gasoline-powered passenger vehicle usage increased from 0.13 to 0.2 vehicle/person. Over the same period, this index in Los Angeles actually decreased from 0.36 to 0.34 vehicle/person. In part, this is due to relatively slow fleet turnover rates for older vehicle model years, but it is primary a response to the rapid introduction of newer vehicles (Zavala et al., 2009b). This is important because of the approximately four million gasoline-powered vehicles in the MCMA, more than 20% are 1990 models or older and do not have emission control technologies. About 7% of MCMA gasoline vehicles are 1991–1992 models that have 2-way catalytic converters designed to reduce CO and VOCs but not NO_x, and the rest have three-way catalytic converters that are designed to reduce all three pollutants (SMA-GDF, 2008a). In addition, diesel vehicles constitute only around 4% of the vehicle fleet, but contribute disproportionally to NO_x, PM, and selected VOCs emissions.

During MILAGRO/MCMA-2006, direct measurements of mobile emissions were obtained using the Aerodyne mobile laboratory, which contained an extensive set of sensitive, fast response (1–2 s measurement times) trace gas and fine PM instruments (Zavala et al., 2009b; Thornhill et al., 2009).These fast time response instruments were used during mobile lab transits between sites to obtain on-road vehicle emissions data (see Fig. 7). The comparison of the 2006 results to similar on-road measurements conducted during MCMA-2003 (Zavala et al., 2006) indicates some interesting trends. While the NO emission factors have remained within the measured variability ranges, emission factors of aldehyde and aromatic species were reduced in 2006 relative to 2003. The comparison with the 2006 mobile emissions inventory indicate an over-prediction of mean emissions inventory motor vehicle estimates on the order of 20–28% for CO and 14–20% for NO. However, these measurements also suggest that the emissions inventory underpredicts total VOC emissions from mobile sources by a factor of 1.4 to 1.9. For speciated VOC compounds: the inventory estimates of benzene and toluene emissions from mobile sources are within the uncertainties of the corresponding measured on-road emissions estimates. This is in contrast to the results for the aldehydes from mobile emissions. Compared to on-road measurements, the 2006 inventory underpredicts formaldehyde (HCHO) and acetaldehyde (CH_3CHO) by factors of 3 and 2, respectively (Zavala et al., 2009b).

Additional information on the chemical and physical characteristics of emissions from mobile sources has been obtained from source apportionment analysis of stationary data at T0 (Aiken et al., 2009, 2010; Paredes-Miranda et al., 2009), area-averaged emission fluxes at the SIMAT tower

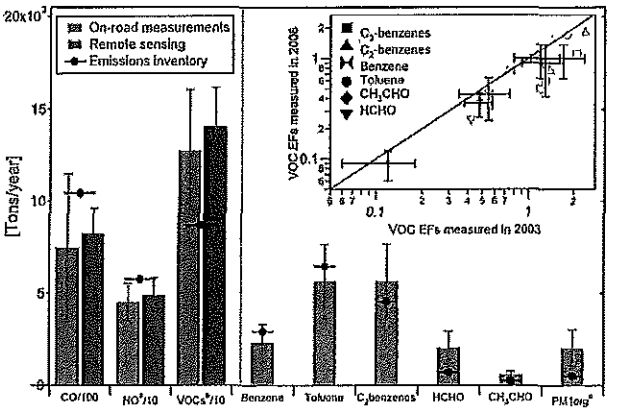

Fig. 7. Comparison among LDGV on-road mobile emissions estimated during MILAGRO, remote sensing measurements in 2006 (Schifter et al., 2008) and the mobile emissions inventories (SMA-GDF, 2008a, b). The uncertainty bars displayed are standard errors of the means. For clarity, emissions of CO, NO, and VOCs are divided by factors of 100, 10 and 10, respectively. The upper-corner inset shows a comparison of on-road VOCs fuel based emission factors (EFs, g/kg) measured in 2003 and 2006 with the ARI mobile laboratory in Mexico City for SAG (green), TRA (blue) and CRU (red) driving conditions (see Zavala et al 2009a for definitions of driving conditions). Error bars are shown for TRA driving conditions and represent one standard deviation of the measured values. Notes: [a] NO_x (expressed as NO_2) emissions in the inventory were assumed 90% NO and 10% NO_2 in mass. [b] Total VOCs emissions from the inventory include evaporative emissions. The corresponding on-road VOC's are inferred rather than measured scaling CO emissions by a remote-sensing-based VOC/CO ratio (Schifter et al., 2008). Estimated organic mass of particles in the non-refractory PM_1 range. The PM mass from the emissions inventory refers to $PM_{2.5}$.

site (Velasco et al., 2009), and aircraft measurements (Karl et al., 2009; Gilardoni et al., 2009; DeCarlo et al., 2010). Analysis of the data at T1 showed higher hydrocarbon emissions relative to CO than in the US, but similar emission ratios were found for most oxygenated VOCs and organic aerosol (de Gouw et al., 2009). Using eddy covariance techniques coupled with fast response analytical sensors, Velasco et al. (2009) showed that a representative residential district of Mexico City is a net source of CO_2, olefins, aromatics and oxygenated VOCs with substantial contributions from mobile sources (see Fig. 8). Comparisons of the measured fluxes with the emissions reported in the emissions inventory for the monitored footprint (on average 1.15 km covering an area of 7.6 km^2) indicate that the toluene and C2-benzenes (xylene isomers + ethyl-benzene) emissions from gasoline vehicles are overestimated in the inventory. In contrast, it appears that methanol is emitted by mobile sources, but is not included in the 2006 emissions inventory.

Measurements of organic mass emissions of PM_1 particles from gasoline-powered vehicles suggested a large

underprediction of $PM_{2.5}$ emissions in the inventory from on-road sources (Zavala et al., 2009b). This underprediction of PM emissions from mobile sources is consistent with the results of Positive Matrix Factorization (PMF) analysis of the high resolution organic aerosol (OA) spectra of submicron aerosol measured at T0 (Aiken et al., 2009). Components of organic aerosols derived by PMF analysis of data from several Aerodyne Aerosol Mass Spectrometer (AMS) instruments deployed both at ground sites and on research aircraft were used to evaluate the WRF-Chem model during MILAGRO (Fast et al, 2009). Modeled primary OA (POA) was consistently lower than the measured OA at the ground sites due to lack of an SOA model, whereas a much better agreement was found when modeled POA was compared with the sum of primary anthropogenic and biomass burning components derived from PMF analyses on most days.

5.3 Fixed site emissions measurements

Several studies have reported that the high concentrations of propane, butane and other low molecular weight alkanes are due to liquefied petroleum gas (LPG) leakages (e.g., Blake and Rowland, 1995; Bishop et al., 1997; Mugica et al., 1998, 2003; Velasco et al., 2007). LPG is the main fuel for cooking and water heating in Mexican households. In 2006, GC-FID and PIT-MS measurements of VOCs at T1 suggested that high alkane emissions from LPG usage may be responsible for photochemical formation of acetone (de Gouw et al., 2009). A small fraction of vehicles, particularly small buses used as public transport, are powered by LPG and also contribute to the emissions of low molecular weight alkanes (Schifter et al., 2003; Velasco et al., 2007).

The Eddy covariance flux measurements at the SIMAT tower site during MILAGRO/MCMA-2006 showed that evaporative emissions from commercial and other anthropogenic activities were also important sources of toluene, C2-benzenes and methanol (Velasco et al., 2009). Within the monitoring footprint extending several km around the site, the data show that the emissions inventory is in reasonable agreement with measured olefin and CO_2 fluxes, while C2-benzenes and toluene emissions from gasoline vehicles and evaporative sources are overestimated in the inventory for that particular sector of the city. The SIMAT tower site also included using an Aerodyne Quadrupole Aerosol Mass Spectrometer operated in eddy covariance mode (Nemitz et al., 2008) to obtain fluxes of submicron speciated aerosols by Washington State University, Univ. of Colorado, CEH-Edinburgh, and PNNL groups (see Table 1).

According to the 2006 emissions inventory (EI), about 83% of the energy consumed by the industrial sector within the MCMA is produced by natural gas. The estimated total annual emissions of SO_2 in the 2006 EI are about 7 ktons per year for the MCMA. About 7800 industries considered in the inventory as point sources contribute more than 50% of the SO_2 emissions within the MCMA. However, a current

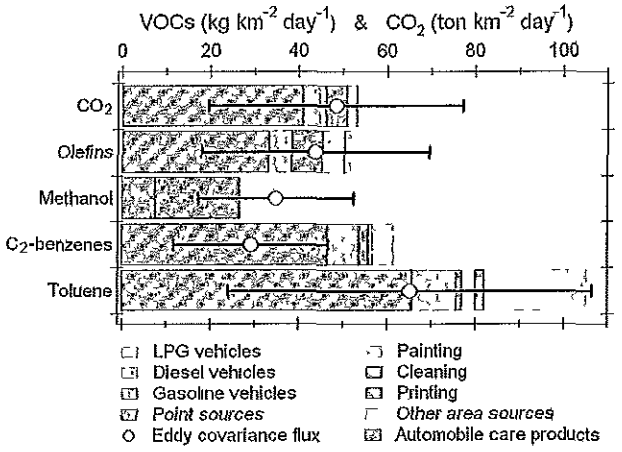

Fig. 8. Total daily measured fluxes at the SIMAT site compared to the disaggregated emissions by source type in the official 2006 emissions inventory. The emission profiles of CO_2 and 4 VOCs are included (provided by E. Velasco, 2009).

challenge is quantification of the contributions of SO_2 emissions from the Tula industrial complex, located 60 km northwest of the MCMA and not included in the inventory, to the high SO_2 levels observed in the northern part of the city, especially during the winter season (de Foy et al., 2009b). Total vertical columns of SO_2 and NO_2 were measured during plume transects in the neighborhood of the Tula industrial complex using DOAS instruments (Rivera et al., 2009). Vertical profiles of wind speed and direction obtained from pilot balloons and radiosondes were used to calculate SO_2 and NO_2 fluxes in the plume. Average emissions fluxes for SO_2 and NO_2 were estimated to be 140 ± 38 and 9 ± 3 ktons per year, respectively; the standard deviation is due to actual variations in the observed emissions from the refinery and power plant, as well as the uncertainty in the wind fields at the time of the measurements. These values are in good agreement with available datasets obtained during MCMA-2003 and with simulated trajectory plumes (de Foy et al., 2007, 2009b).

Due to its location (60 km south-east of Mexico City), the Popocatepetl volcano can contribute substantially to regional levels of SO_2, as well as subsequent sulfate particle formation and radiative scattering properties, although the high altitude of emission injection can also favor long-range transport. Therefore, it is important to understand the contributions from this source to the air quality levels at regional scales (de Foy et al., 2009b). SO_2 emissions from the Popocatépetl volcano were measured and imaged during MILAGRO using stationary scanning DOAS (Grutter et al., 2008). An average emission rate of 894 ± 507 ktons per year of SO_2 was estimated from all the daily averages obtained during the month of March 2006, with large variations in maximum and minimum daily averages of 5.97 and 0.56 Gg/day, respectively. A scanning imaging

infrared spectrometer was used for the first time for plume visualization of a specific volcanic gas, confirming observed SO_2 emission plumes through 2-D scanning. In the same study, a frequency analysis of the 48-h forward trajectories calculated from the North American Regional Reanalysis (NARR) model outputs from National Centers for Environmental Prediction (NCEP) suggests that the emissions from Popocatepetl were transported towards Puebla/Tlaxcala approximately 63% of the time during March 2006.

Christian et al. (2010) measured initial emission ratios and emission factors for trace gas and particle species from five potentially important but little-studied combustion sources: wood cooking fires, garbage burning, brick and charcoal making kilns, and crop residue burning in central Mexico during the spring of 2007, as a complementary study to the biomass burning measurements during 2006 MILAGRO (Yokelson et al., 2007). This study estimated a fine particle emission factor ($EFPM_{2.5}$) for garbage burning of $\sim 10.5 \pm 8.8$ g/kg, and a large HCl emission factors in the range 2–10 g/kg. Garbage burning $PM_{2.5}$ was found to contain levoglucosan and K in concentrations similar to those for biomass burning (BB); galactosan was the anhydrosugar most closely correlated with biomass burning species. Brick kilns produced low total $EFPM_{2.5}$ (~1.6 g/kg), but very high EC/OC ratios (6.72). The dirt charcoal kiln $EFPM_{2.5}$ was ~1.1 g/kg; some $PM_{2.5}$ may be scavenged in the walls of dirt kilns. The fuel consumption and emissions due to industrial biofuel use are difficult to characterize regionally because of the diverse range of fuels used. However, the results suggest that cooking and garbage fires can be a major source of several reactive gases and fine particles with the potential for severe local impacts on air quality. Previous study by Mugica et al. (2001) in the MCMA focused on VOCs characterized by GC-FID; it has been documented in other city that meat cooking also produces carbonyls (Ho et al., 2006) (see also Sect. 8.2).

5.4 Aircraft measurements

Aircraft measurements can serve to develop top-down constraints for the validation of emissions inventories. The spatial variability of selected VOC emissions within MCMA was evaluated during the MILAGRO field campaign for the first time by disjunct eddy covariance flux measurements of toluene and benzene from the NCAR/NSF-C-130 aircraft (Karl et al., 2009). Twelve flights were carried out at midday across the northeast section of the city where the industrial district and the airport are located. Median toluene and benzene fluxes of $14.1 \pm 4.0\,mg\,m^{-2}\,h^{-1}$ and $4.7 \pm 2.3\,mg\,m^{-2}\,h^{-1}$, respectively, were measured along these flights. For comparison the 2004 EI adjusted emission inventory used by Lei et al. (2007) estimates toluene fluxes of $10\,mg\,m^{-2}\,h^{-1}$ along the footprint of the flight-track. These flights evidenced the strong contribution of fuel evaporation and industrial sources to the toluene emissions. Karl et al. (2009) observed peak toluene to benzene flux ratios ranging from 10 to 15, with a mean ratio of 3.2 ± 0.5. The ground flux measurements at the SIMAT site reported a mean toluene to benzene flux ratio of 4.2 ± 0.5, and a ratio of 7.0 ± 1.2 during the application of a paint resin to the sidewalks near the tower by the local district city maintenance workers (Velasco et al., 2009). Using the VOC data collected during these flights and a tracer model, it was found that vehicle exhaust, industrial and evaporative sources are the major sources (>87%) of the BTEX compounds (benzene, toluene, ethylbenzene and m,p,o-xylenes) in Mexico City; in contrast to biomass burning, which contributes between 2% and 13%.

Several previous studies have found that many fires occur in and around the MCMA, particularly in the pine forests on the mountains surrounding the city, both inside and outside the basin (Bravo et al., 2002; Johnson et al., 2006; Salcedo et al., 2006). Many of these fires are of human origin and can affect air quality. During MILAGRO, an instrumented US Forest Service (USFS) Twin Otter aircraft measured the emissions from 63 fires throughout south-central Mexico (Yokelson et al., 2007). The data indicate that while the emissions of NH_3 are about average for forest burning, the emissions of NO_x and HCN per unit amount of fuel burned in the pine forests that dominate the mountains surrounding the MCMA are about 2 times higher than normally observed for forest burning. The data showed that molar emission ratios of HCN/CO for the mountain fires were 2–9 times higher than widely used literature values for biomass burning. The nitrogen enrichment in the fire emissions may be due to deposition of nitrogen containing pollutants in the outflow from the MCMA, suggesting that this effect may occur worldwide wherever biomass burning coexists with large urban area or industrial pollution sources. PM emissions from biomass burning are summarized in Sect. 8.3 below.

NASA DC-8 flights conducted around Mexico City to measure gas-phase elemental mercury (Hg) during 2006 showed highly concentrated pollution plumes (with mixing ratios as large as 500 ppqv) originating from the MCMA (Talbot et al., 2008). These high concentrations were related to combustion tracers such as CO but not SO_2 (which is emitted mainly from fuel-oil burning, refineries, and volcanoes) suggesting that widespread multi-source urban/industrial emissions may have a more important influence on Hg than specific point sources for this region.

6 Organic molecules in the atmosphere: the complexity of Mexico City Volatile Organic Compounds

Megacities, such as the MCMA, produce a complex array of emissions including hundreds of different VOCs. Measurable VOCs considered here consist primarily of non-methane hydrocarbons (NMHCs) and oxygenated volatile organic compounds (OVOCs). NMHCs have primary anthropogenic emission sources which can include evaporative,

exhaust, industrial, biogenic, liquefied petroleum gas (LPG), and biomass burning emissions. Sources of OVOCs include primary anthropogenic emissions, primary biogenic emissions, biomass burning, and secondary photochemical formation from anthropogenic, biogenic, and biomass burning sources.

An excellent summary of the knowledge about VOCs in Mexico City before MILAGRO is provided by Velasco et al. (2007). During the MILAGRO field campaign, the complexity of VOCs in the MCMA was investigated using an impressive array of state-of-science measurement methods deployed at a number of fixed ground sites and in several airborne sampling platforms. In this section, the results from these varied measurement efforts are summarized to document the distribution, magnitude, and reactivity of VOCs in the photochemical environment within and downwind of Mexico City.

6.1 Methods and sites

VOC data were obtained from near the city center at the SIMAT tower site, from the T0 urban site, the T1 downwind site, the Aerodyne mobile laboratory platform, and with canisters collected at various city locations. VOCs were measured with various real-time and sampling/post analysis techniques on the NCAR C-130, DOE G-1, NASA DC-8, and the USFS Twin Otter aircraft.

At the SIMAT tower site, VOC concentrations and fluxes – obtained via eddy covariance methods – were measured using a PTR-MS, a continuous chemiluminescent analyzer calibrated for olefin measurements (Fast Olefin Sensor, FOS) and canister samples associated with updrafts and downdrafts which were analyzed off-line by gas chromatography (GC) separation and flame ionization detection (FID) (Velasco et al., 2009). Canister samples were collected for subsequent analyses by the UC Irvine group at the T0 and T1 sites. Each sample was analyzed for more than 50 trace gases comprising hydrocarbons, halocarbons, dimethyl sulfide (DMS), and alkyl nitrates. At T0, a quadrupole PTR-MS (de Gouw and Warneke, 2007) measured 38 mass-to-charge ratios associated with VOCs including select NMHC (alkenes and aromatics), a variety of OVOCs and acetonitrile (Fortner et al., 2009). Two research grade long-path Differential Optical Absorption Spectroscopy (LP-DOAS) instruments measured numerous aromatic VOC, HCHO and glyoxal, following protocols developed in MCMA-2003 (Volkamer et al., 2005, 2010). In addition, vertical column concentrations of HCHO and glyoxal were measured by Multi-Axis DOAS (MAX-DOAS). At T1, a PTR-MS using an ion trap mass analyzer (PIT-MS) (de Gouw et al., 2009) made continuous VOC measurements of a similar but not identical subset of VOCs and a GC-MS continuously measured a wide range of NMHCs. VOC measurements were obtained by the Aerodyne mobile laboratory at various locations using a quadrupole PTR-MS and canister sampling, analyzed by the US EPA, and several Mini-MAX DOAS instruments were deployed within and near the city at various locations (see Table 1). Formaldehyde was measured continuously at the T0 and T1 sites using a commercial instrument operated by IFU (Junkermann and Burger, 2006) and with a mobile DOAS instrument to estimate HCHO city plume mass flow rates (Johannson et al., 2009). Ambient samples of 13 VOCs were also measured at CENICA site (Wöhrnschimmel et al., 2010).

Onboard the C-130, there were three techniques for VOC measurements: (i) the NCAR Trace Organic Gas Analyzer (TOGA) which is a fast GC-MS system (Apel et al., 2003, 2010); (ii) the NCAR quadrupole PTR-MS (Karl et al., 2009); and (iii) UCI canister sampling with post-flight analyses. For the TOGA instrument, 32 compounds were targeted including OVOCs (methanol, ethanol, methyl tertiary butyl ether, C2–C5 aldehydes, C2–C5 ketones), NMHC (C4–C9), and halogenated VOC compound classes and also acetonitrile. Simultaneous measurements were obtained for all compounds every 2.8 min. The PTR-MS targeted OVOCs (mass to charge ratios associated with the detection of methanol, acetaldehyde, (acetone+propanal), (MEK+butanal), acetonitrile, benzene, toluene, and C8 and C9 aromatics for analysis as well as the more polar species acetic acid and hydroxyacetone. The measurement frequency was variable but the suite of species was typically recorded each minute; during some city runs the instrument recorded benzene and toluene measurements at 1 Hz in order to obtain vertical flux profiling by eddy covariance over the MCMA. The UCI canisters were analyzed for a full range of VOCs in the C2–C10 range including NMHCs, halogens, and organic nitrates. The time resolution was limited by the number of canisters available for each flight (72). For co-measured NMHC species, the TOGA NMHCs and halogenated VOCs showed excellent agreement with the UCI canisters. Agreement between TOGA and the PTR-MS was also generally good (usually within 20%) for co-measured species but with greater overall differences than with the canister/TOGA measurements. Formaldehyde was continuously measured on the C-130 with a difference frequency generation absorption spectrometer (Weibring et al., 2007).

The DOE G-1 was equipped with a quadrupole PTR-MS that measured similar species to the NCAR PTR-MS system. A limited number of canister samples were also collected on the G-1 and analyzed for a suite of NMHCs by York University. The majority of the DOE G-1 flight hours were carried out in and around the MCMA at altitudes ranging from 2.2 to 5 km. An in-flight comparison was conducted between the G-1 PTR-MS and the C-130 TOGA and NCAR PTR-MS and the results showed good agreement for benzene but discrepancies on the order of 30% for other species (Apel et al., 2010).

The NASA DC-8 was equipped with a canister collection system operated by UCI. After transporting the canisters back to the laboratory, these were analyzed for a full

range of VOCs in the C2–C10 range including NMHCs, halogens, and organic nitrates. One hundred sixty eight canisters were available for each flight. The NASA Ames group operated PANAK (PAN-Aldehydes-Alcohols-Ketones), an in-situ three-channel gas chromatographic instrument used to measure acetone, methylethylketone, methanol, ethanol, acetaldehyde, propionaldehyde and also hydrogen cyanide and acetonitrile. Formaldehyde was continuously measured on the DC-8 aircraft using tunable diode laser spectroscopy (Fried et al., pers. comm., 2009). The DC-8 was flown out of Houston, TX with a primary objective to measure aged outflow from the MCMA although several flights sampled fresh emissions from the MCMA basin and the surrounding area.

The USFS Twin Otter was equipped with an airborne Fourier transform infrared spectrometer (AFTIR) with the primary objective of sampling biomass burning emissions within the region (Yokelson et al., 2007). Species measured included hydrogen cyanide, methane, ethene, acetylene, formaldehyde, methanol, acetic acid and formic acid. Canisters were also collected which were subsequently analyzed by the University of Miami group using GC-FID for methane, ethane, ethene, ethyne, propane, propene, isobutane, n-butane, t-2 butene, 1-butene, isobutene, c-2-butene, 1,3 butadiene, cyclopentane, isopentane, and n-pentane, with detection limits in the low pptv range. Other canisters were filled for analysis by the Forest Service Fire Sciences Laboratory by GC/FID/RGD for CO_2, CO, CH_4, H_2, and several C2–C3 hydrocarbons.

6.2 VOC emissions

During the MILAGRO campaign, direct VOC emissions measurements were obtained using (i) the Aerodyne mobile laboratory during driving traverses (Zavala et al., 2009b); (ii) a fixed site (SIMAT) flux measurement study (Velasco et al., 2009); and (iii) disjunct eddy covariance (DEC) fluxes onboard the C-130 aircraft (Karl et al., 2009). In addition, emission ratios (pptv VOC)/(ppbv CO) were obtained for a variety of compounds at the T0 and T1 sites (e.g., de Gouw et al., 2009). The flux measurements were analyzed in terms of diurnal patterns and vehicular activity and were compared with the most recent gridded local emissions inventory. The results show that the urban surface of Mexico City is a net source of VOCs with substantial contributions from vehicular traffic. The canister samples collected at the SIMAT tower site were used to calculate fluxes of selected NMHCs by the Disjunct Eddy Accumulation (DEA) technique (see Table 1) (Velasco et al., 2009). Results from the flux study aboard the C-130 aircraft indicate high toluene to benzene flux ratios above an industrial district (e.g., 10–15 g/g) including the Benito Juarez International Airport (e.g., 3–5 g/g) and a mean flux (concentration) ratio of 3.2 ± 0.5 g/g (3.9 ± 0.3 g/g) across Mexico City, which confirm an important role for evaporative fuel and industrial emissions for aromatic compounds in the basin (Karl et al., 2009). Previous indications for solvent sources have been obtained during the MCMA-2003 field campaign from comparisons between in-situ PTR-MS and GC-FID canister measurements with LP-DOAS measurements (Jobson et al., 2010). While the DOAS data agreed within 20% with both point measurements for benzene, concentrations measured by DOAS were on average a factor of 1.7 times greater than the PTRMS data for toluene, C2-alkylbenzenes, naphthalene, and styrene. The level of agreement for the toluene data was a function of wind direction, establishing that spatial gradients – horizontal, vertical, or both – in VOC mixing ratios were significant, and up to a factor of 2 despite the fact that all measurements were conducted above roof level. This analysis highlights the issue of representative sampling in an urban environment.

Spatial concentration gradients complicate the sampling of hydrocarbons and possibly other pollutants in urban areas for comparison with photochemical models (Jobson et al., 2010). More details on the VOCs measurements are provided in Sect. 4 on emissions.

6.3 VOC distributions and patterns

At the SIMAT tower site, and at both the T0 and T1 ground sites, VOC mixing ratios are quite high compared to typical levels in US cities, such as New York (Shirley et al., 2006). The low molecular weight alkanes are prevalent, with propane being the most abundant species with mean daytime mixing ratios of approximately 30 ppbv at T0 and approximately 8 ppbv at T1, which has previously been attributed to widespread use of LPG (e.g., Blake and Rowland, 1995; Velasco et al., 2007). The most important source of alkenes is believed to be vehicular emissions (Doskey et al., 1992; Altuzar et al., 2005; Velasco et al., 2005), but LPG and industrial emissions can also be important. Aromatics result from vehicle emissions but are also widely used in paints, and industrial cleaners and solvents. Aldehydes result from fossil fuel combustion and are formed in the atmosphere from the oxidation of primary NMHCs (Atkinson, 1990). Volkamer et al. (2005) measured glyoxal for the first time directly in the atmosphere during MCMA-2003. Glyoxal is mostly formed from VOC oxidation, and provides advantages over traditional tracers for VOC oxidation, as it is less affected by primary emissions. Garcia et al. (2006) used these unique tracer properties in a tracer ratio method to discern primary emissions of HCHO from photochemically produced HCHO in the MCMA. They concluded that while primary emissions dominate in the early morning, secondary HCHO is responsible for up to 80% of the ambient HCHO for most of the day.

The two most prevalent ketones, acetone and methylethylketone, are believed to have sources similar to the aromatic compounds. They exhibit strong correlation with CO. However, there is also evidence for ketone contributions from paints and solvents. Less is known about the emissions of the alcohols. Methanol is one of the most

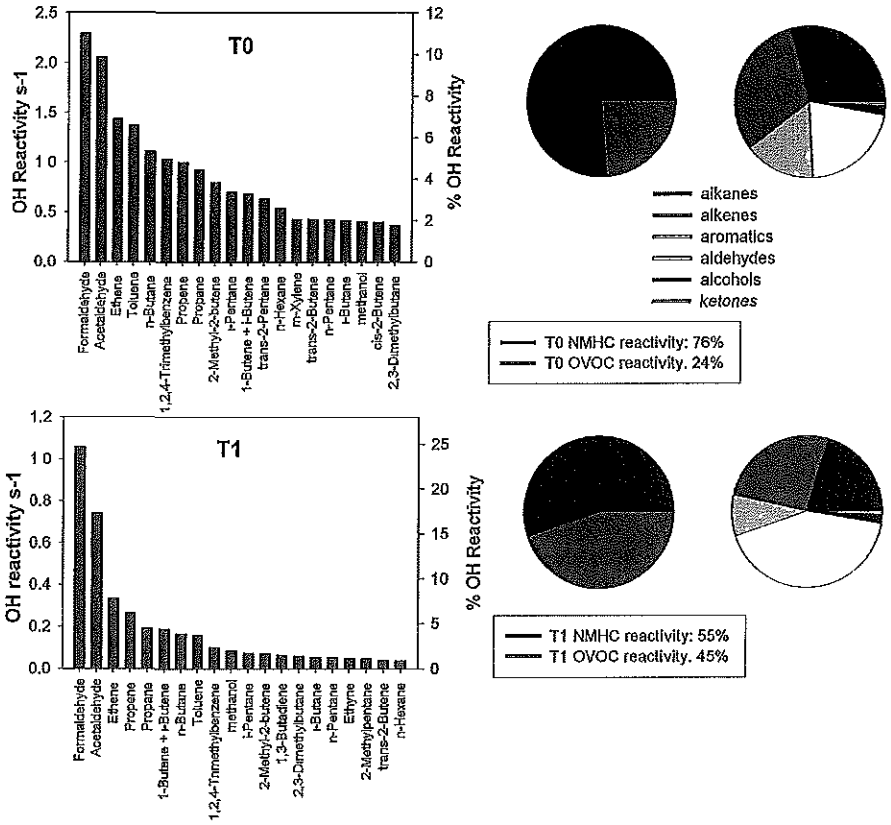

Fig. 9. The top 20 compounds measured at the supersites T0 (top panel) and T1 (bottom panel) in terms of OH reactivity between 09:00 and 18:00 local time averaged over the month of March, 2006. Shown in the first pie chart to the right of each bar graph is the breakdown for the relative contributions from NMHCs and OVOCs for T0 and T1, respectively. Shown in the second pie chart is the breakdown in terms of each compound class.

prevalent VOCs with average mixing ratios of approximately 20 ppbv at T0, 17 ppbv at the SIMAT tower site, and 4 ppbv at T1, during a season when biogenic emissions are believed to be low. During the morning rush hour at the T0 site impacted by industrial emissions and diesel fuel exhaust, methanol concentrations averaged $\cong$ 50 ppbv (Fortner et al., 2009) but no more than 20 ppbv at the SIMAT tower site located in a residential neighborhood (Velasco et al., 2009). The aldehydes are present in relatively higher amounts at T1 versus the T0 site. Biomass burning tracers measured by several investigators suggested that biomass burning is a minor source of VOCs at T0 or T1 relative to mobile and industrial emissions (e.g., de Gouw et al., 2009).

In terms of enhancement ratios, many hydrocarbon species relative to CO were higher in Mexico City than in the US (de Gouw et al., 2009; Apel et al., 2010), and similar enhancement ratios were found for most oxygenated VOCs (de Gouw et al., 2009). The higher hydrocarbon enhancement ratios in Mexico City compared to the US are due to the widespread use of LPG and higher industrial and evaporative emissions of aromatics.

Heald et al. (2008) compiled all the gas and particle phase organic measurements into the newly defined "Total Observed Organic Carbon", which had a daytime mean of 456 μgC m^{-3} at T0 and 17 μgC m^{-3} for the C-130. The T0 levels are an order-of-magnitude higher than those measured in Pittsburgh (28-45 μgC m^{-3}), while those measured in the C-130 are typical of polluted airmasses in the US sampled from aircraft. The organic aerosol PM contribution increased from ~3% of the TOOC at T0 to 9% for the C-130, due to SOA formation and the larger contribution of biomass burning to regional airmasses.

The total daytime average OH reactivity from measured VOC compounds was found to be 19.7 s^{-1} at T0 and 4.4 s^{-1} at T1 (Apel et al., 2010). The OH reactivity determined at T0 is broadly consistent with the results from the MCMA-2003 study at the CENICA supersite located approximately 7 km SE of downtown Mexico City. During MCMA-2003 Shirley et al. (2006), using the Total OH Loss Measurement instrument (TOHLM), reported an average daily OH reactivity of 33 s^{-1}, and estimated that 72% of it (~24 s^{-1}) was due to VOCs. NMHCs provide the majority of the measured daytime averaged VOC reactivity for T0 and T1 (75%

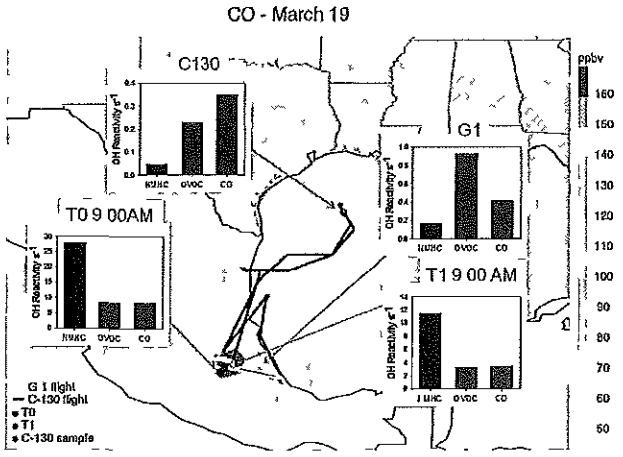

Fig. 10. MOZART depiction of the of the CO outflow from the 19 March 2006 plume. Superimposed on the plume are flight tracks from the G-1 on 18 March and from the C130 on 19 March. The G-1 intercepted the plume as it was emerging from the city during a transect that occurred between the times of 14:20 and 15:20 local time on the 18th and the C-130 which intercepted the plume on the afternoon of the 19th. The OH reactivity distributions in terms of NMHCs, OVOCs, and CO at 09:00 a.m. are shown for the T0 and T1 sites, the G-1 during the transect, and the C130 during the plume interception that occurred at the furthest point from the city.

and 56%, respectively), and OVOCs provide the remaining VOC reactivity with 25% and 44%, respectively. However, the two most important measured VOCs in terms of OH reactivity were formaldehyde and acetaldehyde. The distribution of OH reactivity among VOC classes is shown in Fig. 9. The third most important VOC was ethene which reacts relatively quickly to form formaldehyde (e.g., Wert et al., 2003) and is therefore an important contributor to secondary formaldehyde formation (Garcia et al., 2006). On-road vehicle emissions of acetaldehyde were reported by Zavala et al. (2006) who found substantial levels of this species in vehicle exhaust, although the levels were found to be lower than formaldehyde emissions by a factor of 5 to 8.

6.4 In-basin VOC chemistry

Measurements at T1 (de Gouw et al., 2009) show that diurnal variations of hydrocarbons were dominated by a high peak in the early morning when local emissions accumulated in a shallow boundary layer, and a minimum in the afternoon when the emissions were diluted in an expanded boundary layer and, in the case of reactive gases, removed by OH. In comparison, diurnal variations of species with secondary sources, such as the aldehydes and ketones, stayed relatively high in the afternoon indicating photochemical formation. Photochemical formation of acetone is important in Mexico City due to high emissions of alkane precursors, principally propane, from the widespread use of LPG. The influence of biomass burning was investigated at T1 using the measurements of acetonitrile, which was found to correlate with levoglucosan in the particle phase. Diurnal variations of acetonitrile indicate a contribution from local burning sources. Scatter plots of acetonitrile versus CO suggest that the contribution of biomass burning to the enhancement of most gas and aerosol species was not dominant and perhaps not dissimilar from observations in the US Measurements of the biomass burning influence on Mexico City and the surrounding area were made on the C-130 (Crounse et al., 2009) and the US Forest Service Twin Otter (Yokelson et al., 2007). During the measurement period, fires contributed one third of the enhancement in benzene in the outflow from the Central Mexican Plateau, and by implication, contributed to the enhancement of all VOCs that are produced in fires.

6.5 Long-range VOC transport out of the basin

Apel et al. (2010) have summarized the overall pattern of VOC measurements during MILAGRO in terms of a diurnal process associated with the daily flushing of the MCMA basin: following morning emissions from traffic, industry, cooking, etc., into a shallow boundary layer, the boundary layer deepens rapidly and air is mixed with cleaner air aloft and eventually transported downwind of the city by strong synoptic winds. Figure 10 illustrates some features of the outflow pattern. During the MIRAGE-Mex flight on 19 March, the C-130 intercepted three times an MCMA outflow plume that had been sampled a day earlier by the G-1 over the source region. This was a typical NE transport event at altitudes ranging from 3–5 km. Air was sampled that had aged between 1–2 days. The figure shows the results of a MOZART (Model for Ozone and Related chemical Tracers) simulation of the CO outflow from the plume. Superimposed on the plume are flight tracks from the G-1 on 18 March and from the C-130 on 19 March. The G-1 intercepted the plume as it was emerging from the city during a transect that occurred between 14:20 and 15:20 local time and the C-130 which intercepted the plume on the afternoon of the 19th. Also shown in the figure are the OH reactivity distributions in terms of NMHCs, OVOCs, and CO for the T0 and T1 sites at 09:00 a.m., the G-1 during the transect, and the C-130 during the plume interception that occurred at the furthest point from the city. It is interesting to note the extent of the plume into the US at 620 hPa ($\cong$ 4 km altitude). The total VOC reactivity is dominated by NMHCs in the basin in the morning with CO playing a relatively minor role compared to the VOCs. The total measured OH+VOC reactivity at 09:00 a.m. at T0 is 50 s^{-1} and 14 s^{-1} at T1. A large part of the OH reactivity is provided by alkenes and aromatics (50% of total VOC-OH reactivity, with 30% from alkenes and 20% from aromatics at T0, not shown in the figure), species that have relatively short lifetimes under the conditions present in the basin. It is apparent from the data that rapid photochemistry occurs, quickly transforming the OH-VOC reactivity initially

from being dominated by NMHCs to being dominated by OVOCs aloft (G-1) and further downwind (C-130 plumes). CO plays a relatively more important role in OH reactivity compared to VOCs as the plume ages. At the C-130 plume interception point, approximately 60% of the CO reactivity is from the background CO.

For the C-130 flights conducted over the city, the most abundant species measured was methanol, followed by propane and other NMHC and OVOC species. Eight of the top 20 measured VOCs were OVOCs. Similar to T0 and T1, the two most important VOCs in terms of reactivity were formaldehyde and acetaldehyde.

7 Urban and regional photochemistry

7.1 Urban photochemistry

The production of ozone and secondary organic aerosols (SOA) in the atmosphere involves chemical reactions of NO_x and VOCs in the presence of sunlight (although dark reactions with e.g. NO_3 and O_3 can play a role in SOA formation). The suite of measurements designed to examine the complex photochemistry in the MCMA during MILAGRO expanded upon previous measurements in 2003 (Molina et al., 2007). At T0, measurements were made of NO_x, several VOCs, O_3, OH and HO_2, as well as several radical precursors and indicators for fast NO_x and VOC oxidation processes such as HONO, HCHO and glyoxal.

The median of the daily measured maximum NO_x mixing ratios at T0 was approximately 200 ppbv during the morning rush hour (Dusanter et al., 2009a), which was approximately a factor of 2 greater than that observed at the CENICA supersite during MCMA-2003 (Molina et al., 2007), and thus may reflect the influence of local sources at this site. During both campaigns, direct atmospheric measurements of NO_2 were conducted by LP-DOAS (Volkamer et al., 2005). Such measurements are free from interferences that are known to be issues with commercial NO_x instruments (Dunlea et al., 2007), in particular during afternoons. In the afternoon, NO_x was approximately 20 ppb, similar to that observed during MCMA-2003. *Median peak VOC concentrations at T0 during* the morning rush hour (1600 ppbC) were similar to that measured during MCMA-2003 (1500 ppbC) (Shirley et al., 2006; Velasco et al., 2007; Dusanter et al., 2009a), while plumes of elevated toluene as high as 216 ppbv and ethyl acetate as high as 183 ppbv were often observed during the late night and early morning hours at T0, indicating the possibility of significant industrial sources in the region around this site (Fortner et al., 2009).

7.1.1 Radical sources and budget

Measured concentrations of OH by Laser-Induced Fluorescence (LIF) were similar to that measured in other urban areas, with median midday values of approximately 4.6×10^6 cm^{-3}. These OH concentrations are approximately a factor of two lower than the corrected values measured during MCMA-2003 (Shirley et al., 2006; Mao et al., 2009; Dusanter et al., 2009a). The median diurnal maximum HO_2 concentration was 1.9×10^8 cm^{-3}, which was lower than the corrected values observed during MCMA-2003 (Shirley et al., 2006; Mao et al., 2009; Dusanter et al., 2009a). The lower measured concentrations of OH and HO_2 are consistent with the higher observed NO_x at T0, which would reduce OH and HO_2 through the OH + NO_2 and HO_2 + NO reactions.

A 0-D box model based on the Regional Atmospheric Chemistry Mechanism (RACM) of the HO_x (OH + HO_2) radical concentrations constrained by measurements of radical sources and sinks was used to test the ability of this mechanism to reproduce the observed radical concentrations and to perform a radical budget analysis (Dusanter et al., 2009b). Constraining the simulation to measured values of glyoxal with additional constraints on the estimated concentrations of unsaturated dicarbonyl species resulted in modeled HO_x concentrations in good agreement with measured values during the afternoon. However, consistent with other urban measurements, HO_x concentrations were underpredicted during the morning hours when NO_x is high (Dusanter et al., 2009b). During the MCMA-2003 campaign, results from a constrained 2-D flexible top box model based on the Master Chemical Mechanism found that modeled HO_x concentrations compared favorably with measured concentrations for most of the day (Volkamer et al., 2010; Sheehy et al., 2010). However, the model also underpredicted the concentrations of radicals in the early morning, which could lead to an underprediction of the integrated amount of ozone produced by a factor of two (Sheehy et al., 2010). This detailed testing of chemical models at the radical level highlights the fact that in addition to uncertainties associated with emissions and meteorology, there are additional uncertainties associated with the chemical mechanisms used in current models (Sheehy et al., 2010; Dusanter et al., 2009b; Hofzumahaus et al., 2009). The parameterization associated with the prediction of ozone by these models may mask this uncertainty and may cause models to give the right answer for the wrong reason.

During MCMA-2006, the modeling analysis predicts that the gross photolysis of HONO (35%), photolysis of HCHO (24%), O_3-alkene reactions (19%) and photolysis of dicarbonyls (8%) are the main sources of radicals during the daytime at T0, while O_3 photolysis is predicted to contribute 6% of the total radical initiation (Dusanter et al., 2009b). During MCMA-2003, a similar radical source analysis found that the photolysis of secondary OVOCs other than HCHO (33%) was the largest contribution to the total radical production rate, followed by O_3 photolysis (19%), HCHO photolysis (19%), O_3-alkene reactions (15%), and HONO photolysis (12%) (Volkamer et al., 2010). The larger contribution of HONO photolysis to radical initiation at T0 is due to

the higher median HONO concentrations measured in 2006 as a result of the higher NO_x concentrations at this site. Notably, both studies suggest that HCHO is an important radical source in the MCMA that can have a substantial impact on radical and ozone production, especially during the morning (Lei et al., 2009), while O_3-alkene reactions help jump start the photochemistry shortly after sunrise, and indirectly sustain radical production in the mid- morning by forming HCHO and other OVOCs (Volkamer et al., 2010).

The relative importance of HONO as a radical source varies by location in the MCMA, and even at a given location can vary from day to day. During a period characterized by elevated daytime HONO mixing ratios, Li et al. (2010) used the WRF-Chem model to investigate the relative contribution of several HONO sources and their impact on the formation of photochemical pollutants. The model included homogeneous production of HONO from the gas phase reaction of OH with NO and four other heterogeneous sources. Heterogeneous conversion of NO_2 by condensed semivolatile organic compounds was found to be the main source of HONO in the MCMA, accounting for 75% of the measured ambient concentrations. Inclusion of these additional heterogeneous sources improved the agreement between the measured and modeled HONO and HO_x concentrations and enhanced the production of O_3 and SOA (Li et al., 2010).

Radical termination at T0 was dominated by OH + NO_x reactions, with the formation of HNO_3, HONO, and organic nitrates contributing to 60, 20, and 14% of the total radical termination rate respectively (Dusanter et al., 2009b). Radical termination through the formation of peroxyacetyl nitrates (PANs) and subsequent reaction with OH was calculated to be negligible assuming PANs are in steady-state due to the rapid thermal dissociation of PAN species leading to the formation of RO_2 radicals (Dusanter et al., 2009b). However, a modeling analysis of PAN formation using the Comprehensive Air Quality Model with extensions (CAMx) suggest that PAN is not in chemical-thermal equilibrium during photochemically active periods, and could lead to significant outflow of PAN from the urban area (Lei et al., 2007). Measurements of gaseous HNO_3 reached a peak value of 0.5 to 3 ppb in the early afternoon, which was less than that predicted from the rate of HNO_3 production based on measured OH and NO_2 concentrations (Zheng et al., 2008). However, the measured HNO_3 mixing ratio was found to anti-correlate with submicron-sized aerosol nitrate, suggesting that gas-particle partitioning has a substantial effect on the gas phase concentration of HNO_3 in the MCMA (Zheng et al., 2008), consistent with results from MCMA-2003 (Salcedo et al., 2006; San Martini et al., 2006a, b). Irreversible HNO_3 uptake on dust was also reported by several groups (e.g., Querol et al., 2008) and was an important sink of HNO_3. Gas phase HNO_3 contributed a smaller fraction of oxidized NO_x products (NO_z = NO_y− NO_x), while particulate nitrate comprised a large fraction due to high concentrations of NH_3 and dust (Querol et al., 2008; Wood et al., 2009). Aircraft measurements of total alkyl nitrates in the immediate vicinity of Mexico City were found to be a substantial fraction (approximately 10%) of total NO_y (Perring et al., 2010).

The HO_2/OH ratio can be used as a measure of the efficiency of radical propagation. During MCMA-2006, observed HO_2/OH ratios varied from 1 to 120 for measured NO mixing ratios between 1–120 ppb. These ratios are lower than those measured during MCMA-2003, but may reflect the higher NO_x environment at T0 resulting in greater rates of radical termination and lower HO_2 concentrations (Shirley et al., 2006; Sheehy et al., 2010; Dusanter et al., 2009a). Model predicted HO_2/OH ratios are in generally good agreement with the measurements during the afternoon when NO was between 1 and 5 ppb. However, the model underestimates the measured ratios by approximately a factor of 2–5 at higher NO mixing ratios between 10–100 ppb observed during the morning (Dusanter et al., 2009b). This behavior is consistent with that observed for MCMA-2003 (Shirley et al., 2006; Sheehy et al., 2010) as well as other field campaigns, suggesting that a process converting OH into peroxy radicals may be missing from the chemical mechanism.

The net instantaneous rate of ozone production from HO_2 radicals ($P(O_3) \approx k_{HO_2+NO}$ (HO_2) (NO)) can provide insight into the chemical processes that produce ozone in the MCMA. At T0, $P(O_3)$ was as high as 80 ppb/h in the early morning (Dusanter et al., 2009a). These instantaneous values were lower than during MCMA-2003 (Sheehy et al., 2010), where early morning values reached 120 ppb/hr and are higher than those reported for other urban areas (see references in Sheehy et al., 2010; Kleinman et al., 2005; Mao et al., 2009). An observed ozone production rate from all production mechanisms (HO_2, RO_2, etc.) of approximately 50 ppb/h was observed at a mountain-top site (Pico de Tres Padres) located within and 700 m above the Mexico City basin (Wood et al., 2009). These values are among the highest observed anywhere in the world and are consistent with the extremely high VOC reactivity observed in the MCMA compared to other locations (Shirley et al., 2006; Sheehy et al., 2010; Mao et al., 2009; Wood et al., 2009).

7.1.2 Modeling urban ozone production and sensitivity

Several chemical transport models and analysis of measurements indicate that ozone production in the MCMA is generally VOC-limited in the urban area (Lei et al., 2007, 2008; Song et al., 2010; Tie et al., 2007; Zhang and Dubey, 2009). Measurements of the production of hydrogen peroxide, which is a main radical termination product under NO_x-limited conditions, was found to be negligible in the MCMA (Volkamer et al., 2010; Sheehy et al., 2010) and only increased slightly just outside of the urban area, consistent with ozone production being VOC-limited (Nunnermacker et al., 2008). A comparison of calculated radical production rates with the observed production rate of NO_z also suggests that ozone production in the MCMA is VOC-limited, with the

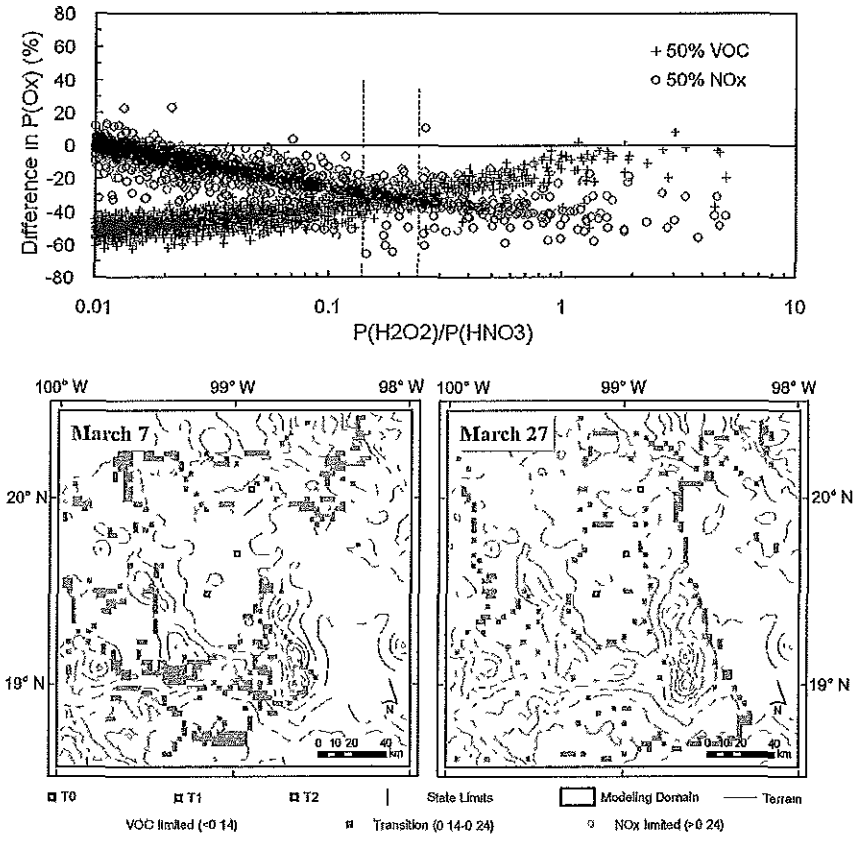

Fig. 11. Top panel: The percentage change in O_X formation rate as a function of the indicator, ratio of H2O2 production rate to HNO3 production rate at 12.00–17:00 LT during the episodes (weekends are shown in gray) within the urban area. The dashed bars envelop the transition regime. Bottom panel: Spatial distribution of the ratio at 14:00 LT on 7 and 27 March 2006 indicating the NO_X-VOC sensitivity (source: Song et al., 2010).

main radical termination reactions involving NO_X oxidation (Wood et al., 2009). An analysis of ratio of radical loss from the formation of nitric acid and organic nitrates to the total radical production for MCMA 2003 also suggests that ozone production is VOC-limited in the early morning and late afternoon, but becomes NO_X-limited during the early afternoon (Mao et al., 2009).

Sensitivity analyses of ozone production to precursor emissions under different meteorological conditions during MCMA-2006, along with a chemical indicator analysis using the chemical production ratios of H_2O_2 to HNO_3, demonstrate that the MCMA urban core region is VOC-limited for all meteorological episodes, while the surrounding areas with relatively low-NO_X emissions can be either NO_X- or VOC-limited regime depending on the episode (Song et al., 2010) (see Fig. 11). Precursor emissions were constrained by the comprehensive data from the MCMA-2006 study and the RAMA network, while the simulated plume mixing and transport were examined by comparison with aircraft measurements. The CAMx model was able to reproduce the observed concentrations of ozone and precursors and suggest that controls on VOC emissions would be a more effective way to reduce ozone levels in the urban area, consistent with previous results from MCMA-2003 (Lei et al., 2007, 2008). However, the degree of VOC-limitation increased for MCMA-2006 due to lower VOCs, lower VOC reactivity and moderately higher NO_X emissions. Furthermore, meteorological conditions led to large variations in regime for the relatively low-NO_X emitting area, implying that the effectiveness of particular emission control strategies would depend on location and meteorology (Song et al., 2010).

An analysis of the weekly pattern of surface concentrations of CO, NO_X, particulate matter (PM_{10}) and O_3 between 1987 and 2007 show a distinct weekend effect, as morning concentrations of CO, NO_X and PM_{10} were lower on Saturdays and Sundays compared to the rest of the week. However, afternoon ozone concentrations showed minimal changes over the weekend with occasional increases, providing direct empirical evidence that ozone production is VOC-limited and NO_X-inhibited during workdays. Decreases in the concentrations of CO (and VOCs) over the past decade have decreased the CO/NO_X and VOC/NO_X ratios, increasing the VOC-limitation of ozone production in the urban area (Stephens et al., 2008). A 3-D CAMx chemical transport

model including the estimated historical changes in ozone precursors was able to adequately reproduce the historical trends in the observed concentrations, and indicated that ozone production is currently VOC-limited. The modeled ozone concentrations were particularly sensitive to aromatics, higher alkenes, and formaldehyde emissions (Zavala et al., 2009a).

Simulations of ozone and other chemical species (CO, NO, NO_2 and NO_y) in the MCMA using WRF-Chem model compare favorably with surface measurements from the RAMA monitoring network with the exception of SO_2 (Zhang et al., 2009; Zhang and Dubey, 2009). Reductions of the total emissions rates of 15%, 25% and 10% for Saturday, Sunday and holidays, respectively, also led to predicted concentrations of the main chemical species that compared favorably to measurements (Zhang et al., 2009). Incorporating 3-D variational data assimilation into meteorological simulations of an air quality episode during the MCMA-2003 campaign significantly improved the magnitude of the peak O_3 concentration, as well as the timing of the O_3 peak on most days of the episode, especially during the daytime (Bei et al., 2008). These results illustrate the importance of applying this technique to ozone simulations in the Mexico City Basin. Bei et al. (2010) further investigated the sensitivity of ozone concentration predictions to meteorological initial uncertainties and PBL parameterization schemes on four selected days during MCMA-2006 through ensemble forecasts. Their results demonstrate that uncertainties in meteorological initial conditions have significant impacts on O_3 predictions, including the peak O_3 concentration, as well as the horizontal and vertical O_3 distributions, and temporal variations. The ensemble spread of the simulated peak O_3 concentration averaged over the city's ambient monitoring sites can reach up to 10 ppb. The magnitude of the ensemble spread also varies with different PBL schemes and meteorological episodes.

7.2 Regional photochemistry

The composition of the regional atmosphere was sampled primarily by aircraft-based instruments, and to some extent from surface stations outside Mexico City. Many of these measurements are still being analyzed, but some general features of the character of the regional atmosphere are beginning to emerge.

Free tropospheric O_3 concentrations in background air (i.e., air not obviously influenced by Mexico City) ranged between 30 and 80 ppb as measured from the C-130 with an average value of 60 ppb (Tie et al., 2009), and ~35–55 ppb over the Gulf of Mexico observed from the DC-8 (region 1, Singh et al., 2009). Ozone sondes launched from the T1 site showed boundary layer values ranging from 30 to 80 ppb, but free tropospheric values of only 40–60 ppb (one standard deviation), likely due to advection of cleaner air from the Pacific (Thompson et al., 2008). Vertical profiles of O_3 calculated with the global MOZART-4 model show good agreement with measurements obtained from both the DC-8 and C-130 aircraft, including a marked peak between 2 and 4 km asl associated with the Mexico City plume outflow (Emmons et al., 2010). In the same study, Emmons et al. used tagged emissions to identify the contribution of various sources to the regional CO and O_3 distribution. Biomass burning was found to have an influence on regional chemistry, although not a dominant one. Emissions from Mexico City were important over Central Mexico but had negligible influence beyond Mexico borders.

Substantial enhancements of O_3 above background were observed in plumes that could be traced back to Mexico City (Tie et al., 2009; Mena-Carrasco et al., 2009; Emmons et al., 2010). This is particularly evident for the quasi-Lagrangian episode of 18–19 March, where air was sampled on 18 March by the G-1 near Mexico City, and on 19 March was intercepted and again sampled far downwind by the C-130 (Voss et al., 2010). Apel et al. (2010) examined correlations between CO and ozone, acetone, or benzene observed in the near-field plume (on 18 March) and in the same plume a day later (19 March). Slopes of O_3 vs. CO were markedly steeper in the aged plume, indicating that considerable O_3 production occurred during the transport time. Some acetone production was also inferred by slightly higher acetone vs. CO slopes, while benzene vs. CO slopes were essentially identical, consistent with the longer lifetime of both compounds.

Photochemical modeling shows that regional O_3 production is sensitive to NO_x as well as to VOCs and CO (Tie et al., 2009), and also to the reduced availability of UV radiation because of the heavy aerosol loadings (Barnard et al., 2008; Mena-Carrasco et al., 2009). WRF-Chem simulations by Tie et al. indicate that the regional OH reactivity is dominated by oxygenated organics and CO, and to a lesser extent the hydrocarbons; the high levels of OVOCs lead to large concentrations of organic peroxy radicals in the plume, typically exceeding those of HO_2. Simulations with the MOZART-4 model (Emmons et al., 2010) tend to underpredict observed concentrations of OVOCs, but even these lower values dominate the regional OH reactivity and O_3 production. Measurements from the G-1 and C-130 during the 18–19 March episode confirm the importance of OVOCs and CO, with OVOCs being dominant in the near field outflow (Apel et al., 2010) and CO increasing in relative importance for ozone production further downwind. OH concentrations measured from the DC-8 are somewhat higher than predicted by MOZART-4, while HO_2 concentrations show better agreement.

Ozone production efficiencies, defined as the number of O_3 molecules produced per NO_x consumed, and estimated from O_3 vs. NO_z correlations measured from the C-130 aircraft, ranged from 4.5–4.6 in air recently influenced by biomass burning or the Tula industrial complex, 5.3 to 5.9 over land influenced by Mexico City, and 8.5 in the marine free troposphere (Shon et al., 2008). These observation-based estimates can be compared with

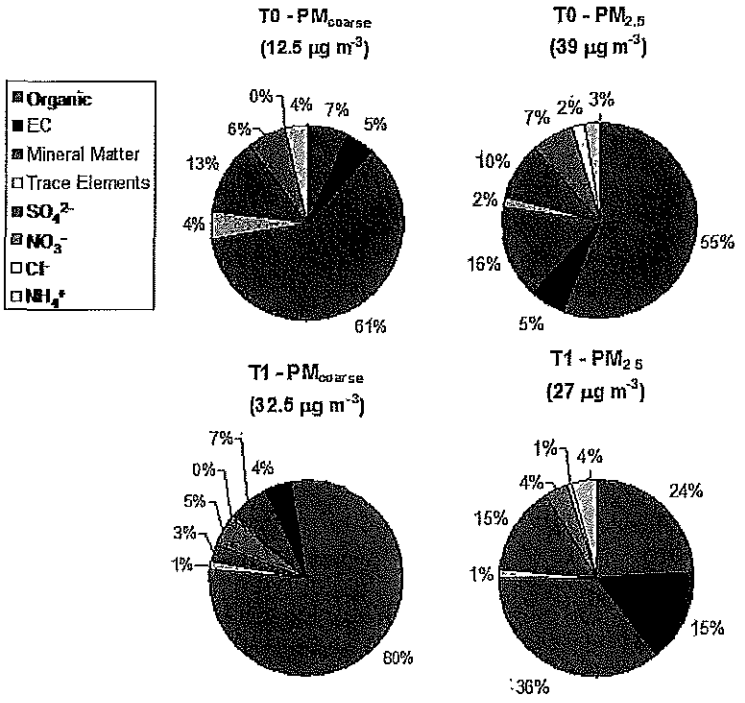

Fig. 12. Average composition of PM_{coarse}(PM_{10}–$PM_{2.5}$) and $PM_{2.5}$ at the T0 and T1 supersites, based on the results of Querol et al. (2008). OA was calculated from the measured OC based on the average measured OA/OC ratio of 1.75 at T0 (Aiken et al., 2008). The T1 site was affected by local resuspension of dust, which explains the unusually large contribution of mineral matter at this site.

model-based estimates by Mena-Carrasco et al. (2009) (STEM model: 4.9 within 100 km of the city, 7.9 outside that radius) and Tie et al. (2009) (WRF-Chem model: 3.3 near the city, increasing to 5.5 on the regional scale). A separate analysis of the C-130 observations, utilizing only data for which NO_y concentrations were in the range 2–6 ppb to filter out very aged air and fresh plumes, yielded an average Ox vs. NO_z slope of 5.9 ± 0.3, in good agreement with the previously cited regional values but somewhat lower than the value of 9.1 ± 0.3 predicted from the MOZART-4 model (Emmons et al., 2010), as might be expected due to this model's lower spatial resolution.

Long-range export of reactive nitrogen from Mexico City was discussed by Mena-Carrasco et al. (2009) and found to take place primarily via the formation of PANs, in agreement with observations from the C-130. PANs can thermally decompose on the regional scale providing a source of NO_x and therefore contribute to regional O_3 formation. The relatively high regional NO_x concentrations are consistent with low or even negative formation rates for hydrogen peroxide observed from the G-1 aircraft over most of the Mexican plateau, with higher values found only in the relatively humid coastal areas (Nunnermacker et al., 2008).

Measurements at a surface station (Altzomoni) located at high altitude (4010 m a.s.l.) 60 km SW of Mexico City were made by Baumgardner et al. (2009). Pollutant concentrations were elevated not only when the synoptic flow came directly from Mexico City but also from the east, suggesting that other pollution sources in Central Mexico and large scale recirculation of Mexico City pollutants may be impacting regional air quality. Recirculation of pollution to the Gulf of Mexico and back over Central Mexico was identified in the modeling study of Emmons et al. (2010). Influences of biomass burning and the nearby Popocatepetl volcano were also observed.

8 Ambient particulate matter

Particulate matter (PM) impacts human health (Pope and Dockery, 2006) visibility (Watson et al., 2002), climate (Forster et al., 2007), and ecosystems (Zambrano et al., 2009). Negative impacts of PM on human health have been documented in the MCMA (e.g., Romieu et al., 1996; Osornio-Vargas et al., 2003; Evans et al., 2002) as discussed in more detail in Section 10 below. PM concentrations observed during the MILAGRO-2006 Campaign were similar to previous studies that measured PM in the MCMA during the late winter and early spring (Chow et al., 2002; Vega et al., 2002; Salcedo et al., 2006; Molina et al., 2007), and similar to concentrations reported by the RAMA monitoring network (http://www.sma.df.gob.mx/simat2). PM_{10} concentrations, as measured from filter samples, were higher at the urban sites with 24-hour averages ranging between 50–56 μg m^{-3}, and lower concentrations at

rural sites ranging from 22 to 35 $\mu g\,m^{-3}$ (Querol et al., 2008). $PM_{2.5}$ concentrations were in the range of 24–46 $\mu g\,m^{-3}$ and 13–25 $\mu g\,m^{-3}$ at the urban and rural sites, respectively (Querol et al., 2008). This is consistent with previous studies (Chow et al., 2002; Vega et al., 2002, 2004) that also found $PM_{2.5}$ made up approximately 50% of the PM_{10} in the MCMA, and with mobile lidar measurements that indicate the PM concentrations in the Mexico City basin are about twice as high as outside the basin (Lewandowski et al., 2010). PM_1 and $PM_{2.5}$ concentrations were similar as the amount of mass between $PM_{2.5}$ and PM_1 was a small fraction of the total $PM_{2.5}$ (Querol et al., 2008; Aiken et al., 2009), consistent with results from MCMA-2003 (Salcedo et al., 2006).

The fractional compositions of $PM_{2.5}$ and PM_{coarse} are illustrated in Fig. 12. Querol et al. (2008) found that mineral matter made up about 25% of the PM_{10} at the urban sites and a larger fraction at the suburban and rural sites. Mineral matter was found to make up a smaller, yet important, fraction of the $PM_{2.5}$ at the urban and rural sites accounting for 15% and 28% of the $PM_{2.5}$, respectively. The current study found about 50% of the $PM_{2.5}$ and the PM_1 was comprised of organic matter in the city (Querol et al., 2008; Aiken et al., 2009), which is similar or larger than reported in other cities (e.g., Zhang et al., 2007). About 25% of the $PM_{2.5}$ mass was due to secondary inorganic ions (sulfate, nitrate, ammonium), and the remaining $PM_{2.5}$ mass was elemental carbon and mineral matter (Querol et al., 2008; Aiken et al., 2009). These percentages are consistent with those in previous studies (Chow et al., 2002; Vega et al., 2004; Salcedo et al., 2006). A strong "weekend effect" with higher weekday than weekend concentrations has been observed for PM_{10} over several years, which is consistent with the large impact of human activities on PM concentrations in the MCMA (Stephens et al., 2008). The vertical structure of the PM concentrations was characterized with lidar, aircraft, and a tethered balloon and found to be relatively well-mixed during the day, although often with substantial horizontal gradients (Hair et al., 2008; DeCarlo et al., 2008; Lewandowski et al., 2010; Rogers et al., 2009; Greenberg et al., 2009).

The PM levels in the MCMA are among the highest in North America although with substantially lower levels than the most polluted Asian megacities (Querol et al., 2008; Hopke et al., 2008), e.g. 200 and 330 $\mu g\,m^{-3}$ annual average concentrations of $PM_{2.5}$ and PM_{10} respectively, in Lahore, Pakistan, about five times the levels in Mexico City during MILAGRO (Stone et al., 2010b). As in the case of many Asian megacities, carbonaceous aerosols are important contributors to $PM_{2.5}$ in Mexico City. An important scientific and air quality management question in many of these megacities is quantifying the relative contributions to concentrations of PM from different sources such as mobile, industrial, biogenic, biomass burning, etc., as well as separating the contributions from primary emissions vs. secondary processes, both of which were an important objective of the MILAGRO Campaign. MILAGRO was not only able to advance the understanding of the sources and atmospheric processing of PM, but was also able to improve the scientific understanding of the tools that can be used for this purpose. These advancements were made in part by the use of new aerosol measurement instruments that had not been used in large field campaigns in the past, and through the simultaneous application of a diverse set of measurement and data analysis tools that had not been widely applied in parallel. The following sections highlight the new PM measurement instruments deployed during MILAGRO, the key scientific results about different PM components, and the needs for future research. Some of the PM findings from MILAGRO have been described in other relevant sections, such as Sect. 5 (Emissions) above.

8.1 Instruments deployed to Mexico City for the first time

Although a very large number of instruments and PM samplers were used as part of the MILAGRO Campaign for both ground-based and aircraft measurements, many of these instruments had been used in similar field studies in Mexico City in the past. Tables 1–4 summarize the PM measurements and instruments deployed during the campaign. This study was the first time that organic aerosol (OA) functional group concentrations by FTIR (Liu et al., 2009; Gilardoni et al., 2009; Baumgardner et al., 2009), particle-phase organic molecular markers (Stone et al., 2008, 2010a), Scanning Transmission X-Ray Microscopy (STXM) spectra of collected particles (Moffet et al., 2010), and ^{14}C content of carbon fractions (organic carbon, elemental carbon, water-soluble OC (WSOC), and water-insoluble OC (WIOC)) (Aiken et al., 2010) were measured in the MCMA. In addition to the new measurements applied to collected particles, several real-time measurements of PM were deployed to the MCMA for the first time. These instruments included:

- An Aerosol-Time-of-Flight Mass Spectrometer (ATOFMS) (Moffet et al., 2008a, b).
- A Thermal Desorption Chemical Ionization Mass Spectrometer (TDCIMS) for measurement of the composition of particles as small as 10 nm (Smith et al., 2008).
- A Particle-Into-Liquid Sampler followed by Ion Chromatography and Water-Soluble Organic Carbon detection (PILS-IC and PILS-WSOC) (Hennigan et al., 2008).
- Two High-Resolution Time-of-Flight Aerosol Mass Spectrometers (HR-ToF-AMS) (DeCarlo et al., 2008; Aiken et al., 2009; Dunlea et al., 2009), one of which sampled behind an aerosol concentrator (Khlystov et al., 2005) during part of the campaign.
- Three compact Time-of-Flight Aerosol Mass Spectrometers (C-ToF-AMS) (Canagaratna et al., 2007;

Kleinman et al., 2008; Herndon et al., 2008; de Gouw et al., 2009).

- A Time-of-Flight Aerosol Mass Spectrometer with an internal light scattering module (LS-ToF-AMS) (Cross et al., 2009).
- A thermodenuder-AMS combination (Huffman et al., 2009a).
- A photoacoustic spectrometer (Paredes-Miranda et al., 2009).
- A TSI Fast Mobility Particle Sizer (FMPS, A. Clarke, pers. comm., 2006).
- A hygroscopicity tandem differential mobility analyzer (HTDMA) (Gasparini et al., 2004).

These measurements taken together have helped improve our understanding of physical and chemical characteristics of PM in the MCMA, as well as their primary and secondary sources.

8.2 Primary inorganic aerosols

Dust and metals in PM samples were studied by several research groups and were found to be relatively high compared to other Megacities in North America (Querol et al., 2008; Moffet et al., 2008a, b; Moreno et al., 2008a, b; Gilardoni et al., 2009; Salcedo et al., 2010). High levels of anthropogenic metals were observed in the urban sites, including arsenic, chromium, zinc, copper, lead, tin, antimony, and barium (Querol et al., 2008). These metals had strong temporal variations in concentration (Moreno et al., 2008a, b; Moffet et al., 2008a, b; Salcedo et al., 2010) and were largely associated with industrial and mobile sources. Hg seemed to have a regional rather than an urban origin (Querol et al., 2008). Rutter et al. (2009) identified possible industrial source regions of gaseous and particulate mercury associated with measurements at T0 and T1. Moreno et al. (2008b) report on the sources of lanthanoid elements (Lanthanum to Lutetium) in Mexico City, which are related to crustal particles, but also to some anthropogenic sources. Christian et al. (2010) reported emissions of 17 metals from source measurements of open trash burning, of which antimony (Sb) was the most unique, consistent with a previous report at the US-Mexico border (Garcia et al., 2006). Fine particle Sb may be a useful tracer for $PM_{2.5}$ from this source in the MCMA, although this topic requires further research as many other Sb sources also exist (Reff et al., 2009). Christian et al. (2010) also reported on the emissions from brick kilns, charcoal kilns, and cooking fires. Adachi and Buseck (2010) reported that nanosized metal-bearing particles (<50 nm diameter) in Mexico City aircraft samples using transmission electron microscopy. Most were attached to larger (several hundreds of nm) host particles, and contained Fe, Zn, Mn, Pb, Hg, Sn, Cr, Ni, Ti, V, and Ag. Hg nano-particles were especially prominent. Salcedo et al. (2010) report the first use of an HR-ToF-AMS to detect Pb in PM_1. These authors found that different chemical forms of Pb had different source regions in the MCMA.

8.3 Primary carbonaceous aerosols

Elemental carbon (EC) is an important tracer for combustion sources (Schauer, 2003) and is an important component of atmospheric PM in terms of climate forcing (Forster et al., 2007; Ramanathan et al., 2007). The optical properties of PM containing EC are strongly dependent on the mixing state of the different species, and were investigated during MILAGRO by several different approaches. Moffet et al. (2008a, 2009) used ATOFMS measurements to show that fresh EC particles were observed during rush-hour periods. However, the majority of EC particles were coated with nitrate, sulfate, and organic carbon, which are expected to increase the light absorption of these particles per unit of EC. Adachi and Buseck (2008) found similar results with laboratory-based transmission electron microscope (TEM) measurements of particles collected during aircraft overflights of the MCMA. These results are both consistent with those of Johnson et al. (2005) using electron microscopy during MCMA-2003. Somewhat surprisingly, however, very little difference in EC mass absorption efficiencies could be observed through direct measurements by Doran et al. (2007) using a pseudo-lagrangian study comparing observations at the T1 and T2 sites and Subramanian et al. (2010) using single particle soot photometer measurements in the C-130 aircraft. Adachi et al. (2010) obtained 3-D images of embedded soot particles and found that many of them have open, chain-like shapes similar to those of freshly emitted soot, and are located in off-center positions within their host materials. The absorption by these geometries is ~20% lower than for the commonly assumed core-shell morphology, and may help explain the lack of a larger increase in mass absorption efficiencies reported by Doran et al. (2007) and Subramanian et al. (2009). In contrast with reports at other locations, Paredes-Miranda et al. (2009) only found a small positive bias of a filter-based absorption measurement due to oxygenated organic aerosols (OOA).

Polycyclic Aromatic Hydrocarbons (PAH) are a family of species, some of which are highly mutagenic and carcinogenic, that are generally associated with EC as their emissions are largely from combustion sources. Thornhill et al. (2008) measured PAH at six locations across the MCMA and found similar levels to those measured during MCMA-2003 (Marr et al., 2006; Dzepina et al., 2007), but with considerable variability in concentrations and PAH distributions across sites. This is consistent with the notion that sources of PAH vary spatially as a result of the spatial distribution of combustions sources across the metropolitan area.

Significant efforts have been directed at understanding the sources of $PM_{2.5}$ and PM_1 organic aerosols and apportioning the observed organic matter into primary organic aerosol (POA) and secondary organic aerosol (SOA) during MILAGRO. Important POA sources were found to include mobile and other combustion sources, biomass burning (BB), and a minor contribution of local (presumably industrial) sources at T0 (Yokelson et al., 2007; Stone et al., 2008; DeCarlo et al., 2008, 2010; Aiken et al., 2008, 2009, 2010; Gilardoni et al., 2009; Liu et al., 2009). Stone et al. (2008), using chemical mass balance of organic molecular markers (Schauer et al., 1996), estimated POA from mobile sources to account for approximately 30–40% of the OC concentrations in MCMA. This result appears consistent with results of Aiken et al. (2009), using positive matrix factorization of high-resolution AMS spectra (Ulbrich et al., 2009), who reported a contribution of "hydrocarbon-like OA" (HOA, which includes vehicle emissions) of ~30% of the PM_1 OA. Food cooking POA may also be apportioned as part of HOA (Mohr et al., 2009) and has been reported as an important contributor of urban POA in some previous studies elsewhere (e.g., Hildemann et al., 1994). Mugica et al. (2009) report a contribution of food cooking to $PM_{2.5}$ of about 10% (~5 $\mu g\,m^{-3}$), which would represent about 20% of the OA, although this study was not able to separately quantify biomass burning and the authors suggest that that problem may have inflated the contribution of other sources. Two measurement-based studies (Zavala et al., 2009b; Aiken et al., 2009) and one 3-D modeling study (Fast et al., 2009) have concluded that the 2006 MCMA emissions inventory (SMA-GDF, 2008a) underestimates POA and primary $PM_{2.5}$ emissions. The emission profiles of gas and particle emissions from biofuel use (biomass used directly as fuel for e.g. cooking) and open trash burning in Mexico City have been reported by Christian et al. (2010). The high emission factors of cooking with biofuels and open trash burning suggest a potentially important contribution to surface concentrations which is being further investigated. Open trash burning is not included in the 2006 MCMA emissions inventory (SMA-GDF, 2008a).

Wildfires in the hills and mountains near Mexico City were unusually intense during MILAGRO, with fire counts being about twice the March climatological average of recent years. Emissions from these fires made a substantial contribution to OA and other species. Aiken et al. (2010) report a good correlation between the different fire tracers (acetonitrile, levoglucosan, AMS levoglucosan-equivalent mass, and total K in $PM_{2.5}$), although total K has a non-wildfire background of ~2/3 of its average concentration. These authors also compared the different estimates of biomass burning OA at the surface inside the city (Stone et al., 2008; Querol et al., 2008; Aiken et al., 2009, 2010), which are consistent in that BB was highly variable in time and accounted on average for 12–23% (range of the different estimates) of the OA during the MILAGRO Campaign inside the city. A similar estimate was derived for data from the IMADA-AVER campaign (Vega et al., 2009). These results are consistent with those of de Gouw et al. (2009) at T1 who report that BB was not a dominant contributor to OC at that site, and perhaps not dissimilar to previous observations by the same group in the Eastern US. The lowest estimate was derived by Liu et al. (2009), who report a contribution of biomass burning to OA in the range 0–8%. Moffet et al. (2008a) report a larger impact of about 40% to particle number at the upper end of the accumulation-mode, based on the particles containing K.

Crounse et al. (2009) and DeCarlo et al. (2010) concluded that the relative impact of BB was substantially larger aloft over the Central Mexican Plateau (up to 2/3 of OA) than at the surface inside the city, This is analogous to the situation for SO_2, for which urban emissions contribute a major fraction of the concentrations inside the urban area, despite being far smaller than the nearby regional sources (de Foy et al., 2009b). Yokelson et al. (2007) reported an estimate of a $50 \pm 30\%$ contribution of the wildfires to the total fine PM outflow (rather than just the OA) from the Mexico City region, whose central value is higher than the Crounse and DeCarlo estimates. The discrepancy may be due to the fact that this study used the MCMA inventory to quantify urban PM, which is known to be substantially underestimated as discussed in Sect. 5 of this overview. The wildfires near Mexico City were estimated to contribute ~2–3% of the fine PM at the surface as an annual average, and their larger importance during MILAGRO arises from the timing of the campaign during the warm dry season and the unusual intensity of these fires during 2006 (Aiken et al., 2010). We do note that the BB season continues through April and peaks in May, so that higher contributions of BB may be expected during those months in the average year. BB impacts during the other 9 months are expected to be much smaller. BB in the Yucatan is a larger regional PM source (Yokelson et al., 2009), but its impact in the MCMA was very small during MILAGRO as these emissions were relatively weak and transported elsewhere (Yokelson et al., 2009; Aiken et al., 2010). This contrasts with a larger impact during the latter half of the MCMA-2003 campaign (Salcedo et al., 2006; Molina et al., 2007). Emmons et al. (2010) conclude from a large-scale modeling study that open fires made some, but not a dominant, impact on the atmospheric composition in the region around Mexico City, when averaged over the MILAGRO period.

Aiken et al. (2010) and DeCarlo et al. (2010) report a good comparison between the time trends of biomass burning OA (BBOA) at T0 and the C130, respectively and the predictions of a FLEXPART-based dispersion model. Fast et al. (2009) and Hodzic et al. (2010a) concluded that BBOA concentrations arising from some large fires are substantially overestimated in their 3-D models when using a custom inventory based on satellite fire counts. Both model studies fail to capture the early morning BBOA impact which is better reproduced by the FLEXPART study of Aiken et al. (2010), presumably due to the improved treatment of the

evening/nighttime smoldering emissions. The MODIS satellite instrument misses some fires for various reasons (cloud cover, smoke cover, fires that are too small, timing issues) (Yokelson et al., 2007; Crounse et al., 2009), so the use of additional data from the GOES satellite instrument may help explain the better predictions of Aiken et al. (2010). The combination of these observations suggests that either the fires missed by the satellite counts only contribute a small fraction of the emissions (e.g. because they tend to be smaller fires), or that the overestimation of the emissions from some fires partially compensates the lack of emissions from the missed fires. Aiken et al. (2010) report that the wildfire BB emissions near Mexico City were nearly 20 times larger than in the 2006 MCMA emissions inventory, which uses a static value and is not based on the fire counts (SMA-GDF, 2008a), although a substantial fraction of these emissions occurred just outside of the MCMA inventory area.

^{14}C measurements have been reported by two groups. Marley et al. (2009a) report that 45–78% of the total carbon at T0 (TC=EC+OC) arises from modern sources. Aiken et al. (2010) report TC modern fractions that range from an average of 46% during the high BB period to 30% during the low BB period. The reasons for the differences of about 15% in the modern carbon fractions at T0 are unclear (Marley et al., 2009a; Aiken et al., 2010). Marley et al. (2009a) did not account explicitly for the extra ^{14}C stored in forests due to the bomb radiocarbon (~124% modern carbon), which needs to be taken into consideration when interpreting that dataset (for example for a modern carbon measurement of 60%, if half of it arises from wood burning, the contemporary carbon fraction would be 54%). During the high BB periods both datasets reported increases of modern carbon of about 15% of the total OC (Aiken et al., 2010), which is consistent with the estimates from several other apportionment techniques as discussed above. A substantial fraction of non-fossil organic carbon ($\geq$37%, (Aiken et al., 2010) is present during very low wildfire periods, which suggests the importance of urban sources of modern carbon such as food cooking or biofuel use (Hildemann et al., 1994; Mugica et al., 2009; Christian et al., 2010) and/or regional sources such as biogenic SOA (e.g., Stone et al., 2010a; Hodzic et al., 2009) and others. Hodzic et al. (2010b) present the first comparison of modern carbon measurements with the predictions of a 3-D model, and find that the observed concentrations are similar to the measurements of Aiken et al. (2010) but lower than those of Marley et al. (2009a). The model explains the observed modern carbon as the sum of similar contributions from regional biogenic SOA, biomass burning POA and SOA, and POA and SOA from urban sources of modern carbon (Hildemann et al., 1994). Sources of "hot" aerosol carbon (enriched in ^{14}C) in the Mexico City area and/or stored in forests could produce a bias in this method and need to be further investigated (Vay et al., 2009).

8.4 Secondary Inorganic Aerosols (SIA)

Secondary inorganic species contribute about 1/4 of the fine PM in the MCMA (Querol et al., 2008; Aiken et al., 2009). Sulfates in PM_1 are generally neutralized by ammonium although they can be in more acidic forms in fresh plumes and have a regional character consistent with the large petrochemical and volcanic sources of SO_2 (Moya et al., 2003; DeCarlo et al., 2008; Aiken et al., 2009), consistent with previous studies (Salcedo et al., 2006; San Martini et al., 2006a, b). The urban area and BB in the Yucatan are also substantial sources of SO_2, although smaller than the petrochemical and volcanic sources (de Foy et al., 2007, 2009b; DeCarlo et al., 2008; Yokelson et al., 2009). The emissions and impacts of different SO_2 sources have been studied by several groups (Grutter et al., 2008; Rivera et al., 2009; de Foy et al., 2009b).

Rapid and intense formation of submicron ammonium nitrate is observed during the morning with important evaporation in the afternoon (Zheng et al., 2008; Hennigan et al., 2008; Aiken et al., 2009), consistent with previous studies (Salcedo et al., 2006). PM_1 nitrate also accounts for a high portion of the NO_z budget in Mexico City, exceeding 20% at times (Wood et al., 2009). Ammonium nitrate is highly correlated with CO and has low correlation with HCN, indicating that urban sources are dominant and BB sources are a small contributor to this species (DeCarlo et al., 2008). Evaporation also plays an important role as airmasses are advected away from Mexico City with the nitrate/ΔCO ratio dropping by about a factor of 4 (DeCarlo et al., 2008). HNO_3 also reacts with dust to form supermicron nitrates, which contribute about a third of the total nitrate during dry periods (Querol et al., 2008; Fountoukis et al., 2009; McNaughton et al., 2009), consistent with a recent 3-D modeling study using MCMA-2003 data (Karydis et al., 2010). The suppression of dust (and thus of this HNO_3 sink) by precipitation during the latter part of MILAGRO led to an increase of NH_4NO_3 concentrations by over 50% after March 23rd (Aiken et al., 2009). Model-predicted submicron nitrate levels inside Mexico City are often sensitive to the aerosol physical state (solid vs. liquid) assumption during periods with ambient RH less than 50% (Fountoukis et al., 2009; Karydis et al., 2010).

Chloride is also a relevant species in Mexico City although its concentrations are generally below 1 $\mu g\, m^{-3}$ and typically much lower than those of sulfate, nitrate, and ammonium (Querol et al., 2008; Aiken et al., 2009). During MCMA-2003 ammonium chloride was the dominant form of chloride in PM_1 at the CENICA site (Salcedo et al., 2006; Johnson et al., 2008), but during MILAGRO the influence of metal or refractory chlorides was larger (Moffet et al., 2008a), on the order of one half of the submicron chloride (Huffman et al., 2009a). Open trash and crop residue burning had high chloride emission factors and are potentially important sources of this component (Christian et al., 2010). However some of the chloride is not associated with OA as it would be the

case for burning sources (Salcedo et al., 2006), so other non-combustion urban sources are also important for chloride. Both forest fires and the urban area were important PM_1 chloride sources based on aircraft data during MILAGRO (DeCarlo et al., 2008). Chlorine-containing organic species in the particle phase have not been reported to our knowledge, despite the detection of substantial concentrations of chlorinated VOCs in the MCMA (Velasco et al., 2007).

8.5 Secondary Organic Aerosols (SOA)

Intense SOA formation in PM_1 was observed during MILAGRO (Kleinman et al., 2008, 2009; Herndon et al., 2008; DeCarlo et al., 2008, 2010; Hennigan et al., 2008; de Gouw et al., 2009; Aiken et al., 2008, 2009) at levels much higher than predicted with traditional SOA models (Kleinman et al., 2008; de Gouw et al., 2009; Hodzic et al., 2009, 2010a, b; Fast et al., 2009; Wood et al., 2010). This is consistent with previous observations and modeling from MCMA-2003 (Volkamer et al., 2006, 2007; Dzepina et al., 2009; Tsimpidi et al., 2010) and the emerging consensus from studies at other polluted locations using a variety of apportionment methods (e.g., Docherty et al., 2008; Hallquist et al., 2009; de Gouw and Jimenez, 2009). These results were consistent between the WSOC (Hennigan et al., 2008) and AMS techniques (e.g., Kleinman et al., 2008) as has been observed elsewhere (Kondo et al., 2007; Docherty et al., 2008). The substantial contribution of SOA was reported not only in the city, but also at the Altzomoni site located 2 km above basin level (Baumgardner et al., 2009) and from aircraft (DeCarlo et al., 2008, 2010; Kleinman et al., 2008). It is also supported by the large underprediction of afternoon OA concentrations when only POA (from urban and BB sources) is considered (Fast et al., 2009, Hodzic et al., 2009; Tsimpidi et al., 2010). The combined formation of SIA and SOA contributes about 75% of the fine PM mass at T0 in the afternoons during MILAGRO, and has a large impact on the aerosol radiative properties such as single-scattering albedo (Paredes-Miranda et al., 2009). The correlation of SOA with odd-oxygen ($O_x = O_3 + NO_2$) (Herndon et al., 2008; Wood et al., 2010) suggests that the use of better-characterized ozone chemistry may help constrain and provide a target for modeling of SOA production. One group (Yu et al., 2009) applied the EC-tracer method to estimate SOA in Mexico City, although it is not possible to separate SOA from primary BBOA with that method only, due to their similar and very high OC/EC ratios (Hallquist et al., 2009).

The formation of SOA from biogenic precursors within the Mexico City basin was small, consistent with previous studies (Volkamer et al., 2006; Dzepina et al., 2009). Most of the isoprene observed in the urban area is likely of anthropogenic origin (Hodzic et al., 2009), consistent with results at other urban locations (Borbon et al., 2001). Other anthropogenic alkenes add little organic mass to SOA, but indirectly add to SOA by reacting to produce radicals for the processing of other SOA precursor VOCs. This indirect SOA contribution of alkenes, i.e., to significantly add to oxidant fields, is likely to be much larger than their direct contribution to SOA mass (Volkamer et al., 2010). A modeling study (Hodzic et al., 2009) and tracer measurements (Stone et al., 2010a) indicate that biogenic SOA formed over forested areas on the coastal mountain ranges and advected over the Central Mexican Plateau contributes ~1–1.5 $\mu g\,m^{-3}$ of SOA background to Mexico City (out of a total SOA background of ~4–5 $\mu g\,m^{-3}$), with relatively low temporal variability. The biogenic SOA source contributes to, but is insufficient to explain, the high fraction of modern carbon in OA observed in Mexico City (30–45%, Aiken et al., 2010) during periods in which BB is suppressed by rain. Biogenic SOA formation may be larger in this region during the wet season.

The predicted SOA from emissions of traditional precursors (aromatics, isoprene, terpenes) from BB are very small (Hodzic et al., 2009, 2010a), although these precursor emissions may be underestimated in current inventories (C. Wiedinmyer, pers. comm., 2009). There is some variability in the net effect of SOA on OA mass observed in the field from BB emissions (Capes et al., 2008; Yokelson et al., 2009; de Gouw and Jimenez, 2009). The only reported chamber study which used woodstove emissions (rather than open-fire emissions) has shown substantial SOA formation in most cases that could not be explained from the traditional precursors and was attributed to semivolatile and intermediate volatility species (Grieshop et al., 2009). SOA formation for the emissions from the forest fires near Mexico City was estimated to add a net amount of OA equivalent to ~37% of the primary BBOA, and it makes a contribution to the outflow of OA from the region (DeCarlo et al., 2010), which should be largest in the late afternoon. Net SOA formation was also observed in BB plumes in the Yucatan where the net relative effect was larger (addition of SOA equivalent to ~100% of the primary BBOA) (Yokelson et al., 2009), perhaps due to the much lower POA emissions from the Yucatan fires compared to those near Mexico City. The impact of BB SOA at the ground inside Mexico City was smaller than for the regional outflow. This was likely due to the fact that BBOA concentrations inside the city peaked in the early morning from emissions in the previous evening and photochemistry was not active during most of the transport period. In contrast, BBOA and acetonitrile levels at T0 were at a minimum during mid-day when OOA was highest (Aiken et al., 2009, 2010). The limited impact of BB SOA to the urban area is also consistent with the limited net SOA formation reported by DeCarlo et al. (2010). An exception was the period around 20–22 March , when substantial SOA from BB emissions was observed at the T0 site (Aiken et al., 2010; Stone et al., 2010a). The lack of a significant decrease of OOA between the high BB and low BB periods confirms that SOA from BB sources was not a dominant contributor to OOA concentrations within the city during most of the campaign (Aiken et al., 2010).

A recently-proposed mechanism postulates the importance of SOA formation from primary semivolatile and intermediate volatility (S/IVOC) precursors from anthropogenic combustion and biomass burning (Robinson et al., 2007). This mechanism has been implemented in a modeling study for MILAGRO (Hodzic et al., 2010a, b), with results similar to two recent studies which compared to MCMA-2003 data (Dzepina et al., 2009; Tsimpidi et al., 2010). The Robinson et al. (2007) version of this mechanism produces approximately the right amount of SOA in the near field, but its O/C is too low and the SOA formed is too volatile (Hodzic et al., 2010a; Dzepina et al., 2009). The Grieshop et al. (2009) update to this mechanism produces too much SOA, especially in the far field, although the O/C prediction is much closer to the observations (Hodzic et al., 2010a; Dzepina et al., 2009). The amount of SOA from anthropogenic S/IVOC reaching T0 and T1 is predicted to be much larger than that from BB sources (Hodzic et al., 2010a). The modern carbon predicted by the model is closer to the observations when S/IVOC precursors are considered compared with when only SOA from VOCs is implemented (Hodzic et al., 2010b). However, there are only weak constraints on the amount and reactivity of primary S/IVOC in Mexico City based on gaps in OH-reactivity and integral FTIR C-H stretches (Sheehy et al., 2010; Dzepina et al., 2009), so it is not clear whether these mechanisms close the SOA budget for the right reasons. Direct measurements of primary and oxidized S/IVOC are critically needed for further progress in this area. The uptake of glyoxal is an alternative mechanism which can produce SOA of high O/C ratios (Volkamer et al., 2009), although it is thought to contribute only the order of ~15% to total SOA in Mexico City (Volkamer et al., 2007).

The current uncertainties on the OA budget led to the proposal of a new quantity, Total Observed Organic Carbon (TOOC), which groups together the carbon from organic gas and particle phase species (Heald et al., 2008). Levels of TOOC in Mexico City are dominated by gas-phase species and are much higher than at other North American locations (Heald et al., 2008). TOOC may be a useful quantify for comparison of measurements and models. However unmeasured species are not included in TOOC and are poorly constrained at present.

The volatility of PM_1 OA components in Mexico City was characterized for the first time using a thermodenuder + AMS combination (Huffman et al., 2008; Faulhaber et al., 2009). Both POA and SOA are semivolatile in Mexico City, with POA being at least as volatile as SOA (Huffman et al., 2009b). These results are consistent with sampling in the Los Angeles area and source tests, and contradict the traditional representation of POA as non-volatile in models (Robinson et al., 2007; Huffman et al., 2009ab). The results from the thermodenuder-AMS system have been used to produce volatility distributions ("basis sets") for the total OA and the OA components (e.g., HOA, OOA, BBOA) (Cappa and Jimenez, 2010). This analysis concludes, using two different techniques, that a substantial fraction (50-80%) of the OA (especially the aged OOA) is essentially non-volatile and will not evaporate under any atmospheric conditions. However a semivolatile fraction is also present (Cappa and Jimenez, 2010), and Hennigan et al. (2008) reported that some of the SOA detected at the T1 site using WSOC measurements evaporated in the afternoons, although to a lesser extent than ammonium nitrate.

The elemental composition of the PM_1 OA was characterized with high time-resolution (down to 10 seconds from aircraft) and high-sensitivity for the first time using a new technique based on high-resolution aerosol mass spectrometry (Aiken et al., 2007). The diurnal cycle of the O/C atomic ratio at T0 peaked with the afternoon photochemistry (~0.5, OA/OC~1.8) and reached the lowest values during the morning rush hour (~0.3, OA/OC~1.6). H/C was anticorrelated with O/C. N/C was low (~0.02) and higher during the morning than the afternoon indicating a more important association with POA (Aiken et al., 2008), although organonitrates are not included in the AMS N/C (Farmer et al., 2010). Regional trends observed from the C-130 aircraft were consistent with those in the city, with increasing O/C away from the city (DeCarlo et al., 2008, 2010; Aiken et al., 2008). The chemical aging trends of OA and SOA observed in Mexico City are consistent with those at multiple other locations (Jimenez et al., 2009; Ng et al., 2010; Heald et al., 2010). Organic species with higher O/C were less volatile on average than those with lower O/C (Huffman et al., 2009a). FTIR functional group analyses showed that in the urban area the molar ratio of oxidized functional group (carboxylic acid) to saturated hydrocarbon functional group (typical of primary organic aerosol) measured with FTIR varied between 0.04 and 0.14, and ratios higher than 0.08 were observed for aged particles (Gilardoni et al. 2009). The correlation of primary metals and carboxylic acid functional groups indicated relatively rapid (less than 12 h since emission) formation of SOA (Liu et al., 2009). The average OA/OC ratios estimated from FTIR at SIMAT and Altzomoni were 1.8 and 2.0, respectively. Gilardoni et al. (2009) observed a larger fraction of oxygenated functional groups in samples collected inside the urban plume compared to background samples, which contrasts with the findings of Aiken et al. (2008) and DeCarlo et al. (2008) who found that urban samples were less oxygenated. The FTIR technique did not observe organonitrates or organosulfates in the particles above the respective detection limits (Gilardoni et al., 2009). Concentrations of organosulfates of ~5 nmol m^{-3} were, however, detected from T0 and T1 samples using LC-MS/MS (Stone et al., 2009).

8.6 New particle formation

New particle formation (NPF) is important for climate (Spracklen et al., 2008), and freshly nucleated particles could affect health (Oberdorster et al., 2005). Very intense NPF

events were observed within the Mexico City basin during MILAGRO consistent with a previous study (Dunn et al., 2004; Molina et al., 2007) in which sulfates and oxygenated organics were observed in the growing particles. Growth rates of freshly nucleated particles were typically about ten times higher than could be explained by the condensation of sulfuric acid alone (Iida et al., 2008). The TDCIMS instrument provided chemical composition measurements for smaller particles than had been characterized before (10–33 nm), and it demonstrated that the high growth rates were dominated by the uptake of nitrogen-containing organic compounds, organic acids, and hydroxy organic acids, while sulfate was a minor contributor to the observed growth (Smith et al., 2008).

8.7 Aerosol CCN activity

Wang et al. (2010) performed a closure study between the measured CCN and those calculated using Kohler theory with the measured aerosol size distributions and composition. Their results suggest that the mixing of non-hygroscopic POA and BC with photochemically produced hygroscopic species takes place in a few hours during daytime, which is consistent with the results of Moffet et al. (2009, 2010). This rapid process suggests that during daytime, a few tens of kilometers away for POA and BC sources, N_{CCN} may be derived with sufficient accuracy by assuming an internal mixture, and using bulk chemical composition. One of the implications is that while physically unrealistic, external mixtures, which are used in many global models, may also sufficiently predict N_{CCN} for aged aerosol, as the contribution of non-hygroscopic POA and BC to overall aerosol volume is often substantially reduced due to the condensation of secondary species.

In situ measurements made from the C-130 aircraft during MILAGRO were examined in an attempt to link the aerosol optical properties to cloud condensation nuclei (CCN) activity (Shinozuka et al., 2009). The wavelength dependence of visible light extinction was found to be negatively correlated with the organic fraction of submicron non-refractory aerosol mass (OMF) over Central Mexico. The OMF was, in turn, anti-correlated with the CCN activity of particles for the urban, industrial and biomass burning aerosols over Central Mexico and the US West Coast. The wide range of OMF means a stronger impact of the aerosol chemical composition in determining the CCN concentration over the regions we investigated compared to fixed-point studies elsewhere. These analyses provide an improved context for understanding the capabilities and limitations for inferring CCN from spectral remote sensing.

Further studies of CCN impacts from water soluble fractions of filter samples have been analyzed using Kohler theory (Padro et al., 2010). This study found that organics were causing a surface tension depression of 10–15%. Lower molar masses (~200 MW) were found for daytime samples with approximately twice that size being found in nighttime samples. This has been interpreted as being due to aging of the aerosols. The overall changes in surface tension appear to partially compensate for changes in the mean molar volume yielding an observed constant hygroscopicity and lead to the consideration that the volume/volume fraction of water-soluble organics is the key compositional parameter in predicting CCN activity.

Ervens et al. (2010) have compared the CCN activity of Mexico City (T0) aerosols to those at other polluted and remote locations, and concluded that CCN can be predicted within a factor of two assuming either externally or internally mixed soluble OA, although these simplified compositions/mixing states might not represent the actual properties of ambient aerosol populations. Under typical conditions, a factor of two uncertainty in CCN concentration translates to an uncertainty of ~15% in cloud drop concentration, which might be adequate for large-scale models given the much larger uncertainty in cloudiness.

9 Aerosol optical properties and radiative influences

Aerosol radiative forcing has been identified as one of the largest uncertainties in climate change research (IPCC, 2007). Aerosol radiative impacts include direct and indirect effects. Direct effects include scattering of incoming solar radiation that can lead to cooling, and absorption of solar radiation that can lead to warming. Indirect effect of aerosol is tied to their ability to act as CCN and form cloud droplets. Absorption of longwave radiation can also lead to forcing by the aerosols and is another area of active research aimed at reducing the uncertainties in these processes. The amount of forcing depends on their physical (size and shape) and chemical properties (surface chemistry, hygroscopicity, etc.) and on their residence times in the troposphere. As aerosol production is tied to energy from combustion of fossil fuels, particularly in large metropolitan areas, the role of megacities as sources of these aerosols and their future evolution in terms of aerosol properties and source strengths is an area where a better fundamental understanding of aerosols is needed for improved regional and global modeling.

During MILAGRO, the MAX-Mex component was specifically focused on making measurements to examine how variable the chemical and physical properties of the megacity aerosols were and how these properties affected the scattering and absorption by the aerosol related to climate. Three surface supersites were instrumented to examine the aerosol plume evolution. As described in Sect. 7 above, the T0 and T1 sites were set up with state-of-the-art aerosol spectrometers and samplers for characterization of chemical and physical properties including the scattering and absorption of aerosols, particularly in the submicrometer fractions that are anticipated to have the longest lifetimes and have the most impact on regional and potentially global climate

forcing. Measurements were also conducted using several airborne platforms: the DOE G-1 that obtained precursor gas and aerosol measurements; a NASA King Air equipped with a High Spectral Resolution Lidar (HSRL) to measure profiles of aerosol extinction, backscattering, and depolarization (Hair et al., 2008; Rogers et al., 2009); NCAR C-130 and the NASA J-31 (see Sect. 10). Rogers et al. (2009) describe the King Air flight operations and show the King Air flight tracks during MILAGRO.

Key findings related to aerosol optical properties obtained during MILAGRO are presented below. Some of the measurements and results related to this topic have been described also under Sect. 8 (Ambient PM).

MILAGRO provided the first-ever deployment of an airborne HSRL on a comprehensive field campaign. Unlike standard backscatter lidars, the HSRL technique enables an accurate and unambiguous measurement of aerosol extinction. Rogers et al. (2009) compared the HSRL aerosol extinction measurements with aerosol extinction derived from simultaneous measurements from the NASA Ames Airborne Sun Photometer (AATS-14) (Redemann et al., 2009) and in situ scattering and absorption measurements from the Hawaii Group for Environmental Aerosol Research (HiGEAR) (McNaughton et al., 2009) in situ instruments and found bias differences between HSRL and these instruments to be less than 3% ($0.001\,km^{-1}$) at 532 nm; root-mean-square (rms) differences at 532 nm were less than 50% ($0.015\,km^{-1}$). These differences are well within the typical state-of-the-art systematic error of 15–20% at visible wavelengths (Schmid et al., 2006). Airborne HSRL measurements of aerosol intensive properties were used to identify aerosol types and partition the measured extinction into cumulative Aerosol Optical Depth (AOD) for each type (Ferrare et al., 2007). The aerosol type consisting of a mix of dust and urban aerosols accounted for nearly half of the AOD measured by the HSRL with urban/biomass aerosol types accounting for approximately 35% of the AOD (see Fig. 13). In contrast, during subsequent HSRL field missions over the Houston region (Parrish et al., 2009b) and the eastern US, urban/biomass aerosols accounted for 80–90% of the AOD.

While scattering by aerosols is fairly well understood and is principally dependent on size and shape of the aerosols, absorption of solar radiation by atmospheric aerosols is a major uncertainty in assessing radiative balance on regional scales. Carbonaceous aerosols are of particular concern as they are among the major light absorbing species in the troposphere. Incomplete combustion of hydrocarbon fuels leads to the formation of carbon soots or black carbon, which have been well known as a significant, if not the major, absorbing aerosol species in the troposphere (Marley, et al., 2007; Marr, et al., 2006). Fossil fuel combustion, particularly in diesel engines, has received significant attention as the major source of black carbon aerosols. Other sources of absorbing carbonaceous aerosols (i.e., black carbon and other UV-Vis active species such as PAH, conjugated ketones and other partially combusted organics) include biomass burning of agricultural fields and forest fires as well as the formation of potentially light-absorbing absorbing SOA from anthropogenic, biomass burning, and biogenic precursors. Light absorption by SOA is an active research topic (e.g., Andreae and Gelencser, 2006; Barnard et al., 2008).

Results from both ground-based and airborne measurements confirm that Mexico City is a significant source of both primary and secondary aerosols at the regional scale (Doran, et al., 2007; 2008; Fast, et al., 2009, Kleinman, et al., 2008; DeCarlo et al., 2008). Single scattering albedos in the MCMA and downwind are substantially lower than in other areas (such as the eastern United States) (Doran et al., 2007, 2008; Kleinman et al., 2008; Marley et al., 2009a; Paredes-Miranda et al., 2009; Thornhill et al., 2008). These results are consistent with the significant amounts of black carbon and light-absorbing PAH coatings observed during these studies as well as during MCMA-2003 (Marr, et al., 2006; Marley et al., 2007; Stone et al., 2008; Querol et al., 2008). Carbon-14 and stable carbon-13 measurements also have indicated that a major fraction of the total carbonaceous aerosol is coming from recent carbon sources including biomass and agricultural burning activities (Marley et al., 2009a; Aiken et al., 2010). As discussed in Sect. 7, modern carbon measurements are about 15% higher during the high biomass burning periods compared to those in which BB is suppressed by rain (Aiken et al., 2010). Thus other urban and regional sources of modern carbon are important in Central Mexico, such as biogenic SOA (Hodzic et al., 2009), food cooking (Mugica et al., 2009), and other anthropogenic open burning activities (e.g., trash burning and biofuel use (Christian et al., 2010)). Larger relative amounts of biomass burning aerosols were noted at the T1 regional site than the urban T0 site (Stone et al., 2008; Marley et al., 2009b), consistent with the megacity having a significant fossil fuel input, but both sites were heavily impacted by recent carbon sourced carbonaceous aerosols from local and regional burning and also other modern carbon-containing sources as discussed above.

As noted, light scattering and absorption measurements in the UV-visible region found that the ground-based T0 and T1 surface sites single scattering albedo (SSA) was frequently in the 0.7–0.8 range with some early morning values having even lower SSA (Marley, et al., 2009b; Paredes-Miranda et al., 2009). Aircraft results from several platforms (NASA King Air, DOE G-1, and NCAR C-130) aerosol instruments all indicate that there was significant transport of aerosols and that most of this aerosol is in the lower layer of the atmosphere consistent with the ground sourcing of primary aerosols and secondary aerosol precursors. Aircraft SSA values were typically found to be higher than ground-based measurements, but still lower than those typically seen in the eastern US due to absorbing aerosols (Kleinman et al., 2008). The aircraft measurements also found that substantial amounts of aerosols (primary and secondary) can be transported aloft and exported to regional and global scales via

the free troposphere during venting events that were anticipated by pre-campaign modeling studies (Fast et al., 2007). Substantial vertical layering of the aerosol and regional differences in the Valley of Mexico for aerosol scattering and extinction was also found. Enhanced UV absorption (300–450 nm) of incoming solar radiation was found to be substantial and was likely due to both SOA formation as well as from biomass burning sources (Corr et al., 2009; Marley et al., 2009b), consistent with a previous study during MCMA-2003 (Barnard et al., 2008). The wavelength dependence of absorption measured at 470, 530 and 660 nm on the C-130 was higher with higher organic fraction of non-refractory mass of submicrometer particles, and this relationship was more pronounced under high single scattering albedo, as expected for the interplay between soot and colored weak absorbers (some organic species and dust) (Shinozuka et al., 2009). The slope of SSA spectra also varied with the submicrometer aerosol composition. These observations from the C130 aircraft are consistent with, and extend, the results obtained elsewhere using AERONET ground-based remote sensing and airborne radiometric techniques (Russell et al., 2010). J-31 measurements of aerosol absorption over the broader wavelength range 350–~1650 nm (Bergstrom et al., 2010) also indicated the combined presence of black carbon, organic matter and possibly mineral dust and their influence on the wavelength dependence of absorption.

A strong correlation was found between the absorption Angstrom exponent (AAE) and the modern carbon content (radioactive ^{14}C) in aerosols. The AAE values were derived from a simple exponential fit of the broadband aerosol absorption spectra obtained from either a seven-channel wavelength Aethalometer (5-min time resolution) or from 12-h integrated submicrometer aerosols samples by using an integrating sphere/spectrometer to obtain complete UV-visible-NIR spectra (Marley et al., 2009b). This result showed the significant impact that grass fires had in the region during the MILAGRO campaign on the lower atmospheric aerosol radiative forcing. Rain events during the latter portion of the campaign were found to put out the fires and both lower ^{14}C content and reduced UV-visible absorption were seen in the data (Marley et al., 2009a; Marley et al., 2009b; Aiken et al., 2010). Both biomass-burning and SOA sources are likely to add significant absorption in the UV-VIS-NIR region. These more complete spectral evaluations of aerosol absorption indicate the importance of multi-wavelength if not complete spectral characterization for absorbing carbonaceous aerosols. Previous work using single wavelengths, particularly at wavelengths longer than 500 nm, did not detect these changes in absorption in the 300 to 500 nm range that are primarily due to oxidized organics (both aged primary and SOA coatings).

Studies from MILAGRO have reported significant enhanced UV-Visible absorption from biomass burning, secondary organics, and aged carbonaceous aerosol components. It will be important to add this spectral information to direct effect climate modeling efforts for these classes of organic aerosols, as this enhanced absorption will lead to warming of the atmosphere. This includes improved modeling of SOA production from megacity environments (Fast et al., 2009; Hodzic et al., 2009, 2010a, b; Dzepina et al., 2009). The importance of absorbing aerosols on regional radiative forcing has also been seen in other major field studies such as INDOEX (Ramanathan et al., 2001) and is an indication of the increasing potential importance that SOA and biomass burning aerosols may have on regional climate direct forcing, even in megacity environments. With anticipated increases in the growing seasons, reduced precipitation in summer months, and warmer climates, increases in forest and grass fires are predicted for many regions (IPCC, 2007). The potential increases in agricultural burning due to future increases in biofuel production constitute land use change that may add to carbonaceous aerosol impacts. The connection between biomass and agricultural burning with enhanced UV-visible absorbing aerosols identified during MILAGRO will need to be added to future regional climate modeling efforts.

Infrared forcing of these aerosols, particularly in the boundary layer is another area that has been identified as potentially important (Marley et al., 1993; Gaffney and Marley, 1998). FTIR and mass spectral studies have been reported that indicate that humic-like substances (HULIS) are contributing to the carbonaceous aerosols (Stone et al., 2009) and that these have strong absorption bands in the mid-IR region consistent with their HULIS structures (Marley et al., 1996, 2009a). The mid-IR absorption of carbonaceous aerosols will also add to the heating of the lower atmosphere and megacity sources of these aerosols along with associated higher greenhouse gases certainly add to urban heat island effects (Marley et al., 1993; Gaffney and Marley, 1998).

10 INTEX-B flights over Mexico City and the Gulf

This section presents an overview of methods and results of the Jetstream 31 (J-31) which participated in MILAGRO as part of the NASA-led INTEX-B study. As described by Singh et al. (2009), the major INTEX-B aircraft was a DC-8, which flew in two phases: 1–21 March (focused on Mexico and the Gulf during MILAGRO), and 17 April–15 May (focused on trans-Pacific Asian pollution transport). Methods and results of all DC-8 flights in INTEX-B are summarized by Singh et al. (2009).

10.1 J-31 overview

For INTEX-B/MILAGRO the J-31 was equipped to measure many properties of solar radiant energy and how that energy is affected by atmospheric constituents and Earth's surfaces. Table 7 gives more information on J-31 instruments and the properties retrieved from their measurements. Because solar

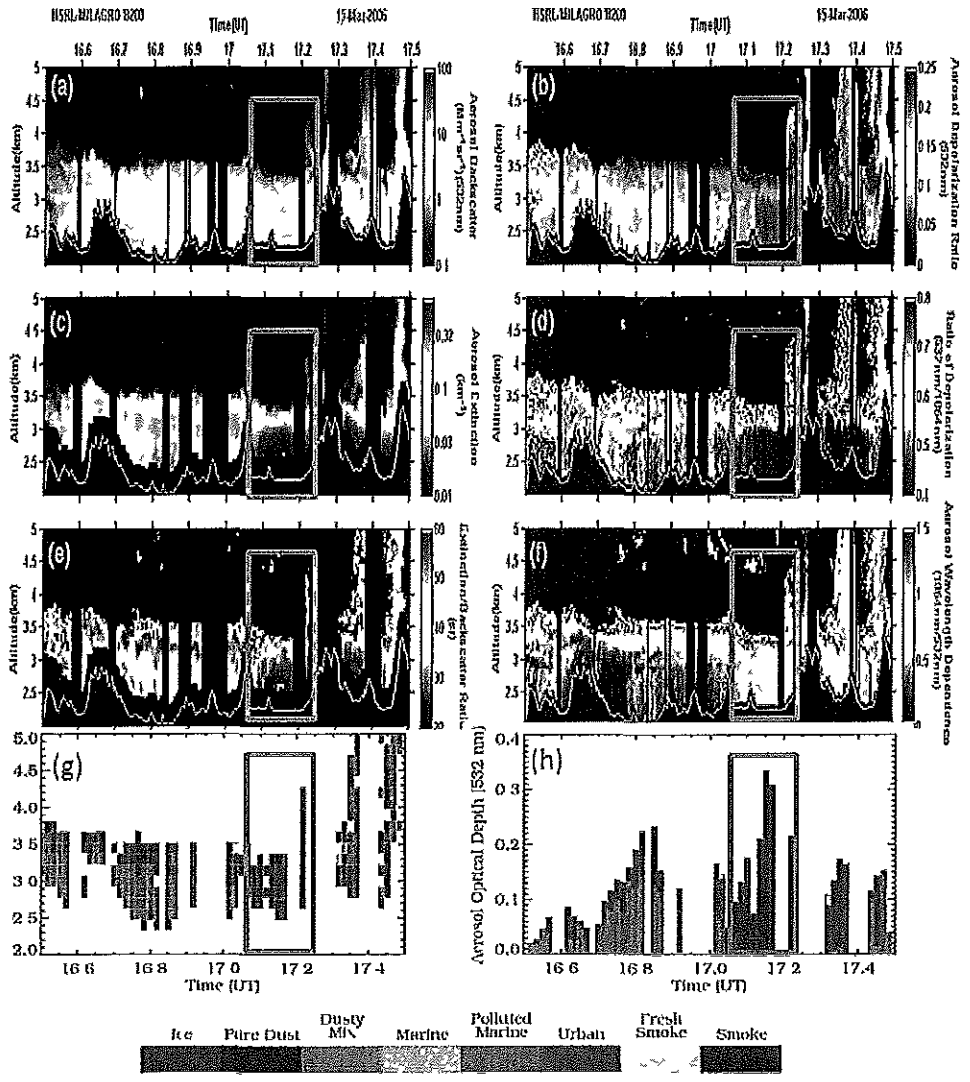

Fig. 13. Suite of airborne HSRL aerosol measurements acquired on 15 March 2006 in the Mexico City region. **(a)** aerosol backscatter (532 nm), **(b)** aerosol depolarization (532 nm), **(c)** aerosol extinction (532 nm), **(d)** ratio of aerosol depolarization (532/1064 nm), **(e)** aerosol extinction/backscatter ratio, **(f)** backscatter wavelength dependence (1064/532 nm), **(g)** aerosol type inferred from the HSRL measurements, and **(h)** aerosol optical thickness (532 nm) contributed by each aerosol type. In (h), the total length of the bar represents the total aerosol optical thickness. The color bar at the bottom denotes the various aerosol types. The purple box between 17:05–17:25 UT indicates when the King Air flew directly over the city from northwest to southeast. Prior to that time, the King Air flew to the north and east of the Mexico City region. Over the city, the HSRL measurements indicate that urban (polluted) aerosols had the greatest contribution to AOD; in contrast, outside the city, a mixture of dust and urban aerosols had the greatest contribution to AOD.

energy drives Earth's climate, the J-31 suite of measurements helps show how changing atmospheric and surface properties can change the climate.

Constituents retrieved from J-31 measurements in INTEX-B/MILAGRO include aerosol particles, water vapor, and clouds, in addition to properties of a variety of Earth surfaces. Specific scientific goals of these measurements were to:

- Characterize the distributions, properties, and effects of aerosol PM and water vapor advecting from Mexico City and biomass fires toward and over the Gulf of Mexico, including:
  - Aerosol optical depth and extinction spectra (354–2138 nm).
  - Water vapor columns and profiles.
  - Aerosol radiative impacts: in clear sky (direct effect) & via clouds (indirect effect).

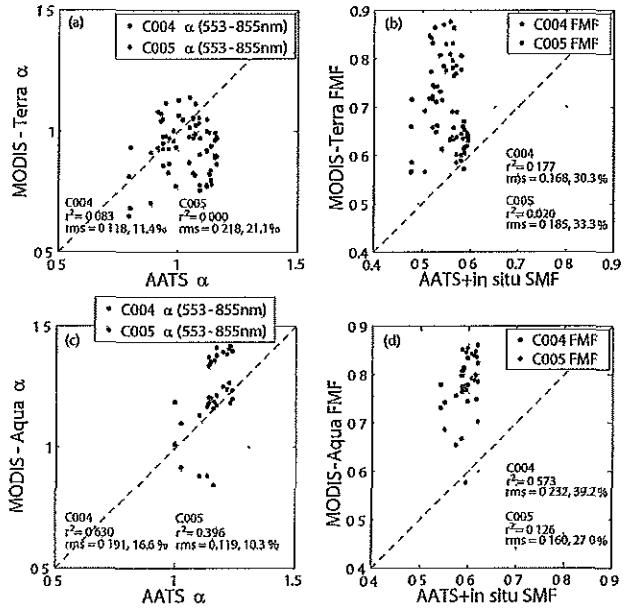

Fig. 14. **(a)** Comparison of MODIS-Terra and AATS-14 derived AOD Angstrom exponent for MODIS Collection 4 (C004, blue circles) and Collection 5 (C005, red circles). **(b)** Same as (a), but for the MODIS-Terra derived fine mode fraction, FMF, versus the AATS + in situ derived sub-micron fraction of AOD. **(c–d)** same as (a–b), but for MODIS-Aqua. The AATS + in situ derived sub-micron fraction of AOD uses DC-8 INTEX-B measurements as described by Redemann et al. (2009).

- Test the ability of Aura, other A-Train & Terra satellite sensors, and airborne lidar, to retrieve aerosol, cloud, and water vapor properties.
- Characterize surface spectral albedo and bidirectional reflectance distribution function (BRDF) to help improve satellite retrievals.
- Quantify the relationships between the above and aerosol amount and type.

The J-31 made 13 successful flights totaling 43 flight hours out of Veracruz airport during MILAGRO. Scientific results are presented in several papers referenced below.

10.2 Results from J-31 flights and related measurements

Coddington et al. (2008) used J-31 Solar Spectral Flux Radiometer (SSFR) measurements of upward and downward irradiance to determine spectral surface albedo at ground stations and along the flight track, thereby linking flight-level retrieved measurements to larger-scale satellite observations in the polluted Mexico City environment. As they point out, these spectral surface albedo values strongly affect Earth's radiation balance and are also boundary conditions that need to be accurately known for aerosol remote sensing, aerosol radiative forcing, and radiative transfer calculations. Their approach involves iteratively adjusting the surface albedo input of an SSFR-specific radiative transfer model until the modeled upward irradiance matches the SSFR measurements at flight level. They also compared spectral surface albedos derived from the SSFR, Multi-Filter Rotating Shadowband Radiometer (MFRSR), and the Moderate Resolution Imaging Spectroradiometer (MODIS) instrument onboard the NASA-EOS Terra and Aqua satellites, obtaining differences of 6–10% and 0.025–0.05 units, respectively. Along-track comparisons between the SSFR and MODIS show that two instruments (aircraft and satellite) can capture inhomogeneous surface albedo scene changes.

A related MILAGRO/MCMA-2006 study on surface reflectance in the Mexico City metropolitan area was conducted by de Almeida Castanho et al. (2007). Their approach included using radiances from the MODIS satellite sensor at 1.5 km spatial resolution over distinct surfaces in the area to determine ratios of visible (VIS) to shortwave infrared (SWIR) reflectance for those surfaces. They also measured AOD using sunphotometers at 5 different locations over the urban area, as well as the CIMEL from the global AERONET located at the three supersites. They found that use of their derived VIS/SWIR surface reflectance ratios in the MODIS AOD retrieval algorithm greatly improved agreement between AOD measured from the surface and retrieved from MODIS.

J-31 Research Scanning Polarimeter (RSP) measurements have been used in studies of both Earth surface properties and aerosols. Chowdhary et al. (2010) use RSP measurements over the open ocean at low and high altitudes, and at azimuth angles close to and away from the solar principal plane, to show that reflectances are sensitive to variations in chlorophyll*a* concentrations in the ocean, and that they can be matched using their hydrosol model over the full range of viewing geometries and observational heights and over the entire solar spectrum. In that study aerosol optical thickness values used in radiative transfer calculations are varied to match data from the Ames Airborne Tracking Sunphotometer (AATS) on the J-31. Cairns et al. (2009) use RSP measurements made over Mexico City to demonstrate for the first time the accurate retrieval of aerosol accumulation mode particle size, complex refractive index and spectral optical depth using downward looking passive measurements above an urban environment.

Livingston et al. (2009) use J-31 AATS measurements acquired over the Gulf of Mexico and Mexico City to evaluate retrievals of AOD from measurements by the Ozone Monitoring Instrument (OMI) aboard the Aura satellite and from the MODIS aboard the Aqua satellite. They show that MODIS and AATS AODs agree to within root mean square (RMS) differences of 0.00–0.06, depending on wavelength, but that OMI and AATS AODs can differ by considerably more. They explore how these OMI-AATS differences

depend on the OMI retrieval algorithm used (near-UV vs. multiwavelength), on the retrieved aerosol model, and on other factors.

Redemann et al. (2009) compare J-31 AATS measurements of AOD and related aerosol properties to results from MODIS-Aqua and MODIS-Terra, with emphasis on differences between the older MODIS Collection 4 (C4) and the new Collection 5 (C5) data set, the latter representing a reprocessing of the entire MODIS data set completed during 2006. They find notable differences between MODIS C4 and C5 in AOD, Angstrom exponent, and aerosol fine mode fraction (FMF), and they explore how those differences depend on MODIS instrument (Aqua vs. Terra), on wavelength, and on other factors. An example result is shown in Fig. 14. They conclude that differences in MODIS C4 and C5 in the limited J-31 INTEX-B/MILAGRO data set can be traced to changes in the sensor calibration and recommend that they be investigated with a globally more representative data set.

Schmidt et al. (2010) introduce a method for deriving aerosol spectral radiative forcing, along with single scattering albedo, asymmetry parameter and surface albedo from airborne vertical profile measurements of shortwave spectral irradiance and spectral aerosol optical thickness. Using data collected by the SSFR and the AATS-14 on the J-31, they validate an over-ocean spectral aerosol forcing efficiency from the new method by comparing with the traditional method. Retrieved over-land aerosol optical properties are compared with in-situ measurements and AERONET retrievals. The spectral forcing efficiencies over ocean and land are remarkably similar, and agree with results from other field experiments.

Gatebe et al. (2010) use measurements by CAR on the J-31 and an AERONET sun-sky photometer on the ground to test a new method for simultaneously retrieving aerosol properties and surface reflectance properties from combined airborne and ground-based direct and diffuse radiometric measurements. Results are shown from four campaigns at four sites having different surface characteristics and aerosol types. As an example, for 6 March 2006 over Mexico City, they retrieve an aerosol size distribution that is trimodal above the J-31 and bimodal below. Although submicrometer particles appear to dominate in both layers, there is a significant contribution to the total optical thickness from particles with $r > 1$ μm. Results for single scattering albedo and complex refractive index above and below the aircraft are also presented.

Bergstrom et al. (2010) combine J-31 measurements of solar radiation spectra by SSFR and AOD spectra by AATS to derive spectra of aerosol SSA and aerosol absorption optical depth (AAOD) for two flights over the Gulf of Mexico and three flights over Mexico City for wavelengths from 350 to ~1650 nm. They describe the results in terms of three different wavelength regions: The 350–500 nm region where the aerosol absorption often falls off sharply presumably due to organic carbonaceous matter and windblown dust; the 500–1000 nm region where the decrease with wavelength is slower, presumably due to black carbon; and the near infrared spectral region (1000 nm to 1650 nm) where it is difficult to obtain reliable results since the aerosol absorption is relatively small and the gas absorption dominates. However, there is an indication of a small and somewhat wavelength independent absorption in the region beyond 1000 nm. For one of the flights over the Gulf of Mexico near the coastline it appears that a cloud/fog formation and evaporation led to an increase of absorption possibly due to a water shell remaining on the particles after the cloud/fog had dissipated. For two of the Mexico City cases, the single scattering albedo is roughly constant between 350–500 nm consistent with other Mexico City results. In three of the cases a single absorption Angstrom exponent (AAE) fits the aerosol absorption optical depth over the entire wavelength range of 350 to 1650 nm relatively well ($r^2 > 0.86$).

Additional results on Mexico City aerosol absorption wavelength dependence from C-130 measurements in MILAGRO are presented by Russell et al. (2010), who also present an analysis from previous AERONET measurements in Mexico City and other locations.

11 Health studies

There is strong evidence from around the world that urban air pollution affects human health (Samet and Krewski, 2007). Health effects have been associated predominately with at least one of the so-called criteria pollutants that are routinely measured to assess air quality in most cities around the world. Ozone and PM represent a common persistent problem in several cities, with important effects on public health (Craig et al., 2008). Although recent attention has been brought towards understanding the role of multipollutants interactions in air pollution related health effects (Mauderly and Samet, 2009), current methodological approaches have focused on ozone (Samoli et al., 2009) and, more importantly, in PM as the criteria pollutant with stronger associations with most of the described health effects.

Adverse health outcomes include: increased mortality, hospital admissions, altered pulmonary function, cancer, asthma, etc. (Pope and Dockery, 2006). However, PM effects are heterogeneous and vary with PM size, season and location (Bell et al., 2008; Dominici et al., 2006; Peng et al., 2005). Recent evidence at the experimental and population level indicates that variations in the PM mixture chemical composition could account for the heterogeneous health effects observed (Alfaro-Moreno et al., 2010; Dominici et al., 2007; Lippmann et al., 2006). For example, Ni and V content have been linked to increased cardiovascular disease. Local conditions, however, can drive stronger associations, as in the case of New York City where local sources could be responsible for high Ni content, causing health effects both locally and at downwind locations as due to "imported" pollution

(Dominici et al., 2007; Lippmann et al., 2006). The emerging issue of the role of PM composition will require studies using more comprehensive data on air pollution components, e.g., EPA's Speciation Trends Network (Lippmann, 2009), and their chemical "evolution" during emission, atmospheric dispersion and transport.

The MCMA has been the subject of previous pollution-related health studies. Evidence on mortality and school absenteeism was first published in the 1990s (Borja-Aburto et al., 1997; Romieu et al., 1992). More recent evidence has been focused on children's health, e.g., the participation of genetic polymorphisms (Romieu et al., 2006), systemic damage (Calderon-Garciduenas et al., 2007), lung growth retardation (Barraza-Villarreal et al., 2008) and the participation of other variables such as education (O'Neill et al., 2008). Some of the published results from Mexico City describe situations relevant to information revealed by MILAGRO. Among them are the importance of coarse particles on mortality (Castillejos et al., 2000) or the existence of PM toxicological profiles depending on where the samples were obtained (Osornio-Vargas, et al., 2003) and the relative effects of their components (Rosas-Perez et al., 2007). See Sect. 8 for further information on MCMA PM levels and characteristics.

Many MILAGRO observations are relevant to human exposure and health impact. However, it is difficult to relate them directly to health effects due to the short length of the campaign, compared to the typical length for human health effects studies. The MILAGRO findings are certainly useful for the design of future health studies, including effects related to long range transport of pollutants (see e.g., Hashizume et al., 2010).

Two health-related studies were carried out during MILAGRO: one on human exposure and another at the cellular level; each are described briefly below:

(1) The human exposure study done by Tovalin et al. (2010) aimed to evaluate the contribution of regionally transported air pollutants from the MCMA to the children's personal exposure (age 9–12) and their parents during the campaign. This study included: collection of personal and microenvironmental samples of air pollutants (ozone, fine and ultrafine particles, CO, VOCs) at three selected sites in urban, suburban and rural areas; comparison of the indoor and outdoor concentrations and personal exposures to air pollutants at the three sites; determination of the association between the exposures and the level of oxidative stress markers among the study populations; and analysis of the relationship between the exposures and their respiratory health. Results indicate that children near T0 have decreased levels of respiratory and olfactory function as well as enhanced indicators for oxidative stress and inflammation. However, the lack of clear gradient effects between urban, suburban and rural areas suggests that local sources are also playing a role on health effects. Pollutants such as benzene, O_3, NO_2, SO_2, PM_{10} showed statistical associations with biomarkers of oxidative stress. The study design and the duration of the study did not allow for discrimination between acute and cumulative effects.

(2) Osornio-Vargas el at. (2008) described the oxidative potential of PM_{10} collected at T0 and T1 using Electron Paramagnetic Resonance (EPR) technique in the presence of DMPO as an OH trap to correlate with in vitro PM_{10}-induced membrane disruption and degradation of isolated DNA. Daily samples were pooled and analyzed accordingly to the influence/non-influence dispersion patterns of T0 on T1, as defined by de Foy (2008) during MILAGRO using back trajectories. PM_{10} samples from T0 had a higher oxidative potential than those from T_1. During T0 $\rightarrow$ T1 influence days, the oxidative potential of T1 samples was lower than for other days. Additionally, PM_{10} samples were analyzed for elemental content and oxidative potential correlated with PM_{10} Cu and Zn levels. However biological effects did not correlate with oxidative potential and were different by site, probably as a result of local influences such as PM_{10} composition, suggesting that oxidative stress is not the only mechanism involved in PM-toxicity. Other MILAGRO findings support these observations, for example: (1) Mexico City's air pollution "footprint" influences the receptor site, but not further than 200 km (Kleinman et al., 2008; Mena-Carrasco et al., 2009); (2) The plume dilutes and ages as it moves towards the receptor site (Kleinman et al., 2008); and (3) MCMA is photochemically very active and produces large amount of OH from various radical sources. The highly reactive OH controls lifetime and fate of most ambient trace gases (Dusanter et al., 2009a). Mugica et al. (2009) also describe the variability of PM oxidative potential in relation to composition, sources and meteorological conditions.

Several studies on different PM size fractions give useful information on PM composition and its evolution or aging, as described in Sect. 8 of this Overview. Of particular interest for health studies are the results on metals and PAHs, many of which have known toxic effects. Another important observation is that persistent organic pollutants (POPs) collected with passive samples had similar indoor and outdoor concentrations in Mexico City (Bohlin et al., 2008). These are important points worth keep in mind when considering human exposures.

12 Summary and conclusions

The MILAGRO Campaign was designed to investigate the extremely vigorous atmospheric photochemistry of North America's most populous metropolitan area. The observation phase of MILAGRO/INTEX-B has provided an extremely rich data set that will likely take years to fully analyze and evaluate. Many interesting aspects of atmospheric chemistry in and near the MCMA are emerging and have already added to our understanding of the chemical and physical properties of the city's reactive atmosphere and its

regional impacts. Results from 2006, as well as the earlier 2002/2003 studies, have been presented at international conferences and communicated to Mexican government officials. In this paper we have reviewed over 120 papers resulting from MILAGRO/INTEX-B Campaign that have been published or submitted, as well as additional relevant papers from MCMA-2003, with the aim of providing a road map for the scientific community interested in understanding the emissions from a megacity such as the MCMA and their impacts on air quality and climate.

12.1 Summary of key findings

Key findings from the analysis and evaluation of the extensive MILAGRO and relevant MCMA-2003 results obtained to date are summarized below.

12.1.1 Meteorology and dynamics

- The overall synoptic conditions and boundary layer circulations were similar to those reported by MCMA previous studies and consistent with prior climatology, suggesting that results from MILAGRO are applicable to general conditions in the MCMA.
- Meteorological measurements at the surface and aloft coupled with measurements of trace gases and aerosols indicate that the synoptic-scale transport of the Mexico City pollutant plume was predominantly towards the northeast, although regional-scale circulations transported pollutants to the surrounding valleys and basins on some days.
- On the basin-scale, morning winds from the north transported the plume towards the south. On certain days, this was transported over the basin rim or through the mountain pass in the southeast. An afternoon gap flow from the south reversed the flow direction in the mountain pass and contributed to flushing the MCMA plume towards the northeast.
- Surface and airborne lidars, as well as airborne meteorological measurements have shown multiple layers of particulate matter resulting from complex mixing processes over central Mexico.
- Drainage flows at night have a strong impact on air pollution transport and accumulation in the basin leading to high pollutant concentrations.
- Biomass burning plumes were found to be transported into the MCMA from the surrounding basin and outlying regions.
- The Popocatepetl volcano has very limited impacts on the air quality in the MCMA because of the elevation of the emissions and the vertical stratification in the wind flows. However, these impacts can be larger at regional scales.
- CMET balloon trajectories found strong layering of the urban plume persisting as far as the Gulf of Mexico, with very rapid transport at high altitude.
- Mesoscale meteorological models were found to capture the main features of the basin wind transport and were of sufficient accuracy to assist in data analysis and interpretation.
- The combination of Radar Wind Profiler analysis and modeling studies assisted in suggesting possible source areas of heavy metals. Further analysis could be used to identify these more precisely.

12.1.2 MCMA emissions of gases and fine PM:

- MILAGRO demonstrated the synergy of using multiple bottom-up and top-down analysis techniques with data obtained from multiple platforms and instruments to evaluate emissions inventories. The combined process helps to reduce the associated uncertainties in the emissions estimates and provides guidance for setting priorities for improving further development and refinement of the emissions inventories.
- Several studies showed that some mobile emissions from gasoline vehicles in the MCMA decreased in recent years, CO in particular, but that mobile emission sources are still the main contributors of gaseous pollutants and a major contributor to PM pollution in the city.
- The relative contribution of diesel vehicles to overall NO_x levels has increased over time in the city. This is expected and consistent with observations in the US, and is partially due to the increases in diesel fuel consumption and to the introduction of very effective control technologies for gasoline vehicle emissions, which have not been matched by similarly effective diesel emission control technologies (Harley et al., 2005; Ban-Weiss et al., 2008).
- The measurements of mobile emissions during MILAGRO identified several discrepancies between the observations and the emissions estimates in the emissions inventory. These include slight overpredictions of CO and NO (<30% and <20%, respectively), and a probable underprediction of VOCs by a factor of 1.4 to 1.9 in the inventory. Similarly, there is modeling and observational evidence that the current PM emissions estimates are severely underestimated.
- The direct flux measurements at the SIMAT tower site in the city center suggest that the local emissions inventory estimates of CO_2, olefins and selected aromatic and

oxygenated VOCs are accurate for emissions from combustion sources, but overestimate the evaporative emissions from area sources within several km footprint of the measurement site. In contrast, the aircraft flux measurements indicate an underestimation of the toluene and benzene emissions reported in the emissions inventory for the northeast industrial sector of the city.

- The surface and airborne flux measurements carried out during MCMA-2003 and MILAGRO-2006 demonstrated that the eddy covariance techniques coupled with fast response sensors can be used to evaluate directly emission inventories in a way that is not possible with other indirect evaluation methods, making them valuable tools for improving the air quality management process.
- Due to the uncertainties on the current estimates of PM emissions in the emissions inventory, it is important to better characterize the PM contributions from the diesel and gasoline mobile emissions sources in the MCMA.
- Additional sources from informal commerce and road side food preparation need to be characterized. The results show that there is potential for severe local impacts on air quality from cooking and garbage fires, as they can be major sources of several reactive gases and fine particles.
- The widespread multi-source urban/industrial emissions may have an important influence on Hg in the MCMA. Nevertheless, other species not addressed in this review (e.g., NH_3, dust, metals) warrant further study in the MCMA.

12.1.3 MCMA volatile organic compounds

- Evaporative fuel and industrial emissions are important sources for aromatic VOCs in the basin.
- LPG use continues to be an important source of low molecular weight alkanes.
- Many hydrocarbon emissions show greater enhancement ratios to CO in the MCMA than the US due to the widespread use of LPG and higher industrial and evaporative emissions of aromatics in Mexico City.
- Total OH reactivity due to VOCs in the MCMA remains largely unchanged from the 2003 study; however the speciated attribution is quite different. Formaldehyde and acetaldehyde were the two most important measured VOC species in terms of OH reactivity in the MCMA.
- Diurnal variations suggest that photochemical formation of secondary VOCs is very important in the MCMA basin.
- Fires are a modest source of VOCs measured at surface sites.
- Rapid photochemistry transforms the VOC OH reactivity distribution from NMHCs domination in the morning hours in the MCMA basin to OVOCs domination aloft and downwind.
- There are large non-biogenic sources of methanol in the MCMA basin.

12.1.4 Urban and regional photochemistry

- Measured concentrations of OH and HO_2 in the MCMA were higher than predicted in the morning when NO_X is high, suggesting that there may be a significant source of radicals missing from current atmospheric chemistry models of polluted environments.
- Photolysis of HONO and HCHO and ozonolysis of alkenes are important sources of radicals in the MCMA, while photolysis of ozone is a minor contributor to total radical production. Inclusion of heterogeneous sources of HONO improves substantially the agreement between measured and modeled HONO and HO_x concentrations and enhanced the production of O_3 and SOA.
- The net instantaneous rate of ozone production from HO_2 radicals as well as the observed rate of ozone production from all production mechanisms are among the highest observed anywhere.
- Several chemical transport models and analyses of measurements indicate that ozone production in the MCMA is generally VOC-limited.
- On the regional scale, significant enhancements of O_3 above background were observed in plumes that could be traced back to Mexico City, with indications that significant O_3 production occurred during the plume transport time.
- Regional O_3 production appears to be sensitive to NO_X as well as to VOCs and CO, with the regional OH radical reactivity dominated by oxygenated organics and CO.
- Long-range export of reactive nitrogen from Mexico City was found to take place primarily via the formation of PANs, which can thermally decompose leading to regeneration of NO_X contributing to regional O_3 formation.
- Biomass burning was found to have a significant influence on regional chemistry, contributing more than half of the organic aerosol and about one third of the benzene, reactive nitrogen, and carbon monoxide to the regional outflow.

12.1.5 Ambient particulate matter

- During the study, PM_{10} and $PM_{2.5}$ concentrations in the urban area were about double the concentrations in the rural areas surrounding Mexico City.
- $PM_{2.5}$ made up about half of the PM_{10} concentrations, with small amounts of mass in the $PM_{2.5}$–$PM_{1.0}$ range.
- Mineral matter made up approximately 25% of the PM_{10} and on average 15% and 28% of the $PM_{2.5}$ in the urban and rural areas, respectively. Approximately 25% of the $PM_{2.5}$ was secondary inorganic ions with the remaining $PM_{2.5}$ mass being comprised of largely carbonaceous aerosol.
- Except for surface measurements at the central sampling sites in Mexico City, the elemental carbon mass absorption efficiency was relatively constant for aircraft and surface measurements throughout the study.
- Although different organic aerosol source apportionment methods had some differences, there was agreement that the dominant sources of carbonaceous aerosol were secondary organic aerosol, biomass burning, and vehicle exhaust emissions.
- The impact of biomass burning on the aerosol outflow from the region was much larger than on the surface concentrations inside the city.
- SOA formation from primary semivolatile and intermediate volatility precursors has the potential to close the gap in predicted vs. measured SOA. However these predictions are poorly constrained by the data and more specific measurements are needed in future campaigns.
- Biogenic SOA advected from the coastal ranges contributes about $1\,\mu g\,m^{-3}$ to concentrations in the MCMA.
- Anthropogenic alkenes add little organic mass to SOA, but indirectly add to SOA by reacting to produce radicals for the processing of other SOA precursor VOCs.
- Additional work is needed to fully quantify the sources of substantial modern carbon in organic aerosols during low biomass burning periods. Discrepancies between the two ^{14}C datasets deserve further study. A modeling study suggests that the observed modern OC may be due to a combination of regional biogenic SOA, biomass burning OA, and POA and SOA from urban sources of modern carbon.
- Primary OA from anthropogenic and biomass burning sources was found to be semivolatile, while secondary OA was less volatile than POA and aged SOA was essentially non-volatile, in contrast with current models.
- Growth rates of new particle formation in Mexico City were very large and found to be impacted by nitrogen containing organic compounds, organic acids, and hydroxyl organic acids, with only a smaller fraction of sulfate aerosol.
- CCN can be predicted well with an internal mixing assumption after a few hours of photochemical aging, which is shorter than scales in most global models.

12.1.6 Optical properties and remote measurements of aerosol and earth surfaces

- At the T0 and T1 surface sites single scattering albedos (SSA) were frequently in the 0.7–0.8 range with some early morning values having even lower SSA. This is consistent with high absorbing aerosol concentrations from both fossil and biomass burning sources during MILAGRO.
- Aerosol contributions from biomass burning sources contained both black carbon and oxidized organics that yielded enhanced UV absorption. This observation indicated biomass burning activities can have important impacts on the absorption or heating by carbonaceous aerosols in megacity (urban) as well as regional scales.
- Oxidized organics from primary fires and from secondary aerosol formation were also found to have strong absorption in the 300–400 nm region that leads to enhanced optical absorption by these aerosols over that anticipated from black carbon alone.
- Comparisons of the HSRL aerosol extinction measurements with aerosol extinction derived from simultaneous airborne Sun photometer and in situ scattering and absorption measurements found bias differences between HSRL and these instruments to be less than 3% (0.01 km-1) at 532 nm; root-mean-square (rms) differences at 532 nm were less than 50% ($0.015\,km^{-1}$). These differences are well with range of current state-of-the-art instrumentation.
- Measurements of surface albedo and reflectance in the Mexico City metropolitan area showed that many urban surfaces are more reflective than assumed in common satellite retrieval algorithms, and that use of larger visible surface reflectance in algorithms can produce more accurate retrieved aerosol optical depth (AOD).
- Comparisons between AOD from airborne sunphotometer (AATS) and from the satellite sensors OMI and MODIS show that MODIS and AATS AODs agree to within root mean square (RMS) differences of 0.00–0.06, depending on wavelength, but that OMI and AATS AODs can differ by considerably more.

– Other comparisons between AATS and MODIS aerosol properties show notable differences between the older MODIS Collection 4 and the new Collection 5 in terms of AOD, Angstrom exponent, and aerosol fine mode fraction, with differences traceable to changes in sensor calibration.

13 Future research

As described above, a very large number of instruments were used in the MCMA during MILAGRO for both ground-based and aircraft measurements; and some innovative instruments and measurement techniques were deployed for the first time. The MILAGRO campaign has shown the synergy of using multiple measuring platforms, instrumentation, and data analysis techniques for obtaining an improved understanding of the physical and chemical characteristics of emissions in a megacity.

Furthermore, the deployment of a significant number of advanced instruments, many operating with sensitive, fast ($\sim$s) response times, along with a large number of established air quality monitoring instruments deployed on aircraft and at surface sites, as well as onboard several mobile laboratories, have provided significant opportunities to intercompare and evaluate a number of instruments in a highly polluted environment. Several papers documenting and/or cross comparing the performance of instruments have been published as well.

Despite the use of many advanced PM techniques during MILAGRO, some questions remain unanswered or strongly debated and should be the focus of further research. The fraction of dust due to road resuspension vs. natural sources is unclear. There is a need for characterizing the dust source regions and the soil characteristics for those regions, not only for the Mexico City Valley, but for the entire Central Mexican plateau. The impact of gas-particle reactions is important, for example for nitrate uptake into the coarse dust mode, but needs to be further investigated to reach a quantitative understanding, including through 3-D modeling. The identities of industrial sources of metals and organic aerosols and of the urban chloride sources remain unclear. High time-resolution quantitative analyses of dust and metals may yield very useful information for source identification.

The 2006 MCMA emissions inventory underestimates primary $PM_{2.5}$ and needs to be updated with the information arising from MILAGRO and other studies. Forest fire $PM_{2.5}$ appears to be underestimated by an order of magnitude in the official MCMA inventory (although a fraction of the fires occur just outside the inventory area), but perhaps overestimated about two-fold on a custom satellite-based inventory used in 3-D modeling. The impact of some POA sources such as food cooking, biofuel use, and open trash burning may be important, but remains poorly characterized. Some differences in the apportionment of biomass burning PM between different approaches were observed and need further research, as these techniques together represent the state of the art for source apportionment. The differences in the relative oxidation of OA in urban vs. background samples between the FTIR and AMS techniques need to be further investigated.

Further study is needed of the reasons for the differences between the two datasets of modern carbon. The mix of sources that contribute to 30–45% modern carbon in OC during low regional fire periods need to be identified, including a quantification of the urban sources of modern carbon. The influence of "hot" sources of radiocarbon in aerosols needs to be further investigated as it could bias assessments of fossil vs. modern carbon. SOA from traditional precursors such as aromatics is much smaller than the observed SOA in the Mexico City urban area, but the dominant sources of anthropogenic SOA are still poorly characterized. SOA from biomass burning sources, although not dominant in the city, remains poorly characterized and appears to be underpredicted by traditional models. The relative impacts of MCMA vs. regional sources for the different components deserve further study. The sources and chemical species leading to the very intense new particle formation events observed are only starting to be characterized.

Measurements of aerosol optical absorption in Mexico City and downwind also benefitted from the variety of techniques applied during MILAGRO, leading to several results summarized above. However, not all results are in perfect agreement, and lack of perfect spatiotemporal coincidence between different measurements makes it impossible to say whether different results stem from different techniques or from different aerosols sampled. Future campaigns need increased focus on spatiotemporal coincidence between different techniques, to help resolve these questions. There are also persistent differences among different satellite retrievals of aerosols, as well as between results from satellite and suborbital techniques. This is an area that requires continued effort, with attention not only to spatiotemporal coincidence of different techniques, but also to statistical significance and geophysical representativeness of comparison data sets.

In summary, observations from MILAGRO/INTEX-B have provided extremely comprehensive characterization on the urban and regional atmospheric composition and chemistry of the Mexico Megacity. All data sets and publications are available to the scientific community interested in evaluating the impact of urban emissions on human health, ecosystem viability, and climate change. We anticipate new results from MILAGRO/INTEX-B will continue to contribute to our understanding of megacity air pollution and its potential impacts on human health, ecosystem viability, and climate change on urban, regional, and even hemispheric scales. This information will improve significantly the scientific understanding that decision makers in Mexico will need to craft effective policies as well as provide insights to air pollution problems in other megacities around the world.

Appendix A

List of acronyms

AAE	Absorption Angstrom Exponent
AATS	Ames Airborne Tracking Sunphotometer
ACP	Atmospheric Chemistry and Physics
AERONET	AErosol RObotic NETwork
AMS	Aerosol Mass Spectrometer
ANL	Argonne National Laboratory
AOD	Aerosol Optical Depth
APS	Aerosol Polarimetry Sensor
ARI	– Aerodyne Research, Inc
ATOFMS	Aerosol Time of Flight Mass Spectrometer
BBOA	Biomass Burning Organic Aerosol
BNL	Brookhaven National Laboratory
BTEX	Benzene, Toluene, Ethylbenzene and m p,o Xylenes
CAM	*Comision Ambiental Metropolitana* (Metropolitan Environmental Commission)
CCN	*Cloud Condensation Nuclei*
CEH	Center for Ecology and Hydrology, Edingburgh
CENICA	*Centro Nacional de Investigation y Capcitacion Ambiental* (National Center for Environmental Research and Training)
CIMS	Chemical Ionization Mass Spectrometer
CMET	Controlled Meteorological balloons
CONACyT	*Consejo Nacional de Ciencia y Technología* (National Council for Science and Technology)
CPC	Condensation Particle Counter
CSIC	Consejo Superior de Investigaciones Científicas, Spain
CTM	Chemical Transport Model
DEC	Disjunct Eddy Covariance
DOAS	Differential Optical Absorption Spectroscopy
FMPS	Fast Mobility Particle Sizer
FOS	Fast Olefin Sensor
GC FID	Gas Chromatography / Flame Ionization Detection
HOA	Hydrocarbon like Organic Aerosol
HR ToF AMS	High Resolution Time-of Flight Aerosol Mass Spectrometer
HSRL	High Spectral Resolution Lidar
HTDMA	Hygroscopicity Tandem Differential Mobility Analyzer
HULIS	Humic like Substances
IC MS	Ion Chromatography Mass Spectrometry
IGMA	*Inclined Grid Mobility Analyzer*
IMK–IFU	Institute for Meteorology and Climate Research, Atmospheric Environmental Research, Karlsruhe Institute of Technology
IMP	*Instituto Mexicano del Petroleo* (Mexican Petroleum Institute)
INE	*Instituto Nacional de Ecologia* (National Institute of Ecology)
INTEX B	Intercontinental Chemical Transport Experiment Phase B
IRGA	Infrared Gas Analyzer
ITESM	*Instituto Tecnologico y de Estudios Superiores de Monterrey* (TEC)
LBNL	– Lawrence Berkeley National Laboratory
LPG	liquefied Petroleum Gas
MAX Mex	Megacity Aerosol Experiment Mexico City
MCE2	Molina Center for Energy and the Environment
MCMA	Mexico City Metropolitan Area
MFRSR	Multi Filter Rotating Shadowband Radiometer
MILAGRO	Megacity Initiative Local And Global Research Observations
MIRAGE Mex	Megacity Impacts on Regional and Global Environments Mexico
MISR	Multiangle Imaging Spectroradiometer
MODIS	Moderate Resolution Imaging Spectroradiometer
MOZART	Model for OZone And Related chemical Tracers
MSU	*Montana State University*
NARR	North American Regional Reanalysis
NASA	National Aeronautics and Space Administration
NCAR	National Center for Atmospheric Research
NCEP	National Centers for Environmental Prediction
NTDMA	Nanoparticle Tandem Differential Mobility Analyzer
OA	Organic Aerosol
OC	Organic Carbon
OMI	Ozone Monitoring Instrument
OOA	Oxygenated organic aerosol
OPC	Optical Particle Counter
OVOC	Oxygenated Volatile Organic Chemicals
PAHs	Polycyclic Aromatic Hydrocarbons
PANs	Peroxyacetyl Nitrates
PAS	Photoacoustic Absorption Spectrometer
PEMEX	*Petroleos Mexicanos* (Mexican Petroleum)
PMF	Positive Matrix Factorization
PNNL	Pacific Northwest National Laboratory
POA	Primary Organic Aerosol
POPs	Persistent Organic Pollutants
PSAP	Particle Soot Absorption Photometer
PSU	– Pennsylvania State University
PTR MS	Proton Transfer Reaction Mass Spectrometry
RAMA	*Red Automatica de Monitoreo Atmosferico* (Ambient Air Quality Monitoring Network)
RSP	Research Scanning Polarimeter
SEMARNAT	*Secretaria de Medio Ambiente y Recursos Naturales* (Mexican Ministry of the Environment and Natural Resources)
SIMAT	*Sistema de Monitoreo Atmosferico* (Atmospheric Monitoring System)
S/IVOC	Semivolatile and Intermediate Volatility Organic Compounds
SMA GDF	*Secretaria de Medio Ambiente Gobierno del Distrito Federal (Environmental Secretariat Government of the Federal District)*
SMN	*Servicio Meteorologico Nacional* (National Weather Service)
SMPS	Scanning Mobility Particle Sizer
SOA	Secondary Organic Aerosol
SSA	Single Scattering Albedos
SSFR	Solar Spectral Flux Radiometer
STEM (Model)	Sulfur Transport and Deposition Model
STEM (Technique)	Scanning Transmission Electron Microscopy
STXM	Scanning Transmission X Ray Microscopy
TDCIMS	Thermal Desorption Chemical Ionization Mass Spectrometry
TDMA	Tandem Differential Mobility Analyzer,
TD LIF	Thermal Dissociation Laser Induced Fluorescence
TEM	Transmission Electron Microscope
TOOC	Total Observed Organic Carbon
TSP	Total Suspended Particles
UAH	University of Alabama at Huntsville
UAM A	*Universidad Autonoma Metropolitana – Azcapotzalco*
UNAM	*Universidad Nacional Autonoma de Mexico*
UTC	Coordinated Universal Time
VT	Virginia Tech
WIOC	Water insoluble Organic Carbon
WSU	Washington State University
WRF Chem (Model)	Weather Research and Forecast (WRF) model coupled with Chemistry
WSOC	Water Soluble Organic Carbon

Acknowledgements The MILAGRO/INTEX-B Campaign is the collaborative efforts of a large number of participants with the support of multi-national agencies The MILAGRO/INTEX-B participants would like to thank the governments of the Federal District, the States of Mexico, Hidalgo and Veracruz, the Mexican Ministries of the Environment, Foreign Relations, Defense and Finance, the US Embassy in Mexico and the Molina Center for Energy and the Environment for their logistical support, IMP, U-Tecámac, and Rancho La Bisnega for hosting the supersites as well as many other Mexican institutions for their support The MILAGRO/INTEX-B participants are grateful for funding from the Mexican Metropolitan Environmental Commission, Mexican Ministry of the Environment, CONACyT, PEMEX, NSF Atmospheric Chemistry Program, DOE Atmospheric Science Program and NASA Tropospheric Chemistry and Radiation Science Programs

We would like to thank many MILAGRO investigators for reviewing the manuscript and for their comments and suggestions We are grateful to R Ramos, A Retama and the operators and analyst personnel of the RAMA Monitoring Network for administering and gathering the surface air quality and meteorological data, and

M. Rosengaus and the personnel of the Mexican National Meteorological Service for providing EMA and radiosonde data. We thank E. Velasco for preparing Fig. 8, C. Hostetler for contributing to the King Air section and C. Kolb for helpful discussion.

Edited by: U. Pöschl

References

Adachi, K. and Buseck, P. R.: Internally mixed soot, sulfates, and organic matter in aerosol particles from Mexico City, Atmos. Chem. Phys., 8, 6469–6481, doi:10.5194/acp-8-6469-2008, 2008.

Adachi, K., Chung, S. H., and Buseck, P. R.: Shapes of soot aerosol particles and implications for their effects on climate, J. Geophys. Res.-Atmos., 115, D15206, doi:10.1029/2009JD012868, 2010.

Adachi, K. and Buseck, P. R.: Hosted and Free-Floating Metal-bearing Atmospheric Nanoparticles in Mexico City, Environ. Sci. Technol., 44, 2299–2304, 2010.

Aiken, A. C., DeCarlo, P. F., and Jimenez, J. L.: Elemental Analysis of Organic Species with Electron Ionization High-Resolution Mass Spectrometry, Anal. Chem., 79, 8350–8358, *doi:10.1021/ac071150w, 2007.*

Aiken, A. C., DeCarlo, P. F., Kroll, J. H., Worsnop, D. R., Huffman, J. A., Docherty, K. S., Ulbrich, I. M., Mohr, C., Kimmel, J. R., Sueper, D., Sun, Y., Zhang, Q., Trimborn, A., Northway, M., Ziemann, P. J., Canagaratna, M. R.,, Onasch, T. B., Alfarra, M. R., Prevot, A. S. H., Dommen, J., Duplissy, J, Metzger, A., Baltensperger, U., and Jimenez, J. L.: O/C and OM/OC Ratios of Primary, Secondary, and Ambient Organic Aerosols with High Resolution Time-of-Flight Aerosol Mass Spectrometry, Environ. Sci. Technol., 42, 4478–4485, doi:10.1021/es703009q, 2008.

Aiken, A. C., Salcedo, D., Cubison, M. J., Huffman, J. A., DeCarlo, P. F., Ulbrich, I. M., Docherty, K. S., Sueper, D., Kimmel, J. R., Worsnop, D. R., Trimborn, A., Northway, M., Stone, E. A., Schauer, J. J., Volkamer, R. M., Fortner, E., de Foy, B., Wang, J., Laskin, A., Shutthanandan, V., Zheng, J., Zhang, R., Gaffney, J., Marley, N. A., Paredes-Miranda, G., Arnott, W. P., Molina, L. T., Sosa, G., and Jimenez, J. L.: Mexico City aerosol analysis during MILAGRO using high resolution aerosol mass spectrometry at the urban supersite (T0) – Part 1: Fine particle composition and organic source apportionment, Atmos. Chem. Phys., 9, 6633–6653, doi:10.5194/acp-9-6633-2009, 2009.

Aiken, A. C., de Foy, B., Wiedinmyer, C., DeCarlo, P. F., Ulbrich, I. M., Wehrli, M. N., Szidat, S., Prevot, A. S. H., Noda, J., Wacker, L., Volkamer, R., Fortner, E., Wang, J., Laskin, A., Shutthanandan, V., Zheng, J., Zhang, R., Paredes-Miranda, G., Arnott, W. P., Molina, L. T., Sosa, G., Querol, X., and Jimenez, J. L.: Mexico city aerosol analysis during MILAGRO using high resolution aerosol mass spectrometry at the urban supersite (T0) – Part 2: Analysis of the biomass burning contribution and the non-fossil carbon fraction, Atmos. Chem. Phys., 10, 5315–5341, doi:10.5194/acp-10-5315-2010, 2010.

Alfaro Moreno, E., García Cuellar, C., De Vizcaya Ruiz, A., Rojas-Bracho, L., and Osornio-Vargas, A. R.: Cellular Mechanisms behind Particulate Matter Air Pollution Related Health Effects, in: Air Pollution: Health & Environmental Impacts, edited by: Gurjar, R., Molina, L. T., and Ojha, C. S. P., Taylor & Francis, Chapter 9, 249–274, 2010.

Altuzar, V., Tomás, S. A., Zelaya-Angel, O., Sánchez-Sinencio, F., and Arriaga, J. L.: Atmospheric ethene concentrations in Mexico City: Indications of strong diurnal and seasonal dependences, Atmos. Env., 39, 5219–5225, 2005.

Andreae, M. O. and Gelencsér, A.: Black carbon or brown carbon? The nature of light-absorbing carbonaceous aerosols, Atmos. Chem. Phys., 6, 3131–3148, doi:10.5194/acp-6-3131-2006, 2006.

Andreae, M. O. and Gelencsér, A.: Black carbon or brown carbon? The nature of light-absorbing carbonaceous aerosols, Atmos. Chem. Phys., 6, 3131–3148, doi:10.5194/acp-6-3131-2006, 2006.

Apel, E. C., Emmons, L. K., Karl, T., Flocke, F., Hills, A. J., Madronich, S., Lee-Taylor, J., Fried, A., Weibring, P., Walega, J., Richter, D., Tie, X., Mauldin, L., Campos, T., Weinheimer, A., Knapp, D., Sive, B., Kleinman, L., Springston, S., Zaveri, R., Ortega, J., Voss, P., Blake, D., Baker, A., Warneke, C., Welsh-Bon, D., de Gouw, J., Zheng, J., Zhang, R., Rudolph, J., Junkermann, W., and Riemer, D. D.: Chemical evolution of volatile organic compounds in the outflow of the Mexico City Metropolitan area, Atmos. Chem. Phys., 10, 2353–2375, doi:10.5194/acp-10-2353-2010, 2010.

Apel, E. C., Hills, A. J., Lueb, R., Zindel, S., Eisele, S. and Riemer, D. D.: A Fast-GC/MS system to measure C_2 to C_4 carbonyls, and methanol aboard aircraft, J. Geophys. Res., 108, 8794, doi:10.1029/2002JD003199, 2003.

Atkinson, R.: Gas phase tropospheric chemistry of organic compounds: a review, Atmos. Environ., 24A, 1–41, 1990.

Ban-Weiss, G. A., McLaughlin, J. P., Harley, R. A., Lunden, M. M., Kirchstetter, T. W., Kean, A. J., Strawa, A. W., Stevenson, E. D., and Kendall, G. R.: Long-term changes in emissions of nitrogen oxides and particulate matter from on-road gasoline and diesel vehicles, Atmos. Environ., 42, 220–232, 2008.

Barnard, J. C., Volkamer, R., and Kassianov, E. I.: Estimation of the mass absorption cross section of the organic carbon component of aerosols in the Mexico City Metropolitan Area, Atmos. Chem. Phys., 8, 6665–6679, doi:10.5194/acp-8-6665-2008, 2008.

Barraza-Villarreal, A., Sunyer, J., Hernandez-Cadena, L., Escamilla-Nunez, M. C., Sienra-Monge, J. J., Ramirez-Aguilar, M., Sienra-Monge, J. J., Cortez-Lugo, M., Texcalac, J. L., del Rio-Navarro, B., and Romieu, I.: Air pollution, airway inflammation, and lung function in a cohort study of Mexico City schoolchildren, Environ. Health Perspect., 116, 832–838, 2008.

Baumgardner, D., Grutter, M., Allan, J., Ochoa, C., Rappenglueck, B., Russell, L. M., and Arnott, P.: Physical and chemical properties of the regional mixed layer of Mexico's Megapolis, Atmos. Chem. Phys., 9, 5711–5727, doi:10.5194/acp-9-5711-2009, 2009.

Bei, N., de Foy, B., Lei, W., Zavala, M., and Molina, L. T.: Using 3DVAR data assimilation system to improve ozone simulations in the Mexico City basin, Atmos. Chem. Phys., 8, 7353–7366, doi:10.5194/acp-8-7353-2008, 2008.

Bei, N., Lei, W., Zavala, M., and Molina, L. T.: Ozone predictabilities due to meteorological uncertainties in the Mexico City basin using ensemble forecasts, Atmos. Chem. Phys., 10, 6295–6309, doi:10.5194/acp-10-6295-2010, 2010.

Bell, M. L., Ebisu, K., Peng, R. D., Walker, J., Samet, J. M.,

Zeger, S. L., and Dominici, F.: Seasonal and regional short-term effects of fine particles on hospital admissions in 202 US counties, 1999–2005, Am. J. Epidemiol., 168(11), 1301–1310, doi:10.1093/aje/kwn252, 2008.

Bergstrom, R. W., Schmidt, K. S., Coddington, O., Pilewskie, P., Guan, H., Livingston, J. M., Redemann, J., and Russell, P. B.: Aerosol spectral absorption in the Mexico City area: results from airborne measurements during MILAGRO/INTEX B, Atmos. Chem. Phys., 10, 6333–6343, doi:10.5194/acp-10-6333-2010, 2010.

Bishop, G. A., Stedman, D. H., de la Garza, J., and Davalos, F.: On road remote sensing of vehicle emissions in Mexico, Environ. Sci. Technol., 31, 3505–3510, 1997.

Blake, D. R. and Rowland, F. S.: Urban leakage of liquefied petroleum gas and its impact on Mexico City air quality, Science, 269, 953–956, 1995.

Bohlin, P., Jones, K. C., Tovalin, H., and Strandberg, B.: Observations on persistent organic pollutants in indoor and outdoor air using passive polyurethane foam samplers, Atmos. Environ., 42, 7234–7241, 2008.

Borbon, A., Fontaine, H., Veillerot, M., Locoge, N., Galloo, J. C., and Guillermo, R.: An investigation into the traffic-related fraction of isoprene at an urban location, Atmos. Environ., 35, 3749–3760, 2001.

Borja-Aburto, V. H., Loomis, D. P., Bangdiwala, S. I., Shy, C. M., and Rascon-Pacheco, R. A.: Ozone, suspended particulates, and daily mortality in Mexico City, Am. J. Epidemiol., 145, 258–268, 1997.

Bravo, A., Sosa, E., Sanchez, A., Jaimes, P., and Saavedra, R.: Impact of wildfires on the air quality of Mexico City, 1992–1999, Environ. Pollut., 117, 243–253, 2002.

Cairns, B., Waquet, F., Knobelspiesse, K., Chowdhary, J., and Deuzé, J. L.: Polarimetric remote sensing of aerosols over land surfaces, in Aerosol Remote Sensing over Land edited by: Kokhanovsky, A. A. and de Leeuw, G., Springer, 295–325, 2009.

Calderon-Garciduenas, L., Franco-Lira, M., Torres-Jardon, R., Henriquez-Roldan, C., Barragan-Mejia, G., Valencia-Salazar, G. González-Maciel A., Reynoso-Robles, R., Villarreal-Calderón, R., and Reed, W.: Pediatric respiratory and systemic effects of chronic air pollution exposure: Nose, lung, heart, and brain pathology, Toxicol. Pathol., 35, 154–162, 2007.

Canagaratna, M. R., Jayne, J. T., Jimenez, J. L., Allan, J. D., Alfarra, M. R., Zhang, Q., Onasch, T. B. Drewnick, F., Coe, H., Middlebrook, A., Delia, A., Williams, L. R., Trimborn, A. M., Northway, M. J., DeCarlo, P. F., Kolb, C. E., Davidovits, P., and D. R. Worsnop: Chemical and Microphysical Characterization of Ambient Aerosols with the Aerodyne Aerosol Mass Spectrometer, Mass Spec. Rev., 26, 185–222, 2007.

Cappa, C. D. and Jimenez, J. L.: Quantitative estimates of the volatility of ambient organic aerosol, Atmos. Chem. Phys., 10, 5409–5424, doi:10.5194/acp-10-5409-2010, 2010.

Capes, G., Johnson, B., McFiggans, G., Williams, P. I., Haywood, J., and Coe, H.: Aging of biomass burning aerosols over West Africa: aircraft measurements of chemical composition, microphysical properties, and emission ratios, J. Geophys. Res., 113, D00C15, doi:10.1029/2008JD009845, 2008.

Castillejos M., Borja-Aburto, V. H., Dockery, D. W., Gold, D. R., and Loomis, D.: Coarse Particles and Mortality in Mexico City, Inhal. Toxicol., 12, 61–72, 2000.

CEC 2009, Comprehensive Assessment of North American Air Emissions Inventories and Ambient Air Monitoring Networks, available at: http://www.cec.org/Storage/88/8537_Air_Assessment_Report_en.pdf, last access: 15 August 2010.

Chow, J. C., Watson, J. G., Edgerton, S. A., and Vega, E.: Chemical composition of $PM_{2.5}$ and PM_{10} in Mexico City during winter 1997, Sci. Total Environ., 287, 177–201, 2002.

Chowdhary, J., Cairns, B., Waquet, F., Knobelspiesse, K., Ottaviani, M., Redemann, J., Travis, L., and Mishchenko, M.: Sensitivity of multiangle, multispectral polarimentric remote sensing over open oceans to water-leaving radiances: Analyses of RSP data acquired during the MILAGRO campaign10, submitted to Remote Sens. Environ., June, 2010.

Christian, T. J., Yokelson, R. J., Cárdenas, B., Molina, L. T., Engling, G., and Hsu, S.-C.: Trace gas and particle emissions from domestic and industrial biofuel use and garbage burning in central Mexico, Atmos. Chem. Phys., 10, 565–584, doi:10.5194/acp-10-565-2010, 2010.

Coddington, O., Schmidt, K. S., Pilewskie, P., Gore, W. J., Bergstrom, R. W., Roma'n, M., Redemann, J., Russell, P. B., Liu, J. and Schaaf, C. C.: Aircraft measurements of spectral surface albedo and its consistency with ground-based and space-borne observations, J. Geophys. Res., 113, D17209, doi:10.1029/2008JD010089, 2008.

Corr, C. A., Krotkov, N., Madronich, S., Slusser, J. R., Holben, B., Gao, W., Flynn, J., Lefer, B., and Kreidenweis, S. M.: Retrieval of aerosol single scattering albedo at ultraviolet wavelengths at the T1 site during MILAGRO, Atmos. Chem. Phys., 9, 5813–5827, doi:10.5194/acp-9-5813-2009, 2009.

Craig, L., Brook, J. R., Chiotti, Q., Croes, B., Gower, S., Hedley, A., Krewski, D., Krupnick, A., Krzyzanowski, M., Moran, M. D., Pennell, W., Samet, J. M., Schneider, J., Shortreed, J., Williams, M.: Air pollution and public health: a guidance document for risk managers, J. Toxicol. Environ. Health A, 71, 588–698, 2008.

Cross, E. S., Onasch, T. B., Canagaratna, M., Jayne, J. T., Kimmel, J., Yu, X.-Y., Alexander, M. L., Worsnop, D. R., and Davidovits, P.: Single particle characterization using a light scattering module coupled to a time-of-flight aerosol mass spectrometer, Atmos. Chem. Phys., 9, 7769–7793, doi:10.5194/acp-9-7769-2009, 2009.

Crounse, J. D., DeCarlo, P. F., Blake, D. R., Emmons, L. K., Campos, T. L., Apel, E. C., Clarke, A. D., Weinheimer, A. J., McCabe, D. C., Yokelson, R. J., Jimenez, J. L., and Wennberg, P. O.: Biomass burning and urban air pollution over the Central Mexican Plateau, Atmos. Chem. Phys., 9, 4929–4944, doi:10.5194/acp-9-4929-2009, 2009.

de Almeida Castanho, A. D., Prinn, R., Martins, V., Herold, M., Ichoku, C., and Molina, L. T.: Analysis of Visible/SWIR surface reflectance ratios for aerosol retrievals from satellite in Mexico City urban area, Atmos. Chem. Phys., 7, 5467–5477, doi:10.5194/acp-7-5467-2007, 2007.

DeCarlo, P. F., Kimmel, J. R., Trimborn, A., Northway, M. J., Jayne, J. T., Aiken, A. C, Gonin, M., Fuhrer, K., Horvath, T., Docherty, K. S., Worsnop, D. R., and Jimenez, J. L.: Field-Deployable, High-Resolution, Time-of-Flight Aerosol Mass Spectrometer, Anal. Chem., 78, 8281–8289, 2006.

DeCarlo, P. F., Dunlea, E. J., Kimmel, J. R., Aiken, A. C., Sueper, D., Crounse, J., Wennberg, P. O., Emmons, L., Shinozuka, Y., Clarke, A., Zhou, J., Tomlinson, J., Collins, D. R., Knapp, D.,

Weinheimer, A. J., Montzka, D. D., Campos, T., and Jimenez, J. L.: Fast airborne aerosol size and chemistry measurements above Mexico City and Central Mexico during the MILAGRO campaign, Atmos. Chem. Phys., 8, 4027–4048, doi:10.5194/acp-8-4027-2008, 2008.

DeCarlo, P. F., Ulbrich, I. M., Crounse, J., de Foy, B., Dunlea, E. J., Aiken, A. C., Knapp, D., Weinheimer, A. J., Campos, T., Wennberg, P. O., and Jimenez, J. L.: Investigation of the sources and processing of organic aerosol over the Central Mexican Plateau from aircraft measurements during MILAGRO, Atmos. Chem. Phys., 10, 5257–5280, doi:10.5194/acp-10-5257-2010, 2010.

de Foy, B., Caetano, E., Magañaa, V., Zitácuaro, A., Cárdenas, B., Retama, A., Ramos, R., Molina, L. T., and Molina, M. J.: Mexico City basin wind circulation during the MCMA-2003 field campaign, Atmos. Chem. Phys., 5, 2267–2288, doi:10.5194/acp-5-2267-2005, 2005.

de Foy, B., Clappier, A., Molina, L. T., and Molina, M. J.: Distinct wind convergence patterns in the Mexico City basin due to the interaction of the gap winds with the synoptic flow, Atmos. Chem. Phys., 6, 1249–1265, doi:10.5194/acp-6-1249-2006, 2006.

de Foy, B., Varela, J. R., Molina, L. T., and Molina, M. J.: Rapid ventilation of the Mexico City basin and regional fate of the urban plume, Atmos. Chem. Phys., 6, 2321–2335, doi:10.5194/acp-6-2321-2006, 2006b.

de Foy, B., Lei, W., Zavala, M., Volkamer, R., Samuelsson, J., Mellqvist, J., Galle, B., Martínez, A.-P., Grutter, M., Retama, A., and Molina, L. T.: Modelling constraints on the emission inventory and on vertical dispersion for CO and SO_2 in the Mexico City Metropolitan Area using Solar FTIR and zenith sky UV spectroscopy, Atmos. Chem. Phys., 7, 781–801, doi:10.5194/acp-7-781-2007, 2007.

de Foy, B., Fast, J. D., Paech, S. J., Phillips, D., Walters, J. T., Coulter, R. L., Martin, T. J., Pekour, M. S., Shaw, W. J., Kastendeuch, P. P., Marley, N. A., Retama, A., and Molina, L. T.: Basin-scale wind transport during the MILAGRO field campaign and comparison to climatology using cluster analysis, Atmos. Chem. Phys., 8, 1209–1224, doi:10.5194/acp-8-1209-2008, 2008.

de Foy, B., Zavala, M., Bei, N., and Molina, L. T.: Evaluation of WRF mesoscale simulations and particle trajectory analysis for the MILAGRO field campaign, Atmos. Chem. Phys., 9, 4419–4438, doi:10.5194/acp-9-4419-2009, 2009a.

de Foy, B., Krotkov, N. A., Bei, N., Herndon, S. C., Huey, L. G., Martínez, A.-P., Ruiz-Suárez, L. G., Wood, E. C., Zavala, M., and Molina, L. T.: Hit from both sides: tracking industrial and volcanic plumes in Mexico City with surface measurements and OMI SO2 retrievals during the MILAGRO field campaign, Atmos. Chem. Phys., 9, 9599–9617, doi:10.5194/acp-9-9599-2009, 2009b.

de Gouw, J. and Warneke, C.: Measurements of volatile organic compounds in the earths atmosphere using proton-transfer-reaction mass spectrometry, Mass Spec. Rev. 26, 223–257, 2007.

de Gouw, J. A., Welsh-Bon, D., Warneke, C., Kuster, W. C., Alexander, L., Baker, A. K., Beyersdorf, A. J., Blake, D. R., Canagaratna, M., Celada, A. T., Huey, L. G., Junkermann, W., Onasch, T. B., Salcido, A., Sjostedt, S. J., Sullivan, A. P., Tanner, D. J., Vargas, O., Weber, R. J., Worsnop, D. R., Yu, X. Y., and Zaveri, R.: Emission and chemistry of organic carbon in the gas and aerosol phase at a sub-urban site near Mexico City in March 2006 during the MILAGRO study, Atmos. Chem. Phys., 9, 3425–3442, doi:10.5194/acp-9-3425-2009, 2009.

de Gouw, J. and Jimenez, J. L.: Organic Aerosols in the Earth's Atmosphere, Environ. Sci. Technol., 43, 7614–7618, doi:10.1021/es9006004, 2009.

Docherty, K. S., Stone, E. A., Ulbrich, I. M., DeCarlo, P. F., Snyder, D. C., Schauer, J. J, Peltier, R. E., Weber, R. J., Murphy, S. M., Seinfeld, J. H., Grover, B. D., Eatough, D. J., and Jimenez, J. L.: Apportionment of Primary and Secondary Organic Aerosols in Southern California during the 2005 Study of Organic Aerosols in Riverside (SOAR), Environ. Sci. Technol., 42, 7655–7662, doi:10.1021/es8008166, 2008.

Dominici, F., Peng, R. D., Bell, M. L., Pham, L., McDermott, A., Zeger, S. L. and Samet, J. M.: Fine particulate air pollution and hospital admission for cardiovascular and respiratory diseases, JAMA, 295, 1127–1134, 2006.

Dominici, F., Peng, R. D., Ebisu, K., Zeger, S. L., Samet, J. M., Bell, M. L.: Does the effect of PM_{10} on mortality depend on PM nickel and vanadium content?, A reanalysis of the NMMAPS data, Environ. Health Perspect., 115, 1701–1703, 2007.

Doran, J. C., Fast, J. D., Barnard, J. C., Laskin, A., Desyaterik, Y., and Gilles, M. K.: Applications of lagrangian dispersion modeling to the analysis of changes in the specific absorption of elemental carbon, Atmos. Chem. Phys., 8, 1377–1389, doi:10.5194/acp-8-1377-2008, 2008.

Doran, J. C., Barnard, J. C., Arnott, W. P., Cary, R., Coulter, R., Fast, J. D., Kassianov, E. I., Kleinman, L., Laulainen, N. S., Martin, T., Paredes-Miranda, G., Pekour, M. S., Shaw, W. J., Smith, D. F., Springston, S. R., and Yu, X.-Y.: The T1-T2 study: evolution of aerosol properties downwind of Mexico City, Atmos. Chem. Phys., 7, 1585–1598, doi:10.5194/acp-7-1585-2007, 2007.

Doran, J. C., Abbott, S., Archuleta, J., Bian, X., Chow, J., Coulter, R. L., de Wekker, S. F. J., Edgerton, S., Elliott, S., Fernandez, A., Fast, D. J., Hubbe, J. M., King, C., Langley, D., Leach, J., Lee, J. T., Martin, T. J., Martinez, D., Martinez, J. L., Mercado, G., Mora, V., Mulhearn, M., Pena, J. L., Petty, R., Porch, W., Russell, C., Salas, R., Shannon, J. D., Shaw, W. J., Sosa, G., Tellier, L., Templeman, B., Watson, J. G., White, R., Whiteman, C. D., and Wolfe, D.: The IMADA-AVER boundary-layer experiment in the Mexico City area, B. Am. Meteor. Soc., 79, 2497–2508, 1998.

Doskey, P. V., Porter, J. A., and Scheff, P. A.: Source fingerprints for volatile non-methane hydrocarbons, J. Air Waste Manag. Assoc., 42, 1437–1445, 1992.

Dunlea, E. J., DeCarlo, P. F., Aiken, A. C., Kimmel, J. R., Peltier, R. E., Weber, R. J., Tomlinson, J., Collins, D. R., Shinozuka, Y., McNaughton, C. S., Howell, S. G., Clarke, A. D., Emmons, L. K., Apel, E. C., Pfister, G. G., van Donkelaar, A., Martin, R. V., Millet, D. B., Heald, C. L., and Jimenez, J. L.: Evolution of Asian aerosols during transpacific transport in INTEX-B, Atmos. Chem. Phys., 9, 7257–7287, doi:10.5194/acp-9-7257-2009, 2009.

Dunlea, E. J., Herndon, S. C., Nelson, D. D., Volkamer, R. M., San Martini, F., Sheehy, P. M., Zahniser, M. S., Shorter, J. H., Wormhoudt, J. C., Lamb, B. K., Allwine, E. J., Gaffney, J. S., Marley, N. A., Grutter, M., Marquez, C., Blanco, S., Cardenas, B., Retama, A., Ramos Villegas, C. R., Kolb, C. E., Molina, L. T., and Molina, M. J.: Evaluation of nitrogen dioxide chemilumines-

cence monitors in a polluted urban environment, Atmos. Chem. Phys., 7, 2691–2704, doi:10.5194/acp-7-2691-2007, 2007.

Dunn, M., Jimenez, J. L., Baumgardner, D., Castro, T., McMurry, P. H., and Smith, J. N.: Measurements of Mexico City nanoparticle size distributions: Observations of new particle formation and growth, Geophys. Res. Lett., 31, L10102, doi:10.1029/2004GL019483, 2004.

Dusanter, S., Vimal, D., Stevens, P. S., Volkamer, R., and Molina, L. T.: Measurements of OH and HO_2 concentrations during the MCMA-2006 field campaign – Part 1: Deployment of the Indiana University laser-induced fluorescence instrument, Atmos. Chem. Phys., 9, 1665–1685, doi:10.5194/acp-9-1665-2009, 2009a.

Dusanter, S., Vimal, D., Stevens, P. S., Volkamer, R., Molina, L. T., Baker, A., Meinardi, S., Blake, D., Sheehy, P., Merten, A., Zhang, R., Zheng, J., Fortner, E. C., Junkermann, W., Dubey, M., Rahn, T., Eichinger, B., Lewandowski, P., Prueger, J., and Holder, H.: Measurements of OH and HO2 concentrations during the MCMA-2006 field campaign – Part 2: Model comparison and radical budget, Atmos. Chem. Phys., 9, 6655–6675, doi:10.5194/acp-9-6655-2009, 2009b.

Dzepina, K., Arey, J., Marr, L.C., Worsnop, D. R., Salcedo, D., Zhang, Q., Onasch, T. B., Molina, L. T., Molina, M. J., and Jimenez, J. L.: Detection of Particle-Phase Polycyclic Aromatic Hydrocarbons in Mexico City using an Aerosol Mass Spectrometer, Int. J. Mass Spec., 263, 152–170, 2007.

Dzepina, K., Volkamer, R. M., Madronich, S., Tulet, P., Ulbrich, I. M., Zhang, Q., Cappa, C. D., Ziemann, P. J., and Jimenez, J. L.: Evaluation of recently-proposed secondary organic aerosol models for a case study in Mexico City, Atmos. Chem. Phys., 9, 5681–5709, doi:10.5194/acp-9-5681-2009, 2009.

Edgerton, S. A., Bian, X., Doran, J. C., Fast, J. D., Hubbe, J. M., Malone, E. L., Shaw, W. J., Whiteman, C. D., Zhong, S., Arriaga, J. L., Ortiz, E., Ruiz, M., Sosa, G., Vega, E., Limon, T., Guzman, F., Archuleta, J., Bossert, J. E., Elliot, S., Lee, J. T., McNair, L. A., Chow, J. C., Watson, J. G., Coulter, R. L., , Doskey, P. V., Gaffney, J. S., Marley, N. A., Neff, W., and Petty, R.: Particulate Air pollution in Mexico City: A Collaborative Research Project, J. Air Waste Manag. Assoc., 49, 1221–1229, 1999.

Emmons, L. K., Apel, E. C., Lamarque, J.-F., Hess, P. G., Avery, M., Blake, D., Brune, W., Campos, T., Crawford, J., DeCarlo, P. F., Hall, S., Heikes, B., Holloway, J., Jimenez, J. L., Knapp, D. J., Kok, G., Mena-Carrasco, M., Olson, J., O'Sullivan, D., Sachse, G., Walega, J., Weibring, P., Weinheimer, A., and Wiedinmyer, C.: Impact of Mexico City emissions on regional air quality from MOZART-4 simulations, Atmos. Chem. Phys., 10, 6195–6212, doi:10.5194/acp-10-6195-2010, 2010.

Ervens, B., Cubison, M. J., Andrews, E., Feingold, G., Ogren, J. A., Jimenez, J. L., Quinn, P. K., Bates, T. S., Wang, J., Zhang, Q., Coe, H., Flynn, M., and Allan, J. D.: CCN predictions using simplified assumptions of organic aerosol composition and mixing state: a synthesis from six different locations, Atmos. Chem. Phys., 10, 4795–4807, doi:10.5194/acp-10-4795-2010, 2010.

Evans, J., Levy, J., Hammitt, J., Santos-Burgoa, C., Castillejos, M., Caballero-Ramirez, M., Hernandez-Avila, M., Riojas-Rodriguez, H., Rojas-Bracho, L., Serrano-Trespalacios, P., Spengler, J. D., and Suh, H.: Health benefits of air pollution control, in: "Air Quality in the Mexico Megacity: an Integrated Assessment", edited by: Molina, L. T. and Molina, M. J. , Kluwer Academic Publishers, 103–136, 2002.

Farmer, D. K., Matsunaga, A., Docherty, K. S.,Surratt, J. D., Seinfeld, J. H., Ziemann, P. J., and Jimenez, J. L.: Response of the Aerosol Mass Spectrometer to organonitrates and organosulfates and implications for field studies, P. Natl. Acad. Sci. USA, 107, 6670–6675, doi:10.1073/pnas.0912340107, 2010.

Fast, J. D. and Zhong, S., Meteorological factors associated with inhomogeneous ozone concentrations within the Mexico City basin, J. Geophys. Res., 103, 18927–18946, 1998.

Fast, J., Aiken, A. C., Allan, J., Alexander, L., Campos, T., Canagaratna, M. R., Chapman, E., DeCarlo, P. F., de Foy, B., Gaffney, J., de Gouw, J., Doran, J. C., Emmons, L., Hodzic, A., Herndon, S. C., Huey, G., Jayne, J. T., Jimenez, J. L., Kleinman, L., Kuster, W., Marley, N., Russell, L., Ochoa, C., Onasch, T. B., Pekour, M., Song, C., Ulbrich, I. M., Warneke, C., Welsh-Bon, D., Wiedinmyer, C., Worsnop, D. R., Yu, X.-Y., and Zaveri, R.: Evaluating simulated primary anthropogenic and biomass burning organic aerosols during MILAGRO: implications for assessing treatments of secondary organic aerosols, Atmos. Chem. Phys., 9, 6191–6215, doi:10.5194/acp-9-6191-2009, 2009.

Fast, J. D., de Foy, B., Acevedo Rosas, F., Caetano, E., Carmichael, G., Emmons, L., McKenna, D., Mena, M., Skamarock, W., Tie, X., Coulter, R. L., Barnard, J. C., Wiedinmyer, C., and Madronich, S.: A meteorological overview of the MILAGRO field campaigns, Atmos. Chem. Phys., 7, 2233–2257, doi:10.5194/acp-7-2233-2007, 2007.

Faulhaber, A. E., Thomas, B. M., Jimenez, J. L., Jayne, J. T., Worsnop, D. R., and Ziemann, P. J.: Characterization of a thermodenuder-particle beam mass spectrometer system for the study of organic aerosol volatility and composition, Atmos. Meas. Tech., 2, 15–31, doi:10.5194/amt-2-15-2009, 2009.

Ferrare, R., Hostetler, C., Hair, J., Cook, A., Harper, D., Burton, S., Clayton, M. Clarke, A., Russell, P., Redemann, J.: Airborne High Spectral Resolution Lidar Aerosol Measurements During MILAGRO and TEXAQS/GoMACCS, Ninth Conference on Atmospheric Chemistry, 2007 Annual AMS Conference, San Antonio, TX, http://ams.confex.com/ams/pdfpapers/119758.pdf, January 2007.

Forster, P., Ramaswamy, V., Artaxo, P., et al.: Changes in Atmospheric Constituents and in Radiative Forcing, in: "Climate Change 2007: the Physical Science Basis. Contribution of Working Group I to the Fourth Assessment Report of the Intergovernmental Panel on Climate Change", edited by: Solomon, S., Qin, D., Manning, M., Chen, Z., Marquis, M., Averyt, K. B., Tignor, M., and Miller, H. L., Cambridge University Press, Cambridge, United Kingdom and New York, NY, USA, 2007.

Fortner, E. C., Zheng, J., Zhang, R., Berk Knighton, W., Volkamer, R. M., Sheehy, P., Molina, L., and André, M.: Measurements of Volatile Organic Compounds Using Proton Transfer Reaction – Mass Spectrometry during the MILAGRO 2006 Campaign, Atmos. Chem. Phys., 9, 467–481, doi:10.5194/acp-9-467-2009, 2009.

Fountoukis, C., Nenes, A., Sullivan, A., Weber, R., Van Reken, T., Fischer, M., Matas, E., Moya, M., Farmer, D., and Cohen, R. C.: Thermodynamic characterization of Mexico City aerosol during MILAGRO 2006, Atmos. Chem. Phys., 9, 2141–2156, doi:10.5194/acp-9-2141-2009, 2009.

Gaffney, J. S. and Marley, N. A.: Uncertainties of aerosol effects in global climate models, Atmospheric Environment, 32, 2873–

2874, 1998.

Garcia, J. H., Li, W. W., Cardenas, N., Arimoto, R., Walton, J., and Trujillo, D.: Determination of $PM_{2.5}$ sources using time-resolved integrated source and receptor models, Chemosphere, 65, 2018–2027, 2006.

Gasparini, R., Li, R. J., and Collins, D. R.: Integration of size distributions and size-resolved hygroscopicity measured during the Houston Supersite for compositional categorization of the aerosol, Atmos. Environ., 38(20), 3285–3303, 2004.

Gatebe, C. K., Dubovik, O., King, M. D., and Sinyuk, A.: Simultaneous retrieval of aerosol and surface optical properties from combined airborne- and ground-based direct and diffuse radiometric measurements, Atmos. Chem. Phys., 10, 2777–2794, doi:10.5194/acp-10-2777-2010, 2010.

Gilardoni, S., Liu, S., Takahama, S., Russell, L. M., Allan, J. D., Steinbrecher, R., Jimenez, J. L., De Carlo, P. F., Dunlea, E. J., and Baumgardner, D.: Characterization of organic ambient aerosol during MIRAGE 2006 on three platforms, Atmos. Chem. Phys., 9, 5417–5432, doi:10.5194/acp-9-5417-2009, 2009.

Greenberg, J. P., Guenther, A. B., and Turnipseed, A.: Tethered balloon-based soundings of ozone, aerosols, and solar radiation near Mexico City during MIRAGE-MEX, Atmos. Environ., 16, 2672–2677, doi:10.1016/j.atmosenv.2009.02.019, 2009.

Grieshop, A. P., Logue, J. M., Donahue, N. M., and Robinson, A. L.: Laboratory investigation of photochemical oxidation of organic aerosol from wood fires 1: measurement and simulation of organic aerosol evolution, Atmos. Chem. Phys., 9, 1263–1277, doi:10.5194/acp-9-1263-2009, 2009.

Grutter, M., Basaldud, R., Rivera, C., Harig, R., Junkerman, W., Caetano, E., and Delgado-Granados, H.: SO_2 emissions from Popocatépetl volcano: emission rates and plume imaging using optical remote sensing techniques, Atmos. Chem. Phys., 8, 6655–6663, doi:10.5194/acp-8-6655-2008, 2008.

Gurjar, B. R., Butler, T. M., Lawrence, M. G., and Lelieveld, J.: Evaluation of emissions and air quality in megacities, Atmos. Environ., 42, 1593–1606, 2008.

Hair, J. W., Hostetler, C. A., Cook, A. L., Harper, D. B., Ferrare, R. A., Mack, T. L., Welch, W., Isquierdo, L. R., and Hovis, F. E.: Airborne high spectral resolution Lidar for profiling aerosol optical properties, Appl. Opt., 47, 6734–6752, 2008.

Hallquist, M., Wenger, J. C., Baltensperger, U., Rudich, Y., Simpson, D., Claeys, M., Dommen, J., Donahue, N. M., George, C., Goldstein, A. H., Hamilton, J. F., Herrmann, H., Hoffmann, T., Iinuma, Y., Jang, M., Jenkin, M. E., Jimenez, J. L., Kiendler-Scharr, A., Maenhaut, W., McFiggans, G., Mentel, Th. F., Monod, A., Prévôt, A. S. H., Seinfeld, J. H., Surratt, J. D., Szmigielski, R., and Wildt, J.: The formation, properties and impact of secondary organic aerosol: current and emerging issues, Atmos. Chem. Phys., 9, 5155–5236, doi:10.5194/acp-9-5155-2009, 2009.

Harley, R. A., Marr, L. C., Lehner, J. K., and Giddings, S. N.: Changes in motor vehicle emissions on diurnal to decadal time scales and effects on atmospheric composition, Environ. Sci. Technol., 39, 5356–5362, 2005.

Hashizume, M., Ueda, K., Nishiwaki, Y., Michikawa, T., and Onozuka, D.: Health effects of Asian dust events: a review of the literature, Nippon Eiseigaku Zasshi, 65, 13–421, 2010.

Heald, C. L., Goldstein, A. H., Allan, J. D., Aiken, A. C., Apel, E., Atlas, E. L., Baker, A. K., Bates, T. S., Beyersdorf, A. J., Blake, D. R., Campos, T., Coe, H., Crounse, J. D., DeCarlo, P. F., de Gouw, J. A., Dunlea, E. J., Flocke, F. M., Fried, A., Goldan, P., Griffin, R. J., Herndon, S. C., Holloway, J. S., Holzinger, R., Jimenez, J. L., Junkermann, W., Kuster, W. C., Lewis, A. C., Meinardi, S., Millet, D. B., Onasch, T., Polidori, A., Quinn, P. K., Riemer, D. D., Roberts, J. M., Salcedo, D., Sive, B., Swanson, A. L., Talbot, R., Warneke, C., Weber, R. J., Weibring, P., Wennberg, P. O., Worsnop, D. R., Wittig, A. E., Zhang, R., Zheng, J., and Zheng, W.: Total observed organic carbon (TOOC) in the atmosphere: a synthesis of North American observations, Atmos. Chem. Phys., 8, 2007–2025, doi:10.5194/acp-8-2007-2008, 2008.

Heald, C. L., Kroll, J. H., Jimenez, J. L., Docherty, K. S., DeCarlo, P. F., Aiken, A. C., Chen, Q., Martin, S. T., Farmer, D. K., and Artaxo, P.: A simplified description of organic aerosol composition and implications for atmospheric aging, Geophys. Res. Lett., 37, L08803, doi:10.1029/2010GL042737, 2010.

Hennigan, C. J., Sullivan, A. P., Fountoukis, C. I., Nenes, A., Hecobian, A., Vargas, O., Peltier, R. E., Case Hanks, A. T., Huey, L. G., Lefer, B. L., Russell, A. G., and Weber, R. J.: On the volatility and production mechanisms of newly formed nitrate and water soluble organic aerosol in Mexico City, Atmos. Chem. Phys., 8, 3761–3768, doi:10.5194/acp-8-3761-2008, 2008.

Herndon, S. C., Onasch, T. B., Wood, E. C., Kroll, J. H., Canagaratna, M. R., Jayne, J. T., Zavala, M. A., Knighton, W. B., Mazzoleni, C., Dubey, M.K., Ulbrich, I. M., Jimenez, J.L., Seila, R. de Gouw, J. A., de Foy, B., Fast, J., Molina, L. T., Kolb, C. E., and Worsnop, D. R.: The correlation of secondary organic aerosol with odd oxygen in a megacity outflow, Geophys. Res. Lett., 35, L15804, doi:10.1029/2008GL034058, 2008.

Hildemann, L. M., Klinedinst, D. B., Klouda, G. A., Currie, L. A., and Cass, G. R.: Sources of Urban Contemporary Carbon Aerosol, Environ. Sci. Technol., 28, 1565–1576, 1994.

Ho, S. S. H., Yu, J. Z., Chu, K. W. and Yeung, L. L.: Carbonyl Emissions from Commercial Cooking Sources in Hong Kong, J. Air Waste Manage. Assoc., 56, 1091–1098, 2006.

Hodzic, A., Jimenez, J. L., Madronich, S., Aiken, A. C., Bessagnet, B., Curci, G., Fast, J., Lamarque, J.-F., Onasch, T. B., Roux, G., Schauer, J. J., Stone, E. A., and Ulbrich, I. M.: Modeling organic aerosols during MILAGRO: importance of biogenic secondary organic aerosols, Atmos. Chem. Phys., 9, 6949–6981, doi:10.5194/acp-9-6949-2009, 2009.

Hodzic, A., Jimenez, J. L., Madronich, S., Canagaratna, M. R., DeCarlo, P. F., Kleinman, L., and Fast, J.: Modeling organic aerosols in a megacity: potential contribution of semi-volatile and intermediate volatility primary organic compounds to secondary organic aerosol formation, Atmos. Chem. Phys., 10, 5491–5514, doi:10.5194/acp-10-5491-2010, 2010a.

Hodzic, A., Jimenez, J. L., Prvt, A. S. H., Szidat, S., Fast, J. D., and Madronich, S.: Can 3-D models explain the observed fractions of fossil and non-fossil carbon in and near Mexico City?, Atmos. Chem. Phys. Discuss., 10, 14513–14556, doi:10.5194/acpd-10-14513-2010, 2010b.

Hofzumahaus, A., Rohrer, F., Lu, K., Bohn, B., Brauers, T., Chang, C., Fuchs, H., Holland, F., Kita, K., Kondo, Y., Li, X., Lou, S., Shao, M., Zeng, L., Wahner, A. and Zhang, Y.: Amplified Trace Gas Removal in the Troposphere, Science, 324, 1702–1704, 2009.

Hopke, P. K., Cohen, D. D., Begum, B. A., Biswas, S. K., Ni, B.,

Pandit, G. G., Santoso, M., Chung, Y.-S., Davy, P., Markwitz, A., Waheed, S., Siddique, N., Santos, F. L., Pabroa, P. C. B., Seneviratne, M. C. S., Wimolwattanapun, W., Bunprapob, S., Vuong, T. B., Hien, P. D., and Markowicz, A.: Urban air quality in the Asian region, Sci. Total Environ., 404, 103–112, 2008.

Huffman, J. A., Ziemann, P. J., Jayne, J. T., Worsnop, D. R., and Jimenez., J. L.: Development and Characterization of a Fast-Stepping/Scanning Thermodenuder for Chemically-Resolved Aerosol Volatility Measurements, Aerosol Sci. Technol., 42, 395–407, 2008.

Huffman, J. A, Docherty, K. S., Mohr, C., Cubison, M. J., Ulbrich, I. M., Ziemann, P. J., Onasch, T. B., and Jimenez, J. L: Chemically-Resolved Volatility Measurements of Organic Aerosol from Different Sources, Environ. Sci. Technol., 43, 5351–5357, doi:10.1021/es803539d, 2009a.

Huffman, J. A., Docherty, K. S., Aiken, A. C., Cubison, M. J., Ulbrich, I. M., DeCarlo, P. F., Sueper, D., Jayne, J. T., Worsnop, D. R., Ziemann, P. J., and Jimenez, J. L.: Chemically-resolved aerosol volatility measurements from two megacity field studies, Atmos. Chem. Phys., 9, 7161–7182, doi:10.5194/acp-9-7161-2009, 2009b.

IMP (Instituto Mexicano el Petróleo), Investigación sobre materia particulada y deterioro atmosférico, Subdirección de Protección Ambiental, 1994–1998, 1998.

IPCC, Fourth Assessment Report: Climate Change 2007. Intergovernmental Panel on Climate Change, 4 volumes, http://www.ipcc.ch/publications_and_data/publications_and_data_reports.htm #1, last access: 15 August 2010.

Iida, K., Stolzenburg, M. R., McMurry, P. H., and Smith, J. N.: Estimating nanoparticle growth rates from size-dependent charged fractions – Analysis of new particle formation events in Mexico City, J. Geophys. Res., 113, D05207, doi:10.1029/2007JD009260, 2008.

Jáuregui ,E.: El Clima de la Ciudad de México, Publisher Instituto de Geografia – UNAM, 129 pp., ISBN: 968-856-819-8 (in Spanish), 2000.

Jimenez, J. L., Canagaratna, M. R., Donahue, N. M., et al.: Evolution of Organic Aerosols in the Atmosphere, Science, 326, 1525–1529, doi:10.1126/science.1180353, 2009.

Jobson, B. T., Volkamer, R. A., Velasco, E., Allwine, G., Westberg, H., Lamb, B. K., Alexander, M. L., Berkowitz, C. M., and Molina, L. T.: Comparison of aromatic hydrocarbon measurements made by PTR-MS, DOAS and GC-FID during the MCMA *2003 Field Experiment, Atmos. Chem. Phys., 10, 1989–2005,* doi:10.5194/acp-10-1989-2010, 2010.

Johansson, M., Rivera, C., de Foy, B., Lei, W., Song, J., Zhang, Y., Galle, B., and Molina, L.: Mobile mini-DOAS measurement of the outflow of NO_2 and HCHO from Mexico City, Atmos. Chem. Phys., 9, 5647–5653, doi:10.5194/acp-9-5647-2009, 2009.

Johnson, K. S., Zuberi, B., Molina, L. T., Molina, M. J., Iedema, M. J., Cowin, J. P., Gaspar, D. J., Wang, C., and Laskin, A.: Processing of soot in an urban environment: case study from the Mexico City Metropolitan Area, Atmos. Chem. Phys., 5, 3033–3043, doi:10.5194/acp-5-3033-2005, 2005.

Johnson, K. S., de Foy, B., Zuberi, B., Molina, L. T., Molina, M. J., Xie, Y., Laskin, A., and Shutthanandan, V.: Aerosol composition and source apportionment in the Mexico City Metropolitan Area with PIXE/PESA/STIM and multivariate analysis, Atmos. Chem. Phys., 6, 4591–4600, doi:10.5194/acp-6-4591-2006, 2006.

Johnson, K. S., Laskin, A., Jimenez, J. L., Shutthanandan, V., Molina, L. T., Salcedo, D., Dzepina, K., and Molina, M. J.: Comparative Analysis of Urban Atmospheric Aerosol by Particle-Induced X-ray Emission (PIXE), Proton Elastic Scattering Analysis (PESA), and Aerosol Mass Spectrometry (AMS), Environ. Sci. Technol, 42, 6619–6624, doi:10.1021/es800393e, 2008.

Junkermann, W. and Burger, J. M.: A new portable instrument for continuous measurement of formaldehyde in ambient air, J, Atmos, Ocean, Tech, 23, 38–45, 2006.

Karl, T., Apel, E., Hodzic, A., Riemer, D. D., Blake, D. R., and Wiedinmyer, C.: Emissions of volatile organic compounds inferred from airborne flux measurements over a megacity, Atmos. Chem. Phys., 9, 271–285, doi:10.5194/acp-9-271-2009, 2009.

Karydis, V. A., Tsimpidi, A. P., Fountoukis, C., Nenes, A., Zavala, M., Lei, W., Molina, L. T. and Pandis, S.: Simulating the fine and coarse inorganic particulate matter concentrations in a polluted Megacity, Atmos. Environ., 44, 608–620, 2010.

Kleinman, L. I., Daum, P. H., Lee, Y. N., Nunnermacker, L. J., Springston, S. R., Weinstein-Lloyd, J., and Rudolph, J.: A comparative study of ozone production in five US metropolitan areas, J. Geophys. Res.-Atmos., 110, D02301, doi:10.1029/2004JD005096, 2005.

Kleinman, L. I., Springston, S. R., Daum, P. H., Lee, Y.-N., Nunnermacker, L. J., Senum, G. I., Wang, J., Weinstein-Lloyd, J., Alexander, M. L., Hubbe, J., Ortega, J., Canagaratna, M. R., and Jayne, J.: The time evolution of aerosol composition over the Mexico City plateau, Atmos. Chem. Phys., 8, 1559–1575, doi:10.5194/acp-8-1559-2008, 2008.

Kleinman, L. I., Springston, S. R., Wang, J., Daum, P. H., Lee, Y.-N., Nunnermacker, L. J., Senum, G. I., Weinstein-Lloyd, J., Alexander, M. L., Hubbe, J., Ortega, J., Zaveri, R. A., Canagaratna, M. R., and Jayne, J.: The time evolution of aerosol size distribution over the Mexico City plateau, Atmos. Chem. Phys., 9, 4261–4278, doi:10.5194/acp-9-4261-2009, 2009.

Khlystov, A., Zhang, Q., Jimenez, J. L., Stanier, C., Pandis, S. N., Canagaratna, M. R., Fine, P., Misra, C., and Sioutas. C.: In-situ concentration of semi-volatile aerosol using water-condensation technology, Journal of Aerosol Science, 36, 866–880, doi:10.1016/j.jaerosci.2004.11.005, 2005.

Kondo, Y., Miyazaki, Y., Takegawa, N., Miyakawa, T., Weber, R. J., Jimenez, J. L., Zhang, Q., and Worsnop, D. R.: Oxygenated and water-soluble organic aerosols in Tokyo, J. Geophys. Res., 112, *D01203, doi:10.1029/2006JD007056, 2007.*

LANL/IMP (Los Alamos National Laboratory and Instituto Mexicano del Petróleo). Mexico City Air Quality Research Initiative. Los Alamos, NM, 1994.

Lawrence, M. G., Butler, T. M., Steinkamp, J., Gurjar, B. R., and Lelieveld, J.: Regional pollution potentials of megacities and other major population centers, Atmos. Chem. Phys., 7, 3969–3987, doi:10.5194/acp-7-3969-2007, 2007.

Lei, W., de Foy, B., Zavala, M., Volkamer, R., and Molina, L. T.: Characterizing ozone production in the Mexico City Metropolitan Area: a case study using a chemical transport model, Atmos. Chem. Phys., 7, 1347–1366, doi:10.5194/acp-7-1347-2007, 2007.

Lei, W., Zavala, M., de Foy, B., Volkamer, R., and Molina, L. T.: Characterizing ozone production and response under different

meteorological conditions in Mexico City, Atmos. Chem. Phys., 8, 7571–7581, doi:10.5194/acp-8-7571-2008, 2008.

Lei, W., Zavala, M., de Foy, B., Volkamer, R., Molina, M. J., and Molina, L. T.: Impact of primary formaldehyde on air pollution in the Mexico City Metropolitan Area, Atmos. Chem. Phys., 9, 2607–2618, doi:10.5194/acp-9-2607-2009, 2009.

Lewandowski, P. A., Eichinger, W. E., Holder, H., Prueger, J., Wang, J., and Kleinman, L. I.: Vertical distribution of aerosols in the vicinity of Mexico City during MILAGRO-2006 Campaign, Atmos. Chem. Phys., 10, 1017–1030, doi:10.5194/acp-10-1017-2010, 2010.

Lezama, J. L., Favela, R., Galindo, L. M., Ibarrarán, M. E., Sánchez, S., Molina, L. T., Molina, M. J., Connors, S. R., and Fernandez Bremauntz, F.: Forces driving pollutant emissions in the MCMA, in: "Air Quality in the Mexico Megacity: an Integrated Assessment", edited by: Molina, L. T. and Molina, M. J., Kluwer Academic Publishers, 61–104, 2002.

Li, G., Lei, W., Zavala, M., Volkamer, R., Dusanter, S., Stevens, P., and Molina, L. T.: Impacts of HONO sources on the photochemistry in Mexico City during the MCMA-2006/MILAGO Campaign, Atmos. Chem. Phys., 10, 6551–6567, doi:10.5194/acp-10-6551-2010, 2010.

Lippmann, M.: Semi-continuous speciation analyses for ambient air particulate matter: An urgent need for health effects studies, J. Expo. Sci Environ. Epidemiol., 19, 235–247, 2009.

Lippmann M., Ito, K., Hwang, J. S., Maciejczyk, P., and Chen, L. C.: Cardiovascular effects of nickel in ambient air, Environ. Health Perspect., 114, 1662–1669, 2006.

Liu, S., Takahama, S., Russell, L. M., Gilardoni, S., and Baumgardner, D.: Oxygenated organic functional groups and their sources in single and submicron organic particles in MILAGRO 2006 campaign, Atmos. Chem. Phys., 9, 6849–6863, doi:10.5194/acp-9-6849-2009, 2009.

Livingston, J. M., Redemann, J., Russell, P. B., Torres, O., Veihelmann, B., Veefkind, P., Braak, R., Smirnov, A., Remer, L., Bergstrom, R. W., Coddington, O., Schmidt, K. S., Pilewskie, P., Johnson, R., and Zhang, Q.: Comparison of aerosol optical depths from the Ozone Monitoring Instrument (OMI) on Aura with results from airborne sunphotometry, other space and ground measurements during MILAGRO/INTEX-B, Atmos. Chem. Phys., 9, 6743–6765, doi:10.5194/acp-9-6743-2009, 2009.

Mao, J., Ren, X., Chen, S., Brune, W. H., Chen, Z., Martinez, M., Harder, H., Lefer, B., Rappengluck, B., Flynn, J., and Leuchner, M.: Atmospheric oxidation capacity in the summer of Houston 2006: comparison with summer measurements in other metropolitan studies, Atmos. Environ., doi:10.1016/j.atmosenv.2009.01.013, in press, 2009.

Marley, N. A., Gaffney, J. S., and Cunningham, M. M.: Aqueous Greenhouse Species in Clouds, Fogs, and Aerosols. Environ. Sci. Technol., 27, 2864–2869, 1993.

Marley, N. A., Gaffney, J. S., and Orlandini, K. A.: Characterization of Aquatic Humic and Fulvic Materials by Cylindrical Internal Reflectance Infrared Spectroscopy. Chapter 7, Humic/Fulvic Acids and Organic Colloidal Materials in the Environment, ACS Symposium Series 651, American Chemical Society, Washington, D.C., 96–107, 1996.

Marley, N. A., Gaffney, J. S., Ramos-Villegas, R., and Cárdenas González, B.: Comparison of measurements of peroxyacyl nitrates and primary carbonaceous aerosol concentrations in Mexico City determined in 1997 and 2003, Atmos. Chem. Phys., 7, 2277–2285, doi:10.5194/acp-7-2277-2007, 2007.

Marley, N. A., Gaffney, J. S., Ramos-Villegas, R., and Cárdenas González, B.: Comparison of measurements of peroxyacyl nitrates and primary carbonaceous aerosol concentrations in Mexico City determined in 1997 and 2003, Atmos. Chem. Phys., 7, 2277–2285, doi:10.5194/acp-7-2277-2007, 2007.

Marley, N. A., Gaffney, J. S., Tackett, M., Sturchio, N. C., Heraty, L., Martinez, N., Hardy, K. D., Marchany-Rivera, A., Guilderson, T., MacMillan, A., and Steelman, K.: The impact of biogenic carbon sources on aerosol absorption in Mexico City, Atmos. Chem. Phys., 9, 1537–1549, doi:10.5194/acp-9-1537-2009, 2009a.

Marley, N. A., Gaffney, J. S., Castro, T., Salcido, A., and Frederick, J.: Measurements of aerosol absorption and scattering in the Mexico City Metropolitan Area during the MILAGRO field campaign: a comparison of results from the T0 and T1 sites, Atmos. Chem. Phys., 9, 189–206, doi:10.5194/acp-9-189-2009, 2009b.

Marr, L. C., Dzepina, K., Jimenez, J. L., Reisen, F., Bethel, H. L., Arey, J., Gaffney, J. S., Marley, N. A., Molina, L. T., and Molina, M. J.: Sources and transformations of particle-bound polycyclic aromatic hydrocarbons in Mexico City, Atmos. Chem. Phys., 6, 1733–1745, doi:10.5194/acp-6-1733-2006, 2006.

Mauderly, J. L. and Samet, J. M.: Is there evidence for synergy among air pollutants in causing health effects?, Environ. Health Perspect, 117, 1–6, 2009.

McNaughton, C. S., Clarke, A. D., Kapustin, V., Shinozuka, Y., Howell, S. G., Anderson, B. E., Winstead, E., Dibb, J., Scheuer, E., Cohen, R. C., Wooldridge, P., Perring, A., Huey, L. G., Kim, S., Jimenez, J. L., Dunlea, E. J., DeCarlo, P. F., Wennberg, P. O., Crounse, J. D., Weinheimer, A. J., and Flocke, F.: Observations of heterogeneous reactions between Asian pollution and mineral dust over the Eastern North Pacific during INTEX-B, Atmos. Chem. Phys., 9, 8283–8308, doi:10.5194/acp-9-8283-2009, 2009.

Melamed, M. L., Basaldud, R., Steinbrecher, R., Emeis, S., Ruz-Surez, L. G., and Grutter, M.: Detection of pollution transport events southeast of Mexico City using ground-based visible spectroscopy measurements of nitrogen dioxide, Atmos. Chem. Phys., 9, 4827–4840, doi:10.5194/acp-9-4827-2009, 2009.

Mena-Carrasco, M., Carmichael, G. R., Campbell, J. E., Zimmerman, D., Tang, Y., Adhikary, B., D'allura, A., Molina, L. T., Zavala, M., García, A., Flocke, F., Campos, T., Weinheimer, A. J., Shetter, R., Apel, E., Montzka, D. D., Knapp, D. J., and Zheng, W.: Assessing the regional impacts of Mexico City emissions on air quality and chemistry, Atmos. Chem. Phys., 9, 3731–3743, doi:10.5194/acp-9-3731-2009, 2009.

Moffet, R. C., de Foy, B., Molina, L. T., Molina, M. J., and Prather, K. A.: Measurement of ambient aerosols in northern Mexico City by single particle mass spectrometry, Atmos. Chem. Phys., 8, 4499–4516, doi:10.5194/acp-8-4499-2008, 2008a.

Moffet, R., Desyaterik, Y., Hopkins, R. J., Tavanski, A. V., Gilles, M. K., Wang, Y., Shutthanandan, V., Molina, L. T., Gonzalez, R., Johnson, K. S., Mugica, V., Molina, M. J., Laskin, A., Prather, K. A., Characterization of Aerosols Containing Zn, Pb, and Cl from an Industrial Region of Mexico City, Environ. Sci. Technol., 42, 7091–7097, 2008b.

Moffet, R. C. and Prather, K. A.: In-situ measurements of the mix-

ing state and optical properties of soot with implications for radiative forcing estimates, P. Natl. Acad. Sci. USA, 106, 11872–11877, 2009.

Moffet, R. C., Henn, T. R., Tivanski, A. V., Hopkins, R. J., Desyaterik, Y., Kilcoyne, A. L. D., Tyliszczak, T., Fast, J., Barnard, J., Shutthanandan, V., Cliff, S. S., Perry, K. D., Laskin, A., and Gilles, M. K.: Microscopic characterization of carbonaceous aerosol particle aging in the outflow from Mexico City, Atmos. Chem. Phys., 10, 961–976, doi:10.5194/acp-10-961-2010, 2010.

Mohr, C., Huffman, J. A., Cubison, M. J., Aiken, A. C., Docherty, K. S., Kimmel, J. R., Ulbrich, I. M., Hannigan, M., Garcia, J., and Jimenez, J. L.: Characterization of Primary Organic Aerosol Emissions from Meat Cooking, Trash Burning, and Motor Vehicles with High-Resolution Aerosol Mass Spectrometry and Comparison with Ambient and Chamber Observations, Environ. Sci. Technol., 43, 2443–2449, doi:10.1021/es8011518, 2009.

Molina, L. T. and Molina, M. J.: Air Quality in the Mexico Megacity: An Integrated Assessment, Kluwer Academic Publishers: Dordrecht, The Netherlands, 384 pp., 2002.

Molina L. T., Molina, M. J., Favela, R., Fernandez Bremauntz, F., Slott, R., and Zavala, M. A., Cleaning the Air: A Comparative Study, in: "Air Quality in the Mexico Megacity: An Integrated Assessment", edited by: Molina, L. T. and Molina, M. J., Kluwer Academic Publishers, 21–59, 2002.

Molina, L. T., Molina, M. J., Slott, R., Kolb, C. E., Gbor, P. K., Meng, F., Singh, R., Galvez, O., Sloan, J. J., Anderson, W., Tang, X. Y., Shao, M., Zhu, T., Zhang, Y. H., Hu, M., Gurjar, B. R., Artaxo, P., Oyola, P., Gramsch, E., Hidalgo, P., and Gertler A.: 2004 Critical Review Supplement: Air Quality in Selected Megacities, J. Air Waste Manage. Assoc, http://www.awma.org, 2004.

Molina, L. T., Kolb, C. E., de Foy, B., Lamb, B. K., Brune, W. H., Jimenez, J. L., Ramos-Villegas, R., Sarmiento, J., Paramo-Figueroa, V. H., Cardenas, B., Gutierrez-Avedoy, V., and Molina, M. J.: Air quality in North America's most populous city – overview of the MCMA-2003 campaign, Atmos. Chem. Phys., 7, 2447–2473, doi:10.5194/acp-7-2447-2007, 2007.

Molina, M. J. and Molina, L. T.: 2004 Critical Review: Megacities and atmospheric pollution, J. Air Waste Manage. Assoc., 54(6), 644–680, 2004.

Moreno ,T., Querol, X., Alastuey, A.: Lanthanoid geochemistry of urban atmospheric particulate matter, Environ. Sci. Technol., 42, 6502–6507, 2008a.

Moreno T., Querol X., Pey J., Pey, J., Minguillon, M. C., Perez, N., Bernabe, R. M., Blanco, S., Cerdenas, B., Eichinger, W., Salcido, A., and Gibbons, W.: Spatial and temporal variations in inhalable CuZnPb aerosols within the Mexico City pollution plume, J. Environ. Monitoring, 10, 370–378, 2008b.

Moya, M., Castro, T., Zepeda, M., and Baez, A.: Characterization of size-differentiated inorganic composition of aerosols in Mexico City, Atmos. Environ., 37, 3581–3591, 2003.

Mugica, V., Vega, E., Arriaga, J. L., Ruiz, M. E.: Determination of motor vehicle profiles for non-methane organic compounds in the Mexico City Metropolitan Area, J. Air Waste Manage. Assoc., 48, 1060–1068, 1998.

Mugica, V., Vega, E., Chow, J., Reyes, E., Sánchez, G., Arriaga, J., Egami, R. and Watson, J. (), Speciated non-methane organic compounds emissions from food cooking in Mexico, Atmos. Eviron, 35, 1729–1734, 2001.

Mugica, V., Ruiz, M. E., Watson, J., and Chow, J.: Volatile aromatic compounds in Mexico City atmosphere: levels and source apportionment, Atmosfera, 16, 15–27, 2003.

Mugica V., Ortiz, E., Molina L., De Vizcaya-Ruiz A., Nebot A., Quintana R., Aguilar J., and Alcantara, E.: PM Composition and Source Reconciliation in Mexico City, Atmos. Environ. 43, 5068–5074, 2009.

NARSTO, (North American Research Strategy for Tropospheric Ozone): Improving emissions inventories for effective air quality management across North America, a NARSTO assessment, NARSTO-05-001, 2005.

Nemitz, E., Jimenez, J. L., Huffman, J. A., Canagaratna, M. R., Worsnop, D. R., and Guenther, A. B.: An eddy-covariance system for the measurement of surface/atmosphere exchange fluxes of submicron aerosol chemical species – first application above an urban area, Aerosol Sci. Technol., 42, 636–657, 2008.

Ng, N. L., Canagaratna, M. R., Zhang, Q., Jimenez, J. L., Tian, J., Ulbrich, I. M., Kroll, J. H., Docherty, K. S., Chhabra, P. S., Bahreini, R., Murphy, S. M., Seinfeld, J. H., Hildebrandt, L., Donahue, N. M., DeCarlo, P. F., Lanz, V. A., Prévôt, A. S. H., Dinar, E., Rudich, Y., and Worsnop, D. R.: Organic aerosol components observed in Northern Hemispheric datasets from Aerosol Mass Spectrometry, Atmos. Chem. Phys., 10, 4625–4641, doi:10.5194/acp-10-4625-2010, 2010.

Nunnermacker, L. J., Weinstein-Lloyd, J. B., Hillery, B., Giebel, B., Kleinman, L. I., Springston, S. R., Daum, P. H., Gaffney, J., Marley, N., and Huey, G.: Aircraft and ground-based measurements of hydroperoxides during the 2006 MILAGRO field campaign, Atmos. Chem. Phys., 8, 7619–7636, doi:10.5194/acp-8-7619-2008, 2008.

O'Neill, M. S., Bell, M. L., Ranjit, N., Cifuentes, L. A., Loomis, D., Gouveia, N. and Borja-Aburto V. H.: Air pollution and mortality in Latin America: The role of education, Epidemiology, 19, 810–819, 2008.

Oberdorster, G., Oberdorster, E., and Oberdorster, J.: Nanotoxicology: An emerging discipline evolving from studies of ultrafine particles, Environ. Health Persp., 113, 823–839, 2005.

Osornio-Vargas, A. R., Bonner, J. C., Alfaro-Moreno, E., Martínez L., García-Cuellar C., Ponce-de-León Rosales S., Miranda J., and Rosas, I.: Proinflammatory and cytotoxic effects of Mexico City air pollution particulate matter in vitro are dependent on particle size and composition, Environ. Health Perspect., 111, 1289–1293, 2003.

Osornio-Vargas, A. R, Quintana, R., Gómez, V., Serrano, J., Vázquez, I., Flores, G., Miranda, J., Vega, E., Ruiz, H., Escalona, S., de Foy, B., De Vizcaya-Ruiz, A., Garcia, C., Rosas, I., and Molina, L. T.: Oxidative potential and cellular effects induced by PM_{10} obtained in Mexico City and at a receptor site (2077). The Toxicologist CD, 102(S1), 427, 2008.

Padró, L. T., Tkacik, D., Lathem, T., Hennigan, C. J., Sullivan, A. P., Weber, R. J., Huey, L. G., and Nenes, A.: Investigation of CCN properties and droplet growth kinetics of water-soluble aerosol fraction in Mexico City, J. Geophys. Res., 115, D09204, doi:10.1029/2009JD013195, 2010.

Paredes-Miranda, G., Arnott, W. P., Jimenez, J. L., Aiken, A. C., Gaffney, J. S., and Marley, N. A.: Primary and secondary contributions to aerosol light scattering and absorption in Mexico City during the MILAGRO 2006 campaign, Atmos. Chem. Phys., 9, 3721–3730, doi:10.5194/acp-9-3721-2009, 2009.

Parrish D. D., Kuster W. C., Shao M., Yokouchi Y., Kondo Y.,

Goldan P. D., deGouw J. A., Koike M., and Shirai T., Comparison of air pollutant emissions among mega-cities, Atmos. Environ., 43, 6435–6441, 2009a.

Parrish, D. D., Allen, D. T., Bates, T. S., Estes, M., Fehsenfeld, F. C., Feingold, G., Ferrare, R., Hardesty, R. M., Meagher, J. F., Nielsen-Gammon, J. W., Pierce, R. B., Ryerson, T. B., Seinfeld, J. H., and Williams, E. J. : Overview of the Second Texas Air Quality Study (TexAQS II) and the Gulf of Mexico Atmospheric Composition and Climate Study (GoMACCS), J. Geophys. Res., *114, D00F13, doi:10.1029/2009JD011842, 2009b.*

Peng, R. D., Dominici, F., Pastor-Barriuso, R., Zeger, S. L., and Samet, J. M.: Seasonal analyses of air pollution and mortality in 100 US cities, Am. J. Epidemiol., 161, 585–594, doi:10.1093/aje/kwi075, 2005.

Perring, A. E., Bertram, T. H., Farmer, D. K., Wooldridge, P. J., Dibb, J., Blake, N. J., Blake, D. R., Singh, H. B., Fuelberg, H., Diskin, G., Sachse, G., and Cohen, R. C.: The production and persistence of $\sum$RONO$_2$ in the Mexico City plume, Atmos. Chem. Phys., 10, 7215–7229, doi:10.5194/acp-10-7215-2010, 2010.

Pope, C. A. and Dockery, D. W.: Health effects of fine particulate air pollution: lines that connect, Journal of Air and Waste Management Assoc., 56, 709-742, 2006.

Querol, X., Pey, J., Minguillón, M. C., Pérez, N., Alastuey, A., Viana, M., Moreno, T., Bernabé, R. M., Blanco, S., Cárdenas, B., Vega, E., Sosa, G., Escalona, S., Ruiz, H., and Artíñano, B.: PM speciation and sources in Mexico during the MILAGRO-2006 Campaign, Atmos. Chem. Phys., 8, 111–128, doi:10.5194/acp-8-111-2008, 2008.

Ramanathan, V., Crutzen, P. J., Kiehl, J. T., and Rosenfeld, D.: Aerosols, Climate, and the Hydrological Cycle, Science, 294, 2119–2124, 2001.

Ramanathan, V., Ramana, M. V., Roberts, G., Kim, D., Corrigan, C., Chung, C., and Winker, D.: Warming trends in Asia amplified by brown cloud solar absorption, Nature, 448, 575–578, 2007.

Redemann, J., Zhang, Q., Livingston, J., Russell, P., Shinozuka, Y., Clarke, A., Johnson, R., and Levy, R.: Testing aerosol properties in MODIS Collection 4 and 5 using airborne sunphotometer observations in INTEX-B/MILAGRO, Atmos. Chem. Phys., 9, 8159–8172, doi:10.5194/acp-9-8159-2009, 2009.

Reff, A., Bhave, P. V., Simon, H., Pace, T. G., Pouliot, G. A., Mobley, J. D., and Houyoux, M.: Emissions Inventory of PM$_{2.5}$ Trace Elements across the United States, Environ. Sci. Technol., 43, 5790–5796, 2009.

Rivera, C., Sosa, G., Wöhrnschimmel, H., de Foy, B., Johansson, M., and Galle, B.: Tula industrial complex (Mexico) emissions of SO_2 and NO_2 during the MCMA 2006 field campaign using a mobile mini-DOAS system, Atmos. Chem. Phys., 9, 6351–6361, doi:10.5194/acp-9-6351-2009, 2009.

Robinson, A. L., Donahue, N. M., Shrivastava, M. K., Weitkamp, E. A., Sage, A. M., Grieshop, A. P., Lane, T. E., Pandis, S. N., Pierce, J. R.: Rethinking organic aerosols: Semivolatile emissions and photochemical aging, Science, 315, 1259–1262, 2007.

Rogers, R. R., Hair, J. W., Hostetler, C. A., Ferrare, R. A., Obland, M. D., Cook, A. L., Harper, D. B., Burton, S. P., Shinozuka, Y., McNaughton, C. S., Clarke, A. D., Redemann, J., Russell, P. B., Livingston, J. M., and Kleinman, L. I.: NASA LaRC airborne high spectral resolution lidar aerosol measurements during MILAGRO: observations and validation, Atmos. Chem. Phys., 9, 4811–4826, doi:10.5194/acp-9-4811-2009, 2009.

Romieu, I., Lugo, M. C., Velasco, S. R., Sanchez, S., Meneses, F., and Hernandez, M.: Air pollution and school absenteeism among children in Mexico City, Am. J. Epidemiol., 136, 1524–1531, 1992.

Romieu, I., Meneses, F., Ruiz, S., Sienra, J. J, Huerta, J., White, M. C., and Etzel, R. A.: Effects of air pollution on the respiratory health of asthmatic children living in Mexico City, Am. J. Resp. Crit. Care Med. 154, 300–307, 1996.

Romieu. I., Ramirez-Aguilar, M., Sienra-Monge, J. J., Moreno-Macias, H., del Rio-Navarro, B. E., David, G., Marzec, J., Hernández-Avila, M., and London, S.: GSTM1 and GSTP1 and respiratory health in asthmatic children exposed to ozone, Eur. Respir. J., 28(5), 953–959, doi:10.1183/09031936.06.00114905, 2006.

Rosas-Perez, I., Serrano, J., Alfaro-Moreno, E., Baumgardner, D., García-Cuella, C., Miranda-Martin del Campo, J., Raga, G. B., Castillejos, M., Drucker-Colín, R., and Osornio-Vargas, A.: Relations between PM$_{10}$ composition and cell toxicity: a multivariate and graphical approach, Chemosphere, 67, 1218–1228, 2007.

Russell, P. B., Bergstrom, R. W., Shinozuka, Y., Clarke, A. D., DeCarlo, P. F., Jimenez, J. L., Livingston, J. M., Redemann, J., Dubovik, O., and Strawa, A.: Absorption Angstrom Exponent in AERONET and related data as an indicator of aerosol composition, Atmos. Chem. Phys., 10, 1155–1169, doi:10.5194/acp-10-1155-2010, 2010.

Rutter, A. P., Snyder, D. C., Stone, E. A., Schauer, J. J., Gonzalez-Abraham, R., Molina, L. T., Márquez, C., Cárdenas, B., and de Foy, B.: In situ measurements of speciated atmospheric mercury and the identification of source regions in the Mexico City Metropolitan Area, Atmos. Chem. Phys., 9, 207–220, doi:10.5194/acp-9-207-2009, 2009.

Salcedo, D., Onasch, T. B., Dzepina, K., Canagaratna, M. R., Zhang, Q., Huffman, J. A., DeCarlo, P. F., Jayne, J. T., Mortimer, P., Worsnop, D. R., Kolb, C. E., Johnson, K. S., Zuberi, B., Marr, L. C., Volkamer, R., Molina, L. T., Molina, M. J., Cardenas, B., Bernabé, R. M., Márquez, C., Gaffney, J. S., Marley, N. A., Laskin, A., Shutthanandan, V., Xie, Y., Brune, W., Lesher, R., Shirley, T., and Jimenez, J. L.: Characterization of ambient aerosols in Mexico City during the MCMA-2003 campaign with Aerosol Mass Spectrometry: results from the CENICA Supersite, Atmos. Chem. Phys., 6, 925–946, doi:10.5194/acp-6-925-2006, 2006.

Salcedo, D., Onasch, T. B., Dzepina, K., Canagaratna, M. R., Zhang, Q., Huffman, J. A., DeCarlo, P. F., Jayne, J. T., Mortimer, P., Worsnop, D. R., Kolb, C. E., Johnson, K. S., Zuberi, B., Marr, L. C., Volkamer, R., Molina, L. T., Molina, M. J., Cardenas, B., Bernab, R. M., Márquez, C., Gaffney, J. S., Marley, N. A., Laskin, A., Shutthanandan, V., Xie, Y., Brune, W., Lesher, R., Shirley, T., and Jimenez, J. L.: Characterization of ambient aerosols in Mexico City during the MCMA-2003 campaign with Aerosol Mass Spectrometry: results from the CENICA Supersite, Atmos. Chem. Phys., 6, 925–946, doi:10.5194/acp-6-925-2006, 2006.

Salcedo, D., Onasch, T. B., Aiken, A. C., Williams, L. R., de Foy, B., Cubison, M. J., Worsnop, D. R., Molina, L. T., and Jimenez, J. L.: Determination of particulate lead using aerosol mass spectrometry: MILAGRO/MCMA-2006 observations, Atmos. Chem. Phys., 10, 5371–5389, doi:10.5194/acp-10-5371-

2010, 2010.

Samet, J. and Krewski, D.: Health effects associated with exposure to ambient air pollution, J. Toxicol. Environ. Health A, 70, 227–242, 2007.

Samoli, E., Zanobetti, A., Schwartz, J., Atkinson, R., LeTertre, A., Schindler, C., Perez, L., Cadum, E., Pekkanen, J., Paldy, A., Touloumi, G., Katsouyanni, K.: The temporal pattern of mortality responses to ambient ozone in the APHEA project, J. Epidemiol Community Health, 63(12), 960–966, 2009.

San Martini, F. M., Dunlea, E. J., Volkamer, R., Onasch, T. B., Jayne, J. T., Canagaratna, M. R., Worsnop, D. R., Kolb, C. E., Shorter, J. H., Herndon, S. C., Zahniser, M. S., Salcedo, D., Dzepina, K., Jimenez, J. L., Ortega, J. M., Johnson, K. S., McRae, G. J., Molina, L. T., and Molina, M. J.: Implementation of a Markov Chain Monte Carlo method to inorganic aerosol modeling of observations from the MCMA-2003 campaign – Part II: Model application to the CENICA, Pedregal and Santa Ana sites, Atmos. Chem. Phys., 6, 4889–4904, doi:10.5194/acp-6-4889-2006, 2006.

San Martini, F. M., Dunlea, E. J., Volkamer, R., Onasch, T. B., Jayne, J. T., Canagaratna, M. R., Worsnop, D. R., Kolb, C. E., Shorter, J. H., Herndon, S. C., Zahniser, M. S., Salcedo, D., Dzepina, K., Jimenez, J. L., Ortega, J. M., Johnson, K. S., McRae, G. J., Molina, L. T., and Molina, M. J.: Implementation of a Markov Chain Monte Carlo method to inorganic aerosol modeling of observations from the MCMA-2003 campaign Part II: Model application to the CENICA, Pedregal and Santa Ana sites, Atmos. Chem. Phys., 6, 4889–4904, doi:10.5194/acp-6-4889-2006, 2006b.

Schauer, J. J.: Evaluation of elemental carbon as a marker for diesel particulate matter, J. Expos. Anal. Environ. Epidemiol, 13, 443–453, 2003.

Schauer, J. J., Rogge, W. F., HildemannL, M., Mazurek, M. A., Cass, G. R., and Simoneit, B. R. T.: Source Apportionment of Airborne Particulate Matter Using Organic Compounds as Tracers, Atmos. Environ., 30, 3837–3855, 1996.

Schifter, I., Diaz, L., Duran, J., Guzman, E., Chavez, O., and Lopez-Salinas, E.: Remote sensing study of emissions from motor vehicles in the Metropolitan Area of Mexico City, Environ. Sci. Technol., 37, 395–401, 2003.

Schifter, I., Díaz, L., Rodríguez, R., Duran, J., and Chavez. O.: Trends in exhaust emissions from in-use Mexico City vehicles, 2000–2006. A remote sensing study, Environ. Monit. Assess., 137, 459–470, doi:10.1007/s10661-007-9781-4, 2008.

Schmid, B., Ferrare, R., Flynn, C., Elleman, R., Covert, D., Strawa, A., Welton, E., Turner, D.,Jonsson, H., Redemann, J., Eilers, J., Ricci, K., Hallar, A. G., Clayton, M., Michalsky, J.,Smirnov, A., Holben, B., and Barnard, J.: How well do state-of-the-art techniques measur-ing the vertical profile of tropospheric aerosol extinction compare?, J. Geophys. Res., 111, D05S07, doi:10.1029/2005JD005837, 2006.

Schmidt, K. S., Pilewskie, P., Bergstrom, R., Coddington, O., Redemann, J., Livingston, J., Russell, P., Bierwirth, E., Wendisch, M., Gore, W., Dubey, M. K., and Mazzoleni, C.: A new method for deriving aerosol solar radiative forcing and its first application within MILAGRO/INTEX-B, Atmos. Chem. Phys. Discuss., 10, 2731–2767, doi:10.5194/acpd-10-2731-2010, 2010.

SEMARNAT: Inventario Nacional de Emisiones de Mexico, 1999, Instituto Nacional de Ecologia, available at: http://www.ine.gob.mx/dgicur/calaire/inem.html, 2006.

Shaw, W. J., Pekour, M. S., Coulter, R. L., Martin, T. J., and Walters, J. T.: The daytime mixing layer observed by radiosonde, profiler, and lidar during MILAGRO, Atmos. Chem. Phys. Discuss., 7, 15025–15065, doi:10.5194/acpd-7-15025-2007, 2007.

Sheehy, P. M., Volkamer, R., Molina, L. T., and Molina, M. J.: Oxidative capacity of the Mexico City atmosphere – Part 2: A RO_X radical cycling perspective, Atmos. Chem. Phys., 10, 6993–7008, doi:10.5194/acp-10-6993-2010, 2010.

Shinozuka, Y., Clarke, A. D., DeCarlo, P. F., Jimenez, J. L., Dunlea, E. J., Roberts, G. C., Tomlinson, J. M., Collins, D. R., Howell, S. G., Kapustin, V. N., McNaughton, C. S., and Zhou, J.: Aerosol optical properties relevant to regional remote sensing of CCN activity and links to their organic mass fraction: airborne observations over Central Mexico and the US West Coast during MILAGRO/INTEX-B, Atmos. Chem. Phys., 9, 6727–6742, doi:10.5194/acp-9-6727-2009, 2009.

Shirley, T. R., Brune, W. H., Ren, X., Mao, J., Lesher, R., Cardenas, B., Volkamer, R., Molina, L. T., Molina, M. J., Lamb, B., Velasco, E., Jobson, T., and Alexander, M.: Atmospheric oxidation in the Mexico City Metropolitan Area (MCMA) during April 2003, Atmos. Chem. Phys., 6, 2753–2765, doi:10.5194/acp-6-2753-2006, 2006.

Shon, Z.-H., Madronich, S., Song, S.-K., Flocke, F. M., Knapp, D. J., Anderson, R. S., Shetter, R. E., Cantrell, C. A., Hall, S. R., and Tie, X.: Characteristics of the NO-NO2-O3 system in different chemical regimes during the MIRAGE-Mex field campaign, Atmos. Chem. Phys., 8, 7153–7164, doi:10.5194/acp-8-7153-2008, 2008.

Singh, H. B., Brune, W. H., Crawford, J. H., Flocke, F., and Jacob, D. J.: Chemistry and transport of pollution over the Gulf of Mexico and the Pacific: spring 2006 INTEX-B campaign overview and first results, Atmos. Chem. Phys., 9, 2301–2318, doi:10.5194/acp-9-2301-2009, 2009.

SMA-GDF (Secretaría del Medio Ambiente del Gobierno del Distrito Federal): Inventario de emisiones criterio para el año de 2006 de la Zona Metropolitana del Valle de México, Secretaría del Medio Ambiente, Gobierno de México, México, available at: http://www.sma.df.gob.mx/, 2008a.

SMA-GDF (Secretaría del Medio Ambiente del Gobierno del Distrito Federal): Inventario de emisiones toxicas para el año de 2006 de la Zona Metropolitana del Valle de México, Secretaría del Medio Ambiente, Gobierno de México, México, available at: http://www.sma.df.gob.mx/, 2008b.

SMA-GDF (Secretaría del Medio Ambiente del Gobierno del Distrito Federal): Inventario de emisiones de gases de efecto invernadero para el año de 2006 de la Zona Metropolitana del Valle de México, Secretaría del Medio Ambiente, Gobierno de México, México, available at: http://www.sma.df.gob.mx/, 2008c.

Smith, J. N., Dunn, M. J., VanReken, T. M., Iida, K., Stolzenburg, M. R., McMurry, P. H., and Huey, L. G.: Chemical composition of atmospheric nanoparticles formed from nucleation in Tecamac, Mexico: Evidence for an important role for organic species in nanoparticle growth, Geophys. Res. Lett., 35, L04808, doi:10.1029/2007GL032523, 2008.

Song, J., Lei, W., Bei, N., Zavala, M., de Foy, B., Volkamer, R., Cardenas, B., Zheng, J., Zhang, R., and Molina, L. T.: Ozone response to emission changes: a modeling study during the MCMA-2006/MILAGRO Campaign, Atmos. Chem. Phys., 10,

3827–3846, doi:10.5194/acp-10-3827-2010, 2010.

Spracklen, D. V., Carslaw, K. S., Kulmala, M., Kerminen, V.-M., Sihto, S.-L., Riipinen, I., Merikanto, J.,. Mann, G. W, Chipperfield, M. P., Wiedensohler, A., Birmili, W., and Lihavainen, H.: Contribution of particle formation to global cloud condensation nuclei concentrations, Geophys. Res. Lett., 35, L06808, doi:10.1029/2007GL033038, 2008.

Stephens, S., Madronich, S., Wu, F., Olson, J. B., Ramos, R., Retama, A., and Muñoz, R.: Weekly patterns of Mxico City's surface concentrations of CO, NO_X, PM_{10} and O_3 during 1986–2007, Atmos. Chem. Phys., 8, 5313–5325, doi:10.5194/acp-8-5313-2008, 2008.

Stone, E. A., Snyder, D. C., Sheesley, R. J., Sullivan, A. P., Weber, R. J., and Schauer, J. J.: Source apportionment of fine organic aerosol in Mexico City during the MILAGRO experiment 2006, Atmos. Chem. Phys., 8, 1249–1259, doi:10.5194/acp-8-1249-2008, 2008.

Stone, E. A., Hedman, C. J., Sheesley, R. J., Shafer, M. M., and Schauer, J. J.: Investigating the chemical nature of humic-like substances (HULIS) in North American atmospheric aerosols by liquid chromatography tandem mass spectrometry, Atmos. Environ., 43, 4205–4213, 2009.

Stone, E. A., Hedman, C. J., Zhou, J., Mieritz, M., and Schauer, J. J.: Insights into the Nature of Secondary Organic Aerosol in Mexico City during the MILAGRO Experiment 2006, Atmos. Environ., 44, 312–319, 2010a.

Stone, E. A., Schauer, J. J., Quraishi, T. A., and Mahmood, A.: Chemical Characterization and Source Apportionment of Fine and Coarse Particulate Matter in Lahore, Pakistan, Atmos. Environ., 44, 1062–1070, 2010b.

Stremme, W., Ortega, I., and Grutter, M.: Using ground-based solar and lunar infrared spectroscopy to study the diurnal trend of carbon monoxide in the Mexico City boundary layer, Atmos. Chem. Phys., 9, 8061–8078, doi:10.5194/acp-9-8061-2009, 2009.

Streit, G. E. and Guzman, F.: Mexico City Air Quality: Progress of an International Collaborative Project to Define Air Quality Management Options. Atmos. Environ., 30, 723–733, 1996.

Subramanian, R., Kok, G. L., Baumgardner, D., Clarke, A., Shinozuka, Y., Campos, T. L., Heizer, C. G., Stephens, B. B., de Foy, B., Voss, P. B., and Zaveri, R. A.: Black carbon over Mexico: the effect of atmospheric transport on mixing state, mass absorption cross-section, and BC/CO ratios, Atmos. Chem. Phys., 10, 219–237, doi:10.5194/acp-10-219-2010, 2010.

Talbot, R., Mao, H., Scheuer, E., Dibb, J., Avery, M., Browell, E., Sachse, G., Vay, S., Blake, D., Huey, G., and Fuelberg, H.: Factors influencing the large-scale distribution of Hg^o in the Mexico City area and over the North Pacific, Atmos. Chem. Phys., 8, 2103–2114, doi:10.5194/acp-8-2103-2008, 2008.

Thompson, A. M., Yorks, J. E., Miller, S. K., Witte, J. C., Dougherty, K. M., Morris, G. A., Baumgardner, D., Ladino, L., and Rappenglück, B.: Tropospheric ozone sources and wave activity over Mexico City and Houston during MILAGRO/Intercontinental Transport Experiment (INTEX-B) Ozonesonde Network Study, 2006 (IONS-06), Atmos. Chem. Phys., 8, 5113–5125, doi:10.5194/acp-8-5113-2008, 2008.

Thornhill, D. A., de Foy, B., Herndon, S. C., Onasch, T. B., Wood, E. C., Zavala, M., Molina, L. T., Gaffney, J. S., Marley, N. A., and Marr, L. C.: Spatial and temporal variability of particulate polycyclic aromatic hydrocarbons in Mexico City, Atmos. Chem. Phys., 8, 3093–3105, doi:10.5194/acp-8-3093-2008, 2008.

Thornhill, D. A., Williams, A. E., Onasch, T. B., Wood, E., Herndon, S. C., Kolb, C. E., Knighton, W. B., Zavala, M., Molina, L. T., and Marr, L. C.: Application of positive matrix factorization to on-road measurements for source apportionment of diesel- and gasoline-powered vehicle emissions in Mexico City, Atmos. Chem. Phys., 10, 3629–3644, doi:10.5194/acp-10-3629-2010, 2010.

Tie, X., Madronich, S., Li, G. H., Ying, Z. M., Zhang, R., Garcia, A., Lee-Taylor, J., and Liu, Y.: Characterizations of chemical oxidants in Mexico City: a regional chemical/dynamical model (WRF-Chem) study, Atmos. Environ., 41, 1989–2008, 2007.

Tie, X., Madronich, S., Li, G., Ying, Z., Weinheimer, A., Apel, E., and Campos, T.: Simulation of Mexico City plumes during the MIRAGE-Mex field campaign using the WRF-Chem model, Atmos. Chem. Phys., 9, 4621–4638, doi:10.5194/acp-9-4621-2009, 2009.

Tovalin, H., Herbarth, O., Sierra-Vargas, M. P., Strandberg, B., Blanco, S., Vega ,L., Sioutas, C. Hicks, J., Marroquín, R., Acosta, G., Guarneros, M., Hernández, V., Estrada-Muñiz, E., Olivares, I., Pérez, D., Torres-Ramos, Y., Ulrich, F., Hudson, R., Reyes, E., Rodríguez, T., Elizondo, G., and Cantellano, E.: Air pollutants exposure and health effects: A multi-pollutant approach during the MILAGRO-MCMA2006 campaign, in: "Air Pollution: Health & Environmental Impacts", edited by: Gurjar, B. R., Molina, L. T., Ojha, C. S. P., Taylor & Francis, 203–228, 2010.

Tsimpidi, A. P., Karydis, V. A., Zavala, M., Lei, W., Molina, L., Ulbrich, I. M., Jimenez, J. L., and Pandis, S. N.: Evaluation of the volatility basis-set approach for the simulation of organic aerosol formation in the Mexico City metropolitan area, Atmos. Chem. Phys., 10, 525–546, doi:10.5194/acp-10-525-2010, 2010.

Ulbrich, I. M., Canagaratna, M. R., Zhang, Q., Worsnop, D. R., and Jimenez, J. L.: Interpretation of organic components from Positive Matrix Factorization of aerosol mass spectrometric data, Atmos. Chem. Phys., 9, 2891–2918, doi:10.5194/acp-9-2891-2009, 2009.

Vay, S. A., Tyler, S. C., Choi, Y., Blake, D. R., Blake, N. J., Sachse, G. W., Diskin, G. S., and Singh, H. B.: Sources and transport of $\Delta^{14}C$ in CO2 within the Mexico City Basin and vicinity, Atmos. Chem. Phys., 9, 4973–4985, doi:10.5194/acp-9-4973-2009, 2009.

Vega, E., Reyes, E., Sanchez, G., Ortiz, E., Ruiz, M., Chow, J., Watson, J., and Edgerton, S.: Basic statistics of $PM_{2.5}$ and PM_{10} in the atmosphere of Mexico City, Sci. Total Environ., 287, 167–176, 2002.

Vega, E., Reyes, E., Ruiz, H., García, J., Sánchez, G., Martínez-Villa, G., González, U., Chow, J. C., and Watson, J. G.: Analysis of $PM_{2.5}$ and PM_{10} in the Atmosphere of Mexico City during 2000–2002, J. Air & Waste Manage. Assoc., 54, 786–798, 2004.

Vega, E., Lowenthal, D. H., Ruiz, H., Reyes, E., Watson, J. G., Chow, J. C., Viana, M., Querol, X., and Alastuey, A.: Fine Particle Receptor Modeling in the Atmosphere of Mexico City, J. Air Waste Manage. Assoc., 59, 1417–1428, 2009.

Velasco, E., Lamb, B., Pressley, S., Allwine, E., Westberg, H., Jobson, B. T., Alexander, M., Prazeller, P., Molina, L. T., and Molina, M. J.: Flux measurements of volatile organic compounds from an urban landscape, Geophys. Res. Lett., 32, L20802, doi:10.1029/2005GL023356, 2005.

Velasco, E., Lamb, B., Westberg, H., Allwine, E., Sosa, G., Arriaga-Colina, J. L., Jobson, B. T., Alexander, M. L., Prazeller, P., Knighton, W. B., Rogers, T. M., Grutter, M., Herndon, S. C., Kolb, C. E., Zavala, M., de Foy, B., Volkamer, R., Molina, L. T., and Molina, M. J.: Distribution, magnitudes, reactivities, ratios and diurnal patterns of volatile organic compounds in the Valley of Mexico during the MCMA 2002 & 2003 field campaigns, Atmos. Chem. Phys., 7, 329–353, doi:10.5194/acp-7-329-2007, 2007.

Velasco, E., Márquez, C., Bueno, E., Bernabé, R. M., Sánchez, A., Fentanes, O., Wöhrnschimmel, H., Cárdenas, B., Kamilla, A., Wakamatsu, S., and Molina, L. T.: Vertical distribution of ozone and VOCs in the low boundary layer of Mexico City, Atmos. Chem. Phys., 8, 3061–3079, doi:10.5194/acp-8-3061-2008, 2008.

Velasco, E., Pressley, S., Grivicke, R., Allwine, E., Coons, T., Foster, W., Jobson, B. T., Westberg, H., Ramos, R., Hernández, F., Molina, L. T., and Lamb, B.: Eddy covariance flux measurements of pollutant gases in urban Mexico City, Atmos. Chem. Phys., 9, 7325–7342, doi:10.5194/acp-9-7325-2009, 2009.

Velasco, E., Pressley, S., Grivicke, R., Allwine, E., Molina, L. T., and Lamb, B.: Energy balance in urban Mexico City: observation and parameterization during the MILAGRO/MCMA-2006 field campaign, Theor. Appl. Climatol., 102, doi:10.1007/s00704-010-0314-7, 2010.

Volkamer, R., Molina, L. T., Molina, M. J., Shirley, T., and Brune, W. H.: DOAS measurement of glyoxal as an indicator for fast VOC chemistry in urban air, Geophys. Res. Lett., 32, L08806, doi:10.1029/2005GL022616, 2005.

Volkamer, R., Jimenez, J. L., San Martini, F., Dxepina, K., Zhang, Q., Salcedo, D., Molina, L. T., Worsnop, D. R., and Molina, M. J.: Secondary Organic Aerosol Formation from Anthropogenic Air Pollution: rapid and Higher than Expected, Geophys. Res. Lett, 33, L17811, doi:10.1029/2006GL026899, 2006.

Volkamer, R., San Martini, F., Molina, L. T., Salcedo, D., Jimenez, J. L., and Molina, M. J.: A Missing Sink for Gas-Phase Glyoxal in Mexico City: formation of Secondary Organic Aerosol, Geophys. Res. Lett., 34, L19807, doi:10.1029/2007GL030752, 2007.

Volkamer, R., Sheehy, P., Molina, L. T., and Molina, M. J.: Oxidative capacity of the Mexico City atmosphere – Part 1: A radical source perspective, Atmos. Chem. Phys., 10, 6969–6991, doi:10.5194/acp-10-6969-2010, 2010.

Volkamer, R., Ziemann, P. J., and Molina, M. J.: Secondary Organic Aerosol Formation from Acetylene (C_2H_2): seed effect on SOA yields due to organic photochemistry in the aerosol aqueous phase, Atmos. Chem. Phys., 9, 1907–1928, doi:10.5194/acp-9-1907-2009, 2009.

Voss, P. B., Zaveri, R. A., Flocke, F. M., Mao, H., Hartley, T. P., DeAmicis, P., Deonandan, I., Contreras-Jiménez, G., Martínez-Antonio, O., Figueroa Estrada, M., Greenberg, D., Campos, T. L., Weinheimer, A. J., Knapp, D. J., Montzka, D. D., Crounse, J. D., Wennberg, P. O., Apel, E., Madronich, S., and de Foy, B.: Long-range pollution transport during the MILAGRO-2006 campaign: a case study of a major Mexico City outflow event using free-floating altitude-controlled balloons, Atmos. Chem. Phys., 10, 7137–7159, doi:10.5194/acp-10-7137-2010, 2010.

Wallace, L.: Indoor sources of ultrafine and accumulation mode particles: Size distributions, size-resolved concentrations, and source strengths, Aerosol Sci. Technol., 40, 348–360, 2006.

Wang, J., Cubison, M. J., Aiken, A. C., Jimenez, J. L., and Collins, D. R.: The importance of aerosol mixing state and size-resolved composition on CCN concentration and the variation of the importance with atmospheric aging of aerosols, Atmos. Chem. Phys., 10, 7267–7283, doi:10.5194/acp-10-7267-2010, 2010.

Watson, J. G.: Visibility: science and regulation, J. Air Waste Manag. Assoc., 52(6), 628–713, 2002.

Weibring, P., Richter, D., Walega, J. G., and Fried, A.: Airborne difference frequency spectrometer for ultra sensitive formaldehyde measurements, in Conference on Lasers and Electro-Optics/Quantum Electronics and Laser Science Conference and Photonic Applications Systems Technologies, OSA Technical Digest Series (CD), Optical Society of America, 2007.

Wert, B. P., Trainer, M., Fried, A., Ryerson, T. B., Henry, B., Potter, W., Angevine, W. M., Atlas, E., Donnelly, S. G., Fehsenfeld, F. C., Frost, G. J., Goldan, P. D., Hansel, A., Holloway, J. S., Hubler, G., Kuster, W. C., Nicks Jr., D. K., Neuman, J. A., Parrish, D. D., Schauffler, S., Stutz, J., Sueper, D. T., Wiedinmyer, C., Wisthaler, A.: Signatures of terminal alkene oxidation in airborne formaldehyde measurements during TexAQS 2000, J. Geophys. Res., 108, 4104, doi:10.1029/2002JD002502, 2003.

Wöhrnschimmel, H., Magaña, M., Stahel, W. A., Blanco, S., Acuña, S., Pérez, J. M., González, S., Gutiérrez, V., Wakamatsu, S., and Cárdenas, B.: Measurements and receptor modeling of volatile organic compounds in south-eastern Mexico City, 20002007, Atmos. Chem. Phys. Discuss., 10, 3319–3346, doi:10.5194/acpd-10-3319-2010, 2010.

Wood, E. C., Herndon, S. C., Onasch, T. B., Kroll, J. H., Canagaratna, M. R., Kolb, C. E., Worsnop, D. R., Neuman, J. A., Seila, R., Zavala, M., and Knighton, W. B.: A case study of ozone production, nitrogen oxides, and the radical budget in Mexico City, Atmos. Chem. Phys., 9, 2499–2516, doi:10.5194/acp-9-2499-2009, 2009.

Wood, E. C., Canagaratna, M. R., Herndon, S. C., Kroll, J. H., Onasch, T. B., Kolb, C. E., Worsnop, D. R., Knighton, W. B., Seila, R., Zavala, M., Molina, L. T., DeCarlo, P. F., Jimenez, J. L., Weinheimer, A. J., Knapp, D. J., Jobson, B. T., Stutz, J., Kuster, W. C., and Williams, E. J.: Investigation of the correlation between odd oxygen and secondary organic aerosol in Mexico City and Houston, Atmos. Chem. Phys. Discuss., 10, 3547–3604, doi:10.5194/acpd-10-3547-2010, 2010.

Yokelson, R. J., Urbanski, S. P., Atlas, E. L., Toohey, D. W., Alvarado, E. C., Crounse, J. D., Wennberg, P. O., Fisher, M. E., Wold, C. E., Campos, T. L., Adachi, K., Buseck, P. R., and Hao, W. M.: Emissions from forest fires near Mexico City, Atmos. Chem. Phys., 7, 5569–5584, doi:10.5194/acp-7-5569-2007, 2007.

Yokelson, R. J., Crounse, J. D., DeCarlo, P. F., Karl, T., Urbanski, S., Atlas, E., Campos, T., Shinozuka, Y., Kapustin, V., Clarke, A. D., Weinheimer, A., Knapp, D. J., Montzka, D. D., Holloway, J., Weibring, P., Flocke, F., Zheng, W., Toohey, D., Wennberg, P. O., Wiedinmyer, C., Mauldin, L., Fried, A., Richter, D., Walega, J., Jimenez, J. L., Adachi, K., Buseck, P. R., Hall, S. R., and Shetter, R.: Emissions from biomass burning in the Yucatan, Atmos. Chem. Phys., 9, 5785–5812, doi:10.5194/acp-9-5785-2009, 2009.

Yu, X.-Y., Cary, R. A., and Laulainen, N. S.: Primary and secondary organic carbon downwind of Mexico City, Atmos. Chem. Phys.,

9, 6793–6814, doi:10.5194/acp-9-6793-2009, 2009.

Yuan, T., Li, Z., Zhang, R., and Fan, J.: Increase of cloud droplet size with increasing aerosol loading, J. Geophys. Res., 113, D04201, doi:10.1029/2007JD008632, 2008.

Zambrano García, A., Medina Coyotzin, C., Rojas Amaro, A., López Veneroni, D., Chang Martínez, L., and Sosa Iglesias, G.: Distribution and sources of bioaccumulative air pollutants at Mezquital Valley, Mexico, as reflected by the atmospheric plant Tillandsia recurvata L., Atmos. Chem. Phys., 9, 6479–6494, doi:10.5194/acp-9-6479-2009, 2009.

Zavala, M., Herndon, S. C., Slott, R. S., Dunlea, E. J., Marr, L. C., Shorter, J. H., Zahniser, M., Knighton, W. B., Rogers, T. M., Kolb, C. E., Molina, L. T., and Molina, M. J.: Characterization of on-road vehicle emissions in the Mexico City Metropolitan Area using a mobile laboratory in chase and fleet average measurement modes during the MCMA-2003 field campaign, Atmos. Chem. Phys., 6, 5129–5142, doi:10.5194/acp-6-5129-2006, 2006.

Zavala, M., Lei, W., Molina, M. J., and Molina, L. T.: Modeled and observed ozone sensitivity to mobile-source emissions in Mexico City, Atmos. Chem. Phys., 9, 39–55, doi:10.5194/acp-9-39-2009, 2009a.

Zavala, M., Herndon, S. C., Wood, E. C., Onasch, T. B., Knighton, W. B., Marr, L. C., Kolb, C. E., and Molina, L. T.: Evaluation of mobile emissions contributions to Mexico City's emissions inventory using on-road and cross-road emission measurements and ambient data, Atmos. Chem. Phys., 9, 6305–6317, doi:10.5194/acp-9-6305-2009, 2009b.

Zaveri, R., Chapman, E. G., Easter, R. C., Fast, J. D., Flocke, F., Kleinman, L. I., Madronich, S., Springston, S. R., Voss, P. B., and Weinheimer, A.: Modeling gas-aerosol processes during MILAGRO 2006, Fall American Geophysical Union Meeting, San Francisco, CA, A33D-1570, 2007.

Zhang, Q., Jimenez, J. L., Canagaratna, M. R., Allan, J. D., Coe, H., Ulbrich, I., Alfarra, M. R., Takami, A., Middlebrook, A. M., Sun, Y. L., Dzepina, K., Dunlea, E., Docherty, K., DeCarlo, P. F., Salcedo, D., Onasch, T., Jayne, J. T., Miyoshi, T., Shimono, A., Hatakeyama, S., Takegawa, N., Kondo, Y., Schneider, J., Drewnick, F., Borrmann, S., Weimer, S., Demerjian, K., Williams, P., Bower, K., Bahreini, R., Cottrell, L., Griffin, R. J., Rautiainen, J., Sun, J. Y., Zhang, Y. M., and Worsnop, D. R.: Ubiquity and dominance of oxygenated species in organic aerosols in anthropogenically-influenced Northern Hemisphere midlatitudes, Geophys. Res. Lett., 34, L13801, doi:13810.11029/12007GL029979, 2007.

Zhang, Y., Dubey, M. K., Olsen, S. C., Zheng, J., and Zhang, R.: Comparisons of WRF/Chem simulations in Mexico City with ground-based RAMA measurements during the 2006-MILAGRO, Atmos. Chem. Phys., 9, 3777–3798, doi:10.5194/acp-9-3777-2009, 2009.

Zhang, Y., and Dubey, M. K.: Comparisons of WRF/Chem simulated O_3 concentrations in Mexico City with ground-based RAMA measurements during the MILAGRO period, Atmos. Environ., 43, 4622–4631, 2009.

Zheng, J., Zhang, R., Fortner, E. C., Volkamer, R. M., Molina, L., Aiken, A. C., Jimenez, J. L., Gaeggeler, K., Dommen, J., Dusanter, S., Stevens, P. S., and Tie, X.: Measurements of HNO_3 and N_2O_5 using ion drift-chemical ionization mass spectrometry during the MILAGRO/MCMA-2006 campaign, Atmos. Chem. Phys., 8, 6823–6838, doi:10.5194/acp-8-6823-2008, 2008.

RESERVE THIS SPACE

Climate Impacts from Agricultural Emissions: Greenhouse Species and Aerosols

Jeffrey S. Gaffney* and Nancy A. Marley
University of Arkansas at Little Rock
2801 S. University Avenue,
Little Rock, AR 72204-1099
jsgaffney@ualr.edu

Abstract

Climate forcing has become a concern due to the increasing concentrations of a number of well recognized greenhouse gases in the atmosphere, such as carbon dioxide, nitrous oxide, and methane. All three of these well-known greenhouse gases have connections to agriculture, particularly nitrous oxide and methane from rice production. However, these gases are not the only radiatively important species, as tropospheric ozone and aerosols are also important in climate change. Carbonaceous aerosols are increasing in importance, particularly as some inorganic aerosols such as sulfate are being successfully controlled. The impacts of these agriculturally important greenhouse species are overviewed here, and discussed in light of recent work using carbon isotopic measurements to examine the potential impacts of biogenic aerosols on climate. Examples from Mexico City, Chicago and Arkansas are given, which suggest that grass fires and agricultural burning can be significant sources of carbonaceous aerosols. Spectroscopic characterization of these aerosols in the UV-NIR-IR regions has clearly shown that a significantly enhanced absorption, particularly in the UV and IR, can occur from aerosols produced in agricultural and forest burning. The aerosol species responsible for this enhanced absorption has been described as "humic-like" substances (HULIS). The use of natural carbon isotope variations (^{13}C and ^{14}C) along with optical characterizations can be useful in examining the impacts of this type of burning practices, especially for corn and sugar cane (C4-plants). Combustion of agricultural biowaste as a biofuel source instead of uncontrolled field burning is suggested as an alternative to current practices in the U.S.

RESERVE THIS SPACE

Introduction

While the emission of the well-known greenhouse gases such as carbon dioxide, nitrous oxide, and methane are well defined and have been identified as being directly tied to specific agricultural processes, a number of other greenhouse species produced from agricultural activities are not. Ozone, which plays an important role in tropospheric air quality, is also a climate forcing greenhouse gas. Agricultural practices that involve standard field burning to remove unused debris is a major problem in the Southern, Southeast, and Midwestern U.S. and a large source of reactive hydrocarbons and nitrogen oxide which react in the atmosphere to produce elevated ozone levels on regional scales.

Atmospheric aerosols have been identified as a major uncertainty in climate forcing due to their direct and indirect effects on radiative balance. Both scattering and absorption of radiation by aerosols are of concern in determining the impact of the aerosol direct effect. The ability of aerosols to act as cloud condensation nuclei leads to their indirect effect, as the aerosols impact both cloud formation and type. Biogenic carbonaceous aerosol sources have been found to be major contributors to both primary and secondary organic aerosols (SOA) on regional scales. Biogenic SOA are produced from the reaction of reactive biogenic hydrocarbons emitted by both natural and agricultural vegetation with ozone. These SOA biogenic precursors include isoprene, monoterpenes, and sesquiterpenes. Agricultural burning is also a large source of primary carbonaceous aerosols as well as reactive biogenic hydrocarbons which produce SOA.

The direct impacts of the strongly absorbing carbonaceous aerosols on climate will depend on their wavelength dependent optical properties. The degree to which atmospheric aerosols and clouds prevent the transmission of light through the atmosphere is commonly reported as the optical thickness, also known as optical extinction or atmospheric turbidity. The wavelength dependence of atmospheric extinction is traditionally described by Ångstrom's turbidity formula as $\tau = \beta \cdot \lambda^{-\alpha}$, where β, known as the Ångstrom t urbidity coefficient, is the value of τ at a wavelength of 1 μm and α, known as the Ångstrom exponent, represents the wavelength dependence of the optical extinction. The total atmospheric extinction is the sum of scattering, which produces a cooling effect, and absorption, which produces a local warming effect, as $\tau = \beta_s \cdot \lambda^{-\alpha}s + \beta_a \cdot \lambda^{-\alpha}a$, where α_s is the Ångstrom exponent for aerosol scattering and α_a is the Ångstrom exponent for aerosol absorption. The values of the aerosol α_a give a measure of their

wavelength dependent absorption profiles and their ability to cause local heating of the atmosphere. In addition, since the value of α_a is dependent on the chemical composition of the absorbing aerosol, it can serve as an indication of the type of absorbing aerosol present (1).

Past work assumed that the dominant light absorbing aerosol species was carbonaceous soot produced from incomplete combustion of fossil fuel. Carbon soot is a broad band absorber with an absorption strength that decreases monotonically with wavelength ($1/\lambda$) yielding an α_a of 1 (2, 3). Recently, other important light absorbing species have been observed in atmospheric aerosols including the water soluble polycarboxylic acids known as "humic-like" substances, or HULIS (4). Aerosol HULIS can be produced directly from biomass burning (5) or by *atmospheric oxidation of biogenic hydrocarbons (6) and are therefore* biogenic in nature. They can comprise up to 50% of the water soluble organic aerosol species at both urban and rural sites (7). Like the aquatic humic acids they are named for, HULIS contain polycarboxylic acid groups along with other unsaturated sites in an extended conjugation system. This results in intense absorbances below 400 nm (8) which cause the HULIS to be yellow to brown in color, leading to their being referred to as "brown carbon" (5, 9). This enhanced shortwave absorption gives the aerosols containing HULIS α_a values that are greater than 1. Pure HULIS materials isolated from biomass burning aerosols have very high α_a values in the range of 6 – 7 (5). Mixed atmospheric aerosols produced from biomass burning have intermediate values for the α_a values of about 2-3 (5,10).

Atmospheric aerosol α_a values measured in Mexico City were observed to increase in the afternoon over the values measured in the morning *(11). This was attributed to the photochemical formation of highly* absorbing SOA in the afternoon. The α_a values were also observed to increase during periods of biomass burning. Local grass fires resulted in α_a values around 2-3 (12), while aged biomass burning aerosols transported long distances from the Yucatan resulted in α_a values of 1.6 (11). Measurement of aerosol carboxylic acid content by FTIR spectroscopy coupled with carbon isotopic analysis indicated that the enhanced α_a values observed were due to increased HULIS content of the aerosols (13, 14). These results clearly indicate that there is a significant impact from biomass derived carbonaceous aerosol sources even in the large urban area of Mexico City and that these aerosols have absorption profiles that are enhanced in the shortwave region over those derived from fossil fuel combustion. This enhanced shortwave absorption

can lead to local heating of the atmosphere and changes in climate and weather patterns.

Carbon Isotopic Measurements

The measurement of radiocarbon (^{14}C) in atmospheric aerosol samples can give a measure of the amounts of aerosol carbon produced from fossil fuel and non-fossil fuel sources. All biogenic materials are labeled with a relatively constant initial $^{14}C/^{12}C$ ratio (15). Aerosols produced from the combustion of this biogenic material will have the same ^{14}C content as the source material. The aerosols produced from the combustion of fossil fuels contain no ^{14}C because the age of the fuel is much greater than the 5730-year half-life of the ^{14}C. Therefore, the ^{14}C content in atmospheric aerosols, reported as the fraction of modern carbon, provides a direct measure of the relative contributions of carbonaceous materials derived from fossil fuels and that derived from modern biomass sources. The ^{14}C content of atmospheric aerosols determined in samples collected in a number of areas are shown in Table I.

Early measurements made in Barrow, AK (16), Los Angeles (17) and Denver (18) previous to the year 2000 showed a lower modern carbon content than those made later reflecting a higher percentage of fossil fuel derived aerosols during that time (17,18). Later measurements have resulted in larger modern carbon fractions reflecting a lower percentage of fossil-derived carbon in atmospheric aerosols. This is possibly a result of implementing tighter controls on motor vehicle emissions and the growing use of biofuels compounded by little control of open burning in many areas (19).

The high levels of modern carbon reported in Table I for Launceston, Tasmania were attributed to high levels of residential wood burning in the wintertime (20). The high modern carbon levels observed in Nashville (21), Tampa (22), and the park sites of Yosemite, Brigantine National Wildlife Refuge (BNW), Mt. Rainier, Rocky Mountain National Park, and Tonto National Monument (TNM) (23) were attributed to biogenic SOA formation. The very high values for fraction modern carbon (> 1.0) observed in some rural areas may have been due to contributions from the burning of older trees which contained "bomb carbon" from nuclear testing in the 1950s resulting in $^{14}C/^{12}C$ ratios higher than seen in modern biomass.

The fraction of modern carbon measured in the aerosols collected in Mexico City in 2006 was found to be consistently larger than 0.5 (> 50%)

suggesting a large biogenic contribution to the carbonaceous aerosols even in this large urban area (12, 24). Other measurements have also found significant biogenic aerosol sources in this area particularly for the low molecular weight and water soluble fractions of the aerosols (25). The modern carbon aerosol content observed at Tecamac, a suburban, rural site located 18 miles north of Mexico City, was higher than that observed in the city due to impacts from local grass fires. The biogenic impacts in this area were observed to be as high as 90%.

Table I. The fraction of modern carbon in atmospheric aerosols reported for some urban areas.

Location	Year	Modern C		Reference
		Range	Average	
Barrow, AK	1982	0.42-0.46	0.4	16
Long Island, NY	1982	0.37-0.40	0.4	16
Los Angeles, CA	1982	0.20-0.43	0.3	17
Denver, CO	1996-97	0.05-0.69	0.3	18
Nashville, TN	1999	0.56-0.80	0.7	21
Houston, TX	2000	0.27-0.77	0.5	26, 27
Look Rock, TN	2000-01	0.54-0.83	0.7	28
Tampa, FL	2002	0.55-0.95	0.7	22
Zurich,CH	2002	0.60-0.67	0.6	29
Yosemite, CA	2002	0.80-1.05	0.9	30
Tokyo, JP	2002-04	0.31-0.52	0.4	31
Aveiro, PT	2002-04	0.77-0.92	0.8	32
Puy de Dôme, FR	2002-04	0.72-0.87	0.8	32
Schauinsland, DE	2002-04	0.79-0.84	0.8	32
Mexico City, MX	2003	0.56-0.86	0.7	12
Launceston, AU	2003-04	0.96-1.11	0.9	20
Seattle, WA	2004-05	0.38-0.69	0.6	23
BNW, NJ	2004-05	0.30-0.99	0.8	23
Mt. Rainier, WA	2004-05	0.75-1.10	0.9	23
Tokyo, JP	2004-05	0.31-0.54	.0.4	33
Phoenix, AZ	2005-06	0.49-0.75	0.6	23
Rocky Mt NP, CO	2005-2006	0.78-1.11	1.0	23
TNM, AZ	2005-2006	0.64-1.04	0.8	23
Mexico City, MX	2006	0.42-0.75	0.6	12
Tecamac, MX	2006	0.55-0.96	0.8	12

BNW = Brigantine National Wildlife Refuge; TNM = Tonto National Monument

The fraction of modern carbon was determined in the organic carbon (OC) and elemental carbon (EC) aerosol fractions in Mexico City by using thermal fractionation methodologies described previously (16, 34). The results shown in Figure 1 indicate that the EC fraction, which is made up of the high molecular weight soots generated by incomplete combustion, contain less modern carbon than the smaller molecular weight OC fractions while the results for the total aerosol carbon are generally shown to be midway beween the EC and OC values. Similar results have been reported in studies in Okinawa, Japan where the black carbon (BC) aerosol component was found to be 67% modern compared to 94% modern in the OC fraction (35). Overall, the fraction of modern carbon in the EC aerosol component was 0.67 in Mexico City and 0.75 at Tecamac. The corresponding results for the OC component were 0.75 in Mexico city and 0.85 at Tecamac. This is consistent with input from the local grass fire sources at Tecamac and diesel soot being a major source of EC in the Mexico City urban area. In any case, data obtained in Mexico City as well as the many other areas listed in Table 1, suggests that the biogenic contributions to carbonaceous aerosols are becoming significant world wide and their effects on radiative balance will need to be considered.

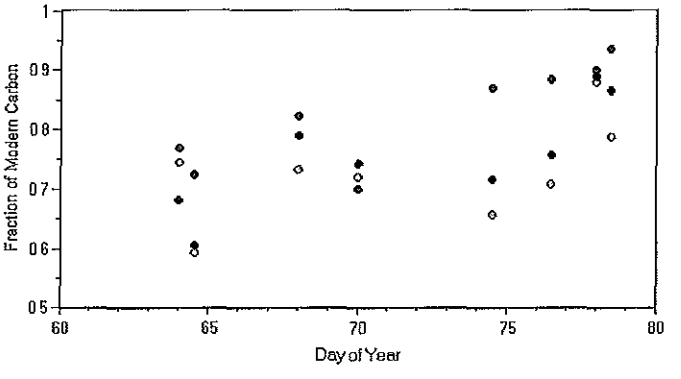

Figure 1. Fraction of modern carbon in organic carbon (red) elemental carbon (green), and total carbon (blue) fractions of aerosol samples collected in Mexico City and Tecamac in 2006.

Organic Reactivity and SOA

It is important to recognize that the volatile organics emitted from both fossil fuel sources and from biogenics have very different reactivities with

OH, nitrate radical and ozone. A comparison of the reactivity for some common organics and natural hydrocarbons with OH is given in Table II. In general, the alkenes are more reactive than the alkanes and aromatic hydrocarbons. This is due to the ability of OH radicals to add to the olefinic double bond. Another trend is that the presence of functional groups that donate electrons to the double bond increases the reactivity. Thus, larger alkenes react faster than smaller ones. Alkanes react with OH by abstraction and those with more secondary and tertiary protons will be more reactive. Therefore, as with the alkenes, larger alkanes will react faster. Oxidized organics are typically less reactive with OH, as in

Table II. Reaction rates of some important volatile hydrocarbons with OH (36).

Hydrocarbon	rate x 10^{12} cm^3 $molecule^{-1}$ s^{-1}
Alkenes	
Ethene	8.5
Propene	26
1-butene	31
1-pentene	31
1-hexene	37
cis-2-butene	56
trans-2-butene	67
2-methyl-2-butene	87
2,3-dimethyl-2-butene	110
2-methylpropene	51
Cyclohexene	68
1,3-butadiene	67
2-methyl-1,3-butadiene (isoprene)	101
Limonene	171
beta-caryophyllene	collisional
Alkanes	
Ethane	0.03
n-Butane	2.5
Cyclohexane	7.4
Others	
Acetylene	0.08
Benzene	1.3

most cases they react by abstraction and are therefore their reactivities are comparable to the small alkanes. The ozone and nitrate radical reactivities for these hydrocarbons also follow the same general trend as the OH reactivities as they are all electrophilic reagents.

Since fossil fuel sources have been identified as "anthropogenic", we have implemented control strategies for the volatile organics emitted from both mobile and stationary sources in order to reduce ozone formation in urban areas. One important control strategy is the use of of catalytic converters for mobile sources. This same reactivity trends listed in discussed above also occur in catalytic oxidation. Thus, in catalytic converters the more reactive alkenes and larger alkanes are most effectively removed yielding emissions primarily composed of the much less reactive hydrocarbons. With time, these measures have led to the reduction of the most reactive anthropogenic volatile organic compounds (VOCs) leading to a reduction in the overall reactivity of the emissions. While the organic reactivity of the emissions from motor vehicles and energy related stationary sources has been reduced, the nitrogen oxide emissions have not been lowered. Thus, the result of this reduction in anthropogenic VOC reactivity has led to a slower production of ozone and a transition from the formation of high ozone levels in urban areas to elevated ozone concentrations on regional scales.

Note in Table II that the biogenic hydrocarbons isoprene, d-limonene and beta-caryophyllene are very, very reactive compared to the anthropogenic hydrocarbons. The biogenic hydrocarbons, isoprene (C5 hemiterpene), the monoterpenes (C10), and especially the sesquiterpenes (C15) have atmospheric lifetimes typically of minutes to hours in urban environments and hours to days in regional areas. The less reactive anthropogenic organic emissions tend to have lifetimes on the order of hours to days in urban environments, and days to months on regional scales (36). Unless they are photochemically reactive, the oxidized organic hydrocarbons have atmospheric lifetimes that are are typically much longer. For comparison, at a OH radical concentration of 1.0×10^6 molecules per cc, typical of an urban environment, the lifetime of ethane is 43 days, ethene is 1.4 days, and cis-2-butene is 5 hours, while the biogenic hydrocarbons have lifetimes of minutes to hours. Indeed, the sesquiterpenes are so reactive with OH and ozone that they are typically very difficult to measure directly in the atmosphere and have to be inferred from measurements of their reaction products.

These very reactive biogenic hydrocarbons are emitted from living vegetation including natural as well as anthropogenically managed

agricultural areas. The estimated total emission rate in the U.S. is 30.7 Mt annually with more than half of these emissions occurring in summer, and approximately half in the Southeast and Southwestern U.S (37). The actual fraction of land used for agricultural purposes in the Midwestern, Southern, and Southeastern U.S. is considerable as compared to land left in the "natural state". While the percentage of cropland in the U.S., excluding Alaska, was approximately 23% in 2002 (38), this fraction approaches or exceeds 40-50% in many portions of the midwest and south.

As we increase controls on the VOC emissions from fossil fuel sources, and the overall hydrocarbon emission reactivity from these sources is lowered, ozone formation rates as well as the SOA formation rates from these sources are lowered. At the same time the nitrogen oxide emissions have not been controlled and the atmospheric levels remain high so that ozone levels are increasing regionally. This has the effect of increasing the ozone reactions with the very reactive biogenic hydrocarbons and increasing the formation rates of the biogenic SOA reaction products. This expected increase in biogenic SOA is a contributing factor to the observed increases in fraction modern carbon observed in carbonaceous aerosols over the years.

Primary Combustion Aerosols

Carbonaceous aerosols from leaf burning and regional agricultural burning practices are a substantial source of carbonaceous aerosols in the Southern U.S., with Arkansas, Louisiana, and Florida contributing more than 75% of all agricultural burning in the southeast (39). In 2004, results from the Moderate Resolution Imaging Spectroradiometer (MODIS) satellite data showed that 73% of all the fire activity in Arkansas was due to agricultural burning with the highest activities occurring in June and October – January (39). As part of an effort to evaluate the aerosol optical properties in this region, a number of instruments have been operated at the Chemistry Department of the University of Arkansas at Little Rock (UALR), Little Rock, AR. These included a 7-wavelength aethalometer to measure aerosol absorption, aerosol α_a, and BC aerosol levels. The instrumentation and methods used have been described previously in detail (11, 12).

Figure 2 shows the BC concentrations measured at UALR from October to December, 2010 compared to measurements made by the same methods at The University of Chicago (U of C) from October to December, 2007. . During this time period the biogenic VOC

emissions would be minimal in both areas decreasing the input from SOA formation. The observed BC would therefore be primarily from fossil fuel or biogenic combustion. The BC levels observed at The U of C were *significantly lower than at UALR by a factor of 2-3. The overall average in* Chicago during this period was 0.4 $\mu g/m^3$ compared to 0.8 $\mu g/m^3$ at UALR and the maximum levels observed were 2.8 $\mu g/m^3$ in Chicago and 7.9 $\mu g/m^3$ in Little Rock. The site The U of C was located in Southside Chicago and highly impacted by diesel truck traffic from the nearby expressways as well as campus traffic, while the site in Little Rock was located on the heavily wooded UALR campus in Southwestern Little Rock and not heavily impacted by local traffic. The only source of biomass combustion in Chicago would be wood burning fireplaces, which are minimal in this area. However, there are no open burning controls in

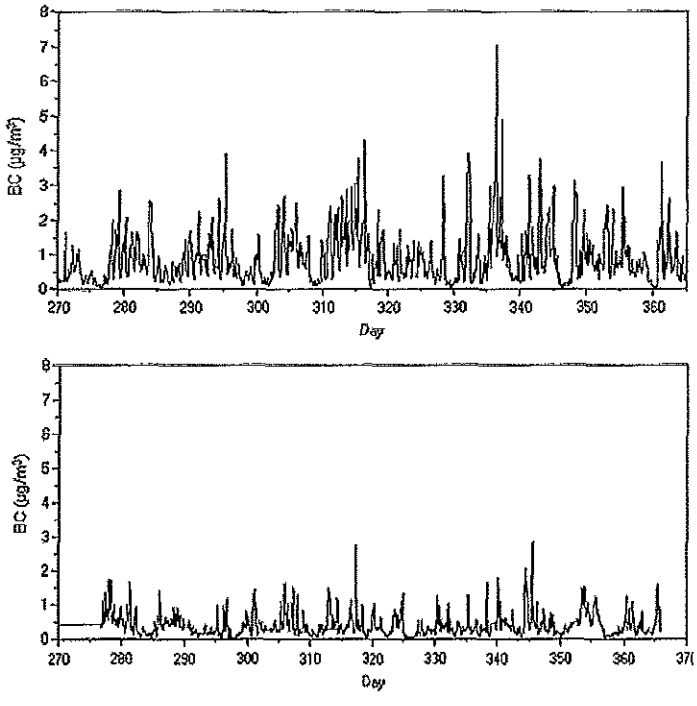

Figure 2. Black carbon (BC) levels measured at the University of Arkansas at Little Rock (top) and at The University of Chicago (bottom) from October to December 2010 (UALR) and 2007 (U of C).

Arkansas and leaf and trash burning as well as agricultural burning are common during this time period. The hgher BC levels observed in Little Rock would therefore indicate a significantly higher level of combustion aerosols in Little Rock compared to the large urban area of Chicago. Note the population of Little Rock is approximately 190,000 as compared to Chicago's population of 2.85 million.

It should also be noted that in addition to the production of high levels of carbonaceous aerosols, these open burning practices common in the Southern U.S. also produce regional ozone from nitrogen oxide and reactive organic emissions released during combustion. Ozone is a regulated atmospheric pollutant and a recognized human health hazard as well as a greenhouse gas. In addition, open burning also produces significant amounts of carbon monoxide and aldehydes. Aldehydes (e.g. formaldehyde, acetaldehyde, acrolein, crotonaldehyde, etc.) are considered air toxics and have immediate high level eye-irritation or lachyrmator potential along with long term carcinogenic exposure potential to downwind populations.

Natural Isotopic Labeling to Assess Agricultural Burning Sources

The natural labeling of vegetation with different ratios of stable carbon isotopes ($^{13}C/^{12}C$) due to their different photochemical pathways can also help to identify the biomass aerosol sources. The C-3 plants, which utilize the Calvin-Benson photosynthetic cycle, have a more selective chemistry and fractionate the heavier carbon isotope (^{13}C) by about 12-14 parts per thousand as compared to the less selective C-4 or Hatch-Slack photosynthetic pathway. The C-3 and C-4 plants will therefore be labeled with different $^{13}C/^{12}C$ ratios. The C-3 plants are most abundant and comprise most tree species, shrubs, and cool temperate grasses and sedges, while the C-4 plants consist mostly of warm temperate to tropical grasses (40). The $^{13}C/^{12}C$ ratios are commonly expressed as $\delta^{13}C$ values in per-mil (‰), and represent the difference between the measured ratios and that of a carbon isotope standard, typically CO_2 prepared from Peedee belemnite carbonate. The measured $^{13}C/^{12}C$ ratios of organic matter are generally ^{13}C-depleted compared to that of the standard and are therefore reported as negative values. These resulting $\delta^{13}C$ values can be used to estimate the relative contributions from C-3 ($\delta^{13}C = -27 \pm 6$) and C-4 ($\delta^{13}C = -13 \pm 4$) plant sources to the carbonaceous aerosols.

Taken together with ^{14}C measurements these determinations can allow for the impacts from specific agricultural burning activities to be

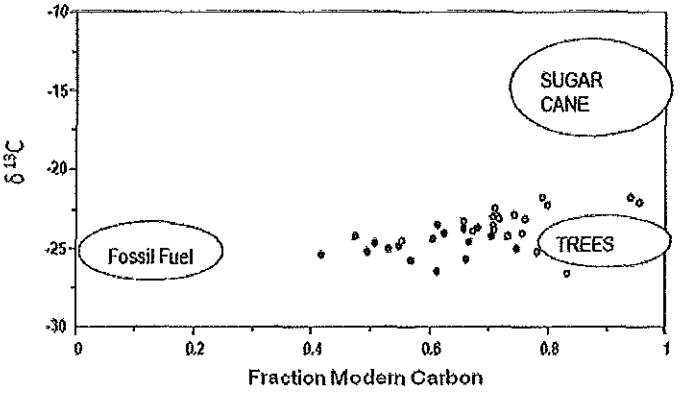

Figure 3. Carbon isotopic ratios of fine aerosols in Mexico City (red) and Tecamac (green) in 2006. Results expected from the combustion of fossil fuel, sugar cane, and trees and grasses are indicated with ovals.

assessed. A comparison of the ^{13}C *ratios with the fraction of modern* carbon is shown in Figure 3 for fine aerosols collected in Mexico City and Tecamac in 2006 (12, 24). The results of -25 ‰ $\delta^{13}C$ and near the 100 % fraction modern carbon observed at Tecamac are indicative of combustion of biomass with both C-3 and C-4 grasses. The results shown for the Mexico City aerosols are typical of fossil fuel combustion mixed with biomass burning aerosols. Mexico City was impacted both by grass fires to the north and widespread forrest fires in the Yuccatan during this period (41, 42). The values expected from carbonaceous aerosols produced from the combustion of different sources are also shown in Figure 3. For instance, the practice of burning sugar cane debris (C4 plant) in the Southern U.S. will lead to the release of carbonaceous soot aerosols and reactive organics enriched in ^{13}C and ^{14}C content (-12 ‰ $\delta^{13}C$ and a 100% fraction modern C). This is contrasted with that expected from the combustion of wood (C3 plant) producing aerosols more depleted in ^{13}C (-25 ‰ $\delta^{13}C$ and 100% fraction modern carbon) and that from fossil fuel combustion yieldin aerosols depleted in both ^{13}C and ^{14}C (-25 ‰ $\delta^{13}C$ and 0% fraction modern). Therefore, measurements of the carbon isotopic content of the fine aerosols produced during a burning event of sugarcane debris from agricultural fields will give isotopic signitures that are distinct from that produced from these other sources, as represented in Figure 3.

The integrated nature of the carbon isotopic measurements also allows for the actual mass fraction of aerosols produced from combustion of different materials to be assessed during these events. Similarly, the use of carbon isotopes can be combined with other tracers of opportunity such as fine potassium or halogen content to assess the impacts from other types of agricultural burn events. These methods have recently been applied to aid in source determination for long range transported aerosols impacting the pacific northwest (43).

Alternative Uses for Biomass

Agricultural field stubble removal by open combustion processes currently in use are not necessarily the best option when considering the potential impacts on regional ozone production from nitrogen oxide and reactive organic emissions as well as the climate impacts from released greenhouse gases and carbonaceous aerosols associated with these burning events. Alternate approaches to disposing of these unused materials should be considered. One option is the potential use of this agricultural debris as a direct biofuel replacement for coal as a cleaner energy source. A simple comparison of the energy content of the different types of agricultural materials and wood debris to coal and oil used for power plant fuels is given in Table III (44).

TABLE III. Energy content in gigajoules per metric tone (GJ/T) of some biomass and fossil fuels.

Carbonaceous Fuel Source	Energy Content (GJ/T)
Biomass	
Dry Wood	18-22
Wet Wood – (20% moisture content)	15
Ag residues – Wet	10-17
Charcoal (from 90-180 GJ original wood content)	30
Ethanol	26.7
Biodiesel	37.8
Fossil	
Gasoline	47.3
Diesel –	42.8
Coal - anthracite	27-30
Coal – bituminous	27
Lignite	15-19

The agricultural (Ag) residues listed in Table III include sugar cane bagasse, rice straw, and wheat and corn stover. It should be noted that the energy content listed for ethanol and biodiesel is for the final product and does not take into account the energy costs to produce the final liquid fuel.

The data shown in Table III indicate the potential energy content in these unused agricultural residues. This is a potentially renewable fuel source which should not be neglected. While the use of this material to produce alcohols, biodiesel, and other liquid fuels is being explored, the direct, controlled, high temperature combustion of dried agricultural carbon residues from crops should be considered where open field burning is common. In this case, controlled combustion of these materials as an alternative to open burning could lead to the reduction of greenhouse species as well as to reduce the agricultural impacts on regional ozone formation while providing an alternative source of energy. This would help to obtain a sustainable energy situation for agriculture.

Organics in Precipitation

Precipitation samples were collected at UALR on the roof-top of the Science Lab Building during 2009 and 2010 using an automated wet-dry sample collector. The total dissolved organic carbon (DOC) was measured in each rain sample using a Shimadzu DOC analyzer. Figure 4 shows the total amount of rain recorded at the site and the DOC in each rain sample after filtration through a 0.45 membrane filter to remove suspended particulates.

The DOC levels were observed to increase beginning in May (day 140) and continue through August (day 245). The average DOC observed during this time period was 4 ppm with a maximum of 8.5 ppm in June. Note that this in peak time for both biogenic emissions and agricultural burning activities (34, 39). Analysis of the rain samples using mass spectrometry found that the water soluble organics present in the samples are less than 500 daltons molecular weight (45). This is also consistant with results found on aerosol HULIS (46). The area near Little Rock is heavily forested with deciduous (isoprene emitting) and coniferous (monoterpene emitting) trees. A comparison of the reaction products of ozone with beta-caryophyllene have found them to be of similar molecular weight. These results suggest that a significant amount of the dissolved organics in the rainfall may be due to low molecular weight oxidation products of biogenic hydrocarbons. However, it should also be noted that the organics produced from open burning will likely be

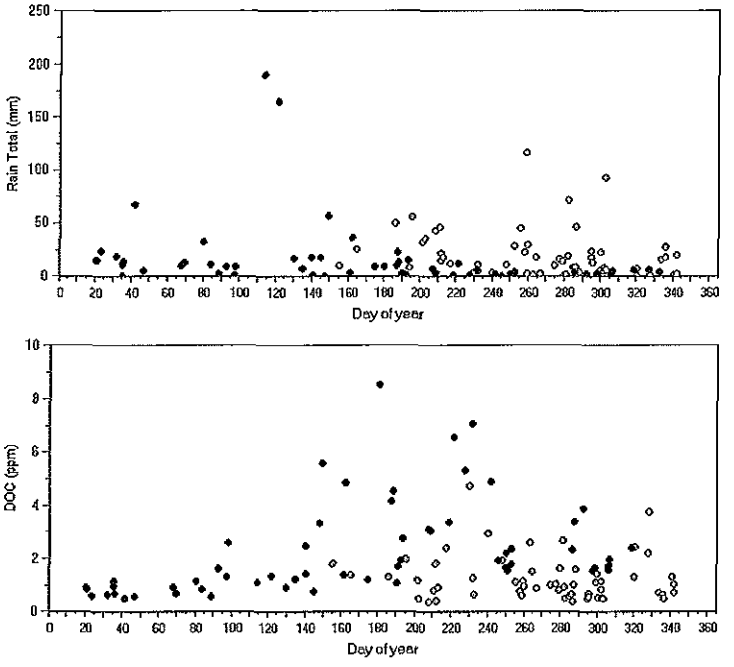

Figure 4. Total amount of rain (mm) and dissolved organic carbon (DOC) concentration in rainwater samples collected at UALR in 2009 (green) and 2010 (blue).

a mix of oxidized compounds that will be of similar structure to those produced from the low temperature atmospheric oxidations by OH *radical and other oxidants in the troposphere.*

There are very few measurements of ^{14}C in DOC in rainwater. However, the few that have been reported in coastal North Carolina have found the DOC to contain 76-96 % modern carbon (47). This is again consistent with a biomass source for the soluble organic compounds in the rainwater. The input of this biogenic DOC from rainwater into surface waters can be important on regional scales. For example, the flux of these oxidized organics into Lake Maumelle, a Little Rock drinking water source, is estimated to be approximately one ton of carbon per average rain event.

The BC concentrations and the aerosol α_a determined from a 7 wavelength aethalometer as described previously (11) are shown in Figure 5 along with total rain amounts measured at the UALR site from August to December 2010. Examination of the data shows that there is significant amounts of carbon that remain in the atmosphere during rain events. However, the aerosol α_a are closer to a value of 1 during and immediately following significant rain events. An α_a of 0.9 to 1.0 is typical for diesel soot, while α_a higher than 1.0 indicate the presence of UV absorbing compounds such as HULIS that are produced from biogenic VOC reactions with OH and ozone or from biomass burning (12). This

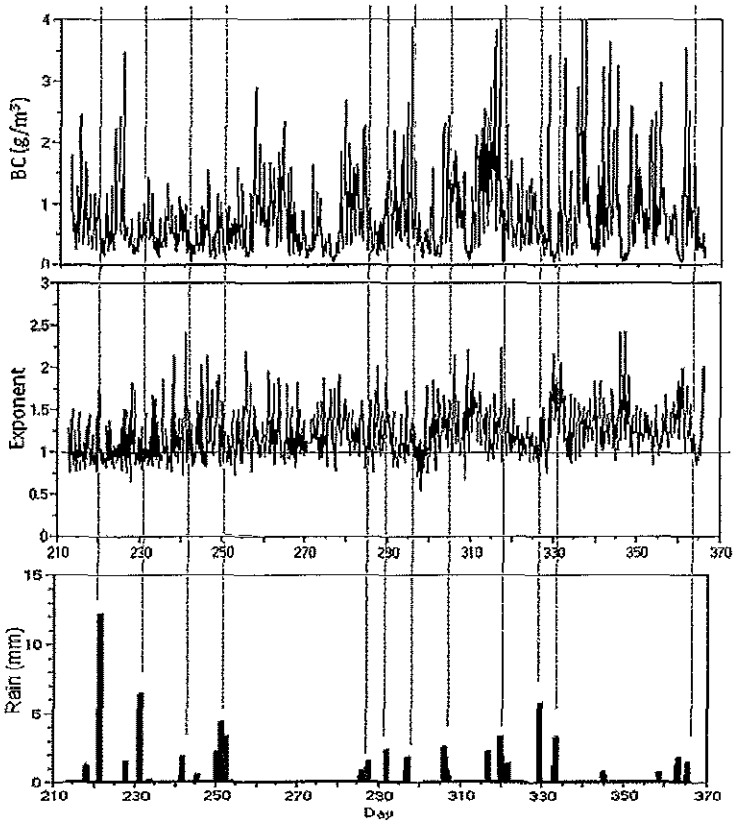

Figure 5. Black carbon concentrations, Ångstrom exponents for aerosol absorption, and total rain amount measured at UALR during August-December, 2010.

indicats that the rain preferentially removes the water soluble aerosol components with enhanced shortwave absorption, typical of HULIS, leaving behind the more hydrophobic BC. It is likely this occurs due to partitioning of semi-volatiles between the surfaces of aerosols and water droplets thus allowing for the removal of the oxidized organics through wet deposition and the observed lowering of the absorption exponents to the base diesel values during rain events.

A significant amount of the carbonaceous aerosols in the submicron region is not removed during the rain events and this will lead to longer lifetimes for these more hydrophobic species. It also indicates that the remaining BC would be transported over much longer distances than the oxidized reaction products which are more readily removed from the atmosphere by wet deposition.

Climate Impacts of Biogenic Aerosols

Measurements of the mass absorption coefficient (B_a) of the atmospheric carbonaceous aerosols in Mexico City have been reported as 10.9±2.1 m^2/g at 660 nm (48). The wavelength dependent absorption profiles from 290 to 600 nm for a diesel soot type BC aerosol with this absorption strength and an α_a value of 1 is shown in Figure 6 compared to the wavelength dependent absorption profile for a mixed fossil fuel + biomass burning type aerosol with an α_a of 1.6, as measured in Mexico City previously (11).

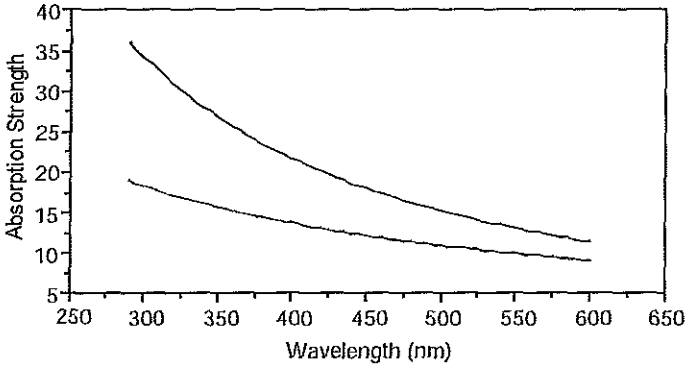

Figure 6. Absorption strengths (m^2/g) for a soot type BC aerosol (green) and a biomass type BC aerosol (blue).

In order to estimate the atmospheric heating potential of the BC aerosols shown in Figure 6, the relative energy absorbed can be calculated from the wavelength dependent solar irradiance at ground level (Figure 7A). Note that the irradiance at ground level is reduced from that anticipated at the top of the atmosphere due to absorption by atmospheric gases. For example, absorption by stratospheric ozone removes a significant amount of short-wave radiation in the 280-300 nm wavelength range preventing it from reaching ground level. It should also be noted that while the number of photons reaching the ground in the UVB and UVA regions is significantly lower than that expected at 550 nm, there is significant energy associated with these photons and thus the ground level irradiance peaks at around 450 nm. The relative amounts of energy absorbed by equal amounts of the two types of BC aerosols in Figure 6 can be obtained by multiplying the solar irradiance (Figure 7A) by the wavelength dependent B_a of the two types of BC aerosols

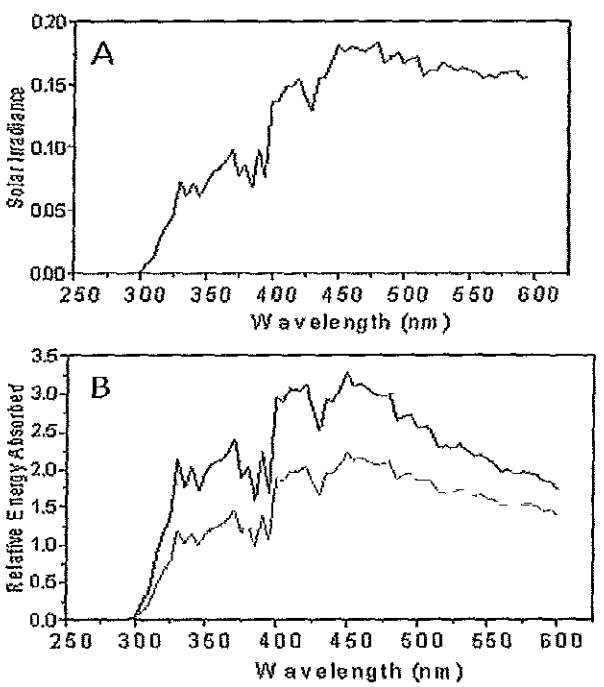

Figure 7. A) Solar irradiance at ground level (W/cm^2-μm). B) relative energy absorbed by a soot type BC aerosol (green) and a biomass type BC aerosol (blue) present in the lower atmosphere.

(Figure 6). The result shown in Figure 7B demonstrates that the biomass type aerosol absorbs approximately 1.5 times more energy than the soot type aerosol at the irradiance peak of 450 nm and 1.7 times more energy in the UVA region (350 nm). An integration of the energy curves from 290 to 600 nm yields a total absorption ratio in the UV-visible region of 1.46 to 1 for the biomass to the diesel soot type aerosols indicating that the biomass type BC would trap 46 % more energy in the lower atmosphere than the same amount of diesel soot type BC aerosols due to their enhanced shortwave absorption. This clearly shows the potential for biomass burning BC aerosols containing HULIS as well as similar oxidized compounds found in biogenic SOA to impact energy absorption in the region of 290-600 nm.

Conclusions

In assessing the impacts of agricultural practices on climate, the current focus is on carbon dioxide as the major greenhouse species, although some attention is now being given to methane and nitrous oxide, particularly in rice production where anaerobic bacterial emissons of these gases can be significant during flooding. However, there is currently significant evidence that agricultural burning practices are leading to the uncontrolled releases of significant levels of nitrogen oxide, reactive organics, and carbonaceous aerosols (both primary and secondary), as well as oxygenates such as aldehydes, on large scales. These emissions need to be controlled as they have significant impacts on climate as well as on regional air quality. The release of nitrogen oxide and reactive organics leads to the production of tropospheric ozone, a regulated air pollutant and greenhouse gas. Carbonaceous aerosols that absorb in the UV – Visible regions, will add to regional heating and changes in local climate and weather. These same organics are water soluble and removed by rainfall events which adds to the organic loadings in surface waters.

In addition, climate change may lead to enhanced production of absorbing carbonaceous aerosols and biogenic SOA produced from the oxidations of isoprene, monoterpenes, and sesquiterpene emissions from deciduous and pine forests. While forest fires and biogenic hydrocarbon emissions are natural processes, they are likely to be impacted indirectly by anthropogenic factors. These include increases in carbon dioxide that act to "fertilize" plant growth and climate warming and precipitation changes that are known to lead to enhanced emissions of biogenic hydrocarbons, as well as earlier springs and longer growing seasons that lead to increases in brush and forest fires. This all serves to

increase production of both primary and secondary biogenic aerosols and in-turn these aerosols have UV and IR absorption that may impact radiation balance on regional scales.

While the current practices of agricultural combustion are continuing particularly in the Southeastern and Midwestern U.S., serious consideration should be placed on developing alternative uses of these wastes. In particular, the potential use of agricultural waste as an alternate fuel for power plant operation should be considered. This would lead to a more sustainable energy source and would be a means of controlling one environmental problem while producing a source of cleaner energy than the combustion of coal.

Acknowledgement

This work was conducted as part of the Department of Energy's Atmospheric Systems Research. This research was supported by the Office of Science (BER), U.S. Department of Energy Grant No. DE-FG02-07ER64329. The authors acknowledge Dr. John Frederick of The University of Chicago for helpful discussion and calculations of UV-Visible absorption. Dr. Tom Guilderson of the Center for Accellerator Mass Spectrometry and Dr. Neil Sturchio of the University of Illinois at Chicago are also thanked for assistance in obtaining carbon isotope data noted in this work. Ms. Gail Bridges is acknowledged for collecting precipitation samples and performing DOC analyses.

References

1. Bergstrom, R. W., Pilewskie, P., Russell, P. B., Redemann, J., Bond, T. ., Quinn, P. K., Sierau, B. *Atmos. Chem. Phys.* **2007,** 7, 5937-5943.
2. Bergstrom, R. W., Russell, P. B., Hignett, P. B. *J. Atmos. Sci.* **2002,** 59, 567-577.
3. Marley, N. A., Gaffney, J. S., Baird, J. C., Blazer, C. A., Drayton, P. J., Frederick, J. E. *Aerosol Sci. Technol.* **2001,** 34, 535-549.
4. Cappiello, A., De Simoni, E., Fiorucci, C., Mangani, F., Palma, P., Trufelli, H., Decesari, S., Facchini, M. C., Fuzzi, S. *Environ. Sci. Technol.* **2003,** 37, 1229-1240.
5. Hoffer, A., Gelencer, A., Guyon, P., Kiss, G., Schmid, O., Frank, G. P., Artaxo, P., Andreae, M. O. *Atmos. Chem. Phys.* **2006,** 6, 3563-3570.
6. Iinuma, Y., Muller, C., Boge, O., Gnauk, T., Herrmann, H. *Atmos. Environ.* **2007,** 41, 5571-5583.

7. Limbeck, A., Kulmala, M., Puxbaum, H. *Geophys. Res. Lett.* **2003,** 30, doi:10.1029/2003GL017738.
8. Gaffney, J. S., Marley, N. A., Clark, S. B. In *Humic and Fulvic Acids, Isolation, Structure, and Environmental Role;* Gaffney, J. S., Marley, N. A., Clark, S. B. Eds.; American Chemical Society, Washington, DC, 1996; Chapter 1.
9. Andreae, M. O., Geleneser, A. *Atmos. Chem. Phys.* **2006,** 6, 3131-3148.
10. Kirchstetter, T.W., Novakov, T., Hobbs, P.V. *J. Geophys. Res.* **2004,** 109, D21208, doi:10.1029/2004JD004999.
11. Marley, N. A., Gaffney, J. S., Castro, T., Salcido, A., Frederick, J. *Atmos. Chem. Phys.* **2009**, 9, 189-206.
12. Marley, N. A., Gaffney, J. S., Tackett, M., Sturchio, N. C., Heraty, L., Martinez, N., Hardy K. D. , Marchany-Rivera, A., Guilderson, T., MacMillan, A., Steelman, K. *Atmos. Chem. Phys.* **2009,** 9, 1537-1549.
13. Marley, N. A., Gaffney, J. S., Kelley, K. L., Sarkar, A., Bridges, G. L. *Eos Trans. AGU Fall Meet. Suppl.* **2009,** 90, A13C-0241.
14. Marley, N. A., Kelley, K. L., Smith, K. J., Sarkar, A., Gaffney' J. S. *Appl. Spectros.***2011,** in preparation.
15. Currie, L. A., Klouda, G. A., Gerlach, R. W. In *Proceedings of the 1981 International Conference on Residential Solid Fuels: Environmental Impacts and Solutions.* Cooper, J. A., Malek, D., Eds., Oregon Graduate Center, Beaverton, OR, **1982**; pp 365-385.
16. Gaffney, J. S., Tanner, R. L., Phillips, M. *Sci. Tot. Environ.* **1984,** 36, 53-60.
17. Hildemann, L. M., Klinedinst, D. B., Klouda, G. A., Currie, L. A., Cass, G. R. *Environ. Sci.Technol.* **1994,** 28, 1565-1576.
18. Klinedinst, D. B., Currie, L. A. *Environ. Sci.Technol.* **1999,** 33, 4146-4154.
19. Gaffney, J. S., Marley, N. A. In *Air Pollution Reviews: Volume 1, Alternate Fuels.* P. Brimblecombe and R. Maynard, Eds., Imperial College Press, London, U.K., **2000,** Chapter 6, pp 195-246.
20. Jordan, T. B., Seen, A. J., Jacobson, G. E., Gras, J. L. *Atmos. Environ.* **2006,** 40, 2575-2582.
21. Lewis, C. W., Klouda, G. A., Ellenson, W. D. *Atmos. Environ.* **2004,** 38, 6053-6061.
22. Lewis, C. W., Stiles, D. C. *Aerosol Sci. Technol.* **2006,** 40, 189-196.
23. Bench, G., Fallon, S., Schichtel, B., Malm, W., McDade, C. *J. Geophys. Res.* **2007,** 112, D10205, doi:10.1029/2006JD007708.
24. Gaffney, J.S., Marley, N.A., Tackett, M., Gunawan, G., Sturchio, N.C.. Heraty, L., Martinez, N., Hardy, K. *Proceedings of the AMS National Meeting, New Orleans.* **2008,** Paper J1.1.

25. Aiken, A. C., de Foy, B., Wiedinmyer, C., DeCarlo, P. F., Ulbrich, I. M., Wehrli, M. N., Szidat, S., Prevot, A. S. H., Noda, J., Wacker, L., Volkamer, R., Fortner, E., Wang, J., Laskin, A., Shutthanandan, V., Zheng, J., Zhang, R., Paredes-Miranda, G., Arnott, W. P., Molina, L. T., Sosa, G., Querol, X., Jimenez, J. L. *Atmos. Chem. Phys.,* **2010**, 10, 5315-5341.
26. Allen, D. Progress Report, Environmental Protection Agency Technology Transfer Network Ambient Monitoring Technology Information Center. **2001,** http://www.epa.gov/ttnamti1/houprog.html.
27. Lemire, K. R., Allen, D. T., Klouda, G. A., Lewis, C.W. *J. Geophys. Res.* **2002,** 107, 4613-4620.
28. Tanner, R. L., Parkhurst, W. J., McNicol, A. P. *Aerosol. Sci. Technol.* **2004,** 38, 133-139.
29. Szidat, S., Jenk, T. M., Gäggeler, H. W., Synal, H. -A., Fisseha, R., Baltensperger, U., Kalberer, M., Samburova, V., Wacker, L., Saurer, M., Schwikowski, M., Hajdas, I. *Radiocarbon* **2004,** 46, 475-484.
30. Bench, G. *Environ. Sci. Technol.* **2004,** 38, 2424-2427.
31. Yamamoto, N., Muramoto, A., Yoshinaga, j., Shibata, K., Endo, M., Endo, O., Hirabayashi, M., Tenabe, K., Goto, S., Yoneda, M., Shibata, Y. *Environ. Sci. Technol.* **2007,** 41, 6357-6362.
32. May, B., Wagenbach, D., Hammer, S., Steier, P., Puxbaum, H., Pio, C. *Tellus* **2009,** 61, 461-472.
33. Takahashi, K., Hirabayashi, M., Tanabe, K , Shibata, Y., Nishikawa, M., Sakamoto, K. *Water Air Soil Poll.* **2007,**185, 305-310.
34. Tanner, R. L., Gaffney, J. S., Phillips, M. F. *Anal. Chem.* **1982,** 54, 1627-1630.
35. Handa, D., Nakajima, H., Arakaki, T., Kumata, H., Shibata, Y., Uchida, M. *Nucl. Instrum. Methods B.* **2010,** 268, 1125-1128.
36. Finlayson-Pitts, B. J., Pitts, J.N. In *Chemistry of the Upper and Lower Atmosphere*; Academic Press, San Francisco, CA; **2000.**
37. Lamb, B., Guenther, A., Gay, D., Westberg, H. *Atmos. Environ.* **1987,** 21, 1695-1705.
38. Lubowski, R.N., Versterby, M., Bucholtz, S., Baez, A., Roberts, M.J. *USDA publication EIB14.* **2002.** http://www.ers.usda.gov/publications/EIB14/eib14a.pdf.
39. McCarty, J. L., Justice, C. O., Korontzi, S. *Remote Sens. Environ.* **2007,** 108, 151-162.
40. Sage, R. F. *Plant Biol.* **2001,** 3, 202-213.
41. Yokelson, R. J., Urbanski, S. P., Atlas, E. L., Toohey, D. W., Alvarado, E. C., Crounse, J. D., Wennberg, P. O., Fisher, M. E., Wold, C. E., Campos, T. L., Adachi, K., Buseck, P. R., Hao, W. M. *Atmos. Chem. Phys.,* **2007,** 7, 5569–5584.

42. Yokelson, R., Crounse, J.D., DeCarlo, P.F., Karl T., Urbanski, S., Atlas, E., Campos, T., Shinozuka, Y., Kapustin, V., Clarke, A. D., Weinheimer, A., Knapp, D. J., Montzka, D. D., Holloway, J., Weibring, P., Flocke, F., Zheng, W., Toohey D., Wennberg, P. O., Wiedinmyer, C., Mauldin, L., Fried, A., Richter, D., Walega, J., Jimenez, J. L., Adachi, K., Buseck, P. R., Hall, S. R., Shetter R. *Atmos. Chem. Phys.* **2009,** 9, 5785-5812.
43. Fischer, E. V., Jaffe, D. A., Marley, N. A. Gaffney, J. S., Marchany-Rivera, A. *J. Geophys. Res.* **2010,** 115, D20209. doi:10.1029/2010JD013943.
44. ORNL, Oak Ridge National Laboratories, *Bioenergy Information Feedstock Network* **2010**, http://bioenergy.ornl.gov/.
45. Marley, N. A., Gaffney, J. S., Kelley, K. L., Sarkar, A., Bridges, G. L. *Eos Trans. AGU, Fall Meet. Suppl.* **2009,** *90*, A13C-0241.
46. Garber, E. R., Rudich, Y. *Atmos. Chem. Phys.* **2006,** 6, 729-753.
47. Avery, G. B, Willey, J. D., Kieber, R. J. *Atmos. Environ.* **2006,** 40, 7539-7544.
48. Subramanian, R., Kok, G. L., Baumgardner, D., Clarke, A., Shinozuka, Y., Campos, T. L., Heizer, C. G., Stephens, B. B., de Foy, B., Voss, P. B., Zaveri, R. A. *Atmos. Chem. Phys.,* **2010**, 10, 219-237.

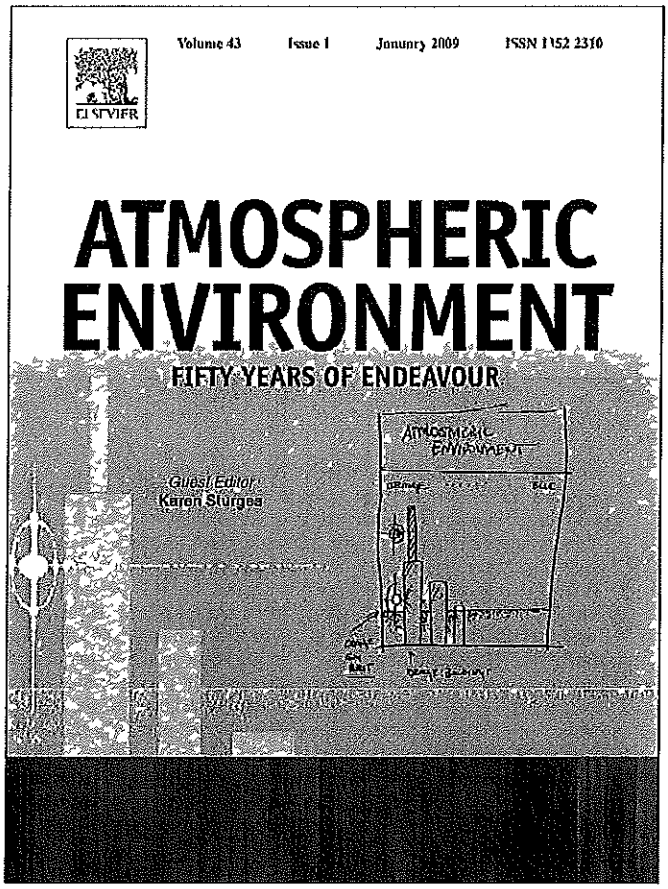

Atmospheric Environment 43 (2009) 23–36

Contents lists available at ScienceDirect

Atmospheric Environment

journal homepage: www.elsevier.com/locate/atmosenv

The impacts of combustion emissions on air quality and climate – From coal to biofuels and beyond

Jeffrey S. Gaffney*, Nancy A. Marley

University of Arkansas at Little Rock, 2801 South University Avenue SCLB 451, Little Rock, AR 72204-1099, United States

Keywords:
Fossil fuels
Emissions
Coal
Petroleum
Biofuels
Biodiesel
Oxyfuels
Combustion products
Natural gas
Liquefied petroleum gas
Nitrogen oxides
VOCs
Sulfur dioxide
Mercury
Natural radioactivity

A B S T R A C T

Combustion processes have inherent characteristics that lead to the release in the environment of both *gaseous and particulate pollutants that have primary and secondary impacts on air quality, human* health, and climate. The emissions from the combustion of fossil fuels and biofuels and their atmospheric impacts are reviewed here with attention given to the emissions of the currently regulated pollutant gasses, primary aerosols, and secondary aerosol precursors as well as the emissions of non-regulated pollutants. Fuels ranging from coal, petroleum, liquefied petroleum gas (LPG), natural gas, as well as the biofuels; ethanol, methanol, methyl tertiary-butyl ether (MTBE), ethyl tertiary-butyl ether (ETBE), and biodiesel, are discussed in terms of the known air quality and climate impacts of the currently regulated pollutants. The potential importance of the non-regulated emissions of both gasses and aerosols in air quality issues and climate is also discussed with principal focus on aldehydes and other oxygenated organics, polycyclic aromatic hydrocarbons (PAHs), and nitrated organics. The connection between air quality and climate change is also addressed with attention given to ozone and aerosols as potentially important greenhouse species.

1. Introduction

Since man first discovered that he could control fire and combust fuels for heat and cooking, he has had to deal with the byproducts of the combustion of organic fuels. These byproducts include the major *combustion products of carbon dioxide (CO_2) and water vapor (H_2O)*, along with a variety of trace gasses and aerosol emissions that have many impacts on air quality, human health, and climate. When man's population levels were at a more or less constant level of a few million for the first two million years of his existence on the planet, and his fuel usage was limited to the combustion of wood in simple campfires, the impacts of the emitted pollutants were limited to the near vicinity of the combustion. Research has found that continual exposure of early man to campfires used as heat sources in enclosed areas contributed to increased incidences of nasal cancer (Zimmerman, 2004). As the human population grew and the combustion of wood and coal became more widespread, the air pollution impacts of combustion emissions were still generally limited to the major cities where the population and combustion levels were concentrated into confined areas.

Air pollution has been recognized for some time as an urban problem. Moses Maimonides, a Jewish leader, philosopher, and physician living in the middle ages in Cairo, Egypt from 1165 to 1204, noted in his writings (Finlayson-Pitts and Pitts, 1986):

> "...Comparing the air of cities to the air of deserts and arid lands is like comparing waters that are befouled and turbid to waters that are fine and pure. In the city, because of the height of its buildings, the narrowness of its streets, and all that pours forth from its inhabitants and their superfluities... the air becomes stagnant, turbid, thick, misty, and foggy... If there is no choice in this matter, for we have grown up in the cities and have become accustomed to them, you should... select from the cities one of open horizons... endeavor at least to dwell at the outskirts of the city..."

His discussion clearly indicates that, in the twelfth century, air pollution was already associated with urban environments and their higher population densities.

During the fourteenth century, coal burning had become such a problem in London, that King Edward I passed a law banning coal burning when the English Parliament was in session (Freese, 2003). This was the first known legislation aimed at reducing human exposures to air pollution. In 1661, John Evelyn Esquire was commissioned by King Charles II to write an assessment of the air

* Corresponding author. Tel.: +1 501 569 8840; fax: +1 501 569 8838.
E-mail address: jsgaffney@ualr.edu (J.S. Gaffney).

1352-2310/$ – see front matter © 2008 Elsevier Ltd. All rights reserved.
doi:10.1016/j.atmosenv.2008.09.016

quality in London due to the combustion of coal (Evelyn, 1661). His comments on the effects of air quality included:

> "...This horrid Smoake which obscures our Church and makes our Palaces look old, which fouls our Cloth and corrupts the Waters, so as the very Rain, and refreshing Dews which fall in the several seasons, precipitate to impure vapour, which, with its black and tenacious quality, spots and contaminates whatever is exposed to it... it is evident to everyone who looks on the yearly Bill of Mortality, that near half the children that are born in London die under two years of age."

He further noted in his work, that children born in a Country Village had an even chance of living 40 years. To combat the pollution problem, Evelyn proposed moving such industries as breweries and lime-burners to locations far outside of London to prevent the soot from settling in the city. In addition to relocating polluting industries, Evelyn also encouraged gardens and orchards to be planted on the city's periphery.

In 1775, English surgeon and physician, Percival Pott observed that young boys employed as chimney sweeps were at risk to develop cancer later in life due to their occupational exposures to chimney soot containing coal tars, ash, and other combustion products (Finlayson-Pitts and Pitts, 1986). This was the first suggestion of the association of "substances" in the environment with the development of cancer in a particular occupational group. These early works indicated the severity of the problem of air pollution in urban centers, even in pre-industrial times.

During the late 1940s and early 1950s, the combustion of high-sulfur coal led to the so-called "killer smogs" in Donora, Pennsylvania and London, England (Finlayson-Pitts and Pitts, 2000). The emissions from coal combustion from industry and domestic heating fires resulted in high levels of sulfur dioxide (SO_2) and atmospheric aerosols or particulate matter (PM). At the same time, meteorological conditions resulted in thermal inversions that served to trap the pollutants in a small air volume near the surface. This led to extremely high concentrations of the pollutants and exposure of inhabitants to very high levels resulting in the deaths of thousands. These fatal events occurred during low-lying foggy periods in which the smoke from coal combustion and fogs combined. The term coined to describe these events was "smog". Until that time, air pollution was viewed as the price of progress. The disasters, however, demonstrated the lethal potential of air pollution and led to the passage of new regulations and legislature that were put in place to restrict the use of dirty fuels in industry and ban uncontrolled emissions of black smoke. This groundbreaking legislation for cleaner urban air included the City of London (Various Powers) Act of 1954 and the United States Clean Air Acts of 1956 and 1968.

A different type of smog was observed for the first time in early 1950s in the Los Angeles air basin in southern California. Farmers began to observe serious damage to some crops, especially to romaine lettuce and parsley in the San Gabriel Valley. Rubber products were found to deteriorate at an accelerated rate. John Middleton, a professor of plant pathology at the University of California first noted that, unlike the London smog, SO_2 was not the cause of the observed damage and that the atmospheric processes occurring involved oxidation not reduction (Middleton et al., 1950; Middleton, 1961). At the same time Arie Haagen-Schmit was able to reproduce the observed plant pathology by exposing plants to the photochemical products of nitrogen dioxide (NO_2) and gasoline exhaust containing hydrocarbons demonstrating that the solar photolysis could produce the oxidant ozone (Haagen-Smit, 1950; Haagen-Smit et al. 1952a, 1952b). Therefore, the Los Angeles smog became known as "photochemical smog" (Stephens, 1987).

With the advent of the industrial revolution, the use of fossil and biomass-derived fuels have led to man's ability to grow his population through the use of enhanced agricultural practices and the rapid transportation of goods. This has led to the development of huge cities and industrial centers worldwide contributing to exponentially increasing population densities, and in turn, an exponential increase in our combustion of carbonaceous fuels to meet an exponentially increasing thirst for energy. In 1800 only 3% of the world's population lived in urban areas. This increased to 47% by the end of the 20th century. This trend has led to the formation of megacities, large urban and suburban centers whose populations exceed ten million inhabitants. These megacities are steadily increasing worldwide with the most rapid growth in the tropical areas of South America and Asia. In 1950 there were 83 cities with populations exceeding one million and New York City was the only megacity (UNEP/WHO, 1992). By 2007 there were 468 urban centers of more than one million and of these 14 are classified as meagacities, with the largest metropolitan complexes centered at Tokyo, Japan, and Mexico City, Mexico (Molina and Molina, 2002). If this trend continues, the world's urban populations will double every 38 years and within the next 10–15 years it is predicted that there will be more than 30 megacities worldwide.

These megacities suffer from high levels of pollution and degraded air quality due to the high demand for energy and the associated combustion in mobile and stationary sources. They are therefore huge sources of air pollutants into the surrounding regional areas. Mexico City is a classic example of a megacity with a population approaching 30 million inhabitants. The mass of air pollution emissions from the Mexico City air basin has been estimated to yield 3,000 metric tons of ozone and 40,000 metric tons of particulate matter less than 2.5 micron (PM-2.5) per day (Gaffney et al., 1999). This corresponds to 1.1 megatons of ozone and 15 megatons of PM-2.5 per year. In addition, the transport of reactive species such as nitrogen oxides (NO_x) and volatile organic hydrocarbons (VOCs) may lead to the substantial formation of ozone and other oxidants in the surrounding regions. Therefore, megacities are very large sources of pollutants that lead to the degradation of air quality and the modification of climate on regional scales.

The present review deals with the emissions from combustion of the various fuels used for energy generation focusing principally on the emissions from fuels used for transportation and electric power generation. These fuels are compared with respect to their impacts on air quality and climate in an attempt to evaluate them in light of what we have learned over the past 50 years. Attention is given to the emissions of the so-called "criteria pollutants" or the currently regulated pollutant gasses, and aerosols. The criteria pollutants are those that have been identified as representing a direct environmental health risk such as carbon monoxide (CO) and ozone or as being strongly connected indirectly to an environmental health risk such as the ozone precursors, NO_x, and the VOCs. For example, because ozone is associated directly with an environmental health risk, it is considered to be a direct pollutant and its precursors are considered to be indirect pollutants. All are criteria pollutants. Although other important pollutants are associated with the combustion of fuels, the criteria pollutants are those that are subject to regulation in the U.S. by the Clean Air Act Amendment of 1990 (CAAA).

The discussions here also include both primary and secondary pollutants. The primary pollutants are those that are produced directly by the combustion process and are emitted into the atmosphere immediately after combustion. The pollutants that are formed in the atmosphere from the reactions of primary pollutants after emission are the secondary pollutants. Future issues are also addressed here especially with respect to the emissions of the pollutants that are not currently included as criteria pollutants and are therefore not regulated at this time. Discussions also include the need for development of alternatives for these carbonaceous fuels in order to avoid the occurrence of further air pollution and climate problems associated with their continued use.

2. Coal

Coal is a fossil fuel formed in swamp ecosystems where plant remains were saved from oxidization and biodegradation by water and mud. During the coal formation process, the deposited plant remains undergo a sequence of physical, biochemical, and chemical changes, which include dehydration, loss of oxygen containing functional groups, alkylation, and oligomerization (Van Krevelen, 1961). This results in coals of increasing rank or geologic maturity depending on the degree of completion of this series of chemical reactions. The general structural characteristics of coal include; fused benzene rings (polycyclic aromatic structures) with associated functional groups linked together by ether, sulfur, or alkyl (CH_2 or CH_2CH_2) bridges (Tillman, 1991). As the coal maturity increases, the degree of aromaticity increases and the number of linkages decreases. The number of methylate (OCH_3), carboxylic (COOH) and hydroxyl (OH) functional groups also decreases while the number of carbonyl groups (C=O) increases and the nitrogen containing functional groups change into more condensed structures (pyridines, quinolines, pyroles, and carbazoles) (Oros and Simoneit, 2000).

Coal rankings with increasing progression of maturity are peat, lignite or brown coal, sub-bituminous, bituminous, anthracite, and graphite. Peat is considered to be a coal precursor and has only limited application as a fuel in some countries such as Ireland and Finland. Lignite is the lowest rank of coal and used almost exclusively as fuel for steam-electric power generation. Sub-bituminous coal has variable properties ranging from those of lignite to those of bituminous coal and is also used primarily as fuel for steam-electric power generation. Bituminous coal is a dense black or brown coal used in steam-electric power generation, heat generation and power applications in manufacturing. Anthracite is a harder glossy black coal used primarily for residential and commercial space heating. Graphite, technically the highest rank of coal, is difficult to ignite and therefore not commonly used as fuel.

Coal used in space heating is usually burned in an open flame under low temperature combustion conditions. When coal is used for electricity generation, it is usually pulverized and then burned in a furnace with a boiler. The furnace heat converts boiler water to steam, which is then used to spin turbines, which turn generators and create electricity. In general, there are three types of coal-fired boiler furnaces used in the electric utility industry. They are referred to as dry-bottom boilers, wet-bottom boilers, and cyclone furnaces. The most common type of coal burning furnace is the dry-bottom boiler.

The combustion temperature determines the molecular alterations and transformations of the organic material within the coal. Under flaming conditions (>300 °C), the alkyl and ether linkages are broken first. This is immediately followed by loss of functional groups, resulting in the release of the non-condensable gasses CO_2, H_2O, SO_2, NO_2, and methane (CH_4). Under smoldering conditions (<300 °C), organic compounds and their altered products are released by a volatilization and steam stripping effect. The extent of this process is dependent on the coal moisture content, which is higher for less mature coals (Oros and Simoneit, 2000).

The non-combustible components of coal remain behind as bottom ash. The physical properties of bottom ash are similar to those of natural sand with particle sizes ranging from fine gravel to fine sand with low percentages of silt and clay-sized particles. When pulverized coal is combusted in either a dry-bottom boiler or a cyclone furnace, about 80% of all the ash leaves the furnace as fly ash, entrained in the flue gas. In a wet-bottom furnace, 50% of the ash formed leaves the furnace as fly ash (McKerall et al., 1982). Electrostatic precipitators are used for particulate control to remove the fly ash from the flue gasses. Although these systems have efficiency rates of nearly 99.9%, considerable amounts of fly ash are still emitted to the atmosphere due to the large amounts of coal required for electric power generation. A 1000 MW power station with a normal consumption of 12,000 tons per day (t d^{-1}) of sub-bituminous coal, has a mean combustion fly ash production of about 2,400 (t d^{-1}). Even with a particulate removal efficiency of 99.9%, almost 900 tons per year (t yr^{-1}) are emitted to the atmosphere as primary PM (Querol et al., 1998). In 1997, approximately 165,000 tons of PM-2.5 were emitted from the combustion of coal for electric power generation (Nizich and Pope, 1998).

The PM that escapes the electrostatic precipitators is primarily in the reparable range of 0.8–2 micron (Linak et al., 2000a). Since these particles are very small they have long atmospheric residence times and can therefore travel long distances because the diffusional and depositional loss mechanisms are at a minimum in this size range (Finlayson-Pitts and Pitts, 1986). The FLAME (Fly-Ash and Metals in Europe) project, undertaken to determine the sources and special distribution of fly ash pollution throughout Europe, determined that a large portion of the fly ash deposition to lakes was attributed to long-range transport (Alliksaar and Punning, 1998; Rose et al., 1998). This aerosol size range is also very effective in scattering solar radiation and therefore impacts both visibility and climate.

The composition of fly ash is determined by the composition of the coal burned. The normal composition of fly ash from the combustion of various ranks of coal is given in Table 1 (Meyers et al., 1976; McKerall et al., 1982). The principal components of bituminous coal fly ash are silica, alumina, iron oxide, and calcium, with varying amounts of carbon. Lignite and sub-bituminous coal fly ashes contain higher concentrations of calcium and magnesium oxides and reduced percentages of silica and iron oxide, as well as lower carbon content, compared with bituminous coal fly ash. Lignite and sub-bituminous coal fly ashes may have a higher concentration of sulfate compounds than bituminous coal fly ashes. Since very little anthracite coal is used in utility boilers there is little data on anthracite coal fly ash.

In addition to the major constituents listed in Table 1, fly ash also contains a number of potentially toxic trace materials. These can include heavy metals and radionuclides. The transition metals are of particular importance due to results that show cardiopulmonary damage associated with the inhalation of these elements (Dreher et al., 1996). In addition, the elemental speciation may influence this toxicity as some species are significantly more water-soluble and therefore more bioavailable than others (Dreher et al., 1997). Some of the important trace species in fly ash generated from the combustion of three different coals are listed in Table 2 (Linak et al., 2000a). These include the water-soluble transition metals copper, iron, nickel, vanadium, and zinc and the toxic metals lead and cadmium. The contribution of coal combustion to the total atmospheric lead emissions is conservatively estimated at 6% (Block and Dams, 2004).

Fly ash also contains increased concentrations of some natural radionuclides (UNSCEAR, 1982) as indicated by the total gamma radioactivities listed in Table 2, which range from 218 to 293 mBq g^{-1}

Table 1
Chemical composition of fly ash from coal combustion expressed as a percentage by weight (Meyers et al., 1976; McKerall et al., 1982).

Component	Bituminous	Sub-bituminous	Lignite
SiO_2	20–60	40–60	15–45
Al_2O_3	5–35	20–30	10–25
Fe_2O_3	10–40	4–10	4–15
CaO	1–12	5–30	15–40
MgO	0–5	1–6	3–10
SO_3	0–4	0–2	0–10
Na_2O	0–4	0–2	0–6
K_2O	0–3	0–4	0–4

Table 2
Trace element concentrations in fly ash particulate matter (PM) from the combustion of Western Kentucky bituminous, Montana sub-bituminous, and Utah bituminous coals (Linak et al., 2000a, 2000b; Furr et al., 1977).

Trace element	Concentration (μg/g)		
	Western Kentucky	Montana	Utah
Arsenic	200	108	149
Cadmium	12	<1	<1
Chromium	240	38	189
Copper	126	152	147
Lead	51	142	52
Nickel	196	70	148
Vanadium	686	196	418
Zinc	813	173	184
Unburned Carbon (%)	20	1	23
Radioactivity (mBq/g)	243	218	293

of fly ash (Furr et al., 1977). The enrichment factors for the radionuclides in fly ash vary from a factor of 31 for the most volatile nuclides such as polonium-210 and lead-210 to a factor of 2 for radium-228 (Weng and Chu, 1992). The activity concentrations of radionuclides in fly ash from a coal-fired power plant in Kentucky burning high-sulfur and low-sulfur coals are listed in Table 3 (Zielinski and Budahn, 1998). The more volatile lead-210 appears in the highest concentration and is nearly a factor of two higher in the high-sulfur fuel. This enrichment of the radionuclides can result in an elevation of background levels of radioactivity by as much as 20% (Greiner et al., 1983). Therefore, it has been hypothesized that fly ash may be a likely candidate for the toxic fine particulates that play a significant role in the demonstrated association of adverse health effects with atmospheric fine PM (Linak et al., 2000a).

Coal-fired power plants are also major sources of the primary pollutants SO_2 and NO_x. The production of SO_2 occurs from the direct oxidation of sulfur contained in the fuel and is therefore dependent on the sulfur content of the coal. There are two major mechanisms of NO_x production. It can be formed directly from oxidation of nitrogen contained in the coal (fuel NO_x) and from the thermal oxidation of diatomic nitrogen in air (thermal NO_x). In coal combustion, fuel NO_x is the major source, contributing as much as 80% to the total NO_x emissions. Coal-fired power plants are the largest source of SO_2 emissions in the United States, contributing approximately 60% to the total SO_2 burden. They are second only to motor vehicles in emissions of NO_x accounting for 18% of the total U.S. emissions (US-EPA, 2003).

In addition to primary fly ash PM, gas to particle conversion gives rise to considerable amounts of acidic secondary PM from the atmospheric oxidation of SO_2 and NO_2 emissions. Conversion ratios of SO_2 to sulfuric acid in power plant plumes may reach up to 40% at conversion rates of 1–6% per hour (Hidey, 1994) while conversion rates of NO_2 to nitric acid are in the range of 3–6% per hour depending on atmospheric conditions (Lin and Cheng, 2007). Therefore, power plants with high SO_2 and/or NO_2 emissions result in the formation of secondary PM several orders of magnitude higher than the emissions of the primary fly ash PM (Hidey, 1994; Gillani et al., 1981). Moreover, since these secondary particles are very small (<1 micron) they have long atmospheric residence times and can travel long distances (Finlayson-Pitts and Pitts, 1986). This aerosol size range is also very effective in scattering solar radiation and can impact both visibility and climate. Highly scattering aerosols, such as sulfates and nitrates, have been shown to have an overall effect of cooling in the lower atmosphere by scattering the incoming solar radiation (Charlson and Wigley, 1994). The cooling effect from anthropogenic sulfate aerosols in the Northern Hemisphere has been estimated to be comparable in magnitude to the atmospheric warming produced from increases in the major greenhouse gas, CO_2 (Kiel and Briegleb, 1993). In addition, the presence of more numerous hygroscopic aerosol particles in the atmosphere increases the lifetime of clouds by competing for the available water vapor resulting in more numerous but smaller cloud droplets (Twomey, 1977, 1991). This has the overall effects of regional cooling due to scattering of solar radiation by the longer-lived clouds and diminished rainfall from these clouds. Upon deposition, these secondary acidic aerosols generated from coal combustion are also the principal cause of acid rain, which alters the acidity of lakes and streams and promotes deterioration of buildings and construction materials.

Another toxic emission from coal-fired power plants that has received much attention lately is mercury. Currently, mercury is a non-regulated air pollutant and coal-fired power plants are not required to reduce their emissions of this toxic metal. In 1999 the emissions of mercury from coal-fired power plants were estimated to be 49 t yr^{-1}, which accounted for 42% of the total U.S. emissions inventory (US-EPA, 1999a). In addition, mercury emissions are expected to increase based on projections of increased energy production and increased coal usage. Mercury is emitted from power plants in one of three forms, vapor phase elemental mercury, vapor phase oxidized mercury, or adsorbed onto particulate surfaces (UNEP/Chemicals, 2002). Each of these three forms has a different atmospheric fate. While elemental mercury can be transported over long distances with residence times of a few months up to one year, oxidized mercury and particle bound mercury have much shorter lifetimes with removal by wet or dry deposition within a few days (US-EPA, 1999b). Due to the potential for long-range transport of elemental mercury, it has been estimated that up to 20–80% of all mercury deposited in the U.S. comes from non-U.S. sources with the highest non-U.S. input occurring west of Minnesota (Levin, 2002).

In addition to the air toxics, electric power plants account for over 40% of total U.S. CO_2 emissions, the major contributor to global warming (US-DOE, 2000). Coal has the highest carbon content of all fossil fuels and therefore has the highest output rate of CO_2 per kilowatt hour (kwh) generating 2.1 lbs CO_2 per kwh resulting in the release of 1.8×10^9 metric tons of CO_2 in 1998. Along with the CO_2 emissions, coal-fired power plants are also major sources of CH_4 and nitrous oxide (N_2O), also greenhouse gasses.

Table 3
Activity concentrations (mBq/g) of radionuclides in fly ash from a Kentucky coal-fired power plant burning high-sulfur and low-sulfur coals (Zielinski and Budahn, 1998).

Radionuclide	High sulfur	Low sulfur
Uranium-238	181	161
Radium-226	189	143
Lead-210	315	178
Radium-228	76	125

3. Fuel oil

Approximately 40% of the world electricity production uses coal. A much smaller fraction uses residual fuel oil. Only 3% of the U.S. electricity is generated by fuel oil-fired power plants and residual fuel oils are used in significant quantities in only selected regions of the U.S., primarily in the northeast and southeast (Linak et al., 2000a; US-DOE, 2007). In 1997, 35,000 tons of primary PM-2.5 were emitted from plants using residual fuel oils, in comparison with 165,000 tons from coal combustion (Nizich and Pope, 1998).

There are two major types of fuel oil burned by combustion sources; distillate oils and residual oils. These fuel types are further distinguished by grade number. Numbers 1 and 2 are distillate oils and Numbers 5 and 6 are residual oils. Number 4 is often a mixture

of distillate and residual oils. Number 6 fuel oil is sometimes referred to as Bunker C (Smith, 1962). Distillate oils are more volatile and less viscous than residual oils. They have negligible nitrogen and ash content and usually contain less than 0.3% sulfur. Distillate oils are most often used in domestic applications and include kerosene and diesel fuels. The heavier residual oils are produced from the residue remaining after the lighter fractions have been removed from the crude oil by distillation. They contain significant amounts of ash, nitrogen, and sulfur (Danielson, 1973). Residual oils are used mainly in utility, industrial and large commercial applications. The major boiler designs for fuel oil combustion are water-tube, fire-tube, cast iron, and tubeless. The tube designs are relatively small and are most often used primarily in residential and small industrial applications, while the tubeless designs are most often used for power generation (US-EPA, 1982).

The primary PM emissions from residual oil combustion are related to sulfur content of the fuel. The low-sulfur fuel exhibits substantially lower viscosity, reduced asphaltine content, lower ash as well as lower sulfur content. This results in better atomization of the fuel and more complete combustion (Sigmund, 1969). Table 4 shows the composition of PM from combustion of high-sulfur Number 6 fuel oil in a fire-tube boiler and a tubeless combustor (Linak et al., 2000a). The high metal content of the particulates from the high temperature combustor arises from vaporization of the metals under the high combustion temperatures followed by nucleation, coagulation and condensation onto existing particles (Linak et al., 2000b). The extent of metal vaporization is dependent on the extent of carbon combustion. For cases of incomplete combustion, a substantial fraction of metals remain trapped in the unburned carbon particles, and never reach the vapor phase. The PM formed in the lower temperature fire-tube boiler shown in Table 4 was reported to consist of a significant amount of large porous carbonaceous material indicating a substantial amount of incomplete combustion (Linak et al., 2000a). Particulate matter formed in the tubeless combustor was about half that formed in the fire-tube boiler and contained very few large particles. These small particles consisted primarily of trace species that contained copper, iron, nickel, vanadium, and zinc, along with 3.2% sulfur as sulfate.

Since the majority of the residual fuel oil used today is of high-sulfur content, oil-fired power plants have high SO_2 emissions. The residual fuel oils contain approximately 2–5 % by weight of sulfur whereas coal contains from 0.5 to 5% (Linak et al., 2000a; Sawyer et al., 2000). Due to their small numbers, the total SO_2 emissions from oil-fired power plants are less than 20% of those produced by the coal-fired plants (Hauser, 1986). Oil-fired power plants are also large sources of CO_2. Nearly all the fuel carbon (99%) is converted directly to CO_2 during the combustion process. The fuel carbon not converted to CO_2 is emitted as primary carbonaceous PM as a result of incomplete combustion. However, due to their small numbers, oil-fired plants are responsible for only 5% of the total U.S. CO_2 emitted by the electric utility sector.

Another major user of fuel oil is aircraft. About 9% of the fuel used by mobile sources in the U.S. goes to jet aircraft (Sawyer et al., 2000). Some regions have a higher consumption than others. In California, 17% of the mobile fuel use goes to aircraft. Jet fuel is a kerosene grade distillate fuel and therefore has very low-sulfur content and does not generate significant SO_2 emissions. However, jet engines are high NO_x emitters, especially during take-off when emissions range from 30 to 45 g NO_x per kg of fuel, which is 10–20 times that of an automobile (Baughcum, 1996). However, normal cruise emissions are a factor of 10 lower and the emissions of NO_x in North America from jet aircraft are estimated to be less than 1% of the total NO_x emissions (Sawyer et al., 2000).

Large ocean-going vessels, including cargo and container ships, cruise ships, and oil tankers can utilize either diesel or bunker fuels. However, since there are no emission controls on marine transport, they usually choose the less expensive, high sulfur, Number 6 residual oil. Therefore, as with the oil-fired power plants, they have high SO_2 emissions and are the only important mobile source of SO_2. It has been estimated that large ships generate 16% of the global sulfur emissions (Corbett and Fischbeck, 1997). The SO_2 emissions from ships are responsible for 54% of the total sulfate aerosol column burden over the Mediterranean (Marmer et al., 2007). They are also high NO_x emitters, with about 70 g of NO_x produced per kg of fuel burned.

Commercial shipping vessels are also large sources of carbonaceous particulate matter, or black carbon (BC) from incomplete combustion of the residual fuel. It has been estimated from fuel consumption data that the global contribution of carbonaceous aerosols from shipping is 133 Gg yr^{-1} or about 1.7% of the total global emissions (Lack et al., 2007). Like the sulfate aerosols, the BC particles are in the size range that has the longest atmospheric lifetimes and can therefore travel long distances from the emission source. Carbonaceous soot particles are also in a size range that efficiently scatters incoming solar radiation. However, unlike the sulfate aerosols, they are also strong absorbers of incoming solar radiation. While sulfate aerosols are the dominant light scattering species, BC is the dominant light-absorbing aerosol in the atmosphere with a broadband absorption profile and a $1/\lambda$ dependence over the entire spectral region from UV to the near IR (Marley et al., 2001). Atmospheric aerosols containing BC can absorb as much as 20–25% of the incoming solar radiation leading to heating of the particles and local warming of the boundary layer (Hermann and Hanel, 1997).

Much of the overall impacts of the emissions from shipping are due to the fact that they occur over the open oceans, where there are no other sources of pollutants. It has been estimated that if the arctic shipping lanes should become open for longer periods due to global warming and melting of the sea ice, the increased emissions of these light-absorbing aerosols would significantly add to warming in the arctic (Lack et al., 2007).

Table 4
Trace element concentrations in particulate matter (PM) from the combustion of high-sulfur Number 6 fuel oil in a fire-tube burner and a refractory lined combustor (Linak et al., 2000a, 2000b).

Trace element	Concentration (μg/g)	
	Fire-tube burner	Refractory lined combustor
Total PM (mg m^{-3})	184	93
PM-2.5 (%)	39.5	1
Arsenic	45	
Cadmium	21	
Chromium	101	
Copper	1272	2346
Iron	6150	13,993
Lead	1084	
Magnesium	8410	19989
Manganese	116	
Nickel	10,290	16,518
Vanadium	78,800	13,5718
Zinc	23,740	34,245

4. Gasoline

Considerable attention has been given to the impact of motor vehicle fuels on air quality specifically as it relates to the criteria pollutants. The primary criteria pollutants that are currently regulated as direct health-related hazards are CO and lead. Lead is added to gasoline as an octane enhancer and is emitted from the tailpipe as inorganic lead halides (>90%) and to a lesser extent organolead compounds (Finlayson-Pitts and Pitts, 1986). Lead was banned as gasoline additive for on-road vehicles in the United

States in 1996 due to its extreme toxicity, particularly in children. However, it is still allowed for off-road uses including aircraft, racing cars, farm equipment and marine engines. With the mandated use of unleaded fuels in on-road vehicles, the levels of airborne lead particulate matter have been lowered drastically in the United States. However, leaded fuels are still in use in other areas of the world and can be a substantial health problem. With the removal of lead from gasoline, other additives have been used to enhance octane, such as aromatics or branched alkylated compounds, and these may lead to other atmospheric problems especially in vehicles without catalytic converters.

Carbon monoxide is of concern because it is a direct toxin. It acts efficiently to bind with hemoglobin in the blood, forming a very stable and irreversible carboxyhemoglobin complex. In this manner CO prevents the hemoglobin from functioning in its normal oxygen-binding capacity. At levels of low parts per million (ppm), CO exposure can lead to stress for many individuals who suffer from respiratory or coronary dysfunctions. The addition of catalytic converters to automobiles has reduced substantially the emissions of CO from the combustion of conventional gasoline and diesel fuels. However, CO emissions during the "cold start" of engines, when the catalyst is cold and has not reached operating temperature, can still be substantial, even for those vehicles that are equipped with catalytic converters.

The indirect primary pollutants that are regulated include the VOCs and NO_x. In contrast to coal combustion, NO_x is produced in gasoline combustion primarily as thermal NO_x, which is generally emitted as NO, with smaller amounts of NO_2 and other nitrogen oxide species. The VOCs are emitted directly from the tailpipe from incomplete combustion. They are also emitted to the atmosphere from loss of unburned fuel. This loss of unburned fuel can occur through (1) spillage during fueling; (2) diurnal evaporative losses (occurring as the fuel tank is heated during the day, followed by cooling at night, resulting in "breathing" of air and trapped hydrocarbons); (3) hot soak evaporative losses (occurring when the engine is shut off and residual heat is transferred to the fuel system); and (4) running evaporative losses (Calvert et al., 1993). The evaporative losses can be high at high ambient temperatures or for vehicles that run abnormally hot.

The NO_x and VOC emissions react in the presence of sunlight by way of a series of photochemical reactions involving hydroxyl-, peroxy-, and alkoxy radicals, to form the secondary pollutant ozone (Finlayson-Pitts and Pitts, 2000). Therefore, the emissions of NO_x and total VOCs are currently regulated in vehicle exhaust in order to control the formation of ozone in the atmosphere. However, the atmospheric reactivities of the VOCs vary dramatically. The VOCs emitted from gasoline-fueled vehicles arise from uncombusted or partially combusted fuel and typically include cyclohexane, octanes, and aromatics. The most reactive VOCs are the very reactive olefins and the natural hydrocarbons, isoprene and alpha-pinene. Estimations are made of the ozone formation potential for the VOCs in an urban environment by studying the organic compounds in smog-chamber systems under varying concentrations of VOCs and NO_x, followed by using chemical modeling to predict the amount of ozone formed. The ozone-forming potentials of different hydrocarbons have been calculated as reactivity adjustment factors by using the maximum incremental reactivity (MIR) scale developed by Carter (Carter and Atkinson, 1989; Carter, 1994). These so-called ozone production factors are usually referred to in units of grams of ozone per gram of non-methane hydrocarbon emitted into the atmosphere.

Of course, ozone is not the only oxidant formed from the reactions of NO_2 and the VOCs in the atmosphere. Other atmospheric oxidants are also formed such as hydrogen peroxide (H_2O_2), which can react with SO_2 to form sulfuric acid aerosol, aldehydes, organic acids, nitric acid, and the peroxyacyl nitrates (PANs). Although not currently regulated, these secondary pollutants are of concern because of their potential roles in acidic deposition, as plant toxins, and as health hazards in their own right. The PANs are particularly interesting because they are known to be potent phytotoxins and eye irritants. They are produced directly from the reaction of peroxyacyl radicals with NO_2, both of which are in equilibrium with the PANs (Gaffney et al., 1989).

$$RC(=O)-OO + NO_2 \rightarrow RC(=O)-OO-NO_2 \quad (1)$$

The most prevalent of the PANs is the methyl derivative, peroxyacetyl nitrate (PAN). This secondary pollutant is produced along with ozone in the process of urban photochemical smog formation.

A number of air toxics are also emitted as primary pollutants from gasoline combustion. Air toxics are those compounds that are of concern at low levels primarily because of their potential carcinogenic properties. The air toxics that have been targeted by the CAAA of 1990 are benzene, 1,3-butadiene, formaldehyde, acetaldehyde, and polycyclic organic matter (POM) (Health Effects Institute, 1996). Benzene dominates the total emissions (65%–80%) of air toxics in the current fleet of gasoline-fueled vehicles (Gorse et al., 1991). Benzene is also the only mobile source air toxic thus far classified as a known human carcinogen by the United States Environmental Protection Agency (US-EPA) because of its ability to cause leukemia in humans at relatively high exposure levels (US-EPA, 1994). The US-EPA has added that benzene may produce developmental effects at exposure levels as low as 1 ppm. In response to this, the US-EPA has adopted new limits on benzene emissions, to take effect between 2009 and 2011, that would reduce toxic emissions of benzene and other pollutants from passenger vehicles by up to 80 percent in the next two decades.

Light duty cars and trucks are responsible for 10% of the CO_2 emissions globally. The U.S. alone is responsible for 45% of this total (IEA, 2005). This amounted to 314 million metric tons of CO_2 or 5.3 lbs per gallon of fuel burned in 2004. Small cars (compacts, subcompacts and 2-seaters) were responsible for 25% of the total emissions, followed by SUVs at 21% (DeCicco and Fung, 2006). Since 1970, the U.S. has achieved a 60% reduction in primary emissions of the criteria pollutants due to catalyst based emission controls (US-EPA, 2005). However, in that same time, the emissions of CO_2 from automobiles have increased by 70% (FHWA, 2006). The only way to reduce the CO_2 emissions from gasoline combustion is to decrease the fuel use rate by either increasing fuel economy or decreasing the number of miles driven through the use of car-pooling or public transportation. In addition to the primary CO_2 emissions, CO and NO_x can also act to trap heat in the atmosphere and are therefore greenhouse species. Many of the secondary pollutants generated by the photochemical oxidation of gasoline emissions, including ozone and PAN are also greenhouse gasses.

5. Diesel fuel

Diesel fuel is a distillate oil and as such usually contains <0.3% sulfur by weight. The combustion of diesel fuel is therefore not a significant source of atmospheric SO_2 (Smith, 1962). However, diesel engines are a major source of NO_x. Tunnel studies have estimated that diesel engines produce five times the amount of NO_x per mass of fuel burned when compared to gasoline vehicles (Kirchstetter et al., 1998). Although heavy-duty diesel trucks make up only 1% of all on-road vehicles in California, motor vehicle emission inventory indicates that are responsible for 21% of the NO_x emissions from on-road vehicles statewide (CARB, 1996). The same emission inventory estimates that heavy-duty diesel trucks were responsible for 75% of the exhaust PM from on-road vehicles. These estimates do not include off-road diesel engines, which can also be a major source of PM (Sawyer et al., 2000).

In general, diesel engines produce more carbonaceous particulate matter than spark-ignition engines. This is due to the way the fuel is injected and ignited in the diesel engine. The fuel is injected later in the compression cycle than in gasoline engines and ignited spontaneously from pressure. Consequently, the air and fuel do not have a chance to mix thoroughly before ignition. The presence of fuel dense pockets in the mixture results in incomplete combustion of the fuel and the production of carbon soot or BC particulate matter. The amount and chemical composition of diesel particulate matter depends on the operational parameters, such as speed, motor load, engine and vehicle type, tuning and age of the engine, fuel composition, ambient air temperature, and relative humidity (Sjogren et al., 1996; Lloyd and Cackette, 2001). The typical composition of diesel particulate matter obtained from a medium-duty diesel truck in a dynamometer study was 30.8% elemental carbon, 19.7% organic carbon, 1% sulfur, 0.7% aluminum, 0.2% nitrate, and 0.96% other metals (in order of concentration; silicon, aluminum, zinc, cadmium, indium, and lead) (Schauer et al., 1998).

Diesel exhaust contains hundreds of gas-phase, semi-volatile, and particle phase organic compounds. Small carbonyls, including acetaldehyde, formaldehyde, and acetone, make up the largest fraction, accounting for more than half of the organic emissions (Schauer et al., 1998). Also included in diesel exhaust are air toxics such as POM compounds, which are defined by the CAAA as a class of organic compounds having more than one benzene ring and a boiling point of 100 °C or higher. This includes polycyclic aromatic hydrocarbons (PAHs), substituted PAHs (e.g., nitro-PAHs and alkyl-PAHs), and heterocyclic compounds (e.g., azo-arenes, thio-arenes, and lactones).

The particulates associated with diesel exhaust are very small (<1 micron). Along with their small size, these particulates have a very large surface area onto which other organic contaminants present in the diesel exhaust can adsorb. Polycyclic organic matter compounds with five or more membered rings are usually associated with the diesel PM. Nitroarenes, nitrolactones, and oxy-polycyclic aromatic compounds can be produced as primary pollutants associated with diesel soot or as secondary pollutants produced by heterogeneous reactions of other gas-phase POM on particulate surfaces in VOC/NO_x-polluted atmospheres (Pitts et al., 1980; Pitts, 1993). Many POM compounds are mutagenic and some are carcinogenic. The best known of these is benzo(α)pyrene, a powerful human carcinogen (Phillips, 1983). It has been known for some time that PAHs are potential carcinogens and the nitroarenes show a much higher mutagenic activity than other PAHs. The combination of PAHs in both particulate and vapor phases appears to be responsible for a substantial portion of the mutagenic activity of the atmosphere (Pitts et al., 1978). Thus, POM compounds adsorbed on the diesel PM may add to the total carcinogenicity of the diesel emissions to an extent that is currently undetermined. Due to their small size, diesel PM can lodge deep in the respiratory tract and increase the risk of lung cancer. There has been a consistent causal relationship observed between the occupational exposure to diesel exhaust and lung cancer (Lloyd and Cackette, 2001).

Emissions of BC particulate matter from diesel engines are thought to be the largest source of light-absorbing aerosols worldwide. Some model calculations suggest that the contribution to global warming from diesel soot aerosols may be as much as 0.3–0.4 °C, rivaling the contributions from atmospheric methane (Jacobson, 2004; Chung and Seinfeld, 2005). The presence of large amounts of BC aerosols such as has been observed in Mexico City (Marley et al., 2007; Raga et al., 2001) and over the Indian Ocean (Ramanathan et al., 2005) can therefore lead to regional warming of the atmosphere and substantially offset the cooling effect of the light scattering aerosols in certain areas (Jacobson, 2002). It has been suggested that the most effective and possibly the quickest method of slowing global warming is to control the emissions of particulate black carbon from fossil fuel combustion (Jacobsen, 2002).

In addition to their climate effects, atmospheric BC particles absorb UV radiation very efficiently in the wavelength range that promotes photochemistry. Therefore, in areas where BC emissions are high, such as in megacities like Mexico City, the formation rates of secondary pollutants, such as ozone, may be slowed (Castro et al., 2001). In these cases, transport of the primary pollutants from the city into the surrounding areas where BC aerosols are less dominant will result in the production of secondary pollutants on regional scales. In contrast, areas that are dominated by light scattering aerosols, like sulfate, may have increased UV radiation due to multiple scattering effects of the aerosols, which may lead to an increased formation of the secondary photochemical pollutants (Marley et al., 2008).

6. Alcohol fuels

Alcohols, principally methanol and ethanol, along with their gasoline blends, have received considerable attention as alternative fuels. The principal drawback of alcohol fuels, from an air quality standpoint, is the production of aldehydes during combustion. Under cold-start conditions, alcohols crack to produce aldehydes, principally formaldehyde in the case of methanol and acetaldehyde in the case of ethanol. It is these aldehyde emissions from alcohols that make their potential impacts on air quality different from the non-oxygenated fuels. On the positive side, the use of alcohols and alcohol/petroleum blends in diesel engines has been shown to reduce emissions of the potentially carcinogenic carbonaceous soot particles (Gaffney et al., 1980; Wang et al., 1997). However, the PM emissions from alcohol fuel combustion have not been well characterized with regard to any changes in chemical, physical, and health-related properties, as compared with diesel PM.

The use of methanol has been considered for some time as an alternative to gasoline. This is primarily because methanol can be produced fairly cheaply by catalytic reduction of CO with hydrogen using methane or coal as the feedstock. For reasons of safety and engine material (i.e., corrosion and degradation of plastic fuel lines), methanol/gasoline blends of up to 85% have been studied for use. The convention has been to refer to the methanol/gasoline blends as M85 for 85% methanol, M50 for 50% methanol, and so on up to neat gasoline (M0).

Comparison studies of gasoline-fueled conventional vehicles and M85-fueled variable fuel vehicles (VFVs) showed the total organic emissions were 37% lower with M85 than with M0, (Auto/Oil Air Quality Improvement Research Program, 1992). In the same study, CO was 31% lower with M85 than with M0, while NO_x was 23% higher. The emissions of the air toxics benzene, 1,3-butadiene, and acetaldehyde, were lower with M85 than M0 by 84%, 93%, and 70%, respectively. The decreases corresponded roughly to the dilution effect of methanol in M85. Exhaust methanol emissions were higher with both M10 and M85 as expected, and formaldehyde emissions were about 5 times higher with M85 when compared with M0.

Formaldehyde is a carcinogen and an eye irritant, as well as being a photochemically active compound. Methanol itself has a lower atmospheric reactivity than gasoline. In comparison, methanol's combustion product, formaldehyde, reacts much more rapidly to form ozone (Atkutsu et al., 1991). Thus, the ozone-forming potential of methanol-fueled emissions is very dependent upon the formaldehyde emissions, which increase with increasing methanol content (Gabele, 1990). If the highly soluble gaseous formaldehyde is emitted in the presence of aqueous aerosols, it can be found to be present in relatively high concentrations in the aerosol phase in the form of the hydrated species, methylene glycol (Klippel and Warneck, 1980; Finlayson-Pitts and Pitts, 1986). In

addition, aqueous reactions with SO_2 emissions can lead to the formation of hydroxymethane sulfonate ions, while aqueous oxidation forms formic acid, both of which are highly toxic (Boyce and Hoffmann, 1984; Finlayson-Pitts and Pitts, 1986). These aqueous-phase reactions of formaldehyde and the resulting concentrations in inhalable aerosols are an aspect of these air pollutants that also must be considered when evaluating the air quality impacts of methanol fuels.

Of all of the oxygenated fuels, ethanol has had the greatest worldwide application. Ethanol, similar to methanol, can crack during combustion to form acetaldehyde in the exhaust emissions. Dynamometer studies of the use of gasahol (10% ethanol in gasoline) in motor vehicles report an average decrease in total hydrocarbon emissions of 5%, a decrease in CO emissions of 13% with an increase in NO_x emissions of 5% (Health Effects Institute, 1996). The same studies showed a decrease in the emissions of the air toxics, benzene and 1,3-butadiene, of 12% and 6%, while acetaldehyde emissions increased by 159%. Although the atmospheric reactivity of ethanol is much lower than that of gasoline, no significant change was reported in the overall atmospheric reactivity (MIR) of the exhaust emissions from gasahol when the higher reactivity of acetaldehyde is included. The evaporative emissions of hydrocarbons also increased when ethanol was added to the fuel. Diurnal hydrocarbon emissions increased by 30% while hot soak hydrocarbon emissions increased by 50%. The atmospheric reactivity of these evaporative emissions represents an increase of 30% for diurnal and a decrease of 19% for hot soak when compared to gasoline alone. This study also determined that, similar to methanol, most of the emissions in catalyst-equipped cars occurred during the cold start.

A number of field studies have examined the air quality impacts of increased levels of aldehydes caused by the use of ethanol/gasoline blends. In Brazil, when 20–30% ethanol/gasoline blends were used in the motor vehicle fleets with little or no use of catalytic converters, studies have found increased atmospheric levels of acetaldehyde and formaldehyde (Tanner et al., 1988; Grosjean et al., 1990). Field studies in Albuquerque, New Mexico also indicate elevated atmospheric aldehyde levels, albeit at a lower level than was observed in Brazil, when 10% ethanol/gasoline blends were used in vehicles with catalytic converters (Popp et al., 1995; Gaffney et al., 1997). Similar studies conducted in Denver, Colorado have concluded that oxygenated fuel usage has not had a major effect on ambient concentrations of acetaldehyde (Anderson et al., 1995, 1997). However, the data show a significant increase in reported acetaldehyde concentrations since 1994, when ethanol had obtained 80% of the oxyfuel market in the Denver area.

As indicated earlier, aldehydes are quite photochemically reactive and can lead to the formation of secondary atmospheric pollutants. While primary emissions of formaldehyde from methanol combustion leads to increased production of ozone, H_2O_2, formic acid, and CO, depending upon the atmospheric levels of NO/NO_2, primary acetaldehyde from ethanol combustion leads to the formation of these same products, as well as PAN, acetic acid, and peracetic acid (Atkutsu et al., 1991; McNair et al., 1992). The observation of elevated levels of PAN has been used as an indicator for primary acetaldehyde emissions (Tanner et al., 1988; Popp et al., 1995; Gaffney et al., 1997). The increases in PAN may have impacts on regional scale ozone production because the PANs can act to transport NO_2 over long distances (Gaffney et al., 1993). The major pathway for the thermal decomposition of PAN leads to the formation of peroxyacetyl radical and NO_2. This decomposition depends upon the temperature and NO_2 concentrations and leads to the formation of ozone in the presence of NO. Under low-NO conditions, decomposition of PAN leads to the formation of H_2O_2, and organic oxidants, such as peracetic acid and organic hydroperoxides (Gaffney et al., 1987; Gaffney and Marley, 1992).

Table 5
Energy content and CO_2 emissions of different fuels (Gushee, 1992a, 1992b; Chang et al., 1991).

Fuel	BTU/gallon	Miles/gallon	CO_2 (g mile^{-1})
Gasoline	115,000	34	315
Diesel	102,000–156,000	39–48	315–252
Methanol	56,000	22	272
Ethanol	76,000	28	243
Methane	20,000[a]	8	301
Propane	94,000[b]	31	229

[a] Fuel stored at 2000 psi.
[b] Fuel stored at 200 psi.

Therefore, similar to the case for methanol, the emissions of acetaldehyde from the combustion of ethanol/gasoline blends will strongly affect the ozone-forming potential of the exhaust emissions. A Canadian assessment of the use of 10% ethanol/gasoline blends estimates that usage will lead to 0.4–1.6% increases in ozone, 1–5% increases in formaldehyde, approximately 2.7% increase in acetaldehyde, and 2.9–4.5% increase in levels of PAN, with an approximate 15% reduction in CO (Singleton et al., 1998). This estimate is in fairly good agreement with field data obtained in the United States (Gaffney et al., 1997).

As with any hydrocarbon fuel, the alcohol fuels release the greenhouse gas CO_2 upon combustion. The important values to consider when determining the overall greenhouse impact of any fuel is the amount of CO_2 produced per gallon, which will vary with the carbon content of the fuel, and the fuel economy of the vehicle (Chang et al., 1991). Although the alcohol fuels have less carbon content than the fossil fuels, they have lower energy content (see Table 5) and therefore require more fuel to travel the same distance (Gushee, 1992a, 1992b). Consequently, their resulting CO_2 production per mile is not significantly different than for gasoline or diesel. It is important when comparing CO_2 emissions from different fuels to include contributions through the total life cycle (Wang, 2003). When considering the CO_2 emissions from the entire life cycle of the fuels, those fuels that use less fossil carbon than the petroleum fuels they are replacing will lead to improvements in the overall CO_2 budget. The biomass-derived fuels like ethanol are likely to reduce these emissions, provided that significant fossil fuel is not involved in the production process. Therefore, oxygenated fuels from these renewable sources will lead to reductions in overall CO_2 releases. The use of methanol derived from coal will lead to more CO_2 emissions than the use of methanol derived from biomass.

Other climate impacts can arise from the primary pollutant emissions or secondary pollutants formed from them. The aldehydes can act as greenhouse species in both the vapor and the aerosol phases (Marley et al., 1993). The aerosols formed from these primary emissions can contribute to atmospheric cooling by increased light scattering. The atmospheric reactions of the peroxy radicals formed from the aldehyde emissions will also likely lead to increased acidic aerosol production contributing to light scattering aerosol species. Once dissolved in aerosols, the aldehydes are also strong infrared absorbers, and can contribute to local heating of the atmosphere (Gaffney and Marley, 1992). The overall impact of the aerosol formation on climate will depend on their concentrations, atmospheric lifetimes and distributions.

7. Branched chain ether additives

The CAAA of 1990 mandated the use of fuels containing 2–2.7% oxygen by weight in order to reduce the emissions of the criteria pollutants CO and the ozone forming precursors NO_x and VOCs in U.S. non-attainment areas (Calvert et al., 1993). In order to meet these demands, oxygenated compounds, such as ethanol, methyl tertiary-butyl ether (MTBE), ethyl tertiary-butyl ether (ETBE), and

tertiary-amyl methyl ether (TAME) were blended with gasoline. The resulting fuels were called "reformulated gasoline". Since the regulations also mandated the reduction of the concentrations of benzene and other aromatics in the fuels, the branched chain ethers were popular choices since they also served to enhance the octane number lost by decreasing the aromatic content of the fuel. Neither ETBE or TAME gained as wide-spread use as MTBE due to the higher cost of production.

Methyl tertiary-butyl ether is manufactured from isobutene and methanol (Maxwell and Naber, 1992). Upon combustion, it can crack to yield the starting products, which are emitted in the exhaust during incomplete combustion. Similarly, ETBE is manufactured from ethanol and isobutene and TAME is made from methanol and isopentene. Therefore, similar to the alcohol fuels, MTBE and TAME can lead to increased formaldehyde emissions and ETBE can lead to increased emissions of acetaldehyde (Kaiser et al., 1991). The addition of MTBE to California reformulated gasoline resulted in an increase of formaldehyde emissions of 21% in the current fleet (Auto/Oil Air Quality Improvement Research Program, 1992). In tunnel studies, formaldehyde levels increased by 13% and isobutene increased by 87% during the period when MTBE was in use compared to periods when oxygenates were not added to the fuel (Kirchstetter et al., 1996). Similar tunnel studies in the California South Coast Air Basin have reported a formaldehyde to isobutene molar ratio of 1 in emissions where MTBE was in use indicating a common source (Gertler et al., 1997; Zielinska et al., 1997).

Field studies in Mexico City reported atmospheric levels of formaldehyde increased by approximately 3 ppb, after the use of MTBE/gasoline blends (Bravo et al., 1991). Moreover, the time of peak concentrations changed from midday (previous to MTBE use) to the morning hours, indicating a primary source of formaldehyde. Ozone levels also increased in morning and evening hours, with higher levels occurring more frequently after the introduction of MTBE. These field studies indicate that, similar to ethanol/gasoline blends, MTBE use will lead to primary emissions of the photochemically reactive formaldehyde, as well as isobutene, thus increasing the atmospheric reactivity of the emissions and increasing secondary ozone formation.

The major atmospheric oxidation products from MTBE and ETBE are formaldehyde and the formates and acetates (Japar et al., 1990; Smith et al., 1991; Tuazon et al., 1991; Wallington and Japar, 1991). The heterogeneous photooxidation of MTBE adsorbed onto aerosols leads to the production of formaldehyde and acetone (Idriss and Seebauer, 1996; Idriss et al., 1997). Both the acetates and the formates are expected to undergo hydrolysis in wet aerosols and in precipitation to form tertiary-butyl alcohol. The reaction of nitrate radical (NO_3) with ETBE is an important nighttime loss mechanism and is equivalent to the daytime loss by reaction with hydroxyl radical (Finlayson-Pitts and Pitts, 1986). Lifetimes for ETBE were estimated to be approximately 30 h in a moderately polluted urban area (Langer et al., 1996). Products from the reaction initiated by NO_3 included tertiary-butyl formate, tertiary-butyl acetate, formaldehyde, and methyl nitrate (Langer et al., 1996).

The U.S. federal requirement that fuels contain oxygen was dropped on May 6, 2006 and MTBE use is being phased out due to issues with contamination of ground water. Studies of the reductions of CO and ozone from the addition of oxygenated compounds to gasoline were inconclusive. Reductions in atmospheric CO levels reported after the use of oxygen containing fuels correlated better with the number of cars using catalytic converters than with the number of cars burning the reformulated gasolines (Gaffney and Marley, 2000). The reduction in emissions of the ozone precursors from the use of oxygenated fuels was also unclear. Results of emission studies of total hydrocarbons and NO_x produced varying results with different fuels and fleets (Health Effects Institute, 1996). One study reported a decrease in total hydrocarbon emissions of 20% and an increase in NO_x emissions of 2% with the addition of MTBE to gasoline (Noorman, 1993). Another study reported a decrease of 7% for total hydrocarbon emissions and no significant change in NO_x emissions with 15% MTBE fuel (Reuter et al., 1992) while studies of the use of a 9.5% MTBE/gasoline blend found no general pattern of reduction of tailpipe emissions when compared with the unoxygenated fuel (Stump et al., 1994). In all cases, formaldehyde emissions were greater with the fuel containing MTBE. Therefore, similar to the case for methanol, the emissions of the photochemically reactive aldehydes from the combustion of ether/gasoline blends will strongly affect the atmospheric reactivity and the ozone-forming potential of the exhaust emissions.

8. Natural gas and liquified petroleum gas

Methane (natural gas), propane, and the butanes all have been proposed as clean alternatives to conventional liquid gasoline and diesel fuels. Natural gas is primarily composed of methane but can contain small amounts of alkenes. Natural gas is typically handled as a compressed gas and is usually referred to as compressed natural gas (CNG). Methane is an attractive fuel in many ways. It has a low atmospheric reactivity and therefore has low ozone-forming potential. Propane and the butanes, as liquefied petroleum gas (LPG), are also of reasonably low atmospheric reactivity and low ozone-forming potential. Reductions in CO, reactive hydrocarbon emissions, and nitrogen oxides are all feasible with the use of these fuels, particularly if engines are designed for the fuels and make use of three-way catalysts for emission control (Fowler et al., 1991; Stodolsky and Santini, 1993; Tabata et al., 1995; Chang and McCarty, 1996).

Methane, propane, and the butanes have low reactivities with hydroxyl radical, leading to long atmospheric lifetimes and low ozone-forming potential (Finlayson-Pitts and Pitts, 1986, 1993). However, the associated olefins, such as ethene, propene, and the butenes are quite reactive with hydroxyl radical. Thus, these highly reactive alkenes, present in LPG at low concentrations, can cause considerable problems in emissions of unburned fuel. These emissions can occur in leakage from LPG containers or during transfer of the fuel between containers. When used as a transportation fuel, releases of uncombusted olefins also result during cold starts or in vehicles without catalytic converters. The widespread use of LPG in Mexico City and other foreign cities for heating and cooking has led to some concern regarding the potential for the formation of ozone due to the olefin contents of these fuels (Blake and Rowland, 1995). Alkenes also can react with ozone leading to increases in secondary aldehyde production and the formation of PANs. Many of these problems can be resolved but will require reformulation of the LPG to reduce the alkene content if these fuels are to be used in vehicles on large scales.

Since CO emission rates are a function of the air/fuel ratio, vehicles which utilize gaseous fuels have a potential for lower CO emissions because they can operate on a stoichiometric air/fuel ratio during cold start, when CO emissions are at their highest. Studies comparing vehicles using CNG, LPG, methanol, ethanol, and gasoline fuels showed that the LPG and CNG vehicles have, in general, the lowest emissions of CO, benzene, 1,3-butadiene, and aldehydes (Gabele, 1995). Total reactive VOC emissions were also reduced with CNG and LPG when compared with gasoline or the alcohol fuels. Although all CNG and LPG fuels were >99% alkane, the olefin content of the hydrocarbon emissions varied from 1.6 to 22% for CNG and from 2 to 14% for LPG. The atmospheric reactivity of the organic emissions was decreased by 26–83% for CNG and by 51–78% for LPG when compared to gasoline. This variation in olefin content of the exhaust corresponded roughly to their overall atmospheric reactivities. The major reactive component of the emissions from these fuels is therefore the alkenes.

Other issues arise when considering changing from liquid fuels to CNG or LPG (Eckhoff, 1994). The single biggest drawback for methane lies in its very low reactivity. Its atmospheric lifetime has been estimated at approximately 10 years (Senum and Gaffney, 1985). Methane is a very strong greenhouse gas with many natural sources. However, the potential for releases of methane from fossil sources would have a major impact on climate change. The use of the fossil-based CNG and LPG would also increase CO_2 emissions, albeit by lesser amounts than with the use of gasoline or diesel fuels. In addition, methane is the major source of stratospheric water vapor, and increases in the troposphere would likely lead to increases in stratospheric clouds and the associated catalytic destruction of stratospheric ozone.

9. Biodiesel

There has been considerable interest in the use of vegetable oils as an alternative to diesel fuel (Peterson and Reece, 1996). Animal fats have also been considered as diesel substitutes (Muniyappa et al., 1996). However, the high viscosity and high molecular weight of the raw oils and fats cause poor fuel atomization and low volatility leading to incomplete combustion and severe engine deposits (Bagby, 1987). One way to improve the fuel properties of the oils and fats is through transesterification (Peterson, 1986; Peterson et al., 1991). Transesterification converts the large molecular weight organic acid esters in the oils and fats to smaller esters of the same acid using an alcohol in the presence of a catalyst. These so-called biodiesel fuels are typically the methyl esters of rapeseed, soybean, safflower, peanut, sunflower, coconut, cottonseed, or other vegetable oils. In Germany, the most common biodiesel is rapeseed oil methyl ester, while in the U.S. it is mainly soy methyl ester (Krahl et al., 2002a).

Studies of the comparisons of emissions from combustion of biodiesel or biodiesel blends to diesel fuel vary depending on the fuel and the vehicle. In general biodiesel has up to 60% lower CO emissions with an increase in NO_x of up to 80% (Chang and McCarty, 1996; Dorado et al., 2003; Schumacher et al., 1996) and an overall increase in the ozone-forming potential of the biodiesel emissions (Krahl et al., 2001). Emissions of benzene and aldehydes are also reported to increase with the biodiesel fuels (Geyer et al., 1984; Krahl et al., 2002a, 2002b; Mittlelbach et al., 1985). Since these fuels are methyl esters, cracking of the fuel during incomplete combustion leads to the formation of formaldehyde (Turrio-Baldassarri et al., 2004).

Emissions of PM from biodiesel also vary widely depending on the fuel and vehicles tested. In general, PM emissions are seen to increase with the use of biodiesel. However, the biodiesel particulates have a much higher organically extractable fraction (Krahl et al., 2002b). The BC content of the biodiesel PM is therefore lower. The total PAH and nitro-PAH emissions are not significantly different with biodiesel and the overall mutagenicity of the emissions are seen to be similar for biodiesel and low-sulfur diesel fuels (Bunger et al., 2000; Krahl et al., 2002b; Turrio-Baldassarri et al., 2004). It is clear from these studies that, similar to the oxygenated alternative fuels, the potential emissions of aldehydes and PAHs, along with other non-criteria pollutants, need to be investigated in order to assess the overall air quality impacts of the use of biofuels in diesel engines.

The biodiesel fuels contain approximately 10% by weight of oxygen. Similar to the case with the alcohol fuels, since they have less carbon content, their combustion results in lower CO_2 emissions per gallon of fuel burned (Lin and Lin, 2006). However, more fuel must be combusted to travel similar distances as with diesel fuel. The CO_2 emissions per mile are similar for both fuels. When considering the CO_2 emissions from the entire life cycle of the fuels, the biomass-derived fuels are likely to result in lower overall CO_2 emissions. However, since the methyl esters are produced from transesterification with methanol, this impact would depend on the source of the methanol. The use of methanol derived from coal will lead to more CO_2 emissions than the use of methanol derived from biomass.

10. Future needs

It is becoming increasingly more obvious that we need to decrease our fossil fuel combustion to address the impacts on both air quality and climate change. The first attempt at accomplishing this has been to attempt to convert to the renewable biofuels, such as alcohol fuels and biodiesel. However, studies indicate that while combustion of these renewable fuels may, in some cases, result in a reduction in the criteria pollutants, the emissions may contain significant amounts of currently unregulated yet equally important pollutants. In general, the oxygenated fuels and their gasoline blends will lead to increases in cold-start aldehyde emissions, which will increase the photochemical reactivity of the exhaust gas, leading to the increased production of ozone and the PANs. The use of alcohol fuels may lead to some reductions in CO and VOC emissions, with a corresponding increase in NO_x emissions. The use of alcohols and biofuels in diesel engines may have some advantages in reducing light-absorbing BC emissions. However, any impact on the resulting toxicity of the PM, particularly for the biodiesel fuels, is not necessarily a direct consequence of this reduction. Since most of the emissions of CO, aldehydes, and exhaust hydrocarbons occur during the cold start of the engine, when the catalyst is not sufficiently heated to operating temperatures, research aimed at improving catalyst performance and incorporating preheated catalytic system designs will be important in reducing emissions from both fossil and biofuels.

The reduction of CO_2 emissions from the renewable biofuels is also unclear. Although the emission of CO_2 per gallon of fuel burned is lower than for fossil fuels, the CO_2 emissions per mile are not. Also, care must be taken in considering the entire life cycle of the fuel and other potential greenhouse gas emissions when determining the overall climate impacts of these alternate fuels. While the combustion of fossil-derived methane will lead to increased CO_2 emissions, the combustion of biomass-derived methane likely will lead to net CO_2 emission reductions. From a global environmental perspective, the biomass-derived fuels that act to recycle CO_2 are attractive as a means of reducing combustion-related CO_2 emissions. However, a complete assessment of the bio-derived fuels needs to include the fossil fuels used in their production to accurately determine net CO_2 reductions.

Compressed natural gas is certainly a cleaner fuel than gasoline. Its biggest drawbacks are in handling and distributing the CNG and in associated safety issues. Methane releases will be of concern as a greenhouse gas with a fairly long lifetime, and so the main use of natural gas is likely to be in stationary power plants where the fugitive emissions can be better controlled. Incomplete combustion of methane does lead to formaldehyde emissions, but this can be controlled with use of catalytic converters. Liquefied petroleum gas is not as clean as CNG but is easier to handle, although one of the major issues with both of these fuels is high NO_x emissions. Indeed, all of the internal combustion systems that make use of either spark-ignition or diesel configurations will lead to the emission of thermal NO_x.

With all considered, the use of a fuel-cell-powered electric vehicle would seem to be the longer-term "best" answer to the air quality problems facing most major urban centers in the world. Fuel cells convert the gaseous fuels such as hydrogen or natural gas directly into electricity by an electrochemical process. The key components of a fuel cell are an anode, to which fuel is supplied, a cathode, to which the oxidant is supplied, and an electrolyte, which permits the flow of ions between the anode and cathode. Fuel cells operate like batteries but since the fuel and oxidant are

not integral parts of the fuel cell, they do not need to be recharged and will continually produce power when supplied with fuel and oxidant. The chemical reaction occurring within the fuel cell is exactly the same as when the fuel is burned, but the chemical conversion process occurs at a much lower temperature than in an internal combustion engine, so there is no NO_x formation, and since there are no lubricating oils, there are also no hydrocarbons or CO emissions. In short, fuel cells can be used to operate zero emitting vehicles (ZEV).

The most efficient fuel for fuel cells is hydrogen. It can be supplied directly from refueling stations, or indirectly from on-board generation systems. Due to infrastructure compatibility, safety considerations, and optimum driving range of the vehicles, on-board generation of hydrogen from gasoline or methanol is more widely favored (Kartha and Grimes, 1994; Kordesch and Simader, 1995; Hohlein et al., 1996). Increases in fuel economy of approximately 50% with very low CO, NO_x, and VOC emissions appear to be feasible with this approach. In addition, the increased projected fuel economy would lead to lower CO_2 emissions, particularly if biomass-derived fuels are used as a feedstock. However, the methanol reaction does produce CO, which has to be removed catalytically (Schmidt et al., 1994).

Most of the attention regarding the combustion impacts on air quality and climate has centered on motor vehicles and the transportation fuels. However, coal-fired power plants are a major source of PM, SO_2 and NO_x, the toxic metal mercury, and the greenhouse gasses CO_2, CH_4, and N_2O worldwide. Clearly, in order to decrease the impact of combustion on air quality and climate, we need to convert to other energy sources for electricity generation. Solar, hydroelectric and wind can all be used on small scales in areas where the source of energy is available and reliable. The only energy source that has the potential for eliminating the effects of combustion emissions and can be used on a wide scale is nuclear power. Currently, nuclear power provides approximately 17% of the world's electricity with the U.S., France and Japan accounting for 57%. Most estimates suggest that in order to have a significant impact on carbon emissions, carbon-free sources of electrical energy, such as nuclear power would have to expand by factors of 3–10 by 2050 (Ewing, 2005).

There are many available types of nuclear reactors and nuclear fuel cycles used in nuclear power generation. The different fuel cycles represent different strategies for making use of the nuclear materials. The open-cycle treats the spent nuclear fuel as a waste without any attempt at reclaiming it. This results in the need to dispose of the spent fuel after one pass through the reactor. The closed-cycle reprocesses the spent fuel and retrieves about 99% of the nuclides for reuse in the reactor. The breeder-reactor cycle creates more fissile material in the spent fuel than was contained in the original fuel and involves multiple cycles of fuel reprocessing and reuse, greatly reducing the amount of waste (Ewing, 2005). In 1977 nuclear materials reprocessing was halted in the U.S. due to concerns regarding nuclear proliferation. Today, reprocessing is not pursued because it is more expensive than the simpler strategy of direct disposal of the spent fuel in a nuclear repository (Bunn et al., 2003). There are several problems associated with this strategy. The U.S. has not agreed on where and how to dispose of the spent fuel, consequently, the waste is currently stored at some 100 commercial reactor sites. Meanwhile, since the long delayed Yucca Mountain Repository is not likely to accept waste before 2020, the U.S. is already getting close to the cap set for the Yucca Mountain site of 63,000 metric tons of commercially generated waste (C&E News, 2007). The only solution to this problem is reprocessing the spent fuel. Since there are currently no financial incentives to put this technology into practice, it will most likely take government regulation of the waste generation process to provide the needed motivation.

Overall, nuclear power plants produce far less waste than fossil fuel based plants. Coal-fired plants in particular generate very large amounts of toxic and radioactive bottom ash. This ash is typically disposed of in landfills or used as fill material in road construction where the trace metals and radionuclides can leach into ground or surface waters. It has been estimated that these practices result in more radioactive waste being released into the environment than from nuclear power. The population effective dose equivalent from radiation from coal-fired power plants is 100 times as much as for nuclear plants (McBride et al., 1978; Ren et al., 1998).

We have been aware for some time that in order to avoid or at least minimize the air quality and climate impacts of fossil fuel combustion, alternatives must be put in place. However, no matter how dire the predictions associated with inaction, there has been major resistance to change. Even with gasoline prices skyrocketing, vehicle fuel economy has not been increased and the currently available hybrid vehicles have not been popular. The key to successful application of new technologies such as fuel cells or electric vehicles will be the development of the infrastructure and the commercialization and replacement of the current fleets (Serfass et al., 1994; Appleby, 1996; Chalk et al., 1996). After all, the internal combustion engines have the benefit of 100 years of evolution and infrastructure development. Therefore, even with the current environmental pressures, the establishment of alternative vehicles in the market will not occur overnight and will likely require government support considering the magnitude of the investment required.

Acknowledgments

The authors wish to acknowledge the current support of the U.S. Department of Energy's Atmospheric Science Program, Office of Science (BER), U.S. Department of Energy Grant No. DE-FG02-07ER64329.

References

Alliksaar, T., Punning, J.-M., 1998. The spatial distribution of characterized fly-ash particles and trace metals in lake sediments and catchment mosses: Estonia. Water, Air, and Soil Pollution 106, 219–239.

Anderson, L.G., Wolfe, P., Barnell, R.A., Lanning, J.A., 1995. The effects of oxygenated fuels on the atmospheric concentrations of carbon monoxide and aldehydes in Colorado. In: Sterrett, F.S. (Ed.), Alternative Fuels and the Environment. Lewis Publishers, Boca Raton, FL, pp. 75–102.

Anderson, L.G., Lanning, J.A., Wilkes, E., Wolfe, P., Jones, R.H., 1997. Effects of using oxygenated fuels on carbon monoxide, formaldehyde and acetaldehyde concentrations in Denver. Paper 97-RP139.05. In: The Air and Waste Management Association 90th Annual Meeting, Toronto, Canada, 11 pp.

Appleby, A.J., 1996. Issues in fuel cell commercialization. Journal of Power Sources 69, 153–176.

Atkutsu, Y., Toyoda, F., Tomita, K.-I., Yoshizawa, F., Tamura, M., Yoshida, T., 1991. Effect of exhaust from alcohol fuel on ozone formation in the atmosphere. Atmospheric Environment 25A, 1383–1389.

Auto/Oil Air Quality Improvement Research Program, 1992. Gasoline Reformulation and Vehicle Technology Effects on Exhaust Emissions. In: Technical Bulletin Number 17. Coordinating Research Council, Atlanta, Georgia, pp. 1–18.

Bagby, M.O., 1987. Vegetable oils for diesel fuel: Opportunities for development. American Society for Automotive Engineering, Paper No. 87-1588. St. Joseph, MI.

Baughcum, S.L., 1996. Subsonic aircraft emission inventories. In: Thompson, A.M., Friedel, R.R., Wesoky, H.L. (Eds.), Atmospheric Effects of Aviation: First Report of the Subsonic Assessment Project. NASA Reference Publication 1385, Chapter 2.

Blake, D.R., Rowland, F.S., 1995. Urban leakage of liquefied petroleum gas and its impacts on air quality in Mexico City. Science 269, 953–956.

Block, C., Dams, R., 2004. Lead contents of coal, coal ash and fly ash. Water, Air, and Soil Pollution 5, 207–211.

Boyce, S.D., Hoffmann, M.R., 1984. Kinetics and mechanism of the formation of hydroxymethanesulfonic acid at low pH. Journal of Physical Chemistry 88, 4740–4746.

Bravo, H.A., Camancho, R.C., Roy-Ocotla, G.R., Sosa, R.E., Torres, R.J., 1991. Analysis of the change in atmospheric urban formaldehyde and photochemical activity as a result of using methyl-t-butyl-ether (MTBE) as an additive in gasoline of the metropolitan area of Mexico City. Atmospheric Environment 25B, 285–288.

Bunger, J., Muller, M.M., Krahl, J., Baum, K., Weigel, A., Hallier, E., Schults, T.G., 2000. Mutagenicity of diesel exhaust particles from two fossil and two plant oil fuels. Mutagenesis 15, 391–397.

Bunn, M., Fetter, S., Holdren, J.P., van der Zwaan, B., 2003. The economics of reprocessing vs. direct disposal of spent nuclear fuel. Project on Managing the Atom, Final Report. DE-FG26–99FT4028, 127 pp.
C&E News, 2007. Reprocessing key to nuclear plan. Chemical and Engineering News, American Chemical Society (June 18), 48–54.
Calvert, J.G., Heywood, J.B., Sawyer, R.F., Seinfeld, J.H., 1993. Achieving acceptable air quality: Some reflections on controlling vehicle emissions. Science 261, 37–45.
CARB, 1996. Predicted California on-road motor vehicle emissions. In: EMFAC7G, vol. I. Mobile Source Emission Inventory Branch, California Air Resources Board, Sacramento, CA.
Carter, W.P.L., Atkinson, R., 1989. A computer modeling study of incremental hydrocarbon reactivities. Environmental Science and Technology 23, 864–880.
Carter, W.P.L., 1994. Development of ozone reactivity scales for volatile organic compounds. Journal of the Air and Waste Management Association 44, 881–889.
Castro, T., Madronich, S., Rivale, S., Muhlia, A., Mar, B., 2001. The influence of aerosols on photochemical smog in Mexico City. Atmospheric Environment 35, 1765–1772.
Chalk, S.G., Patil, P.G., Venkateswaran, S.R., 1996. The new generation of vehicles: market opportunities for fuel cells. Journal of Power Sources 61, 7–13.
Chang, T.Y., Hammerle, R.H., Japar, S.M., Salmeen, I.T., 1991. Alternative transportation fuels and air quality. Environmental Science and Technology 25, 1190–1197.
Chang, Y.-F., McCarty, J.G., 1996. Novel oxygen storage components for advanced catalysts for emission control in natural gas fueled vehicles. Catalysis Today 30, 163–170.
Charlson, R.J., Wigley, T.M.L., 1994. Sulfate aerosol and climate change. Scientific American (February), 48–57.
Chung, S.H., Seinfeld, J.H., 2005. Climate response of direct radiative forcing of anthropogenic black carbon. Journal of Geophysical Research 110, D11102–11127.
Corbett, J.J., Fischbeck, P.S., 1997. Emissions from ships. Science 278, 823–824.
Danielson, J.A., 1973. Air Pollution Engineering Manual, second ed. US-EPA, Research Triangle Park, NC. AP-40.
DeCicco, J., Fung, F., 2006. Global warming on the road: the climate impact of America's automobiles. http://www.environmentaldefense.org.
Dorado, M.P., Ballesteros, E., Arnal, J.M., Gomez, J., Lopez, F.J., 2003. Exhaust emissions from a diesel engine fuelled with transesterified waste olive oil. Fuel 82, 1311–1315.
Dreher, K., Jaskot, R., Richards, J.H., Lehmann, J.R., Winsett, D., Hoffman, A., Costa, D., 1996. Acute pulmonary toxicity of size-fractionated ambient air particulate matter. American Journal of Respiratory and Critical Care Medicine 153, A15.
Dreher, K., Jaskot, R., Lehmann, J.R., Richards, J.H., McGee, J.K., Ghio, A.J., Costa, D.L., 1997. Soluble transition metals mediate residual oil fly ash induced lung injury. Journal of Toxicology and Environmental Health 50, 285–305.
Eckhoff, R.F., 1994. New safety issues when moving from liquid fuels to natural gas. Marine Pollution Bulletin 29, 304–306.
Evelyn, J., 1661. Fumifugium: Or the Inconvenience of the Aer and Smoak of London, Dissapated. Together with Some Remedies Humbly Proposed to His Sacred Majestie and the Parliament Now Assembled. Published by His Majesties Command. Lucret. I. VI.802.
Ewing, R.C., 2005. The nuclear fuel cycle versus the carbon cycle. The Canadian Mineralogist 43, 2099–2116.
FHWA, January 2006. Highway statistics 2004. Department of Transportation, Federal Highway Administration, Washington, DC.
Finlayson-Pitts, B.J., Pitts Jr., J.N., 1986. Atmospheric Chemistry: Fundamentals and Experimental Techniques. John Wiley & Sons, New York.
Finlayson-Pitts, B.J., Pitts Jr., J.N., 1993. Volatile organic compounds: Ozone formation, alternate fuels and toxics. Chemistry and Industry (October 18), 796–800.
Finlayson-Pitts, B.J., Pitts Jr., J.N., 2000. Chemistry of the Upper and Lower Atmosphere: Theory, Experiments, and Applications. Academic Press, San Diego.
Fowler, T., Lander, D., Broomhall, D.B., 1991. Reduced NO_x emissions from internal combustion engines fuelled by natural gas. Fuel 70, 499–502.
Freese, B., 2003. Coal: A Human History. Preseus Books Group, Cambridge, MA.
Furr, A.K., Parkinson, T.F., Hinrichs, R.A., Van Campen, D.R., Bache, C.A., Gutenmann, W.H., St. John, L.E., Pakkala, I.S., Lisk, D.J., 1977. National survey of elements and radioactivity in fly ash-soil mixtures. Environmental Science and Technology 11, 1194–1201.
Gabele, P.A., 1990. Characterization of emissions from a variable gasoline/methanol fuelled car. Journal of the Air and Waste Management Association 40, 296–304.
Gabele, P.A., 1995. Exhaust emissions from in-use alternate vehicles. Journal of the Air and Waste Management Association 45, 770–777.
Gaffney, J.S., Sapienza, R., Butcher, T., Krishna, C., Marlow, W., O'Hare, T., 1980. Soot reduction in diesel engines: a chemical approach. Combustion Science and Technology 24, 89–92.
Gaffney, J.S., Streit, G., Spall, W.D., Hall, J.H., 1987. Beyond acid rain: do soluble oxidants and organic toxins interact with SO_2 and NO_x to increase ecosystem effects? Environmental Science and Technology 21, 519–524.
Gaffney, J.S., Marley, N.A., Prestbo, E.W., 1989. Peroxyacyl nitrates (PANs): their physical and chemical properties. Handbook of Environmental Chemistry, 4/ Part B, pp. 1–38.
Gaffney, J.S., Marley, N.A., 1992. Potential changes in atmospheric chemistry in the decades ahead: Climate and biosphere interactions and feedbacks. In: Schwartz, S.E., Slinn, W.G.N. (Eds.), Precipitation Scavenging and Atmosphere-Surface Exchange. The Summers Volume: Applications and Appraisals, vol. 3. Hemisphere Publishing Corporation, Washington, DC, pp. 1735–1743.
Gaffney, J.S., Marley, N.A., Prestbo, E.W., 1993. Measurement of peroxyacetyl nitrate (PAN) at a remote site in southwestern United States. Environmental Science and Technology 27, 1905–1910.
Gaffney, J.S., Marley, N.A., Martin, R.S., Dixon, R.W., Reyes, L.G., Popp, C.J., 1997. Potential air quality effects of using ethanol-gasoline fuel blends: a field study in Albuquerque, New Mexico. Environmental Science and Technology 31, 3053–3061.
Gaffney, J.S., Marley, N.A., Cunningham, M.M., Doskey, P.V., 1999. Measurements of peroxyacyl nitrates (PANs) in Mexico City: implications for megacity air quality impacts on regional scales. Atmospheric Environment 33, 5003–5012.
Gaffney, J.S., Marley, N.A., 2000. Alternative fuels. In: Brimblecombe, P., Maynard, R. (Eds.), Air Pollution Reviews. The Urban Air Atmosphere and Its Effects, vol. 1. Imperial College Press, London, UK, pp. 195–246. Chapter 6.
Gertler, A.W., Sagebiel, J.C., Dippel, W.A., O'Connor, C.M., 1997. Impact of reformulated gasoline on ambient air quality in the South Coast Air Basin, California. In: The Fifth Chemical Congress of North America, Cancun, Quintana Roo, Mexico, Paper 2090.
Geyer, S.M., Jacobus, M.J., Lestz, S.S., 1984. Comparison of diesel engine performance and emissions from neat and transesterified vegetable oils. Transactions of the American Society of Agricultural Engineers 27, 375–381.
Gillani, N.V., Kohli, S., Wilson, W.E., 1981. Gas to particle conversion of sulfur in power plant plumes I, Parameterization of the conversion rate for dry, moderately polluted ambient conditions. Atmospheric Environment 15, 2293–2313.
Gorse, R.A., Benson, J.D., Burns, V.R., Hochhauser, A.M., Koehl, W.J., Painter, L.T., Reuter, R.M., Rippon, B.H., 1991. Toxic air pollutant vehicle emissions with reformulated gasolines, Society of Automotive Engineers Technical Paper Number 912324.
Greiner, N.R., Williams, M.D., Wagner, P., 1983. Estimation of radionuclide releases from specific large coal-fired industrial and utility boilers. Technical Report No. LA-9845-MS, Los Alamos National Laboratory, Los Alamos, NM.
Grosjean, D., Miguel, A.H., Taveres, T.M., 1990. Urban air pollution in Brazil: acetaldehyde and other carbonyls. Atmospheric Environment 24B, 101–106.
Gushee, D.E., 1992a. Alternative fuels for cars: are they cleaner than gasoline? Part 1. Chemtech 22, 406–411.
Gushee, D.E., 1992b. Alternative fuels for cars: are they cleaner than gasoline? Part 2. Chemtech 22, 470–476.
Haagen-Smit, A.J., 1950. The air pollution problem in Los Angeles. Engineering and Science XIV, 7–13.
Haagen-Smit, A.J., Bradley, C.E., Fox, M.M., 1952a. Formation of ozone in Los Angeles smog. In: Proceedings of the Second National Air Pollution Symposium, pp. 54–56.
Haagen-Smit, A.J., Darley, E.F., Zaitlin, M., Hull, H., Noble, W., 1952b. Investigation on injury to plants from air pollution in the Los Angeles basin. Plant Physiology 27, 18–34.
Hauser, R.B., 1986. Emissions of Sulfur dioxide and nitrogen oxides and trends for Eastern North America. Acid Deposition Long Term Trends. National Academy Press, Washington, DC.
Health Effects Institute, 1996. The potential health effects of oxygenates added to gasoline: a review of the current literature. Health Effects Institute, Cambridge, MA.
Hermann, P., Hanel, G., 1997. Wintertime optical properties of atmospheric particles and weather. Atmospheric Environment 31, 4053–5062.
Hidey, G.M., 1994. Atmospheric Sulfur and Nitrogen Oxides. Academic Press, San Diego, California.
Hohlein, B., Boe, M., Bogild-Hansen, J., Brockerhoff, P., Colsman, G., Emonts, B., Menzer, R., Riedel, E., 1996. Hydrogen from methanol for fuel cells in mobile systems: development of a compact reformer. Journal of Power Sources 61, 143–147.
IEA, 2005. CO_2 Emissions from Fuel Combustion 1971–2005. International Energy Agency, ISBN 978-92-64-02771-8.
Idriss, H., Seebauer, E.G., 1996. Fast photoreactions of oxygenates on tropospheric fly ash particles. Journal of Vacuum Science and Technology 14, 1627–1632.
Idriss, H., Miller, A., Seebaur, E.G., 1997. Photoreactions of ethanol and MTBE on metal oxide particles in the troposphere. Catalysis Today 33, 215–225.
Jacobson, M.Z., 2002. Control of fossil-fuel particulate black carbon and organic matter, possibly the most effective method of slowing global warming. Journal of Geophysical Research 107 (D19), 4410–4431.
Jacobson, M.Z., 2004. Climate response of fossil fuel and biofuel soot, accounting for soot's feedback to snow and sea ice albedo and emissivity. Journal of Geophysical Research 109, D21201. doi:10.1029/2004JD004945.
Japar, S.M., Wallington, T.J., Richert, J.F.O., Ball, J.C., 1990. The atmospheric chemistry of oxygenated fuel additives: t-butyl alcohol, dimethyl ether, and methyl t-butyl ether. International Journal of Chemical Kinetics 22, 1257–1269.
Kaiser, E.W., Andino, J.M., Siegl, W.O., Hammerle, R.H., Butler, J.W., 1991. Hydrocarbon and aldehyde emissions from an engine fueled with ethyl-t-butyl ether. Journal of the Air and Waste Management Association 41, 195–197.
Kartha, S., Grimes, P., 1994. Fuel cells: Energy conversion for the next century. Physics Today November, 54–61.
Kiel, J.T., Briegleb, B.P., 1993. The relative roles of sulfate aerosols and greenhouse gasses in climate forcing. Science 260, 311–314.
Kirchstetter, T.W., Singer, B.C., Harley, R.A., Kendall, G.R., Chain, W., 1996. Impact of oxygenated gasoline use on California light-duty vehicle emissions. Environmental Science and Technology 30, 661–670.
Kirchstetter, W.T., Miguel, H.A., Harley, A.R., 1998. On-road comparison of exhaust emissions from gasoline and diesel engines. In: Proceedings of the Eighth CRC On-road Vehicle Emissions Workshop, April 20–22, San Diego, CA.

Klippel, W, Warneck, P, 1980 Formaldehyde content of the atmospheric aerosol Atmospheric Environment 14 809
Kordesch, K V, Simader, G R 1995 Environmental Impact of fuel cell technology Chemical Reviews 95, 191–207
Krahl, J Baum, K., Hackbarth U, Jeberien, H-E., Munack A Schutt, C Schroder, O, Walter, N, Bunger J, Muller M M, Weigel, A 2001 Gaseous compounds, ozone precursors, particle number and particle size distributions and mutagenic effects due to biodiesel Transactions of the American Society of Automotive Engineers 44, 179–191
Krahl J, Bunger, J, Schroder, O, Munack, A, Knothe, G, 2002a. Exhaust emissions and health effects of particulate matter from agricultural tractors operating on rapeseed oil methyl ester Journal of the American Oil Chemists Society 79 717–723
Krahl, J Munack A Schroder, O Bunger, J, Bahadir M, 2002b Environmental impacts and health impacts due to biodiesel exhaust gas Fresenius Environmental Bulletin 11, 823–828
Lack, D.A Lerner, B, Granier, C, Massoli P Baynard T, Lovejoy E, Ravishankara, A, Williams, E, 2007 Light absorbing carbon emissions from commercial shipping impacts for local air quality and the Arctic In EOS Transactions American Geophysical Union, 88, Fall Meeting Supplement Abstract A32A 05
Langer, S Ljungstrom E., Wangberg I, Wallington TJ, Hurley M D, Nielsen, O J, 1996 Atmospheric chemistry of di-tert-butyl ether Rates and products of the reactions with chlorine atoms, hydroxyl radicals, and nitrate radicals International Journal of Chemical Kinetics 26, 299–306
Levin I, December 4 2002 Mercury science an update Electric Power Research Institute, Presentation to the Edison Electric Institute
Lin, C-Y Lin, H-A, 2006 Diesel engine performance and emission characteristics of biodiesel produced by the peroxidation process Fuel 85, 298 305
Lin, YC Cheng M T, 2007 Evaluation of formation rates of NO_2 to gaseous and particulate nitrate in the urban atmosphere Atmospheric Environment 41, 1903–1910
Linak, WP, Miller, C A Wendt, J O L. 2000a Comparison of particle size distributions and elemental partitioning from the combustion of pulverized coal and residual fuel oil Journal of the Air and Waste Management Association 50, 1532–1544
Linak, W P Miller, C A Wendt, J O L., 2000b Fine particle emissions from residual fuel oil combustion Characterization and mechanisms of formation Proceedings of the Combustion Institute 28, 2651–2658
Lloyd, A C Cackette, T A, 2001 Diesel engines environmental impact and control Journal of the Air and Waste Management Association 51, 809–847
Marley, N A, Gaffney, J S, Cunningham M M 1993 Aqueous greenhouse species in clouds fogs, and aerosols Environmental Science and Technology 27, 2864–2869
Marley N A Gaffney, J S, Baird, J C, Blazer, C A, Drayton P J Frederick, J E. 2001 The determination of scattering and absorption coefficients of size-fractionated aerosols for radiative transfer calculations Aerosol Science and Technology 34, 535–549
Marley, N A, Gaffney, J S, Ramos-Villegas, R., González B C 2007 Comparison of measurements of peroxyacyl nitrates and primary carbonaceous aerosol concentrations in Mexico City determined in 1997 and 2003 Atmospheric Chemistry and Physics 7, 2277–2285
Marley, N A Gaffney, J S, Stuchio, N C, Heraty, L.J Martinez, N, Guilderson T Castro T, Salcido A 2008 Measurements of aerosol absorption and scattering in Mexico City during the MILAGRO field campaign a comparison of results from the T0 and T1 sites Atmospheric Chemistry and Physics Discussions 8, 1–32
Marmer, E, Vignati E, Langmann, B, Dentener F, Hjorth J Velchev, K, Cavalli, F, van Aatdenne J A 2007 Assessment of impact of ship emissions over the summertime Mediterranean EOS Transactions American Geophysical Union 88, Fall Meeting Supplement, Abstract A14D 08
Maxwell, I E, Naber, J E., 1992 New and improved catalytic processes for clean fuels Catalysis Letters 12 105–116
McBride, J P, Moore, R E, Witherspoon J P, Blanco, R E, 1978 Radiological Impact of Airborne Effluents of Coal and Nuclear Plants Science 8 1045–1050
McKerall, W C, Ledbetter, W B Teague, D J, 1982 Analysis of Fly Ashes Produced in Texas Texas Transportation Institute, Research Report No 240-1 Texas A&M University, College Station, Texas
McNair, L Russell A, Odman, M T, 1992 Airshed calculation of the sensitivity of pollutant formation to organic compound classes and oxygenates associated with alternative fuels Journal of the Air and Waste Management Association 42, 174–178
Meyers, J F, Pichumani, R, Kapples, B S, 1976 Fly ash A Highway Construction Material Federal Highway Administration, Report No FHWA-IP-76 16 Washington, DC.
Middleton, J T, Kendrick J B, Schwalm, H W 1950 Injury to herbaceous plants by smog or air pollutants Plant Disease Reports 34 245–252
Middleton, J T, 1961 Photochemical air pollution damage to plants Annual Reviews of Plant Physiology 12, 431–448
Mittlelbach, M, Tritthart, H Junek, K, 1985 Diesel fuel derived from vegetable oils II Emission tests using rape oil methyl ester Energy in Agriculture 4, 207–215
Molina, L.T, Molina, M J, 2002 Air quality impacts local and global concern In Molina, L.T, Molina M J (Eds) Air quality in the Mexico MegacityAn integrated Assessment Kluwer Academic, Netherlands
Muniyappa, P R, Bramer, S C, Noureddini, H 1996 Improved conversion of plant oils and animal fats into biodiesel and co-product. Bioresource Technology 56, 19–24
Nizich, S V, Pope, C A 1998 National air pollution emission trends update 1970–1997 EPA 454/E-98-007 US Environmental Protection Agency, Office of Air Quality and Standards Research Triangle Park, NC, December
Noorman, M T, 1993 The Effect of MTBE, DIPE, and TAME on Vehicle Emissions Society of Automotive Engineers Technical Series Paper Number 932668 Society for Automotive Engineers, Warrendale, Pennsylvania
Oros, D R, Simoneit, B R T, 2000 Identification and emission rates of molecular tracers in coal smoke particulate matter Fuel 79, 515–536
Peterson, C L., 1986 Vegetable oil as a diesel fuel Status and research priorities Transactions of the American Society of Agricultural Engineers 29 1413–1422
Peterson, C L., Feldman M, Korus, R., Auld, D L., 1991 Batch type transesterification process for winter rape oil Applied Engineering in Agriculture 7, 711–716
Peterson C L., Reece, D, 1996 Emissions characteristics of ethyl and methyl ester of rapeseed oil compared with low sulfur diesel control fuel in a chassis dynamometer test of a pickup truck Transactions of the American Society of Agricultural Engineers 39 805–816
Phillips, D H, 1983 Fifty years of benzo(a)pyrene Nature 303, 468–472
Pitts Jr, J N, Van Cauwenberghe, K A, Grosjean D, Schmid, J P, Fitz, D R, Belser, W L, Knudson G P, Hynds P M, 1978 Atmospheric reactions of polycyclic aromatic hydrocarbons facile formation of mutagenic nitro derivatives Science 202, 515–519
Pitts Jr J N Lokensgard, D M Ripley, P S, Van Cauwenberghe K A, Van Veck, L, Shaffer, S D Thill, A J Belser Jr, W L., 1980 Atmospheric epoxidation of benzo(a)pyrene by ozone formation of the metabolite benzo(a)pyrene-4 5-oxide Science 210 1347–1349
Pitts Jr, J N 1993 Anthropogenic ozone acids and mutagens half a century of Pandora s NO_x Research on Chemical Intermediates 19, 251–298
Popp, C J, Zhang, L., Gaffney, J S 1995 Organic carbonyl compounds in Albuquerque, New Mexico an A preliminary study of the effects of oxygenated fuel use In Stenlett F S (Ed), Alternative Fuels and the Environment Lewis Publishers, Boca Raton, FL, pp 61–74
Querol, X, Alastuey, A, Puicercus, J A, Mantilla, E Miro, J V, Lopez-Soler, A, Plana, F Artinano, B, 1998 Seasonal evolution of suspended particles around a large coal-fired power station particulate levels and sources Atmospheric Environment 32, 1963–1978
Raga, G B, Baumgardner, D, Castro, T, Martínez-Arroyo, A, Navarro-Gonzalez R, 2001 Mexico City air quality a qualitative review of gas and aerosol measurements (1960–2000) Atmospheric Environment 35 4041–4058
Ramanathan V Chung, C, Kim, D Bettge, t, Buja L., Kiel J T Washington, W M Fu Q., Sikka, D R, Wild M, 2005 Atmospheric brown clouds impacts on South Asian climate and hydrological cycle Proceedings of the National Academy of Science USA 102, 5326–5333
Ren, T, Li, Y Fang D, Li, H, 1998 Comparative health risk assessment of nuclear power and coal power in China Journal of Radiological Protection 18, 29–36
Reuter, R M Benson, J D, Burns, V R Gorse, R A Hochhauser A M, Koel, W J, Painter, J, Rippon, B H, Rutherford, J A, 1992 Effects of Oxygenated Fuels and RVP on Automotive Emissions, Society of Automotive Engineers Technical Paper Number 920326, Society of Automotive Engineers, Warrendale, Pennsylvania
Rose N L., Alliksaar, T, Bowman, J J, Fott J, Harlock, S, Punning J-M St Clair-Gribble, K, Vukic J, Watt, J, 1998 The FLAME project general discussions and conclusions Water, Air, and Soil Pollution 106, 329–351
Sawyer, R.F, Harley R A Cadle, S H Norbeck, J M, Slott, R., Bravo, H A, 2000 Mobile sources critical review 1998 NARSTO assessment Atmospheric Environment 34 2161–2181
Schauer J Kleeman, M, Cass, G, 1998 Characterization and control of organic compounds emitted from air pollution sources Report Number 93-329, California air resources board, Sacramento, CA
Schmidt, V M, Brockerhoff, P Hohlein B, Menzer, R, Stimming U 1994 Utilization of methanol for polymer electrolyte fuel cells in mobile systems Journal of Power Sources 49, 299–313
Schumacher L.G, Borgelt, S C, Fosseen D, Goetz, W Hires W G, 1996 Heavy-duty engine exhaust emission tests using methyl ester soybean oil/diesel fuel blends Bioresource Technology 57, 31–36
Senum, G I, Gaffney, J S, 1985 In Sundquist, E T, Broecker, W S (Eds) The Carbon Cycle and Atmospheric CO_2: Natural Variations Achaean to Present Geophysical Monograph 32 American Geophysical Union, Washington, DC, pp 61–69
Serfass, J A Bergman M K, Rodenhiser, W 1994 Commercial, environmental and legislative factors that influence the implementation of fuel cells Journal of Power Sources 49, 193–208
Sigmund, C W 1969 Will desulfurized fuels help? Journal of the American Society of Heating Refrigeration and Air Conditioning Engineers 11, 29–33
Singleton, D L. Britton, A Jiang, W McLaren, R, Lamy, S, 1998 Primary and secondary air toxics from gasoline-alcohol transportation fuels International Journal of Vehicle Design 20, 263–273
Sjogren, M, Li, H, Rannug, U, Westerholm R, 1996 Multivariate analysis of exhaust emissions from heavy duty diesel fuels Environmental Science and Technology 30 38–48
Smith, D F, Kleindienst, T E., Hudgens, E.E., McIver, C.D, Bufalini J J 1991 The photooxidation of methyl tertiary butyl ether International Journal of Chemical Kinetics 23 907–924
Smith, W S 1962 Atmospheric emissions from fuel oil combustion an inventory guide Report Number 999-AP-2, US-Environmental Protection Agency, Research Triangle Park, NC
Stephens, E R., 1987 Smog studies of the 1950s EOS Transactions 68, 91–93
Stodolsky, F, Santini, D J, 1993 Fueling up with natural gas Chemtech 23 54–59

Stump, F.D., Knapp, K.T., Ray, W.D., Siudak, P.D., Snow, R.F., 1994. Influence of oxygenated fuels on the emissions from three pre-1985 light duty passenger vehicles. Journal of the Air and Waste Management Association 44, 781–786.

Tabata, T., Baba, K., Kawashima, H., 1995. Deactivation by poisoning of three-way catalyst for natural gas-fueled engines. Applied Catalysis B: Environmental 7, 19–32.

Tanner, R.L., Miguel, A.H., deAndrade, J.B., Gaffney, J.S., Streit, G.E., 1988. Atmospheric chemistry of aldehydes: Enhanced peroxyacetyl nitrate formation from ethanol-fueled vehicular emissions. Environmental Science and Technology 22, 1026–1034.

Tillman, D.A., 1991. Combustion characteristics of lignite and coal: the dominant solid fossil fuels. The Combustion of Solid Fuels and Wastes. Academic Press, London.

Tuazon, E.C., Carter, W.P.L., Aschmann, S.M., Atkinson, R., 1991. Products of the gas phase reactions of methyl-tert-butyl ether with OH radical in the presence of NO_x. International Journal of Chemical Kinetics 23, 1003–1015.

Turrio-Baldassarri, L., Battistelli, C.L., Conti, L., Crebelli, R., De Berardis, B., Iamiceli, A.L., Gambino, M., Iannaccone, S., 2004. Emission comparison of urban bus engine fueled with diesel oil and 'biodiesel' blend. Science of the Total Environment 327, 147–162.

Twomey, S., 1977. The influence of pollution on the shortwave albedo of clouds. Journal of Atmospheric Science 34, 1149–1152.

Twomey, S., 1991. Atmospheric clouds and radiation. Atmospheric Environment 25A, 2435–2442.

UNEP/Chemicals, 2002. Global Mercury Assessment – 2002. Inter-Organization Programme for the Sound Management of Chemicals (IOMC), United Nations Environmental Program. http://www.chem.unep.ch/mercury/Report/Final%20Assessment%20report.htm.

UNEP/WHO (United Nations Environmental Program/World Health Organization), 1992. Urban Air Pollution in Megacities of the World. Blackwell, Oxford.

UNSCEAR, 1982. Report of the United Nations Scientific Committee on the Effects of Atomic Radiation, 125, United Nations, New York.

US-DOE, 2000. Carbon dioxide emission from the generation of electric power in the United States. http://www.eia.doe.gov/cneaf/electricity/page/co2_report/co2report.html.

US-DOE, 2007. Electric Power Annual. Energy Information Administration, Office of Statistics of the U.S. Government. http://www.eia.doe.gov/cneaf/electricity/epa/epa_sum.html.

US-EPA, 1982. Emission factor determination for AP-42, US Environmental Protection Agency, Code of Federal Regulations, Title 40, Part 50, US Government Printing Office, Washington, DC.

US-EPA, 1994. Health Risk Perspectives on Fuel Oxygenates, EPA 600/R-94/217, Office of Research and Development, Washington, DC.

US-EPA, 1999a. National Emissions Inventory for Hazardous Air Pollutants. Office of Air Quality and Standards. http://www.epa.gov/ttn/chief/net/1999inventory.html#final3haps.

US-EPA, 1999b. Fate and transport of mercury in the environment. Volume III. Mercury Study Report to Congress, 452/R-97-005.

US-EPA, 2003. National Air Quality and Emissions Report. Appendix A. http://www.epa.gov/air/airtrends/aqtrnd03/.

US-EPA, 2005. Light-duty automotive technology and fuel economy trends, 1975 through 2005. Report EPA420-R-001, Ann Arbor, MI.

Van Krevelen, D.W., 1961. Coal Typology, Chemistry, Physics, Constitution. Elsevier, Amsterdam.

Wallington, T.J., Japar, S.M., 1991. Atmospheric chemistry of diethyl ether and ethyl tert-butyl ether. Environmental Science and Technology 25, 410–415.

Wang, M., 2003. Well-to-wheels energy and emission impacts of vehicle/fuel systems: development and applications of the GREET Model. http://www.transportation.anl.gov/pdfs/TA/273.pdf.

Wang, W.G., Clark, N.N., Lyons, D.W., Yang, R.M., Gautam, M., Bata,M., Loth, J.L., 1997. Emissions comparisons from alternate fuel busses and diesel busses with a chassis dynamometer testing facility. Environmental Science and Technology 31, 3132–3137.

Weng, Y., Chu, T.C., 1992. Concentration of radionuclides of size fractionated fly ash emissions from a thermal power plant using Taiwan coal. Journal of Radiation Research 33, 141–150.

Zielinska, B., Harshfield, G., Shire, J., Sagebiel, J., 1997. Impact of Reformulated Gasoline on Ambient Air Quality in the South Coast Air Basin, California, Paper 1434. In: The Fifth Chemical Congress of North America, Cancun, Quintana Roo, Mexico, November 1997.

Zielinski, R.A., Budahn, J.R., 1998. Radionuclides in flu ash and bottom ash: Improved characterization based on radiography and low energy gamma ray spectrometry. Fuel 77, 259–267.

Zimmerman, M., 2004. Paleopathology and study of ancient remains. In: Encyclopedia of Medical Anthropology, vol. I. Springer, US.